

# UC Riverside

## UC Riverside Electronic Theses and Dissertations

### Title

Skull Growth and Prenatal Development in Baleen Whales: Teeth to Baleen Transition in Ontogeny and Phylogeny

### Permalink

<https://escholarship.org/uc/item/2589031q>

### Author

Lanzetti, Agnese

### Publication Date

2019

Peer reviewed|Thesis/dissertation

UNIVERSITY OF CALIFORNIA  
RIVERSIDE

AND

SAN DIEGO STATE UNIVERSITY

Skull Growth and Prenatal Development in Baleen Whales:  
Teeth to Baleen Transition in Ontogeny and Phylogeny

A Dissertation submitted in partial satisfaction  
of the requirements for the degree of

Doctor of Philosophy

in

Evolutionary Biology

by

Agnese Lanzetti

September 2019

Dissertation Committee:

Dr. Annalisa Berta, Co-Chairperson

Dr. Mark Springer, Co-Chairperson

Dr. John Gatesy

Dr. Kevin Burns

Dr. Thomas Deméré

Copyright by  
Agnese Lanzetti  
2019

The Dissertation of Agnese Lanzetti is approved:

---

---

---

---

Committee Co-Chairperson

---

Committee Co-Chairperson

University of California, Riverside  
San Diego State University



## Acknowledgments

I thank my advisor Annalisa Berta, who believed that I could succeed in a biology program despite my geology background. I also thank my UCR advisor John Gatesy, who patiently taught me many useful skills, and my other committee members Mark Springer, Kevin Burns and Tom Deméré.

For Chapter One, I thank John Gatesy and Michael McGowen for their help in the beaked whale phylogeny project. I thank John Gatesy and Mark Springer who designed the sequencing study process of gene *C4orf26* that I contributed to. I also thank my co-authors for the review paper on mysticete evolution Annalisa Berta, Eric Ekdale and Tom Deméré.

For Chapter Two, I thank my co-authors on the humpback whale development paper Annalisa Berta and Eric Ekdale, and Tim Smith (editor) and two anonymous reviewers for insightful comments on earlier drafts of the manuscript. Also for the humpback whale project, I thank for help handling specimens and the iodine staining Mike Van Patten and John Hansen at San Diego State University, and Daniel Klingberg of the Natural History Museum of Denmark. I thank the curators at the institutions that loaned specimens, in particular Jim Dines LACM, Brian O'Toole AMNH, Chris J. Conroy MVZ, and Morten Tange Olsen ZMUC. Special thanks to Phil Unitt SDNHM who agreed to let me test for the first time the new iodine-enhancement protocol. I also thank the institutions and personnel that performed the CT scanning: Matthew Costa at the Horton Hospital in San Diego, CA, Matt Colbert and Jessie Maisano at UTCT in Austin, TX, and Chiara Villa at the Laboratory of Biological Anthropology of the University of Copenhagen, Denmark. For the minke whale paper, I thank Annalisa Berta and Eric Ekdale and two anonymous reviewers for their thoughtful comments that significantly improved the manuscript. For data collection, a special thanks goes to Yuko Tajima, Tadasu Yamada, Naoki Kohno, Kumiko Matsui, and all the graduate students at the National Museum of Science in Tsukuba,

Japan (NSMT) that granted access to the specimens, and greatly helped me during my visit to the museum. I am also grateful to Daisuke Hasegawa and the rest of the staff at Nippon Veterinary and Life Science University in Tokyo, Japan that worked after hours to allow me to obtain the CT scans of the fetal specimens from NSMT. For access to the specimens at the Natural History Museum of Denmark in Copenhagen (ZMCU), I thank M. T. Olsen and D. Klingberg. I would also like to thank C. Villa at the Laboratory of Forensic Anthropology of the University of Copenhagen, Denmark for the CT scans of the ZMCU specimens. I thank Emily Buchholtz for sharing the CT images of the Smithsonian Institution (USNM) neonate minke, as well as Giacomo Franci for his dissertation work collecting 3D models of postnatal minke whale skull. I also thank Doug Boyer for his help uploading and organizing the data on the MorphoSource database.

For Chapter Three, I thank Annalisa Berta, Eric Ekdale and Tom Deméré for the insightful discussions and help they provided by allowing me to use the scan of *Aetiocetus*† in this project. I also thank Jonathan Geisler and Rachel Racicot for sharing the scan of *Coronodon*† with me. Other specimens were kindly provided by E. Buchholtz, G. Franci and E. Ekdale. For access to the fossil specimens in Japan, I would like to thank N. Kohno and K. Matsui, and the director and staff at the Port of Nagoya Public Aquarium. I also thank again the curators at the various institution that lent me fetal specimens, and the staff at the many CT scan facilities I visited.

This dissertation was supported by iDigBio, the Lerner-Gray Grant for Marine Research awarded by the American Museum of Natural History, the SDSU Graduate Student Travel Fund, the University of California, Riverside Newell Award, Sigma Xi Grants-in-Aid of Research, the American Society of Mammalogists Grants-in-Aid of Research, the Gretchen L. Blechschmidt Award from the Geological Society of America and by the Mid-American Paleontology Society

(MAPS) Outstanding Student Research Award from The Paleontological Society. I also thank the Fulbright Commission of Italy for awarding me the IIE scholarship that allowed me to apply to this JDP and conduct my research in the United States.

Last but not least, I thank my past labmates Giacomo Franci, Reagan Furbish, Meghan Smallcomb Corrie, and Bridget Borce, and all the graduate students in the EB program at SDSU and EEOB at UCR that helped me in many ways throughout my Ph.D.. I also thank the “marine mammal” community for the insightful annual discussions at SVP. Finally, I thank my friends, both the ones I made in these last 5 years and the ones that have always been there, for bearing with me through the good and the bad, and my parents and family for their unconditional love and support.

## **Dedication**

*A Speranza, piccola donna dalla grande forza.*

## ABSTRACT OF THE DISSERTATION

Skull Growth and Prenatal Development in Baleen Whales:  
Teeth to Baleen Transition in Ontogeny and Phylogeny

by

Agnese Lanzetti

Doctor of Philosophy, Graduate Program in Evolutionary Biology  
University of California, Riverside and San Diego State University, September 2019  
Dr. Annalisa Berta and Dr. John Gatesy, Co-Chairpersons

In my dissertation, I aim to add a new ontogenetic perspective to the study of baleen whale's (Mysticeti, Cetacea) skull evolution. In Chapter One, I analyze changes in dentition in closely-related toothed whales (Odontoceti, Cetacea), focusing on beaked whales, and trace the evolution of inactivating mutations in tooth-related genes in Mysticeti. While there is high variability in tooth counts in odontocetes, with many instances of convergent evolution among living and fossil taxa, all modern clades retain the ability to produce full adult dentition. Mysticetes instead present a variety of inactivating mutations in at least eight tooth- and enamel-related genes. Analyzing the complex inactivation patterns of these genes, I hypothesize that loss of function preceded the complete loss of adult teeth in baleen whales. In Chapter Two, I investigate the anatomical changes that occur in the skull of baleen whales in ontogeny, focusing on the teeth-to-baleen transition. The internal anatomy of 15 specimens of minke and humpback whales was analyzed using CT scanning. I provide qualitative descriptions of the specimens and study skull shape changes using 3D geometric morphometrics (GM) methods. Tooth germs resorb completely just before eruption of the of the baleen from the gums, and they are still present for a brief period along with baleen rudiments. GM analyses show that the rostrum

progressively grows in length relative to the braincase, with the two parts of the skull showing different patterns of shape and size development. In Chapter Three, I combine developmental data with fossil evidence to directly analyze the connection between ontogeny and evolution of baleen whales using 3D GM methods. I also investigate possible differences in timing of ossification of skull bones between Cetacea and terrestrial artiodactyls. A general acceleration of skull development is likely responsible for modern mysticetes anatomy. The rostrum was the first part of the skull to increase its growth rate, allowing for the evolution of larger buccal cavity needed for bulk filter feeding. These changes in shape were not accompanied by shifts in the ossification sequence, as they appear mostly conserved among all taxa examined and not connected to their feeding adaptations.

# Table of Contents

<b>Introduction of the Dissertation</b>	<b>p. 1</b>
<b>Chapter One:</b>	
<b>Evolution of Dentition and Genetic Mechanisms of Tooth Loss in Cetacea</b>	<b>p. 5</b>
Introduction	p. 5
Materials and methods	p. 26
Results	p. 30
Discussion	p. 43
Conclusions	p. 55
Literature Cited	p. 58
<b>Chapter Two:</b>	
<b>Prenatal Development of Skull, Teeth and Baleen in Modern Mysticeti</b>	<b>p. 72</b>
Introduction	p. 72
Materials and methods	p. 83
Results	p. 101
Discussion	p. 146
Conclusions	p. 165
Literature Cited	p. 169
<b>Chapter Three:</b>	
<b>Developmental Basis for the Evolution of Skull Shape and Tooth Loss in Mysticeti</b>	<b>p.179</b>
Introduction	p. 179
Materials and methods	p. 198
Results	p. 216
Discussion	p. 246
Conclusions	p. 263
Literature Cited	p. 266
<b>Conclusions of the Dissertation</b>	<b>p. 280</b>
<b>Appendices</b>	
Appendix A: Supplementary Methods/Results for Chapter One	p. 285
Appendix B: Supplementary Tables/Figures for Chapter One	p. 292
Appendix C: Supplementary Methods/Results for Chapter Two	p. 305
Appendix D: Supplementary Tables/Figures for Chapter Two	p. 362
Appendix E: Supplementary Methods/Results for Chapter Three	p. 375
Appendix F: Supplementary Tables/Figures for Chapter Three	p. 394

# List of Figures

## Chapter One:

Figure 1.1 – Convergent loss of enamel and teeth in Mammalia	p. 13
Figure 1.2 – Phylogenetic relationships among modern cetacean families	p. 16
Figure 1.3 – Phylogeny of living species of mysticetes and their feeding adaptations	p. 22
Figure 1.4 – Composite tree of of modern Cetacea with mapped tooth counts	p. 31
Figure 1.5 – Dentition evolution in Ziphiidae	p. 36
Figure 1.6 – Tooth- and enamel-related gene inactivation in modern Mysticeti	p. 40

## Chapter Two:

Figure 2.1 – Comparison of CT slices without and with iodine staining	p. 90
Figure 2.2 – Selected landmarks for GM analyses (16 and 12 configurations)	p. 94
Figure 2.3 – Growth curves of selected Mysticeti and Odontoceti species	p. 102
Figure 2.4 – Growth rates of selected Cetartiodactyla species	p. 105
Figure 2.5 – Ancestral state reconstruction of growth rates and newborn length	p. 106
Figure 2.6 – Specimen He1 external and internal morphology	p. 111
Figure 2.7 – Specimen Hf1 external and internal morphology	p. 113
Figure 2.8 – Specimen Hf2 external and internal morphology	p. 115
Figure 2.9 – Specimen Mf3 external and internal morphology	p. 117
Figure 2.10 – Specimen Hf4 external and internal morphology	p. 119
Figure 2.11 – Specimen Mf6 external and internal morphology	p. 121
Figure 2.12 – Specimen Mf7 external and internal morphology	p. 123
Figure 2.13 – Specimen Mf10 external and internal morphology	p. 125
Figure 2.14 – Growth curves of minke whales, with teeth-to-baleen transition steps	p. 126
Figure 2.15 – “Tooth germs” stage in Mf4	p. 127
Figure 2.16 – “Baleen gums” stage in Mf6	p. 130
Figure 2.17 – “Keel” stage in Mf8	p. 131
Figure 2.18 – “Baleen ridge” stage in Mf10	p. 133
Figure 2.19 – Skull shape growth in the ontogeny of humpback and minke whales	p. 135
Figure 2.20 – Rostrum shape growth in the ontogeny of humpback and minke whales	p. 137
Figure 2.21 – PCA plot for the whole skull (16 landmarks) configuration	p. 139
Figure 2.22 – PCA plot for the rostrum-only (12 landmarks) configuration	p. 140
Figure 2.23 – Distribution of RV coefficients in modularity analysis	p. 141
Figure 2.24 – PLS1 analysis plot comparing scores for rostrum and braincase	p. 142
Figure 2.25 – Regression of PLS1 scores of rostrum and braincase	p. 144
Figure 2.26 – Changes in rostrum and braincase shape relative to skull size	p. 145
Figure 2.27 – Change in mandible curvature in ontogeny of the humpback whale	p. 163
Figure 2.28 – Changes in mandibular canal in ontogeny of minke whales	p. 164
Figure 2.29 – Diagram of changes in the teeth-to-baleen transition of minke whales	p. 167



### Chapter Three:

Figure 3.1 – Phylogeny of extant and extinct Mysticeti	p. 190
Figure 3.2 – Measurements used in 2D allometric analyses	p. 203
Figure 3.3 – Trees mapped in GM analyses	p. 210
Figure 3.4 – 2D changes in proportions of each element to skull length	p. 218
Figure 3.5 – 3D changes in skull shape relative to skull size	p. 219
Figure 3.6 – bgPCA plot for the whole skull (16 landmarks) configuration	p. 222
Figure 3.7 – Box plots of bgPC1 and bgPC2 for the whole skull configuration	p. 224
Figure 3.8 – bgPCA plot for the rostrum-only (12 landmarks) configuration	p. 226
Figure 3.9 – Box plots of bgPC1 and bgPC2 for the rostrum-only configuration	p. 227
Figure 3.10 – Distribution of RV coefficients in modularity analysis	p. 229
Figure 3.11 – PLS1 analysis plot comparing scores for rostrum and braincase	p. 231
Figure 3.12 – Regression of PLS1 scores of rostrum and braincase	p. 232
Figure 3.13 – Changes in ossification sequence of Cetartiodactyla using ACCTAN	p. 235
Figure 3.14 – Changes in ossification sequence of Cetartiodactyla using DELTRAN	p. 237
Figure 3.15 – Ossification sequences of Cetartiodactyla in order of similarity	p. 239
Figure 3.16 – ASR of timing of ossification of maxilla and of tooth mineralization	p. 242
Figure 3.17 – ASR of timing of ossification of dentary and of tooth mineralization	p. 243
Figure 3.18 – ASR of timing of ossification of supraoccipital and EQ values	p. 245
Figure 3.19 – Allometric trajectories in skull growth of minke whales	p. 248
Figure 3.20 – Allometric trajectories of skull shape in extinct and extant Mysticeti	p. 253

# List of Tables

## Chapter Two:

Table 2.1 – List of specimens examined in Chapter Two	p. 86
Table 2.2 – CT scan details for the analyzed specimens	p. 92
Table 2.3 – Landmarks used in GM analyses as depicted in Figure 2.2	p. 94
Table 2.4 – List of postnatal specimens used in GM analyses	p. 96
Table 2.5 –Teeth-to-baleen transition in prenatal humpback whales	p. 108
Table 2.6 –Teeth-to-baleen transition in prenatal minke whales	p. 109
Table 2.7 – Tooth germs relative size in ontogeny of humpback and minke whales	p. 129
Table 2.8 – PCA principal components for 16 and 12 landmark configurations	p. 138

## Chapter Three:

Table 3.1 – List of specimens examined in Chapter Three	p. 200-201
Table 3.2 – Measurements used in 2D allometric analyses	p. 204
Table 3.3 – 2D allometric coefficients and growth patterns	p. 217
Table 3.4 – 3D allometric coefficients and growth patterns	p. 220
Table 3.5 – bgPCA principal components for 16 and 12 landmarks configurations	p. 221
Table 3.6 – Scores for trees mapped on bgPCA for both landmarks configurations	p. 222
Table 3.7 – Scores for trees mapped on PLS1	p. 230

# List of Supplementary Figures

## Chapter One:

Figure S1.1 – Molecular phylogenies of living species of Ziphiidae	p. 302
Figure S1.2 – Total evidence phylogeny of living and fossil Ziphiidae, equal weights	p. 303
Figure S1.3 – Total evidence phylogeny of living and fossil Ziphiidae, k=3	p. 304

## Chapter Two:

Figure S2.1 – Measurements taken on smaller/younger specimens	p. 363
Figure S2.2 – Detailed growth curves of selected Mysticeti and Odontoceti species	p. 364
Figure S2.3 – Growth rates for all selected Cetartiodactyla species	p. 365
Figure S2.4 – Specimen Mf2 external morphology and CT image of rostrum	p. 366
Figure S2.5 – Specimen Hf3 external and internal morphology	p. 367
Figure S2.6 – Specimen Mf4 external and internal morphology	p. 368
Figure S2.7 – Specimen Mf5 external and internal morphology	p. 369
Figure S2.8 – Specimen Mf8 external and internal morphology	p. 370
Figure S2.9 – Specimen Mf9 external and internal morphology	p. 371
Figure S2.10 – PCA plot “by specimen” for the 16 landmarks configuration	p. 372
Figure S2.11 – PCA plot “by specimen” for the 12 landmarks configuration	p. 373
Figure S2.12 – PLS1 analysis plot “by specimen” for rostrum and braincase	p. 374

## Chapter Three:

Figure S3.1 – Selected landmarks for GM analyses (16 and 12 configurations)	p. 396
Figure S3.2 – Tree topology used for ASR heterochrony analyses	p. 397
Figure S3.3 – PCA plot for the whole skull (16 landmarks) configuration	p. 398
Figure S3.4 – PCA plot for the rostrum-only (12 landmarks) configuration	p. 399

## List of Supplementary Tables

### Chapter One:

Table S1.1 – Tooth counts for all modern species of Cetacea	p. 292
Table S1.2 – Sources and GenBank accession numbers for mtDNA genes	p. 301

### Chapter Two:

Table S2.1 – Detailed measurements specimens	p. 362
Table S2.2 – PCA principal components “by specimen” for 16 and 12 configurations	p. 362

### Chapter Three:

Table S3.1 – Equations and p-value of the regressions for 2D allometric analysis	p. 394
Table S3.2 – Landmarks used in GM analyses as depicted in Figure S3.1	p. 394
Table S3.3 – Equations and p-value of the regressions for 3D allometric analyses	p. 395
Table S3.4 – PCA principal components for 16 and 12 landmarks configurations	p. 395

## **Introduction of the Dissertation**

Dentition is a key part of the feeding strategy of vertebrates, allowing them to take advantage of a variety of food resources. However many successful vertebrates including frogs, turtles, birds and edentulous mammals lost teeth and evolved alternative feeding strategies. This change was also accompanied by modifications in the skull, such as the evolution of the horny beak in birds. Loss of teeth and acquisition of related adaptations was made possible in these animals by complex changes in their genomes and in their ontogeny. Particularly for mammals, little information is available on these evolutionary mechanisms, either on an anatomical or molecular level.

Baleen whales (Mysticeti, Cetacea) represent a unique system to study tooth loss and its developmental aspects given their extensive fossil record that documents the transition from teeth to baleen. Together with toothed whales (Odontoceti, Cetacea), they have evolved unique feeding strategies in the marine environment. Compared to their relatives terrestrial Artiodactyla (even-toed ungulates – e.g. hippo, cow), odontocetes have evolved a variety of dental patterns and disparate rostral morphologies used to capture prey in a variety of aquatic environments, from shallow rivers to deep ocean trenches. Alternatively, all extant mysticetes are characterized by distinctive feeding structures, baleen, composed of keratinous filaments developed at the edges of the palate, which have completely replaced adult teeth. The appearance of baleen allowed mysticetes to switch from the ancestral raptorial feeding mode, still partially employed by toothed whales, to bulk filter feeding. The loss of teeth and the need for a more flexible rostrum and mandible resulted in major modifications in the skull of baleen whales, for the most part not shared by odontocetes. Interspecific variation in skull shape is also observed in adults of extant and fossil mysticetes, reflecting differences in filter feeding mode.

Current evidence from the fossil record suggests that the loss of teeth occurred once in the common ancestor of all modern mysticetes after the first appearance of baleen, however there is still controversy on whether extinct lineages retaining full dentition possessed baleen-like structures. Whenever this change occurred, it allowed ancestral taxa to better adapt to bulk filter feeding, following the loss of its primary function, and it was correlated with the acquisition of a kinetic rostrum and mandible. Traditional developmental studies based on descriptive anatomy of mysticete fetuses revealed that they still develop tooth buds in the fetal stages in both upper and lower jaws, but teeth never erupt, and the neonates bear baleen plates. However, very little is known of baleen whale ontogeny, and the available literature on this topic lacks a phylogenetic context and is based on a single species. In this framework, my Ph.D. research aims to collect new qualitative and quantitative data on the anatomical development of modern mysticetes, and to combine this evidence with fossil and genetic information to better understand the role of ontogeny in the evolution of tooth loss and filter feeding in this group.

In my first Chapter, I will investigate the evolutionary origin and genetic drivers of the changes in dentition in Cetacea. First, extreme tooth reduction in Ziphiidae (beaked whales), a distinctive but poorly known family of odontocetes, will be examined in the context of tooth number variation in their fossil relatives and of modern toothed whales as a whole. To achieve this goal, I will construct a novel phylogeny of beaked whales combining molecular and morphological data. This investigation of instances of tooth loss in Odontoceti will serve as general framework for studying tooth loss in mysticetes. Secondly, the genetic basis of edentulism in baleen whales will be examined. Current evidence on tooth- and enamel-related gene sequences in Mysticeti will be reviewed in a phylogenetic context. In particular, I will describe the results of the sequencing of gene *C4orf26* that I have contributed to. This will serve

as a foundation to formulate overarching hypothesis on the mode and tempo of the teeth-to-baleen transition and related skull changes in the ontogeny and evolution of Mysticeti.

In my second Chapter, I will provide the first comprehensive detailed account of skull ontogeny for baleen whales, with emphasis on the transition from tooth germs to baleen, using novel techniques and quantitative methods. The Antarctic and the common minke whale (*Balaenoptera bonaerensis* and *B. acutorostrata*) and the humpback whale (*Megaptera novaeangliae*) were chosen for the study, based on availability and size of the specimens, as well as considering the previously available information on these species. Specifically, I will first compile growth curves for selected species of mysticetes, odontocetes, and terrestrial artiodactyls using published data, to be able to readily compare the anatomy of the analyzed specimens to other taxa. Secondly, I will describe in detail the morphology of five humpback whale and eight Antarctic minke whale and two common minke whale prenatal specimens, focusing on the ossification sequence and shape changes in the skull and the teeth-to-baleen transition. Thirdly, 3D landmark analysis is used to quantify skull shape changes in the developmental series of minke whales and humpback whale, including both prenatal and postnatal specimens of each species. Finally, these results are evaluated in the context of previous research on baleen whales and qualitatively compared with similar data available on the ontogeny of toothed whales as well as terrestrial artiodactyls. This will allow the formulation of hypotheses on the developmental origin of the characteristic traits of Mysticeti, and to highlight the ontogenetic transformations that accompany the teeth-to-baleen transition in these taxa. This knowledge will then be used to interpret the anatomical changes observed in the skull of extinct mysticetes, documenting the role of development in the evolution of this lineage.

In my third Chapter, I will combine the previously collected information on the ontogeny of modern species of baleen whales with data from the fossil record. First, I will identify what

major changes in developmental timing and growth rate have enabled the transition of feeding modes during mysticetes evolution and how they relate to the teeth-to-baleen transition. I will use quantitative methods such as 3D landmark analyses on a dataset that includes modern taxa at different stages of development and fossil specimens. Secondly, newly collected ossification sequence data for Mysticeti will be analyzed with information available in the literature for Odontoceti and living terrestrial artiodactyls using ancestral state reconstruction and independent phylogenetic contrasts methods to identify key heterochronic shifts that characterize Mysticeti and Cetacea as a whole. These analyses will allow to the formulation of hypotheses on how these changes are connected to the transition from a terrestrial to an aquatic environment and to the different feeding mode of toothed and baleen whales.



## ***Chapter One***

# **Evolution of Dentition and Genetic Mechanisms of Tooth Loss in Cetacea**

## **Introduction**

### **Connecting trait loss and prenatal development with evolution**

Charles Darwin was one of the first scientists to take interest in loss of characters in *On the origin of species* (1859), where he noticed how common vestigial and rudimentary structures are in nature, especially observing animals' embryos, and presented them as evidence for natural selection and evolutionary theory (Fong et al., 1995, Cabej, 2012). The study of vestigialization and its causes were not seen as particularly important in the first decades of the 20<sup>th</sup> century (Cracraft, 1990, Fong et al., 1995), even if it was known that the loss of a trait is ten times more common than the appearance of new characters (Haldane in Kimura, 1983, p. 61, Fong et al., 1995).

Lost traits can follow different paths in evolution. Some can be “reverted” and reacquired after being lost or reduced in an ancestor (Hall, 2003). This event was thought to be almost impossible, as the widely accepted evolutionary principle commonly known as “Dollo’s Law” states that complex traits lost in a lineage cannot be regained in the ancestral state later in evolution (Dollo, 1893, Gould, 1970). This “law” held true for many decades after its original formulation in the late 19<sup>th</sup> century, but modern phylogenetic analyses began to question the general validity of the statement (Marshall et al., 1994, Collin and Miglietta, 2008). More commonly traits that lost their function become rudiments, if they can only be observed in the

prenatal stages, or vestiges, if they are still partly recognizable in the adults. When vestiges develop to form complete structures in some adults they are defined as atavisms (Hall, 2003).

Sewall Wright, following R. A. Fisher theories on dominance, proposed that the reduction of traits is due to the onset of inactivating mutations, which can be acted upon by selective forces (Wright, 1929, Wright, 1964, Brace, 1963). These mutations, while very common, would not compromise the general fitness of the organism because of pleiotropic effects of genes and their recessive inheritance (Wright, 1929, Wright, 1964). This simple mechanism was believed to be responsible for trait loss until more experimental evidence accumulated, exposing the fact that mutations could not account for all the structure reduction in evolution. It was discovered how the loss of the same trait could be achieved in multiple ways, and more complex interactions between genotypes and phenotypes were in play (Brace, 1963, Prout, 1964).

It has now been shown that trait reversal and loss do not follow a simple pattern, where genetic mutations are the main driver of evolutionary change (e.g. Fong et al., 1995, Cabej, 2012). Modern molecular studies and improved phylogenetic methods questioned the irreversibility of trait loss in evolution. Marshall et al.'s (1994) survey of studies on pseudogenes found that it was theoretically possible for genes inactivated less than 10 Mya to be reactivated successfully under the right environmental conditions. Instances of regaining lost traits are now commonly documented in many groups of animals, thanks to improvements in ancestral state reconstruction algorithms (Collin and Miglietta, 2008). Striking examples are the recovery of wings in Phasmatodea (stick insects), which are believed to have radiated from wingless ancestors. Three lineages independently regained the ability to fly (Whiting et al., 2003). An exceptional example of reversal specific to ontogeny can be found in the frog genus *Gastrotecha*. Many species of this group independently regained the tadpole stage of development, despite the ancestral condition of direct development (Wiens et al., 2007). Moreover, the species *G.*

*guentheri* was once believed to occupy a basal position in the phylogenetic tree of frogs, since it has mandibular teeth. However, likelihood analyses of molecular evolution support the hypothesis that this species independently re-evolved this trait after 200 million years from the last toothed ancestor (Wiens, 2011).

The causes and evolutionary consequences of trait loss are different for each group, and it is important to investigate their ontogenetic and genetic origin as these processes are deeply linked (Atchley and Hall, 1991, Gilbert and Bolker, 2001, Hall, 2003). Studying rudimentary traits present in the prenatal development of organisms can also help reconstructing their phylogeny (Wiens et al., 2005, Wiens et al., 2007). Additionally, by integrating paleontological evidence with developmental and genetic data, it is possible to determine homology of these traits and understand broad evolutionary mechanisms (Hall, 2002, Hall, 2003, Thewissen et al., 2012).

### **Evolution and loss of teeth in vertebrates**

A wide variety of traits appears to have been lost and regained convergently in the evolution of animals: from eyes and visual pigments in multiple lineages of cave organisms (e.g. arachnids, crustaceans, fishes, salamanders, rats) (e.g. Kos et al., 2001, Jeffrey, 2005, Klaus et al., 2013, Bloom et al., 2014), to forelimbs and hindlimbs in a variety of tetrapod groups such as in amphibians (caecilians), reptiles (snakes) and mammals (whales and dolphins) (Lande, 1978, Greer, 1991, Bejder and Hall, 2002, Thewissen et al., 2006). While these transformations are directly connected with the environment that these organisms have adapted to, other instances of trait loss fundamentally changed the feeding adaptations and ecology of animals. Reduction, loss and replacement of teeth represents the best and most common example of a loss of a trait that alone drastically modified the feeding strategy of multiple lineages, by influencing their cranial morphology, physiology and behavior (Huysseune and Sire, 1998, Stock et al., 2006, Davit-Béal et al., 2009, Huysseune et al., 2009).

Vertebrate teeth are mineralized units consisting of a hard tissue (dentin) attached to the bone, usually covered with a second, more superficial layer of enamel. Teeth typically pass through three main stages of prenatal development: bud, cap, and bell (Teaford et al., 2007). The shape of the teeth is determined by the number and positioning of specialized structures called enamel knots, that appear in the cap stage. They are resorbed completely when dentin and enamel start to form in late bell stage (Catón and Tucker, 2009). Dentition appeared before the evolution of the jaw in the fossil record, more than 500 million years ago (Mya) (Huyseune et al., 2009, Koussoulakou et al., 2009). After their evolution, teeth became a key part of the feeding strategy of vertebrates (Huyseune et al., 2009, Fraser et al., 2010). Therefore, a compelling question in evolutionary studies is how this key trait can be modified, even bringing dentition to disappear in many successful taxa such as frogs, turtles, birds and edentulous mammals (Davit-Béal et al., 2009, Huyseune et al., 2009).

When dentition characteristics change, the skull bones and feeding apparatus must adapt accordingly. The skull of early vertebrates went through many transformations to accommodate for the evolution of teeth in the buccal cavity in the first place. The jaw evolved separately from the teeth as a result of tissue rearrangements in the embryos of early agnathans. The teeth and oral cavity evolved their feeding function before a shared developmental pathway for the jaws was present, as observed in the lamprey (Kuratani, 2004). However, morphologists hypothesize that the development of teeth and jaw bones are correlated, especially in mammals (Thompson, 1917, Davis, 1964, Hall, 2003). Recent experiments with knock-out mice showed that the general structure of the mandible develops even in the absence of important genes related to tooth development, with minor malformations, while the maxilla cannot properly form without dentition. This demonstrates that the jaws have a developmental pathway partially separated from dentition, but they share a more complex ontogenetic link (Paradis et al., 2013, Phen et al., 2018).

Therefore, loss of teeth and skull development should be investigated together to understand the process that characterized the evolution of toothless lineages (Hall, 2003, Davit-Béal et al., 2009, Louchart and Viriot, 2011).

#### *Toothless tetrapods: frogs and birds*

Anurans (frogs, toads) are a clade in which evolutionary transformations of the skull due to lack of teeth have been studied closely. “True toads” are the only completely edentulous group, though most frogs and toads show reduced dentition, having only denticle-like structures in the upper jaws. *Gastrotheca guentheri* is the only species with mandibular teeth, and this is probably a case of re-evolution of a lost structure as mentioned previously (Davit-Béal et al., 2009, Wiens, 2011). Adult frogs use primarily the tongue as an alternative tool for food capture, while denticles are important in feeding during the tadpole stage of life (Davit-Béal et al., 2009). The shifts in diet and living environment associated with the transformation from the tadpole to the adult form are also illustrated by changes in skull shape and ossification sequence. This is particularly evident when studying the development of taxa that marked metamorphosis between tadpole and adult stages. One such group is pipoid frogs, which were found to have an accelerated jaw ossification compared to other anurans due to the absence of metamorphosis and the derived similar ecology of adults and tadpoles (Yeh, 2002, Harrington et al., 2013).

Likely the best studied vertebrate clade relative to loss of dentition are birds (Aves). In particular, most of the genetic and developmental data on tooth loss have been collected experimentally on chickens. Laboratory trials demonstrated that chick embryos are capable of developing tooth primordia when mouse tissue is inserted in their palatal region, indicating that birds still possess some of the genetic material necessary for forming dentition. However the chicken embryos that underwent this treatment died prematurely (Sire et al., 2008, Davit-Béal et al., 2009, Louchart and Viriot, 2011). However, initial experiments supporting the idea that

chicken mouth epithelium still produces enamel-capped teeth, resembling the ancestral condition observed in the fossil record (Kollar and Fisher, 1980) were likely misinterpreted. In fact, most of the tooth and enamel-related gene sequences tested in birds have been found to contain inactivating mutations (Chen et al., 2000, Sire et al., 2008, Meredith et al., 2013). From an evolutionary perspective, the loss of dentition in birds was hypothesized to be a reoccurring process in the lineage, driven by slight changes in developmental timing of expression of regulatory genes, and associated with independent acquisition of the keratinous beak (rhamphotheca) and the muscular gizzard as alternative methods to process food (Sire et al., 2008, Davit-Béal et al., 2009, Louchart and Viriot, 2011). This is supported by fossil evidence, which shows that loss of permanent dentition occurred independently several times in stem lineages of Aves and is sometimes correlated with the development of a horny beak (Louchart and Viriot, 2011, Yang and Sander, 2018). However, in modern birds the loss of teeth likely occurred once in the common ancestor, in conjunction with the evolution of the primitive beak, as molecular data shows that some enamel and tooth related genes have lost function in birds all around the same time (Meredith et al., 2014).

*Mammalian dentition: from increased complexity to tooth loss*

The typical mammalian dentition is heterodont, with teeth of different shapes and sizes along the jaws, very different from uniform and conical dentition of nonmammalian amniotes (Berkovitz and Shellis, 2018b). On a molecular level, heterodonty has been linked to different gradients of signaling proteins from *Hox* genes during the early stages of prenatal development. Proteins of the BMP family are preferentially expressed in the anterior part of the mouth, giving rise to unicuspid incisors, while proteins of the FGF family are mostly present in the posterior part, where the multicuspid molars are located (Jernvall, 2000, Jernvall and Thesleff, 2000, Mitsiadis and Smith, 2006). In stem-mammal lineages, this differential gene expression pattern

might have caused the evolution of more complex tooth germs in the posterior portion of the jaws, that then combined together to form bigger and uneven teeth, the precursors of molars (Butler, 1995, Jernvall, 2000). The evolution of uneven dentition was a key adaptation for early mammals, allowing them to occupy different niches and better process food (Berkovitz and Shellis, 2018b). As dental complexity increased, the total number of teeth and generations decreased. As a result, most modern mammals are now characterized not only by the derived condition of heterodonty, but also by having a small number of teeth compared to other groups such as reptiles (oligodonty) and just one or two tooth generations (monophyodonty or diphyodonty) (McCollum and Sharpe, 2001, Koussoulakou et al., 2009, Berkovitz and Shellis, 2018b). These changes in dentition were also accompanied by modifications in the jaw, particularly in the mandible. While non-mammalian amniotes lower jaw is composed of multiple elements, mammals only present one bone (dentary), and the other bones were instead incorporated in the middle ear as the malleus and incus (Allin, 1975, Ji et al., 2009, Berkovitz and Shellis, 2018b). These transformations led to both improvement in food processing and in sound reception, further helping early mammals to diversify and occupy new niches (Berkovitz and Shellis, 2018b).

Despite these extensive changes and acquired evolutionary advantage, some derived lineages of mammals were able to partially return to the ancestral condition of polyodonty and homodonty, presenting an elevated number of teeth all with a similar conical shape. This is the case for example in armadillos (*Xenarthra*, *Cingulata* – Davit-Béal et al., 2009), and in toothed whales (*Laurasiatheria*, *Cetartiodactyla* – Berkovitz and Shellis, 2018a). This reversion in toothed whales in particular represents a striking example of convergent evolution, as they appear to have acquired a tooth morphology similar to several lineages of fishes, Mesozoic marine reptiles, and crocodiles due to their shared ecology (Massare, 1987, McCurry et al., 2017a). On the opposite

end, other mammalian taxa have reduced or completely lost their dentition and evolved unique structures to best adapt to new feeding niches. Four diverse groups, echidnas, anteaters, pangolins and baleen whales, are completely toothless as adults. Others like armadillos, sloths, aardvark and some toothed whales have enamel-less teeth, while the platypus secondarily loses dentition before reaching maturity (Davit-Béal et al., 2009 – Fig. 1.1).

Available embryological studies show that all lineages of toothless or partially toothless mammals have a full dentition in their prenatal stages, even if the evidence has been debated for the pangolin (Ferreira-Cardoso et al., 2019). Therefore, tooth germs must be reabsorbed before birth in completely edentulous taxa. The only known exception to this pattern is the platypus (*Ornithorhynchus anatinus*), which is hatched with functional teeth that are lost secondarily before adulthood, when the beak develops (Davit-Béal et al., 2009). The developmental mechanism of tooth resorption is mostly unknown in mammals. Ishikawa and Amasaki (1995) and Ishikawa et al. (1999) conducted histological studies on baleen whale fetuses and found that this process, at least in this lineage, resembles the molecular mechanism involved in the replacement of the first generation of teeth in diphyodont mammals. Moreover, the connection between the absence of teeth and changes in their skull development have also not been studied in detail. Given the unique nature of these groups, only limited information is available on their ontogeny, and no experimental analysis can be conducted directly on these species. However, some insight could be drawn using data from mouse models (e.g. Paradis et al., 2013, Phen et al., 2018) if enough information was collected on toothless taxa ontogeny.



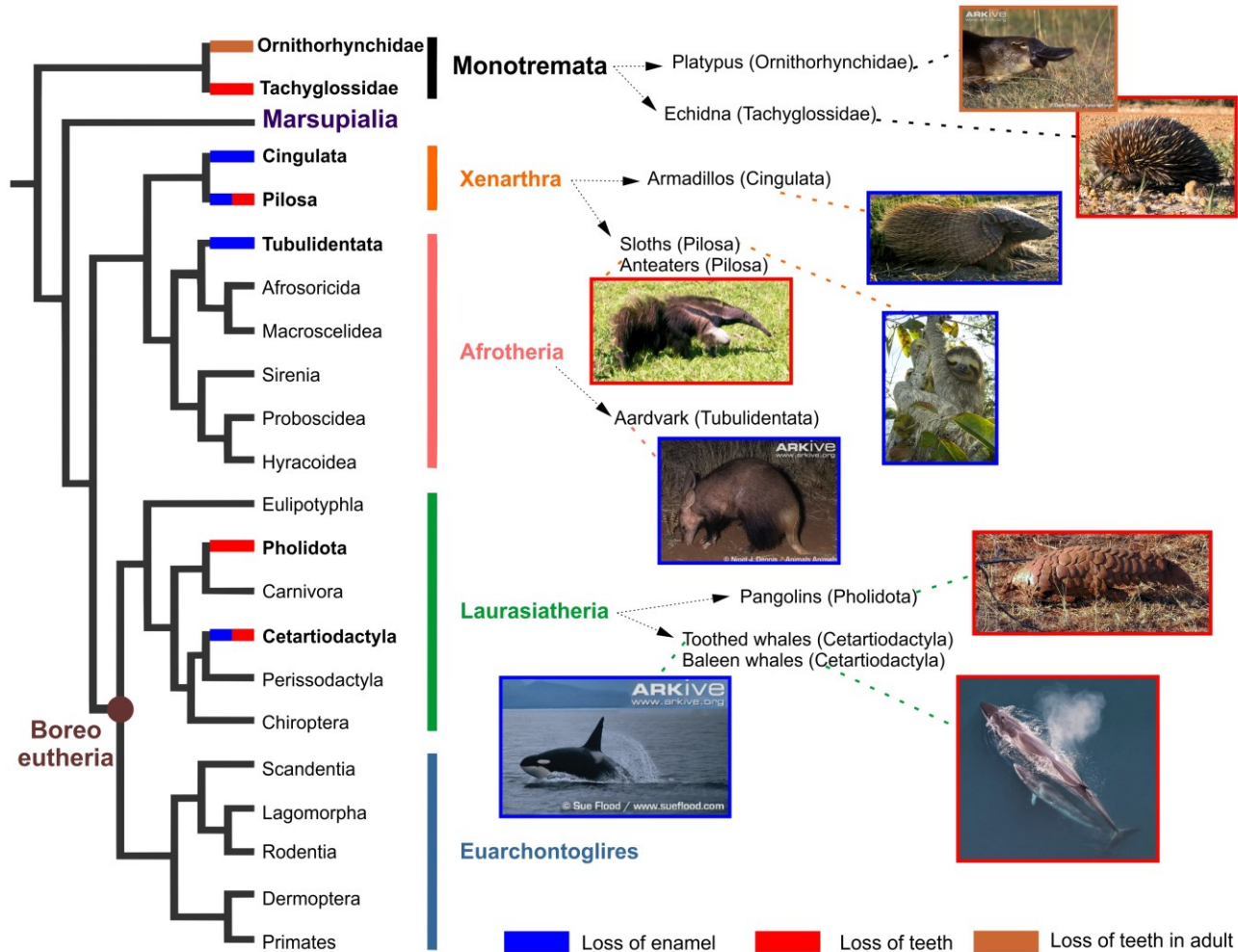


Figure 1.1 – Convergent loss of enamel and teeth in Mammalia. Except Marsupialia and Euarchontoglires, all other lineages have at least one group that has independently acquired reduced dentition. Types of tooth loss are labeled in the figure (enamel=blue, teeth=red, adult teeth=brown). Phylogeny based on Meredith et al. (2011). Data on tooth reduction from Davit-Béal et al. (2009). All images are in the public domain and downloaded from [www.commons.wikimedia.org](http://www.commons.wikimedia.org) and [www.arkive.org](http://www.arkive.org).

From a genetic prospective, recent studies have tried to identify inactivating mutations in genes known in humans and mice to contribute to enamel and tooth formation. Overall, it appears that many of these genes were convergently inactivated both in toothless mammals and other amniotes, however some are still active, likely due to pleiotropic effects (e.g. Meredith et al., 2013, Springer et al., 2016, Springer et al., 2019).

This evidence shows that the loss of dentition is a complex evolutionary process, probably unique for each lineage. Multiple mechanisms at different levels (developmental, genetic, physiological) have to interact to produce the final adult phenotype. Hence, an integrative approach joining ontogenetic data with molecular evidence and observations of the anatomy of extant edentulous taxa and their toothed ancestors is the best approach to study the evolution of edentulism and related adaptations in mammals.

### **Cetacea as a case study for loss of dentition in mammals**

The peculiar characteristics of Cetacea (baleen and toothed whales) make it an exemplary candidate to study evolutionary trends in numerous fields like bioacoustics, physiology, paleontology and molecular evolution (Gatesy et al., 2013). In particular, having adapted to a marine environment from a terrestrial ancestor, they evolved skull morphologies and dentition unique among mammals (Werth, 2006b, Reidenberg, 2007, Kienle et al., 2017, Peredo et al., 2018a, Berta and Lanzetti, in press), becoming a great example of evolution through tooth simplification and loss. Cetacea form a clade within Artiodactyla (even-toed ungulates), and their phylogenetic placement is well-supported in molecular and morphological analyses, with Hippopotamidae representing their closest living ancestor (Gatesy and O'Leary, 2001, Geisler and Sanders, 2003, Gatesy et al., 2013). Cetaceans split from other artiodactyls more than 52 Mya, and fossils reveal that these early forms already pursued at least a partially aquatic lifestyle (Thewissen and Fish, 1997, Thewissen et al., 2007, Gingerich et al., 2009, Uhen, 2010). The first

whales (Pakicetidae, Archaeoceti) were mostly terrestrial, with some degree of adaptation to raptorial feeding and locomotion in shallow water (Uhen, 2010). These extinct whales retained the typical mammal dentition of heterodonty (differentiated teeth) and diphyodonty (deciduous teeth replaced by a permanent one) (Thewissen et al., 2011).

Modern Cetacea (Neoceti) appear in the fossil record around 34 Mya and are completely adapted to the aquatic environment (Uhen, 2010). They are traditionally divided into two subgroups: Odontoceti, which include toothed whales, and Mysticeti or baleen whales (Gatesy et al., 2013). Currently, there are 10 recognized families of Odontoceti, including the likely extinct Chinese river dolphin (Lipotidae – Turvey et al., 2007), and four of families of Mysticeti (Fig. 1.2 – Bannister, 2018, Hooker, 2018). The transition from land to water brought about the radical transformation of numerous traits in these taxa, such as the loss of hind limbs, and the evolution of new features, most notably echolocation in odontocetes and the evolution of baleen in mysticetes (Uhen, 2010). Both groups have unique characteristics and their phylogeny and morphology can give important insights on the mechanisms of tooth loss and the emergence of related feeding adaptations in mammals.

#### *Teeth simplification and reduction in odontocetes: the case of Ziphiidae*

Dentition underwent major modifications from the ancestral terrestrial condition in both lineages. While all baleen whales are characterized by a complete loss of teeth, odontocetes higher trophic and ecological diversity produced many different dental patterns. Teeth and related skull traits are highly correlated with the diet and environment of the species, and therefore present an impressive level of convergence among distantly related lineages both in living and fossil taxa (Werth, 2006a, Bianucci et al., 2016, McCurry et al., 2017b, McCurry and Pyenson, 2018, McCurry et al., 2019, Berta and Lanzetti, in press).

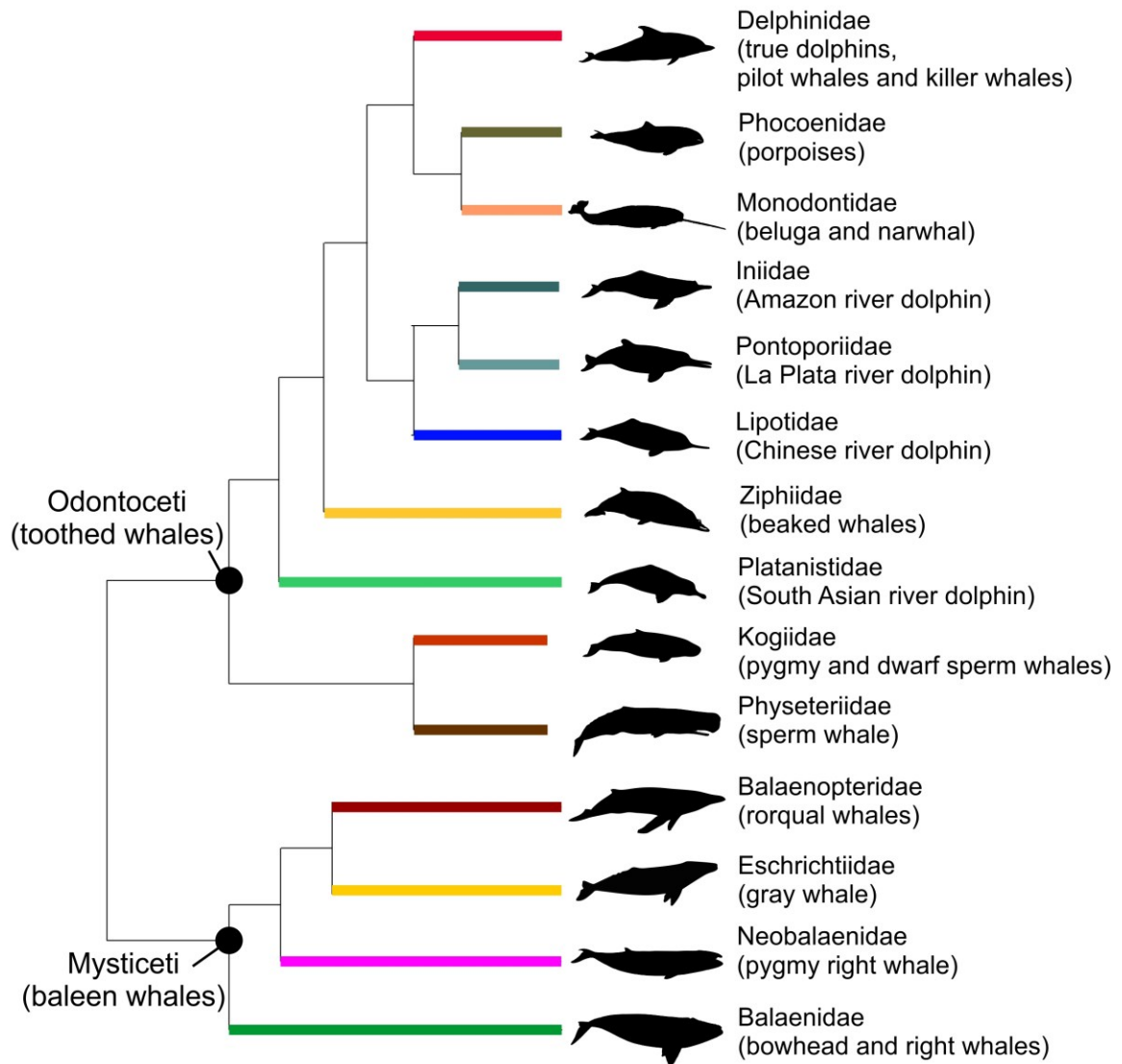


Figure 1.2 – Phylogenetic relationships among modern cetacean families. Topology follows Gatesy et al. (2013).

All extant toothed whales have developed homodonty – teeth that are undifferentiated along the jaws – with a simple conical tooth morphology (Armfield et al., 2013, McCurry et al., 2017b, Peredo et al., 2018a). Some species still rely on teeth to capture food, as it was the case in archaic Cetacea (Archaeoceti – Armfield et al., 2013), in particular those that live in riverine and estuarine habitats (Pauly et al., 1998, McCurry et al., 2017b, McCurry and Pyenson, 2018). Tooth counts are increased (polydonty) in these lineages, and they also present a distinctive skull shape

with an elongated snout and small eyes, similar also to riverine crocodiles (McCurry et al., 2017a, McCurry et al., 2017b, McCurry and Pyenson, 2018). Lineages with these set of traits are the so-called “river dolphins”: Amazon basin river dolphin (Iniidae), La Plata river dolphin (Pontoporiidae), Chinese river dolphin (Lipotidae), South Asian river dolphin (Platanistidae), as well as some Delphinidae that occupy estuarine environments (*Sotalia* spp.) (Hamilton et al., 2001, Werth, 2006a). The high level of convergence displayed in taxa with this “fresh water” morphology has caused issues in phylogenetic analyses before molecular data were used, and only recently modern river dolphins were recognized as descendants of two separate clades (Hamilton et al., 2001, Nikaido et al., 2001, Geisler et al., 2011). On the other hand, many lineages of oceanic odontocetes have a highly reduced dentition, due to their adaptation to suction feeding. In this mode of prey capture, negative pressure is generated in the oral cavity to create a current that draws food towards the mouth. The prey is then swallowed whole or minimally processed, minimizing the role of dentition in feeding (Johnston and Berta, 2011, Hocking et al., 2017, Kienle et al., 2017, Berta and Lanzetti, in press). Thus, in taxa highly specialized for suction feeding sometimes teeth has been transformed into tusks, used for sexual displays and interspecific identification (Dalebout et al., 2008, Nweeia et al., 2012). Some of these groups such as sperm whales (Physeteriidae) lost functional teeth in the upper jaw, and others (e.g. Kogiidae) also lost the enamel cover of the remaining teeth in the lower jaw (Meredith et al., 2009, Loch et al., 2013a, Springer et al., 2019). Other species experienced a severe reduction in tooth counts in both jaws, like beaked whales (Ziphiidae), Risso’s dolphin (Delphinidae) and narwhal (Monodontidae). Tooth reduction is also recorded in numerous fossil lineages (Gatesy et al., 2013, Boessenecker et al., 2017).

Among these groups, the best suited lineage for the study of the evolution of tooth patterning and reduction in odontocetes are Ziphiidae (beaked whales). Due to their deep diving

capacity and elusive behavior, these whales are perhaps the most poorly characterized clade of Cetacea (MacLeod et al., 2003, Dalebout et al., 2004), with most information on this group coming from stranded animals (Dalebout et al., 2008). Ziphiids feed mainly on cephalopods, but also on fish and benthic invertebrates (e.g. mollusks), diving in deep pelagic waters and trenches (MacLeod et al., 2003). This speciose family is comprised by 22 recognized extant species, 15 of them belonging to the genus *Mesoplodon* (e.g. Sowerby's beaked whale, True's beaked whale), two to the genus *Berardius* (giant beaked whales), two to the genus *Hyperoodon* (bottlenose whales), and the remaining three belonging to the monospecific genera *Indopacetus* (tropical bottlenose whale), *Tasmacetus* (Tasman's beaked whale), and *Ziphius* (Cuvier's beaked whale) (Dalebout et al., 2004, MacLeod, 2018). The fossil record of this group is scarce compared to other groups of Cetacea, but recent discoveries have revealed a high genus-level diversity worldwide during the Neogene (23-2.58 Mya) (Bianucci et al., 2008, Buono and Cozzuol, 2013, Lambert et al., 2013, Bianucci et al., 2016). A distinctive feature of most extant ziphiids is an extreme reduction in the number of teeth; only one pair of enlarged teeth – commonly referred to as ‘tusks’ – are usually erupted in male adults in the lower jaws, one per side. They bear a very thin layer of enamel that is quickly eroded away as the animal ages (Loch and Jansen van Vuuren, 2016). Their shape, size, and position changes significantly among species, making this trait significant for taxonomic identification. The main function of the tusks is probably related to sexual selection, both inter- and intra-species (Dalebout et al., 2008). Notable exceptions to this pattern of reduction in dentition are the genus *Berardius* where both adult males and females have two pairs of erupted teeth in the mandible (Balcomb, 1989), and *Tasmacetus shepherdi*, the only species to retain what can be described as a full dentition – 19 pairs in the upper jaw and 23 in the lower on average – in both males and females (Mead, 1989). In males, also two apical tusks are present in the mandible, one per side (Mead and Payne, 1975, Mead, 1989). The dentition of

*Tasmacetus* appears to represent the morphologically ancestral condition, shared by numerous fossil genera like *Messapicetus*†, *Ninoziphius*† and *Notoziphius*†, as well as by most other odontocetes (Buono and Cozzuol, 2013, Bianucci et al., 2016). However, while some molecular analyses conducted on both mitochondrial and nuclear genes agree with morphological phylogenies and place *Tasmacetus* as the earliest diverging lineage of crown Ziphiidae (Steeman et al., 2009), other analyses have positioned *Tasmacetus* in a more apical position within Ziphiidae, with the genus *Berardius* representing the earliest diverging lineage of the group instead (e.g. Dalebout et al., 2004, McGowen et al., 2009, McGowen et al., in press). This would present *Tasmacetus* as a possible exception to Dollo's Law, where a later-diverging taxon has re-evolved an ancestral trait, in this case a complete row of teeth. However, a solid phylogenetic analysis is needed to assess this, especially given the high level of trophic and morphological convergence observed among odontocetes that might bias the results obtained using morphological data alone. While Ziphiidae have been included in larger total evidence (morphological and molecular) studies of Cetacea (e.g. Geisler et al., 2011, Gatesy et al., 2013), no previous study has combined these two lines of evidence to try to resolve this apparent incongruence between methodologies and critically analyze the dentition of *Tasmacetus* based on its phylogenetic placement in a total evidence analysis.

A systematic review of the tooth patterns in Cetacea, as well as a solid reconstruction of the relationship in the family Ziphiidae would greatly contribute to the current understanding of the biological drivers for the loss of teeth in mammals, both ecologically and genetically. A deeper knowledge of the evolution of dentition in this clade would also aid in the investigation of the mechanisms of tooth loss in baleen whales, as these two closely related groups likely share many developmental pathways and genetic mutations.

### *Loss of teeth and evolution of baleen in mysticetes*

Mysticeti represent a unique system to study tooth loss, as they possess an extensive fossil record that documents the transition from teeth to baleen (Deméré et al., 2008, Boessenecker and Fordyce, 2015a, Boessenecker and Fordyce, 2016, Berta et al., 2016) and an increasing amount of genetic data are available for extant species (e.g. Meredith et al., 2011a, Meredith et al., 2013, Springer et al., 2019). Living baleen whales are represented by 14 species divided into four families: Balaenidae (bowhead and right whales), Eschrichtiidae (gray whale), Neobalaenidae (pygmy right whale), and Balaenopteridae (rorquals), the most speciose group that includes humpback, fin, blue and minke whales (Fig. 1.3). All extant baleen whales are characterized by distinctive feeding structures, baleen (Berta et al., 2016, Bannister, 2018). The appearance of baleen, composed of keratinous filaments secreted at the edges of the palate (Pivorunas, 1979), allowed mysticetes to switch to a bulk filter feeding diet from the raptorial feeding mode of Archaeoceti, and still retained by most modern odontocetes (Deméré et al., 2008, Gatesy et al., 2013, Berta et al., 2016, Bannister, 2018). Some extant cartilaginous fishes are filter feeders as well, but at the time of the appearance of baleen-like structures in fossil mysticetes, this niche was mostly unoccupied because of the extinction of bony filter feeding fishes at the K-T boundary (Friedman, 2012, Motani et al., 2015). The loss of teeth and the need of having a more flexible rostrum and mandible resulted in major modifications in the skull of mysticetes, for the most part not shared by toothed whales (Fahlke and Hampe, 2015). Interspecific variation in skull shape is also observed in adults of extant and fossil mysticetes (Nakamura et al., 2012, Pyenson et al., 2013), reflecting differences in feeding mode (Bouetel, 2005, Young et al., 2015). In fact, there are three main modes of bulk filter feeding used by modern taxa: skim, lateral suction and engulfment or lunge feeding (Fig. 1.3). Balaenidae and likely Neobalaenidae are skim feeders: they swim slowly through the water with their mouth open and capture plankton, copepods and



amphipods mostly, using their long baleen plates (Berta et al., 2016, Werth et al., 2018, Berta and Lanzetti, in press). They present an arched upper jaw that allows them to accommodate the long baleen (Bouetel, 2005, Berta et al., 2016). The gray whale (Eschrichtiidae) is primarily a lateral suction feeder: these animals use their baleen as a comb to extract benthic invertebrates from the bottom sediments. They present a mostly flat rostrum, with shorter baleen. Additionally, they have two-three throat grooves that allow for expansion of the buccal cavity during feeding and a semi-synovial joint of the mandible, which is needed to open their mouth widely (Pauly et al., 1998, Bouetel, 2005, El Adli et al., 2014, Berta et al., 2016). Rorqual whales are engulfment or lunge feeders: they feed in gulps, by scooping a large amount of prey in their mouth either by swimming horizontally (engulfment) or by lunging out of the water (lunge). They have a broad and flat rostrum, built to resist the impact of the water during feeding, and blunt baleen plates. They present a high number of throat grooves and completely lost the synovial joint of the mandible in order to be able to enlarge their buccal cavity and engulf 75%-130% of their body mass during each feeding event (Bouetel, 2005, Goldbogen et al., 2010, Goldbogen et al., 2012, Goldbogen et al., 2017, Kahane-Rapport and Goldbogen, 2018). They prey on plankton such as krill but also schooling fish like herring and pollock (Pauly et al., 1998, Berta et al., 2016, Berta and Lanzetti, in press).

Current evidence from the fossil record suggests that, phenotypically, the loss of teeth occurred once in the ancestor of all modern mysticetes, as the common ancestor of both modern clades of Cetacea preserved a full heterodont dentition (Fordyce, 1982, Uhen, 2018). However, there is still controversy on whether this event and the acquisition of baleen occurred independently, or teeth and precursors of baleen coexisted for a brief period before dentition was completely lost (Deméré and Berta, 2008, Marx et al., 2016, Peredo et al., 2018b).

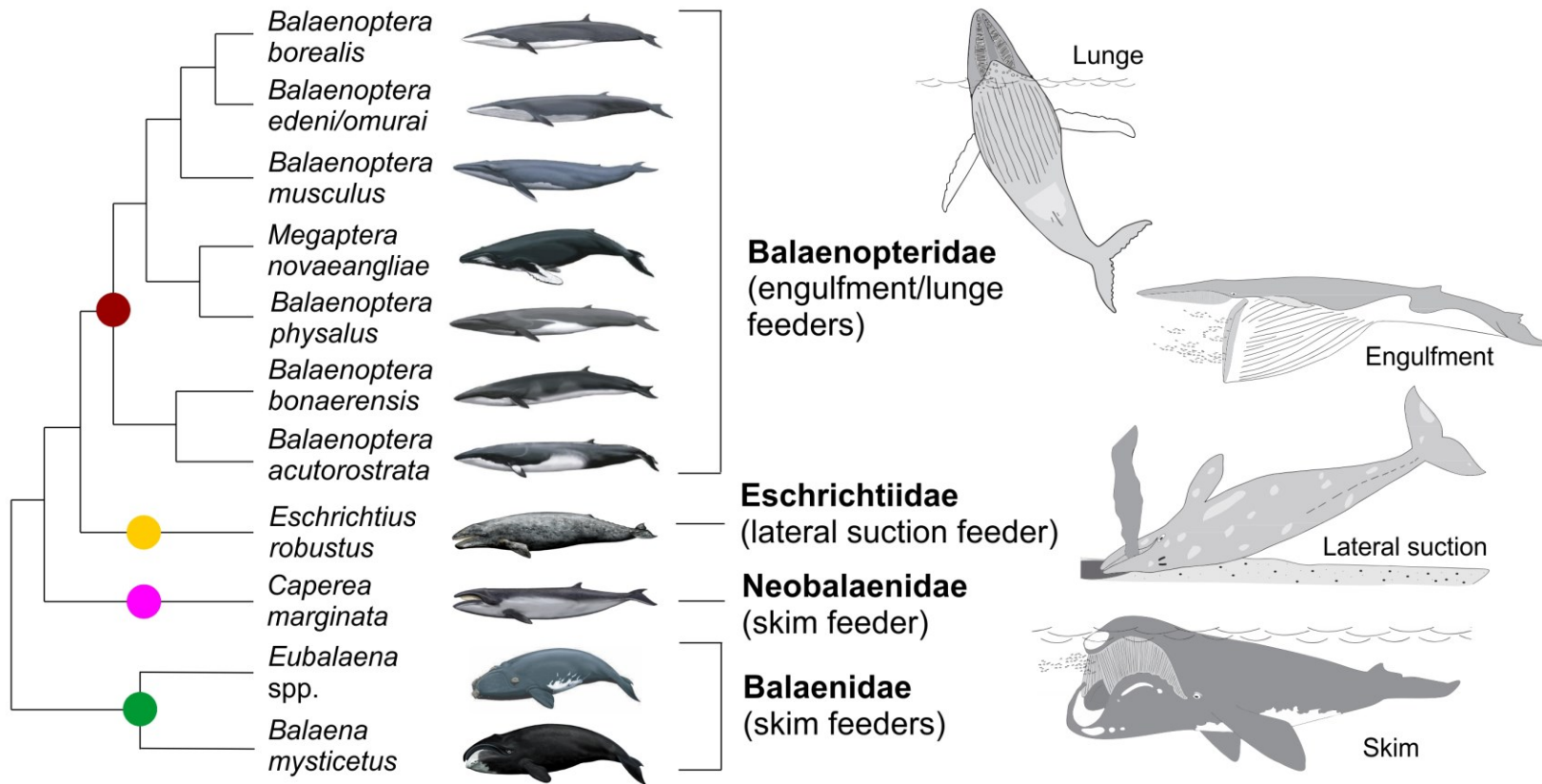


Figure 1.3 – Phylogeny of living species of mysticetes, with relative feeding adaptations. Topology follows Gatesy et al. (2013). *B. edeni* and *B. omurai* are represented on the same branch as the second species was only recently identified and wasn't included in the original study, but it is believed to be the sister taxon to *B. edeni* (Wada et al., 2003). Representation of feeding behavior modified from Berta et al. (2016), drawings of species by Carl Buell from Gatesy et al. (2013).

Independently on how this transition occurred, it allowed ancestral taxa to better adapt to bulk filter feeding, which was also correlated with skull modifications like the acquisition of a flexible rostrum and mandible (Deméré et al., 2008, Boessenecker and Fordyce, 2015a, Boessenecker and Fordyce, 2015b, Berta et al., 2016, Boessenecker and Fordyce, 2016).

Changes in timing (heterochrony) and patterning of cranial ossification during prenatal development, compared to both closely related terrestrial taxa (artiodactyls) and toothed whales, have been hypothesized to follow and allow the transition from teeth to baleen (Armfield et al., 2011, Hampe et al., 2015, Lanzetti et al., 2018, Lanzetti, in press). Nevertheless, which changes in the development of mysticetes are associated with the evolution of their distinctive skull traits, as well as possible ontogenetic differences among species, were never tested with a diverse sample size and rigorous statistical and phylogenetic methods. Descriptive anatomy of mysticete fetuses revealed that they still develop tooth buds in the fetal stages in both upper and lower jaws, but teeth never erupt, and the neonates bear baleen plates (e.g. Ridewood, 1923, Van Dissel-Scherft and Vervoort, 1954, Karlsen, 1962, Tomilin, 1967, Slijper, 1976, Fudge et al., 2009). In the Antarctic minke whale (*Balaenoptera bonaerensis*), the teeth pass through three of the typical mammalian developmental stages before being reabsorbed (Ishikawa and Amasaki, 1995, Ishikawa et al., 1999, Davit-Béal et al., 2009).

Before starting a detailed study of the ontogenetic changes in the skull and teeth of mysticetes, as well as comparing them with other lineages and fossil, it is necessary to understand how genes contributed to the loss of teeth in these taxa. Given that baleen whales possess tooth germs at early ontogenetic stages, they might retain functional tooth-related genes from their toothed ancestors, even if most of these genes might present inactivating mutations (Deméré et al., 2008, Meredith et al., 2013, Springer et al., 2016). For example, previous research on *amelogenesis imperfecta*, a condition that causes abnormal enamel formation in humans,

identified mutations in the *FAM83H*, *WDR72*, and *C4orf26* genes, among others, to be associated with this condition, and therefore these genes were hypothesized to be partially responsible for enamel development (Kim et al., 2008, El-Sayed et al., 2009, Parry et al., 2012). Given this evidence, investigating possible mutations and deletions in these genes in toothless and enamelless mammals such as baleen whales could confirm this functional hypothesis and provide insight on the timing and genetic component on tooth loss in Mysticeti. Several molecular studies on candidate genes like these revealed they are inactivated or deleted in mysticetes and other toothless and enamelless mammals and amniotes (e.g. Meredith et al., 2009, Meredith et al., 2011a, Meredith et al., 2013, Kawasaki et al., 2014), also providing a better understanding of the function and importance of these gene regions. For instance, by analyzing the *MMP20* gene in both toothless baleen whales and enamelless toothed whales (Kogiidae), it was found that this gene is inactivated in both groups, even if Mysticeti has an additional deleterious insertion (Meredith et al., 2011a). This shows that *MMP20* is correlated with enamel formation rather than tooth mineralization in general, but it also highlights the complexity of the genetic bases of dentition development. Not much information is instead available on what genes are responsible for the formation of baleen. Given the tissue's keratinous composition, baleen genes are likely to have originated from hair genes. It is hypothesized that these genes started being expressed in the mouth of these mammals after they lost their primary function of producing hair for body cover in Archaeoceti (Pivorunas, 1979). Specifically, it is possible that an acceleration in the expression of genes of the *WNT* family during development could cause both the hair loss and the growth of baleen in mysticetes (Park et al., 2015). Future investigations into the genetic basis of baleen development will be necessary to more fully understand the tooth to baleen transition in mysticetes (Berta et al., 2016). However, a review of the available information on loss of functionality of putative tooth and enamel genes in Mysticeti can help illuminate the patterns of

tooth loss in this clade, as well explain the retention of tooth germs during prenatal development (Deméré et al., 2008, Thewissen et al., 2017). These data can then be combined with evidence from ontogenetic studies and fossils to create a comprehensive picture of the evolution of filter feeding in baleen whales.

### **Research objectives**

The main goal of this Chapter is to investigate the evolutionary origin and genetic drivers of the unique tooth patterns and edentulism of Cetacea. First, extreme tooth reduction in Ziphiidae will be examined in the context of tooth number variation in their family fossil record and in all modern odontocetes. To achieve this goal, tooth counts of almost all modern species of toothed whales will be inserted into a phylogenetic context to highlight convergent events of tooth loss. Then a total evidence phylogeny of Ziphiidae will be constructed using available molecular data (McGowen et al., in press) and a comprehensive morphological matrix that includes the most complete fossil taxa of this group (Bianucci et al., 2016). Tracing tooth patterns on this novel tree will allow me to determine if full dentition has in fact re-evolved in this clade, in apparent violation of Dollo's Law, or if the variation is line with what is observed in other odontocetes lineages.

This investigation of instances of tooth loss in Odontoceti will serve as general framework for the second objective, where the genetic basis of edentulism in baleen whales will be examined. Current evidence on tooth- and enamel-related gene sequences in Mysticeti will be reviewed in a phylogenetic context. In particular, I will describe the results of the sequencing of gene *C4orf26* that I have contributed to (Springer et al., 2016). This will serve as a foundation to interpret the anatomical changes associated with tooth resorption during the ontogeny of modern baleen whales (Chapter Two) and to then connect genetic and developmental data to the loss of teeth and evolution of baleen detailed in the fossil record of Mysticeti (Chapter Three).

## **Materials and methods**

### **Data collection for Odontoceti**

Tooth counts, as the number of teeth present one side of lower and upper jaw, were collected from the literature for virtually all recognized extant or recently extinct species of Odontoceti (n=74). There is debate on species-level and generic-level taxonomy especially in Delphinidae (e.g. Charlton-Robb et al., 2011, Vollmer et al., 2019). The taxonomic nomenclature follows the list provided by the Society for Marine Mammalogy Committee on Taxonomy ([www.marinemammalscience.org](http://www.marinemammalscience.org)). When data were found for subspecies or putative species, they were also recorded. Tooth numbers were averaged when counts of both sides of each jaw were reported and when multiple specimens were described. These averages are then used in the coding for successive analysis. In taxa where males have erupted teeth and females do not (e.g. Ziphiidae), the number of teeth erupted in males was used. The complete list of tooth counts for all taxa can be found in Table S1.1 (Appendix B), including literature sources and notes on variability between sexes and at different life stages for species where this information is available. The complete list of additional references can be found in Appendix A. Data on presence of teeth or tusks were also collected for the fossil Ziphiidae included in the study.

### **Phylogenetic analysis and ancestral state reconstruction**

To reconstruct the phylogeny of Ziphiidae, a supermatrix that includes molecular and morphological data from multiple sources was compiled. For morphological data, the most complete and up-to-date matrix of Ziphiidae was used, which includes most of the relevant fossil taxa (Bianucci et al., 2016). To match extant taxa in the morphology matrix, molecular data from one species per genus of modern beaked whales (*Berardius bairdii*, *Hyperoodon ampullatus*, *Indopacetus pacificus*, *Mesoplodon bidens*, *Tasmacetus shepherdi*, *Ziphius cavirostris*), as well as

two odontocete outgroup species (*Physeter macrocephalus*, *Tursiops truncatus*) was selected from the matrix presented in McGowen et al. (in press). Mitochondrial DNA sequences (16S, 12S, *CYTB*) for these same taxa were added from GeneBank and from the matrix published in McGowen et al. (2009). These were the only sequences available for *I. pacificus*, which was not included in the McGowen et al. (in press) study. Accession numbers and sources for the mtDNA sequences are reported in Table S1.2 (Appendix B).

The molecular data alone were analyzed first to test if the resulting phylogeny was congruent with previously published molecular trees of Ziphiidae (Dalebout et al., 2004, McGowen et al., 2009, McGowen et al., in press). This analysis was conducted using maximum likelihood in RAxML v.8 (Stamatakis, 2014) with different partitions models (no partitions, nuclear DNA partitioned). Aside from the changing position of *I. pacificus*, likely due to the few genes available for this taxon, the results are the same between different models and in agreement with previously published work (Dalebout et al., 2004, McGowen et al., 2009). Tree topologies with bootstrap support values are reported in Fig. S1.1 (Appendix B) (courtesy of M. McGowen).

The total evidence analysis was performed using maximum parsimony (MP) analysis in PAUP\* 4.0a165 (Swofford, 2003) with 1000 random stepwise-addition replicates and tree bisection reconnection (TBR) branch-swapping. Uninformative characters in the molecular data were excluded from the analysis. Characters were analyzed both under equal weighting and implied weighting using Goloboff's method with  $k=3$ , as this was established to be the best weighting score for the morphological characters in Bianucci et al. (2016). A constraint was applied to root the tree using both the molecular outgroups (*T. truncatus* and *P. macrocephalus*) and the morphological one (*Squalodon*†). Support for nodes was evaluated by calculating decay index, or Bremer's support values (Bremer, 1994).

To determine the states at internal nodes for tooth counts in Odontoceti and presence or absence of teeth and tusk in Ziphiidae, ancestral state reconstructions analyses were performed using ordered parsimony in Mesquite 3.6 (Maddison and Maddison, 2018). The tooth counts for Odontoceti were divided into discrete characters with increments of 5, except state “absent” or “0” which is only used for taxa with no evidence of erupted teeth in that jaw. This categorization was done to produce more clear result in the ancestral state reconstruction and to account for variability among individuals or discrepancies in reported tooth counts in the literature, as only the averages were considered. The resulting matrix is reported in Appendix A. The two characters (upper and lower jaw) were mapped on the topology presented in McGowen et al. (in press). Species not present in that tree but valid and with unequivocal phylogenetic placement (*Indopacetus pacificus*, *Phocoena sinus*, *Lagenorhynchus cruciger*, *Cephalorhynchus hectori*, *C. eutropia*, *Sotalia fluviatilis*) were added to the phylogeny based on their position in McGowen et al. (2009) and McGowen (2011). The species *Delphinus capensis* is positioned where the subspecies *D. d. bairdi* is in the original phylogeny, as these two names have been used interchangeably (Committee on Taxonomy, 2018). *Mesoplodon* (Ziphiidae) is collapsed at the genus level as there is not variation in the number of teeth in the genus. Similarly, Mysticeti are represented as a group as they are all toothless.

The presence/absence of teeth and tusks was reconstructed using the same methodology for Ziphiidae on the novel total evidence topology and on the morphology-only topology from Bianucci et al. (2016). The same matrix used for phylogenetic reconstruction (Bianucci et al., 2016) was used to infer these traits (characters 27 and 28). The coding for these characters was validated with literature sources: Lambert (2005a), Lambert (2005b), Bianucci et al. (2010), Buono and Cozzuol (2013), Lambert et al. (2013), and Bianucci et al. (2016) for fossils, see Table S1.1 (Appendix B) for sources for living taxa. The presence or absence of alveoli is used to assess



the presence of full dentition in most fossils, as teeth not always preserved with the skull. Aside from presence (0) and absence (1) of full dentition, the presence of only mandibular tusks was also coded for the lower jaw (2). Tusks are considered as 1 or 2 enlarged and uniquely shaped teeth present on each side of the jaw. The coding for these traits is reported in Appendix A. Conducting this analysis on both phylogenies will allow to directly compare hypotheses on character history evolution.

### **Sequencing of tooth-related genes in Mysticeti**

To identify additional genetic mutations that are related to the loss of teeth in Mysticeti, the gene *C4orf26*, potentially connected to enamel formation in humans (Parry et al., 2012), was selected to be amplified and sequenced. Based on the examination of the Antarctic minke whale (*Balaenoptera bonaerensis*) genome sequences and BLAST searches, this gene appeared to lack both exon 1 and exon 3 in this species. To investigate this further and understand the evolutionary history of this gene in Mysticeti, three of its regions were selected for PCR amplification and sequencing: exon 1, exon 3 and regions bordering the deletion of these exons in the reference species (Antarctic minke whale). Samples from 11 species representing all the living families of baleen whales were analyzed: Balaenidae (*Balaena mysticetus*, *Eubalaena glacialis*, *Eubalaena australis*), Neobalaenidae (*Caperea marginata*), Eschrichtiidae (*Eschrichtius robustus*), and Balaenopteridae (*Balaenoptera acutorostrata*, *Balaenoptera borealis*, *Balaenoptera edeni*, *Balaenoptera musculus*, *Balaenoptera physalus*, *Megaptera novaeangliae*). The primers and protocol for PCR and sequencing can be found in Springer et al. (2016). I contributed to this analysis by conducting the PCR and gel electrophoresis to amplify the relevant regions of *C4orf26*. To best discuss the results of this investigation, currently available evidence on the inactivation of tooth and enamel-related genes in Mysticeti will also be reviewed.

## Results

### **Patterns of variation of tooth counts in living Odontoceti**

From the ancestral state reconstruction of tooth counts in Odontoceti, complex evolutionary patterns and high variability in tooth numbers emerge (Fig 1.4). True dolphins such as *Stenella* spp. (e.g. spotted dolphins, spinner dolphin), *Delphinus* spp. (common dolphins), and *Sotalia* spp. (tucuxi and Guiana dolphin) present very high tooth counts, with all species of this group having at least 31-35 teeth per row in each jaw. The only exception is *Tursiops* spp. (bottlenose dolphins) that has a markedly lower tooth count (21-25). While this discrepancy has never been specifically addressed before, it might be due to the higher adaptability in habitat preference and prey type displayed by bottlenose dolphins (Perrin, 2018, Wells and Scott, 2018). The other two clades inside Delphinidae also present relatively conserved tooth counts among their member species. The group that includes pilot whales (*Globicephala* spp.) and the false killer whale (*Pseudorca*) presents low tooth counts, with one taxon (*Grampus* – Risso's dolphin) only retaining teeth in the lower jaw. As implied by its tooth pattern, this dolphin is a specialized suction feeder, with a diet composed almost exclusively of cephalopods, while closely related taxa also feed on fish and even higher vertebrates (Pauly et al., 1998, Werth, 2006a). The last clade, which includes Hector's dolphins (*Cephalorhynchus hectori*) and the dusky dolphin (*Lagenorhynchus obscurus*) among others, is characterized by intermediate tooth counts, with most of its members having between 26 and 35 teeth per side of each jaw. The retention of the same number of teeth among these different taxa is particularly interesting as species of the genus *Cephalorhynchus* have a very distinct appearance and skull morphology compared to the rest of the group.

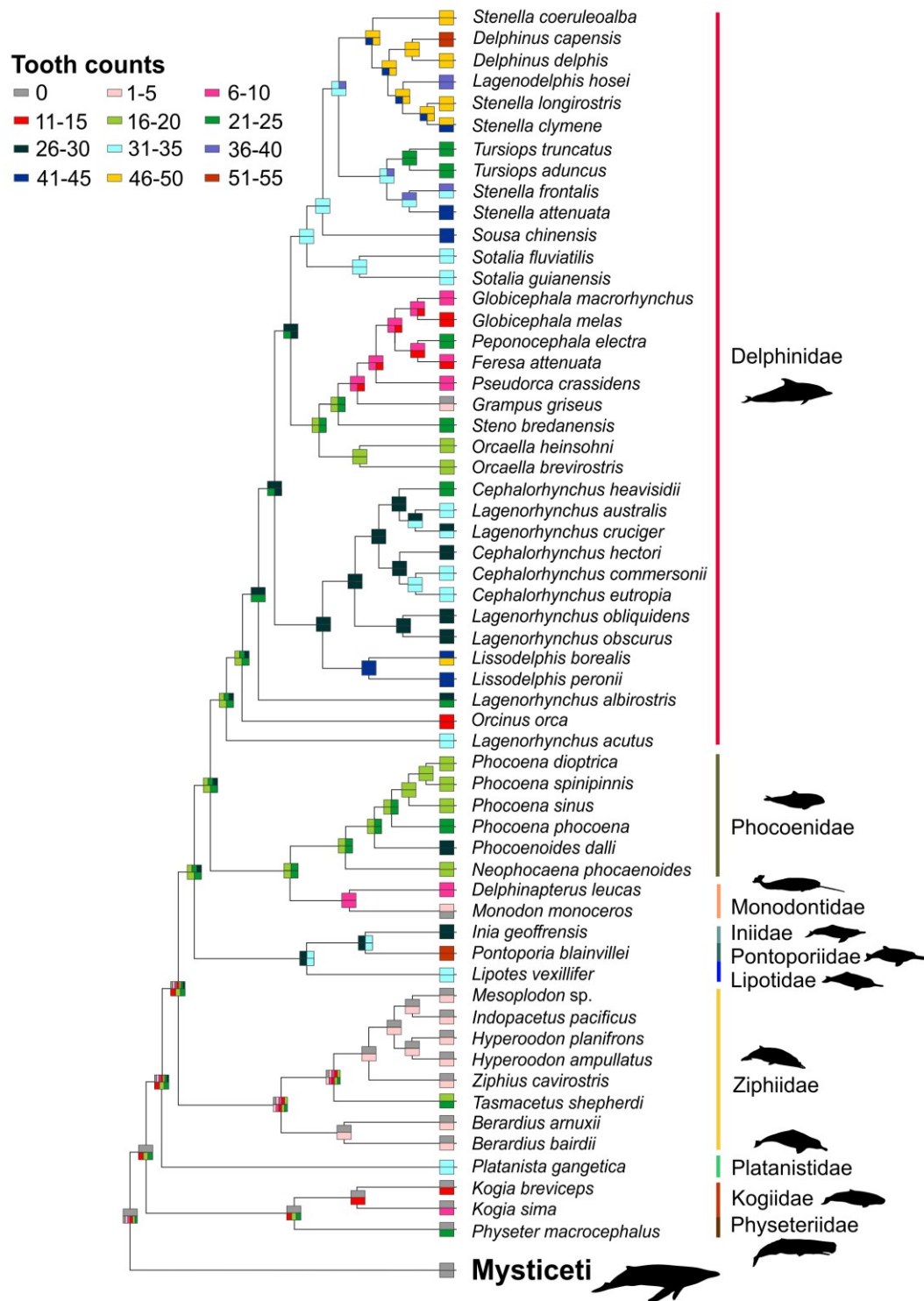


Figure 1.4 –Composite tree of all living species of Cetacea with mapped tooth counts. The upper box represents upper tooth row counts, the lower box counts for the lower jaw; the jaws were coded independently. Colors represent states compiled as tooth number intervals. Details and sources for each species can be found in Table S1.1 (Appendix B), matrix used in Appendix A.

They have a smaller size and blunter rostrum, overall retaining a set of juvenile traits in the adults (Galatius, 2010). Tooth counts seem to be independent from these other factors, possibly representing a trait derived from the common ancestor of the group. However, fossil evidence needs to be evaluated to confirm this hypothesis.

More definitively, phylogenetic constraint appears to play a major role in the distributions of tooth counts in Phocoenidae (porpoises) and Monodontidae (beluga and narwhal). Both these families have fairly conserved tooth numbers, with porpoises ranging from 16-20 to 26-30 teeth per side of the jaw, and monodontids having a reduced dentition. The beluga (*Delphinapterus*) has a diverse diet, including fishes and benthic invertebrates (Pauly et al., 1998), and displays similar tooth counts to pilot whales and related taxa (6-10). The narwhal instead is functionally toothless, with only one tooth modified as a tusk, which fully erupts only in males. While they still have sometimes vestigial teeth in both jaws, especially in the fetal stages, they only rarely erupt and are not used in feeding (Nweeia et al., 2012). As Risso's dolphin, which is also mostly toothless, this species is a specialized suction feeder hunting primarily squids and other cephalopods (Pauly et al., 1998, Werth, 2006a).

Convergent feeding adaptations due to a common habitat instead likely drove the evolution of the elevated tooth counts observed in all four families of river dolphins: Iniidae (Amazon river dolphin), Pontoporiidae (La Plata river dolphin), Lipotidae (Chinese river dolphin), and the early diverging Platanistidae (South Asian river dolphin). These taxa still actively use their teeth, distributed along their elongated and narrow rostrum, to catch prey (mostly fish) with a lateral movement of the head, a feeding adaptation commonly called lateral snapping (Werth, 2006a, Hocking et al., 2017, Page and Cooper, 2017). The Amazon river dolphin is described as heterodont by many authors, as it presents larger teeth of irregular shapes in the posterior portions of the jaws (Best and Da Silva, 1993). However this is not a case of true heterodonty, where there

is a clear functional distinction among teeth in each row, but more likely the product of relaxed selection on tooth shape, as its dental structure does not highly differ from other odontocetes (Stock, 2001, Loch et al., 2013b). This taxon also maintains an enamel structure that is more resembling of stem-Cetacea (Archaeoceti), while the closely related La Plata dolphin does not (Loch et al., 2013a). It is not clear if this is a case of retention of an ancestral trait or re-evolution of lost features, as also many extinct lineages of Odontoceti and early Archaeoceti were adapted to raptorial feeding in a riverine environment (Hamilton et al., 2001, Geisler et al., 2011, McCurry and Pyenson, 2018). Iniidae have an extensive fossil record, supporting the hypothesis that this is the last living representatives of a once-abundant clade, whose traits it still displays (e.g. Pyenson et al., 2015, Murakami, 2016).

As seen in members of Delphinidae and Monodontidae, also specialized suction feeding has evolved multiple times in Odontoceti, accompanied by the reduction or loss of teeth. Extant Physeteriidae and Kogiidae (sperm whales) do not have any erupted teeth in the upper jaws, while they still retain some dentition in the lower jaw (21-25 in Physeteriidae and 6-15 in Kogiidae). Kogiidae also completely lack enamel cover on their teeth, highlighting the loss of functionality in feeding of these structures, as the lack of enamel cover renders the teeth prone to erosion (Bloodworth and Odell, 2008, Meredith et al., 2009). These families descend from a highly diverse lineage, where most taxa were likely macroraptorial feeders like the modern killer whale (*Orcinus*) (Velez-Juarbe et al., 2015, Lambert et al., 2016). The three living species are instead suction feeders, with a diet composed almost entirely of squid (Pauly et al., 1998). Similarly, modern beaked whales (Ziphiidae) also have evolved specialized suction feeding and reduced dentition, retaining only one or two teeth per side in the lower jaw, transformed in tusks. As sperm whales, these species descend from a diverse lineage that included many generalist raptorial-feeding taxa (Lambert et al., 2015). They also share with Physeteriidae and Kogiidae the

ability to dive at great depths to forage, with their preferred prey being squids, but also fishes depending on availability of food sources (Pauly et al., 1998, Pabst et al., 2016). In this clade, *Tasmacetus* (Tasman's beaked whale) stands out for having a high number of teeth in both upper and lower jaws (16-20, 21-25). While all beaked whales, as well as sperm whales, retain vestigial teeth that do not usually erupt (Boschma, 1950a, Boschma, 1950b, Boschma, 1951, Loch and Jansen van Vuuren, 2016), the presence of a full set of teeth in this species has raised many questions on its diet, adaptations and phylogenetic position (Mead, 1989, Dalebout et al., 2004, Best et al., 2014).

Considering the phylogeny of Odontoceti, while there is great variation in tooth counts and feeding adaptations overall, it appears that within groups the taxa share similar tooth numbers and feeding adaptations. Morphological convergence due to similar diets and habitats is detectable among families in several instances. However, these observations do not offer a simple explanation for the anatomy of the Tasman's beaked whale, which is a unique outlier with no other living taxon displaying such high divergence in tooth count relative to other members of its clade. This distinctive pattern warrants further investigation in the evolution of Ziphiidae, by also considering tooth numbers and related adaptations reported for fossil taxa.

### **Convergent loss of teeth in modern and fossil Ziphiidae**

In the total evidence analysis of Ziphiidae, the equal weighting search produced 55 equally parsimonious trees that are slightly shorter (Tree length=54664) than the 9 trees found in the implied weighting k=3 analysis (Tree length= 54666). Other measures of tree fit are the same in both settings (CI=0.722, RI=0.671). Given the higher number of equally parsimonious phylogenies recovered, the strict consensus of the equal weighting analysis produced a less defined topology with six polytomies. The strict consensus topology produced by the k=3 analysis is more defined and compatible with the result of the other search. Therefore, this

topology will be used for ancestral state reconstruction of tooth counts. The two phylogenies with support values are reported in Appendix B (Fig. S1.2-S1.3).

Regardless of the settings used (equal or implied weighting), *Tasmacetus* was found to be nested inside the crown Ziphiidae clade, with *Berardius bairdii* (Baird's giant beaked whale) and its fossil relatives representing the earliest diverging lineage of crown Ziphiidae (Fig. 1.5A). The placement of the other modern taxa is consistent with the results of the molecular phylogenetic analyses, in particular when mt and nu DNA are considered as separate partitions, with *Indopacetus* more closely related to *Hyperoodon* (Fig. S1.1B – Appendix B). Most of the fossil taxa are grouped in a monophyletic clade, informally named the “*Messapicetus*† clade” following Bianucci et al. (2016), which shares some of the same evolutionary trajectories as the crown Ziphiidae clade, such as increase in vertex (i.e. the highest point of the skull measured from the base of the rostrum) elevation and progressive tooth reduction. The most notable difference between the total evidence topology and the morphology-only phylogeny presented by Bianucci et al. (2016) is the position of *Tasmacetus*, which was placed as the first diverging lineage of crown Ziphiidae, with *Nazcacetus*† being the second diverging lineage (Fig 1.5B). *Berardius* and its fossil relatives represented the third lineage. The placement of the other taxa in crown Ziphiidae, both living and fossil, is the same in both topologies.

Considering the ancestral state reconstructions of the dentition states in the total evidence and morphology-only phylogenies (Fig. 1.5), the major difference is in the timing of loss of full dentition in crown Ziphiidae. In the combined tree, loss of teeth in the upper jaw and reduction in the lower jaw occurs in the common ancestor of the clade, and then full dentition is independently re-acquired in *Tasmacetus*. In the morphology-only analysis, it is instead lost in the common ancestor of *Nazcacetus*† and all other taxa in the clade, after the lineage of *Tasmacetus* has diverged.





The accurate phylogenetic placement of this taxon is therefore pivotal to the reconstruction of the evolution of tooth loss in Ziphiidae, and there appears to be a sharp difference between the morphological and combined data. Possible anatomical traits that can support the placement of *Tasmacetus* as a later-diverging lineage in crown Ziphiidae and other implications of this result will be discussed later. As for the “*Messapicetus*† clade”, the ancestral state reconstruction produced the same results, with loss of full dentition occurring in the ancestor of *Aporotus*†. The earlier-diverging genus *Ziphirostrum*† could have only bear vestigial teeth, but the present fossil evidence does not allow for a definitive conclusion and this taxon is coded as ambiguous (Lambert, 2005b). Interestingly, the later-diverging *Beneziphius*† is also coded as ambiguous, as it presents traces of alveoli in the preserved parts of the upper jaw (Lambert, 2005b). This taxon could represent an evolutionary parallel with *Tasmacetus*, as they could have both re-acquired full dentition when their ancestors lacked it.

In sum, both the evolutionary history of Ziphiidae and the distribution of tooth counts in modern Odontoceti present complex patterns of reduction and increases in tooth number. Moreover, dentition is modified in several instances to serve as tusks that have other functions not directly related to feeding, from intraspecific recognition (Dalebout et al., 2008) to sensory organ (Nweeia et al., 2014). This high variability is likely due to the switch from purely raptorial to suction feeding in Archaeoceti, which was a key step in efficiently adapting to an aquatic environment (Hocking et al., 2017, Kienle et al., 2017, Berta and Lanzetti, in press). This change in prey capture style indirectly caused relaxation of the selective pressure on the genes that control tooth formation: precise occlusion was not needed to capture and process prey, making ancestral tooth number and shape not essential for survival in this new environment (Werth, 2006a, Armfield et al., 2013, Peredo et al., 2017, Thewissen et al., 2017). This general framework

provides the foundation to investigate the more radical changes in prey capture and dentition in Cetacea: the vestigialization of teeth and acquisition of baleen in Mysticeti.

### **Genetic bases of tooth loss in Mysticeti**

By investigating the presence of inactivating mutations in tooth- and enamel-related genes in baleen whales, it is possible to identify when these changes occurred in the evolution of Mysticeti. This will aid in the understanding of the complex underlying developmental and genetic processes that are responsible for the evolution of baleen and, at the same time, bulk filter feeding. It can also allow to better identify the function of these genes both in edentulous taxa and in humans.

During this study, the gene *C4orf26* was sequenced and analyzed in detail for the first time in mysticetes. Examining the genome of enameless (aardvark, armadillo, sloth) and toothless taxa (pangolin, baleen whales), Springer et al. (2016) found that the gene was intact in enameless mammals, but not in toothless ones. As this region was originally thought to be related to enamel formation (Parry et al., 2012), this result showed that instead it is most likely connected to the tooth development process more generally (Springer et al., 2016). As *C4orf26* presented significant changes in four species of baleen whales from this preliminary analysis, this gene was sequenced for all families and multiple species to better study the evolution of this gene in Mysticeti. No common mutation was identified in the common ancestor of these species. Additionally, the attempt of sequencing this region in Neobalaenidae (*Caperea*) was unsuccessful, indicating the presence of unique mutations in this taxon. In the other taxa instead, three major inactivation events were discovered. *C4orf26* presents a shared inactivating mutation in Balaenidae (*Balaena* and *Eubalaena*). Both genera then present unique additional inactivating mutations in other regions. In Eschrichtiidae (*Eschrichtius*) and in most examined Balaenopteridae instead the gene is completely deleted, likely in the common ancestor of the

group given the similarity of the sequences leading to and after the missing exons. However, in the blue whale (*B. musculus* – Balaenopteridae) the gene is still present but presents independently evolved inactivating mutations. This possibly indicates the retention of ancestral genetic polymorphism among rorquals. Overall, *C4orf26* was deactivated independently at least three times in the evolution of modern baleen whales, likely four given that it was not possible to recover it in *Caperea*.

While this specific pattern is unique, other tooth-and enamel-related genes present a complex evolutionary history in Mysticeti as well (Fig. 1.6). For example, the gene *ODAM* was recently found to present inactivating mutations and deletions in different exons (Springer et al., 2019). A mutation in exon 4 and a splice site are shared by Balaenidae and Balaenopteridae (*Eschrichtius* +Balaenopteridae) respectively. Other mutations can be found in single genera or in clades, like two changes in exons 4 and 6 shared by minke whales (*B. bonaerensis* and *B. acutorostrata*). As this gene was found to be inactivated in other toothless mammals (pangolin, anteater), but also in enameless ones such as sloths, armadillos and aardvarks, this indicates that its function is likely connected with enamel development. Surprisingly, it also shown inactivating mutations in odontocetes that have enamel-capped teeth. This might be the result of the simpler enamel structure that these taxa present, given that their dentition is not used for primary food processing as described earlier, or might be caused by other related functions of this gene in gingival development.

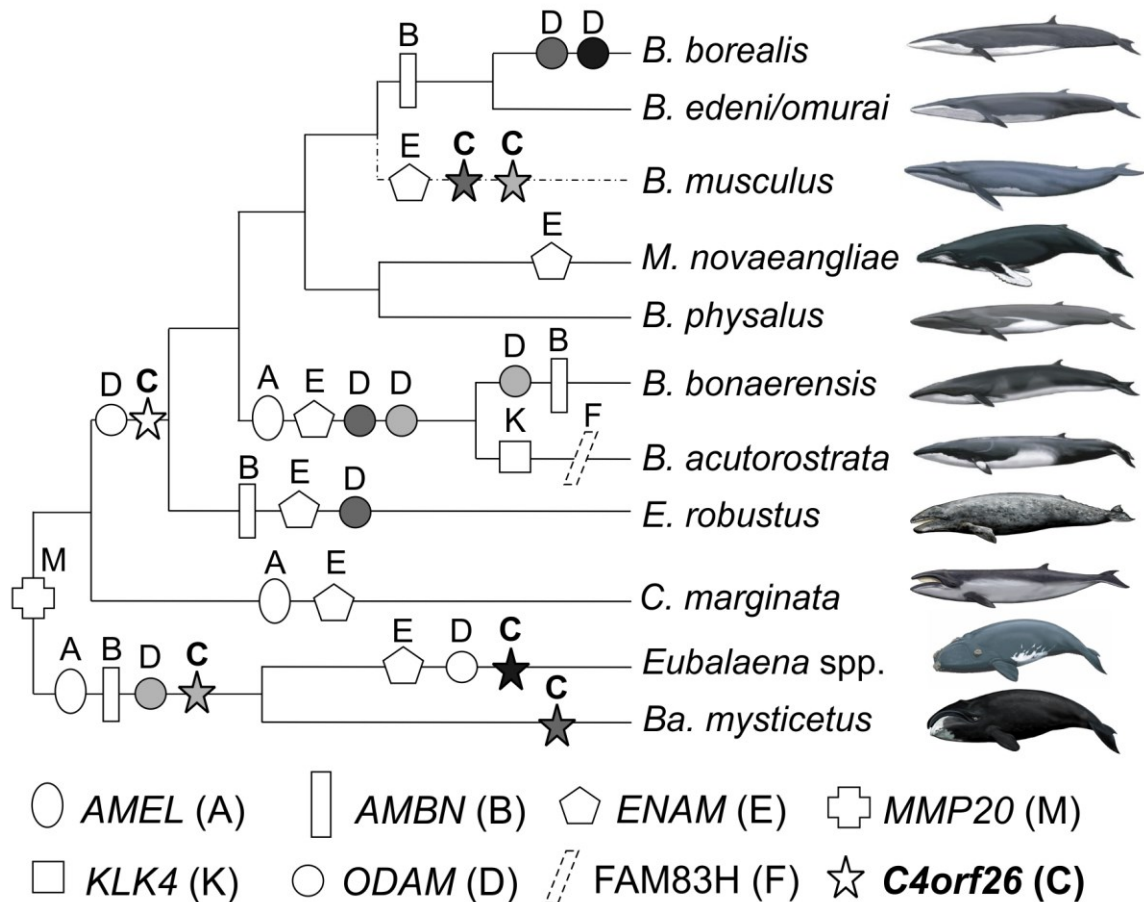


Figure 1.6 – Tooth- and enamel-related gene inactivation in modern Mysticeti. The symbols correspond to the first inactivation of the gene in the lineage or group. Gene *ODAM* has four types of inactivation that can occur concurrently: white circles represent a splice insertion, light gray mutations in exon 4, medium gray mutations in exon 5, dark gray mutation in exon 10. Gene *C4orf26* (bolded) presents three independent inactivations: white stars indicate a shared gene deletion, light gray and medium gray stars signal two different inactivating mutations. *B. musculus* branch is different as this taxon does not share the deletion of *C4orf26* present in other Balaenopteridae, but instead has independently acquired mutations in this gene. Changes in protein sequence (*FAM83H*) are indicated with a dashed shape. Data for *AMEL*, *AMBN*, and *ENAM* from Deméré et al. (2008), Meredith et al. (2009), Meredith et al. (2010), Meredith et al. (2013); *MMP20* from Meredith et al. (2010); *KLK4* from Kawasaki et al. (2014); *ODAM* from Springer et al. (2019); *FAM83H* from Huang et al. (2017); *C4orf26* from Springer et al. (2016). Tree topology after Gatesy et al. (2013). Drawings from Carl Buell from Gatesy et al. (2013).

More enamel-related genes (*AMEL*, *AMBN*, *ENAM*) present unique frameshift mutations in several sites in all families of mysticetes (Deméré et al., 2008, Meredith et al., 2011a). In particular, *ENAM* was discovered to be pseudogenic – having accumulated enough mutations to lose its original coding function – in other toothless and enameless taxa, including in the Odontoceti family Kogiidae, which lacks enamel on teeth (Meredith et al., 2009). These findings strengthen the idea that this region is directly connected with enamel production rather than general tooth formation. Moreover, all three genes are also inactivated in toothless amniotes such as birds and turtles (Meredith et al., 2013). This shows that the genetic bases for tooth loss are shared beyond the mammal clade, and therefore conducting studies on edentulism in baleen whales can have substantial applications in the study of this process in all animals. In contrast with these complex patterns, the enamel-related gene *MMP20* was found to have an inactivating insertion shared by all Mysticeti (Meredith et al., 2011a). After this initial inactivation in the common ancestor of the clade, other mutations arose in several lineages. Also Kogiidae share inactivating mutations, as it was the case for *ENAM*, confirming the enamel-related function of this region. Deleterious mutations were also identified in gene *KLK4* in the common minke whale (*B. acutorostrata*). This gene has an interesting evolutionary history outside of baleen whales. In mammals, *KLK4* was hypothesized to be related specifically to enamel maturation, as it is only found in Boreoeutheria (Laurasiatheria+Euarchontoglires – see Fig. 1.1). This group has an earlier eruption of permanent dentition in postnatal ontogeny compared to other mammals like Afrotheria, a process that, in the light of this findings, appears to be connected to the evolution of this gene (Kawasaki et al., 2014). Deleterious changes can also occur in the protein sequence with only minor changing to the underlying DNA. Conspicuous deletions have been identified in the protein sequence of FAM83H in the common minke whale. Its amino acid sequence was found to be mostly conserved in bowhead whales (*Balaena*) and partial sequences were also recovered in

the genome of Balaenopteridae by Springer et al. (2016). However, Huang et al. (2017) discovered that 59 continuous residues are not present in the examined baleen whale, and other toothless or partially toothless taxa such as the platypus and the armadillo have even larger parts of the sequence missing. The pangolin and the aardvark instead present mostly conserved protein sequences compared to humans and other toothed mammals. These results underscore the need of more research on *FAM83H*, which is a good candidate to be amplified and sequenced in Cetacea and other toothless mammals, in order to better understand its evolutionary history and function in tooth development in Mammalia.

While not exhaustive, the present knowledge on tooth-related gene inactivation in Mysticeti can be used to explain the retention of tooth germs in the fetal stages and to formulate hypotheses on the steps that caused the functional loss of teeth and acquisition of baleen in this group.

## Discussion

### **Feeding strategy and habitat drive tooth count evolution in Odontoceti**

From the analysis of the pattern of distribution of tooth counts in Odontoceti (Fig. 1.4), it emerges that the feeding strategy and habitat play a major role in the evolution of this trait. This is mostly exemplified by the acquisition of a high tooth number convergently in river dolphins. All of these families descended from ancestors that lived in an oceanic environment, and independently acquired traits related to a fresh water habitat, like a long snout and elevated tooth counts to snap prey instead of suction feeding (Hamilton et al., 2001, McCurry et al., 2017a, Page and Cooper, 2017). Given the evidence from the fossil record, it is likely that this transition happened many more times both in ancestral forms of the modern lineages and in extinct groups, always being characterized by the same suit of adaptations (Bianucci et al., 2013a, Pyenson et al., 2015, McCurry and Pyenson, 2018). Another recurring convergent dental pattern in odontocetes is extreme tooth reduction. Sometimes this can occur only in one jaw (e.g. sperm whales) and allow for the remaining teeth to acquire new functions (e.g. narwhal). Tooth reduction is usually also accompanied by a shortening of the rostrum, as dentition and jaws are not employed directly in food capture; this is the opposite evolutionary trajectory observed in river dolphins. Many now-extinct lineages of both stem and crown Odontoceti were also toothless and had a short rostrum (Boessenecker et al., 2017), with some genera such as *Odobenocetops*† evolving tusks (Muizon and Domning, 2002). Ziphiidae and their fossil relatives are likely the best example of convergent evolution of traits in Odontocetes, both in regard to their morphology and associated behavior and physiology. The higher tooth count of *Tasmacetus* stands out as an anomaly in this group of taxa with highly reduced dentition and doesn't have any clear parallel in any other modern clade. Analyzing in detail the evolution of dentition in extant and extinct beaked whales might explain this unique pattern.

Given these observations, the traditional concept of evolutionary irreversibility of a lost trait (Dollo's Law) does not seem to be applicable to the feeding apparatus of toothed whales. The high adaptability to new environments and morphological plasticity of these taxa gave rise to many instances of convergent evolution and drastic changes in tooth counts associated with these adaptations. While certain major traits were lost in the transition from land to water, such as hind limbs, and cannot likely be reacquired, dentition in odontocetes is highly variable but never completely lost. Relaxed selective pressure, due to the acquisition of suction feeding in stem Odontoceti lineages, is responsible for the observed adaptability of tooth counts and rostral shape (Hocking et al., 2017, Kienle et al., 2017, Berta and Lanzetti, in press). In fact, it has been shown that all toothed whales retain dentition in both jaws at least during prenatal ontogeny, with many instances of vestigial dentition also found in adults (Miller, 1929, Boschma, 1938, Boschma, 1950a, Nweeia et al., 2012, Kurihara et al., 2016). Therefore, in Cetacea true loss of teeth, defined as the total absence of adult dentition even as a vestigial character, should be considered as distinct trait from the reduction of number of erupted teeth in adults (Thewissen et al., 2017). Under this definition, only Mysticeti can be considered edentulous. Simple increases in tooth number in odontocetes taxa should not be regarded as a reacquisition of a lost trait, independently of the state of the dentition in the ancestor. Given this premise, it is now possible to better contextualize the evolution of dentition and other related traits in beaked whales and explain their unique tooth count patterns.

### **Independent reacquisition of full dentition in modern and fossil Ziphiidae**

#### *Convergent evolution in the phylogeny of beaked whales*

The analysis of the convergent adaptations of modern and fossil Ziphiidae can shed light on the drivers of convergent evolution in Odontoceti as a whole, thanks to their extensive fossil record. However, their phylogeny needs to be resolved before robust hypotheses on trait



evolution can be formulated. In particular, the conflicting phylogenetic position of *Tasmacetus* needs to be clarified in order to allow an in-depth analysis of the patterns of tooth loss in this clade.

Here, a novel total evidence phylogenetic analysis was performed to try to better resolve the phylogenetic placement of *Tasmacetus* and both fossil and modern beaked whale genera. This taxon was found to be nested in crown Ziphiidae (Fig. 1.5). This result is consistent with some previous molecular analyses (e.g. Dalebout et al., 2004, McGowen et al., 2009), but it has been called into question by other genetic studies (e.g. Steeman et al., 2009) and when morphological data are considered (e.g. Bianucci et al., 2016). One reason of the disagreement between morphological and molecular data might be the lack of significant anatomical differences in the skull of these two genera. In the most up-to-date matrix employed in the present analysis (Bianucci et al., 2016), only 12 of 51 characters differ between the two genera. Of these 12 characters, *Tasmacetus* presents more derived states in four characters, in particular in the degree of fusion of cervical vertebrae (character 51) and possessing only one pair of enlarged mandibular tusk instead of two (character 28). The other eight characters are coded as more derived for *Berardius*, However two of those are autapomorphies of the *Berardius* clade (character 17: intraparietal/frontal form an isolated protuberance on vertex of skull, and character 18: height of supraoccipital relative to vertex) and one is a soft tissue character that cannot be coded for fossil taxa (character 45: stomach anatomy). These genera share a significant similarity that is not present in other Ziphiidae: they have a moderate elevation of the vertex of the skull (character 9), an important trait in the evolution of both modern and fossil beaked whales (Bianucci et al., 2016). Additionally, the presence of full dentition (character 27) is not a reliable character and should not be presented as an example of an ancestral trait conserved in *Tasmacetus*, as also discussed in the previous section for all toothed whales. In Ziphiidae in particular, mandibular

tusks, bore primarily by males of all living species, are modified teeth, and vestigial tooth germs have been found in the upper and lower jaw in almost all “toothless” ziphiid genera (*Mesoplodon*, *Hyperoodon*, and *Ziphius*) in specimens of both sexes (Boschma, 1950b, Boschma, 1951). Loch and Jansen van Vuuren (2016) described in the detail the unerupted teeth of a juvenile Cuvier’s beaked whale (*Ziphius*) and definitively concluded that they are an example of vestiges (i.e. remnants of an ancestral trait – Hall, 2003) rather than atavisms (i.e. rare reappearance of a lost trait – Hall, 2003). This evidence clearly shows that all living beaked whales still possess the genetic information and developmental pathways to produce a full dentition. Furthermore, the closely-related fossil taxon *Nazcacetus*† is only partially toothless, with small teeth having been found associated with the skull, similar in shape and size to the vestigial dentition of modern genera such as *Mesoplodon* (Lambert et al., 2009, Bianucci et al., 2016). This extinct taxon However clearly shares other traits with the Tasman’s beaked whale, supporting the idea that these vestigial structures might have re-acquired some function independently in the living species. If more anatomical characters were identified to distinguish *Tasmacetus* and *Berardius* independently of tooth number, morphological analyses might agree with molecular results and the present total evidence phylogeny.

Some insight on the evolution of extant Ziphiidae and possibly a parallel to the re-acquisition of full dentition in *Tasmacetus* can be found by looking at the convergent evolution of the extinct “*Messapicetus*† clade”. As pointed out by Bianucci et al. (2016) and confirmed here, these fossil taxa form a monophyletic group, which shares many similarities in evolutionary trajectory with crown beaked whales. Both clades display progressive tooth reduction and possible acquisition of lower jaw tusks (Lambert et al., 2010), rostral pachyostosis (i.e. thickening of the facial bones), vertex elevation and increase in body size (Bianucci et al., 2016). While teeth reduction is associated with specialized suction feeding, the other traits are likely connected with

different shared aspects of the physiology and behavior of these taxa. Pachyostosis of the rostrum, due to thickened and more compact bones, might be related to the presence of stronger facial muscles to be employed both in feeding and other behaviors such as male-to-male competition. This behavior is believed to be common in modern beaked whales and also connected to the evolution of tusks (Heyning, 1989, Dalebout et al., 2008, Lambert et al., 2010, Bianucci et al., 2013b, Gol'din, 2014). Elevation of the vertex is probably instead related to sound production and echolocation (Cranford et al., 2008), while increase in body size has been shown in many Cetacea to be beneficial for deep diving and controlling body temperature (Noren and Williams, 2000, Watanabe et al., 2011, Montgomery et al., 2013). Given these similarities, it is possible that also *Tasmacetus* dental morphology, while unique now, is not unprecedented in the context of the evolution of the group.

Indeed, in the “*Messapicetus*† clade”, two taxa stand out in regard to tooth evolution: *Ziphirostrum*† and *Beneziphius*†. These two taxa are recovered as intermediate lineages and present a high number of tooth alveoli in each side of the upper jaw: over 40 in *Ziphirostrum marginatus*† and for *Beneziphius brevirostris*† 14 alveoli are preserved in the posterior part of the rostrum of the holotype (Lambert, 2005b, Bianucci et al., 2016). While these alveoli are interpreted in the literature as vestigial given that they are shallow and small, they are evidence of the presence of a full tooth row even if the teeth might have remained unerupted. It is not possible to determine using the currently available specimens if they were erupted or not, and consequently these taxa are coded in the matrix as ambiguous (character 27). No mandible is known for these species, making it impossible to evaluate the presence of tusks or dentition in the lower jaw. Given this ambiguity, when full dentition was lost in this extinct clade is debatable. *Ziphirostrum*† might have just maintained the ancestral condition, as the earlier diverging lineage (*Messapicetus*†) still retained well-developed teeth in both jaws. But more notable is the position

and morphology of *Beneziphius*†: this taxon is derived from a genus that lacks dentition and alveoli altogether in the upper jaw (*Aporotus*†), but it still had alveoli and possibly erupted teeth. The phylogenetic position of this last taxon in the “*Messapicetus*† clade” seems to mirror the position of *Tasmacetus* in crown Ziphiidae, providing a precedent for the elevated tooth counts observed in this modern taxon.

The parsimony ancestral state reconstruction (Fig. 1.5) of dental characters also supports this hypothesis. According to the total evidence phylogeny, the loss of full dentition in the upper jaw occurs at the *Aporotus*† node in the *Messapicetus*† clade and in the common ancestor crown Ziphiidae, indicating that at least one taxon in each clade (*Tasmacetus* and *Beneziphius*†) with full maxillary dentition might have reacquired this state independently. However, this result might be biased by the preservation status of available fossils and by the absence of molecular data for extinct taxa. As the position of *T. shepherdi* changes drastically when genetic evidence is considered, it is possible that in the *Messapicetus*† clade similar taxa, with an independently reacquired higher tooth count, are present, but they result as earlier diverging based on their tooth count and on the available morphological data. More fossil discoveries could clarify the ancestral state of dentition at the base of crown Ziphiidae and help identify additional phylogenetically-informative morphological characters. Also, reviewing the coding of the present characters taking into consideration the high variability of tooth-related traits might shift the phylogenetic relationships among extinct taxa in the future.

#### *Ecology and behavior explain the tooth count of Tasmacetus*

There are several lines of evidence that could explain the elevated tooth count in the Tasman’s beaked whale and potentially analogous fossil relatives. The diversification of Ziphiidae was relatively rapid, and both molecular and fossil evidence point to the fact that only 2-3 million years separate the *Tasmacetus* clade and the common ancestor of all Ziphiidae, which

it most likely had full dentition (Fig. 1.6 – McGowen et al., 2009, Bianucci et al., 2016). Despite that no detailed analyses on the genetic bases of teeth development have been conducted in Ziphiidae, their phenotype suggests that still retain active tooth-related genes and the developmental toolkit to form dentition, as noted above. Therefore, there are no identifiable intrinsic mechanisms that would prevent an increase in tooth number in a single lineage, which also has precedents in the evolutionary history of Odontoceti as whole.

Extrinsic factors (e.g. ecology, diet, behavior) likely provide the selective pressures to develop and maintain a full dentition. The diet of the Tasman's beaked whale was believed to be composed mostly of fish, based on the evidence provided by the stomach contents of a single individual (Mead, 1989). If fish are its main prey type, the high number of teeth might be employed in feeding, aiding capturing prey in addition to suction feeding (Hocking et al., 2017, Kienle et al., 2017). However, a more recent study described remains of cephalopods in the stomach of a stranded animal, leading the authors to hypothesize that the diet of *Tasmacetus* may vary depending on the time of the day, season, or age of the whale (Best et al., 2014). Additionally, fishes have been identified as prey for most of the other Ziphiidae genera that do not bear a full dentition, and they constitute the main prey type for at least three species of *Mesoplodon* (*M. bidens* – Sowerby's beaked whale, *M. grayi* – Gray's beaked whale, and *M. mirus* – True's beaked whale) (Pauly et al., 1998, MacLeod et al., 2003). Other odontocetes with reduced dentition such as the Risso's dolphin and the narwhal also feed on fish at least occasionally (Pauly et al., 1998). This clearly indicates that the presence of a full row of teeth is not a limiting factor in prey selection (MacLeod et al., 2003). Thus, it is hypothesized that Ziphiidae are generalists and can feed on different types of prey depending on availability, season, geographic location, or competition (MacLeod et al., 2003). For example, some species of the genus *Mesoplodon*, which occur sympatrically to *Hyperoodon* (bottlenose whales) and

*Ziphius*, tend to occupy a different ecological niche by feeding on fish and smaller prey to avoid direct competition from these larger taxa (MacLeod et al., 2003). This could be the case also for *Tasmacetus*, which range also overlaps with *Hyperoodon* and *Ziphius*. Its dentition might represent an advantage in capturing prey not available to these other taxa (MacLeod et al., 2003, Best et al., 2014). Aside from feeding, another important driver of Ziphiidae dentition evolution is sexual selection, which is thought to play a major role, for example, in the differentiation of mandibular tusk shape among males of different species in the genus *Mesoplodon* (Dalebout et al., 2008). Since many of these species co-occur in the same regions for at least part of the year, it is hypothesized that tusks in males are used for species delimitation through sexual selection by female choice (Dalebout et al., 2008). It is possible that the unique dentition pattern of *Tasmacetus* serves the same purpose, by clearly identifying it as a different species in the areas where it co-occurs with other beaked whales.

In sum, a combination of environmental changes, behavior and underlying relaxed selective pressure brought to the independent acquisition of full dentition in the Tasman's beaked whale, and the same factors could have caused the same trait to evolve in unrelated fossil lineages. These are likely the same drivers that produced the disparate tooth counts patterns observed in Odontoceti as whole. Understanding the molecular and developmental mechanisms at the base of these changes would help increasing the resolution of the phylogeny of tooth whales and dating the major phenotypic transitions in feeding adaptations (McGowen et al., 2014). This in turn would help better identify the causes of this great variability and related shifts in feeding mode and habitats (Steeman et al., 2009, Berta and Lanzetti, in press). However, it is first necessary to recognize which gene regions and developmental processes are responsible for tooth formation in Cetacea. Studying inactivated gene regions in edentulous Mysticeti can accomplish

this goal and additionally provide information of the loss of teeth and connected changes in mammals as a whole.

### **Loss of function preceded loss of dentition in Mysticeti**

Reviewing the available information on the inactivation of tooth- and enamel-related genes in modern baleen whales (Fig. 1.6), it is clear that a complex set of mutations in many regions are responsible for the loss of teeth in these taxa, and most of them occurred independently in different lineages, only after the loss of adult functional dentition. While it is possible that a few major changes in the genome of the common ancestor of modern Mysticeti started the process of tooth reduction, these shared mutations still have to be definitively identified (Deméré et al., 2008, Berta et al., 2016). Only one of the eight currently studied genes has an inactivating insert shared by all living baleen whale species (*MMP20*). More research has to be conducted on this topic, to detect and sequence additional genetic regions related to tooth formation that might have initiated the process of tooth loss in the ancestor of modern taxa. However, present data can be used to trace the major steps that characterize postnatal tooth loss in the fossil record, and to explain the retention of rudimental tooth germs prenatally in living species, even after over 35 million years from the acquisition of baleen (Berta et al., 2016).

The majority of the genes sequenced are believed to be involved specifically in enamel development, given that they are also inactivated in toothed but enameless taxa such as Kogiidae, with the exception of *C4orf26* that is tooth-related (Springer et al., 2016). The inactivation of at least one enamel-related gene (*MMP20*) preceded the independent inactivation of this tooth-related gene. However additional knowledge on the genetic and developmental pathways of tooth data appears to be in line with evidence from the fossil record. The first group of baleen-bearing stem-Mysticeti, Eomysticetidae, is in fact hypothesized to have retained some vestigial dentition in the adult or at least juvenile stages, but these teeth were likely enameless (Boessenecker and

Fordyce, 2015a, Boessenecker and Fordyce, 2015b). Earlier stem lineages of toothed mysticetes (e.g. Aetiocetidae) instead have functional dentition with complex enamel, similar to archaic cetaceans (Deméré and Berta, 2008, Loch et al., 2019). Enamel-specific genes being inactivated before tooth-related ones would explain the dental anatomy of these extinct taxa. The progressive loss of function of dentition connected to the evolution of baleen plates and filter feeding could have initiated these changes. This is similar to what is observed in Odontoceti, where the loss of primary function of dentition after the acquisition of specialized suction feeding caused the loss of complex enamel in several lineages (e.g. Kogiidae, Ziphiidae). The hypothesis that loss of function preceded major genetic changes can also explain the convergent evolutionary patterns observed in most enamel- and tooth-related genes in modern baleen whales. Since the loss of function and vestigialization of teeth likely occurred in the common ancestor of both modern Mysticeti and the stem-lineage Eomysticetidae, the genes were not under strong selective pressure by the time that modern groups started diversifying around 4 million years later (Berta et al., 2016). Inactivating mutations could then arise independently in each taxon and be passed on to the next generation without detrimental effects on the fitness of the animal.

Genetic information also fits the characteristics of the tooth germs that develop and then are resorbed in ontogeny in modern species. Histological studies conducted on both Balaenopteridae (*B. physalus* and *B. bonaerensis*) and Balaenidae (*Balaena*) have repeatedly confirmed that the rudimentary tooth germs only grow a dentin layer before being resorbed, and no enamel is recognizable. However, some differences have been noted in the timing of development and shape of tooth germs among families (Karlsen, 1962, Ishikawa and Amasaki, 1995, Ishikawa et al., 1999, Thewissen et al., 2017). The shared absence of enamel can be attributed to the inactivation of enamel-related genes in the ancestors of crown mysticetes. Instead, the disparate morphology of tooth germs can be due to the independently acquired



mutations recorded in many genes. While there is no direct evidence of this, *C4orf26* might be connected with the differences observed in Balaenidae and Balaenopteridae, as it is inactivated in the first group and completely deleted in most species of the second. Focused studies aimed to detect proteins produced by this gene during prenatal development and their effect of tooth formation need to be conducted to test this hypothesis. Other similar genes should also be identified, as tooth development is a complex process regulated by many different regions.

Nevertheless, it is not clear why rudimentary dentition still develops during ontogeny in Mysticeti in the first place. Phylogenetic constraints acting on developmental pathways and genomes are the prevalent explanation for the retention of these rudiments. Sequences of putative enamel genes *WDR72*, *SLC24A4* and *FAM83H* have been found to be mostly intact in mysticetes and other toothless and enameless mammals (Springer et al., 2016). These genes likely have pleiotropic effects and contribute to the proper development of other vital organs, such as heart and kidneys. It is interesting to notice however that FAM83H protein sequence was found to be mutated in the common minke whale, potentially indicating that some functions of this gene have been lost (Huang et al., 2017). Similarly, the DPP domain of the *DSPP* gene, involved in dentin formation, was found to be mostly conserved in the bowhead whale (*Balaena*), However it could not be sequenced for the fin whale (*B. physalus*), suggesting that some mutations might be present in Balaenopteridae that are not shared by Balaenidae (McKnight and Fisher, 2009). This possibility is supported by the fact that this region was also conserved in the platypus, while it was inactivated in anteaters and chickens, highlighting its role on tooth development and viability of inactivating mutations. More recently However, it has been proposed that tooth germs actually play some role in the formation of baleen and jaws in Mysticeti, and do not simply represent a relic of their toothed ancestry. A recent study found that a growth factor commonly associated with tooth growth (FGF-4) might have been co-opted for baleen development, However the

genetic bases of baleen remain unknown (Thewissen et al., 2017). The presence of this “deep homology” in the development of these two feeding structures implies that some features of dentition might still be under selection, especially in the upper jaw where baleen grow. Additionally, the growth of tooth germs might be an integral part of the development of the nerves and blood vessels present in the mandible, which retain important sensorial functions in baleen whales and other toothless taxa (Ferreira-Cardoso et al., 2019).

Overall, the current evidence on the timing and mode of inactivation of enamel- and tooth-related genes fits well with data from the fossil record and presently available developmental observations. However, only a more detailed study of the ontogenetic transformations that occur in teeth, baleen and the surrounding skull bones could provide a better understanding of these processes and what role rudimental dentition plays in the overall ontogeny of the skull. Moreover, a better understanding of prenatal development could help researchers identify possible genes and growth pathways involved in the evolution of the unique features of mysticetes like baleen.

## Conclusions

Trait loss is a major driver in the evolution of animals. Specifically, loss of teeth in order to exploit new feeding niches occurred in many different lineages, from birds to mammals (David-Béal et al., 2009). Among Mammalia, Cetacea present unique adaptations to the aquatic environment, which also include extreme cases of tooth reduction and loss. This study qualitatively demonstrated that the dentition and feeding apparatus of Odontoceti is highly variable, with many instances of convergent evolution. This pattern is likely caused by the relaxation of selective pressures on these traits, followed by adaptations to similar environments and feeding modes. Polyphyletic “river dolphins” present an elevated tooth count and long rostrum, while, on the opposite end, other lineages have a short snout and reduced dentition, like the narwhal and sperm whales. Future research should focus on investigating the underlying genetic and developmental changes that make these variations possible in specific clades, in order to formulate broader hypotheses on the evolutionary drivers of feeding modes and related traits in toothed whales. However, a solid phylogeny of both modern and fossil taxa is needed to conduct an evolutionary study at this scale.

To start this effort, a novel total evidence phylogeny was constructed for beaked whales (Ziphiidae), one of the most poorly known clades of Cetacea. Fossil and modern Ziphiidae represent a good study system to examine the changes in tooth counts and their underlying external causes, due to their unique dental morphology (Dalebout et al., 2004, Dalebout et al., 2008). Based on the phylogenetic analysis of molecular and morphological data combined, the giant beaked whales (*Berardius* spp.) represent the earliest diverging lineage of crown Ziphiidae, and *Tasmacetus*, the only living species retaining a full row of teeth in both jaws, is instead later diverging. Ancestral state reconstruction suggests that this taxon has independently reacquired a full row of teeth, as it probably also occurred convergently in at least one fossil lineage. This

could be possible as genetic bases for teeth development are still preserved in crown Ziphiidae, with all other living beaked whales retaining dentition in the form of mandibular tusks and vestigial teeth having been identified in both jaws of multiple species (Boschma, 1951, Loch and Jansen van Vuuren, 2016). Both sexual selection and intraspecific competition for food resources could explain the presence of full dentition in this species and, at the same time, the great reduction of tooth number in the other modern genera of beaked whales. The collection of additional fossil evidence and data on prey type and behavior of living species will allow for a better picture of tooth pattern evolution in Ziphiidae and of the biological drivers shaping this trait in both extant and extinct clades.

Reacquisition of a full dentition in Ziphiidae should not be considered as an exception to Dollo's Law, as adult teeth are present in some form in all members of Odontoceti. However, given the patterns observed in the evolution of Cetacea, it is not surprising that one group truly lost adult functional dentition: Mysticeti. They only preserve rudimental tooth germs in the prenatal stages of development, and instead they are born with keratinous plates called baleen, which allow them to perform bulk filter feeding instead of the ancestral raptorial feeding (Berta et al., 2016). This major transition in anatomy and feeding mode involved changes on the molecular, phenotypical and developmental levels in order to occur. The impressive fossil record of these taxa provides important insights on the morphological changes that accompanied the evolution of these taxa, but less information is available on the underlying genetic mutations and developmental pathways that caused these transformations. To partially fill the gap on the molecular mechanisms, I contributed to amplify and sequence a putative tooth-related gene (*C4orf26*), which was found to have been independently inactivated or completely deleted in multiple living baleen whale species (Springer et al., 2016). By reviewing the current evidence on other similar genes, this is the only known region directly related to tooth formation to have been

found to present inactivating mutations. Other seven enamel-related genes are inactivated in Mysticeti. Only one of these genes (*MMP20*) presents a mutation shared by all living families, while all others have different inactivations patterns (Meredith et al., 2011a). Given this evidence and fossil data, it is possible to hypothesize that the loss of tooth function, accompanied by a loss of the enamel cap as also seen in some modern toothed whales with reduced dentition, preceded the complete loss of adult dentition. This second step was likely related to the acquisition of baleen plates and the switch to specialized bulk filter feeding. However, presently not enough data are available on the genetic mechanisms of baleen formation to directly test this hypothesis, and future research should focus on identifying molecular changes connected to the acquisition of this unique structure. This genetic pattern of tooth loss can also explain the lack of enamel in the fetal tooth germs and differences in their morphology among families. The retention of this seemingly useless structures was believed to be due to complex pleiotropic effects, as some genes connected to tooth formation are still active in baleen whales (Springer et al., 2016). However, new research showed that tooth germs likely play a role in the development of the jaws and even of the baleen plates (Thewissen et al., 2017, Ferreira-Cardoso et al., 2019). Ontogenetic changes in the skull of modern mysticetes are still understudied, and most data are available for only one or two species. After more developmental data are collected on the anatomical changes connected to the teeth-to-baleen transition that occurs in the fetal stages, they can be united with genetic evidence and morphological data of fossil taxa to present an overarching hypothesis on the drivers and major milestones in the evolution of baleen and filter feeding. Therefore, the data collected in this Chapter on tooth reduction and loss in Cetacea will serve as framework to investigate in detail the prenatal development in Chapter Two and evolution of the skull and feeding mode of Mysticeti in Chapter Three.

## Literature cited

- Allin EF (1975) Evolution of the mammalian middle ear. *J Morphol*, **147**, 403-437.
- Armfield BA, George JC, Vinyard CJ, Thewissen JGM (2011) Allometric patterns of fetal head growth in mysticetes and odontocetes: comparison of *Balaena mysticetus* and *Stenella attenuata*. *Mar Mamm Sci*, **27**, 819-827.
- Armfield BA, Zheng Z, Bajpai S, Vinyard CJ, Thewissen JGM (2013) Development and evolution of the unique cetacean dentition. *PeerJ*, **1**, e24.
- Atchley WR, Hall BK (1991) A model for development and evolution of complex morphological structures. *Biol Rev Camb Philos Soc*, **66**, 101-57.
- Balcomb KCI (1989) Baird's beaked whale - *Berardius bairdii* Stejneger, 1883: Arnoux's beaked whale - *Berardius arnouxii* Duvernoy, 1851. In *Handbook of marine mammals: river dolphins and larger toothed whales* (eds Ridgway SH, Harrison R), pp. 261-288. London: Academic Press.
- Bannister JL (2018) Baleen whales (Mysticeti). In *Encyclopedia of Marine Mammals* (eds Würsig B, Thewissen JGM, Kovacs KM), pp. 62-69. London: Academic Press.
- Bejder L, Hall BK (2002) Limbs in whales and limblessness in other vertebrates: mechanisms of evolutionary and developmental transformation and loss. *Evol Dev*, **4**, 445-458.
- Berkovitz B, Shellis P (2018a) Cetartiodactyla: Cetacea. In *The Teeth of Mammalian Vertebrates*, pp. 249-265. London: Academic Press.
- Berkovitz B, Shellis P (2018b) General Introduction. In *The Teeth of Mammalian Vertebrates*, pp. 1-24. London: Academic Press.
- Berta A, Lanzetti A (IN REVIEW) Feeding in marine mammals: an integration of evolution and ecology through time. *Palaeontol Electron*.
- Berta A, Lanzetti A, Ekdale EG, Deméré TA (2016) From teeth to baleen and raptorial to bulk filter feeding in mysticete cetaceans: the role of paleontological, genetic, and geochemical data in feeding evolution and ecology. *Integr Comp Biol*, **56**, 1271-1284.
- Best PB, Smale MJ, Glass J, Herian K, Von Der Heyden S (2014) Identification of stomach contents from a Shepherd's beaked whale *Tasmacetus shepherdi* stranded on Tristan da Cunha, South Atlantic. *J Mar Biol Assoc UK*, **94**, 1093-1097.
- Best RC, Da Silva VMF (1993) *Inia geoffrensis*. *Mamm Species*, **426**, 1-8.
- Bianucci G, Di Celma C, Urbina M, Lambert O (2016) New beaked whales from the late Miocene of Peru and evidence for convergent evolution in stem and crown Ziphiidae (Cetacea, Odontoceti). *PeerJ*, **4**, e2479.

- Bianucci G, Lambert O, Post K** (2010) High concentration of long-snouted beaked whales (genus *Messapicetus*) from the Miocene of Peru. *Palaeontology*, **53**, 1077-1098.
- Bianucci G, Lambert O, Salas-Gismondi R, et al.** (2013a) A Miocene relative of the Ganges River dolphin (Odontoceti, Platanistidae) from the Amazonian Basin. *J Vert Paleontol*, **33**, 741-745.
- Bianucci G, Miján I, Lambert O, Post K, Mateus O** (2013b) Bizarre fossil beaked whales (Odontoceti, Ziphiidae) fished from the Atlantic Ocean floor off the Iberian Peninsula. *Geodiversitas*, **35**, 105-153.
- Bianucci G, Post K, Lambert O** (2008) Beaked whale mysteries revealed by seafloor fossils trawled off South Africa. *S Afr J Sci*, **104**, 140-142.
- Bloodworth BE, Odell DK** (2008) *Kogia breviceps* (Cetacea: Kogiidae). *Mamm Species*, **819**, 1-12.
- Bloom T, Binford G, A. Esposito L, et al.** (2014) Discovery of two new species of eyeless spiders within a single Hispaniola cave. *J Arachnol*, **42**, 148-154.
- Boessenecker RW, Fordyce RE** (2015a) Anatomy, feeding ecology, and ontogeny of a transitional baleen whale: a new genus and species of Eomysticetidae (Mammalia: Cetacea) from the Oligocene of New Zealand. *PeerJ*, **3**, e1129-e1129.
- Boessenecker RW, Fordyce RE** (2015b) A new genus and species of eomysticetid (Cetacea: Mysticeti) and a reinterpretation of '*Mauicetus lophocephalus*' Marples, 1956: transitional baleen whales from the upper Oligocene of New Zealand. *Zool J Linn Soc*, **175**, 607-660.
- Boessenecker RW, Fordyce RE** (2016) A new eomysticetid from the Oligocene Kokoamu Greensand of New Zealand and a review of the Eomysticetidae (Mammalia, Cetacea). *J Syst Palaeontol*, DOI: 10.1080/14772019.2016.1191045.
- Boessenecker RW, Fraser D, Churchill M, Geisler JH** (2017) A toothless dwarf dolphin (Odontoceti: Xenorophidae) points to explosive feeding diversification of modern whales (Neoceti). *Proc R Soc Lond B Biol Sci*, **284**, 20170531.
- Boschma H** (1938) On the teeth and other particulars of the sperm whale (*Physeter macrocephalus* L.). *Temminckia*, **3**, 155-278.
- Boschma H** (1950a) Absorption of tooth tissue in the sperm whale. *Proc K Ned Akad Wet Ser C Biol Med Sci*, **53**, 289-293.
- Boschma H** (1950b) Maxillary teeth in specimens of *Hyperoodon rostratus* (Muller) and *Mesoplodon grayi* von Haast stranded on the Dutch coasts. *Proc K Ned Akad Wet C*, **53**, 775-786.
- Boschma H** (1951) Rows of small teeth in ziphioid whales. *Zool Meded*, **31**, 139-148.

- Bouetel VV** (2005) Phylogenetic implications of skull structure and feeding behavior in balaenopterids (Cetacea, Mysticeti). *J Mammal*, **86**, 139-146.
- Brace CL** (1963) Structural reduction in evolution. *Am Nat*, **97**, 39-49.
- Bremer K** (1994) Branch support and tree stability. *Cladistics*, **10**, 295-304.
- Buono MR, Cozzuol MA** (2013) A new beaked whale (Cetacea, Odontoceti) from the Late Miocene of Patagonia, Argentina. *J Vert Paleontol*, **33**, 986-997.
- Butler PM** (1995) Ontogenetic aspects of dental evolution. *Int J Dev Biol*, **39**, 25-34.
- Cabej NR** (2012) Evolution by loss. In *Epigenetic Principles of Evolution*, pp. 579-622. London: Elsevier Ltd.
- Catón J, Tucker AS** (2009) Current knowledge of tooth development: patterning and mineralization of the murine dentition. *J Anat*, **214**, 502-515.
- Charlton-Robb K, Gershwin L-a, Thompson R, Austin J, Owen K, McKechnie S** (2011) A new dolphin species, the Burrunan dolphin *Tursiops australis* sp. nov., endemic to southern Australian coastal waters. *PLoS ONE*, **6**, e24047.
- Chen Y, Zhang Y, Jiang TX, et al.** (2000) Conservation of early odontogenic signaling pathways in Aves. *Proc Natl Acad Sci USA*, **97**, 10044-10049.
- Collin R, Miglietta MP** (2008) Reversing opinions on Dollo's law. *Trends Ecol Evol*, **23**, 602-609.
- Cracraft J** (1990) The origin of evolutionary novelties: pattern and process at different hierarchical levels. In *Evolutionary Innovations* (ed Nitecki MH), pp. 21-44. Chicago: University Press.
- Cranford TW, Krysl P, Hildebrand JA** (2008) Acoustic pathways revealed: simulated sound transmission and reception in Cuvier's beaked whale (*Ziphius cavirostris*). *Bioinspir Biomim*, **3**, 016001.
- Dalebout ML, Baker CS, Mead JG, Cockcroft VG, Yamada TK** (2004) A comprehensive and validated molecular taxonomy of beaked whales, family Ziphiidae. *J Hered*, **95**, 459-473.
- Dalebout ML, Steel D, Baker CS** (2008) Phylogeny of the beaked whale genus *Mesoplodon* (Ziphiidae: Cetacea) revealed by nuclear introns: implications for the evolution of male tusks. *Syst Biol*, **57**, 857-75.
- Darwin C** (1859) *On the origins of species by means of natural selection*, Murray, London.
- Davis DD** (1964) The giant panda. A morphological study of evolutionary mechanisms. *Fieldiana*, **3**, 1-339.



- Davit-Béal T, Tucker AS, Sire J-Y** (2009) Loss of teeth and enamel in tetrapods: fossil record, genetic data and morphological adaptations. *J Anat*, **214**, 477-501.
- Deméré TA, Berta A** (2008) Skull anatomy of the Oligocene toothed mysticete *Aetiocetus weltoni* (Mammalia; Cetacea): implications for mysticete evolution and functional anatomy. *Zool J Linn Soc*, **154**, 308-352.
- Deméré TA, McGowen MR, Berta A, Gatesy J** (2008) Morphological and molecular evidence for a stepwise evolutionary transition from teeth to baleen in mysticete whales. *Syst Biol*, **57**, 15-37.
- Dollo L** (1893) The laws of evolution. *Bull Soc Bel Geol Paleontol*, **7**, 164-166.
- El-Sayed W, Parry DA, Shore RC, et al.** (2009) Mutations in the beta propeller *WDR72* cause autosomal-recessive hypomaturation *amelogenesis imperfecta*. *Am J Hum Genet*, **85**, 699-705.
- El Adli JJ, Deméré TA, Boessenecker RW** (2014) *Herpetocetus morrowi* (Cetacea: Mysticeti), a new species of diminutive baleen whale from the Upper Pliocene (Piacenzian) of California, USA, with observations on the evolution and relationships of the Cetotheriidae. *Zool J Linn Soc*, **170**, 400-466.
- Fahlke JM, Hampe O** (2015) Cranial symmetry in baleen whales (Cetacea, Mysticeti) and the occurrence of cranial asymmetry throughout cetacean evolution. *Sci Nat*, **102**, 58.
- Ferreira-Cardoso S, Delsuc F, Hautier L** (2019) Evolutionary tinkering of the mandibular canal linked to convergent regression of teeth in placental mammals. *Curr Biol*, **0**, 1-8.
- Fong DW, Kane TC, Culver DC** (1995) Vestigialization and loss of nonfunctional characters. *Annu Rev Ecol Syst*, **26**, 249-268.
- Fordyce RE** (1982) Dental anomaly in a fossil squalodont dolphin from New Zealand, and the evolution of polydonty in whales. *N Z J Zool*, **9**, 419-426.
- Fraser GJ, Cerny R, Soukup V, Bronner-Fraser M, Streelman JT** (2010) The odontode explosion: the origin of tooth-like structures in vertebrates. *Bioessays*, **32**, 808-17.
- Friedman M** (2012) Parallel evolutionary trajectories underlie the origin of giant suspension-feeding whales and bony fishes. *Proc R Soc Lond B Biol Sci*, **279**, 944-951.
- Fudge DS, Szewciw LJ, Schwalb AN** (2009) Morphology and development of blue whale baleen: an annotated translation of Tycho Tullberg's classic 1883 paper. *Aquat Mamm*, **35**, 226-252.
- Galatius A** (2010) Paedomorphosis in two small species of toothed whales (Odontoceti): how and why? *Biol J Linn Soc*, **99**, 278-295.
- Gatesy J, Geisler JH, Chang J, et al.** (2013) A phylogenetic blueprint for a modern whale. *Mol Phylogen Evol*, **66**, 479-506.

- Gatesy J, O'Leary Ma** (2001) Deciphering whale origins with molecules and fossils. *Trends Ecol Evol*, **16**, 562-570.
- Geisler JH, McGowen MR, Yang G, Gatesy J** (2011) A supermatrix analysis of genomic, morphological, and paleontological data from crown Cetacea. *BMC Evol Biol*, **11**, 112-112.
- Geisler JH, Sanders AE** (2003) Morphological evidence for the phylogeny of Cetacea. *J Mamm Evol*, **10**, 23-129.
- Gilbert SF, Bolker JA** (2001) Homologies of process and modular elements of embryonic construction. *J Exp Zool*, **291**, 1-12.
- Gingerich PD, ul-Haq M, von Koenigswald W, Sanders WJ, Holly Smith B, Zalmout IS** (2009) New protocetid whale from the Middle Eocene of Pakistan: birth on land, precocial development, and sexual dimorphism. *PLoS ONE*, **4**, e4366-e4366.
- Gol'din P** (2014) 'Antlers inside': are the skull structures of beaked whales (Cetacea: Ziphiidae) used for echoic imaging and visual display? *Biol J Linn Soc*, **113**, 510-515.
- Goldbogen JA, Cade DE, Calambokidis J, et al.** (2017) How baleen whales feed: the biomechanics of engulfment and filtration. *Ann Rev Mar Sci*, **9**, 367-386.
- Goldbogen JA, Calambokidis J, Croll DA, et al.** (2012) Scaling of lunge-feeding performance in rorqual whales: mass-specific energy expenditure increases with body size and progressively limits diving capacity. *Funct Ecol*, **26**, 216-226.
- Goldbogen JA, Potvin J, Shadwick RE** (2010) Skull and buccal cavity allometry increase mass-specific engulfment capacity in fin whales. *Proc R Soc Lond B Biol Sci*, **277**, 861-868.
- Gould SJ** (1970) Dollo on Dollo's law: irreversibility and the status of evolutionary laws. *J Hist Biol*, **3**, 189-212.
- Greer AE** (1991) Limb reduction in squamates: identification of the lineages and discussion of the trends. *J Herpetol*, **25**, 166-173.
- Hall BK** (2002) Palaeontology and evolutionary developmental biology: a science of the nineteenth and twenty-first centuries. *Palaeontology*, **45**, 647-669.
- Hall BK** (2003) Descent with modification: the unity underlying homology and homoplasy as seen through an analysis of development and evolution. *Biol Rev*, **78**, 409-433.
- Hamilton H, Caballero S, Collins aG, Brownell RL** (2001) Evolution of river dolphins. *Proc R Soc Lond B Biol Sci*, **268**, 549-556.
- Hampe O, Franke H, Hipsley CA, Kardjilov N, Muller J** (2015) Prenatal cranial ossification of the humpback whale (*Megaptera novaeangliae*). *J Morphol*, **276**, 564-582.

- Harrington SM, Harrison LB, Sheil CA** (2013) Ossification sequence heterochrony among amphibians. *Evol Dev*, **15**, 344-364.
- Heyning JE** (1989) Comparative facial anatomy of beaked whales (Ziphiidae) and a systematic revision among the families of extant Odontoceti. *Contrib Sci (Los Angel)*, **405**, 1-64.
- Hocking DP, Marx FG, Park T, Fitzgerald EMG, Evans AR** (2017) A behavioural framework for the evolution of feeding in predatory aquatic mammals. *Proc R Soc Lond B Biol Sci*, **284**, 20162750.
- Hooker SK** (2018) Toothed whales (Odontoceti). In *Encyclopedia of Marine Mammals* (eds Würsig B, Thewissen JGM, Kovacs KM), pp. 1004-1010. London: Academic Press.
- Huang W, Yang M, Wang C, Song Y** (2017) Evolutionary analysis of FAM83H in vertebrates. *PLoS ONE*, **12**, 1-12.
- Huyseune A, Sire JY** (1998) Evolution of patterns and processes in teeth and tooth-related tissues in non-mammalian vertebrates. *Eur J Oral Sci*, **106**, 437-481.
- Huyseune A, Sire JY, Witten PE** (2009) Evolutionary and developmental origins of the vertebrate dentition. *J Anat*, **214**, 465-476.
- Ishikawa H, Amasaki H** (1995) Development and physiological degradation of tooth buds and development of rudimental baleen plate in southern minke whale, *Balaenoptera acutorostrata*. *J Vet Med Sci*, **57**, 665-670.
- Ishikawa H, Amasaki H, Dohguchi H, Furuya A, Suzuki K** (1999) Immunohistological distributions of fibronectin, tenascin, type I, III and IV collagens, and laminin during tooth development and degeneration in fetuses of minke whale, *Balaenoptera acutorostrata*. *J Vet Med Sci*, **61**, 227-232.
- Jeffrey WR** (2005) Adaptive evolution of eye degeneration in the mexican blind cavefish. *J Hered*, **96**, 185-196.
- Jernvall J** (2000) Linking development with generation of novelty in mammalian teeth. *Proc Natl Acad Sci USA*, **97**, 2641-2645.
- Jernvall J, Thesleff I** (2000) Reiterative signaling and patterning during mammalian tooth morphogenesis. *Mech Dev*, **92**, 19-29.
- Ji Q, Luo Z-X, Zhang X, Yuan C-X, Xu L** (2009) Evolutionary development of the middle ear in Mesozoic therian mammals. *Science*, **326**, 278-81.
- Johnston C, Berta A** (2011) Comparative anatomy and evolutionary history of suction feeding in cetaceans. *Mar Mamm Sci*, **27**, 493-513.
- Kahane-Rapport SR, Goldbogen JA** (2018) Allometric scaling of morphology and engulfment capacity in rorqual whales. *J Morphol*, **279**, 1256-1268.

- Karlsen K** (1962) Development of tooth germs and adjacent structures in the whalebone whale (*Balaenoptera physalus*). *Hval skrif*, **45**, 5-56.
- Kawasaki K, Hu JCC, Simmer JP** (2014) Evolution of *Klk4* and enamel maturation in eutherians. *Biol Chem*, **395**, 1003-1013.
- Kienle SS, Law CJ, Costa DP, Berta A, Mehta RS** (2017) Revisiting the behavioural framework of feeding in predatory aquatic mammals. *Proc R Soc Lond B Biol Sci*, **284**, 20171035.
- Kim J-W, Lee S-K, Lee ZH, et al.** (2008) *FAM83H* mutations in families with autosomal-dominant hypocalcified *amelogenesis imperfecta*. *Am J Hum Genet*, **82**, 489-494.
- Kimura M** (1983) *The neutral theory of evolution*, Cambridge University Press, Cambridge.
- Klaus S, Mendoza JCE, Liew JH, Plath M, Meier R, Yeo DCJ** (2013) Rapid evolution of troglomorphic characters suggests selection rather than neutral mutation as a driver of eye reduction in cave crabs. *Biol Lett*, **9**, 20121098-20121098.
- Kollar EJ, Fisher C** (1980) Tooth induction in chick epithelium: expression of quiescent genes for enamel synthesis. *Science*, **207**, 993-995.
- Kos M, Bulog B, Szél Á, Röhlich P** (2001) Immunocytochemical demonstration of visual pigments in the degenerate retinal and pineal photoreceptors of the blind cave salamander (*Proteus anguinus*). *Cell Tissue Res*, **303**, 15-25.
- Koussoulakou DS, Margaritis LH, Koussoulakos SL** (2009) A curriculum vitae of teeth: evolution, generation, regeneration. *Int J Biol Sci*, **5**, 226-243.
- Kuratani S** (2004) Evolution of the vertebrate jaw: comparative embryology and molecular developmental biology reveal the factors behind evolutionary novelty. *J Anat*, **205**, 335-347.
- Kurihara N, Amano M, Yamada TK** (2016) Decrease in tooth count in melon-headed whales. *J Zool*, **300**, 8-17.
- Lambert O** (2005a) Phylogenetic affinities of the long-snouted dolphin *Eurhinodelphis* (Cetacea, Odontoceti) from the Miocene of Antwerp, Belgium. *Palaeontology*, **48**, 653-679.
- Lambert O** (2005b) Systematics and phylogeny of the fossil beaked whales *Ziphirostrum* du Bus, 1868 and *Choneziphius* Duvernoy, 1851 (Mammalia, Cetacea, Odontoceti), from the Neogene of Antwerp (North of Belgium). *Geodiversitas*, **27**, 443-497.
- Lambert O, Bianucci G, De Muizon C** (2016) Macroraptorial sperm whales (Cetacea, Odontoceti, Physeteroidea) from the Miocene of Peru. *Zool J Linn Soc*.
- Lambert O, Bianucci G, Post K** (2009) A new beaked whale (Odontoceti, Ziphiidae) from the middle Miocene of Peru. *J Vert Paleontol*, **29**, 910-922.

- Lambert O, Bianucci G, Post K** (2010) Tusk-bearing beaked whales from the Miocene of Peru: sexual dimorphism in fossil ziphiids? *J Mammal*, **91**, 19-26.
- Lambert O, Collareta A, Landini W, et al.** (2015) No deep diving: evidence of predation on epipelagic fish for a stem beaked whale from the Late Miocene of Peru. *Proc R Soc Lond B Biol Sci*, **282**, 20151530.
- Lambert O, Muizon Cd, Bianucci G** (2013) The most basal beaked whale *Ninoziphius platyrostris* Muizon, 1983: clues on the evolutionary history of the family Ziphiidae (Cetacea: Odontoceti). *Zool J Linn Soc*, **167**, 569-598.
- Lande R** (1978) Evolutionary mechanisms of limb loss in tetrapods. *Evolution*, **32**, 73-92.
- Lanzetti A** (in press) Prenatal developmental sequence of the skull of minke whales and its implications for the evolution of mysticetes and the teeth-to-baleen transition. *J Anat*.
- Lanzetti A, Berta A, Ekdale EG** (2018) Prenatal development of the humpback whale: growth rate, tooth loss and skull shape changes in an evolutionary framework. *Anat Rec*, <https://doi.org/10.1002/ar.23990>.
- Loch C, Buono MR, Kalthoff DC, Mörs T, Fernández MS** (2019) Enamel microstructure in Eocene cetaceans from Antarctica (Archaeoceti and Mysticeti). *J Mamm Evol*, <https://doi.org/10.1007/s10914-018-09456-3>.
- Loch C, Duncan W, Simões-Lopes PC, Kieser JA, Fordyce RE** (2013a) Ultrastructure of enamel and dentine in extant dolphins (Cetacea: Delphinoidea and Inioidea). *Zoomorphology*, **132**, 215-225.
- Loch C, Jansen van Vuuren L** (2016) Ultrastructure, biomechanical and chemical properties of the vestigial dentition of a Cuvier's beaked whale. *N Z J Zool*, **4223**, 1-8.
- Loch C, Swain MV, van Vuuren LJ, Kieser Ja, Fordyce RE** (2013b) Mechanical properties of dental tissues in dolphins (Cetacea: Delphinoidea and Inioidea). *Arch Oral Biol*, **58**, 773-9.
- Louchart A, Viriot L** (2011) From snout to beak: the loss of teeth in birds. *Trends Ecol Evol*, **26**, 663-673.
- MacLeod CD** (2018) Beaked Whales, Overview. (eds Würsig B, Thewissen JGM, Kovacs KM), pp. 80-83. London: Academic Press.
- MacLeod CD, Santos MB, Pierce GJ** (2003) Review of data on diets of beaked whales: evidence of niche separation and geographic segregation. *J Mar Biol Assoc UK*, **83**, 651-665.
- Maddison WP, Maddison DR** (2018) Mesquite: a modular system for evolutionary analysis. Version 3.6. <http://mesquiteproject.org>

- Marshall CR, Raff EC, Raff Ra** (1994) Dollo's law and the death and resurrection of genes. *Proc Natl Acad Sci USA*, **91**, 12283-12287.
- Marx FG, Hocking DP, Park T, Ziegler T, Evans AR, Fitzgerald EMG** (2016) Suction feeding preceded filtering in baleen whale evolution. *Mem Mus Vic*, **75**, 71-82.
- Massare JA** (1987) Tooth morphology and prey preference of Mesozoic marine reptiles. *J Vert Paleontol*, **7**, 121-137.
- McCollum M, Sharpe PT** (2001) Evolution and development of teeth. *J Anat*, **199**, 153-159.
- McCurry MR, Evans AR, Fitzgerald EMG, Adams JW, Clausen PD, McHenry CR** (2017a) The remarkable convergence of skull shape in crocodylians and toothed whales. *Proc R Soc Lond B Biol Sci*, **284**, 20162348.
- McCurry MR, Evans AR, Fitzgerald EMG, McHenry CR, Bevitt J, Pyenson ND** (2019) The repeated evolution of dental apicobasal ridges in aquatic-feeding mammals and reptiles. *Biol J Linn Soc*, blz025.
- McCurry MR, Fitzgerald EMG, Evans AR, Adams JW, McHenry CR** (2017b) Skull shape reflects prey size niche in toothed whales. *Biol J Linn Soc*, **121**, 936-946.
- McCurry MR, Pyenson ND** (2018) Hyper-longirostry and kinematic disparity in extinct toothed whales. *Paleobiology*, **45**, 21-29.
- McGowen MR** (2011) Toward the resolution of an explosive radiation—a multilocus phylogeny of oceanic dolphins (Delphinidae). *Mol Phylogen Evol*, **60**, 345-57.
- McGowen MR, Gatesy J, Wildman DE** (2014) Molecular evolution tracks macroevolutionary transitions in Cetacea. *Trends Ecol Evol*, **29**, 336-346.
- McGowen MR, Spaulding M, Gatesy J** (2009) Divergence date estimation and a comprehensive molecular tree of extant cetaceans. *Mol Phylogen Evol*, **53**, 891-906.
- McGowen MR, Tsagkogeorga G, Álvarez-Carretero S, et al.** (in press) Phylogenomic resolution of the cetacean tree of life using target sequence capture. *Syst Biol*.
- McKnight Da, Fisher LW** (2009) Molecular evolution of dentin phosphoprotein among toothed and toothless animals. *BMC Evol Biol*, **9**, 299-299.
- Mead JG** (1989) Shepherd's beaked whale - *Tasmacetus shepherdi* Olivier, 1937. In *Handbook of marine mammals: river dolphins and larger toothed whales* (eds Ridgway SH, Harrison R), pp. 309-320. London: Academic Press.
- Mead JG, Payne RS** (1975) A specimen of the Tasman beaked whale, *Tasmacetus shepherdi*, from Argentina. *J Mammal*, **56**, 213-218.

- Meredith RW, Gatesy J, Cheng J, Springer MS** (2011a) Pseudogenization of the tooth gene enamelysin (*MMP20*) in the common ancestor of extant baleen whales. *Proc R Soc Lond B Biol Sci*, **278**, 993-1002.
- Meredith RW, Gatesy J, Murphy WJ, Ryder Oa, Springer MS** (2009) Molecular decay of the tooth gene enamelin (*ENAM*) mirrors the loss of enamel in the fossil record of placental mammals. *PLoS Genet*, **5**, e1000634.
- Meredith RW, Gatesy J, Springer MS** (2013) Molecular decay of enamel matrix protein genes in turtles and other edentulous amniotes. *BMC Evol Biol*, **13**, 20.
- Meredith RW, Janecka JE, Gatesy J, et al.** (2011b) Impacts of the Cretaceous terrestrial revolution and KPg extinction on mammal diversification. *Science*, **334**, 521-524.
- Meredith RW, Zhang G, Gilbert MTP, Jarvis ED, Springer MS** (2014) Evidence for a single loss of mineralized teeth in the common avian ancestor. *Science*, **346**, 1254390.
- Miller GS** (1929) The gums of the porpoise *Phocoenoides dalli* (True). *Proc US Nat Mus*, **74**, 1-8.
- Mitsiadis TA, Smith MM** (2006) How do genes make teeth to order through development? *J Exp Zool*, **306B**, 177-182.
- Montgomery SH, Geisler JH, McGowen MR, Fox C, Marino L, Gatesy J** (2013) The evolutionary history of cetacean brain and body size. *Evolution*, **67**, 3339-3353.
- Motani R, Chen X-H, Jiang D-Y, Cheng L, Tintori A, Rieppel O** (2015) Lunge feeding in early marine reptiles and fast evolution of marine tetrapod feeding guilds. *Sci Rep*, **5**, 8900.
- Muizon Cd, Domning DP** (2002) The anatomy of *Odobenocetops* (Delphinoidea, Mammalia), the walrus-like dolphin from the Pliocene of Peru and its palaeobiological implications. *Zool J Linn Soc*, **134**, 423-452.
- Murakami M** (2016) A new extinct inioid (Cetacea, Odontoceti) from the Upper Miocene Senhata Formation, Chiba, Central Japan: the first record of Iniioidea from the North Pacific Ocean. *Paleontol Res*, **20**, 207-225.
- Nakamura G, Kato H, Fujise Y** (2012) Relative growth of the skull of the common minke whale *Balaenoptera acutorostrata* from the North Pacific in comparison to other *Balaenoptera* species. *Mamm Study*, **37**, 105-112.
- Nikaido M, Matsuno F, Hamilton H, et al.** (2001) Retroposon analysis of major cetacean lineages: the monophyly of toothed whales and the paraphyly of river dolphins. *Proc Natl Acad Sci USA*, **98**, 7384-7389.
- Noren SR, Williams TM** (2000) Body size and skeletal muscle myoglobin of cetaceans: adaptations for maximizing dive duration. *Comp Biochem Phys A*, **126**, 181-191.

- Nweeia MT, Eichmiller FC, Hauschka PV, et al.** (2014) Sensory ability in the narwhal tooth organ system. *Anat Rec*, **297**, 599-617.
- Nweeia MT, Eichmiller FC, Hauschka PV, et al.** (2012) Vestigial tooth anatomy and tusk nomenclature for *Monodon monoceros*. *Anat Rec*, **295**, 1006-1016.
- Pabst DA, McLellan WA, Rommel SA** (2016) How to build a deep diver: the extreme morphology of mesoplodonts. *Integr Comp Biol*, **56**, 1337-1348.
- Page CE, Cooper N** (2017) Morphological convergence in ‘river dolphin’ skulls. *PeerJ*, **5**, e4090.
- Paradis MR, Raj MT, Boughner JC** (2013) Jaw growth in the absence of teeth: the developmental morphology of edentulous mandibles using the p63 mouse mutant. *Evol Dev*, **15**, 268-279.
- Park JY, An Y-R, Kanda N, et al.** (2015) Cetaceans evolution: insights from the genome sequences of common minke whales. *BMC Genomics*, **16**, 13.
- Parry David A, Brookes Steven J, Logan Clare V, et al.** (2012) Mutations in *C4orf26*, encoding a peptide with in vitro hydroxyapatite crystal nucleation and growth activity, cause *amelogenesis imperfecta*. *Am J Hum Genet*, **91**, 565-571.
- Pauly D, Trites AW, Capuli E, Christensen V** (1998) Diet composition and trophic levels of marine mammals. *J Mar Sci Technol*, **55**, 467-481.
- Peredo CM, Peredo JS, Pyenson ND** (2018a) Convergence on dental simplification in the evolution of whales. *Paleobiology*, **44**, 434-443.
- Peredo CM, Pyenson ND, Boersma AT** (2017) Decoupling tooth loss from the evolution of baleen in whales. *Front Mar Sci*, **4**, 1-11.
- Peredo CM, Pyenson ND, Marshall CD, Uhen MD** (2018b) Tooth loss precedes the origin of baleen in whales. *Curr Biol*, **28**, 3992-4000.
- Perrin WF** (2018) Common dolphin: *Delphinus delphis*. In *Encyclopedia of Marine Mammals* (eds Würsig B, Thewissen JGM, Kovacs KM), pp. 205-209. London: Academic Press.
- Phen A, Greer J, Uppal J, Der J, Boughner JC** (2018) Upper jaw development in the absence of teeth: new insights for craniodental evo-devo integration. *Evol Dev*, **20**, 146-159.
- Pivorunas A** (1979) The feeding mechanisms of baleen whale. *Am Sci*, **67**, 432-440.
- Prout T** (1964) Observations on structural reduction in evolution. *Am Nat*, **98**, 239-249.
- Pyenson ND, Goldbogen JA, Shadwick RE** (2013) Mandible allometry in extant and fossil Balaenopteridae (Cetacea: Mammalia): the largest vertebrate skeletal element and its role in rorqual lunge feeding. *Biol J Linn Soc*, **108**, 586-599.



- Pyenson ND, Vélez-Juarbe J, Gutstein CS, Little H, Vigil D, O’Dea A** (2015) *Isthminia panamensis*, a new fossil inioid (Mammalia, Cetacea) from the Chagres Formation of Panama and the evolution of ‘river dolphins’ in the Americas. *PeerJ*, **3**, e1227.
- Reidenberg JS** (2007) Anatomical adaptations of aquatic mammals. *Anat Rec*, **290**, 507-513.
- Ridewood WG** (1923) Observations on the skull in foetal specimens of whales of the genera *Megaptera* and *Balaenoptera*. *Philos Trans R Soc Lond B Biol Sci*, **211**, 209-272.
- Sire J-Y, Delgado SC, Girondot M** (2008) Hen's teeth with enamel cap: from dream to impossibility. *BMC Evol Biol*, **8**, 246.
- Slijper EJ** (1976) *Whales*, Hutchinson, London.
- Springer MS, Emerling CA, Gatesy J, et al.** (2019) Odontogenic ameloblast-associated (*ODAM*) is inactivated in toothless/enamelless placental mammals and toothed whales. *BMC Evol Biol*, **19**, 31.
- Springer MS, Starrett J, Morin PA, Lanzetti A, Hayashi C, Gatesy J** (2016) Inactivation of *C4orf26* in toothless placental mammals. *Mol Phylogen Evol*, **95**, 34-45.
- Stamatakis A** (2014) RAxML version 8: a tool for phylogenetic analysis and post-analysis of large phylogenies. *Bioinformatics*, **30**, 1312-1313.
- Steeman ME, Hebsgaard MB, Fordyce RE, et al.** (2009) Radiation of extant cetaceans driven by restructuring of the oceans. *Syst Biol*, **58**, 573-585.
- Stock DW** (2001) The genetic basis of modularity in the development and evolution of the vertebrate dentition. *Philos Trans R Soc Lond B Biol Sci*, **356**, 1633-1653.
- Stock DW, Jackman WR, Trapani J** (2006) Developmental genetic mechanisms of evolutionary tooth loss in cypriniform fishes. *Development*, **133**, 3127-3137.
- Swofford DL** (2003) PAUP\*: Phylogenetic Analysis Using Parsimony (\*and Other Methods). Version 4. Sinauer Associates, Sunderland, Massachusetts.
- Taxonomy Co** (2018) List of marine mammal species and subspecies. Society for Marine Mammalogy, [www.marinemammalscience.org](http://www.marinemammalscience.org), accessed on 04-23-2019
- Teaford MF, Smith MM, Ferguson MWJ** (2007) *Development, function, and evolution of teeth*, Cambridge University Press, Cambridge.
- Thewissen JGM, Cohn MJ, Stevens LS, Bajpai S, Heyning J, Horton WE** (2006) Developmental basis for hind-limb loss in dolphins and origin of the cetacean bodyplan. *Proc Natl Acad Sci USA*, **103**, 8414-8418.
- Thewissen JGM, Cooper LN, Behringer RR** (2012) Developmental biology enriches paleontology. *J Vert Paleontol*, **32**, 1223-1234.

- Thewissen JGM, Cooper LN, Clementz MT, Bajpai S, Tiwari BN** (2007) Whales originated from aquatic artiodactyls in the Eocene epoch of India. *Nature*, **450**, 1190-1194.
- Thewissen JGM, Fish FE** (1997) Locomotor evolution in the earliest cetaceans: functional model, modern analogues, and paleontological evidence. *Paleobiology*, **23**, 482-490.
- Thewissen JGM, Hieronymus TL, George JC, Suydam R, Stimmelmayer R, McBurney D** (2017) Evolutionary aspects of the development of teeth and baleen in the bowhead whale. *J Anat*, **230**, 549-566.
- Thewissen JGM, Sensor JD, Clementz MT, Bajpai S** (2011) Evolution of dental wear and diet during the origin of whales. *Paleobiology*, **37**, 655-655.
- Thompson DAW** (1917) *Growth and Form*, Cambridge University Press, Cambridge.
- Tomilin AG** (1967) *Mammals of the USSR and adjacent countries, Volume IX, Cetacea*, Israel Program for Scientific Translations, Jerusalem.
- Turvey ST, Pitman RL, Taylor BL, et al.** (2007) First human-caused extinction of a cetacean species? *Biol Lett*, **3**, 537-540.
- Uhen MD** (2010) The origin(s) of whales. *Annu Rev Earth Planet Sci*, **38**, 189-219.
- Uhen MD** (2018) Dental morphology. In *Encyclopedia of Marine Mammals* (eds Würsig B, Thewissen JGM, Kovacs KM), pp. 246-250. London: Academic Press.
- Van Dissel-Scherft MC, Vervoort W** (1954) Development of teeth in fetal *Balaenoptera physalus*. *Proc K Ned Akad Wet Ser C Biol Med Sci*, **57**, 196-210.
- Velez-Juarbe J, Wood AR, De Gracia C, Hendy AJW** (2015) Evolutionary patterns among living and fossil kogiid sperm whales: evidence from the Neogene of Central America. *PLoS ONE*, **10**, e0123909.
- Vollmer NL, Ashe E, Brownell RL, et al.** (2019) Taxonomic revision of the dolphin genus *Lagenorhynchus*. *Mar Mamm Sci*, **00**, 1-101.
- Watanabe YY, Sato K, Watanuki Y, et al.** (2011) Scaling of swim speed in breath-hold divers. *J Anim Ecol*, **80**, 57-68.
- Wells RS, Scott MD** (2018) Bottlenose dolphin, *Tursiops truncatus*, common bottlenose dolphin. In *Encyclopedia of Marine Mammals* (eds Würsig B, Thewissen JGM, Kovacs KM), pp. 118-125. London: Academic Press.
- Werth AJ** (2006a) Mandibular and dental variation and the evolution of suction feeding in odontoceti. *J Mammal*, **87**, 579-588.
- Werth AJ** (2006b) Odontocete suction feeding: experimental analysis of water flow and head shape. *J Morphol*, **267**, 1415-1428.

- Werth AJ, Potvin J, Shadwick RE, Jensen MM, Cade DE, Goldbogen JA** (2018) Filtration area scaling and evolution in mysticetes: trophic niche partitioning and the curious cases of sei and pygmy right whales. *Biol J Linn Soc*, **125**, 264-279.
- Whiting MF, Bradler S, Maxwell T** (2003) Loss and recovery of wings in stick insects. *Nature*, **421**, 264-267.
- Wiens JJ** (2011) Re-evolution of lost mandibular teeth in frogs after more than 200 million years, and re-evaluating Dollo's law. *Evolution*, **65**, 1283-1296.
- Wiens JJ, Bonett RM, Chippindale PT** (2005) Ontogeny discombobulates phylogeny: paedomorphosis and higher-level salamander relationships. *Syst Biol*, **54**, 91-110.
- Wiens JJ, Kuczynski CA, Duellman WE, Reeder TW** (2007) Loss and re-evolution of complex life cycles in marsupial frogs: does ancestral trait reconstruction mislead? *Evolution*, **61**, 1886-1899.
- Wright S** (1929) Fisher's theory of dominance. *Am Nat*, **63**, 274-279.
- Wright S** (1964) Pleiotropy in the evolution of structural reduction and of dominance. *Am Nat*, **98**, 65-69.
- Yang T-R, Sander PM** (2018) The origin of the bird's beak: new insights from dinosaur incubation periods. *Biol Lett*, **14**, 20180090.
- Yeh J** (2002) The evolution of development: two portraits of skull ossification in pipoid frogs. *Evolution*, **56**, 2484-2498.
- Young S, Deméré TA, Ekdale E, Berta A, Zellmer N** (2015) Morphometrics and structure of complete baleen racks in gray whales (*Eschrichtius robustus*) from the eastern North Pacific Ocean. *Anat Rec*, **298**, 703-719.

## *Chapter Two*

# **Prenatal Development of Skull, Teeth and Baleen in Modern Mysticeti**

## **Introduction**

### **General patterns of skull development in mammals**

The prenatal development of the mammalian skull, and its connection with the evolution of this diverse clade, has been a focus of study since the establishment of modern biology (e.g. de Beer, 1937). In recent years, novel techniques such as computed tomography (CT) scanning and geometric morphometrics (GM), as well as quantitative analyses of changes in the sequence of developmental events, have been applied to this discipline, to investigate in more detail how patterns of skull growth contributed to the diversification of mammals at different taxonomic levels. A large body of research is available on the origin of mammalian skull ontogeny and the differences among the three main groups of living mammals: monotremes, marsupials and eutherians. Ancestral mammals quickly adopted a unique developmental sequence, with an earlier onset of ossification of the endochondral bones of the neurocranium relative to other amniotes, possibly connected to the evolution of their larger olfactory receptors (Koyabu et al., 2014, Hoffman and Rowe, 2018). This pattern is clearly observed in the ontogeny of early-diverging lineages such as the echidna (Monotremata), which has an early development of the brain region of the skull but still retains a plesiomorphic ossification timing of the mandible and other elements (Werneburg and Sánchez-Villagra, 2011). After this initial transformations, the other two lineages of mammals evolved their different sequences of bone development and related shape growth patterns, which are mostly conserved in each clade (Bininda-Emonds et al., 2003,

Sánchez-Villagra et al., 2008, Goswami et al., 2012). Marsupials present an early ossification and functional development of the facial region and of parts of the hindlimbs relative to eutherians, likely correlated to their altricial birth (Smith, 1997, Goswami et al., 2009, Goswami et al., 2012, Goswami et al., 2016). In Eutheria, the lack of major constraint in early ontogeny of the facial region allowed for their broader diversification and the evolution of their disparate cranial morphologies (Goswami, 2007, Goswami et al., 2016). In fact, changes in cell division and patterning in embryonic development, the first phase of ontogeny, appear to be connected to the variety of face shapes observed in lineages of this group (Usui and Tokita, 2018). However, shared ontogenetic patterns still heavily influenced the evolution of skull shape in eutherian mammals. The ossification sequence of the skull elements is mostly conserved among all major clades of eutherians, with dermal bones forming earlier and in a more constant sequence relative to the endochondral elements (Koyabu et al., 2014). Across the entire clade, the differential timing of formation in these two types of bones is probably involved in the observed discordant patterns of evolution, or modularity, of the facial and neurocranial regions of the skull, which are primarily composed of dermal and endochondral bones respectively (Goswami and Polly, 2010a, Koyabu et al., 2014). Modularity is broadly defined as the integration of changes in morphological traits: characters belonging to the same module will transform at a similar rate and independently from characters assigned to different modules (Klingenberg, 2010). The shape of neurocranium and rostrum appear to evolve and grow at different rates and relatively independently from each other, However more research on this topic has yet to be conducted to test the presence of developmental modularity in different lineages and its impact on the diversification of all mammals (Porto et al., 2009, Goswami and Polly, 2010a, Koyabu et al., 2011). Changes in onset of ossification in both dermal and endochondral elements seem to occur independently from the state of surrounding bones, therefore more numerous and variable

modules can be identified in the eutherian skull when considering ossification sequences instead of shape (Goswami, 2007, Koyabu et al., 2011). Actually, these variations in timing of development of certain skull bones are more likely correlated not to skull shape, but to more complex traits observed in adult anatomy. For example, the supraoccipital, an endochondral element, has highly variable onset of ossification across Eutheria, and its early formation was found to be correlated with the evolution of larger brains relative to body mass in many lineages, such as primates and dolphins (Koyabu et al., 2014). An early ossification of the vomeronasal portion of the rostrum in moles has been connected with their adaptations for digging (Koyabu et al., 2011). In Cetacea, a relatively early start of ossification of the tympano-periotic complex has been linked to their increased bone thickness in this region, However more comprehensive studies have to be conducted to confirm this observation (Cozzi et al., 2015).

As skull ontogeny appears to be tightly linked with the evolution of numerous distinctive traits of mammals as a whole and with diversity within specific clades (Goswami et al., 2014), it is likely that changes in morphological development of the skull are associated with tooth loss and related characteristic adaptations observed among toothless taxa (echidna, anteaters, pangolin, baleen whales). However very little information is available on the prenatal development of these unique animals, making testing hypotheses on the influence of development in loss of dentition and connected traits challenging (Davit-Béal et al., 2009). In laboratory experiments on mice, the absence of teeth in ontogeny has been correlated with incomplete skeletal development of the upper jaw but not of the lower jaw, indicating that all toothless taxa might still retain tooth germs in development due to functional constraints (Paradis et al., 2013, Phen et al., 2018). This has been shown to be the case in anteaters (Rose, 1892, Davit-Béal et al., 2009) and baleen whales (Hilaire, 1807, Karlsen, 1962), while it is debated if complete tooth germs are formed in pangolins, due to inconsistent accounts (Rose, 1892, Tims, 1908, Ferreira-

Cardoso et al., 2019). The echidna is a different case as it still retains a mineralized tooth at birth, an egg-tooth, which is shed soon after (Davit-Béal et al., 2009). Tooth ontogeny therefore might still play an important role in the development of adult anatomical traits present in these taxa. In fact, recent studies have proposed a correlation between vestigial tooth germ development and presence of keratinous pads in anteaters and baleen whales (Ferreira-Cardoso et al., 2019), and even baleen plates patterning and distribution (Thewissen et al., 2017). Only by acquiring information on both skull ossification and tooth germ development it is possible to formulate hypotheses on the influence of development on tooth loss and study the overall impact of developmental constraints and modifications in the evolution of mammals. In this context, baleen whales are the best candidate to start investigating this complex question, as a consistent body of literature, including mostly traditional accounts of their ontogeny, is already available to use as a comparison with newly assembled detailed description and quantitative data.

### **Previous work on the ontogeny of Cetacea**

The systematic study of ontogeny in baleen and toothed whales started in the early 18<sup>th</sup> century, However those works do not provide sufficient descriptions to be used in modern studies (Thewissen and Heyning, 2007). In the late 1800s and early 1900s, many authors described in detail different aspects of cetacean prenatal development from external appearance (e.g. Müller, 1921) to the brain (e.g. Riese, 1928) and dentition (e.g. Kukenthal, 1893), as well as the skull ossification sequence (e.g. Ridewood, 1923). More recently, quantitative data, histology and computed tomography (CT) scanning have been used to provide exhaustive accounts of different aspects of the ontogeny of whales, dolphins and porpoises (e.g. Ishikawa and Amasaki, 1995, Sterba et al., 2000, Rauschmann et al., 2006, Moran et al., 2011, Hampe et al., 2015). While most of these studies included only one species and lacked an explicit evolutionary approach, their findings can be combined and utilized as a base for comparison for novel observations.

Analyzing the findings of these studies, several transformations that occur during prenatal development of Cetacea appear to directly mirror the acquisition of unique adaptations as they occurred in the evolution of Odontoceti and Mysticeti. For example, the progression of telescoping – the characteristic overlapping of the bones in the braincase of Cetacea (Miller, 1923) – and skull asymmetry in the fetuses follows a similar pattern as what is observed in the fossil record for toothed whales (Rauschmann et al., 2006, Moran et al., 2011, Roston and Roth, 2019). In baleen whales, the development and resorption of tooth germs also matches the progressive loss of teeth and acquisition of baleen observed in fossil taxa of the group (Karlsen, 1962, Ishikawa and Amasaki, 1995, Fudge et al., 2009). Given this, it is not surprising that the two groups have markedly different ontogenetic patterns from very early in their development, as it reflects their diverging adaptations. The external shape of the head and the position of the blowhole is drastically different in dolphins (*Stenella attenuata* – pantropical spotted dolphin) and baleen whales (*Balaena mysticetus* – bowhead whale) fetuses, likely due to the different feeding mode of these taxa, with baleen whales acquiring a larger mouth for filter feeding (Armfield et al., 2011). The two groups of cetaceans also have drastically different rates of development, with baleen whales presenting an unusual accelerated growth rate for mammals especially in the last portion of their gestation (Laws, 1959, Mackintosh, 1965, Frazer and Huggett, 1974). Undoubtedly, many aspects of cetacean prenatal development are unique and warrant in depth analysis to best understand their correlations with the physiology and anatomy of extinct and extant taxa of this group, as it is clear from the vast number of studies conducted in this area.

The present research will focus on the teeth-to-baleen transition and skull transformations in the prenatal development Mysticeti, a topic that has intrigued scientists from the 19<sup>th</sup> century to the present, and that still has many unanswered questions on the morphological changes that occur in the ontogeny of modern taxa and how they differ from the ones in toothed whales and



terrestrial artiodactyls. The first challenge to this study is establishing the gestational age of the specimens that are analyzed for the first time or described in the literature. Several accounts of length and weight of fetuses for several species were recorded during whaling campaigns in the 19<sup>th</sup> and early 20<sup>th</sup> century (e.g. Mackintosh and Wheeler, 1929, Laws, 1959, Tomilin, 1967, Ohsumi et al., 1970, Frazer and Huggett, 1973). However, these accounts are likely unreliable due to the nature of whaling records (Frazer and Huggett, 1973, Clapham and Ivashchenko, 2016, Clapham and Ivashchenko, 2018). Therefore, while growth curves for different species constructed with these data can be used to estimate the age of specimens and compare broad differences among Mysticeti and between this group and other cetaceans or artiodactyls, it is necessary to employ a staging system for the fetuses and embryos to best identify differences in timing of first appearance of traits across species. While a staging system is common practice in embryological studies (Sterba, 1995, Werneburg, 2009), a standardized scale was never described for baleen whales. However, Sterba et al. (2000) and Thewissen and Heyning (2007) developed such system for toothed whales. Their work can then be used as a starting point to classify mysticete specimens and it can be expanded to accommodate the unique characteristics of baleen whale ontogeny.

More accurate information is available on tooth germ development and baleen formation at least in rorquals (Balaenopteridae). The first report of tooth germs in developing baleen whales was actually based on a specimen of bowhead whale (Balaenidae) (Hilaire, 1807). As the study of this topic continued, authors noticed that there was marked difference between the tooth germs of the upper jaw and of the lower jaw. The ones in the mandible were smaller, with an irregular distribution and sometimes appearing to have multiple cusps, instead of the basic conic shape observed in modern Odontoceti and in their rostrum (Eschricht, 1849, Julin, 1880, Weber, 1886). Presence of tooth germs from very early stages of gestation and their general morphology was

confirmed in three species of rorquals by Ridewood (1923), who described early fetal specimens (two-five months from conception) of sei (*Balaenoptera borealis*), blue (*B. musculus*) and humpback whales (*Megaptera novaeangliae*). Kukenthal (1893), in the first detailed account of tooth germs in common minke (*B. acutorostrata*) and fin whale (*B. physalus*) fetuses, proposed that this pattern could be explained by the presence of two generations of teeth, lactal and permanent, that are then both resorbed before birth without erupting from the gums. This interpretation was later challenged and corrected by the histological studies of Van Dissel-Scherft and Vervoort (1954) and Karlsen (1962), who in combination described a complete developmental sequence of tooth germs in fin whales, from the very early embryonic phases to late stages of gestations. They found that the multicuspid teeth were just “double teeth”, formed by the growth of two germs in close proximity or by the division of a larger germ due to resorption, and that only one generation of teeth was developed, at least in this species of baleen whales, before resorption. The authors also noted that while an enamel organ was present, no continuous enamel layer was formed on the tooth germs. The germs were recorded to start resorbing very early in the gestation, around three-four months from conception out of 12 months of total gestation time, but they were only completely absent and resorbed after eight months from conception. These findings are consistent with later histological work on the Antarctic minke whale (*B. bonaerensis* – Ishikawa and Amasaki, 1995, Ishikawa et al., 1999) and the bowhead whale (Thewissen et al., 2017). For both species, the presence of enamel knots but not of a continuous enamel layer on the tooth buds was confirmed, as well as an early start of resorption of the tooth germs (Ishikawa et al., 1999, Thewissen et al., 2017). The dentition that develops in fetal baleen whales is likely homologous to the lactal dentition of terrestrial mammals, due to its similar mode of resorption, but likely some germs in the lower jaw are developed from the dental lamina as permanent teeth (Thewissen et al., 2017). Ishikawa and

Amasaki (1995) also noted in their description of the complete ontogenetic sequence – from young embryos to near term fetuses – of tooth germs for the Antarctic minke whale, that a low-density material, described as “baleen rudiments”, appears near the tooth germs after they start degrading, around six-seven months from conception. The authors did not clearly explain or illustrate their findings, leading to their finding being sometimes misinterpreted (e.g. Marx et al., 2016, Fordyce and Marx, 2018). More data need to be collected to confirm the co-occurrence of teeth and baleen rudiments in minke whales and other mysticetes. However, this work is particularly important as it represents the first account of the direct transition between teeth and baleen in the literature, as previous authors only described tooth germs or baleen separately. Tullberg (1883), translated and annotated in Fudge et al. (2009), provided the primary detailed description of developing baleen plates using histology in blue whale fetuses, However he does not mention their relationship with vestigial dentition. Macroscopically, Slijper (1976) noted that baleen plates developed from a ridge medial to the gums in specimens of fin whales older than eight months. A similar observation was made by Sawamura (2008) in two specimens of Antarctic minke whale also in the late fetal stages. Thewissen et al. (2017) described the development of baleen in bowhead whales from a histological perspective, confirming that also in this species baleen start to form in the medial part of the gums. While the authors did not analyze any specimens that had both resorbing teeth and baleen rudiments, they hypothesized that a shared genetic pathway regulated the growth of tooth germs and baleen in the upper jaw. This would explain the more regular pattern observed in the upper dentition relative to the lower one, and it would also represent an additional reason, aside of developmental constraint, for why tooth germs are still retained in fetal baleen whales.

Descriptions of the ossification sequence and overall development of the skull in baleen whales are scarcer and are usually comprised of only a few specimens in the embryonic or early

fetal stages of development. The species with the best described prenatal skull development is likely the humpback whale. The first description of the skull of an early fetus of this species is found in Eschricht (1849). Honigmann (1917) figured in detail the braincase ossification in an embryonic or early fetal specimen. Later, Ridewood (1923) provided a detailed anatomical account of the changes occurring during the ontogeny of the humpback whale using three embryonic and early fetal specimens. More recently, Hampe et al. (2015) used CT scanning to describe the internal anatomy of six specimens spanning from less than a month to three months from conception that were previously mentioned by Kükenthal (1914). These authors found that the ossification sequence of the humpback whale is overall similar to the data available for other mammals and for the pantropical spotted dolphin, as described in Moran et al. (2011). They based the staging of the specimens on Sterba et al. (2000), but did not compare them with previous description of the same species or other baleen whales to check their assessment. They also did not find mineralized tooth germs in any of the samples, in contrast with previous work by Ridewood (1923). For other rorqual species, only descriptions of few specimens at disparate growth stages are available. Eschricht (1849) and Julin (1880) illustrated ossification and shapes of certain skull elements in early fetuses of common minke whale. Schulte (1916) and Ridewood (1923) provided detailed accounts of the state of ossification of the skull of sei whale using specimens around three-four months in age from conception. Ridewood (1923) also described a skull of an early blue whale fetus. For the most part, these works did not record explicitly the connection between changes in dentition and skull shape or ossification, and accounts of the changes in skull shape in the late fetal stages are lacking entirely for all species. However, these data are invaluable and provide a solid start for a comparative study of the growth of the skull in baleen whales. Novel information can be added to comprehensively illustrate and quantitatively define the developmental sequence of teeth and baleen and of the skull of different modern

mysticetes species. These newly described ontogenetic data can then be used to investigate the role of development in the larger context of the evolution and diversification of Mysticeti.

### **Research objectives**

The primary goal of this research is to provide the first comprehensive detailed account of skull ontogeny, with emphasis on the transition from tooth germs to baleen, for baleen whales with the use of novel techniques and quantitative methods. Among the 14 living recognized species of Mysticeti, the Antarctic and the common minke whale (*Balaenoptera bonaerensis* and *B. acutorostrata*) and the humpback whale (*Megaptera novaeangliae*) were chosen for the study. They were selected based on availability and size of the specimens, as well as considering the previously available information on these species. The humpback whale skull ossification has been previously studied as described earlier, therefore new data can be inserted in a solid context to enrich the knowledge of their ontogeny and aid in the interpretation of the anatomy of less analyzed species. Minke whales warrant a more exhaustive investigation, not only from an anatomical prospective but also from an ecological one. They are the only species still extensively hunted, and the lack of information on their biology and development caused many pregnant females to be caught every year during scientific expeditions, potentially endangering their population growth (Bando et al., 2018). Moreover, the government of Japan recently deciding to abandon the International Whaling Commission (IWC) and resume commercial whaling (Victor, 2018). The implications of this activity are difficult to predict given the paucity of existing data. These species However have the best documented tooth germ ontogenetic sequence (Ishikawa and Amasaki, 1995, Ishikawa et al., 1999), which can be used as reference to age the specimens and interpret the structures observed in this study.

In the context of obtaining solid knowledge of prenatal development of the skull of mysticetes, so that it is possible to better understand the relationship between ontogeny and

evolution in this group, three major objectives are identified. First, in order to readily compare the analyzed specimens to other mysticete species, odontocetes, and terrestrial artiodactyls, growth curves were compiled for selected species of each group using published data. Secondly, a detailed anatomical description of five humpback whale and 10 minke whale (eight Antarctic m.w. and two common m.w.) prenatal specimens is presented. It is focused on the skull ossification sequence and shape changes, and the teeth-to-baleen transition. Data were obtained with traditional CT scanning and diceCT (diffusible iodine-based contrast enhanced computed tomography; Gignac et al., 2016), an emerging technique that provides better density contrasts during CT scanning and may allow study of the tooth germs in more detail (Peredo et al., 2017a). Thirdly, three-dimensional (3D) geometric morphometric (GM) landmark analysis is used to quantify skull shape changes in the developmental series of minke whales and humpback whale, including both prenatal and postnatal specimens of each species. These methods allow to better evaluate cranial shape changes throughout the ontogeny of each species and also to test for general patterns of development such as modularity (Klingenberg, 2010). Finally, these results are evaluated in the context of previous research on baleen whales and qualitatively compared with similar data available on the ontogeny of toothed whales as well as terrestrial artiodactyls. This will allow the formulation of hypotheses on the developmental origin of the characteristic traits of Mysticeti, and to best understand the ontogenetic transformations that accompany the teeth-to-baleen transition in these taxa. These data will then be used to quantitatively assess the role of developmental changes both in skull shape and ontogenetic sequence in the evolution of baleen whales with the inclusion of fossil taxa in Chapter Three.

## Materials and methods

### Growth curves of mysticetes, odontocetes and other artiodactyls

Growth data were compiled from the literature for five species of rorqual whales (gray – *Eschrichtius robustus*, blue, fin, sei, humpback, and Antarctic and common minke whales), four odontocete species (sperm whale – *Physeter macrocephalus*, short-beaked common – *Delphinus delphis*, spinner – *Stenella longirostris*, and pantropical spotted dolphin) and terrestrial artiodactyl taxa (pig – *Sus scrofa*, sheep – *Ovis aries*, and cattle – *Bos taurus*) (Lanzetti et al., 2018). The growth data includes total length and relative estimated gestation age of prenatal specimens, as well as information on total gestation time and average length at birth. This will allow a broad assessment of the age of the specimens of the selected species, humpback and minke whales, before more in depth analysis are conducted, and to estimate the absolute age of specimens described in the literature. It will also permit to assess the differences in growth rate among these taxa by performing a semi-logarithmic transformation of the length data. All the references used to construct the growth curve or rate for each species can be found in Appendix C.

For the growth curves, the total length measurements of specimens (Y-axis) were plotted against the reported age from conception (X-axis) given by the respective authors, following the method employed by Roston et al. (2013). The origins of both axes were set at 0, while the average length at birth along the Y-axis and the average gestation time for each species along the X-axis are the terminal point of the curve. Where possible, these estimated ages were integrated with growth equations calculated independently and other data for the same species available in the literature. The total length measurements of the modern prenatal baleen whale specimens included in this study and in Chapter Three were retrofitted onto the obtained growth trajectories to calculate a general estimate of the age of the specimens. Likewise, the age of specimens

described in the literature was assessed using these curves. As this method relies on inaccurate data (Frazer and Huggett, 1973, Clapham and Ivashchenko, 2016, Clapham and Ivashchenko, 2018), the age of the specimens analyzed here is later confirmed using both external traits (staging) and internal skull ossification. In order to predict when during gestation the teeth-to-baleen transition occurs, information on the first tooth formation, resorption of teeth and first baleen development was placed on the growth curves for the mysticete species that have descriptions of these events in the literature (Appendix C). The growth curves of the two species of minke whales are also provided separately to best visualize the age distribution of the described specimens and summarize the likely timing of the teeth-to-baleen transition in these species according to novel finding of this study, as also reported in Lanzetti (in press), and to Ishikawa and Amasaki (1995).

As these taxa vary greatly in gestation length and size, the Y-axis was transformed into a logarithmic scale (LOG10), while keeping the X-axis at its natural scale. This is a common and reliable method used to study patterns of growth (Glazier, 2013). By calculating the exponential regression coefficient for each taxon in this semi-logarithmic graph, it is possible to simplify the specific growth rate into a simple exponential equation, a conventional approach used to study both cell and organismal growth. Higher coefficients indicate a faster growth rate (Schneidereit, 1985, Stephenson, 2016). This semi-logarithmic graph is not meant to be used to calculate the age of a single specimen given its total length, since it is just an approximation of the average growth rate of the taxon throughout the gestation.

The growth rates calculated as exponential coefficients were also plotted on the phylogeny of the analyzed taxa and compared to the relative newborn length. This analysis was performed using the “Trace Character History” function in Mesquite 3.6 (Maddison and Maddison, 2018). The phylogenetic position of the taxa and divergence dates follow McGowen et



al. (in press). Squared-changed parsimony algorithm was used for the reconstruction. As the sampling is inconsistent among Cetartiodactyla, the possible correlation between the evolutionary transformations in the two traits at internal nodes was not assessed quantitatively. This analysis only provides a visual comparison of the changes in growth rate relative to newborn length, and it can help understand if indeed the growth pattern of mysticetes is distinctive relative to the rest of the clade given their unique adult size and adaptations.

### **Specimens, measurements and staging**

The internal anatomy of 15 prenatal specimens is described, as reported in Lanzetti et al. (2018) and Lanzetti (in press). The sample consists of: one embryonic and four fetal humpback whale (*Megaptera novaeangliae*) specimens, from the American Natural History Museum (AMNH) (New York, NY, USA), the Museum of Vertebrate Zoology, University of California, Berkeley (MVZ) (Berkeley, CA, USA), the San Diego Natural History Museum (SDNHM) (San Diego, CA, USA), and the Zoological Museum, University of Copenhagen (ZMCU) (Copenhagen, Denmark), eight fetal Antarctic minke whale (*Balaenoptera bonaerensis*) specimens, from National Museum of Nature and Science (NSMT) Research Facility (Tsukuba, Japan), and two fetal common minke whale (*B. acutorostrata*) specimens, from ZMCU. In Table 2.1, the list of specimens is reported including their estimated age based on the growth curves.

Table 2.1 – List of specimens described and included in quantitative shape analyses in Chapter Two.

Specimen code	Catalog number	Species	Common name	Age (months)	Age (% gestation time)	TL (cm)	CT scan type	Part of specimen scanned
He1	AMNH232597	<i>Megaptera novaeangliae</i>	humpback whale	2.25	19.6	17	diceCT	whole body
Hf1	AMNH99602	<i>Megaptera novaeangliae</i>	humpback whale	3.3	28.7	31	diceCT	whole body
Hf2	MVZ123560	<i>Megaptera novaeangliae</i>	humpback whale	?3.75	?32.6	?39	diceCT	whole body
Hf3	SDNHM25552	<i>Megaptera novaeangliae</i>	humpback whale	4.75	41.3	70	diceCT	whole body
Hf4 <sup>X</sup>	ZMUC-CN15	<i>Megaptera novaeangliae</i>	humpback whale	5.94	51.7	103	standard CT	head only
Mf1*	NSMT27154	<i>Balaenoptera bonaerensis</i>	Antarctic minke whale	4	42	28	diceCT	whole body
Mf2*	NSMT27149	<i>Balaenoptera bonaerensis</i>	Antarctic minke whale	4.5	47	41	diceCT	whole body
Mf3	ZMCU-CN6x	<i>Balaenoptera acutorostrata</i>	common minke whale	5	48	48	standard CT	whole body
Mf4	NSMTblue10	<i>Balaenoptera bonaerensis</i>	Antarctic minke whale	5.4	57	74	standard CT	head only
Mf5	NSMTwhite11	<i>Balaenoptera bonaerensis</i>	Antarctic minke whale	6.3	66	110	standard CT	head only
Mf6	NSMTwhite15	<i>Balaenoptera bonaerensis</i>	Antarctic minke whale	6.3	66	110	standard CT	head only
Mf7	NSMT27171	<i>Balaenoptera bonaerensis</i>	Antarctic minke whale	6.5	68	115	standard CT	head only
Mf8	ZMCU-CN4x	<i>Balaenoptera acutorostrata</i>	common minke whale	7.7	73	125	standard CT	head only
Mf9	NSMT27175	<i>Balaenoptera bonaerensis</i>	Antarctic minke whale	7.6	80	182	standard CT	head only
Mf10	NSMT27174	<i>Balaenoptera bonaerensis</i>	Antarctic minke whale	8.1	85	212.5	standard CT	head only

X=incomplete 3D model of skull; \*=specimens not included in 3D analyses; AMNH: American Museum of Natural History, New York, NY, USA, MVZ: University of California, Museum of Vertebrate Zoology, Berkeley, CA, USA, NSMT: National Museum of Nature and Science, Tsukuba, Japan, USA, SDNHM: San Diego Natural History Museum, San Diego, CA, USA, ZMUC: Natural History Museum of Denmark, Copenhagen, Denmark

All specimens at NSMT are preserved in a water-based 5% formalin solution, while the specimens from all other institutions are preserved in ethanol 70%. Hf2 total length is unreliable due to apparent compression during storage, therefore its age might be underestimated. Detailed external measurements following Durham (1980) were taken on all described specimens less than 1.21 m in total body length for the minke whales and 1 m for the humpback whale due to the excessive weight and size of larger specimens (Fig. S2.1 – Appendix D). The species assignment of mysticete prenatal specimens reported in museums are tentative since most were collected between the end of the 19<sup>th</sup> century and the beginning of the 20<sup>th</sup> century, and the original labels, when still present, use outdated taxonomic names (Karlsen, 1962). Given that the distinct morphological features of *M. novaeangliae*, such as tubercles and long flippers relative to body size, appear very early in development, it is possible to confidently assign all specimens that have these recognizable characters to this taxon. While it is easy to distinguish the minke whales from other rorquals of the same genus (*Balaenoptera*) due to their small size and distinctive coloration (Perrin et al., 2018), the distinction between the two minke whale species is more subtle. Since the Antarctic minke whale was not recognized as a separate species until recently (Rice, 1998), specimens at both institutions were labeled as either “minke whale” or “*B. acutorostrata*”, as they were collected from the late 1800s to the 1960s. However, most of the specimens had a known collection location, with fetuses from Japan being collected in the Southern Pacific Ocean and those from Denmark being collected in Greenland. The two minke whale species are known to be geographically separated, with the common minke whale largely found in the Northern Hemisphere and the Antarctic only found in the Southern Hemisphere (Brownell et al., 2000, Perrin et al., 2018). This made it possible to confidently assign the Japanese specimens to the Antarctic species, while those from Denmark (ZMCU) were assigned to the northern “common” species. The size, coloration and other external anatomical features of the specimens were also

congruent with the species assignments. Regardless, these species are very closely related (Gatesy et al., 2013) with similar gestation time (Ivashin and Mikhalev, 1978, Masaki, 1979), and erroneous assignment would not undermine the conclusions of this study.

All of the specimens described are assigned Carnegie or Fetal stages using characteristic traits in their external appearance (Lanzetti et al., 2018, Lanzetti, in press). This system was established using the staging developed for the pantropical spotted dolphin (*Stenella attenuata*) as a starting point (Thewissen and Heyning, 2007). The corresponding stage defined by Sterba et al. (2000) is also reported. Since the staging system of Thewissen and Heyning does not cover the later fetal stages, new stages were added to best describe the teeth-to-baleen transition in the oldest specimens in the series (Hf4, Mf6 – Mf10). This method of staging was preferred because it is the most detailed classification available for cetacean embryos and early fetuses, and also makes it possible to compare the developmental sequence of the humpback whale with that published for another cetacean (pantropical spotted dolphin; Moran et al., 2011). Using a staging system based on external features rather than determining the stage of the gestation using measurements such as total length of the specimens also avoids errors introduced through specimen preservation (e.g., shrinkage due to alcohol preservation; Hampe et al., 2015). Therefore, while total length, especially of larger fetuses, can be used to help establish the growth rate of the species, it should not be used alone to estimate gestational stage. Similarly, even though it is a common measurement in embryological studies, the crown-rump length of the specimens was not measured, because of the artefactual changes in form due to long term storage. Applying this standard staging system based on external features allowed direct comparison of samples among species of baleen whales and other taxa.

## **CT scanning and image reconstruction**

The diceCT protocol (Gignac et al., 2016) was used on specimens He1, Hf1, Hf2, Hf3 for the humpback whale and Mf1 and Mf2 for the minke whales. This procedure enhances the contrast in CT images between different tissues such as cartilage, nerves and blood vessels since they have a different level of permeability to iodine. Reconstructions from CT scan images obtained using this technique potentially give comparable resolution as dissection. Given the somewhat contrasting observations in traditional studies (e.g. Ridewood, 1923) and modern CT-based papers (Hampe et al., 2015), implementing this technique for the first time on these samples would likely bring more consistent results. A mostly novel protocol was created for the ethanol-preserved specimens of humpback whale. These samples were immersed in a solution of 70% ethanol and 1% metal iodine for a variable time depending on size, with 12 hours for the smallest specimen (He1) and two weeks for the second largest (Hf3). The progress of the stain was visually checked twice a day for the smaller specimens and once a day for the larger specimens. The staining was completed when the external color of the specimen was uniform and appeared consistent for at least two days for the smaller specimens and four days for the larger. After staining, the specimens were shipped to the University of Texas High-Resolution X-ray CT Facility (UTCT) in Austin, TX and scanned using an NSI CT scanner with a Fein Focus High Power source. When the specimens were returned to San Diego State University, the destaining process was initiated, which consists of immersing the specimens in a 3% sodium thiosulfate ( $\text{Na}_2\text{S}_2\text{O}_3$ ) solution in 70% ethanol. The stain proved to be completely reversible in our specimens, after which no visible differences were apparent compared to the state observed before the iodine procedure. After a maximum of one week, the specimens appeared clear of the stain and were then sent back to the loaning institution. The effects of iodine staining on the resolution of the CT images are clearly visible when scanning the specimens before and after the

staining using similar parameters (Fig. 2.1). For the minke whales, this protocol was slightly modified to accommodate for the different preservation medium (5% formalin).

The staining solution consisted of 1% iodine (1% KI – potassium iodide+0.2% I<sub>2</sub>E – metal iodine) in deionized water.

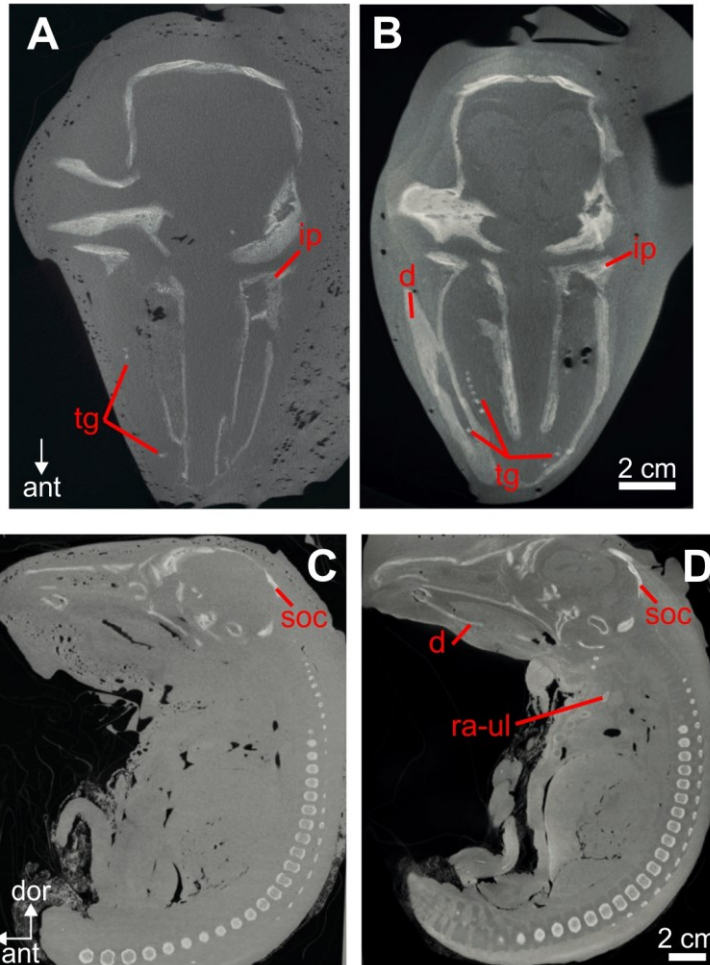


Figure 2.1 – Hf3 (SDNHM25552, TL 70 cm) CT slices without and with iodine staining. A: CT section of the skull in dorsal view without iodine staining, B: comparable CT section of the skull in dorsal view with iodine staining, C: CT section of the entire body in lateral view without iodine staining, D: comparable CT section of the entire body in lateral view with iodine staining. B and D were obtained using the machine and parameters listed in Table 2.2. A and C were obtained using the same machine at UTCT with minimal changes to the settings (voltage 150 kV, current 0.11 mA, slice thickness 145.9  $\mu$ m). In the CT slices with the iodine stain (B, D) partially ossified or cartilaginous elements in the rostrum and neurocranium are recognizable in a slightly lighter grey compared to the other soft tissues. In A and C, these elements are not recognizable. The stain also makes it possible to better distinguish the specimen from the surrounding packaging and highlights internal organs such as the brain and the intestines. Abbreviations: d, dentary; ip, infraorbital process of maxilla; soc, supraoccipital; ra-ul, radius and/or ulna; tg, tooth germs. Modified form Lanzetti et al. (2018).

Specimens were immersed in the staining solution for 10 hours (Mf1) and 24 hours (Mf2) according to their size. After the CT scanning, the samples were immersed in a destaining solution of 3% sodium sulfite ( $\text{Na}_2\text{SO}_3$ ) and deionized water for one hour to eliminate the color of the stain and best preserve these rare specimens for future use. Using diceCT was particularly important for Mf1 and Mf2, since they are the smallest specimens for these species and only a medical-grade CT scanner was available. The CT scan resolution was in fact too poor to create a full 3D reconstruction of the internal skeletal anatomy of these specimens, but this technique allowed recognition of the presence of tooth germs. All other specimens (Hf4, Mf3-Mf10) were not stained given their larger size that would have required very long periods of staining, which might damage the tissues (Metscher, 2009, Gignac et al., 2016).

The CT scans for the specimens from ZMCU and NSMT were performed at local institutions: the samples from the ZMUC were scanned at the Laboratory of Biological Anthropology of the University of Copenhagen, Denmark (KU) using a Siemens Somatom Definition medical-grade CT scanner, and those from the NSMT were scanned at the Nippon Veterinary and Life Science University in Tokyo, Japan (NV) using a Toshiba Aquilon Prime medical-grade CT scanner. All other specimens from the U.S.A. were scanned at UTCT. Only the head was scanned for Hf4 and Mf4-Mf10, owing to their size. Details on the scanning parameters can be found in Table 2.2.

The CT images were created in DICOM or TIFF format depending on the machine used, and then were all converted to 8bit JPEG and cropped in ImageJ (Schneider et al., 2012). They were then imported in Avizo Lite 9.7 (FEI, 2018), where the ossified regions of the skull and – when available – postcranial skeleton, tooth germs and baleen tissue were highlighted and segmented as different materials. Ossification was determined by evaluating the relative gray scale values of the tissues when compared to the surrounding areas.

Table 2.2 – CT scan details for the analyzed specimens.

Specimen code	Catalog number	TL (cm)	CT scan type/facility	Voltage (kV)	Current (mA)	Slice thickness ( $\mu\text{m}$ )	Number of slices	Output format
He1	AMNH232597	17	UTCT X-Ray NSI Fein Focus	150	0.1	49.4	1842	16-bit TIFF
Hf1	AMNH99602	31	UTCT X-Ray NSI Fein Focus	140	0.28	63.1	2953	16-bit TIFF
Hf2	MVZ123560	739	UTCT X-Ray NSI Fein Focus	130	0.09	153.4	893	16-bit TIFF
Hf3	SDNHM25552	70	UTCT X-Ray NSI Fein Focus	150	0.11	145.9	1880	16-bit TIFF
Hf4	ZMUC-CN15	103	KU Siemens Somatom Definition	120	300	400	711	DICOM
Mf1	NSMT27154	28	NV Toshiba Aquilon Prime	120	25	0.3	951	DICOM
Mf2	NSMT27149	41	NV Toshiba Aquilon Prime	120	25	0.3	951	DICOM
Mf3	ZMCU-CN6x	48	KU Siemens Somatom Definition	120	300	0.4	893	DICOM
Mf4	NSMTblue10	74	NV Toshiba Aquilon Prime	120	34	0.3	781	DICOM
Mf5	NSMTwhite11	110	NV Toshiba Aquilon Prime	120	54	0.3	1041	DICOM
Mf6	NSMTwhite15	110	NV Toshiba Aquilon Prime	120	83	0.3	1181	DICOM
Mf7	NSMT27171	115	NV Toshiba Aquilon Prime	120	131	0.3	1281	DICOM
Mf8	ZMCU-CN4x	125	KU Siemens Somatom Definition	120	300	0.4	849	DICOM
Mf9	NSMT27175	182	NV Toshiba Aquilon Prime	120	175	0.3	2571	DICOM
Mf10	NSMT27174	212.5	NV Toshiba Aquilon Prime	120	175	0.21	2939	DICOM



The absolute values in the CT images vary depending on the specimen and on the scanning mode, but for each specimen higher gray scale values (i.e. closer to white) indicate higher tissue density, while darker values (i.e. closer to black) indicate less dense tissue. Using this and knowledge of baleen whale anatomy it is possible to separate ossified areas from surrounding tissues and cartilage. Tooth germs contain dentin, a very dense tissue (Karlsen, 1962, Koussoulakou et al., 2009, Thewissen et al., 2017), and they appear as distinct bright structures. Baleen, instead, is composed of keratin, which has only slightly higher density than most tissues (Pivorunas, 1979), but it is possible to clearly separate it from the surrounding flesh (e.g. Ekdale et al., 2015). DiceCT makes it possible to increase the density difference between ossified and unossified areas, and also to note the presence of cartilage. However, cartilage would always appear darker than ossified tissues. Only relatively bright tissues have been classified as “ossified”.

### **Landmarks and 3D morphometric analyses**

#### *Landmark acquisition and data preparation*

To quantitatively assess shape change throughout the ontogenetic series and to be able to compare the growth of these species, landmark-based 3D geometric morphometric (GM) analyses were performed on the anatomy of the skull, using the landmarks presented in Lanzetti et al. (2018) and Lanzetti (in press). Landmarks were collected in two configurations: one including the entire skull (16 landmarks) and one only including the rostrum, from its anterior tip to the posterior border of the nasals (12 landmarks) (Fig. 2.2, Table 2.3). Specimens Mf1 and Mf2 were excluded from all landmark analyses as the CT scan resolution was too poor to create the D model needed to collect the landmarks. Hf4 is only represented in the 12 landmarks dataset analyses, as the posterior portion of the skull was not recovered in the CT scans.

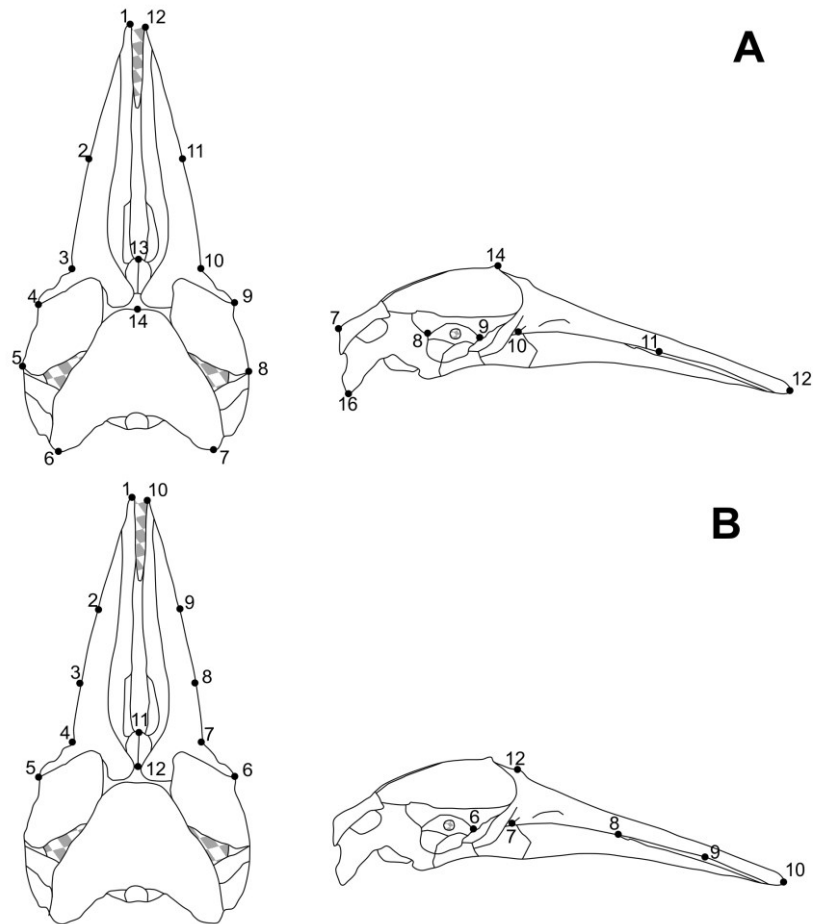


Figure 2.2 – Selected landmarks for the 16-landmark whole skull configuration (A) and the 12-landmark rostrum-only configuration (B) in dorsal and right lateral view of a skull of an adult minke whale. Original of the skull from Nakamura and Kato, 2014, figure modified from Lanzetti et al. (2018). Complete list of landmarks in Table 2.3.

Table 2.3 – List of landmarks used for the 3D GM analyses depicted in Figure 2.2.

<b>A</b>	<u>Landmarks whole skull configuration</u>	<b>B</b>	<u>Landmarks rostrum only configuration</u>
1, 12*	anteriormost point of premaxilla	1, 10*	anteriormost point of premaxilla
2, 11*	lateral midpoint of maxilla	2, 9	lateral one-third of maxilla
3, 10*	antorbital notches	3, 8	lateral two-thirds of maxilla
4, 9*	anterolateral point of the supraorbital process of frontal	4, 7*	antorbital notches
5, 8	posterolateral point of the supraorbital process of frontal	5, 6*	anterolateral point of the supraorbital process of frontal
6, 7*	posterolateral end of the exoccipital	11*	anteromedial point of nasal
13*	anteromedial point of nasal	12	posterior end of nasals
14*	apex of supraoccipital		
15, 16	posteroventral edge of postglenoid process of the squamosal		

\*=landmarks from Tsai and Fordyce (2014)

The rostral portion of the skull is key to the evolution of mysticetes and contains major adaptations related to the different filter feeding modes of each group (Bouetel, 2005, Goldbogen and Madsen, 2018). The second configuration allows more precise comparison of shape change in this region of the skull among specimens of different ages. The whole skull configuration is important to evaluate relative shape changes between rostrum and braincase and the progression of telescoping. Most dentaries of fetal specimens were broken or severely damaged during specimen preservation and storage, and therefore the shape of this bone did not provide useful information in the morphometric analyses. Thus, the dentaries were excluded from the GM analyses. The rest of the skull appeared to be mostly undeformed, with its general shape matching the qualitative descriptions and illustrations of previous authors of other prenatal rorquals specimens (e.g. Eschricht, 1849, Schulte, 1916, Ridewood, 1923). Specifically however, while there are numerous reports of the anatomy of embryonic and early fetal specimens of humpback whale (Ridewood, 1923, Hampe et al., 2015), there are no comprehensive qualitative descriptions of the skull of minke whale fetuses, only partial accounts (Eschricht, 1849, Julin, 1880). Thus, it is not possible to check for deformation by comparing the present observations with direct accounts obtained using traditional methods (i.e. dissection) for these species. Overall, minor levels of deformation might have had an influence on the results of the analyses, and more specimens of similar ontogenetic age are needed to confirm the observations presented in this work.

In order to examine a broader growth series, postnatal specimens of humpback and minke whales were added to the dataset for quantitative analyses: one juvenile of *M. novaeangliae* (Hj1) and two neonates (Mn1-Mn2) and two adults (Ma1-Ma2) of *B. acutorostrata*. The 3D models of these specimens were acquired using CT scanning, laser surface scanning and photogrammetry both during this study and by other researchers, who generously provided their data to use in this

project (Table 2.4). Landmarks were collected on all specimens in Avizo Lite 9.7 using the 3D models of the skulls. Landmark collection was done twice by the same operator (A. Lanzetti) to minimize errors.

Table 2.4 – List of postnatal specimens used in GM analyses.

Specimen code	Catalog number	Common name	TL (m)	Growth stage	Digitalization method	Data provided by
Hj1	LACM097707	humpback whale	800	juvenile	Photogrammetry	A. Lanzetti
Mn1	USNM593554	common minke whale	351	neonate	CT scan	Smithsonian Institution Bio-Imaging Research Center
Mn2	LACM72507	common minke whale	308	neonate	Surface laser scanning	G. Franci (Franci and Berta, 2018)
Ma1	HSU2670	common minke whale	700	adult	Surface laser scanning	G. Franci (Franci and Berta, 2018)
Ma2	CAS23807	common minke whale	800	adult	Surface laser scanning	G. Franci (Franci and Berta, 2018)

CAS: California Academy of Sciences, San Francisco, CA, USA, HSU: Natural History Museum Humboldt State University, Arcata, CA, USA, LACM: Natural History Museum of Los Angeles County, Los Angeles, CA, USNM: National Museum of Natural History, Washington, DC, USA

They were then imported in MorphoJ 1.07a (Klingenberg, 2011) for analysis, separately for each taxon (humpback whale and minke whales). This procedure was performed separately for the two landmark configurations (whole skull and rostrum-only). MorphoJ was chosen since it incorporates the generalized least-squares Procrustes superimposition, which allows to align homologous landmarks in the dataset independently of the orientation and size of the samples (Rohlf and Slice, 1990). All analyses were conducted in this software except when noted. The coordinates were imported assuming object symmetry, as previously done in similar studies on odontocetes (Galatius, 2010, Galatius et al., 2011). It has also been previously shown that both modern and fossil mysticetes, as well as several groups that include the common ancestor of Cetacea, have a symmetrical skull (Fahlke and Hampe, 2015). Consistency between landmark

takes was tested by performing an ANOVA analysis on the shape coordinates, which showed no significant difference between the two replicate sets (Appendix C). After this, the two takes were averaged to obtain a final landmark configuration for each specimen to be used in the subsequent analyses, creating a “by specimen” dataset. For the minke whales, an additional “by stage” dataset was created to best visualize differences in skull shape during growth. To create this dataset, each specimen was classified with their relative fetal stage “FS21/22”, “FS23/24”, “FS25”, “FS26”, “FS27”, “neonate”, “juvenile/adult” and then its shape was averaged with the ones of other samples at the same stage. “Juvenile/adults” are postnatal specimens older than one year, aged according to Walsh and Berta (2011), “neonates” are the other postnatal samples, while the prenatal ones were labeled according to their description provided in this study. This additional dataset was not created for the humpback whale as all stages in its sequence are only represented by one individual.

*Skull shape development in humpback and minke whales (whole skull and rostrum-only)*

Using the averaged configurations, a DA (Discriminant function Analysis) for both the whole skull and rostrum-only landmark configurations was performed. This analysis compares *a priori* data to one other. The results assess whether the groups are significantly different from each other, but also produces landmark configurations all scaled to the same selected “target shape” (Timm, 2002, Klingenberg, 2011). This provides a direct way to visually assess changes in shape through development independently of size, to evaluate major trends in the growth sequence. The “by specimen” dataset was used for both species, However while in the humpback whale the single specimens were compared with the target mature shape (Hj1), for the minke whales, samples were aggregated according to their informal fetal stage (“early fetal”, “late fetal”, “neonate”, “adult”) and compared to the “adult” shape (Lanzetti et al., 2018, Lanzetti, in press). These stages were delimited by analyzing specimens qualitatively, and most noticeably the fetal

period was divided into two stages: “early fetal” and “late fetal”. The late fetal stage encompasses most of the second half of the gestation and it is clearly distinguishable from the previous early fetal period. In the late fetal stage, all major skull bones are ossified almost completely and only the sutures remain open. The tooth germs have clearly started resorption and are more sparse and smaller. There is also a change in the rostrum length to braincase length ratio. Observing this pattern and dividing the specimens accordingly allowed better characterization of the skull shape changes during the prenatal development of the species, even if this subdivision is approximate and should be evaluated for each species separately in an interspecific analysis. Following this growth stage characterization, the minke whale “by specimen” dataset is subdivided as follows: four early fetuses (Mf1-Mf4), six late fetuses (Mf5-Mf10), two neonates (Mn1-Mn2), and two adults (Ma1-Ma2). The humpback whale dataset is only comprised of one embryonic, three “early fetal”, one “late fetal” and one juvenile (“adult”) sample, therefore it was not possible to perform “by stage” comparisons, as most stages are represented by only one individual. This is an additional reason to aggregate the minke whales’ samples, as it allowed to produce comparable results.

For the minke whales, an additional analysis to characterize shape development was conducted given the larger sample size and more even sampling of the sequence. A Principal Component Analysis (PCA) was performed on the “by specimen” and “by stage” dataset in both configurations. This analysis is widely used to reduce the dimensionality of the data into discrete “principal components” so that the variation can be represented in a 2D plot (Goswami and Polly, 2010b, Klingenberg, 2011, Polly et al., 2013). Applying this method to the “by stage” dataset allows identification of complex transformations that occur in skull shape development between the different stages.

### *Skull modularity and within-configuration variation in minke whales (whole skull)*

Exclusively in minke whales, the relative variation in shape and size of braincase and rostrum during development was evaluated by performing several statistical analyses. All methods were applied to the whole skull configuration. First, a modularity test was implemented using the “by specimen” dataset. This methodology allows to test if the coordinates of landmarks contained in the same *a priori* partition change independently to the coordinates of landmarks in the other partition (Klingenberg, 2005, Klingenberg, 2009, Goswami and Polly, 2010b, Klingenberg and Marugán-Lobón, 2013). In this case, it serves to evaluate if the braincase and rostrum develop in shape independently of each other. Two blocks of landmarks were defined within the same configuration to represent the two regions of the skull: landmarks 1-2-3-10-11-12-13 for the rostrum and landmarks 4-5-6-7-8-9-14-15-16 for the braincase. The test measures the relative independence of the two defined partitions of landmarks by comparing them to 10,000 randomly generated contiguous partitions. The result is the RV coefficient, which can vary from 0 to 1, with 0 corresponding to complete independence and 1 to complete integration. MorphoJ also provides a plot of the distribution of all the RV coefficients for the random partitions examined, to best appraise the RV obtained for the *a priori* sets in the context of the overall level of integration present in the dataset (Klingenberg, 2011, Klingenberg and Marugán-Lobón, 2013).

The relative changes in rostrum and braincase shape during ontogeny were then evaluated using a within-configuration Partial Least Squares (PLS) analysis (Goswami and Polly, 2010b). This analysis was performed both in the “by specimen” and on the “by stage” dataset, using the same partitions indicated for the modularity test. The PLS analysis directly examines patterns of covariations between the *a priori* partitions, and also produces a p-value (1,000 permutations) for the hypothesis of independence of the defined landmark sets (Klingenberg, 2009, Goswami and

Polly, 2010b, Klingenberg and Marugán-Lobón, 2013). As in the PCA, performing this analysis on the “by stage” dataset allows to best visualize changes in shape that occur at different developmental stages accounting for individual variation.

To calculate the rate of growth in shape of the rostrum relative to the braincase, a regression analysis was performed using the PLS scores of each partition obtained in the “by specimen” dataset analysis. This provides a regression coefficient and a p-value (10,000 repetitions) to measure the goodness of the fit. A coefficient close to 1 would indicate that the two skull regions develop in shape at similar rates, while higher or lower value would suggest that one component is growing faster than the other. The coefficient was converted in an angular measurement using Microsoft Excel, and the regression line was added graphically using the resulting slope angle. This allows to evaluate which component is growing faster, as the slope would be closer to its axis. Another regression was performed using the PLS scores and the Log-transformed Centroid Size (CS) of the specimens. CS is a measure of size of the landmark configuration of each specimen (Klingenberg, 2011), in this case representing whole skull size. This analysis can assess how the shape of rostrum and braincase grow relative to the overall size of the skull. Also in this case, a regression coefficient and p-value (10,000 repetitions) were produced. The two *a priori* partitions were tested separately against the same variable (LogCS) and then the two resulting plots were combined, and the slope of each regression visualized using Microsoft Excel and graphic software.



## Results

### **Growth curves of mysticetes, odontocetes and other artiodactyls**

Mysticeti, and rorquals in particular, are strikingly diverse in size as adults, a condition also reflected in newborns, which range from 2.5 m in length for the minke whale to 8 m for the blue whale (Laws, 1959, Tomilin, 1967, Frazer and Huggett, 1973). Gestation times vary from 10-12 months (Tomilin, 1967, Slijper, 1976). In Figure 2.3, the growth trajectories of the seven analyzed baleen whale species, constructed using total length and estimated gestational age with published data, are compared with three dolphin species (pantropical spotted, spinner, and short-beaked common dolphin). The major growth stages (“embryo”, “early fetus” and “late fetus”) are indicated on the graph using information provide in Roston et al. (2013), Lanzetti et al. (2018) and Lanzetti (in press). Specimens of baleen whales described in this Chapter and used for analyses in Chapter Three are labeled on the growth curve to indicate their approximate age, along with important events in the teeth-to-baleen transition described in the literature. This graph was simplified by removing the data points used to reconstruct the trajectories. The growth trajectory of each species is best described using a polynomial equation, similar in shape to previous authors’ findings (Frazer and Huggett, 1973, Frazer and Huggett, 1974, Roston et al., 2013). The original graph showing all data points and the relative equations describing the growth curves are available in Appendix D (Fig. S2.2).

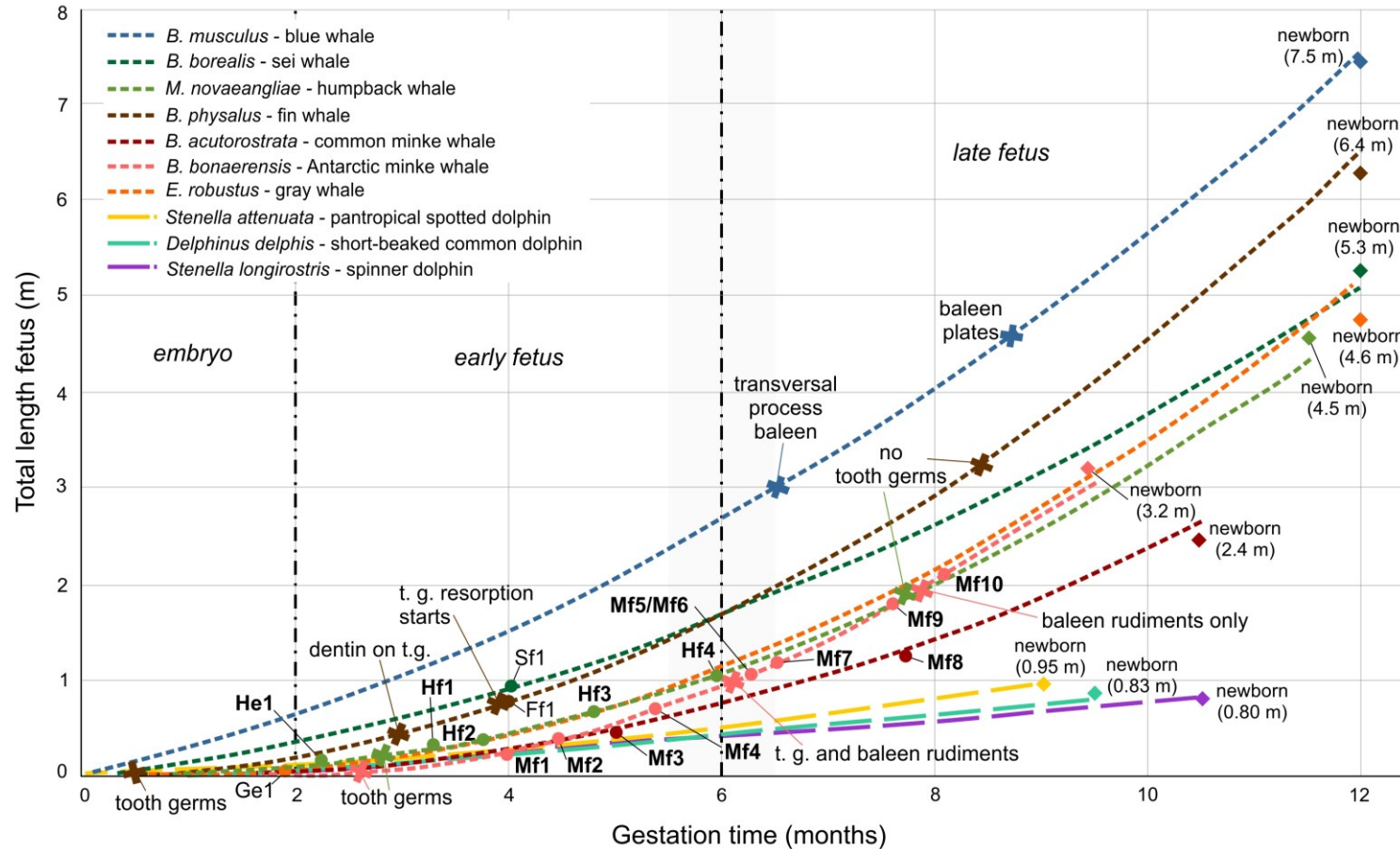


Figure 2.3 – Calculated growth trajectories, using total length (m) and estimated gestational age (months), for seven mysticetes species and three dolphin species. Specimens in bold are described in this Chapter and labeled as in Table 2.1. Circles=specimens included in this study and retro-fitted to the growth curve; crosses=lengths at which important steps in the teeth-to-baleen transition were recorded in the species (not necessarily observed in specimens); diamonds=estimates of length at birth (m). Embryo/fetus line is based on the age estimate for baleenopterygids listed by Roston et al. (2013) (2.1 months). For dolphins the embryonic period ends at 1.7 months (Sterba et al. 2000). Early/late fetus line placed based on observations in the current study and Lanzetti (in press) for baleen whales, with gray area indicating possible variability due to interspecific differences. Data sources listed in Appendix C, detailed graph and equations with  $R^2$  values are available in Appendix D (Fig. S2.2).

The examined baleen whales have a faster growth relative to odontocetes, with a marked increase in growth rate in the last third of gestation, when the teeth-to-baleen transition is likely to take place. This is in agreement with conclusions from other studies (Laws, 1959, Frazer and Huggett, 1973, Frazer and Huggett, 1974, Roston et al., 2013). There seems to be a remarkable variation in growth rate among species, especially in the last stage of pregnancy, and the rate of growth is slower in the smallest species of rorqual (common minke whale) than in other mysticetes. Additionally, several observations can be made on the age of the specimens included in this study for humpback and minke whales and their likely stage of in the teeth and baleen ontogeny. The humpback whale specimens span a range from the embryonic-fetal period (two-three months from conception) to slightly after the midpoint of pregnancy (ca. six months). The smallest specimen (He1) is considered an embryo based on its external characteristics and ossification stage, despite the fact that it plots in the fetal portion of the graph. Since embryonic growth is mostly characterized by the development of major organs rather than size, resulting in an almost flat line in the graph, the age of these specimens cannot be confidently calculated using growth curves, and this is an additional reason to employ a staging system (Sterba, 1995, Moore et al., 2015). Based on available accounts by Ridewood (1923) and Eschricht (1849), all the fetal specimens should preserve tooth germs. The minke whale specimens represent the early and late fetal stages of both species, with the smallest one being around four months in age from conception (Mf1) and the largest one about eight (Mf10). Based on the research by Ishikawa and Amasaki (1995), these specimens should record the transitional phase when tooth germs are resorbed, and baleen start developing.

In order to better contrast the growth rates of mysticetes with odontocetes and artiodactyls, a second graph was made to include two species of mysticetes (humpback whale, minke whale), two species of odontocetes (short-beaked common dolphin, sperm whale) and

three species of terrestrial artiodactyls (pig, sheep, cattle) using a logarithmic scale for the length measurements on the Y-axis (Fig. 2.4). The growth rate was calculated for additional five species of baleen whales and two toothed whales that are included in the non-transformed graph, but they are not shown here to make this plot more easily interpretable. The complete graph including all species in the study and their relative exponential coefficients are available in Appendix D (Fig. S2.3).

By comparing the slope of the exponential trajectories for each species, the data show that mysticetes have a growth rate overall comparable to other artiodactyls, with the sheep and pig having even faster development. This is not surprising given that these animals have one of the shortest gestation times among mammals (Harris, 1937, Marrable and Ashdown, 1967). Interestingly, the two odontocete species exhibit a very slow growth rate. The size of the newborn does not appear to play a role in rate of growth, given that both sperm whales and humpback whale neonates measure between four and five meters (Laws, 1959, Tomilin, 1967), but display strikingly different growth rates. Neonatal size and growth rate do not show any apparent connection also when comparing these two variables in a phylogenetic context (Fig. 2.5). Odontoceti have very slow growth rates, with the sperm whale presenting the lowest values. This might be due to the need of extending the gestation to reach a larger newborn size compared to the smaller dolphin species. Baleen whales instead have somewhat similar growth rates independently of neonatal length. These observations suggest that in both groups of Cetacea the baseline growth rate was inherited by their common ancestor and in modern species it is mostly regulated by external factors rather than by size. It has been proposed that these differences are connected to their migration patterns and seasonal food cycles (Laws, 1959, Tomilin, 1967, Frazer and Huggett, 1973).

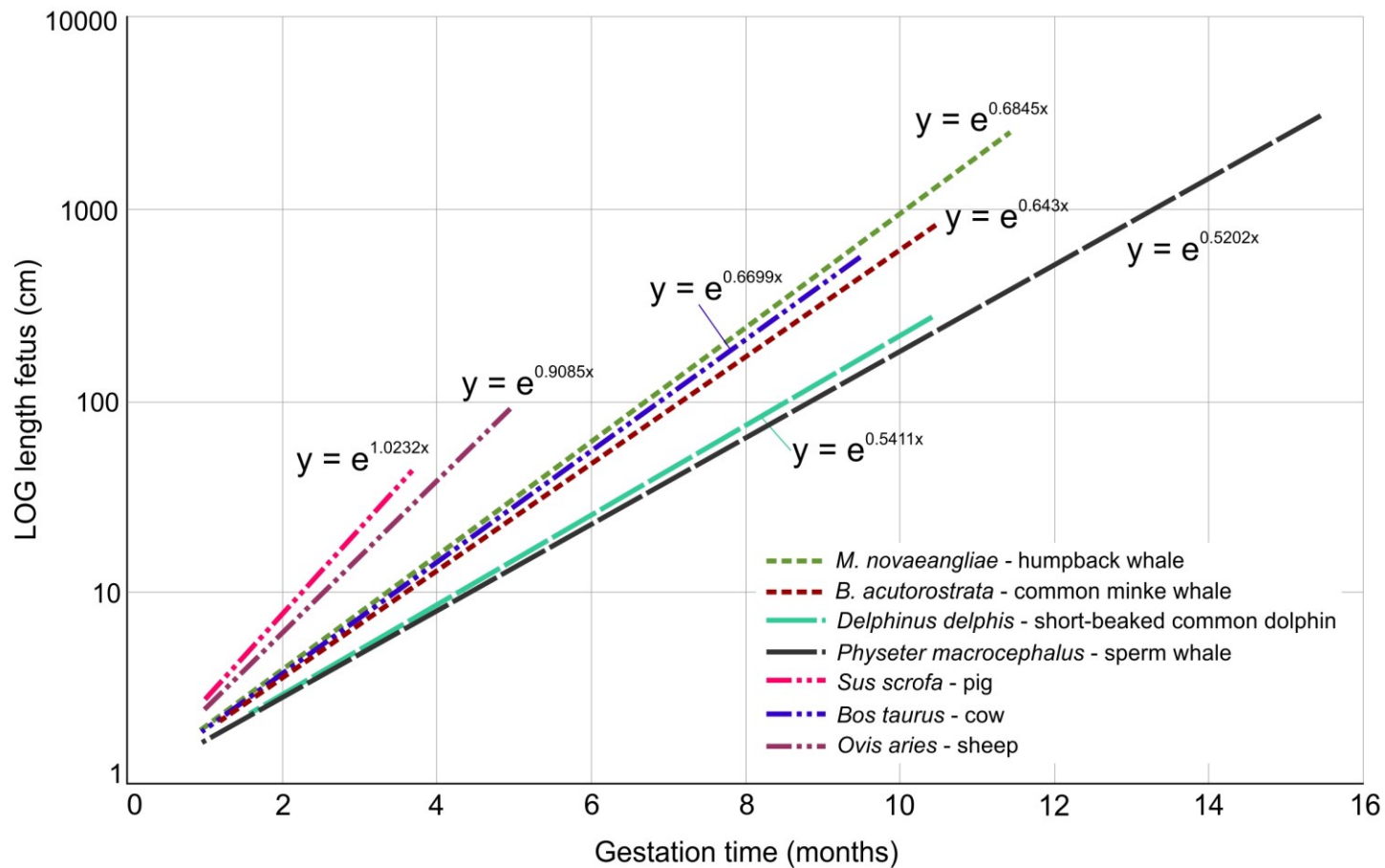


Figure 2.4 – Calculated growth rates, using the LOG-transformed length (cm) and estimated gestational age (months), for two balaenopterid species, two odontocete species, and three terrestrial artiodactyls. The crown-rump length was used for the sheep, cattle and pigs as TL was not provided by the authors. This does not affect the estimation of the growth rate as it was logarithmic transformed. Equations indicating the growth rate for each species are presented on the chart. The higher the X multiplier on the exponent, the faster the rate of growth. Data sources listed in Appendix C, graph including all taxa and equations are available in Appendix D (Fig. S2.3).

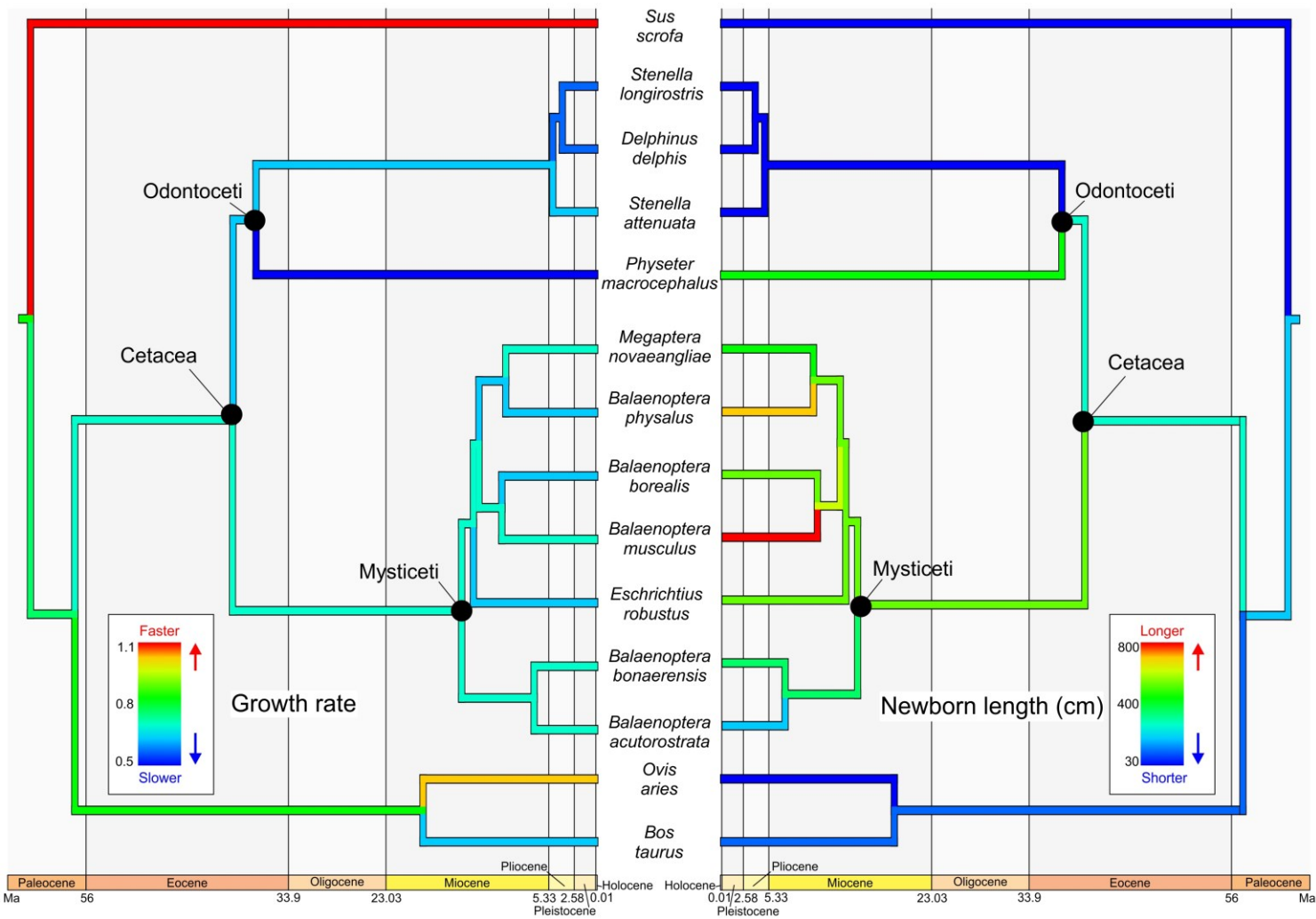


Figure 2.5 – Ancestral state reconstruction of growth rate coefficients (left) and newborn length (right). Warmer colors indicate higher values, cooler colors lower values. Growth rate coefficients were calculated using the transformed semi-logarithmic graph and the newborn length was derived from literature sources, both listed in Appendix D.

However, the teeth-to-baleen transition that occurs in the last stages of pregnancy might also have played a role in the evolution of the accelerated growth rate of Mysticeti (Lanzetti et al., 2018, Lanzetti, in press). The fast development of pigs and sheep might be linked to their domestication, and therefore undomesticated early-diverging taxa (e.g. dromedary) should be added to this dataset to test if growth rate of baleen whales is in line with terrestrial artiodactyls.

Overall, these results confirm previous published accounts of the different rate of development of baleen and toothed whales and confirm that mysticetes possess a characteristic growth trajectory with a marked acceleration in the last stages of the gestation. By estimating the absolute age of the samples included in this project, it will be possible to compare them more reliably with specimens of other taxa described by previous authors. The minke whales ontogenetic sequence likely encompasses the critical phases of tooth resorption and baleen formation and examining these samples will allow to confirm published accounts of these process in these species and to formulate hypotheses on what anatomical changes accompany the teeth-to-baleen transition in Mysticeti as whole and when this transition might happen in other taxa too.

### **Stages of development in the minke and humpback whale**

Both the external characteristics and internal skull anatomy of the 15 fetal baleen whale specimens, five humpback and 10 minke whales (Table 2.1), were examined, as in Lanzetti et al. (2018) and Lanzetti (in press). Since the absolute age of the specimens given in Figure 2.3 is only an approximation, a list of the specimens divided by Carnegie Stage (C), for embryonic development, and Fetal Stage (FS), and a brief description of the distinguishing and diagnostic features of each stage is provided, focusing on changes in head anatomy, skull ossification, suture closure, and major characteristics of teeth and baleen. The descriptions are based on the 3D reconstructions of the internal anatomy derived from the CT images. Therefore, their quality is influenced by imaging resolution, as well as by the status of preservation of the specimens.

However, all bony elements can be recognized and described for each stage. The staging follows the system provided by Sterba et al. (2000) and Thewissen and Heyning (2007), and stages new to this work are marked as such and described in more detail. The anatomical terminology follows Mead and Fordyce (2009).

These descriptions and in particular the presence of teeth and baleen can be contrasted with published accounts. For the humpback, the specimens presented here are comparable to the samples described by Ridewood (1923) and Hampe et al. (2015) (Table 2.5). Hampe et al. (2015) did not identify teeth in most specimens, likely due to preservation of the specimens and CT scan resolution, but Ridewood (1923) accounts are comparable with the present study. This author found a higher number of germs in both jaws, likely due to employing dissection on fresh specimens.

Table 2.5 – Teeth-to-baleen transition in prenatal humpback whales.

Specimen	TL (cm)	Stage	Tooth germs	R (1923) s.c.*	Tooth germs	H et al. (2015) s. c.*	Tooth germs
He1	17	C18/C19	20 u.j. 10 l.j.	X	37 u.j. 36 l.j.	ZMB7522 (IV)- ZMB37783 (V)	?
Hf1	31	C19/FS20	24 u.j. 11 l.j.	-	-	ZMB85514 (VI)	y
Hf2	?39	FS20/FS21	28 u.j. 16 l.j.	Y	35 u.j. 39 l.j.	-	-
Hf3	70	FS21/FS22	29 u.j. 15 l.j.	Z	41 u.j. 37 l.j.	-	-
Hf4	103	FS24	41 u.j. 38 l.j.	-	-	-	-

\*=Ridewood (1923) and Hampe et al. (2015) specimens of similar length; respective codes follow Lanzetti et al. (2018). All specimens are in embryonic (C) or early fetal stages (FS20-24).

The presence of tooth germs and baleen in the minke whale can be evaluated against the descriptions provided by Ishikawa and Amasaki (1995) for specimens of similar total length and approximate gestational age (Table 2.6). Overall, their results fit the observations of tooth germs and baleen in the analyzed specimens, with a few likely presenting baleen rudiments and dentition together. A detailed description of the changes relative to teeth-to-baleen transition in



minke whales are also provided in the next section of the Results, as in the sample the full resorption of teeth and the development of baleen can be observed.

Table 2.6 – Teeth-to-baleen transition in prenatal minke whales. (Lanzetti, in press)

Specimen	TL (cm)	Fetal Stage	Tooth germs	Baleen	I&A (1995) s. n.	Tooth germs	Baleen
Mf1	28	20/21	?	no	16	yes	no
Mf2	41	21/22	yes	no	18	yes	no
Mf3	48	21/22	yes	no	18	yes	no
Mf4	74	23/24	yes	no	20	yes	no
Mf5	110	25	yes	rudiments	21-22	yes	rudiments
Mf6	110	25	yes	rudiments	21-22	yes	rudiments
Mf7	115	26	yes	rudiments	23	yes	rudiments
Mf8	125	26	yes	rudiments	24	yes	rudiments
Mf9	182	27	no	yes	24	no	yes
Mf10	212.5	27	no	yes	n.a.	n.a.	n.a.

\*Ishikawa and Amasaki (1995) specimens with similar TL, numbers follow original publication  
Fetal Stages 20 – 24: “early fetus” growth stage; Fetal Stages 25 – 27: “late fetus” growth stage

Complete descriptions including the ossification state and shape of each major bony element of the skull, and postcrania when possible, and a thorough comparison with previously published specimens are provided in Appendix C. Detailed measurements, when available, and anatomical plates of the specimens not figured here are presented in Appendix D (Figs. S2.4-S2.9, Table S2.1). Only specimens Mf1 is not figured entirely as the CT scan resolution was too poor to recognize any major anatomical features. Other interesting aspects of the skull ontogeny are addressed in the Discussion.

### **Carnegie (embryonic) stage 18/19 (Fig. 2.6)**

Digital ray 3<sup>rd</sup> longer than 2<sup>nd</sup>, globular fluke, distinct beak (Sterba et al. 2000, stage 6)

*Specimen:* He1

*Skull ossification:* rostral ossification has started with all major bone elements in this region distinguishable (premaxilla, maxilla, vomer, palatine). The dentary has also begun ossifying. Supraorbital process of the frontal is the only braincase element visible. Ectotympanic visible, composed of a small horseshoe-shaped lamina.

*Tooth germs:* present and form mostly complete rows in both jaws. More abundant in upper jaw than in dentary.

---

Figure 2.6 (next page) – He1 (AMNH232597; TL 17 cm) external and internal morphology. A: left lateral view, B: left lateral view of 3D rendering of the internal morphology, C: head in ventral view, D: head in left lateral view, E: head in right lateral view. Ossified skull bones in yellow, tooth germs in red, pelvic elements in pink, eye and brain in grey. Ossified elements and tooth germs are labeled in the figures. Abbreviations for Figures 2.6-2.13 and 2.15-2.18: ac, alveolar canal (maxilla and dentary); b, baleen; bhy, basihyoid; bo, basioccipital; br, baleen rudiments; bs, basisphenoid; cp, coronoid process (dentary); d, dentary (=mandibular rami); dif, dorsal infraorbital foramina; ect, ectotympanic; eo, exoccipital; f, frontal; h, humerus; hy, indeterminate hyoid elements; ip, infraorbital process (maxilla); j, jugal; inp, interparietal; l, lacrimal; m, maxilla; ms, mandibular symphysis; n, nasal; p, parietal; pe, pelvic elements; pg, postglenoid process (squamosal); ph, phalanges; pl, palatine; plf, palatine foramina; plp, palatine process (maxilla); pm, premaxilla; pt, pterygoid; ra, radius; rc, rib cage; sc, scapula; shy, stylohyoid; so, supraoccipital; sop, supraorbital process (frontal); sq, squamosal; tg, tooth germs; thy, thyrohyoid; ul, ulna; v, vomer; vr, vertebrae; zp, zygomatic process (squamosal). From Lanzetti et al. (2018).

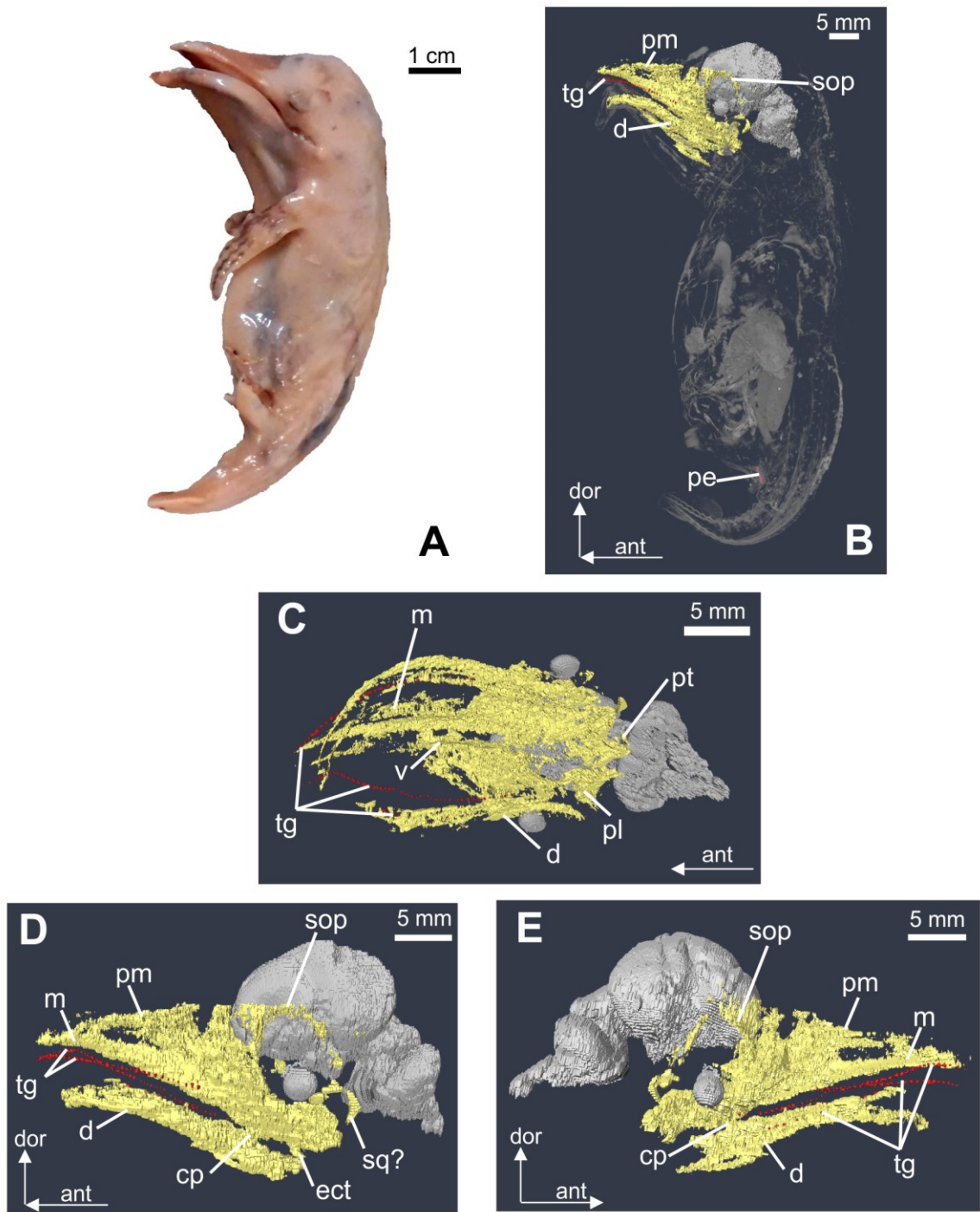


Figure 2.6 – He1 (AMNH232597; TL 17 cm) external and internal morphology. Complete caption previous page.

**Carnegie (embryonic) stage 19/Fetal stage 20 (Fig. 2.7)**

Digital ray 2<sup>nd</sup> longer than 3<sup>rd</sup>, blowhole in the last one-third of head (Sterba et al. 2000, stages 6, 7 and 8)

Notes on staging: FS20 is better characterized by the posterior movement of the external nasal aperture that is now in the last one-third of the head, similar to its adult position. Hyperphalangy noted by Thewissen and Heyning (2007) was already clearly visible at the previous stage, and therefore is not diagnostic.

*Specimen:* Hf1

*Skull ossification:* nasals, parietal, squamosal and most endochondral bones (supraoccipital, basisphenoid, basioccipital) have started ossifying, in addition to the elements present at the earlier stage. The infraorbital process of maxilla is also present. The ectotympanic still presents the same shape, even if the lamina has now grown in size.

*Tooth germs:* present in both jaws. They are more numerous in the upper jaw.

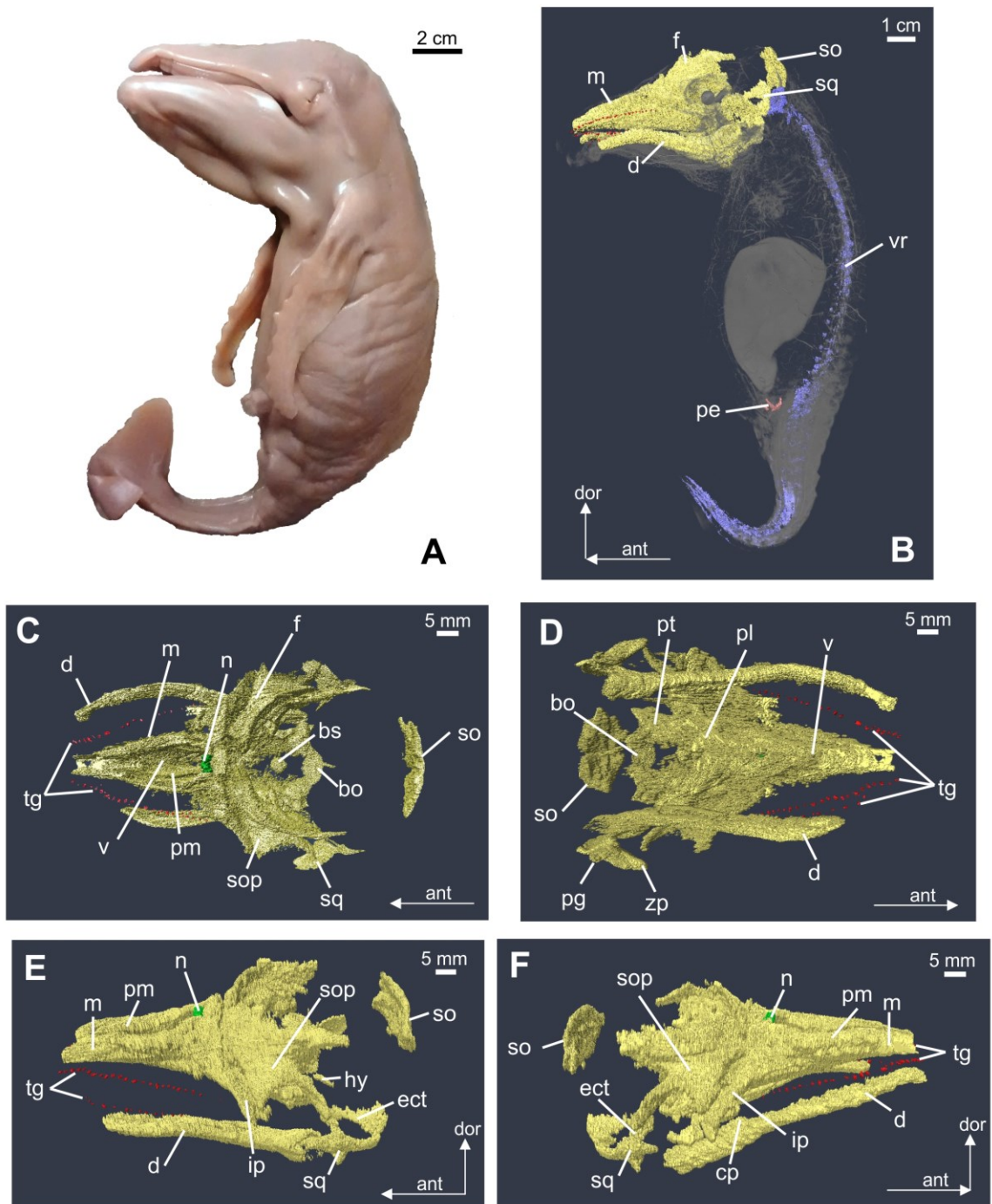


Figure 2.7 – Hfl (AMNH99602; TL 31 cm) external and internal morphology. A: left lateral view, B: left lateral view of 3D rendering of the internal morphology, C: head in dorsal view, D: head in ventral view, E: head in left lateral view, F: head in right lateral view. Ossified skull bones in yellow, tooth germs in red, nasal bones in green, ossified postcranial elements in purple and pink. Ossified elements and tooth germs are labeled in the figures. Abbreviations listed on page 110 (Fig. 2.6). From Lanzetti et al. (2018).

### **Fetal Stages 20/21 (Fig. 2.8)**

Eyelids fused, umbilical hernia retracted/tactile hair present, blowhole in the last one-third of head (Sterba et al. 2000, stages 7, 8 and 9)

*Specimen:* Hf2 – (Mf1)

*Skull ossification:* all major bones are recognizable as they started ossifying, including exoccipital and hyoid. Infraorbital process of maxilla is ossified but not in contact with the frontal.

Interparietal is visible at the top of the neurocranium also in the humpback whale, where it was not identified in previous studies. Ectotympanic has assumed a 3D sigmoid shape and its tucker overall, but still lacks several portions.

*Tooth germs:* present and forming complete rows in both jaws. In the lower jaw they are less numerous and smaller than in the maxilla. They also present a size gradient, becoming smaller towards the tips of the jaw.



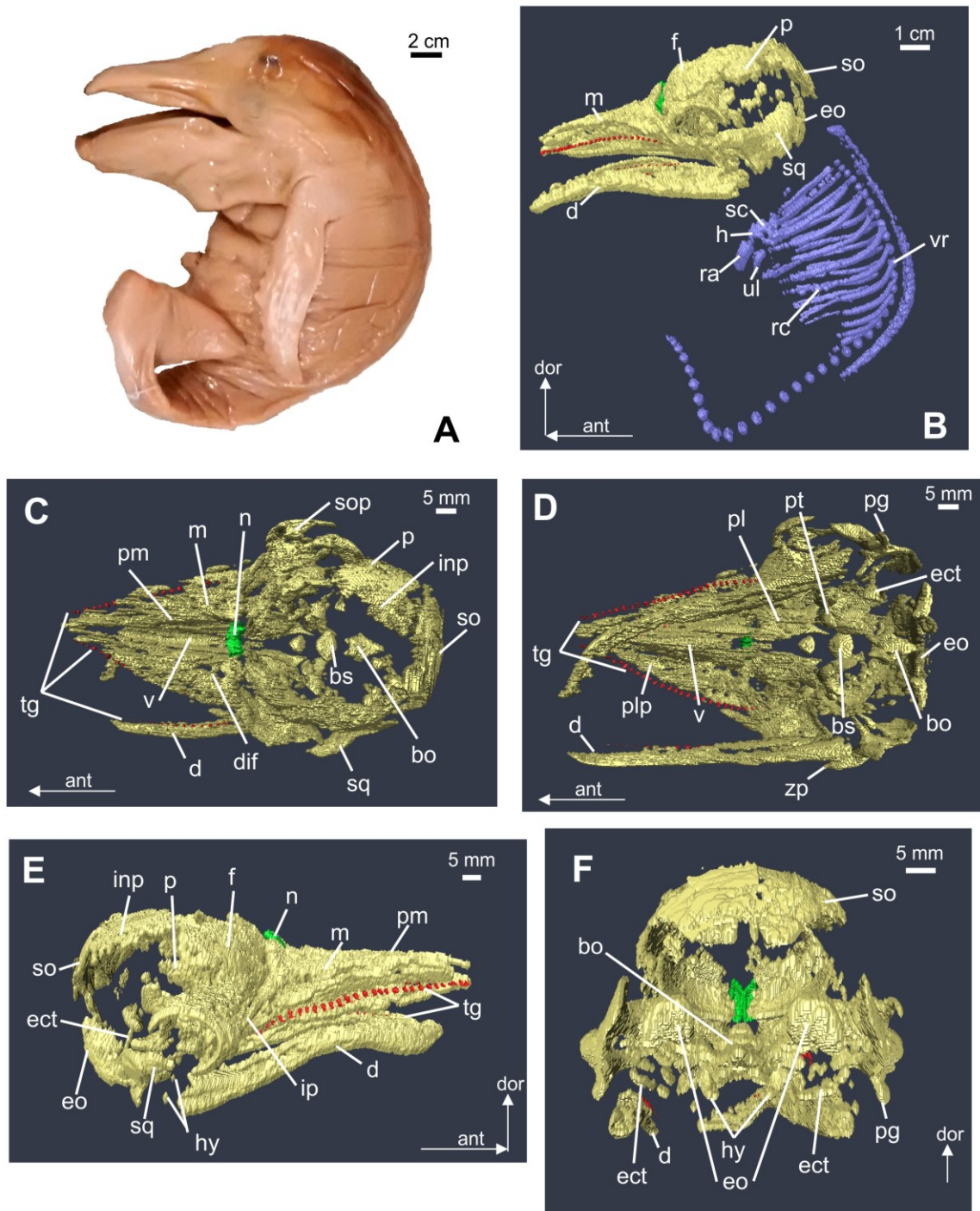


Figure 2.8 – Hf2 (UCB123560, TL 739cm) external and internal morphology, A: left lateral view, B: left lateral view of 3D rendering of the internal morphology, C: head in dorsal view, D: head in ventral view, E: head in right lateral view, F: head in postero-ventral view. Ossified skull bones in yellow, tooth germs in red, nasal bones in green, ossified postcranial elements in purple. Ossified elements and tooth germs are labeled in the figures. Abbreviations listed on page 110 (Fig. 2.6). From Lanzetti et al. (2018).

**Fetal Stages 21/22 (Fig. 2.9 – Figs. S2.4-S2.5)**

Tactile hair present, blowhole in the last one-third of head/eyelids separated, throat grooves present (Sterba et al. 2000, stages 9 and 12)

Notes on staging: FS22 is further characterized in Balaenopteridae by the beginning of development of throat grooves.

*Specimen:* Hf3 – Mf2, Mf3

*Skull ossification:* ossification of all bones is now prominent, with the mandible having complete the process. The infraorbital process of maxilla is still separated from the frontal. Interparietal is visible at the top of the neurocranium, even if in humpback whale is smaller and started suturing to the parietal. Ectotympanic ossification progressed, but still lacks most of the postero-ventral portion. Fontanelles and sutures are open between most elements.

*Tooth germs:* present in both jaws. In the humpback specimen, where they are better recognizable, they maintain a similar pattern as described for FS20/21.



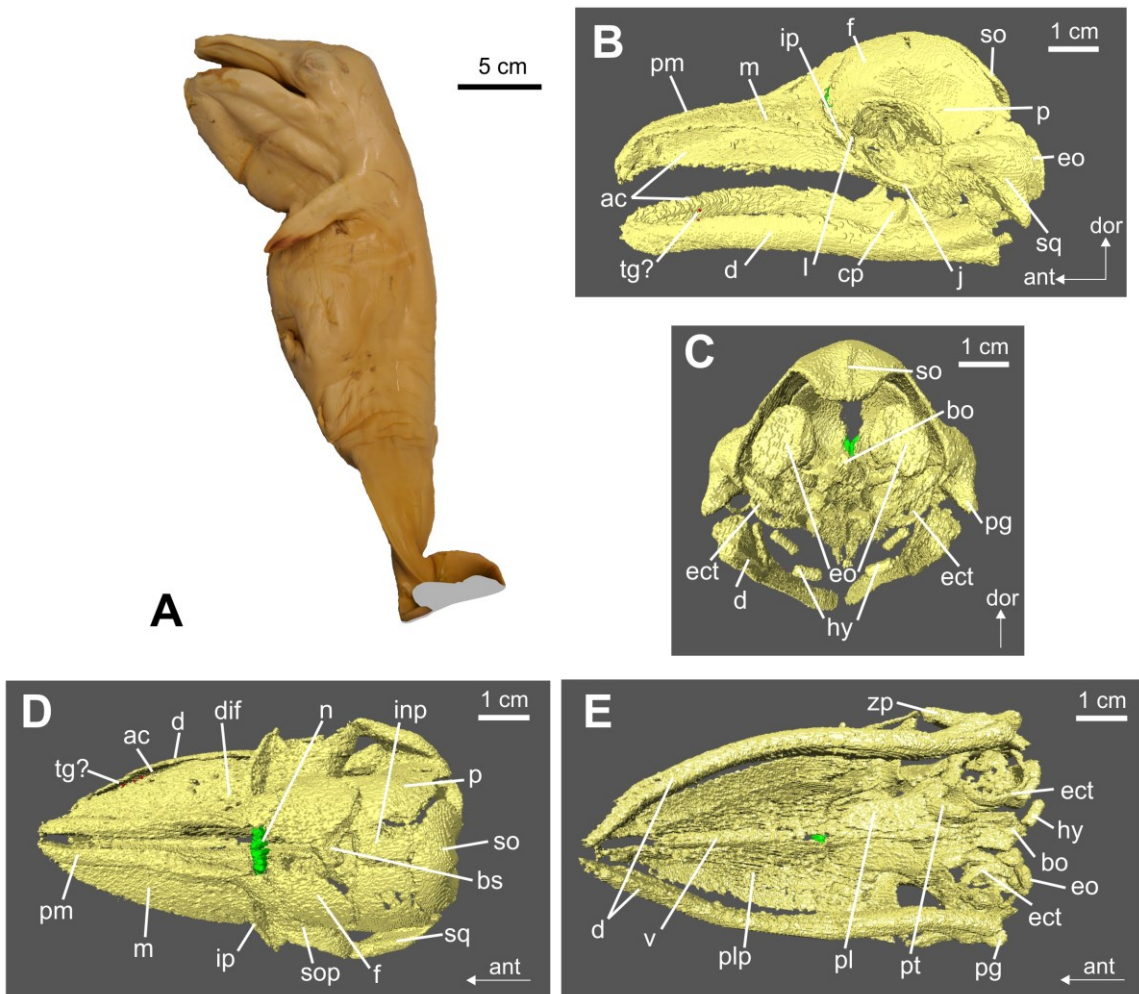


Figure 2.9 – Mf3 (ZMCU-CN6x; TL 48 cm) external and internal morphology. A: left lateral view of external morphology, B: left lateral view of 3D rendering of the internal morphology of head, C: head in postero-ventral view, D: head in dorsal view, E: head in ventral view, Ossified skull bones in yellow, nasal bones in green, tooth germs in red. Ossified elements and tooth germs are labeled in the figures. Abbreviations listed on page 110 (Fig. 2.6). From Lanzetti (in press).

### **Fetal Stages 23/24 – new stage (Fig. 2.10 – Fig. S2.6)**

Pigmentation present (Sterba et al., 2000, stages 10 and 11)/throat grooves well developed, extend below the flippers

Notes on staging: FS24 is a new stage, as the description of Sterba et al. (2000) and Thewissen and Heyning (2007) stopped at FS23. This stage is characterized by the full development of the throat grooves, which extend to at least the insertion of forelimb. This trait can be used to stage balaenopterid specimens only as extensive throat grooves are absent in other extant mysticetes.

*Specimens:* Hf4 (CT images lack posterior end of skull) – Mf4

*Skull ossification:* rostrum is elongated compared to previous stages and has the same length as the mandible, while in FS20-22 the mandible was longer than the rostrum. Nasals are elongated posteriorly. No major changes in the infraorbital process of maxilla. The interparietal is still visible in the minke whale while it is fused to the parietal in the humpback whale. Ectotympanic ossification advanced, but still lacks skull articulation. The supraoccipital shield is extended anteriorly, contacts the interparietal. Pariotic is recognizable in the CT scans and ossified in the minke whale. Dorsal fontanelles still open.

*Tooth germs:* present and forming a complete row in both jaws in the humpback whale. Only a few visible but the bony correlates (open upper and lower alveolar canals) in the minke whale imply that they have similar distribution in this species as well.

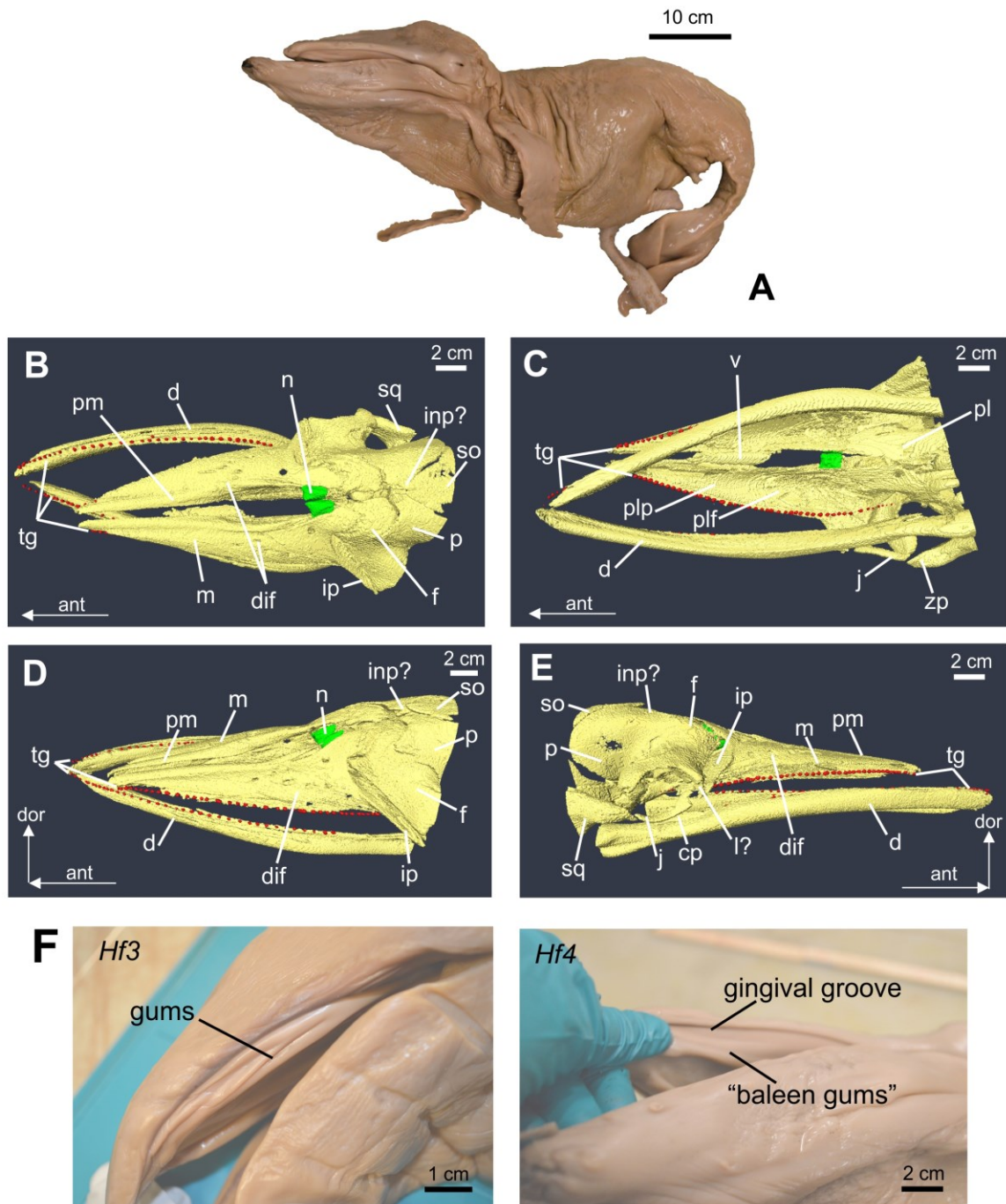


Figure 2.10 – Hf4 (ZMCU-CN15, TL 103 cm) external and internal morphology. A: left lateral view, B: head in dorsal view, C: head in ventral view D: head in right dorso-lateral view, E: head in left lateral view, Ossified skull bones in yellow, tooth germs in red, nasal bones in green. Ossified elements and tooth germs are labeled in the figures. F: comparison of external morphology of the gingiva between specimens Hf3 and Hf4. Abbreviations listed on page 110 (Fig. 2.6). From Lanzetti et al. (2018).

### **Fetal Stage 25 – new stage (Fig. 2.11 – Fig. S2.7)**

Thick baleen gum develops medial to gingival ridge

Notes on staging: this new fetal stage is characterized by the development of a thick gum in the medial part of the palate, especially visible in the posterior portion of the upper jaw (“baleen gum”), that progressively becomes smaller anteriorly. In the anterior one-third of the rostrum, only a groove is visible between the palate and the lip.

*Specimen:* Mf5, Mf6

*Skull ossification:* rostrum is flattened dorso-ventrally. Nasals continue to elongate posteriorly.

The infraorbital process of maxilla is not in contact with the frontal. Interparietal is sutured with parietal but its shape is still recognizable. Ectotympanic has a small portion latero-ventrally that lacks ossification. Mandibular symphysis is probably present. Supraoccipital is in contact with interparietal anteriorly. Pariotic is firmly sutured to the skull.

*Tooth germs/baleen rudiments:* present. A full tooth row is visible in the upper jaw, while only few smaller tooth germs are visible in the lower jaw, where the alveolar canal is also closing.

Denser tissue is present in the posterior one-third of the upper alveolar canal, medial to the teeth and not connected to the bone. This tissue occupies the empty space between the dorsal (rostral) and ventral (palatal) processes of the maxilla.

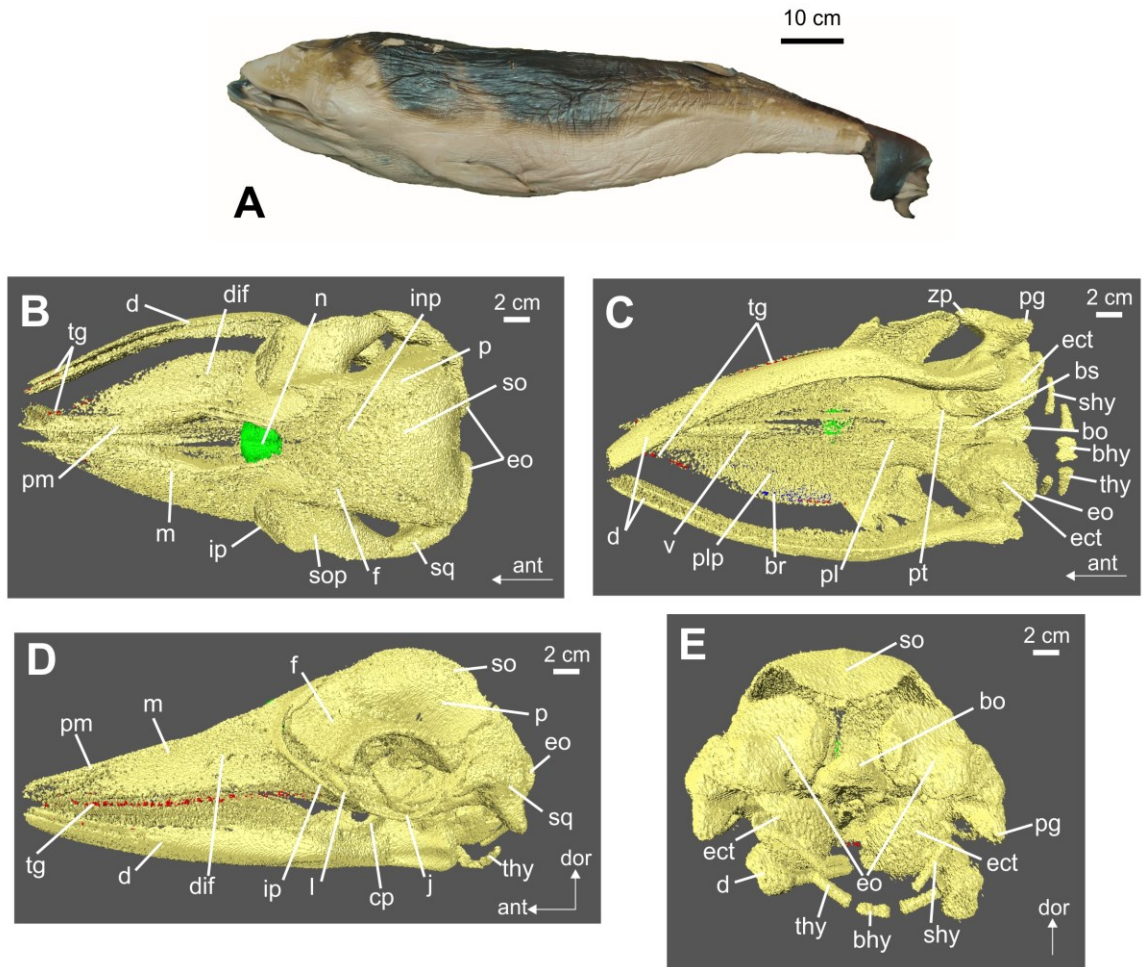


Figure 2.11 – Mf6 (NSMTwhite15, TL 110 cm) external and internal morphology. A: left lateral view of external morphology, B: 3D rendering of internal morphology of head in dorsal view, C: head in ventral view, D: head in left lateral view, E: head in postero-ventral view. Ossified skull bones in yellow, nasal bones in green, tooth germs in red, baleen rudiments in blue. Ossified elements, tooth germs and baleen rudiments are labeled in the figures. Abbreviations listed on page 110 (Fig. 2.6). From Lanzetti (in press).

### **Fetal Stage 26 – new stage (Fig. 2.12 – Fig. S2.8)**

Ridge (keel) forms at the center of the baleen gums.

Notes on staging: this new stage is characterized by the formation of a distinct cartilaginous ridge at the center of the baleen gum. It is most prominent at the posterior end of the rostrum. The gingival groove still borders the baleen gum laterally and it is the only structure present at tip of the rostrum.

*Specimen:* Mf7, Mf8

*Skull ossification:* rostrum is broad and flat. Nasals contact the frontal posteriorly, while the infraorbital process of the maxilla remains not connected to the frontal. Interparietal is not visible anymore, as the supraoccipital shield has extended anteriorly to cover it. Ectotympanic only has a very small unossified segment ventro-laterally, but it is now sutured to the squamosal.

Mandibular rami are united by a short and presumably ligamentous symphysis. Fontanelles are closed. Exoccipital is sutured to the squamosal, and basioccipital and basisphenoid contact the surrounding dermal bones. Periotic has assumed the typical “inflated” shape of mysticetes.

*Tooth germs/baleen rudiments:* tooth germs are present for the entire length of both jaws, however they are less evenly distributed. Upper and lower alveolar canals are narrower than in previous stages. Denser material (baleen rudiments) is present for the entire length of the rostrum, occupying most of the space between the dorsal and ventral processes of the maxilla. In the dorsal part of the rostrum, where the keel occurs externally, this material extends medially and laterally to the tooth germs, covering some of them.



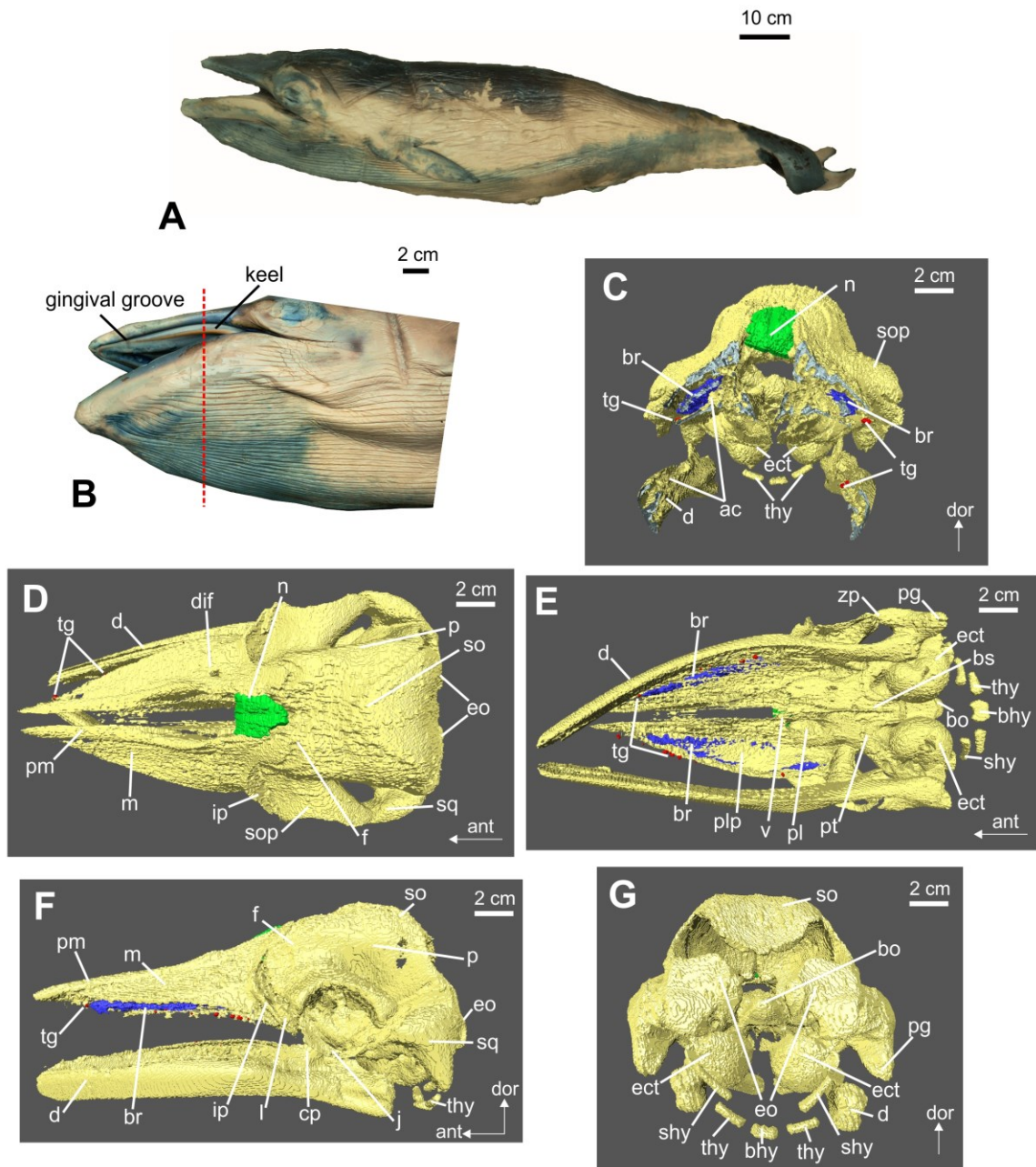


Figure 2.12 – Mf7 (NSMT27171, TL 115 cm) external and internal morphology. A: left lateral view of external morphology, B: left lateral close-up view of head, C: cross section of 3D rendering of internal morphology of head, D: head in dorsal view, E: head in ventral view, F: head in left lateral view, G: head in postero-ventral view. Ossified skull bones in yellow, nasal bones in green, tooth germs in red, baleen rudiments in blue. Ossified elements, tooth germs and baleen rudiments are labeled in the figures. Abbreviations listed on page 110 (Fig. 2.6). From Lanzetti (in press).

### **Fetal Stage 27 – new stage (Fig. 2.13 – Fig. S2.9)**

Transversally oriented rows of connective tissue and baleen visible.

Notes on staging: this new stage is characterized by the presence of the transversal ridges that will form the base of the baleen plates visible in the gums of the upper jaw. They are present for the entire length of the palate except at the anterior end. It is known that this structure represents developing baleen based on the work on blue whale fetuses by Tullberg (1883) (translated and commented by Fudge et al., 2009).

*Specimen:* Mf9, Mf10

*Skull ossification:* the skull has assumed the familiar shape observed in minke whale neonates.

All the dermal bones are at least partially in contact, except the infraorbital process of the maxilla that is still separated from the frontal on one or both sides of the skull. Ectotympanic is completely ossified and sutured to the squamosal for the entire length of its posterior process. Supraoccipital has assumed the characteristic triangular shape of postnatal minke, with its anterior end reaching the midpoint of the orbit and contacting the frontals anteriorly.

Endochondral bones are still not sutured posteriorly, as this process takes places postnatally (Walsh and Berta, 2011).

*Baleen:* no tooth germs are present. Alveolar canal is narrow but open, while the lower alveolar canal is very shallow. However it is still marked for the entire length of the rami. Transversal process of the baleen appears to not have any internal connection with the rest of the skull, However it might be due to preservation issues and CT scan limitations. From both external and internal examination, it appears to be more developed posteriorly and gradually progressing anteriorly.



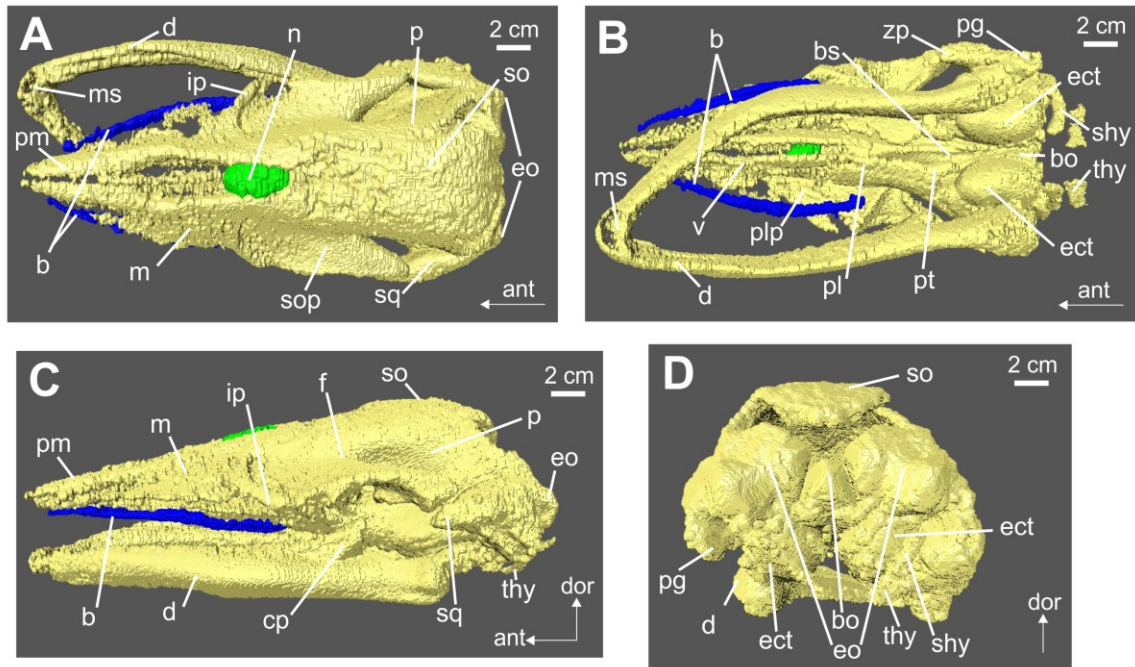


Figure 2.13 – Mf10 (NSMT27174, TL 212.5 cm) internal morphology. A: dorsal view of 3D rendering of the internal morphology of head, B: head in ventral view, C: head in left lateral view, D: head in postero-ventral view. Ossified skull bones in yellow, nasal bones in green, baleen in blue. Ossified elements and baleen are labeled in the figures. Abbreviations listed on page 110 (Fig. 2.6). From Lanzetti (in press).

### **Anatomical aspects of the teeth-to-baleen transition in minke whales' ontogeny**

Based on the external and internal anatomy of the specimens, it is possible to divide the teeth-to-baleen transition in minke whales into three main stages: tooth germs developing, tooth germs resorbing and baleen rudiments, transversal process of baleen erupted with no tooth germs. By plotting these events on the growth curves of these taxa (Fig. 2.14), it shows that how baleen only appears in the very last stages of gestation, along with the deteriorating tooth germs, as hypothesized by Ishikawa and Amasaki (1995). It is likely that dentition starts developing in the embryonic or very early fetal period in these species, as shown in the humpback whale in this work and by other accounts in the literature (e.g. Karlsen, 1962), but the current samples do not allow this assessment. Nonetheless, the present study still provides the unique opportunity to describe in detail the anatomical changes correlated to the transition from teeth to baleen in the

ontogeny of minke whales, particularly focusing on the initial development of baleen plates, a topic that has not yet been explored fully. These observations can then be used as starting point to investigate this event both in other living species and in the evolution of Mysticeti. This entire section, including figures, is reported from Lanzetti (in press) with only minor changes.

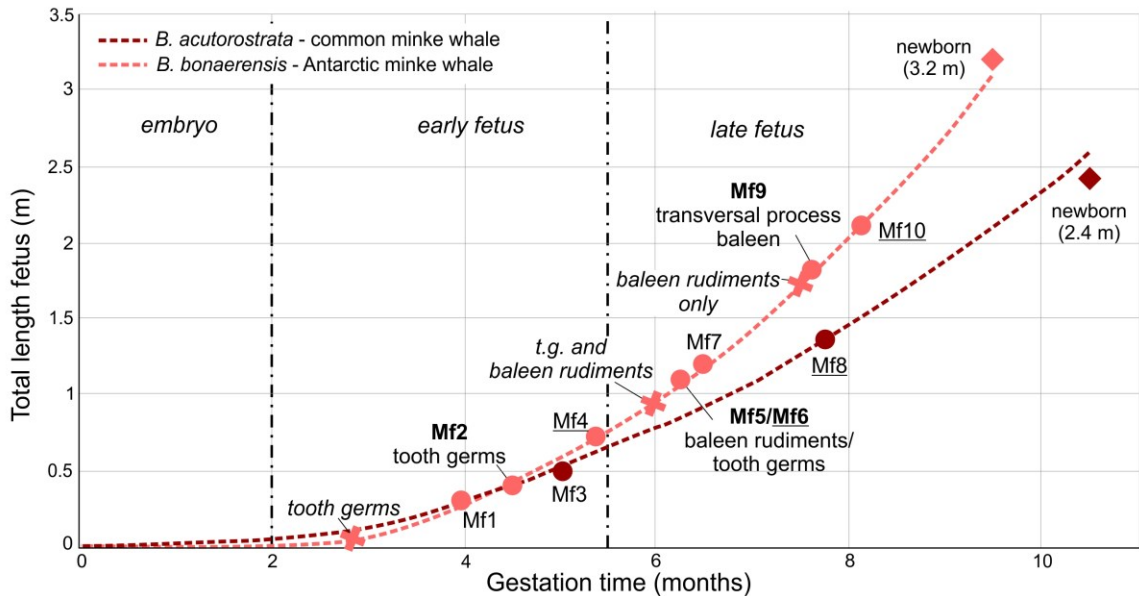


Figure 2.14 – Calculated growth trajectories, using total length (cm) and estimated gestational age (months), for the two minke whale species. Underlined specimens are figured to represent their relative stage in teeth and baleen development in Figs. 2.15-2.18. Circles=specimens included in this study and retro-fitted to the growth curve, with changes in teeth and baleen growth labeled when they are first recorded; crosses=lengths at which important steps in the teeth to baleen transition were recorded in the species by Ishikawa and Amasaki (1995); diamonds=estimates of length at birth. Embryo/fetus line is based on the age estimate for balaenopterids listed by Roston et al. (2013) (2.1 months). Early fetus/late fetus line is based on observations of internal and external anatomy of the specimens and their Fetal Stage (FS 20–24: “early fetus”; FS 25–27: “late fetus”). Specimens labeled as in Table 2.1. Individual data points have been removed to make the graph more legible and highlight the specimens from this study. Equations and data sources are the same as for Fig. 2.3, reported in Appendix C and Fig. S2.2. Modified from Lanzetti (in press).

### *Tooth number, size and distribution*

Specimens spanning from FS20 to FS24 (Mf1, Mf2, Mf3, Mf4) have a distinctive gingival ridge, or gum, that extends throughout each side of the upper jaw (Fig. 2.15). No distinct gum is recognizable on the lower jaw. The ridge is identifiable until FS26 (Mf7, Mf8), However it undergoes significant structural changes after FS24. Paired with the internal anatomical

information from the CT imaging, the appearance of this ridge can help determine the phase of gestation and teeth-to-baleen transition that the specimen occupies.

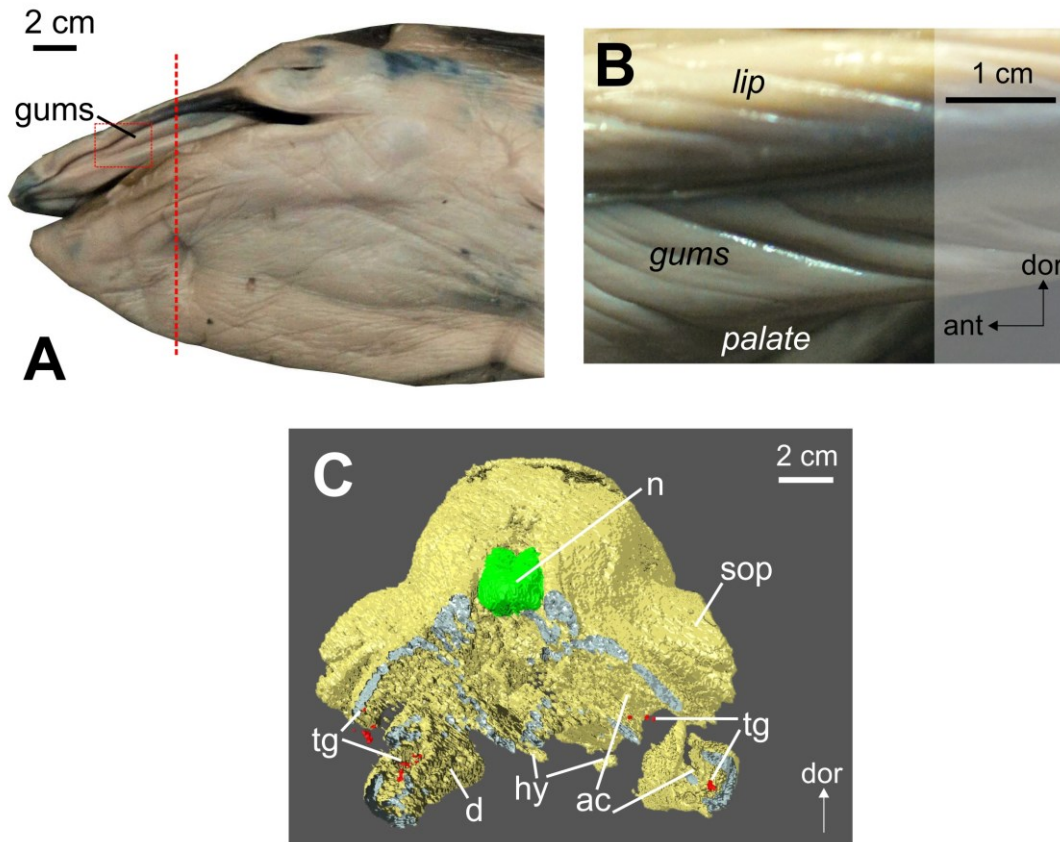


Figure 2.15 – “Tooth germs” stage (FS21-FS24), represented using specimen Mf4. A: left lateral close-up view of head, B: close-up view of gums in the upper jaw, C: cross section of 3D rendering of internal morphology of head. Red dashed line in A represents cross section location and orientation, box represents magnified section of gums. Ossified skull bones in yellow, nasal bones in green, tooth germs in red. Ossified elements and tooth germs are labeled in the figure. Abbreviations listed on page 110 (Fig. 2.6). From Lanzetti (in press).

As anticipated by the external appearance of their gums, starting from Mf2, all specimens have clearly recognizable tooth germs in both jaws, except the two older specimens at FS27 (Mf9 and Mf10). As only medical-grade CT scans were available, presence of teeth in Mf1 could not be assessed due to limited imaging quality, but it is likely that this specimen also had tooth germs based on its external anatomy and the level of development in the dentition of Mf2.

The resolution of the CT images also does not allow for a precise count of the tooth germs in all fetuses or to precisely describe their shape. As many as 35 rounded or conical tooth germs per side in the upper jaw of Mf6 were identified. This elevated number is comparable to the results in Ishikawa and Amasaki (1995) (Table 2.6). None of the lower jaws preserved a visible complete tooth row: this might be due to the poor preservation of these elements and to the relative size of the tooth germs, which have been found to be consistently smaller in the mandible than those in the upper jaw among mysticete fetuses of numerous species (Ridewood, 1923, Karlsen, 1962, Thewissen et al., 2017, Lanzetti et al., 2018). From the presence of a marked alveolar canal along the entire length of the rami in all the specimens up to FS26 and from previous accounts (Eschricht, 1849, Julin, 1880, Ishikawa and Amasaki, 1995), it can be assumed that all specimens up to Mf8 (FS26) have a complete tooth row also in the lower jaws. The characteristic “double teeth”, defined as secondarily fused or very closely spaced tooth germs (Thewissen et al., 2017), are only visible in the lower jaw of Mf8. Julin (1880) described “double teeth” in a mandible of a young minke fetal specimen, tentatively assigned in this work to FS21/22. It is probable that this tooth morphology occurs in the minke whale from very early stages of development, as it has been reported for other mysticetes (Ridewood, 1923, Van Dissel-Scherft and Vervoort, 1954, Karlsen, 1962, Thewissen et al., 2017).

The size of the tooth germs can be used as a proxy to determine when the tooth germs start resorption, especially given that the quality of the CT scans does not allow for direct comparison of other factors such as spacing between germs. The germs stop increasing in size at FS25 (Mf6), indicating the probable start of resorption after mid gestation. In the humpback whale instead, it appears that they start resorbing earlier, likely at FS22 (Hf3) (Table 2.7). The specimens at FS26 (Mf7, Mf8) show similar tooth germs proportions and size to Mf6, and their germs are smaller in proportion than those in FS21/22 (Mf2). Tooth germs do not steeply

decrease in absolute size, but rather they stop growing becoming smaller in proportion due to the growth of the skull and the rest of the fetus. Overall, these observations seem to confirm the results of Ishikawa and Amasaki (1995) who delimited the end of tooth formation and the start of the degradation stage in a specimen close in absolute age to Mf4 and noted high levels of degradation in specimens comparable to Mf5 and Mf6 (Table 2.6).

Table 2.7 – Measurements of tooth germs size relative to skull and TL in humpback and minke whales prenatal specimens.

Specimen	Upper jaw tooth bud diameter (mm)	Distance from tip of snout to eye (mm)	Relative size of tooth bud (%)	TL (mm)	Relative size of tooth bud with TL (%)
He1	0.22	30	0.73	170	0.13
Hf1	1.02	70	1.46	310	0.33
Hf2	1.21	75	1.61	390	0.31
<i>Hf3</i>	<i>1.26</i>	<i>120</i>	<i>1.05</i>	<i>700</i>	<i>0.18</i>
Hf4	2.58	235	1.10	1030	0.25
Mf2	1.8	75	2.40	410	0.44
Mf4	2.6	150	1.73	740	0.35
<i>Mf5</i>	<i>2.6</i>	<i>200</i>	<i>1.30</i>	<i>1100</i>	<i>0.24</i>
Mf6	4.2	230	1.83	1100	0.38
Mf7	4.8	255	1.88	1150	0.42
Mf8	4.8	240	2.00	1250	0.38

Measurements and proportions in italics might be unreliable due to poor preservation of the specimen. Modified from Lanzetti (in press)

### *Baleen rudiments formation and tooth resorption*

Beginning at FS25, a series of external anatomical modifications marks the initiation of baleen formation. First, a thick gum develops in the upper jaw on the medial side of the gum that was visible in earlier stages (Fig. 2.16) and then in FS26 this new gum thickens laterally, fusing to the earlier gums (Fig. 2.17). A deep ridge or keel forms in the center of this expanded “baleen gum”, while the lower jaw does not present any significant changes. The keel appears denser than the normal gum tissue, having a cartilaginous texture. This ridge is more marked posteriorly and fades away in the anterior part of the rostrum, where only a groove is present between the palate and the lip. These structures have been previously described in a single Antarctic minke whale

fetus of comparable age to Mf7 and Mf8 (145 cm TL, ca. 7 months from conception, 74% of gestation) by Sawamura (2008). By dissecting the palate, Sawamura found that the remaining tooth germs occupy the center of the keel. Medial to this, he identified a thick palatal mucosa, which presents high vascularization and innervation, similar to tooth alveoli in humans, and he hypothesized that this tissue was a precursor to baleen formation. He stated that this tissue is part of the periodontal tissue that produces teeth rather than the transversal palatine fold, which produces the soft tissue that covers the hard palate. The present findings confirm that this external morphology exists at this stage of development in both minke whale species, and, given the position of the tooth germs in the CT images, it is likely that they occupy the center of the keel.

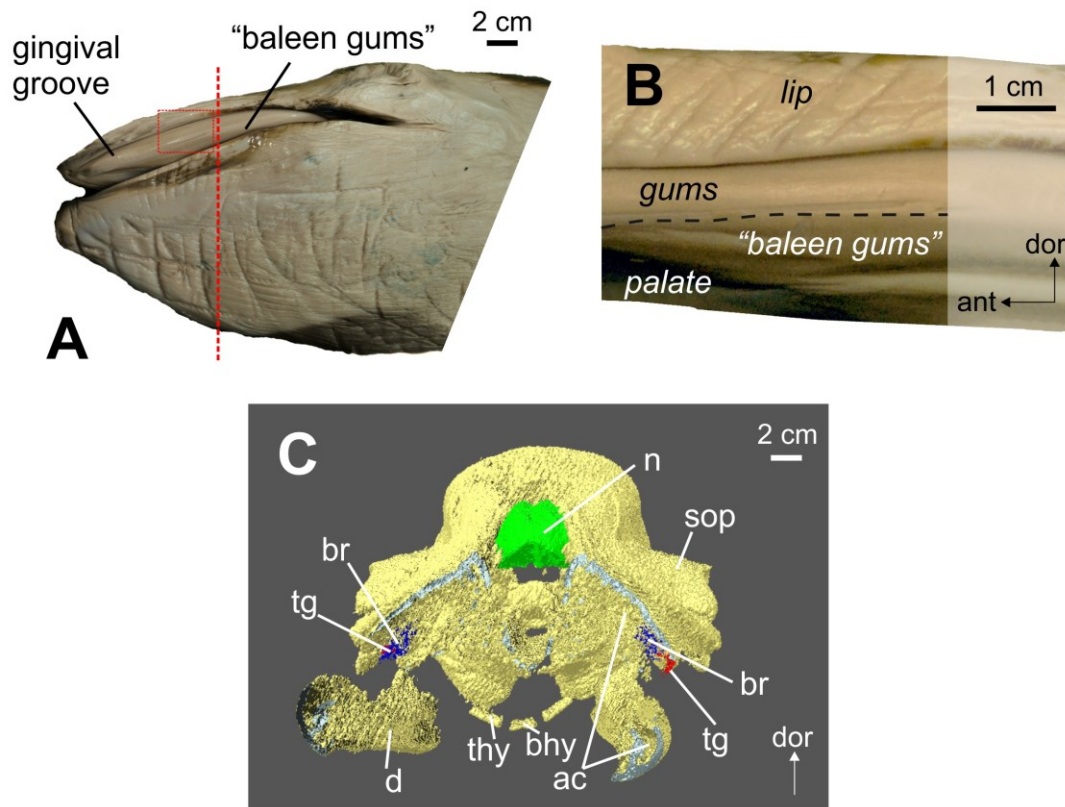


Figure 2.16 – “Baleen gums” stage (FS25), represented using specimen Mf6. A: left lateral close-up view of head, B: close-up view of gums in the upper jaw, C: cross section of 3D rendering of internal morphology of head. Red dashed line in A represents cross section location and orientation, box represents magnified section of gums. Ossified skull bones in yellow, nasal bones in green, tooth germs in red, baleen rudiments in blue. Ossified elements, tooth germs and baleen rudiments are labeled in the figure. Abbreviations listed on page 110 (Fig. 2.6). From Lanzetti (in press).



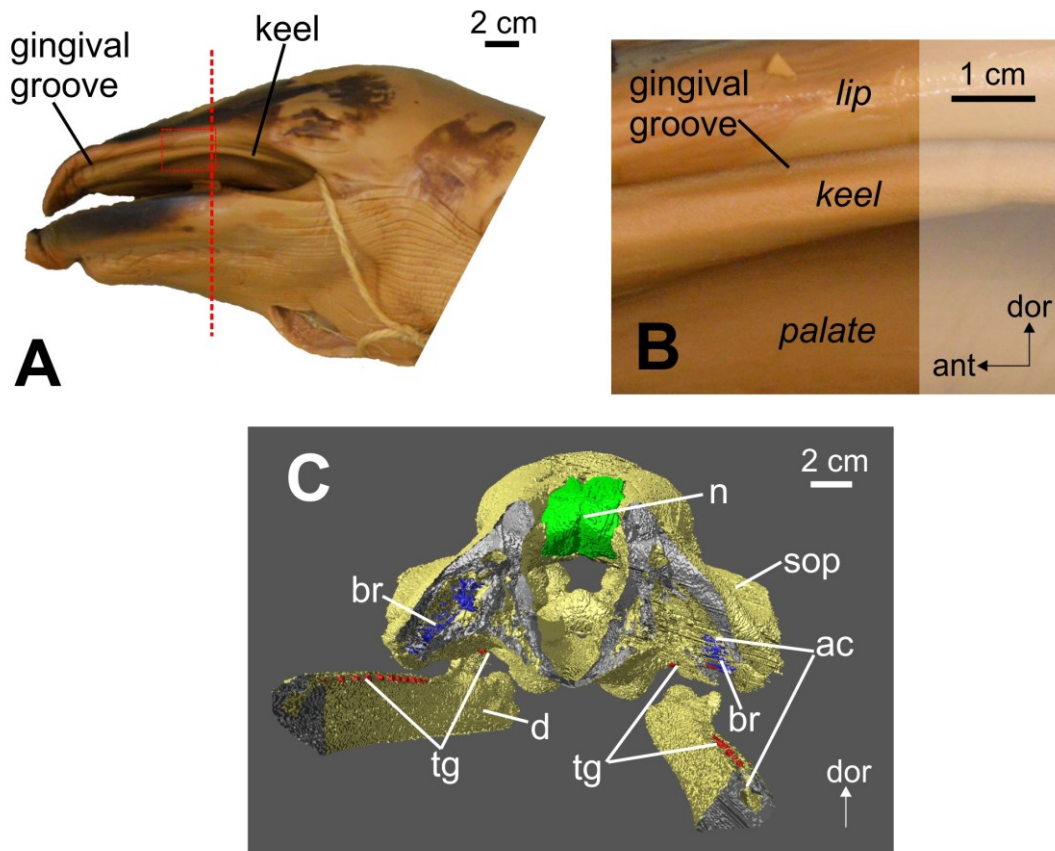


Figure 2.17 – “Keel” stage (FS26), represented using specimen Mf8 (ZMCU-CN4x; TL 125 cm). A: left lateral close-up view of head, B: close-up view of gums in the upper jaw, C: cross section of 3D rendering of internal morphology of head. Red dashed line in A represents cross section location and orientation, box represents magnified section of gums. Ossified skull bones in yellow, nasal bones in green, tooth germs in red, baleen rudiments in blue. Ossified elements, tooth germs and baleen rudiments are labeled in the figure. Abbreviations listed on page 110 (Fig. 2.6). From Lanzetti (in press).

A denser material can be isolated from the CT images medial to the tooth germs starting from specimen Mf6 (Fig. 2.16). It is likely not recognizable in Mf5 due to the poor preservation conditions of the specimen. This tissue does not contact the rostral bones inside the medial part of the alveolar canal. It is present mostly in the posterior part of the rostrum, where most of the foramina are located and also where the enlarged gum is visible externally. In the following stage FS26 (Fig. 2.17), this material is visible along most of the upper jaw and appears, However it is denser in the posterior portions of the alveolar canal. It is now expanded laterally and, in some

regions, it engulfs the tooth germs. It is clearly connected to the visible dorsal and ventral foramina in the posterior parts of the maxilla, as it occupies the space between them. A highly vascularized area was also identified by Sawamura (2008) in the FS26 specimen he dissected. Based on this evidence, and on the findings of Ishikawa and Amasaki (1995), which identified “baleen rudiments” in comparable specimens (Table 2.6), this tissue appears to be a precursor to baleen development. However it is difficult to infer its composition without histological analysis.

#### *Eruption of the transversal process of baleen*

The last two specimens of the series, Mf9 and Mf10 (FS27), display a thick baleen ridge erupted from the upper jaw, with the lower jaw retaining most of the same external morphology as previous stages. No tooth germs are recognizable at this stage and the alveolar canal in both jaws has significantly reduced its size. The baleen ridge is composed of a series of transversal processes, small plates oriented transversally to the main axis of the rostrum, spaced by deep grooves (Fig. 2.18). The baleen recognizable in the CT scan as a structure of intermediate density between the soft tissues and the bone. They do not present any apparent physical connection with the alveolar canal or other parts of the palate. This is to be expected as baleen is not directly surrounded by maxillary bones, but connected to the palate by a network of blood vessels and nerves (Ekdale et al., 2015). The transversal rows of connective tissue appear to have a medial depression in the center, as they “erupted” from the center of the gum towards the sides.

The morphology of the baleen ridge matches the description of Sawamura (2008) for a similar fetus of Antarctic minke whale (175 cm TL, ca. 7.5 months f.c., 80% of gestation). It is also possible to confirm his observation that the baleen appears to develop from the posterior towards the anterior end of the rostrum. This conclusion is supported by the relative thickness of the baleen ridge, which is thicker at posteriorly and becomes progressively less pronounced anteriorly. Additionally, the ridge also appears to be better developed anteriorly in the oldest



specimen, Mf10, compared to Mf9. This pattern of development is congruent with the keel and dense tissue morphology observed in the previous stages since both those structures are more pronounced posteriorly. The overall morphology of the transversal process of baleen matches the observations reported by Fudge et al. (2009) on a blue whale (*Balaenoptera musculus*) fetus of 3 m in total length (6.5 months f.c., 55% gestation).

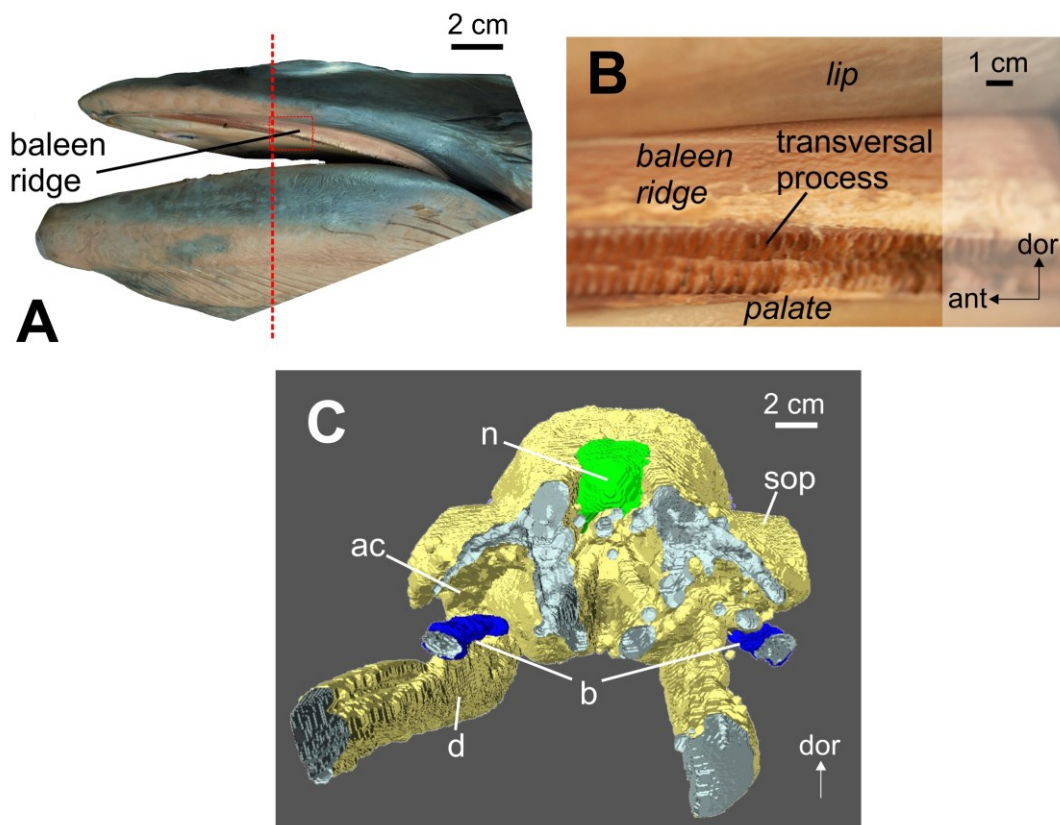


Figure 2.18 – “Baleen ridge” stage (FS27), represented by specimen Mf10. A: left lateral close-up view of head, B: close-up view of baleen ridge, C: cross section of 3D rendering of internal morphology of head. Red dashed line in A represents cross section location and orientation, box represents magnified section of baleen ridge. Ossified skull bones in yellow, nasal bones in green, baleen in blue. Ossified elements and baleen are labeled in the figure. Abbreviations listed on page 110 (Fig. 2.6). From Lanzetti (in press).

## **Skull shape development in humpback and minke whales**

### *Discriminant Analysis (humpback and minke whales)*

For both the whole skull and rostrum-only configurations, no statistically significant differences were found between single specimens in the humpback whale and growth stages in minke whales, but this is most likely due to the low sample size. The detailed results of these analyses can be found in Appendix C. The dataset includes only a few samples of each growth stage and in the case of the humpback, most are only represented by one specimen, making it impossible to conduct reliable statistical tests. However, several important shape changes during growth can be noticed by comparing the average landmark shapes for each growth stage or specimen scaled to the most mature stage or sample in the series in dorsal view (Lanzetti et al., 2018, Lanzetti, in press).

In the whole skull configuration (Fig. 2.19), several structures progressively change with the age of the specimens, and these patterns are overall shared in the two species. Firstly, by comparing Hf3 to the other specimens, it is clear that the rostral shape is deformed, as it deviates visibly by the general growth trend. Given the results of the diceCT scan on this specimen, this is probably a preservation issue, as the internal tissues in this region appear to have been decalcified and damaged by the preservation medium (Fox et al., 1985, Simmons, 1995). Therefore, only the braincase of this specimen can be reliably compared with the rest of the dataset. Also, the humpback embryo has a characteristic shape, with the skull elements having different relative proportions in comparison to fetal and juvenile specimens. The braincase and the rostrum each make up roughly one-half of the entire skull length. Cartilage and other soft tissues that are used to identify the position of the skull vertex, as the supraoccipital is not completely ossified yet, are located more anteriorly. This diverging shape might be a preservation issue of this unossified tissues or might be a real difference between embryonic and fetal development.

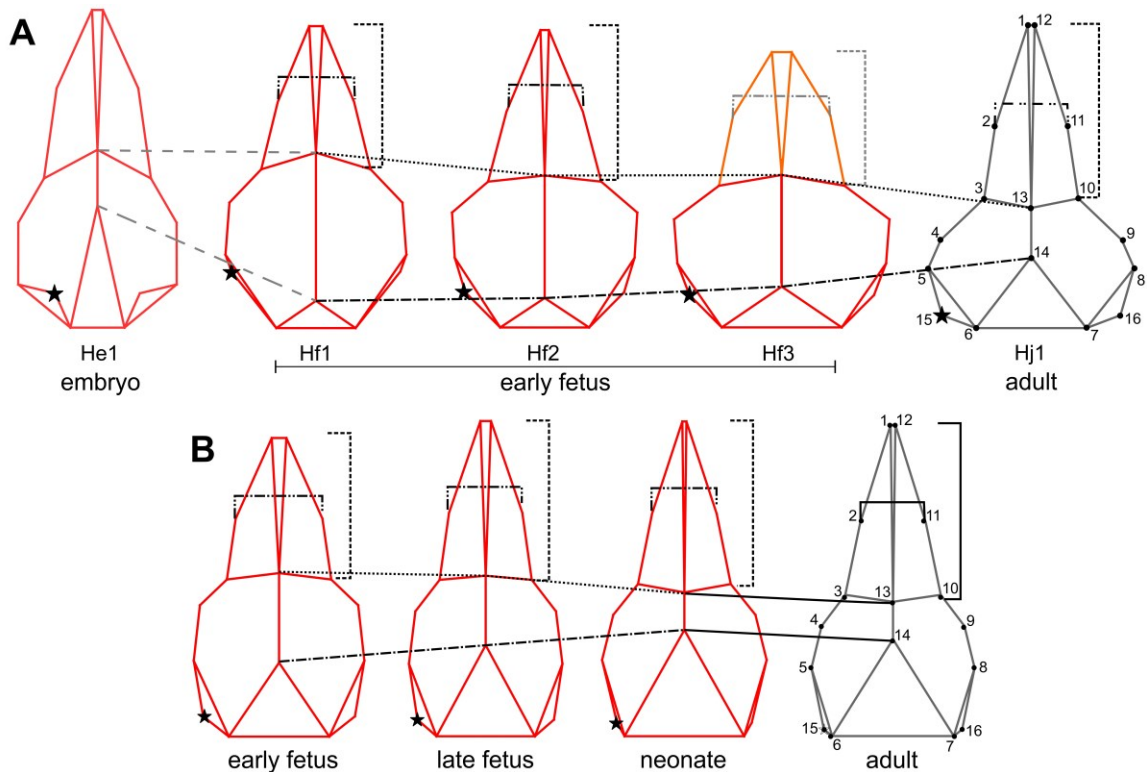


Figure 2.19 – Shape change in the whole skull of humpback (A) and minke (B) whales at different growth stages, visualized using the 16-landmarks configuration in dorsal view with the adult configuration as “target shape”. Configurations are arranged from youngest to oldest from left to right. Progressive elongation of the rostrum is marked by the black dashed lines (landmarks 1-3). Rostral tapering is highlighted by the dash-and-dot line (landmarks 2-11). The two black dot and dash-and-dot lines indicate telescoping, as the relative posterior movement of the anterior end of the nasals (landmark 13) and the anterior movement of the supraoccipital shield (landmark 14). The star highlights the movement of the postglenoid process of the squamosal on the left side (landmark 15). He1 is in light red to indicate its diverging skull shape. Long-dashed gray lines connect it to the other specimens to show the differential pattern of movement of the landmarks between embryonic and fetal stages. Gray lines and orange rostrum and Hf3 highlight that this specimen does not follow the overall growth pattern for preservation issues in the rostral region. Lines that connect neonate and adult shapes of minke whales are full as there is no visible change between these two growth stages in the shapes. Modified from Lanzetti et al. (2018) and Lanzetti (in press).

Additional specimens should be added to the analysis to check the present observations.

Beginning in the early fetal stage and continuing to the most mature individuals, the rostrum appears to become relatively longer compared to the braincase, assuming a more tapered shape by progressively exhibiting a smaller mid length width (landmarks 2-11). Overall, the braincase does not elongate proportionally to the rostrum, and maintains a similar length from the fetal stages to the adult. However, major shape changes occur in this region, with the anterior end of the nasals

moving posteriorly and the anterior end of the supraoccipital shield shifting in the opposite direction, reducing the relative distance between these two landmarks (13-14). This pattern illustrates the process of telescoping (Miller, 1923). The relative movement of the postglenoid process of the squamosal (landmarks 15-16) is evident in both series, but it follows different trajectories, likely due to interspecific differences in the skull shape of the two taxa (Clapham and Mead, 1999, Perrin et al., 2018). In the humpback whale it extends laterally and posteriorly as development progresses, while in the minke whales it shifts medially maintaining the same antero-posterior position. This movement is part of the general pattern of shape change observed in the rest of the braincase: in *M. novaeangliae* the braincase becomes progressively wider than the rostrum while in *B. bonaerensis/acutorostrata* follows the tapering trend of the rostrum.

In the rostrum-only configuration (Fig. 2.20), the same pattern of rostrum tapering and elongation can be detected as noted in the whole skull configuration. He1 and Hf3 were excluded from this comparison due to their mentioned probable deformation or different developmental trend. The nasal bones become more elongated especially early in the fetal development (landmarks 11-12), with the anterior end moving posterior to the antorbital notches (landmarks 4 and 7) in the later stages of growth, between the late fetus and neonate stages in the minke whales and between the late fetus Hf4 and Hj1 in the humpback whale. Both looking at the whole skull and at the rostrum, it appears that there is little change between the neonate and adult stages in the minke whale, suggesting that the changes in postnatal ontogeny might be subtle and not detectable using this dataset. It is likely that this would also be detected in the humpback whale by improving the resolution of the growth series.

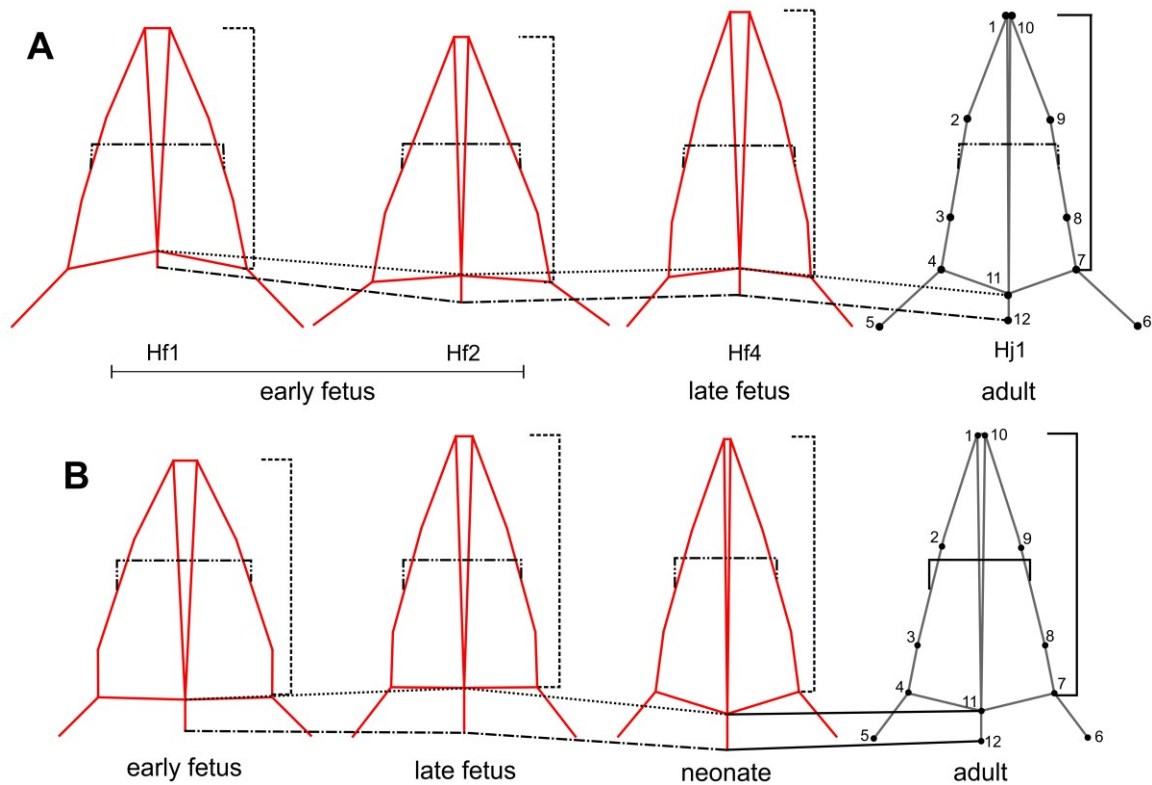


Figure 2.20 – Shape change in the rostrum of humpback (A) and minke (B) at different growth stages, visualized using the 12-landmarks configuration in dorsal view with the adult configuration as “target shape”. Configurations are arranged from youngest to oldest from left to right. Progressive elongation of the rostrum is marked by the black dashed lines (landmarks 1-4). Rostral tapering is highlighted by the dash-and-dot line (half way between landmarks 2-9 and landmarks 3-8). The two black dot and dash-and-dot lines indicate telescoping, as the progressive elongation of the nasal bones (landmarks 11-12). Lines that connect neonate and adult shapes of minke whales are full as there is no visible change between these two growth stages in the shapes. Modified from Lanzetti et al. (2018) and Lanzetti (in press).

### *Principal Component Analyses (minke whales)*

The PCA analysis conducted on the whole skull configuration “by specimen” dataset found 11 principal components, with the first five describing 95% of the variation. The scatter plot of points and complete PCA results can be found in Appendix D (Fig. S2.10, Table S2.2). To best understand transformation during ontogeny independently of the minke whale species and individual specimen variation, a PCA was also conducted on the “by stage” dataset, and these results are presented here. Six components were identified by this analysis, with PC1 and PC2 representing most of the total variation (76.9%) (Table 2.8).

Table 2.8 – PCA principal components for both configurations. Components ordered according to the amount of variation they represent, from largest to smallest.

<u>Whole skull configuration</u>		<u>Rostrum-only configuration</u>	
Principal Component	% Total Variance	Principal Component	% Total Variance
PC1	60.2	PC1	66.4
PC2	16.7	PC2	21.5
PC3	14.4	PC3	6.4
PC4	5.2	PC4	3.0
PC5	2.9	PC5	1.9
PC6	0.5	PC6	0.8

As growth progresses, specimens move from more negative to more positive values on PC1 (Fig. 2.21). This axis represents the major ontogenetic changes also highlighted in the DA results: rostrum elongation and telescoping, represented mostly by the anterior movement of the supraoccipital shield, along with an overall tapering of the skull. PC2 mostly divides the late gestational stages from the neonatal and adult phases of growth. In these later stages, the braincase appears to shorten relative to the rostrum, and the telescoping becomes more pronounced. This sharp difference might also be due to the fact that postnatal specimens in the analysis all belong to the common minke whale, which has a slightly different rostral shape than the Antarctic species (Perrin et al., 2018).

The PCA conducted on the rostrum-only “by specimen” dataset also found 11 components, with the first five representing 95% of the variation. For complete results of this analysis see Appendix D (Fig. S2.11, Table S2.2). In the “by stage” dataset, six components were identified by the PCA, and PC1 and PC2 represent 87.9% of the total variation (Table 2.8). In this analysis (Fig. 2.22), the pattern of distribution of rostral shape in the morphospace is somewhat different from that recovered in the whole skull configuration. PC1 describes the main direction of growth, characterized by rostral tapering and elongation, with younger specimens plotting on more positive values and the adult stages having the most negative ones. However, the first stage (FS21/22) does not have the most extreme values as it would be expected.

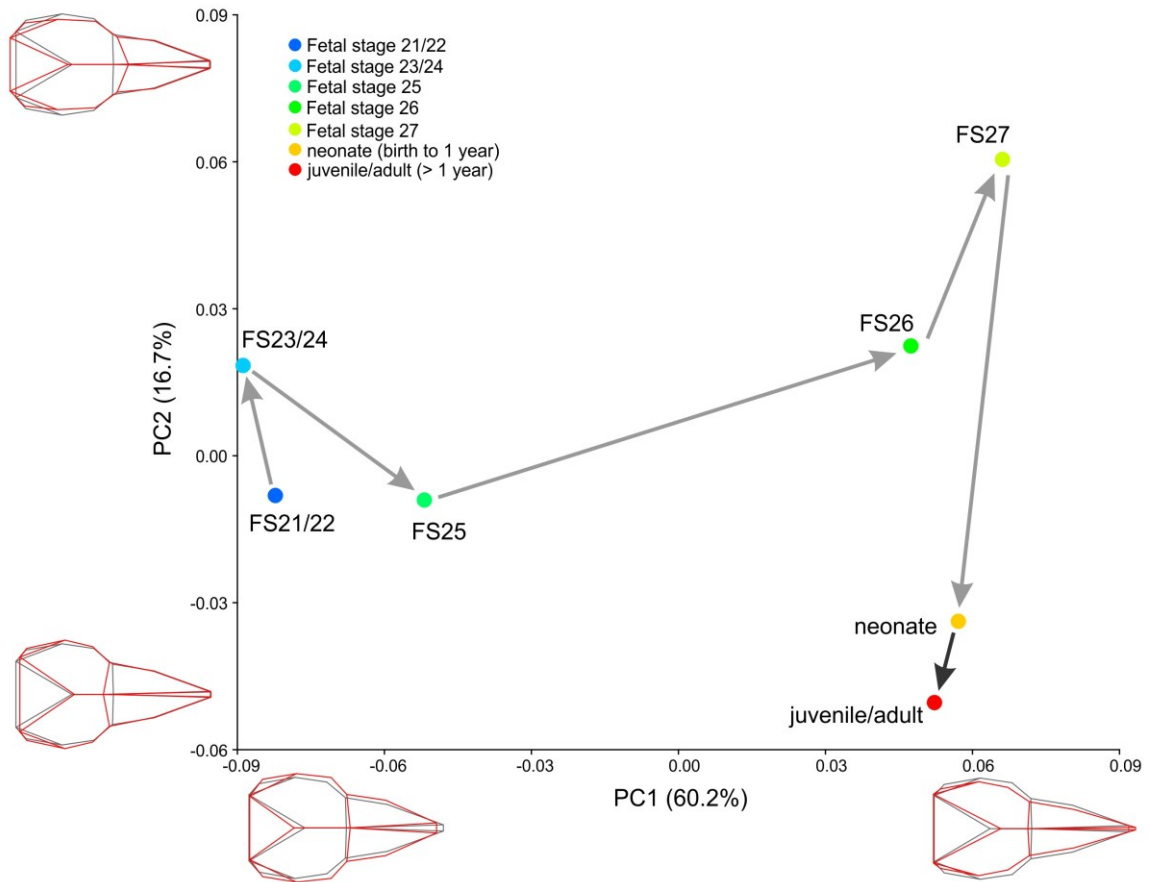


Figure 2.21 – PCA plot for the whole skull configuration. Light gray arrows connect prenatal stages, dark gray postnatal ones. The lines were added graphically to trace the progression of shape change. Average shape at 0 on both axes in light gray wireframe, shape at maximum and minimum values of axes in red wireframe.

It is also characterized by low values of PC2, signaling a more posterior positioning of the anterior end of the nasals, similar to neonates and adults. The somewhat unexpected pattern of distribution of specimens on this axis could be explained by interspecific differences as Mf3, the only sample included in the analysis at FS21/22, and postnatal specimens all belong to the common minke whale. A larger dataset with an even sampling of both minke whale species is needed to test these possible differences in skull shape and growth in the two taxa.

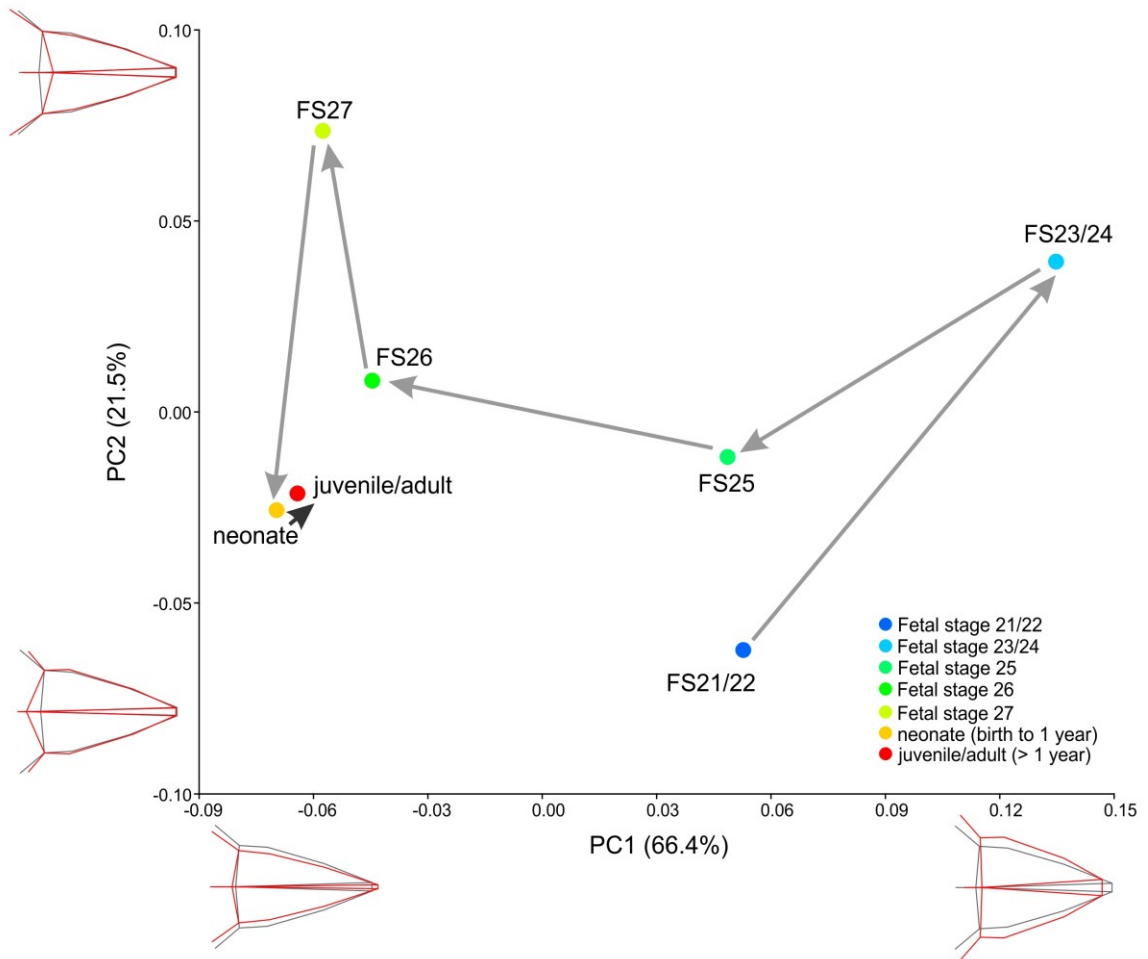


Figure 2.22 – PCA plot for the rostrum-only configuration. Light gray arrows connect prenatal stages, dark gray postnatal ones. The lines were added graphically to trace the progression of shape change. Average shape at 0 on both axes in light gray wireframe, shape at maximum and minimum values of axes in red wireframe.

### *Modularity and Partial Least Square analyses (minke whales)*

The modularity analysis was conducted on the whole skull configuration on the “by specimen” dataset to test whether the braincase and rostrum follow significantly different patterns of shape development and can be analyzed as separate modules. As the modules belong to the same unit, the skull, it is to be expected that the RV coefficient will be generally high. However, if the calculated RV coefficient for the *a priori* hypothesis (rostrum and braincase) falls in the bottom 5% of values of all the coefficients estimated for the random partitions, these two parts



would result to be less connected to each other than other parts of the skull (Klingenberg, 2009, Klingenberg and Marugán-Lobón, 2013). Therefore, it would be possible to interpret the results of the PLS analysis to evaluate how they change in shape during ontogeny relative to each other more confidently. The modules tested have an RV score ( $RV_h=0.678$ ) higher than the lowest possible score computed ( $RV_{min}=0.592$ ).  $RV_h$  is above the bottom 5% of the distribution of the calculated coefficients ( $RV_h>10\%$ ) (Fig. 2.23). However, it still falls on the left side of the distribution, below the median RV value. Therefore, while the development of rostrum and braincase is somewhat connected, for the purpose of this study their shape changes will still be contrasted. A larger sample size might clarify if indeed these two skull blocks can be considered two independent developmental modules in this taxon and in baleen whales in general.

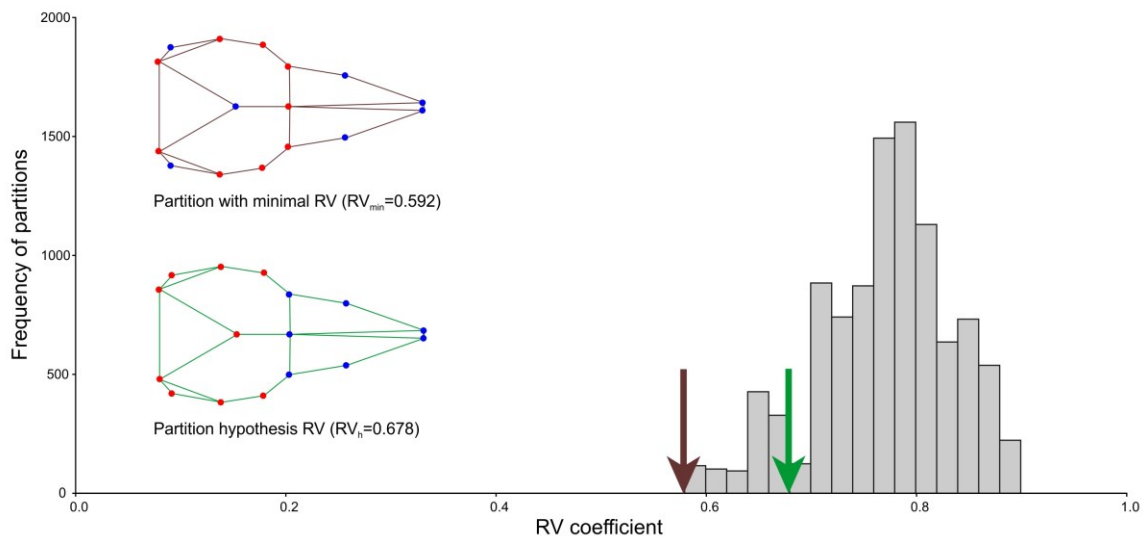


Figure 2.23 – Distribution of RV coefficients for rostrum and braincase modularity analysis. Brown arrow=minimum RV coefficient, green arrow=RV coefficient for partition hypothesis. Distribution of landmark between partitions are figured for the minimum RV (brown wireframe) and for the hypothesis (green wireframe). Partition1 landmarks=red, partition2=blue.

The PLS analysis between the rostrum and the braincase was performed on both the “by specimen” and “by stage” dataset. The first found that the two blocks are significantly correlated ( $p=0.008$ ), as expected by the results of the modularity analysis and by being two parts of the skull (del Castillo et al., 2017). The first component (PLS1) explains most of the shape variation

between the two parts (83.8%). The scatter plot resulting from this analysis is reported in Figure S2.12 (Appendix D), as these data will be used for subsequent regression analysis. The PLS analysis on the “by stage” dataset provided similar results, with the two blocks being significantly correlated ( $p=0.013$ ), and PLS1 describing 89.1% of total relative variation. Analyzing this plot (Fig. 2.24), it is possible to notice that the braincase undergoes a higher degree of shape change ( $-0.08, +0.08$ ) in ontogeny relative to the rostrum ( $-0.06, +0.06$ ). Between stages FS20/21 and FS25, the rostrum changes faster than the neurocranium in shape, which appears to undergo little transformations especially in the early stages.

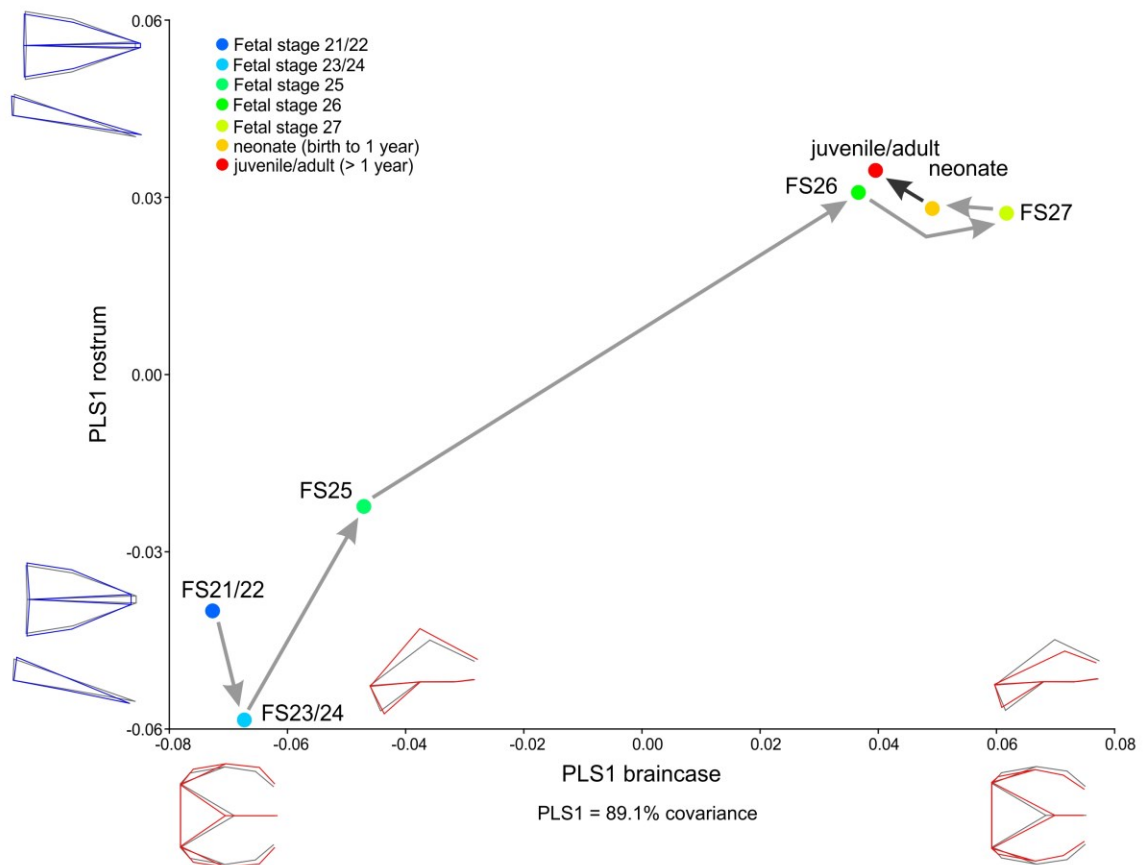


Figure 2.24 – PLS1 analysis plot, comparing scores from the two partitions (rostrum and braincase). Light gray arrows connect prenatal stages, dark gray postnatal ones. The lines were added graphically to trace the progression of shape change. Average shape at 0 on both axes in light gray wireframe. Shape at maximum and minimum values of Y axes in blue wireframe (rostrum) and of X axes in red (braincase).

After this, a large shift in shape occurs in the braincase due to the anterior movement of the supraoccipital shield (telescoping), while the rostrum only elongates and tapers at relatively slow rate. As detected in the DA, rostral shape does not appear to modify significantly after birth relative to the late stages of ontogeny, and only minimal changes can be detected in the neurocranium. This might be due to both taxon sampling or to the selection of landmarks. Larger sample size and a higher number of landmarks or semi-landmarks might be able to identify differences among these stages. However, this analysis still indicates significantly different patterns of development in the two regions of the skull. This might have important implications for the evolution of baleen whales and their interspecific differences, as these two parts could potentially also be able to evolve independently (Klingenberg, 2005, Goswami and Polly, 2010a).

By conducting a regression analysis of the braincase and rostrum PLS scores obtained in the “by specimen” analysis, it is possible to see how the shape of these two components compare in each sample and which one has a relatively faster development. This regression shows that the scores of the components are highly correlated as anticipated ( $p=0.0003$ ), and the resulting coefficient is significantly below 1 (0.6612). By looking at the plot (Fig. 2.25), this coefficient is the results of the braincase growing at a faster pace than the rostrum overall, as it was hypothesized in the earlier PLS “by stage” analysis, with the regression slope nearing its PLS axis. However, the same discordant pattern also emerges, with early fetal specimens presenting higher PLS scores for the rostrum than the braincase, and late fetal stages the opposite. It is interesting that the adults and neonates, despite being the most mature individuals, do not present the highest shape scores for either components. Interspecific differences between the common and Antarctic minke whales might be causing this pattern. However, it could also indicate a drastic change in the development after birth, due to the different environmental pressures.

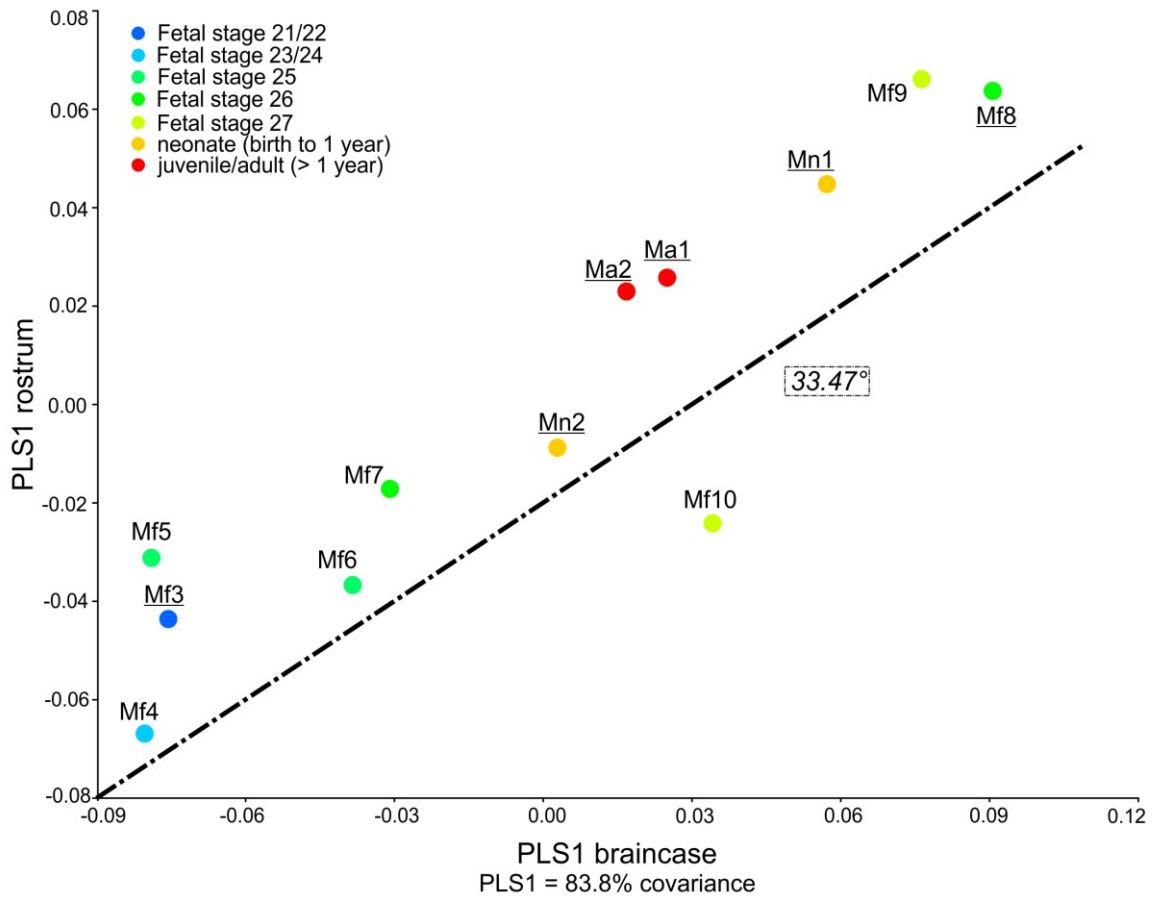


Figure 2.25 – Regression of PLS1 scores of rostrum and braincase. Axes as PLS1 “by specimen” plot (Fig. S2.12). Dash-dotted line=regression line drawn according to the angle calculated using the coefficient provided in the Results. Slope angle is indicated on graph. Specimens colored according to developmental stage. Specimens codes as in Table 2.1, with common minke whale samples underlined.

A faster initial shape change in the rostrum and a later increase in growth rate in the braincase is confirmed when analyzing the regression of the PLS scores of these two components with the total skull size (LogCS) (Fig. 2.26). Both regressions were significant ( $p$ -value braincase=0.0067,  $p$ -value rostrum=0.0113) and had a log-transformed coefficient close to 1 (braincase=1.07, rostrum=1.05). While growth rates seem similar, there is a clear shift in their proportions around FS26 (Mf7-Mf8). At this stage, the braincase starts changing in shape faster than the rostrum, while earlier it was the opposite.

This reversion in shape growth pattern appears to happen in both species, as the change in PLS score in Mf3 and Mf8 (common minke whale) is in line with the other samples. In the most mature specimen of the series (Ma2), the rostrum resents again a higher score than the braincase, reinforcing the idea that during postnatal development an additional shift in growth pattern occurs.

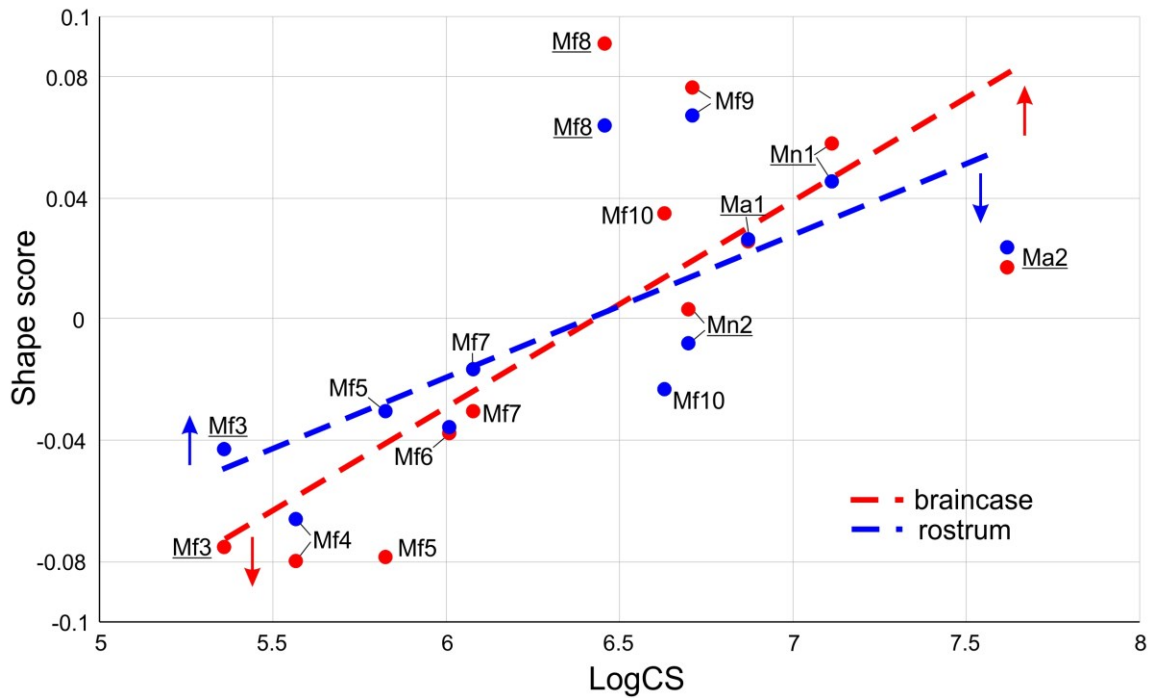


Figure 2.26 – Changes in rostrum and braincase shape relative to skull size. Shape score on Y axis, size as LogCS on X axis. Long-dashed line=regression line drawn according to the angle calculated using the coefficient provided in the Results for each skull region. Arrows indicate relative shifts in growth rate at the beginning and end of the developmental series. Each specimen is represented by two data points, one for the rostrum score one for the braincase. Specimens codes as in Table 2.1, with common minke whale samples underlined.

## **Discussion**

### **Growth rates of mysticetes, odontocetes and terrestrial artiodactyls**

In order to place various ontogenetic events associated with the teeth-to-baleen transition in a broader context, growth curves were constructed to enable comparison of mysticete growth patterns with those of close relatives, namely odontocetes and terrestrial artiodactyls. The growth trajectories compiled in Figure 2.3 in general follow the pattern previously described by Laws (1959) and Frazer and Huggett (1973), with odontocetes having slower growth rates than mysticetes. Frazer and Huggett (1973) argued that mysticete prenatal growth is linear after the embryonic stage, while the results of Laws (1959) are in agreement with the present findings, with an accelerated growth rate in the last portion of gestation. This is mostly due to the different approaches that those previous authors used to construct the growth curves. Authors of both papers agreed that the difference between mysticetes and odontocetes is probably caused by differences in ecology and behavior between these two groups. They argue that odontocetes, for the most part, feed on prey that is available all year round while most mysticetes migrate from polar regions to tropical and temperate waters to follow their prey. Such variations could also be due to diverse ecological adaptations, as for example, some species migrate further than others between breeding and feeding grounds (Corkeron and Connor, 1999). As phylogeny could also play a role, Balaenidae and Neobalaenidae should be included in future studies given their different feeding strategy and more restricted distribution (Rosenbaum et al., 2000, Kemper, 2002, Rugh et al., 2002) in addition to Balaenopteridae and Eschrichtidae represented in this work. As specified earlier, the growth curves provide only a general approximation of the growth pattern, and the ages estimated for the single specimens should be taken with caution. For example, embryonic and early fetal specimens age from conception is harder to estimate given the very small variations in total length of the fetus during these initial stages of gestation.

Very little is known regarding the growth rates of other artiodactyls (Fig. 2.4). One exception is Frazer and Huggett (1974) who compiled a list of growth rates in cetaceans as well as several lineages of placental mammals. Those authors found overall slower growth rates in terrestrial artiodactyls than in cetaceans. The formula they employed however takes into account total gestation time and weight of the fetus as part of the equation. This does not allow for a proper comparison between large mysticetes or sperm whales and smaller ungulates (i.e. cattle, sheep or pigs). Using a logarithmic scale to normalize length data minimizes this problem and therefore allows for a direct comparison of growth rates. By doing this, it emerges that baleen whale grow at similar rates as terrestrial artiodactyls, but faster than toothed whales. It is thus possible to hypothesize that the higher growth rate during gestation in mysticetes, while possibly explained by physiological and environmental factors, such as the water support of their body mass that allows the pregnant mother to spend less energy while carrying the fetus (Frazer and Huggett, 1973, Frazer and Huggett, 1974), might be related to their evolutionary history. The slower growth rate of odontocetes might instead be a characteristic trait of the group. This is also supported by comparing growth rates and neonate length in a phylogenetic context (Fig. 2.5). The size of newborn clearly appears not to have a major influence on gestation length and growth rate in Cetacea, and it is likely that more complex intrinsic (i.e. genetic) and extrinsic (i.e. ecological) factors control this variable. More data are needed to definitively test this hypothesis, but an ancestral state reconstruction using an expanded dataset of the log-transformed growth rates of Cetacea, terrestrial artiodactyls and other related mammals such as perissodactyls could better inform the role of phylogeny in the evolution of growth rates in mammals and their ecological significance. Other features of their ontogeny, such as ossification sequence, should also be tested to understand physiological differences among Cetartiodactyla.

### **Ossification sequence of mysticetes, odontocetes and terrestrial artiodactyls**

The skull ossification sequence described in the humpback specimens is in overall agreement with Ridewood (1923) and Hampe et al. (2015). All dermal and endochondral bones were identified beginning in Hf2 (Fig. 2.8) at Fetal Stage 21 (Ridewood, 1923, Hampe et al., 2015, Lanzetti et al., 2018). The dermal bones of the anterior portion of the skull ossify first, along with the supraorbital process of the frontal. The dentary shows advanced ossification already in the embryonic specimen of the series, so it may be the first element to begin this process. Similarly, in the minke whales all major skull elements have already started to ossify by Fetal Stage 22 (Mf3 – Fig. 2.9), with the mandible being completely ossified at this stage. Given the extent of the ossification, it appears that the dermal bones of the anterior portion of the skull start ossifying earlier than the endochondral and intramembranous elements of the neurocranium also in these taxa. On a larger scale, this is in agreement with the general pattern of mammalian ossification, in which the dermal bones appear to develop before the endochondral ones starting from the earliest common ancestor (Smith, 1997, Koyabu et al., 2014). In related taxa, this was also found to be the case in the pantropical spotted dolphin (Moran et al., 2011), in the sperm whale (Kuzmin, 1976) in and terrestrials artiodactyls such as pigs (Hodges, 1953) and sheep (Harris, 1937), as all show an earlier ossification of the facial elements of the skull, with premaxilla, maxilla, dentary and frontal starting to ossify in the initial stages of the gestation. Similarly, in these animals, the mandible is likely the first element to complete ossification.

The endochondral elements and the intramembranous posterior portion of the skull start ossifying in the early fetal stages, with the supraoccipital, the parietal and the squamosal already being visible between Carnegie stage 19 and Fetal stage 20 (Hf1 – Fig. 2.7) in the humpback whale. The nasals also appear at this stage. It is not possible to recognize any of these elements before Fetal Stage 22 in the minke whales due to CT scan quality, but from their size it appears



that they started ossifying before this stage, likely at the same time as in the humpback whale. In odontocetes (pantropical spotted dolphin and sperm whale), the nasals appear in the last embryonic stages, so slightly earlier than in mysticetes (Kuzmin, 1976, Moran et al., 2011). Aside from this, early ossification sequences of baleen and toothed whales are similar by all available accounts (Lanzetti et al., 2018, Lanzetti, in press). This conclusion is apparently in contrast with Hampe et al. (2015), who instead reported that the baleen whales start ossification of endochondral elements earlier dolphins, based on their specimen description for the humpback whale and Moran et al. (2011) for the pantropical spotted dolphin. However, this result is caused by an incorrect staging of the samples in their study: they assumed that only the two smallest samples in their series lie between the embryonic and fetal stage. However the specimens that Hampe et al. (2015) described were not examined directly, using the evidence collected here it is possible to estimate that all six of their specimens are still in the embryonic stages of development, with the largest one likely in late Carnegie Stage 19, similar to Hf1. Instead, when considering the sequence of pig and sheep ossifications, major differences are undoubtedly found. Both groups of cetaceans have a much earlier onset of ossification of the nasals compared to terrestrial artiodactyls, as in both the pig and sheep they first appear in advanced fetal stages (Harris, 1937, Hodges, 1953). Another bone that appears earlier in Cetacea than in some other artiodactyls is the supraoccipital. In the both baleen and toothed whale taxa examined, it starts ossifying in the embryonic stages (Kuzmin, 1976, Moran et al., 2011, Lanzetti et al., 2018, Lanzetti, in press). In sheep, the supraoccipital begins ossifying relatively early as well, just after the anterior dermal bones (Harris, 1937). In pigs instead, it only starts ossifying with the nasal bones, after the parietal and when the rostral bones are mostly complete (Hodges, 1953). The early onset of the ossification of the endochondral elements in the dolphin has already been quantified as significantly different from the ossification of other artiodactyls using the dataset

presented by Moran et al. (2011). In particular, the early formation of the supraoccipital has been linked to a higher encephalization quotient (EQ) in all mammals, with the pantropical spotted dolphin being a prime example of this, due to its relatively large brain (Koyabu et al. 2014). However, mysticetes do not share the same high EQ present in odontocetes (Boddy et al., 2012). Therefore, given that now two mysticete species were shown to exhibit this trait, one can hypothesize that early ossification of the supraoccipital was acquired in the common ancestor of Neoceti (modern toothed and baleen whales), rather than being convergently evolved by both lineages like telescoping (Churchill et al., 2018). In Chapter Three, this and other hypotheses connected with difference in ossification timing of major skull bone elements will be tested quantitatively, by combining the evidence collected in this work on baleen whales with previously published data for other cetaceans and terrestrial artiodactyls (Kuzmin, 1976, Koyabu et al., 2014).

These new data also shed light on the homology and presence of specific bone elements in rorquals. Starting with specimen Hf2, the interparietal can be identified in all humpback whale specimens. In minke whale, it is visible in the fetuses from FS22 to FS25 (Mf3 to Mf6) and appears to have been covered by the advancing anterior end of the supraoccipital at later stages (Mf7 to Mf10). The presence of this bone in mysticetes has been controversial, while it is clearly identifiable in odontocetes especially in fetuses and juveniles (Mead and Fordyce, 2009, Moran et al., 2011). Eschricht (1849) recognized the bone in a fetal specimen of minke whale and Wada et al. (2003) identified its presence in adult skulls of Omura's whale (*Balaenoptera omurai*), a recently identified species closely related to Bryde's whale (*B. edeni*). Honigsmann (1917) described in detail the ossification of the neurocranium of two early fetal specimens of humpback whale, but does not mention the presence of the interparietal. Ridewood (1923) identified it in a dissected skull of sei whale but clearly states that it does not appear in the humpback whale

specimens he described. Hampe et al. (2015) also did not recognize this bone in their *M. novaeangliae* samples. Given that clearly two ossification centers are present in the area of the parietal in Hf2, Hf3 and Hf4, and that the interparietal is conclusively present in at least some portions of the ontogeny of other three species of rorqual whales, this element should be identified and coded as a separate bone also in humpback whales (Lanzetti et al., 2018, Lanzetti, in press).

Examining instead larger evolutionary patterns, sequence of ossification and suture closure in the skull during prenatal development are probably connected to the peculiar arrangement of the neurocranial bones observed in Cetacea, telescoping (Roston and Roth, 2019). This feature has evolved convergently in both cetacean lineages, However in odontocetes it is more extreme and it has been associated with echolocation (Miller, 1923, Armfield et al., 2011, Churchill et al., 2018, Roston and Roth, 2019). Baleen whales possess an apomorphic structure, the infraorbital process of the maxilla, which probably does not allow for the complete overlap of the maxilla on the frontal as seen in toothed whales (Deméré et al., 2005). In the early fetal specimens of the pantropical spotted dolphin, Moran et al. (2011) recognized the onset of telescoping as an initial overlap of those two bones. The infraorbital process is already ossified in FS22 in the minke whale but does not completely fuse to the frontal posteriorly even in the oldest specimen (Mf10 – Fig. 2.13) (Lanzetti, in press). This is similar to what is observed in the humpback whale, where it is recognizable at the beginning of fetal development (Hf1), but is still not articulated with the frontal posteriorly in the oldest specimen described (Hf4), in line with the findings of Ridewood (1923) and Hampe et al. (2015) (Lanzetti et al., 2018). The lack of suturing between this process and the frontal, as well as the late closure of the fontanelles in the neurocranium, which only ossify at FS26 in minke whales, are probably what allows the partial telescoping observed in mysticetes, together with the anterior movement of the occipital shield.

This pattern is clearly shared at least by rorqual whales, as Ridewood (1923) also found the neurocranial sutures open in a blue whale specimen of comparable age with Hf4 (193 cm TL, ca. 5 months f.c., 42% total gestation time), which also displayed a similar degree of ossification. The late closure of sutures also possibly facilitates rostral elongation in later stages of ontogeny and postnatally, which was shown to occur by Nakamura and Kato (2014). Further investigation of the late stages of prenatal development of both cetacean groups should be done to test this connection. Most available information on suture closure come from the analysis of postnatal ontogeny, where it is known that there are major differences between baleen and toothed whales. In many dolphin species, the braincase elements are already fused at birth, and suturing of rostral elements progresses until the late juvenile stages (Perrin, 1975, Perrin and Heyning, 1993). In mysticetes instead, the rostral bone sutures remain open for their entire life, which might also contribute to the elongation of the rostrum after birth. In the neurocranium, all sutures are closed at birth except those between the occipital elements (supraoccipital/exoccipital, exoccipital/basioccipital, basioccipital/basisphenoid) (Walsh and Berta, 2011). Therefore, analyzing in detail the timing of suture closure prenatally would probably provide more information to understand the differences in development that influence the skull anatomy in adult mysticetes and odontocetes, given that the ossification sequence of the bone elements appears mostly conserved (Lanzetti et al., 2018, Roston and Roth, 2019, Lanzetti, in press).

### **Teeth-to-baleen transition in humpback and minke whales and other mysticetes**

#### *Tooth formation and resorption*

Several shared patterns emerge by the analysis of the dentition morphology in humpback and minke whales. All specimens aged from Carnegie Stage 18 to Fetal Stage 26 possess tooth germs in both jaws, even if image resolution does not allow to observe them in the youngest minke whale specimen of the series (Mf1). While the growth series of humpback whale described

here terminates at FS24 (Hf4 – Fig. 2.10), it is likely that tooth germs are present also in later stages in this species, given the high tooth count observed in the sample and that they were described in a slightly larger specimen by Eschricht (1849) (114 cm TL, ca. 6 months f.c., 53% gestation). Using diceCT it is possible to better visualize the tooth germs compared to traditional CT, as highlighted by comparison of the present data with Hampe et al. (2015), in which no teeth were observed in specimens that should have them based on their estimated age. The number of germs in the lower jaw is always fewer than in the upper jaw. However this might be partly due to preservation given that the dentary is usually broken or damaged in the specimens, it is consistent with previous descriptions of fetal mysticetes. The mandibular tooth germs are also smaller than those in the maxilla (Ridewood, 1923, Karlsen, 1962, Ishikawa and Amasaki, 1995, Ishikawa et al., 1999, Thewissen et al., 2017, Lanzetti et al., 2018, Lanzetti, in press). The dentition in the lower jaw can be defined as heterodont given the presence of “double teeth” and the size gradient of the germs, which become smaller moving toward the anterior end of the rami. In the upper jaw instead, the tooth germs appear to be similar in shape and size along the tooth row, However it is not possible to confidently comment on the precise shape of each visible tooth germ due to CT imaging resolution. Heterodont dentition in the mandible has been observed in all other fetal balaenopterids for which data are available (e.g. Van Dissel-Scherft and Vervoort, 1954, Karlsen, 1962), and its absence in the upper jaw has recently been linked to baleen development in the bowhead whale (Thewissen et al., 2017). The homodont and polyodont tooth pattern in the upper jaw could be linked to this process since tooth germs and baleen share part of their genetic developmental pathway. The growth factor FGF-4 was found to be activated in the tissues surrounding both teeth and rudimental baleen tissue even after all tooth germs were resorbed. This could imply that tooth patterning in the upper jaw is still under selection, due to the need of expressing this gene to develop a full baleen rack. The same constraints do not apply to the

mandibular tooth germs where no baleen is present (Thewissen et al., 2017). Gene expression and focused histological studies are needed to confirm that these conclusions apply to the minke whale as well, but these species could be perfect candidates for such research given the present knowledge on their tooth development.

Regarding the start of tooth resorption, size and count of the germs can be used to estimate when this process begins in the absence of histological data. They increase significantly in size, both absolutely and proportionally relative to the rest of the skull, up to specimen Hf2 (Fetal Stage 20) in *M. novaeangliae* and up to Mf6 (Fetal Stage 25) in *B. bonaerensis/acutorostrata* (Table 2.7). After those stages, the germs grow slightly in absolute diameter – measured as average diameter in dorsal view in the mid portion of the tooth row –, but they did not grow proportionally to the rest of the head or body. However preservation issues and image quality might partially affect this assessment, it is clear that the main phase of tooth formation is concluded by mid-gestation. This is in line with the findings of Ishikawa and Amasaki (1995) and Ishikawa et al. (1999), who observed the termination of tooth development and the start of degradation in specimens of Antarctic minke whale between 70 and 90 cm in TL (5-6 months f.c., 55-66% gestation). The present findings would suggest that in the humpback whale this shift happens slightly earlier, when taking into account the longer gestation time of this species. A larger dataset including more specimens and detailed histological analyses are needed to pinpoint the start of tooth degradation in this species as no previous work is available for direct comparison. In other mysticetes, the start of tooth resorption has been placed at even earlier stages based on direct and indirect evidence. In the fin whale, Van Dissel-Scherft and Vervoort (1954) and Karlsen (1962) identified resorbing germs starting around the fourth month of gestation, at the end of the first third of the pregnancy. However, Karlsen (1962) only noticed the complete absence of teeth in a specimen of eight to nine months of pregnancy, pointing to the fact

that even if resorption starts early, it is only completed in the last one third of gestation. No mention of the presence of baleen is provided in both papers. For the blue whale, from the accounts of Ridewood (1923) and Fudge et al. (2009) it appears that teeth are completely resorbed in this species around mid-gestation (ca. 6.5 months f.c., 55% gestation), when the transversal process of baleen is erupted from the gums. This implies that in taxon the process of tooth resorption either starts earlier or it is highly accelerated, as by the time that the baleen erupt from the gums all germs are resorbed (Fudge et al., 2009, Lanzetti, in press). However, only four specimens at late fetal stages of blue whale are described in the literature. Therefore, these major discrepancies, even with the similar sized fin whale, might be due to the lack of sampling, misidentification or individual variation. An expanded dataset including prenatal specimens of other rorqual species at advanced stages of development is needed to test these hypotheses on the timing of tooth resorption and to understand the possible biological significances of these differences.

Outside of Balaenopteridae, the only description of the teeth-to-baleen transition during ontogeny was provided by Thewissen et al. (2017) for the bowhead whale (Balaenidae). As mentioned earlier, those authors looked at the expression of developmental growth factors in the jaws of bowhead whales. They found no tooth germs present in a specimen of 159 cm in length (ca. 6.5 months f.c., 47% gestation – Reese et al., 2001). Thus, in this species the resorption of teeth would also occur early in the fetal period, at a comparable time as the blue whale.

Phylogenetic constraints, which also concern independent mutations and inactivations in genes involved in tooth and enamel formation (Meredith et al., 2011, Meredith et al., 2013, Springer et al., 2016), as well as physiological differences in gestation timing might be responsible for the hypothesized variation among taxa.

Regarding the development of dentition in dolphins, Armfield et al. (2013) provided definitive evidence that tooth germs only develop in this group after Carnegie Stage 17 by examining histological sections of pantropical spotted dolphin. Moran et al. (2011) found that tooth germs had not yet mineralized in the first fetal stage in the same odontocete species, with the first teeth appearing only in their larger specimen at Fetal Stage 21/22. This places the initial development of tooth germs in dolphins at later stages than in baleen whales, where they are recognizable and mineralized at least at Carnegie Stage 18 (He1 – Fig. 2.6) in the humpback whale, and also present from the embryonic stages in other Balaenopteridae (Karlsen 1962; Ishikawa and Amasaki 1995) and in the bowhead whale (Thewissen et al. 2017). The early formation of dentition in mysticetes might be associated with their later resorption and replacement with baleen. Changes in timing of tooth formation across Cetartiodactyla will be quantitatively analyzed in Chapter Three.

### *Baleen development*

In minke whales, the formation of baleen rudiments as a denser tissue medial to the tooth germs is first observed in FS25 (Fig. 2.16). It is linked to external anatomical changes in the gingival ridge of the upper jaw, which enlarges medially before forming a distinct keel at FS26 (Fig. 2.17) (Lanzetti, in press). This is in line with previous histological evidence presented by Ishikawa and Amasaki (1995) and by the observations reported by Sawamura (2008), and confirms that dentition and early baleen tissue (rudiments) can be found together in the upper palate of fetal minke whales for a short period of their development, between six and 8 months from conception. Baleen formation in ontogeny is poorly understood, and it has not been studied in most species of Mysticeti, due to specimen availability and consequent methodological limitations. Slijper (1976) also noticed the presence of an elevated ridge in early to late fetal specimens of fin whale, while tooth germs are still present (Karlsen, 1962). Thewissen et al.



(2017) noted that baleen tissue starts developing from the medial side of the dental lamina in the bowhead whale, supporting the hypothesis that baleen indeed developed from periodontal tissue rather than from the palatal mucosa. These authors also noted an increased vascularization in the posterior portion of the palate in specimens presenting early developing baleen. In the bowhead whale, early sign of baleen development can be observed in a specimen at FS21 (ca. 2 months f.c., 15% gestation – Reese et al., 2001). This might be an intraspecific difference or might be due to the preservation of the specimens and different study methodologies.

Some information is also available on the early development of baleen plates once they are visible in the gums (FS27 – Fig. 2.18). In both the blue (Fudge et al., 2009) and the minke whale, the connective tissue plates are placed transversely to the main axis of the palate, with depressions between them. There is also a depression at the center of the ridge, which might be connected with the eruption pattern of the baleen from the gum. A major difference between the observations of Fudge et al. (2009) and those made in the minke whale in this work and by Sawamura (2008) is that in the blue whale it appears that baleen starts developing at the center of the palate, with the posterior and anterior ends of the ridge appearing less thickened, while in the minke whale the transversal process appears consistently more developed at the posterior end. This might be an interspecific difference, however all hypotheses should be considered with caution given the very limited available sample size. Thewissen et al. (2017) noted that the zone of baleen growth expands caudally in bowhead fetuses, possibly implying that this species also has a posterior-to-anterior baleen development pattern, even if the adult bowhead has a very different baleen rack structure compared to rorqual whales due to their different filter feeding style (Berta et al., 2016, Werth et al., 2018). Given the available information and the phylogenetic position of these species, with the Balaenidae representing the earliest diverging mysticete lineage and the minke whale the earliest diverging lineage of Balaenopteridae (Gatesy et al.,

2013), it is possible to tentatively hypothesize that the posterior-to-anterior development of baleen is the ancestral condition in mysticetes, and that in the blue whale and possibly in other later diverging rorquals it has been modified, with the center of the palate now developing first. More evidence is needed from other species of balaenopterids and different families (Eschrichtiidae and Neobalaenidae) to confirm this hypothesis.

Overall, these discrepancies in timing of tooth formation, resorption and baleen development appear to be connected both to phylogenetic relationships and to physiological differences, such as gestation length and body size. It would be necessary to analyze with comparable methods ontogenetic sequences of all species of baleen whales, as well as additional odontocetes and terrestrial artiodactyls, to definitively assess when these events occur in the prenatal development of Mysticeti and what is the influence of phylogenetic constraints on this pattern.

### **Skull shape development and implications for baleen whale feeding adaptations**

#### *Braincase ad rostrum*

By analyzing the landmark configurations of the whole skull and the rostrum in dorsal view at different ontogenetic stages in both taxa (Fig. 2.19-2.20), several major patterns stand out: rostral elongation, rostral tapering, telescoping (i.e. relative posterior movement of the nasals and anterior movement of the supraoccipital), and movement of the postglenoid process of the squamosal, which occurs in different directions in the two species (Lanzetti et al., 2018, Lanzetti, in press). Focusing on the minke whales' growth series, the same trends emerge when visualizing the results of the PCA (Fig. 2.21-2.22), with most of the variation representing the characteristic changes through development highlighted in the DA. This is the first time that similar analyses have been performed on prenatal cetacean specimens, therefore a direct comparison with closely related taxa is not possible. However, similar broad trends of rostral elongation and telescoping

characterize the fossil record of Mysticeti (Berta et al., 2016, Lanzetti et al., 2018) and this connection between skull development and evolution will be explored in Chapter Three with the inclusion of extinct taxa in the dataset.

Comparing the development of braincase and rostrum in minke whales, the shape changes in the two regions of the skull result to be connected but still partially independent (Fig. 2.23). Overall, the rostrum undergoes most of its shape development in the early fetal stages, while the braincase mostly transforms in the late fetal period. This is evident when comparing both the two regions to each other (Fig. 2.24-2.25) and when relating them to overall skull size (Fig. 2.26). After birth, it is likely that the developmental patterns switch again, with the rostrum changing more significantly than the braincase. These results are likely influenced by the different nature of the shape modifications in the two skull regions: while the rostrum mostly elongates with only minor changes in curvature, the braincase bones undergo major shifts due to telescoping and the movement of the postglenoid process. The fact that two species are included in the series might also affect these observations. Once again, given that this work is the first attempt to quantitatively analyze skull shape change in cetacean ontogeny, it is not possible to compare these findings with similar studies. However, some research has been done on growth patterns in the skull of postnatal minke whales. During these later phases, the rostrum grows proportionally larger relative to the rest of the skull. This trend has been associated with transformations in feeding strategy, as the calf matures and goes from weaning to actively filter feed. The braincase However does not change proportionally to the rostrum, and even becomes smaller compared to overall skull size (Nakamura and Kato, 2014, Franci and Berta, 2018). These combined trends show that the enlargement of the buccal cavity, a key feature especially for the feeding mode of the rorqual whales, drives the development of the rostral elements. While rostral growth is initiated during early prenatal development, ontogenetic changes are mostly are mostly

concentrated in the braincase region to achieve telescoping in the late fetal stages. As noted before, the sutures in the rostral region of the skull remain open for the entirety of baleen whale life, while most of sutures in the neurocranium are ossified at birth (Walsh and Berta, 2011). This pattern of suture closure, as well as the ossification sequence of the bones, likely drives the recorded pattern of shape change in ontogeny. The sample size of the present study is not sufficient to conduct significant analyses to quantitatively compare the overall skull shape development in the two examined taxa. It is possible However to put this data in the context of mysticetes evolution by including isolated specimens of other living baleen whale taxa in the analysis as well as skulls of extinct stem-mysticetes. This will be done in Chapter Three to test hypothesis on the influence of major processes such as allometry and modularity on the evolution of this group (Goswami and Polly, 2010b, Klingenberg and Marugán-Lobón, 2013).

An analysis of skull shape development in fetal specimens of other species of mysticetes with different filter feeding adaptations should be performed to test if similar patterns are observable in their ontogeny, or if most diverging features appear postnatally. Given the current evidence, it can be hypothesized that the general skull shape growth patterns are shared by at least all Balaenopteridae, as they all employ a similar filter feeding style (Berta et al., 2016, Kahane-Rapport and Goldbogen, 2018). The other living families of Mysticeti employ alternative filter feeding strategies: bowhead and right whales (*Balaena mysticetus* and *Eubalaena* spp. – Balaenidae) and the pigmy right whale (*Caperea marginata* – Neobalaenidae) are skim feeders, as they capture plankton from the water by swimming slowly with their mouth open. Instead the gray whale (Eschrichtiidae) feeds prevalently on benthic invertebrates by filtering its prey from the sediments while lying on one side, utilizing lateral suction feeding (Berta et al, 2016, Werth et al., 2018). These different feeding modes have been shown to require major differences in filtration area and associated buccal size, as well as overall skull shape (Bouetel, 2005, Werth et

al., 2018). Given the strong ecological and evolutionary pressure on adult mouth shape, several developmental processes likely played a role in the evolution of modern mysticete anatomy. A developmental process that has been shown to have driven the evolution of many mammalian lineages is heterochrony, a broad concept that describes all variations in relative timing of development in different features (McNamara, 1986, Smith, 1997, Klingenberg, 1998, Bininda-Emonds et al., 2003, Goswami, 2007). It has been demonstrated that heterochrony, in the form of changes in skull shape development rate after birth, is an important driver of species divergence in many odontocete genera (Galatius, 2010, Sydney et al., 2012, del Castillo et al., 2017). Tsai and Fordyce (2014) hypothesized that this same process is connected to the diversification of modern baleen whale taxa. The authors speculated that the two main types of heterochrony, paedomorphosis and peramorphosis (McNamara, 1986), provided the basis for the characteristic skull shapes observed in two families of modern Mysticeti that occupy different feeding niches, Neobalaenidae and Balaenopteridae. They hypothesized that the pygmy right whale exhibits a paedomorphic skull shape, as the adult seems to retain many features of the juvenile morphology, while Balaenopteridae such as the humpback whale would display the opposite trend, peramorphosis, in which adults undergo a longer or accelerated development that allows them to progressively acquire new traits. Their study focused on few specimens, mainly postnatal, and did not include the common ancestor of the species considered, and therefore the role of heterochrony in the diversification of baleen whales could not be assessed definitively (McNamara, 1986, Klingenberg, 1998). However, it demonstrated that major lineages of baleen whales tend to follow different developmental paths, with their distinctive skull shapes already noticeable in the fetal stages of ontogeny. In Chapter Three, the possible influence of heterochrony on mysticetes evolution will also be tested using the expanded dataset containing fossil taxa.

## *Mandible*

While most research efforts have been focused on the upper jaw anatomy, the mandible, however it is completely toothless and does not present baleen plates or other structures, also plays an important role in feeding among living mysticetes (Pyenson et al., 2013). By qualitatively assessing the dentary shapes in the samples, it is possible to notice that they progressively acquire their characteristic lateral curvature: the minke whale specimens display a clear curvature starting at FS21/22 (Mf3), and the ligamentous symphysis at the anterior end is present starting at FS26 (Mf7, Mf8). While the humpback whale specimens are probably too young to possess a distinguishable symphysis, the lateral curvature of the mandible is evident at FS20 (Hf2) and close to the adult proportions at FS24 (Hf4) (Fig. 2.27 – Lanzetti et al., 2018). It is possible that at this stage the symphysis is also forming, however further specimens must be analyzed to confirm it. Ridewood (1923) also reported that the mandible is the first bone to ossify completely in this species and to assume a progressively more curved shape as the development progresses. Therefore, while the rostrum assumes its adult shape and curvature at late stages of gestation, the dentary seems to reach its final adult proportions and curvature earlier. This has interesting evolutionary implications since among fossil mysticetes evolution of the unfused mandibular symphysis precedes the evolution of distinctive rostral characters of mysticetes, such as the lack of fusion between the premaxilla and maxilla (Deméré and Berta, 2008, Berta et al., 2016). Unfortunately, the mandibles are dislocated or broken in the majority of specimens, so no quantitative analyses can be conducted on the lower jaws. However, some previous hypotheses on the changes that occur in the lower alveolar canal during ontogeny can be tested using the more complete developmental sequence of the minke whales. Peredo et al. (2017b) investigated the internal anatomy of the mandible in baleen and toothed whales compared to terrestrial

artiodactyls, and formulated hypotheses on the homology of the internal mandibular canal in mysticetes.

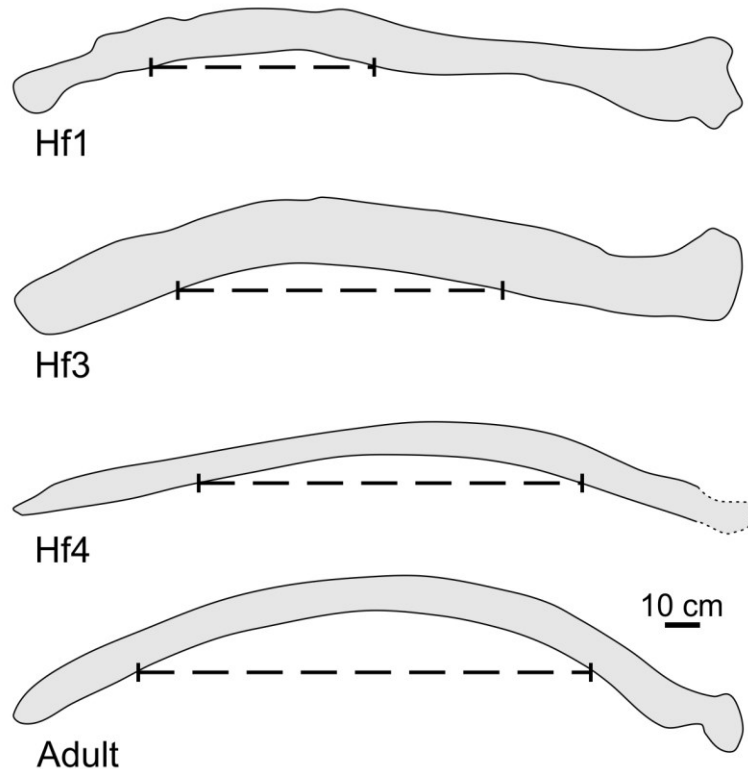


Figure 2.27 – Change in mandible curvature during development of the humpback whale. The curvature is a feature clearly present in Hf3. In Hf4 the dentary is very close to its adult shape. Fetal mandibles are in ventral view while the adult is in dorsal view. The best-preserved ramus was chosen for each specimen. The silhouettes were mirrored to provide a better visual comparison and scaled to the size of the adult. Long-dashed line represents the chord of the arch formed by the curved area. Original of the adult mandible from Clapham and Mead (1999). Figure modified from Lanzetti et al. (2018).

Using the developmental data presented here, their observation that the mandibular canal is positioned more dorsally in mysticetes, and that it moves progressively in this direction during development as the alveolar canal closes and tooth germs resorb can be confirmed. They also hypothesized that the branching canals dorsal to the main mandibular canal in mysticetes are not homologous to those supplying blood to the teeth of toothed whales and terrestrial artiodactyls, given that the process of tooth resorption and associated bone remodeling would not allow them to reach the bone surface in adults. In the minke whales, the dorsal alveolar canal containing the

tooth germs mostly closes by the last stages of gestation, but smaller canals that connect the alveolar canal with the main internal mandibular canal are always visible and do not drastically change before and after tooth resorption (Fig. 2.28). From this evidence and recently collected data on other toothless mammals (Ferreira-Cardoso et al., 2019), the smaller canals appear unequivocally homologous to the ones observed feeding the alveoli in toothed taxa, including Odontoceti. They have therefore been coopted for some other functions in both baleen whales and other toothless taxa such as anteaters.

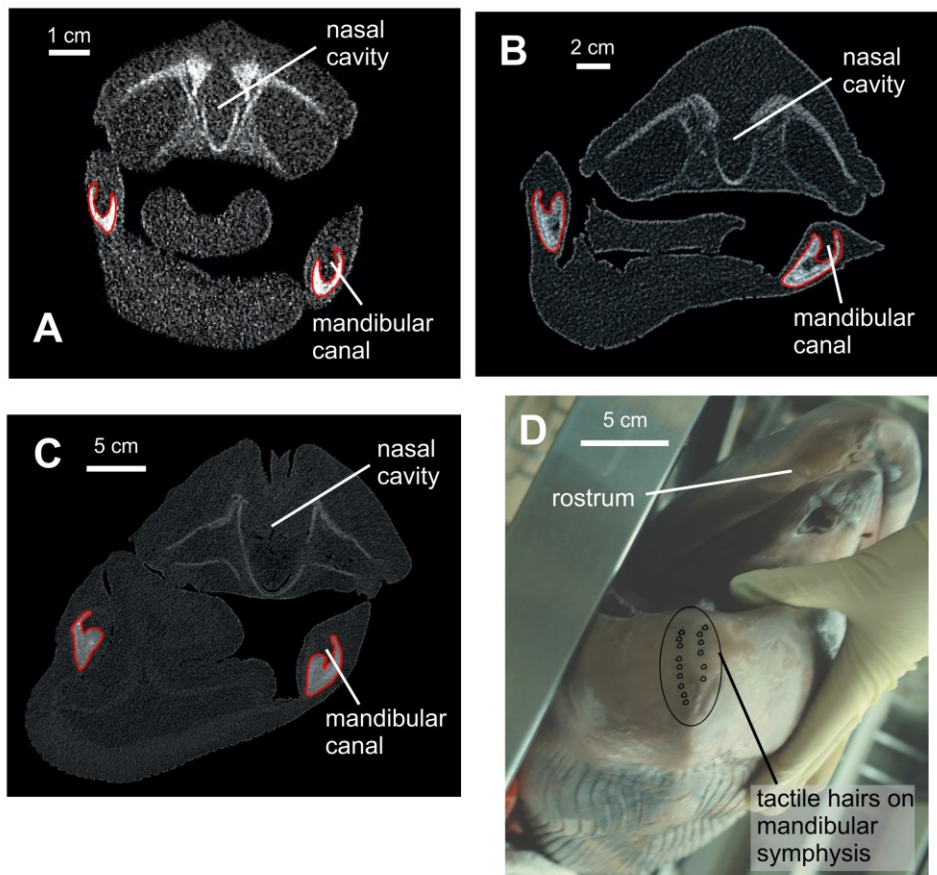


Figure 2.28 – Prenatal changes in mandibular canal and development of sensory organ at anterior end of mandible in minke whales. A: CT slice of cross section at mid-length of rostrum of Mf3, B: CT slice of cross section at mid-length of rostrum of Mf6, C: CT slice of cross section at mid-length of rostrum of Mf10, D: close-up of anterior end of the mandible of Mf9 showing a concentration of tactile hairs. From the youngest (Mf3) to the oldest (Mf10) specimen, the mandibular canal (labeled) becomes smaller and the mandibular bone (delimited in red) grows thicker. From the external morphology of Mf9, it appears that the sensory organ found in adult Balaenopteridae is already present in the late fetal stages at least, and it can explain the retention of a wide mandibular canal even when tooth germs are completely resorbed (Mf10).



The retention of these canals is most likely related to the presence of sensory organs and keratinous structures in the mouth of these animals (Ferreira-Cardoso et al., 2019). As proposed by Peredo et al. (2017b), the canals in adult mysticetes probably supply blood and innervate sensory structures present on the mandible. Many tactile hairs are present at the tip of the symphysis especially in the late developmental stages (Fig. 2.28), hinting to the presence of a sensory organ in this region, as previously observed in adult Balaenopteridae (Pyenson et al., 2012). More data are needed to reconstruct the precise anatomy of the internal mandibular canals during ontogeny, but this dataset could serve as the foundation to directly test the homology of this structure as well as similar questions on other skull features between mysticetes and related taxa. Studies on other baleen whale species are also needed to test these hypotheses in all mysticetes and stem fossil taxa with more confidence.

## Conclusions

This research documents the teeth-to-baleen transition and associated skull changes in baleen whales. The first detailed anatomical description of the ossification sequence of the humpback whale and of skull shape ontogeny of the Antarctic and common minke whales is presented. The observations on the changing features of these species are related to other Cetacea, and Artiodactyla, by combining qualitative and quantitative methods and using newly compiled growth curves to better compare our dataset with previously described specimens.

Primarily, these data help illuminate the pattern of tooth resorption and baleen growth, by confirming and expanding on previous data (e.g. Ishikawa and Amasaki, 1995). Tooth germs appear in the very early fetal stages, then, at least in minke whales, after mid-gestation a denser material, interpreted as a precursor of baleen development and referred as “baleen rudiments”, starts developing medially to the resorbing tooth buds. By the start of the last one-quarter of gestation, the transversal process of the baleen is erupted, starting at the posterior end, and no tooth germs are present (Fig. 2.29). This transition is matched by changes in the external appearance of the borders of the palate: first gums develop, then they enlarge medially, forming a distinct ridge at the center, at the same time as the denser tissue is visible internally, and finally only the ridge containing the baleen is visible (Fig. 2.29). Overall, the skull ossification pattern and shape changes are similar to in the two taxa, However no quantitative comparisons of shape were possible due to the limited sample sizes (Lanzetti et al., 2018, Lanzetti, in press).

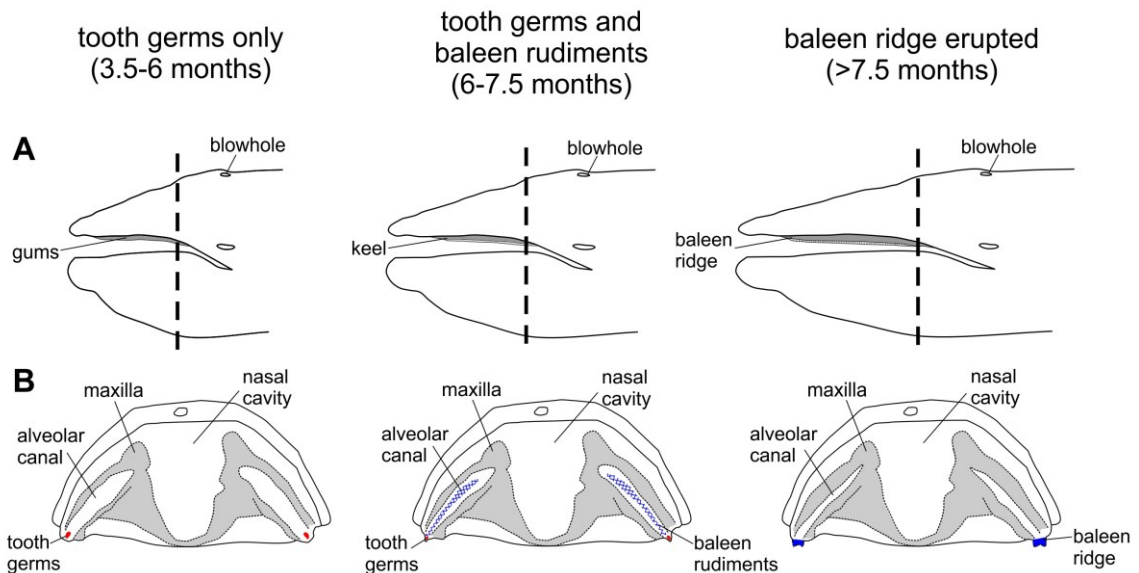


Figure 2.29 – Schematic representation of the external and internal changes during the teeth-to-baleen transition at different stages of development in minke whales. A: simplified lateral view of external morphology of the head of a minke whale fetus at different growth stages, B: simplified cross section of internal morphology of the rostrum of a minke whale fetus at different growth stages. In A, gums region is highlighted in grey to best represent changes. In B, ossified maxilla in grey, tooth germs in red, baleen rudiments area dashed in blue and white, baleen in blue. Dashed line in A indicates the location of the cross section in B for each stage. The drawings are not to scale. From Lanzetti (in press).

Quantitative investigation of skull shape changes shows that development potentially played a key role in the evolution of other characteristic traits of this lineage related to filter feeding, such as their large buccal cavity and elongated rostrum. A complex interaction of heterochronic patterns at different levels could explain the differences among modern species (Tsai and Fordyce, 2014). However, this hypothesis is not directly testable with the current dataset due to limited sample size.

More generally, a novel diceCT protocol was shown to provide better results when examining the internal anatomy of small fetal and embryonic specimens than traditional CT, allowing for a resolution comparable to dissection. The application of 3D morphometrics to the dataset allowed to visualize and quantify changes in internal anatomy, using a method that can be consistently applied in future research enabling direct comparisons among different studies.

A larger dataset consisting of multiple species of both mysticetes and odontocetes should be used to replicate the observations made in this work and to test the hypotheses derived from them. Numerous specimens at each developmental stage for every species should be included to account for intraspecific variation. Data from different species, especially from the other three extant clades of mysticetes, will also highlight interspecific differences in development and help reconstruct the ancestral skull ossification sequence of mysticetes. It would also be useful to employ a consistent method of staging in order to compare phylogenetically distant taxa more closely, but this issue is not unique to the present study (Werneburg, 2009). Future research should also include histological and gene expression analyses on the gum tissues of these specimens or comparable ones, to determine the composition of the denser tissue and confirm its connection with baleen development.

The observations presented here have implications for the evolution of mysticetes, especially regarding the teeth-to-baleen transition in fossil lineages (Deméré and Berta, 2008, Deméré et al., 2008, Peredo et al., 2017a). Therefore, in Chapter Three quantitative analyses of shape change and ossification sequence will be conducted to understand what role developmental mechanisms (e.g. heterochrony, allometry, modularity) played on the evolution of baleen whales. This will be done by integrating the present samples in an expanded 3D dataset including other mysticetes species as well as fossil taxa, and by comparing the ossification sequence information with data from odontocetes and terrestrial artiodactyls. This will allow for more definitive conclusions on the relationship between prenatal and fossil skull morphology in Mysticeti and expand the knowledge on the influence of ontogeny in tooth loss in mammals. The present CT dataset also offers additional possibility to investigate other aspects of prenatal skull ontogeny, such as patterns of suture ossification and soft tissue development, which could be explored in future studies.

## Literature cited

- Armfield BA, George JC, Vinyard CJ, Thewissen JGM** (2011) Allometric patterns of fetal head growth in mysticetes and odontocetes: comparison of *Balaena mysticetus* and *Stenella attenuata*. *Mar Mamm Sci*, **27**, 819-827.
- Armfield BA, Zheng Z, Bajpai S, Vinyard CJ, Thewissen JGM** (2013) Development and evolution of the unique cetacean dentition. *PeerJ*, **1**, e24.
- Bando T, Nakai K, Kanbayashi J, et al.** (2018) Results of the third biological field survey of NEWREP-A during the 2017/18 austral summer season. International Whaling Commission, 1-17.
- Berta A, Lanzetti A, Ekdale EG, Deméré TA** (2016) From teeth to baleen and raptorial to bulk filter feeding in mysticete cetaceans: the role of paleontological, genetic, and geochemical data in feeding evolution and ecology. *Integr Comp Biol*, **56**, 1271-1284.
- Bininda-Emonds ORP, Jeffrey JE, Richardson MK** (2003) Is sequence heterochrony an important evolutionary mechanism in mammals? *J Mamm Evol*, **10**, 335-361.
- Boddy AM, McGowen MR, Sherwood CC, Grossman LI, Goodman M, Wildman DE** (2012) Comparative analysis of encephalization in mammals reveals relaxed constraints on anthropoid primate and cetacean brain scaling. *J Evol Biol*, **25**, 981-994.
- Bouetel VV** (2005) Phylogenetic implications of skull structure and feeding behavior in balaenopterids (Cetacea, Mysticeti). *J Mammal*, **86**, 139-146.
- Brownell RL, Perrin WF, Pastene LA, et al.** (2000) Worldwide taxonomic status and geographic distribution of minke whales (*Balaenoptera acutorostrata* and *B. bonaerensis*). International Whaling Commission, 1-13.
- Churchill M, Miguel J, Beatty BL, Goswami A, Geisler JH** (2018) Asymmetry drives modularity of the skull in the common dolphin (*Delphinus delphis*). *Biol J Linn Soc*, **126**, 225-239.
- Clapham PJ, Ivashchenko YV** (2016) Stretching the truth: length data highlight falsification of Japanese sperm whale catch statistics in the Southern Hemisphere. *Roy Soc Open Sci*, **3**, 160506.
- Clapham PJ, Ivashchenko YV** (2018) Whaling catch data are not reliable for analyses of body size shifts. *Nature*, **2**, 756.
- Clapham PJ, Mead JG** (1999) Megaptera novaeangliae. *Mamm Species*, **604**, 1-9.
- Corkeron PJ, Connor RC** (1999) Why do baleen whales migrate. *Mar Mamm Sci*, **15**, 1228-1245.

- Cozzi B, Podestà M, Vaccaro C, et al.** (2015) Precocious ossification of the tympanoperiotic bone in fetal and newborn dolphins: an evolutionary adaptation to the aquatic environment? *Anat Rec*, **298**, 1294-1300.
- Davit-Béal T, Tucker AS, Sire J-Y** (2009) Loss of teeth and enamel in tetrapods: fossil record, genetic data and morphological adaptations. *J Anat*, **214**, 477-501.
- de Beer GR** (1937) *The development of the vertebrate skull*, The University of Chicago Press, Chicago.
- del Castillo DL, Viglino M, Flores DA, Cappozzo HL** (2017) Skull ontogeny and modularity in two species of *Lagenorhynchus*: morphological and ecological implications. *J Morphol*, **278**, 203-214.
- Deméré TA, Berta A** (2008) Skull anatomy of the Oligocene toothed mysticete *Aetiocetus weltoni* (Mammalia; Cetacea): implications for mysticete evolution and functional anatomy. *Zool J Linn Soc*, **154**, 308-352.
- Deméré TA, Berta A, McGowen MR** (2005) The taxonomic and evolutionary history of fossil and modern balaenopteroid mysticetes. *J Mamm Evol*, **12**, 99-143.
- Deméré TA, McGowen MR, Berta A, Gatesy J** (2008) Morphological and molecular evidence for a stepwise evolutionary transition from teeth to baleen in mysticete whales. *Syst Biol*, **57**, 15-37.
- Durham FE** (1980) External morphology of bowhead fetuses and calves. *Mar Fish Rev*, **42**, 74-80.
- Ekdale E, Deméré TA, Berta A** (2015) Vascularization of the gray whale palate (Cetacea, Mysticeti, *Eschrichtius robustus*): soft tissue evidence for an alveolar source of blood to baleen. *Anat Rec*, **298**, 691-702.
- Eschricht DF** (1849) *Zoologisch-anatomisch-physiologische Untersuchungen über die nordischen Wallthiere*, Verlag von Leopold Voss, Leipzig.
- Fahlke JM, Hampe O** (2015) Cranial symmetry in baleen whales (Cetacea, Mysticeti) and the occurrence of cranial asymmetry throughout cetacean evolution. *Sci Nat*, **102**, 58.
- FEI VSG** (2018) Avizo Lite: 3D analysis software for scientific and industrial data, version 9.5. Berlin: Konrad-Zuse-Zentrum für Informationstechnik
- Ferreira-Cardoso S, Delsuc F, Hautier L** (2019) Evolutionary tinkering of the mandibular canal linked to convergent regression of teeth in placental mammals. *Curr Biol*, **29**, 468-475.
- Fordyce RE, Marx FG** (2018) Gigantism precedes filter feeding in baleen whale evolution. *Curr Biol*, **28**, 1670-1676.
- Fox CH, Johnson FB, Whiting J, Roller PP** (1985) Formaldehyde fixation. *J Histochem Cytochem*, **33**, 845-853.

- Franci G, Berta A** (2018) Relative growth of the skull of the common minke whale (*Balaenoptera acutorostrata*) using a 3D laser surface scanner. *Aquat Mamm*, **44**, 529-537.
- Frazer JFD, Huggett ASG** (1973) Specific foetal growth rates of cetaceans. *J Zool*, **169**, 111-126.
- Frazer JFD, Huggett ASG** (1974) Species variations in the foetal growth rates of eutherian mammals. *J Zool*, **174**, 481-509.
- Fudge DS, Szewciw LJ, Schwalb AN** (2009) Morphology and development of blue whale baleen: an annotated translation of Tycho Tullberg's classic 1883 paper. *Aquat Mamm*, **35**, 226-252.
- Galatius A** (2010) Paedomorphosis in two small species of toothed whales (Odontoceti): how and why? *Biol J Linn Soc*, **99**, 278-295.
- Galatius A, Berta A, Frandsen MS, Goodall RNP** (2011) Interspecific variation of ontogeny and skull shape among porpoises (Phocoenidae). *J Morphol*, **272**, 136-148.
- Gatesy J, Geisler JH, Chang J, et al.** (2013) A phylogenetic blueprint for a modern whale. *Mol Phylogen Evol*, **66**, 479-506.
- Gignac PM, Kley NJ, Clarke JA, et al.** (2016) Diffusible iodine-based contrast-enhanced computed tomography (diceCT): an emerging tool for rapid, high-resolution, 3-D imaging of metazoan soft tissues. *J Anat*, **228**, 889-909.
- Glazier DS** (2013) Log-transformation is useful for examining proportional relationships in allometric scaling. *J Theor Biol*, **334**, 200-203.
- Goldbogen JA, Madsen PT** (2018) The evolution of foraging capacity and gigantism in cetaceans. *J Exp Biol*, **221**, jeb166033.
- Goswami A** (2007) Cranial modularity and sequence heterochrony in mammals. *Evol Dev*, **9**, 290-298.
- Goswami A, Polly PD** (2010a) The influence of modularity on cranial morphological disparity in carnivora and primates (Mammalia). *PLoS ONE*, **5**, e9517.
- Goswami A, Polly PD** (2010b) Methods for Studying Morphological Integration and Modularity. *Paleo Soc Pap*, **16**, 213-243.
- Goswami A, Polly PD, Mock OB, SÁNchez-Villagra MR** (2012) Shape, variance and integration during craniogenesis: contrasting marsupial and placental mammals. *J Evol Biol*, **25**, 862-872.
- Goswami A, Randau M, Polly PD, et al.** (2016) Do developmental constraints and high integration limit the evolution of the marsupial oral apparatus? *Integr Comp Biol*, **56**, 404-415.

- Goswami A, Smaers JB, Soligo C, Polly PD** (2014) The macroevolutionary consequences of phenotypic integration: from development to deep time. *Philos Trans R Soc Lond B Biol Sci*, **369**, 20130254.
- Goswami A, Weisbecker V, Sánchez-Villagra MR** (2009) Developmental modularity and the marsupial-placental dichotomy. *J Exp Zool Part B*, **312B**, 186-195.
- Hampe O, Franke H, Hipsley CA, Kardjilov N, Muller J** (2015) Prenatal cranial ossification of the humpback whale (*Megaptera novaeangliae*). *J Morphol*, **276**, 564-582.
- Harris HA** (1937) The foetal growth of the sheep. *J Anat*, **71**, 516-527.
- Hilaire EGS** (1807) Considerations sur les pieces de la tete osseuse des animaux vertebres, et particulierement sur les celles du crane des oiseaux. *Ann Mus Hist Natur*, **10**, 342-365.
- Hodges PC** (1953) Ossification in the fetal pig. A radiographic study. *Anat Rec*, **116**, 315-325.
- Hoffman EA, Rowe TB** (2018) Jurassic stem-mammal perinates and the origin of mammalian reproduction and growth. *Nature*, **561**, 104-108.
- Honigmann H** (1917) Bau und Entwicklung des Knorpelschadels vom Buckelwal. *Zoologica*, **69**, 1-85.
- Ishikawa H, Amasaki H** (1995) Development and physiological degradation of tooth buds and development of rudimental baleen plate in southern minke whale, *Balaenoptera acutorostrata*. *J Vet Med Sci*, **57**, 665-670.
- Ishikawa H, Amasaki H, Dohguchi H, Furuya A, Suzuki K** (1999) Immunohistological distributions of fibronectin, tenascin, type I, III and IV collagens, and laminin during tooth development and degeneration in fetuses of minke whale, *Balaenoptera acutorostrata*. *J Vet Med Sci*, **61**, 227-232.
- Ivashin MV, Mikhalev YA** (1978) To the problem of the prenatal growth of minke whales *Balaenoptera acutorostrata* of the Southern Hemisphere and of the biology of their reproduction. International Whaling Commission, 201-205.
- Julin C** (1880) Recherches sur l'ossification du maxillaire inferieur et sur la constitution du systeme dentaire chez le foetus de la *Balaenoptera rostrata*. *Arch Biol*, **1**, 75-136.
- Kahane-Rapport SR, Goldbogen JA** (2018) Allometric scaling of morphology and engulfment capacity in rorqual whales. *J Morphol*, **279**, 1256-1268.
- Karlsen K** (1962) Development of tooth germs and adjacent structures in the whalebone whale (*Balaenoptera physalus*). *Hval skrif*, **45**, 5-56.
- Kemper CM** (2002) Distribution of the pygmy right whale, *Caperea marginata*, in the Australasian region. *Mar Mamm Sci*, **18**, 99-111.



- Klingenberg CP** (2005) Developmental constraints, modules, and evolvability. In *Variations* (eds Hallgrímsson B, Hall BK), pp. 219-247. Cambridge: Academic Press.
- Klingenberg CP** (2009) Morphometric integration and modularity in configurations of landmarks: tools for evaluating a priori hypotheses. *Evol Dev*, **11**, 405-421.
- Klingenberg CP** (2010) Evolution and development of shape: integrating quantitative approaches. *Nat Rev Genet*, **11**, 623-635.
- Klingenberg CP** (2011) MORPHOJ: an integrated software package for geometric morphometrics. *Mol Ecol Resour*, **11**, 353-357.
- Klingenberg CP, Marugán-Lobón J** (2013) Evolutionary covariation in geometric morphometric data: Analyzing integration, modularity, and allometry in a phylogenetic context. *Syst Biol*, **62**, 591-610.
- Koussoulakou DS, Margaritis LH, Koussoulakos SL** (2009) A curriculum vitae of teeth: evolution, generation, regeneration. *Int J Biol Sci*, **5**, 226-243.
- Koyabu D, Endo H, Mitgutsch C, et al.** (2011) Heterochrony and developmental modularity of cranial osteogenesis in lipotyphlan mammals. *EvoDevo*, **2**, 21-21.
- Koyabu D, Werneburg I, Morimoto N, et al.** (2014) Mammalian skull heterochrony reveals modular evolution and a link between cranial development and brain size. *Nat Commun*, **5**, 3625.
- Kukenthal W** (1893) *Vergleichend-anatomische und entwicklungsgeschichtliche Untersuchungen an Walthieren*, Gustav Fischer Verlag, Jena.
- Kükenthal W** (1914) Untersuchungen an Walen (Zweiter Teil). *Jen Zei Natur*, **51**, 1-122.
- Kuzmin AA** (1976) Embryogenesis of the osseous skull of the sperm whale. *Investig Cetacea*, **7**, 187-202.
- Lanzetti A** (in press) Prenatal developmental sequence of the skull of minke whales and its implications for the evolution of mysticetes and the teeth-to-baleen transition. *J Anat*.
- Lanzetti A, Berta A, Ekdale EG** (2018) Prenatal development of the humpback whale: growth rate, tooth loss and skull shape changes in an evolutionary framework. *Anat Rec*, <https://doi.org/10.1002/ar.23990>.
- Laws RM** (1959) The foetal growth rates of whales with special reference to the fin whale, *Balaenoptera physalus* Linn. *Disc Rep*, **29**, 281-308.
- Mackintosh NA** (1965) *The stocks of whales*, Fishing News (Books) Ltd., London.
- Mackintosh NA, Wheeler JFG** (1929) Southern blue and fin whales. *Disc Rep*, **1**, 257-529.

- Maddison WP, Maddison DR** (2018) Mesquite: a modular system for evolutionary analysis. Version 3.6. <http://mesquiteproject.org>
- Marrable AW, Ashdown RR** (1967) Quantitative observations on pig embryos of known ages. *J Agric Sci*, **69**, 443-447.
- Marx FG, Hocking DP, Park T, Ziegler T, Evans AR, Fitzgerald EMG** (2016) Suction feeding preceded filtering in baleen whale evolution. *Mem Mus Vic*, **75**, 71-82.
- Masaki Y** (1979) Yearly change of the biological parameters for the Antarctic minke whale. International Whaling Commission, 375-395.
- McGowen MR, Tsagkogeorga G, Álvarez-Carretero S, et al.** (in press) Phylogenomic resolution of the cetacean tree of life using target sequence capture. *Syst Biol*.
- Mead JG, Fordyce RE** (2009) The therian skull: a lexicon with emphasis on the odontocetes. *Smithson Contrib Zool*, **627**, 1-249.
- Meredith RW, Gatesy J, Cheng J, Springer MS** (2011) Pseudogenization of the tooth gene enamelysin (*MMP20*) in the common ancestor of extant baleen whales. *Proc R Soc Lond B Biol Sci*, **278**, 993-1002.
- Meredith RW, Gatesy J, Springer MS** (2013) Molecular decay of enamel matrix protein genes in turtles and other edentulous amniotes. *BMC Evol Biol*, **13**, 20-20.
- Metscher BD** (2009) MicroCT for comparative morphology: simple staining methods allow high-contrast 3D imaging of diverse non-mineralized animal tissues. *BMC Physiol*, **9**, 11.
- Miller GS** (1923) The telescoping of the cetacean skull. *Smit Misc Coll*, **76**, 1-71.
- Moore KL, Persaud TVN, Torchia MG** (2015) *The developing human: clinically oriented embryology - v. 10*, Elsevier Health Sciences, Philadelphia.
- Moran MM, Nummela S, Thewissen JGM** (2011) Development of the skull of the pantropical spotted dolphin (*Stenella attenuata*). *Anat Rec*, **294**, 1743-1756.
- Müller HC** (1921) Zur Entwicklungsgeschichte von *Phocaena communis* Less. *Archiv für Naturgeschichte A*, **7**, 1-113.
- Nakamura G, Kato H** (2014) Developmental changes in the skull morphology of common minke whales *Balaenoptera acutorostrata*. *J Morphol*, **275**, 1113-1121.
- Ohsumi S, Masaki Y, Kawamura A** (1970) Stock of the antarctic minke whale. Whales Research Institute of Tokyo, 75-125.
- Paradis MR, Raj MT, Boughner JC** (2013) Jaw growth in the absence of teeth: the developmental morphology of edentulous mandibles using the p63 mouse mutant. *Evol Dev*, **15**, 268-279.

- Peredo CM, Pyenson ND, Boersma AT** (2017a) Decoupling tooth loss from the evolution of baleen in whales. *Front Mar Sci*, **4**, 1-11.
- Peredo CM, Pyenson ND, Uhen MD, Marshall CD** (2017b) Alveoli, teeth, and tooth loss: Understanding the homology of internal mandibular structures in mysticete cetaceans. *Curr Biol*, **12**, e0178243.
- Perrin WF** (1975) Variation of spotted and spinner porpoise (genus *Stenella*) in the Eastern Pacific and Hawaii. *Bull Scripps Inst Ocean*, **21**, 1-212.
- Perrin WF, Heyning JE** (1993) Rostral fusion as a criterion of cranial maturity in the common dolphin, *Delphinus delphis*. *Mar Mamm Sci*, **9**, 195-197.
- Perrin WF, Mallette SD, Brownell RL, Jr.** (2018) Minke whales: *Balaenoptera acutorostrata* and *B. bonaerensis*. In *Encyclopedia of Marine Mammals* (eds Würsig B, Thewissen JGM, Kovacs KM), pp. 608-613. London: Academic Press.
- Phen A, Greer J, Uppal J, Der J, Boughner JC** (2018) Upper jaw development in the absence of teeth: new insights for craniodental evo-devo integration. *Evol Dev*, **20**, 146-159.
- Pivorunas A** (1979) The feeding mechanisms of baleen whale. *Am Sci*, **67**, 432-440.
- Polly PDPD, Lawing AMM, Fabre A-CAC, Goswami A** (2013) Phylogenetic principal components analysis and geometric morphometrics. *Hystrix*, **24**, 33-41.
- Porto A, de Oliveira FB, Shirai LT, De Conto V, Marroig G** (2009) The evolution of modularity in the mammalian skull I: morphological integration patterns and magnitudes. *Evol Biol*, **36**, 118-135.
- Pyenson ND, Goldbogen JA, Shadwick RE** (2013) Mandible allometry in extant and fossil Balaenopteridae (Cetacea: Mammalia): the largest vertebrate skeletal element and its role in rorqual lunge feeding. *Biol J Linn Soc*, **108**, 586-599.
- Pyenson ND, Goldbogen JA, Vogl AW, Szathmary G, Drake R, L., Shadwick RE** (2012) Discovery of a sensory organ that coordinates lunge feeding in rorqual whales. *Nature*, **485**, 498.
- Rauschmann MA, Huggenberger S, Kossatz LS, Oelschläger HHA** (2006) Head morphology in perinatal dolphins: a window into phylogeny and ontogeny. *J Morphol*, **267**, 1295-1315.
- Reese CS, Calvin JA, George JC, Tarpley RJ** (2001) Estimation of fetal growth and gestation in bowhead whales. *J Am Stat Assoc*, **96**, 915-938.
- Rice D** (1998) *Marine mammals of the world: systematics and distribution*, Society of Marine Mammalogy, USA.
- Ridewood WG** (1923) Observations on the skull in foetal specimens of whales of the genera *Megaptera* and *Balaenoptera*. *Philos Trans R Soc Lond B Biol Sci*, **211**, 209-272.

- Riese W** (1928) Über das Vorderhirn des Walfötus (*Megaptera boops*). *Anat Anz*, **65**, 255-260.
- Rohlf FJ, Slice D** (1990) Extensions of the procrustes method for the optimal superimposition of landmarks. *Syst Zool*, **39**, 40-59.
- Rose C** (1892) Beiträge zur Zahnentwicklung der Edentaten. *Anat Anz*, **7**, 495-512.
- Rosenbaum HC, Brownell RL, Brown MW, et al.** (2000) World-wide genetic differentiation of *Eubalaena*: questioning the number of right whale species. *Mol Ecol*, **9**, 1793-1802.
- Roston RA, Lickorish D, Buchholtz EA** (2013) Anatomy and age estimation of an early blue whale (*Balaenoptera musculus*) fetus. *Anat Rec*, **296**, 709-722.
- Roston RA, Roth VL** (2019) Cetacean skull telescoping brings evolution of cranial sutures into focus. *Anat Rec*, <https://doi.org/10.1002/ar.24079>.
- Rugh DJ, Demaster D, Rooney A, Breiwick JM, Sheldon K, Moore SE** (2002) A review of bowhead whale (*Balaena mysticetus*) stock identity. *J Cetacean Res Manage*, **5**, 267-279.
- Sánchez-Villagra MR, Goswami A, Weisbecker V, Mock O, Kuratani S** (2008) Conserved relative timing of cranial ossification patterns in early mammalian evolution. *Evol Dev*, **10**, 519-530.
- Sawamura H** (2008) The origin of baleen whale-comparative morphology of the toothed mysticetes and the minke whale fetuses. *J Fos Res*, **40**, 120-130.
- Schneider CA, Rasband WS, Eliceiri KW** (2012) NIH Image to ImageJ: 25 years of image analysis. *Nat Methods*, **9**, 671-675.
- Schneidereit M** (1985) Study of fetal organ growth in Wistar rats from day 17 to 21. *Lab Anim*, **19**, 240-244.
- Schulte HVW** (1916) Anatomy of a foetus of *Balaenoptera borealis*. *Mem Am Mus Nat Hist*, **1**, 389-502.
- Simmons JE** (1995) Storage in fluid preservatives. In *Storage of Natural History Collections: A Preventive Conservation Approach* (eds Rose CL, Hawks CA, Genoways HH), pp. 161-186. New York: Society for the Preservation of Natural History Collections.
- Slijper EJ** (1976) *Whales*, Hutchinson, London.
- Smith KK** (1997) Comparative patterns of craniofacial development in eutherian and metatherian mammals. *Evolution*, **51**, 1663-1678.
- Springer MS, Starrett J, Morin PA, Lanzetti A, Hayashi C, Gatesy J** (2016) Inactivation of *C4orf26* in toothless placental mammals. *Mol Phylogen Evol*, **95**, 34-45.
- Stephenson FH** (2016) Cell Growth. In *Calculations for Molecular Biology and Biotechnology* (ed Frank HS), pp. 43-79. London: Elsevier.

- Sterba O** (1995) Staging and ageing of mammalian embryos and fetuses. *Acta Vet Brno*, **64**, 83-89.
- Sterba O, Klima M, Schildger B** (2000) Embryology of dolphins: staging and ageing of embryos and fetuses of some cetaceans. *Adv Anat Embryol Cell Biol*, **157**, 1-133.
- Thewissen JGM, Heyning J** (2007) Embryogenesis and development in *Stenella attenuata* and other cetaceans. In *Reproductive Biology and Phylogeny of Cetacea* (ed Miller DL), pp. 307-329. Boca Raton: CRC Press.
- Thewissen JGM, Hieronymus TL, George JC, Suydam R, Stimmelmayer R, McBurney D** (2017) Evolutionary aspects of the development of teeth and baleen in the bowhead whale. *J Anat*, **230**, 549-566.
- Timm NH** (2002) *Applied multivariate analysis*, Springer, New York.
- Tims HWM** (1908) Tooth-vestiges and associated mouth parts in the Manidae. *J Anat Physiol*, **42**, 375-387.
- Tomilin AG** (1967) *Mammals of the USSR and adjacent countries, Volume IX, Cetacea*, Israel Program for Scientific Translations, Jerusalem.
- Tsai CH, Fordyce RE** (2014) Disparate heterochronic processes in baleen whale evolution. *Evol Biol*, **41**, 299-307.
- Tullberg T** (1883) Bau und Entwicklung der Barten bei Balaenoptera sibbaldii. *Nov Acta Reg Soc Scie Ups*, **3**, 1-36.
- Usui K, Tokita M** (2018) Creating diversity in mammalian facial morphology: a review of potential developmental mechanisms. *EvoDevo*, **9**, 15-15.
- Van Dissel-Scherft MC, Vervoort W** (1954) Development of teeth in fetal *Balaenoptera physalus*. *Proc K Ned Akad Wet Ser C Biol Med Sci*, **57**, 196-210.
- Victor D** (2018) Japan to resume commercial whaling, defying international ban. *The New York Times*, 12-26-2018, <https://www.nytimes.com/2018/12/26/world/asia/japan-whaling-withdrawal.html>
- Wada S, Oishi M, Yamada TK** (2003) A newly discovered species of living baleen whale. *Nature*, **426**, 278-281.
- Walsh BM, Berta A** (2011) Occipital ossification of balaenopteroid mysticetes. *Anat Rec*, **294**, 391-398.
- Weber M** (1886) *Studien über Säugethiere: ein Beitrag zur Frage nach dem Ursprung der Cetaceen*, Gustav Fischer, Jena.
- Werneburg I** (2009) A standard system to study vertebrate embryos. *PLoS ONE*, **4**, e5887.

**Werneburg I, Sánchez-Villagra MR** (2011) The early development of the echidna, *Tachyglossus aculeatus* (Mammalia: Monotremata), and patterns of mammalian development. *Acta Zool*, **92**, 75-88.

**Werth AJ, Potvin J, Shadwick RE, Jensen MM, Cade DE, Goldbogen JA** (2018) Filtration area scaling and evolution in mysticetes: trophic niche partitioning and the curious cases of sei and pygmy right whales. *Biol J Linn Soc*, **125**, 264-279.

## *Chapter Three*

# **Developmental Basis for The Evolution of Skull Shape and Tooth Loss in Mysticeti**

## **Introduction**

### **Connecting evolution and development: heterochrony and allometry**

Ontogeny and phylogeny were hypothesized to be linked before molecular and experimental studies, as Darwin himself saw changes in development as an argument in favor of his theory of descent with modification (Gould, 1977). Possibly the most important concept to bridge evolution and development is heterochrony, broadly defined as changes in the relative timing of appearance or growth rate of characters between the ancestor and its descendants (Gould, 1977, Alberch et al., 1979, McNamara, 1986, Klingenberg, 1998). Heterochronic process can act both on discrete traits, such as changing in timing of bone ossification and suture closure, or on the overall shape and rate of development of the organisms, as well on a molecular level (e.g. regulatory gene expression) (Klingenberg, 1998, Smith, 2002, Smith, 2003, Olsson et al., 2017). Independently of the scale, they can be divided into two broad categories based on their effect on the descendant morphology: paedomorphosis, in which the adult organism retains juvenile characters of the ancestor, and peramorphosis, in which the juvenile of the descendant presents traits that characterized the adult ancestor (Alberch et al., 1979, McNamara, 1986, Klingenberg, 1998). Modifications in developmental rate (neoteny or acceleration), in timing of sexual maturation (progenesis or hypermorphism), and in onset of growth (post- or pre-displacement) are the major categories of physical process that can cause heterochronic changes, whether paedomorphic or peramorphic (Gould, 1977, McNamara, 1986, Klingenberg, 1998).

Understanding which of these specific processes is causing the changes in the descendant phenotype is sometimes impossible when working with extinct lineages, but the effect of heterochronic shifts in development on the evolution of a group are usually well recognizable and can be qualified as paedomorphic or peramorphic changes (McNamara, 1986, McNamara and McKinney, 2005). A good example of a well-studied lineage that shows examples of both types of heterochrony acting at different levels is birds (Aves). The skull of modern birds appears to possess an overall paedomorphic shape, while their postcranial skeleton presents peramorphic features, both relative to extinct non-avian dinosaurs, their closely ancestors (Bhullar et al., 2012, Bhullar et al., 2016). Modern birds appear to share a very similar ossification sequence of the skull bones with their ancestors, but then these elements are fused together to compose the characteristic bird skull with its different shape (Smith-Paredes et al., 2018). Similar evidence of initial bone development followed by fusion was also recovered in their wrist articulation (Botelho et al., 2014). The clearest example of a paedomorphic heterochronic transformation in this lineage is the progressive truncation of ontogenetic tooth development observed in fossil taxa, which eventually resulted in the complete loss of teeth in favor of the beak in the ancestor of modern birds (Wang et al., 2017). These heterochronic features are hypothesized to be related to locomotory and dietary transformations seen in modern species (Bhullar et al., 2016). Taking into consideration heterochrony in the investigation of the evolution of any given group is of key importance to identify the role of development in the rise of new traits and adaptations in both living and extinct organisms, and it can also help clarify phylogenetic relationships based on morphological traits (Wiens et al., 2005, Thewissen et al., 2012).

An important developmental concept that is connected with heterochronic processes is allometry, defined as the relationship between changes in size and shape of a structure during the growth of an organism (Gould, 1977, McNamara, 1986, Klingenberg, 1998). Allometric changes



and trajectories, unlike general heterochronic shifts, are not correlated with time, as they can be recorded during the growth of a single organism or species without considering the timing of these events compared to their ancestor (McKinney, 1988). Initially allometric studies described shape as the absolute dimension of a trait by using discrete linear measurements of traits (Alberch et al., 1979), while presently it can be measured more accurately using geometric morphometrics (GM) methods (Webster and David Sheets, 2010, Klingenberg and Marugán-Lobón, 2013). Size can be defined as both the overall size of the organism or of the specific trait for which the change in shape is considered (e.g. skull) (Alberch et al., 1979, McNamara, 1986). Regardless of how they are measured and what structure they represent, when both shape and size change at the same rate during development, the growth is defined as isometric. When instead shape increases more rapidly than size, it is a case of positive allometry, while the opposite (size increasing faster than shape) is classified as negative allometry (McNamara, 1986, McKinney, 1988, Klingenberg, 1998). The concept of allometry can also be expanded to apply to evolutionary transformations by comparing the size and growth rates of closely related organisms, and it has allowed the identification of heterochronic patterns (Gould, 1977, Cheverud, 1982, Klingenberg, 1998). A clear instance of evolutionary allometry is the gigantism or extreme increase in body size in sauropods (herbivorous non-avian dinosaurs) compared to their ancestors, probably connected to shifts in global climate and resource availability (Sander et al., 2011, Clauss et al., 2013), an example of peramorphosis. On the other hand, a typical case of pedomorphosis in evolutionary allometry is the dwarfism or reduction of body size, as well as brain size, in many mammalian insular species, such as hippos, elephants and humans, which was likely caused by the lack of predators and decrease in diet quality (Weston and Lister, 2009, Herridge and Lister, 2012).

Identifying and quantifying patterns of growth and evolutionary allometry and how they act on different parts of the organism's phenotypes is a key part of studying the role of

heterochrony in the evolution of a lineage (McNamara, 1986, McKinney, 1988, Klingenberg, 1998).

### **Influence of development on morphology and diversity of Cetacea**

In Cetacea, several recent studies investigated different aspects of the contribution of ontogeny to the evolution of this unique clade. Heterochrony on a molecular level, represented by changes in timing and duration of regulatory gene expression early in ontogeny (Smith, 2003), has been found to have had a profound influence on the loss of functional hind limbs in the ancestor of all modern Cetacea (Archaeoceti), a key adaptation to life in water, allowing the evolution of a more efficient swimming mode (Thewissen and Fish, 1997, Thewissen et al., 2006, Thewissen et al., 2012). Progressive decrease in expression in the posterior region of the body of regulatory genes *Shh* and *Hand2* and the early loss – in the first months of gestation – of the apical ectodermal ridge (AER), the embryonic tissue of amniotes that guides the growth of limbs, are probably responsible for the absence of external hind limbs in modern baleen and toothed whales (Thewissen et al., 2006). Similar changes in gene expression have been hypothesized to control the characteristic changes observed in the vertebral column of modern cetaceans (Buchholtz, 2007, Bebej and Smith, 2017).

Alterations in location and timing of gene expression have also been implicated in the evolution of homodont dentition in Odontoceti (Armfield et al., 2013). In the pantropical spotted dolphin (*Stenella attenuata*), the gene *Bmp4*, commonly expressed only in the anterior portion of the jaws of terrestrial mammals, is also found in the caudal regions, where other mammals express only the gene *Fgf8* instead. This process that occurs in the early stages of ontogeny is probably responsible for the pointed and constant shape of the teeth in adult odontocetes. In Mysticeti, Thewissen et al. (2017) hypothesized that an early development and posterior elongation of the dental lamina is associated with the fetal polydonty seen in the prenatal

development of these species, which have convergently evolved a morphologically similar fetal dentition to toothed whales (see Chapter Two for a detailed comparison of tooth development in Cetacea and other mammals).

Postnatal heterochrony on a broader, phenotypic level has been found to have had a strong impact on the phylogeny and diversification of Odontoceti, especially in porpoises and at least one dolphin genus (*Cephalorhynchus*) (Galatius and Kinze, 2003, Galatius, 2010, Galatius et al., 2011). All porpoises (*Phocoena* spp., *Phocoenoides*, *Neophocaena*) have been shown to have a paedomorphic skull shape, with a blunter rostrum, as well as unfused bone sutures, probably due to early sexual maturation (progenesis). This heterochronic pattern seems to be phylogenetically driven, as the common ancestor of the group is hypothesized to have exhibited juvenile traits too (Galatius et al., 2011). The onset of heterochrony seems to be correlated with the habitat of these animals: species that tend to live in a coastal environment present more paedomorphic traits compared to pelagic forms (Galatius, 2010, Galatius et al., 2011). Similar paedomorphic traits appear to have convergently evolved in the genus *Cephalorhynchus*, which is the only genus of its group of oceanic dolphins (Lissodelphininae, Delphinidae – McGowen, 2011) to live prevalently in a coastal environment (Galatius, 2010). Moreover, paedomorphism in the form of delayed or absent ossification of the epiphyseal elements in the flipper has been detected at least in the genus *Phocoena*, including in the critically endangered species *P. sinus* (vaquita) (Galatius and Kinze, 2003, Mellor et al., 2009). Both porpoises and *Cephalorhynchus* tend to have a much smaller body and head size than other dolphins, indicating a tight link between heterochrony and allometry in their evolution, diversification and habitat selection (Galatius, 2010, Galatius et al., 2011). While it was not explicitly tested, paedomorphism might also play a role in the vulnerability of these taxa to environmental change, as it was demonstrated

for other well-studied vertebrates, such as European newts (Denoël et al., 2009) and certain groups of flightless birds (Livezey, 1993, Duncan et al., 2002).

In another genus of dolphins, *Sotalia*, mosaic heterochrony, where different parts of the skull grow in shape and size at different rates resulting in divergent allometric patterns, has been shown to have an impact on species and habitat differentiation (Monteiro-Filho et al., 2002, Sydney et al., 2012). During postnatal ontogeny of *S. guianensis* (Guiana dolphin), the neurocranium and rostrum change shape at different rates, and the rostrum stops growing earlier than the rest of the skull (Sydney et al., 2012). This differential growth is probably one of the driving causes of morphological skull differentiation between this estuarine species from its sister species (*S. fluviatilis* – tucuxi) that instead lives in a riverine environment in the Amazon basin (Monteiro-Filho et al., 2002, Sydney et al., 2012). Therefore, also in these dolphins, changes in skull growth during postnatal development appear to be tightly linked with their feeding strategies and phylogenetic diversification.

In Mysticeti, several studies have focused on postnatal growth and evolutionary allometry of skull features and how it affects the feeding style of the species (Goldbogen et al., 2010, Nakamura et al., 2012, Goldbogen et al., 2012, Pyenson et al., 2013, Nakamura and Kato, 2014, Werth et al., 2018, Franci and Berta, 2018). In rorquals (Balaenopteridae), head size, mandibular length and buccal capacity have been shown to increase allometrically with body size, with larger species having a greater head-to-body size ratio than smaller ones (Goldbogen et al., 2010, Pyenson et al., 2012, Kahane-Rapport and Goldbogen, 2018). This relationship likely has driven the evolution of this group, with taxa progressively modifying their body proportions over time to best adapt to different ecological niches. For example, smaller species like the minke whales (*B. acutorostrata* and *B. bonaerensis*) have higher maneuverability given their smaller head compared to body size and can chase more active prey compared to the giant blue (*B. musculus*)

and fin whales (*B. physalus*) (Goldbogen et al., 2010, Nakamura et al., 2012). It has also been recently shown that filtration area, measured as surface area of baleen, is positively correlated with body size in all living mysticetes (Werth et al., 2018). Different families with diverse filter feeding styles follow separate allometric trajectories as they are constrained by the shape of their rostrum and of the baleen. Interestingly, the sei whale (*B. borealis*) follows an allometric pattern intermediate between balaenids (skim feeders) and rorquals (lunge feeders), warranting the hypothesis that this species is a generalist filter feeder that can switch between both filter feeding styles. The pygmy right whale (*Caperea marginata*) also follows an interesting pattern, as it more closely approximates the trajectory of skim feeders or lunge feeders depending on the metric used. Lack of observational data for this species makes it impossible to formulate a definitive hypothesis on its feeding mode (Werth et al., 2018). On an intraspecific level, disparate allometric trajectories have also been recognized in the growth of the skull of the common minke whale (*B. acutorostrata*). The size of the rostrum has been shown to positively increase through postnatal ontogeny while the size of the neurocranium decreases relative to total skull size (Nakamura and Kato, 2014, Franci and Berta, 2018), suggesting a similar mosaic heterochronic pattern of skull shape growth as seen in the *Sotalia*. However more studies are needed to test this hypothesis. Overall, these findings show that there is a deep connection between head size and shape and the feeding niche of the animal, as well as body size, and that ontogeny plays a role in creating the adult proportions observed through differential growth rates. These data can serve as a baseline to infer feeding mode of extinct mysticete taxa and reconstruct the time of origin of baleen, by comparing the allometric skull proportions of living taxa with the fossils (Pyenson et al., 2013, Werth et al., 2018). While the effects of allometry on the feeding adaptations of baleen whales have been explored in length, very little is known on the influence of heterochronic process on their evolution and diversification. The only study to consider this topic in depth is Tsai and

Fordyce (2014). The authors only compared the skulls of three prenatal and three adult specimens of pygmy right whale (*C. marginata*) to prenatal and adult specimens of rorquals (sei whale and humpback whale) using pictures and drawings. By qualitatively comparing the specimens and conducting 2D geometric morphometric analyses, they determined that the pygmy right whale presents a paedomorphic skull shape, as the adults are similar in shape to the prenatal specimens of the species, while rorquals express peramorphic traits, given their highly different adult skull morphologies compared to their younger specimens. While these hypotheses might be correct, this study is flawed, in part because of the limited sample size and methodology employed, but mostly due to the incorrect application of the terminology. By definition, it is not possible to assess the presence or nature of the heterochronic process at play without considering the supposed or recorded ancestral state of the species studied (McNamara, 1986, McKinney, 1988), and this analysis did not include any living or fossil taxon closely related to all species considered to provide a point of comparison. Therefore, while the small size of the pygmy right whale compared to all other baleen whales (Davies and Guiler, 1957, Pavey, 1992) could suggest that this taxon indeed has paedomorphic features, the peramorphism of rorquals cannot be assessed in contrast to the size and shape of *Caperea* (Gould, 1977, McNamara, 1986). Moreover, all baleen whales appear to have some immature features in their skulls, as many sutures between bones of the rostrum remain open for the entire life of the animal, probably due to the need of a flexible rostrum for efficient filter feeding, and certain sutures in the neurocranium only completely ossify after the first year of life of the individual (Walsh and Berta, 2011, Berta et al., 2016). The presence of these traits makes it harder to determine the impact of discrete heterochronic process on the evolution and diversification of Mysticeti.

From this evidence, it is clear that ontogeny has deeply influenced the evolution of aquatic adaptations, feeding modes and species diversification of Cetacea as a whole and of

Mysticeti and Odontoceti respectively. While information on postnatal development is useful to understand certain anatomical differences among living species, it does not provide information on the basic changes that caused the rise of new adaptations in a lineage (Thewissen et al., 2012). Placing new developmental data directly in the context of the fossil evidence available is key to test which heterochronic and allometric transformations mostly influenced the evolution of skull shape and feeding mode in baleen whales (Peredo et al., 2017, Lanzetti et al., 2018, Lanzetti, in press).

### **Feeding and skull evolution of Mysticeti in the fossil record**

The extensive fossil record of Mysticeti provides a direct account of the anatomical transformations involved in the shift from the ancestral raptorial feeding mode to the modern filter feeding adaptations, including the replacement of teeth with baleen postnatally (Berta et al., 2016, Peredo et al., 2017). While many skull remains of fossil taxa are being described regularly (e.g. Marx et al., 2017b, Peredo et al., 2017), the interpretation of the feeding mode of these extinct animals and their phylogenetic position relative to modern mysticetes is still debated. Aside from the fragmentary nature of fossil specimens that render phylogenetic inference difficult, investigating how these early mysticetes captured food is particularly challenging since baleen plates are rarely preserved in the rocks, due to their keratinous composition that is not suitable for fossilization like bones or other mineralized tissues (Gioncada et al., 2016, Marx et al., 2017a).

Current evidence suggests that, phenotypically, the acquisition of baleen occurred once in the common ancestor of all modern mysticetes, but it is debated whether teeth and baleen-like structures could have co-occurred in the same animal (Deméré and Berta, 2008) or the complete loss of teeth has preceded the evolution of baleen as a functional analog (Peredo et al., 2018b). Consequently, different hypotheses on the evolution of the feeding strategy of mysticetes from

ancestral raptorial forms to the modern filter feeding taxa have been proposed. On one hand, primordial baleen structures could have been employed in filter feeding aided by multicuspid teeth, providing a stepwise pathway to the evolution of modern mysticete feeding behavior (Deméré et al., 2008, Berta et al., 2016, Geisler et al., 2017, Geisler, 2018). However, if dentition was completely lost before the occurrence of baleen, intermediate taxa might have employed a suction feeding strategy more similar to modern odontocete lineages with extreme tooth reduction (e.g. Ziphiidae) before adapting to bulk filter feeding (Marx et al., 2016, Peredo et al., 2017, Peredo et al., 2018b). The relationships among major groups of stem and crown Mysticeti are represented in the cladogram in Figure 3.1, along with their simplified head anatomy and hypothesized feeding mode.

Baleen whales split from Odontoceti around 40 Ma ago (Berta et al., 2016). Earliest diverging mysticete lineages (*Coronodon havensteini*† ~ 34–28 Ma, Llanocetidae†, ~ 37–33 Ma) retain several traits observed in coeval stem-Cetacea (Basilosauridae, Archaeoceti) such as limited telescoping of the skull, defined as the overlapping of the bones of the braincase to allow for the migration of the external nares towards the posterior end of the skull (Miller, 1923), and a short rostrum, compared to the elongated head and mouth of modern baleen whales. Since they retained an ancestral heterodont dentition, they are generally believed to have been suction and raptorial feeders. However, it has been proposed that some of these animals could have used teeth as a functional analog for baleen to filter feed, as seen in some modern seals, due to the highly complex teeth morphology and lack of precise occlusion in these specimens (Fordyce and Marx, 2016, Geisler et al., 2017, Hocking et al., 2017, Fordyce and Marx, 2018, Geisler, 2018). Mammalodontidae (~ 28–24 Ma), which includes the genera *Mammalodon*† and *Janjucetus*†, probably represent a “dead end” in the evolution of mysticetes (Fitzgerald, 2006, Fitzgerald, 2010, Hampe and Baszio, 2010). Both of these taxa share many characteristics with basal



mysticetes, such as low level of telescoping and heterodont, well-developed dentition (Marx, 2011). However, they present skull morphologies and feeding adaptations not seen in any other lineage of this group: *Mammalodon*† was probably a bottom suction feeder, with teeth highly worn by contact with the sediment (Fordyce and Marx, 2016, Fitzgerald, 2010), while *Janjucetus*† was likely an active predator, with complex tooth cusps and forward-facing eyes (Fitzgerald, 2006, Marx, 2011).

Another lineage coeval to Mammalodontidae (Aetiocetidae†, ~ 32–24 Ma) instead evolved some skull features related to filter feeding, while still retaining multicuspid teeth in both jaws. Representatives of these groups, such as *Aetiocetus*† spp., have been hypothesized to bear baleen-like structures or proto-baleen, a bristle-like keratinous organ, in the posterior portion of the rostrum, along with dentition. This conclusion is supported by the presence of a large diastema between teeth and sulci and foramina on the ventral process of the maxilla, which have been identified as possible bony correlates for baleen using observations on modern species (Deméré et al., 2008, Ekdale et al., 2015). This interpretation has sparked the debate on the possibility of co-occurrence of teeth and baleen in these fossil taxa, with several authors dismissing this hypothesis and instead favoring the interpretation that Aetiocetidae† employed suction feeding. This feeding mode would not require precise occlusion, which is not possible with the large diastema observed in these taxa, and the maxillary sulci would be correlated with the presence of enlarged gums (Marx et al., 2015, Marx et al., 2016, Peredo et al., 2017, Fordyce and Marx, 2018). All these taxa also lack important skull features associated with bulk filter feeding (Goldbogen and Madsen, 2018, Werth et al., 2018).

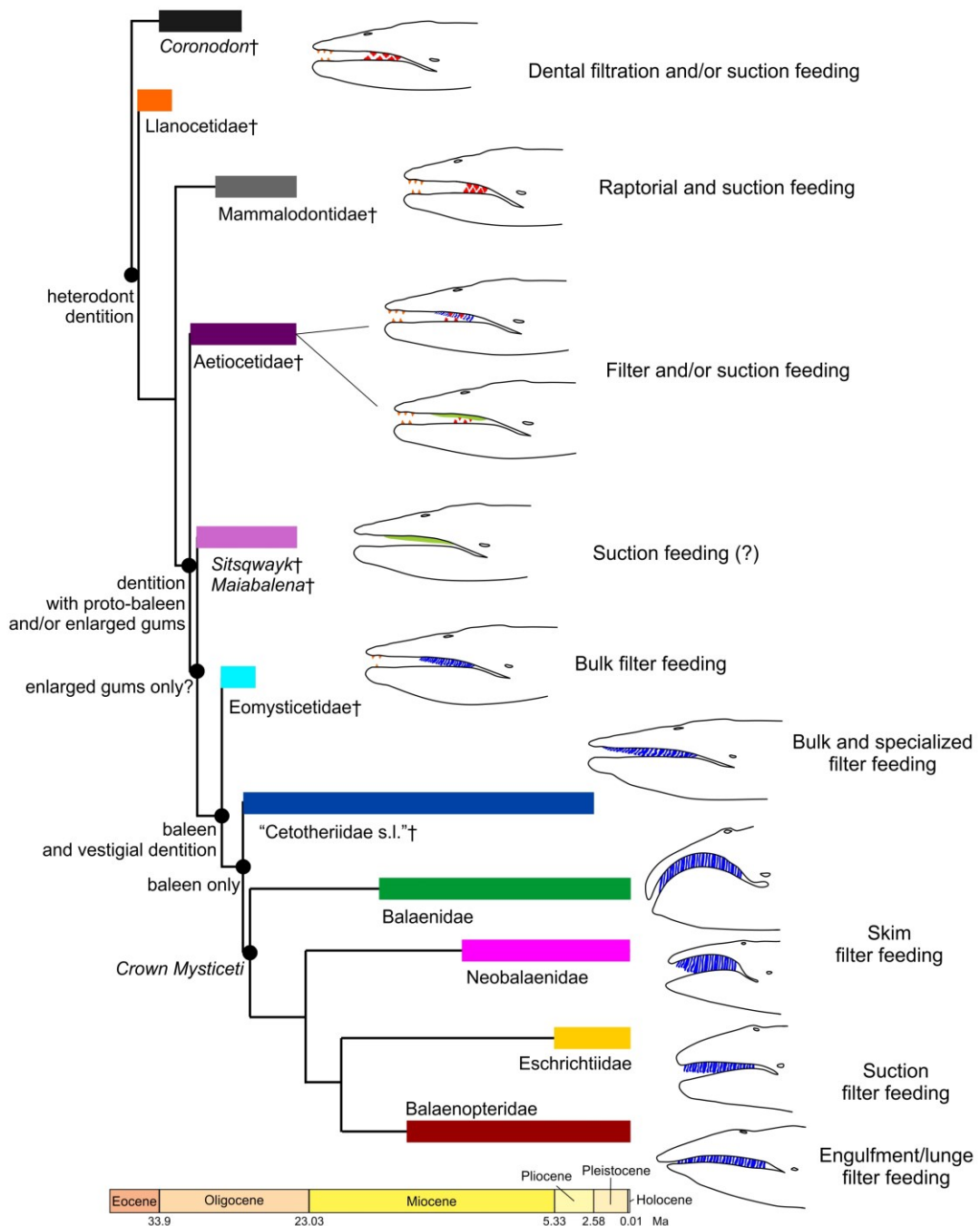


Figure 3.1 – Phylogenetic relationships of major groups of Mysticeti. On the right, reconstructed or observed changes in external anatomy and feeding mode of the taxa. On the left, important steps in the teeth-to-baleen transition at each node. Topology, node and group dates follow Gatesy et al. (2013) and Berta et al. (2016). *Coronodon*†, *Llanocetidae*† and *Sitsqwayk*†/*Maiabalaena*† are added according to phylogenetic position and age presented in Geisler et al. (2017), Fordyce and Marx (2018), Peredo and Uhen (2016b) and Peredo et al. (2018b). Anterior (orange) and posterior (red) teeth are in different colors to represent heterodonty. Baleen in blue and enlarged gums in green. †=fossil taxa

Two recently discovered fossil genera, *Sitsqwayk cornishorum*† (~ 31–24 Ma, Peredo and Uhen, 2016b) and *Maiabalaena nesbittae*† (~ 34–30 Ma, Peredo et al., 2018b), have been included in a separate group of stem Mysticeti, which lacked both teeth and baleen-like structures but might have had enlarged gums (Peredo and Uhen, 2016b, Peredo et al., 2018b). These animals have been therefore hypothesized to have employed a derived form of suction feeding, similar to what is observed in modern beaked whales (Ziphiidae) (Peredo et al., 2018b). This discovery would support the hypothesis of a transition between teeth and baleen mediated by a stage of complete lack of dentition, as proposed by the same authors (Marx et al., 2016, Peredo et al., 2017, Peredo et al., 2018b). However, these specimens preserve sulci and foramina similar to what is observed in Eomysticetidae†, the first group of toothless mysticetes. Therefore, the presence of baleen cannot be *a priori* excluded and would explain the lack of teeth in these specimens. Further studies are needed to corroborate either hypotheses on the feeding mode of these fossils.

The following diverging group (Eomysticetidae†, ~ 29.5–27 Ma) includes the earliest taxa to be functionally toothless and likely possess baleen plates. They had a broad and flat rostrum indicating that they likely employed a bulk filter feeding strategy, and undisputable bony correlates for baleen in the palate, However some species might have still retained vestigial teeth in the anterior portion of the rostrum and mandible (Boessenecker and Fordyce, 2015a, Boessenecker and Fordyce, 2015b, Berta et al., 2016, Boessenecker and Fordyce, 2016). “Cetotheriidae *sensu lato*” † (~ 28–2.5 Ma) are the first to lack teeth completely postnatally. This group contains many heterogeneous taxa and it is most certainly paraphyletic, but the phylogenetic placement of individual genera and their grouping varies greatly in the literature (e.g. Marx, 2011, Bisconti, 2015, Gol’din et al., 2015, Marx and Fordyce, 2015, Marx et al., 2019). Most likely a portion of this taxa belongs in crown mysticetes, and it has been proposed

that the genus *Caperea* should be included in this more derived group of Cetotheriidae (Fordyce and Marx, 2013, Marx and Fordyce, 2016, Marx et al., 2019). Despite this, other analyses have failed to recover this relationship (Gatesy et al., 2013, Bisconti, 2015, Boessenecker and Fordyce, 2015a, Gol'din et al., 2015) and the phylogenetic position of the taxa in this clade remains uncertain (Berta et al., 2016). However, these fossils represent an important step in the evolution of Mysticeti, and the uncertainty over their evolutionary relationships is probably due to convergent evolution of similar filter feeding modes displayed in specimens found in different parts of the world (El Adli et al., 2014, Gol'din and Startsev, 2014, Collareta et al., 2015, Berta et al., 2016). Most representatives of “Cetotheriidae *sensu lato*”† were probably extinct by the end of the Pliocene epoch (2.58 Ma), even if some taxa might have survived until the end of the early Pleistocene (1.8 Ma) (Boessenecker, 2013). The decline of these archaic mysticetes, which share many anatomical characteristics with modern baleen whale families and possibly also shared their filter feeding niches (e.g. *Herpetocetus morrowi*† likely employed lateral suction filter feeding to consume benthic invertebrates similar to the gray whale, *Eschrichtius robustus* – El Adli et al., 2014), was probably connected to drastic change in ocean circulation due to the start of the formation of the Arctic ice sheet (Marx and Fordyce, 2015, Collareta et al., 2017).

Modern Mysticete families originated around 28 Mya (middle Oligocene epoch). The family Balaenidae is recognized in the fossil record starting around 18 Mya (early Miocene), at about the same time when Balaenopteridae also started diversifying (~ 16 Mya – early Miocene) (Gatesy et al., 2013, Berta et al., 2016). These families diversified rapidly, and this is likely the cause of the apparent disagreement of molecular and morphological data in phylogenetic analysis, particularly regarding the position of the gray whale (McGowen et al., 2009, Gatesy et al., 2013, Boessenecker and Fordyce, 2015a) and the pygmy right whale (Marx, 2011, Gatesy et al., 2013, Marx and Fordyce, 2015). This swift radiation in different filter feeding niches of modern

mysticetes track several environmental factors such as abundance of planktonic primary producers (Marx and Uhen, 2010, Berta and Lanzetti, in press). Their increase in body size also seems to be correlated with the establishment of the North Pole ice cap and other climatic events that characterized the Pliocene epoch (Pyenson and Vermeij, 2016, Tsai and Kohno, 2016, Slater et al., 2017, Goldbogen and Madsen, 2018).

In this context, developmental evidence can be used to determine the mechanisms that enabled these major dietary shifts to occur by allowing the evolution of new morphological traits, as well as the rapid increase in head and body size that occurred throughout this lineage (Tsai and Kohno, 2016, Fordyce and Marx, 2018).

### **Ontogenetic evidence for the teeth-to-baleen transition**

Previous studies have tried to reconcile paleontological evidence of the teeth-to-baleen transition with developmental observations on modern species using a qualitative approach (e.g. Deméré et al., 2008, Peredo et al., 2017). Morphologies and adaptations of specimens from the fossil Aetiocetidae† in particular have been discussed in length in relation to developmental evidence (e.g. Deméré and Berta, 2008, Marx et al., 2016, Fordyce and Marx, 2018). Ontogenetic data seems to point to the possibility of coexistence of proto-baleen structures and tooth germs on both an anatomical level, as seen in Chapter Two, and on a gene expression level, as it was shown that genetic pathways commonly used for tooth growth in mammals are co-opted for baleen (Thewissen et al., 2017). On the surface, this fact supports the interpretation of Aetiocetidae† having both teeth and proto-baleen structures as proposed by some authors (Deméré and Berta, 2008, Deméré et al., 2008, Ekdale et al., 2015). However, as it should be expected, many features of the dentition of fossil aetiocetids do not resemble prenatal modern mysticetes tooth germs: these taxa had heterodont teeth, in contrast with the homodont dentition found in the fetuses, and were not polyodont, retaining tooth counts similar to Archaeocetes, the ancestral group to both

baleen and toothed whales, with less than 20 teeth per side of each jaw (Deméré and Berta, 2008, Marx et al., 2015, Marx et al., 2016). This brought other researchers to argue that the shared genetic pathways and overall morphology observed in extant species ontogeny has evolved independently in a separate group of early Mysticeti and concluded that present developmental evidence does not support the co-occurrence of teeth and baleen in Aetiocetidae† (Marx et al., 2016, Peredo et al., 2017, Fordyce and Marx, 2018). While ontogenetic data are clearly meaningful for understating this macroevolutionary change, information collected on modern species should be used with caution when comparing it to adult morphology of extinct taxa. It is important to avoid excessive simplifications and wrong interpretations by directly comparing adult and fetal morphologies. Similar erroneous interpretations were at the base of the now disproven “biogenetic law” (“ontogeny recapitulates phylogeny”), where the fetal stages of the descendant should resemble more ancestral or “less evolved” forms of that lineage of organisms (Haeckel, 1866, Gould, 1977, Alberch, 1985, Olsson et al., 2017). Unless exceptional specimens of prenatal Aetiocetidae† are found, it is not possible to determine if polyodonty was present in this lineage during development. Potentially, higher level of expression of certain growth factors still active in modern species (Thewissen et al., 2017) or the fusion of many single rooted teeth as observed in the lower jaw of the fetal specimens (e.g. Karlsen, 1962) could explain the heterodont dentition in the fossil adults, without precluding the possibility of prenatal polyodonty and seemingly associated baleen tissue in adults. Moreover, prenatal polyodonty and homodonty might have only been acquired after the loss of adult dentition as a developmental precursor to baleen rack formation (Thewissen et al., 2017). In fact, Aetiocetidae† and similar taxa are hypothesized to only have borne proto-baleen, primitive keratinous structures, which probably would not have presented the organized pattern seen in modern species (Deméré and Berta, 2008), in line with the possible absence of the developmental factors needed for the formation of

a complex modern rack (Thewissen et al., 2017). Additionally, the hypothesized occurrence of enlarged gums in Aetiocetidae† and related taxa might also be correlated with the presence of some precursor of baleen, rather than be an alternative morphology (Peredo et al., 2017, Peredo et al., 2018b). This is supported by the anatomical changes observed in the gum of modern fetal mysticetes, which enlarge medially in the late stages of ontogeny when baleen tissue starts to develop around resorbing tooth germs (Sawamura, 2008, Lanzetti et al., 2018, Lanzetti, in press). Based on a more appropriate application of developmental evidence, the presence of some proto-baleen structure cannot be excluded in Aetiocetidae†, along with thick gums. Possibly other toothed mysticete taxa such as the *Llanocetus*† (Llanocetidae†) might have possessed a baleen-like organ, in addition to the hypothesized enlarged gums, as this taxon had also wide gaps between the teeth in both jaws (Fordyce and Marx, 2018). It has been previously hypothesized that baleen precursors would have been mostly developed or only present at the posterior end of the rostrum, as the majority of the palatal foramina are located in the posterior part of the maxilla in fossils (Sawamura, 2008).

The enigmatic taxa belonging to Eomysticetidae† have also sparked interest about the connection between development and evolution of filter feeding. As many of these taxa have only shallow alveoli and present several traits connected with presence of baleen plates, it has been hypothesized that they only retained small, peg-like teeth in the anterior portion of their jaws, possibly losing this vestigial dentition during postnatal ontogeny (Boessenecker and Fordyce, 2015a, Boessenecker and Fordyce, 2015b, Boessenecker and Fordyce, 2016). The baleen plates would only fully develop in the posterior part of the jaw, making these taxa the first obligate filter feeders, even though they probably were not specialized in any particular mode of filtering like modern species (Boessenecker and Fordyce, 2016). While the pattern of baleen development from the posterior to the anterior end of the palate in the minke whales seems congruent with

previous observations on fossils of Eomysticetidae†, as discussed in Chapter Two in other species (i.e. blue whale) baleen starts developing from the center of the jaw, and more research needs to be conducted in modern mysticetes to determine if the pattern of baleen development is analogous to the position of baleen in Eomysticetidae†. The peg-like tooth shape resembles the conical shape of tooth germs in modern fetal mysticetes, However only one tooth is known, and postnatal tooth shape is not directly comparable with developing tooth germs. The evolution of homodont or simplified dentition in concurrence with the evolution of an organized baleen rack would be congruent with current anatomical and genetic developmental evidence (Thewissen et al., 2017, Lanzetti, in press). It is important to stress that the adult morphology observed in Eomysticetidae† does not contradict hypotheses on the feeding anatomy of toothed stem mysticete groups, as these lineages were mostly coeval and might have occupied different feeding niches and evolved independently (Gatesy et al., 2013, Peredo et al., 2017, Tsai and Fordyce, 2018). In addition, the contentious phylogenetic position of many stem mysticete taxa supports the hypothesis that some of these groups might not approximate the ancestral morphology or feeding mode of the common ancestor of modern mysticete families (Geisler et al., 2017, Fordyce and Marx, 2018, Gatesy et al., 2018, Tsai and Fordyce, 2018). While it is not possible to speculate directly on the feeding strategies of fossil groups using developmental evidence, identifying possible heterochronic patterns and allometrical relationships in the skulls of extinct and extant taxa at different developmental stages could help create a more accurate picture of the teeth-to-baleen transition and of the intermediate morphologies that accompanied it.



## **Research objectives**

In the light of the clear contribution of ontogenetic processes to the evolution of Cetacea and Mysticeti in particular and the rich fossil history of this group, this Chapter aims to combine the previously collected information on the ontogeny of modern species of baleen whales with data from the fossil record. First, by using quantitative methods such as 3D geometric morphometrics (GM) analyses on a dataset including modern taxa at different stages of development and fossil specimens, this study will highlight what major changes in developmental timing and growth rate have enabled the transition of feeding modes during mysticete evolution and how they relate to the teeth-to-baleen transition. Secondly, newly collected ossification sequence data for Mysticeti will be analyzed with information available in the literature for Odontoceti and modern terrestrial artiodactyls using ancestral state reconstruction and independent phylogenetic contrasts methods to identify key heterochronic shifts that characterize Mysticeti and Cetacea as a whole. These analyses will allow the formulation of hypotheses on how these changes are connected to the transition from a terrestrial to an aquatic environment and to the different feeding modes of toothed and baleen whales.

## Materials and methods

### Specimens for skull shape analyses

In this Chapter, all previously described specimens for the minke (*B. acutorostrata* and *B. bonaerensis*) and humpback (*M. novaeangliae*) whales were used in the geometric morphometrics (GM) analyses, as well as additional specimens, both prenatal and postnatal, representing two other modern families of baleen whales: the gray whale (*E. robustus* – Eschrichtiidae), the pygmy right whale (*C. marginata* – Neobalaenidae), and two different species of Balaenopteridae: the sei whale (*B. borealis*) and the fin whale (*B. physalus*). Hf4 CT scan lacks the posterior end of the skull and was excluded from some analyses. In order to incorporate these data in an evolutionary perspective, skull specimens representative of each major fossil group were included in the study: early diverging stem Mysticeti (*Coronodon havensteini*† – Geisler et al., 2017), Aetiocetidae† (*Aetiocetus weltoni*† – (Deméré and Berta, 2008), Eomysticetidae† (*Yamatocetus canaliculatus*† – Okazaki, 2012), and “Cetotheriidae *sensu lato*” (*Diorocetus chichibuensis*† – Yoshida et al., 2003). Given the uncertainty on the phylogenetic position of this last taxon, its placement relative to the other species included in the dataset will be optimized in the context of the morphometric analyses performed. Mammalodontidae were not included as the specimens were not readily available and given their disparate morphology, which is likely not directly connected with the evolution of modern filter feeding (Hampe and Baszio, 2010, Marx, 2011). *Yamatocetus*† and *Diorocetus*† specimens were only available as casts, but both specimens are very well preserved, and the casts used were directly molded from the respective holotype. The 3D models of the specimens were obtained using diceCT/CT scanning, laser surface scanning and photogrammetry. The models for certain postnatal specimens were kindly lent by other researchers to use in this study. A total of 27 specimens is included in GM analyses. Allometric growth analyses were conducted on a subset of these data, indicated with a \*

in Table 3.1. A different dataset (described below) was used to investigate developmental sequence heterochrony given the different nature of that part of the study (sequence of ossification of skull bone elements rather than skull shape changes). All the information on the specimens used in this chapter, including their developmental stages and digitization mode, are listed in Table 3.1.

CT images for the additional specimens were processed following the same protocol as illustrated in Chapter Two and Lanzetti et al. (2018) and Lanzetti (in press). The diceCT protocol applied was also the same. 3D models of CT scanned specimens were constructed in Avizo 9.7 (FEI, 2018) following the same procedure illustrated previously for the minke (Lanzetti, in press) and humpback whales (Lanzetti et al., 2018). For *Coronodon*†, the 3D model of the skull was originally divided in two parts, rostrum and braincase, and the final model was assembled using MeshLab 2016 (Cignoni et al., 2008). Photographs for all photogrammetry models were taken using a Nikon D3200 camera. These models were rendered and cleaned using ReCap software by Autodesk. The surface models provided were not modified. Photogrammetry and surface models were scaled according to their reported or directly measured skull (condylobasal) length with MeshLab.

Table 3.1 – List of specimens included in quantitative shape analyses in Chapter Three.

Specimen code	Catalog number	Species	Family	TL (cm)	Growth stage	Digitalization method	Data provided by
He1	AMNH232597	<i>Megaptera novaeangliae</i>	Balaenopteridae	17	embryo	diceCT	AL
Hf1*	AMNH99602	<i>Megaptera novaeangliae</i>	Balaenopteridae	31	early fetus	diceCT	AL
Hf2	MVZ123560	<i>Megaptera novaeangliae</i>	Balaenopteridae	79	early fetus	diceCT	AL
Hf3*	SDNHM25552	<i>Megaptera novaeangliae</i>	Balaenopteridae	70	early fetus	diceCT	AL
Hf4* <sup>x</sup>	ZMUC-CN15	<i>Megaptera novaeangliae</i>	Balaenopteridae	103	late fetus	CT scan	AL
Hj1*	LACM097707	<i>Megaptera novaeangliae</i>	Balaenopteridae	800	juvenile	Photogrammetry	AL
Mf3*	ZMUC-CN6x	<i>Balaenoptera acutorostrata</i>	Balaenopteridae	48	early fetus	CT scan	AL
Mf4*	NSMTblue10	<i>Balaenoptera bonaerensis</i>	Balaenopteridae	74	early fetus	CT scan	AL
Mf5*	NSMTwhite11	<i>Balaenoptera bonaerensis</i>	Balaenopteridae	110	late fetus	CT scan	AL
Mf6*	NSMTwhite15	<i>Balaenoptera bonaerensis</i>	Balaenopteridae	110	late fetus	CT scan	AL
Mf7*	NSMT27171	<i>Balaenoptera bonaerensis</i>	Balaenopteridae	115	late fetus	CT scan	AL
Mf8*	ZMUC-CN4x	<i>Balaenoptera acutorostrata</i>	Balaenopteridae	125	late fetus	CT scan	AL
Mf9*	NSMT27175	<i>Balaenoptera bonaerensis</i>	Balaenopteridae	182	late fetus	CT scan	AL
Mf10*	NSMT27174	<i>Balaenoptera bonaerensis</i>	Balaenopteridae	212.5	late fetus	CT scan	AL
Mn1*	USNM593554	<i>Balaenoptera acutorostrata</i>	Balaenopteridae	351	neonate	CT scan	Smithsonian Institution Bio-Imaging Research Center

Mn2*	LACM72507	<i>Balaenoptera acutorostrata</i>	Balaenopteridae	308	neonate	Surface laser scanning	G. Franci (Franci and Berta, 2018)
Ma1*	HSU2670	<i>Balaenoptera acutorostrata</i>	Balaenopteridae	700	adult	Surface laser scanning	G. Franci (Franci and Berta, 2018)
Ma2*	CAS23807	<i>Balaenoptera acutorostrata</i>	Balaenopteridae	800	adult	Surface laser scanning	G. Franci (Franci and Berta, 2018)
Ff1	ZMUC-CN43	<i>Balaenoptera physalus</i>	Balaenopteridae	85	early fetus	CT scan	AL
Sf1	MVZ125084	<i>Balaenoptera borealis</i>	Balaenopteridae	88	early fetus	diceCT	AL
Pn1	NMNZ012998	<i>Caperea marginata</i>	Neobalaenidae	191	neonate	CT scan	Emily Buchholtz Smithsonian Institution Bio-Imaging Research Center
Ge1	USNM504752	<i>Eschrichtius robustus</i>	Eschrichtiidae	15	embryo	CT scan	Eric G. Ekdale
Gn1	SDNHM25307	<i>Eschrichtius robustus</i>	Eschrichtiidae	394	neonate	CT scan	Eric G. Ekdale
<i>Coronodon</i> †*	CCNHM108	<i>Coronodon havensteini</i> †	n.a.	500	adult	CT scan	Jonathan H. Geisler
<i>Aetiocetus</i> †*	UCMP122900	<i>Aetiocetus weltoni</i> †	Aetiocetidae	500	adult	CT scan	Eric G. Ekdale
<i>Yamatocetus</i> †*	KMNH-VP-000.017	<i>Yamatocetus canaliculatus</i> †	Eomysticetidae	500	adult	Photogrammetry	AL
<i>Diorocetus</i> †*	SMNH-VeF-68	<i>Diorocetus chichibuensis</i> †	"Cetotheriidae s.l."	600	adult	Photogrammetry	AL

X=incomplete 3D model of skull; \*=specimens used in 2D allometry analysis; AMNH: American Museum of Natural History, New York, NY, USA, CAS: California Academy of Sciences, San Francisco, CA, USA, CCNHM: Natural History Museum, College of Charleston, Charleston, SC, USA, HSU: Natural History Museum Humboldt State University, Arcata, CA, USA, KMNH: Kitakyushu Museum of Natural History and Human History, Kitakyushu, Japan, LACM: Natural History Museum of Los Angeles County, Los Angeles, CA, USA, MVZ: University of California, Museum of Vertebrate Zoology, Berkeley, CA, USA, NMNZ: Museum of New Zealand Te Papa Tongarewa, Wellington, New Zealand, NSMT: National Museum of Nature and Science, Tsukuba, Japan, SDNHM: San Diego Natural History Museum, San Diego, CA, USA, SMNH: Saitama Prefectural Museum of Nature, Nagatoro, Japan, UCMP: University of California, Museum of Paleontology, Berkeley, CA, USA, ZMUC: Natural History Museum of Denmark, Copenhagen, Denmark

## **2D measurements and allometric growth analyses**

To test how the size of different parts of the skull change during growth, selected measurements of skull features were compared to the total condylobasal length (CBL) of the whale specimens. This method was selected to replicate the study of Nakamura et al. (2012) and Nakamura and Kato (2014) on the postnatal allometric growth of minke whales and other balaenopterids. 2D measurements were collected on the 3D reconstructed internal morphology of the skulls of minke (*B. acutorostrata* and *B. bonaerensis*) and humpback (*M. novaeangliae*) whale specimens. Only specimens that were not clearly deformed and that could be reliably measured were used. All measurements were taken on the 3D renderings of the skulls of the specimens in cm using the software MeshLab (Cignoni et al., 2008). The skull measurements, selected from the ones collected in Nakamura and Kato (2014), are the following: rostral length (RL), rostral width (RW), greatest width of the occipital bone (GWOB), and skull height (SH). A new measurement not present in the original study was added to test the allometric growth of the braincase compared to the whole skull (BCL) (Figure 3.2). The specimens used and their measurements are reported in Table 3.2. Measurements for Hf4 were estimated based on external features where the CT scan images did not include the posterior end of the skull.

For the analyses, all measurements were transformed in the natural logarithmic scale and then a linear regression of each measurement on CBL was performed. All variables were significantly correlated with CBL for the minke whales, instead only RL, GWOB and BCL showed a significant correlation in the humpback whale (Table S3.1 – Appendix F). This is probably an artifact of the low sample size and disparate ontogenetic age of the specimens. In any case, RW and SH for the humpback whale were excluded from the subsequent analysis.

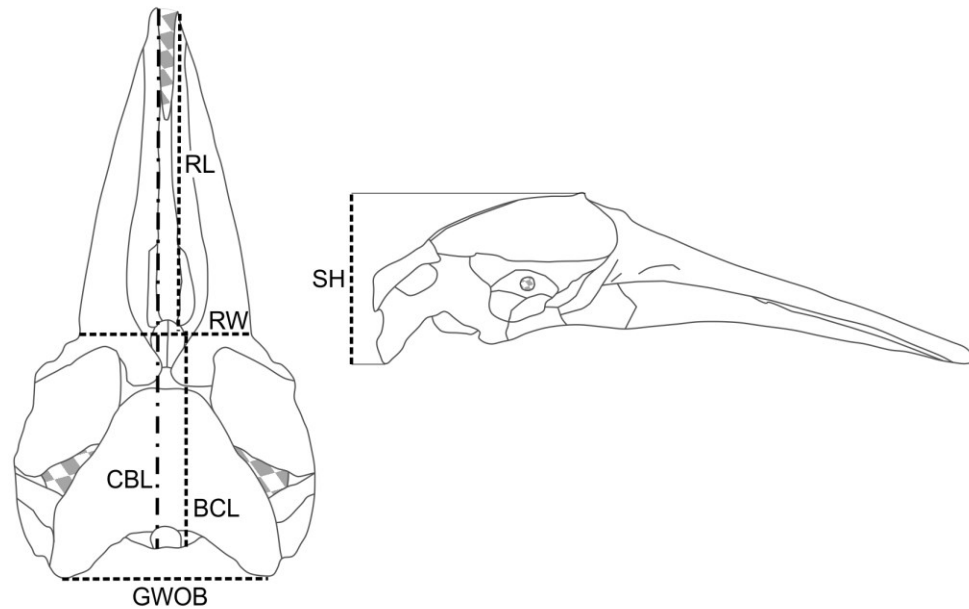


Figure 3.2 – Measurements used in 2D allometric analyses. Silhouette of adult minke whale skull from Lanzetti et al. (2018).

The linear correlation test produced the parameters (constant and allometric coefficients) needed to demine the allometric growth equation for each part of the skull measured, employed by Nakamura and Kato (2014):

$$\text{Log}Y = \text{Log}\beta + \alpha * \text{Log}CBL \Rightarrow Y = \beta X^\alpha$$

where  $X$  represents CBL,  $Y$  the analyzed skull measurements,  $\alpha$  is the allometric coefficient and  $\beta$  the constant. For the significant correlations, the values of  $\alpha$  (lower bound, mean, upper bound) were analyzed for each skull measurements using a 1-sample t-test to test if the allometric coefficient was significantly different from 1 ( $t \neq 1$ ). If the null hypothesis could not be rejected (t-test  $p > 0.05$ ), then the growth of the skull component can be defined as isometrical to the rest of the skull. If the null hypothesis was rejected, the growth was considered positive allometric if  $\alpha\text{-mean} > 1$ , and negative allometric if less than 1. Coefficients were calculated and tested separately for the two groups of species (minkes and humpback whales).

Table 3.2 – Measurements used in 2D allometric analyses (cm). Specimen codes as Table 3.1.

Specimen code	CBL	RW	SH	GWOB	RL	BCL
Hf1	9.83	3.05	4.2	2.8	7	5.63
Hf3	16.16	7.49	7.32	4.98	7.36	8.84
Hf4	28*	9.95	18.59	7*	10.6	9.41
Hj1	223	61.4	130	83	107	93
Mf3	13.85	4.75	6.97	6.78	6.85	6.88
Mf4	20.93	9.48	11.26	8.44	11.42	9.67
Mf5	27.8	10.88	14.32	9.29	13.47	13.48
Mf6	33.73	12.6	17.6	11.82	13.06	16.13
Mf7	33.11	11.7	17.44	11.52	16.05	15.67
Mf8	34.22	7.78	17.91	7.57	9.94	16.31
Mf9	49.94	13.73	28.46	17.06	15.77	21.48
Mf10	49.5	13.9	21.2	16.71	17.76	28.3
Mn1	92.43	27.33	50.58	36.33	31.54	41.85
Mn2	54.51	18.86	28.92	24.25	21.55	25.59
Ma1	66.85	20.38	37.29	26.43	24.92	29.56
Ma2	135.93	43.86	77.11	58.3	51.38	58.82
<i>Coronodon</i> †	63.86	19.82	32.15	30.7	19.23	31.71
<i>Aetiocetus</i> †	78.88	24.4	48.07	27.4	23.35	30.81
<i>Yamatocetus</i> †	109.67	24.92	83.8	33.51	28.25	25.87
<i>Diorocetus</i> †	133.38	31.67	82.01	31.98	29.24	51.37

Independently of these previous analyses, the change of size in each skull component during growth was visualized relative to CBL, plotting the % of the measurement for that skull component relative to CBL on the Y axis and CBL on the X axis. The species were plotted together, and a power regression line was calculated for each to best represent their growth pattern for that feature on the plot. Measurements of the corresponding features of the fossil skulls (*Coronodon*†, *Aetiocetus*†, *Yamatocetus*†, *Diorocetus*†) were also added to these plots, to see how their skull proportions relate to the ones of the modern species during ontogeny. All analyses were conducted in Microsoft Excel and XSTAT (Addinsoft, 2019).



## **Landmarks and 3D morphometrics analyses**

### *Landmark acquisition and data preparation*

To quantitatively assess the relationship between developmental and evolutionary shape changes, landmark-based 3D geometric morphometric (GM) analyses were performed using the same landmarks and workflow described in Chapter Two and in previous work (Lanzetti et al., 2018, Lanzetti, in press). Landmarks were collected using Avizo 9.7 (FEI, 2018) for all specimens in both configurations except Hf4. The CT scanning of this specimen lacks the posterior end of the skull and therefore it was only included in the rostrum-only analyses. Landmark collection was repeated twice by the same operator (A. Lanzetti) to minimize errors. Two configurations were analyzed: one including the whole skull (16 landmarks) and one including only the rostrum (12 landmarks) (Fig. S3.1, Table S3.2 – Appendix F). The whole skull configuration allows the evaluation of the shape changes in the braincase compared to the rostrum, while the rostrum-only dataset makes it possible to better relate changes in shape to different feeding adaptations. The dentaries were not included in these landmark analyses as well as they are deformed or broken in many prenatal and fossil specimens. Embryonic and fetal specimens might be slightly deformed due to preservation, as discussed for the minke and humpback specimens in Chapter Two (Lanzetti et al., 2018, Lanzetti, in press). However, also for the additional specimens included here, the deformations appear to be minimal and they do not affect the analysis. Fossils are also subject to deformation during diagenesis, therefore the specimens were selected taking this factor into account. The fossil specimens used in this study are among the best preserved representatives of each group and represent the most suitable specimens for comparison that were available (Deméré and Berta, 2008, Gol'din et al., 2015, Boessenecker and Fordyce, 2016, Geisler et al., 2017).

The landmark coordinates for the two configurations, whole skull and rostrum-only, were imported separately into MorphoJ 1.07a (Klingenberg, 2011) for analysis. As for Chapter Two, this software was chosen since it incorporates the generalized least-squares Procrustes superimposition, which aligns the homologous landmark collected on the specimens correcting for the different sizes and orientations (Rohlf and Slice, 1990). The landmarks were imported assuming object symmetry, as the skulls of both modern and fossil mysticetes were proven to be symmetrical (Fahlke and Hampe, 2015). The same analysis workflow described below was applied to both landmark configurations. The data were analyzed starting from the same protocol described in Chapter Two: first, consistency between landmark takes was tested by performing an ANOVA analysis on the shape coordinates (Appendix E). Secondly, after confirming that the two takes were statistically identical, the two takes were averaged to obtain an average landmark configuration representing the skull shape of each specimens, creating an averaged “by specimen” dataset. A separate dataset with skull shapes averaged “by species” was also created to use in other analyses.

### *3D skull shape allometry (whole skull)*

To quantify the allometric changes in skull shape relative to its size during ontogeny, regression analyses were performed in the whole skull configuration for the same humpback and minke whales’ specimens used in the 2D analyses, as listed in Table 3.2, plus He1 and Hf2 but excluding Hf4. This test, conducted in MorphoJ, compared the symmetric component of skull shape of the samples of each species with their size, expressed as Log Centroid Size (LogCS). The regression for the minke whales was significant ( $p=0.0036$ ), while the one for the humpback whale was not significant, probably because of the low sample size and uneven ontogenetic sampling ( $p=0.3015$ ). As MorphoJ does not directly provide a regression coefficient for this analysis, the regression scores representing each specimen and their LogCS were then exported

and the linear regression coefficients (*Loga*) and intercept (*b*) were calculated independently for the two species in Microsoft Excel and XLSTATS. If the back-transformed regression coefficient *a* is very close to 1, it indicates that the shape and size are changing at a similar rate (isometrically). If it is measurably higher or lower, then one of the two variables is changing at a higher rate relative to the other (Klingenberg, 1998, Klingenberg, 2005). The type of allometric growth pattern was then determined performing a one sample t-test as done for the 2D data ( $t \neq 1$ ). To compare the shape growth of modern species with the fossils, a separate regression was conducted in MorphoJ including only the fossil specimens. These shape scores and relative LogCS values were then exported and displayed on the same plot as the minke and humpback specimens to understand how their skull shape related to their size, as in the 2D graphs.

#### *Skull shape variation (whole skull and rostrum-only)*

After this initial set of tests, all other GM analyses were conducted on the entire dataset (Table 3.1). Since multiple species at different developmental stages are included, the influence of allometry must be taken into account in the following analyses. An “allometric correction” was applied to each dataset, “by specimen” and “by species”, using the same regression analysis employed to evaluate 3D shape variation in the minke and humpback whales (symmetric shape data vs LogCS). As this regression was highly significant in both datasets, showing a strong correlation between shape and size (Table S3.3 – Appendix F), the residuals of the regression, representing the shapes corrected for evolutionary and growth allometry, were used in subsequent analyses. This method is widely applied in GM studies of evolutionary and developmental shape changes, as the residual shapes can be compared to find characteristic changes in shape without the confounding variable of size-related variation (Drake and Klingenberg, 2008, Klingenberg and Marugán-Lobón, 2013).

For both the whole skull and rostrum-only configurations, a Principal Component Analysis (PCA) was conducted to visualize the variation in the “by specimen” dataset on a few major axes (Klingenberg, 2011, Klingenberg and Marugán-Lobón, 2013). As this study only contains 27 samples (26 for the whole skull configuration) and some species are only represented by a single specimen, in order to best visualize differences in shape among species, additional analyses are warranted to test if the difference among species was captured correctly by this analysis. A separate PCA was performed on the dataset averaged “by species” using the residual shapes after allometric correction, following the methodology detailed by Mitteroecker and Bookstein (2011). The PC scores representative of the different species obtained were then applied to the residual shapes of the dataset averaged “by specimen”. This method creates a “between groups PCA” (bgPCA), where differences among the chosen groups, in this case species, are highlighted. Similar results could be obtained by performing a CVA (Canonical Variate Analysis) but having only one sample for certain species precludes this option (Klingenberg, 2011, Mitteroecker and Bookstein, 2011).

A set of phylogenies was mapped on the PC axes of the bgPCA to best visualize how shape changed through phylogenetic time in Mysticeti (Klingenberg and Gidaszewski, 2010, Klingenberg, 2011). Given that this study includes many prenatal specimens, this analysis also provides a direct comparison between developing skull shape in living species and adult fossil morphology by showing the relative position of the fossils to prenatal specimens of modern species. Using these observations, it will be possible to formulate hypotheses on the heterochronic processes at play in the evolution of mysticetes such as paedomorphism and peramorphism. MorphoJ uses squared-change parsimony to calculate the position of the taxa on the trees mapped on the bgPCA plot, allowing to test the fit of different phylogenetic hypotheses to the data (Klingenberg, 2011). Therefore, using a p-value calculated in 10,000 permutations and

the total tree length, it was possible to identify the best phylogeny for the taxa included in the dataset among the ones assembled considering different relationships proposed in the literature (Figure 3.3). This method allows the formulation of the most accurate hypotheses given the data and taxa sampled.

The bgPCA scores were also visualized using box plots to highlight how fossil skull shapes compare to the skull at different stages of development in modern species. The scores of the two components representing most of the variation for the whole skull and rostrum-only analyses were exported and the box plots were built using XLSTAT in Microsoft Excel.

#### *Skull modularity and within-configuration variation (whole skull)*

To evaluate if the braincase and the rostrum change shape independently both during evolution and development, a modularity test was performed on the whole skull configuration (Klingenberg, 2005, Klingenberg, 2009, Goswami and Polly, 2010b, Klingenberg and Marugán-Lobón, 2013). The analysis was performed on the residual shapes of the dataset averaged “by specimen” using the same blocks identified in Chapter Two: the rostrum (landmarks 1-2-3-10-11-12-13) and the braincase (landmarks 4-5-6-7-8-9-14-15-16), considered within the same configuration. The resulting RV coefficient, a measure of independence of the position of the landmarks representing the analyzed skull components, was calculated comparing these *a priori* partitions with 10,000 randomly generated contiguous partitions.

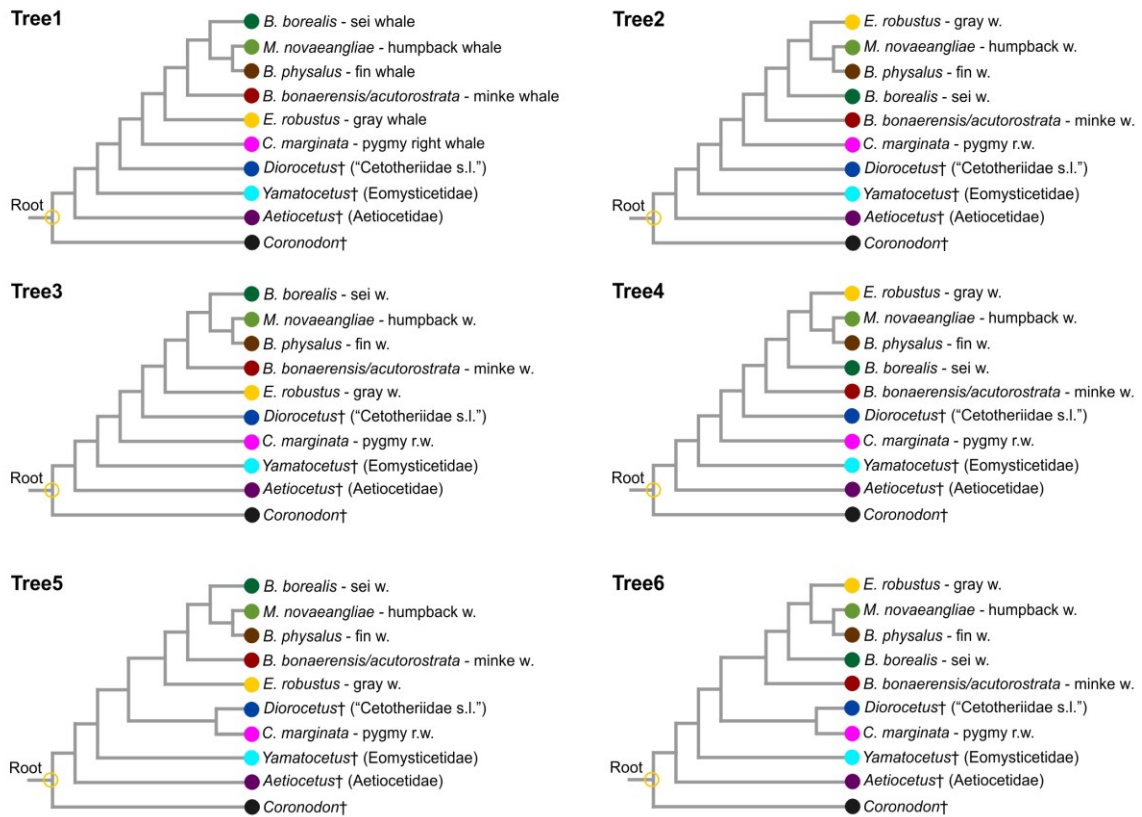


Figure 3.3 – Phylogenetic relationships tested in GM analyses. Tree topologies are assembled to reflect the different phylogenetic placements of the genera *Eschrichtius*, *Caperea* and *Diorocetus*†. Sources: Marx (2011), Gatesy et al. (2013), Marx and Fordyce (2015), Berta et al. (2016), and Marx et al. (2019). Colors for taxa used here are the same in all other figures.

Modularity and the connection between shape changes in the rostrum and the braincase were investigated further by performing a within-configuration Partial Least Squares (PLS) analysis (Goswami and Polly, 2010b). This analysis was conducted on the same dataset and using the same partitions as the modularity test. This method also tests the hypothesis of independence between these two partitions by calculating a p-value (1,000 permutations) (Goswami and Polly, 2010b, Klingenberg and Marugán-Lobón, 2013). The same set of trees used for the bgPCA analyses was also mapped on the PLS axes to visualize how the rostrum and the braincase change relative to each other in evolution and identify heterochronic patterns specifically connected to one of the two parts of the skull. The fit of the tree was evaluated with the same method

employed in the bgPCAs. Also similar to Chapter Two, a regression analysis was conducted between the rostrum and braincase PLS scores to quantify the evolutionary allometric relationship between these two partitions. MorphoJ in this case provides a coefficient for the regression as well as a p-value to evaluate the goodness of the fit (10,000 repetitions). If the coefficient is close to 1, the shape of two partitions would be evolving at the same rate. Lower or higher values indicate relative differential rates of evolution of the braincase and rostrum. The slope was added graphically to the plot after converting the coefficient in an angular measurement using Microsoft Excel.

### **Ossification sequence heterochrony data and analyses**

#### *Taxa selection and ossification sequence matrix*

Ossification sequence heterochrony was tested using the dataset provided by Koyabu et al. (2014) (abbreviated as KEA2014 from here). This work included all mammalian lineages, but for the present study only members of Cetartiodactyla were included. The taxa selected from KEA2014 matrix are the following: *Bos taurus* (cattle), *Ovis aries* (domestic sheep), *Capra (aegagrus) hircus* (domestic goat), *Capreolus* (European roe deer), *Stenella attenuata* (pantropical spotted dolphin), *Sus scrofa (domesticus)* (domestic pig), *Camelus dromedaries* (dromedary). The species *Dama dama* (fallow deer) was excluded from this study as its ossification sequence in the KEA2014 matrix is not well defined. Its sequence only includes three stages of ossification, and this can negatively affect the ancestral state reconstruction of ossification timing, as detailed below. Two additional species of Cetacea were added to the KEA2014 dataset: *Physeter macrocephalus* (sperm whale), and *Megaptera novaeangliae* (humpback whale). The sequence for the sperm whale was described by Kuzmin (1976), while the one of the humpback whale is detailed in Chapter Two and in Lanzetti et al. (2018). The humpback was the only baleen whale species that can be used for these analyses, as all specimens

of minke whales examined are in the fetal period, when most centers of ossification have already appeared. Moreover, the ossification sequence of these two species is likely identical given their close phylogenetic relationship (both in the Balaenopteridae). The phylogenetic placement of the taxa and node dates follow Gatesy (2009) and Bininda-Emonds et al. (2007), as in KEA2014 (Fig. S3.2 – Appendix F).

The ossification sequences were coded by noting the first appearance or description of an ossification center in the area where that bone element is present in the adult. Bones that start ossifying at the same stage present the same number, while the progression of numbers (ontogenetic ranks) indicates when the ossification of those elements occurs in comparisons to the other bones. Higher ontogenetic ranks indicate that ossification starts later in the developmental process compared to lower ranks. This is the standard procedure to code ossification sequences as done in KEA2014 and other studies (e.g. Fröbisch et al., 2007, Sánchez-Villagra et al., 2008). When the KEA2014 coding was derived from the literature, their matrix was checked against the original source. The sequences used include all major skull bone elements. Certain bone elements not recognizable in the humpback whale were removed from the KEA2014 matrix (orbitosphenoid, alisphenoid, goniale), but the total number of ranks for the taxa previously coded was left unchanged. The start of tooth mineralization was added to the matrix using data from the literature and direct observation for the humpback whale, as this trait, even if not due to an ossification event, is of interest in this study. It was ranked consistently with the bone elements. The final matrix contains 9 taxa and 19 developmental events. It can be found in Appendix E, including the literature references used to infer the coding.

#### *Heterochronic changes in ossification sequences*

Firstly, this matrix was used to highlight heterochronic changes in the skull ossification sequence during evolution. In KEA2014 this was accomplished using the PGi algorithm



(Harrison and Larsson, 2008). However, this method is computationally intensive, and the results can be compromised if there are a similar number of ontogenetic ranks and taxa (Harrison and Larsson, 2008, Maxwell and Harrison, 2009). The package is also not currently available from the R library ([www.cran.r-project.org](http://www.cran.r-project.org)). Given these challenges and the preliminary nature of this study, as it includes only three species of Cetacea, the group of interest, the heterochrony analysis was conducted in PAUP\* 4.0a164 (Swofford, 2003) using maximum parsimony (MP). Parsimony has been found to be an overall reliable, but conservative, method to estimate heterochronic changes (Maxwell and Harrison, 2009). This has been accomplished mostly by using event-pairing methods (e.g. Jeffery et al., 2002a, Jeffery et al., 2002b) to uniform ossification sequences of distantly related taxa with a wide range of developmental time (e.g. skull elements ossification heterochrony between eutherian and marsupial mammals – Smith, 1997). In this case However, the taxa considered are all relatively closely related to each other and with fairly conserved developmental sequences, therefore the matrix can be used as-is, similar to what is done with the PGI algorithm, to produce more informative results (Jeffery et al., 2002b, Maxwell and Harrison, 2009). The ossification sequence matrix and the selected phylogeny (Gatesy, 2009) were imported in PAUP\*, and the heterochronies were identified using the “Apomorphy list” function from the “Describe tree” command under the “Tree” menu. This function displays the change in characters’ state occurring on any branch of the tree. The characters represent the skull elements and the states are the ontogenetic rankings. If the ontogenetic rank goes from a higher number to a lower number on the branch, than that element starts ossifying earlier in the descendants of that branch, resulting in an acceleration of the start of its development. If the opposite is true – the ontogenetic rank goes from a lower to a high number on the branch – then the element has delayed ossification in the descendants. The heterochronic changes were tested using both ACCTRAN and DELTRAN optimizations, as the algorithm can affect the results of the analysis

(Maxwell and Harrison, 2009). PAUP\* was also used to calculate developmental sequence similarity under the MP model. A heuristic search was performed using TBR branch-swapping algorithm, with simple addition using the dromedary as reference taxon, since it represents the earliest diverging lineage of the group in the phylogeny employed in the study (Gatesy, 2009). Also in this case both ACCTRAN and DELTRAN algorithms were used, and they produced the same taxon arrangement with equal parameters. These analyses, while producing a tree, do not have phylogenetic value. This step was useful to order the developmental sequences by similarity and highlight the shifts of interest among the analyzed taxa. The results were then used to create a graphical representation of the ossification sequences and the relative changes in timing of ossification of skull elements in different taxa, similar to Figure 9 in Olori (2013).

*Ossification timing ancestral states and correlation of heterochronic changes*

Secondly, the matrix was transformed from standard to continuous characters, using the method outlined in KEA2014, to allow for ancestral state reconstruction of the ossification timing of each element on the phylogeny. By using the formula:

$$(r - 1) / (r_{max} - 1)$$

where  $r$  represents the developmental rank (state) of a given element (character), and  $r_{max}$  is the total number of ranks for that species, the states become continuous and uniform across all taxa, independently of the total rank number of each species, which is usually an artifact of the resolution of the ossification sequence data (Koyabu et al., 2011, Koyabu et al., 2014). The first elements to ossify will be coded as 0 while the last ones will be coded as 1, with all the others falling in that range. This method can only be applied for sequences with >3 ranks, and this brought to the exclusion of *Dama* from the analyses. Encephalization quotient (EQ) was added to the matrix as it was found to be correlated with supraoccipital ossification heterochrony by KEA2014. The values were either reported in the original work or derived from Ridgway et al.

(2017) for the taxa unique to this study (humpback and sperm whale). The transformed matrix and the EQ values are also provided in Appendix E. The continuous matrix and the phylogeny with branch lengths were then imported in Mesquite 3.6 (Maddison and Maddison, 2018) for analysis. The protocol followed for the ancestral state reconstruction (ASR) was similar to the one described in Chapter Two. The ASR was conducted using squared-change parsimony, which assumes that the character evolves under a Brownian motion model (Maddison, 1991). Each element was traced separately on the tree. After this step, the fit of each character's reconstructed states to the evolution model was tested using the PDAP package (Midford et al., 2005). All characters' state changes resulted to be congruent with the evolutionary model. In Appendix E the results of this analysis for the characters of interest (maxilla, dentary, supraoccipital, teeth, EQ) are reported. Using PDAP, Felsenstein's phylogenetic independent contrasts were calculated for the following pairs of characters of interest: maxilla and teeth, dentary and teeth, supraoccipital and EQ. Changes in timing of ossification of maxilla and dentary and tooth mineralization might be correlated with each other and could play a role in the teeth-to-baleen transition. As it was amply discussed in KEA2014, also the relationship between ossification of the supraoccipital and EQ was tested. All of the three tests that were performed failed to recover a significant relationship between the changes of states of the two characters (Appendix E). As this study used a limited sample size with only eight contrasts to compare and PDAP has limited statistical capabilities (PDAP user manual – Midford et al., 2005), the results of these analyses were exported to be further analyzed in Microsoft Excel using XLSTAT. The exported unstandardized contrasts were first converted in standardized contrasts (PDAP user manual – Midford et al., 2005) and then a Pearson correlation test was performed between the same pairs listed above to test if a significant correlation could be detected.

## Results

### **Allometric changes in skull proportions in Mysticeti**

In 2D allometric analyses, all measured skull elements for the minke whales were found to grow isometrically with the skull length, with an allometric coefficient ( $\alpha$ ) not significantly different from 1 (Table 3.3). This result is different from what was reported by Nakamura and Kato (2014) for the postnatal ontogeny of the common minke whale. These authors found that only GWOB has an isometric growth relative to the skull, with all other elements having positive allometric increase during development, except BCL that was included in the study. The present finding also differ from the ones of Franci and Berta (2018), which employed the same methodology as Nakamura and Kato (2014) on the same species and growth stage but with a smaller sample size. They found a positive growth allometry only for RL, and all other components had a negative relationship with CBL, again without considering BCL. They also tested the relative changes between multiple measurements that represented the braincase area relative and the rostral area relative to skull size. In this analysis, the rostrum and braincase showed opposite allometric patterns, with the rostrum still having positive allometry, while the braincase has a negative rate. Given this evidence, it is possible that during prenatal development the growth both in size and shape of the parts of the skull is isometrical, while this pattern mostly changes after birth, causing the differences in allometric trends described here. However, the present analysis might have been influenced by the fact that both species of minke whales (Antarctic and common) were considered together, and minor differences in their development might skew the results. While the results of the allometric analyses conducted here differ from both previous studies, they are in line with the 3D analysis of rostrum and braincase shape changes in Chapter Two, in which both elements changed isometrically with total size. It is

notable However that RL has a higher allometric coefficient than BCL, implying faster growth. The 3D analysis in Chapter Two showed the opposite pattern, with the braincase growing in shape faster than the rostrum.

Table 3.3 – 2D allometric coefficients and growth patterns in minke (M) and humpback (H) whales.

Measurement	$\alpha$	$\beta$	t-test p-value	Growth pattern relative to CBL
GWOB-H	1.081	0.241	0.440	Isometric
RL-H	1.098	0.343	<b>0.043</b>	Positive
BCL-H	0.898	0.725	<b>0.011</b>	Negative
RW-M	0.893	0.480	0.450	Isometric
SH-M	0.816	0.798	0.234	Isometric
GWOB-M	1.015	0.349	0.926	Isometric
RL-M	1.040	0.453	0.504	Isometric
BCL-M	0.952	0.563	0.427	Isometric

p-value<0.05 corresponds to  $\alpha \neq 1$  in t-test. Significant values in bold.

The humpback whale instead was found to have a positive allometric growth of the rostrum (RL) relative to CBL and a negative allometric growth of the braincase (BCL) (Table 3.3). While there are no previous studies on this species, this finding is congruent with the patterns recovered in postnatal common minke whales (Nakamura and Kato, 2014, Franci and Berta, 2018). As this study is the first attempt to analyze allometry in the skull of humpback whales, these results will need to be validated using a larger sample size and separating prenatal and postnatal ontogeny as they might show different allometric patterns as hypothesized for the minke whales that are not recovered here due to the disparate ontogenetic sampling.

Both species have comparable growth trajectories for the proportions of skull elements relative to CBL. Considering how these relate to the proportions in the fossil taxa, it is interesting to notice that both *Aetiocetus*† and *Coronodon*† have similar ratios of the different components to late fetal and neonatal specimens of minke whales for all variables measured (Figure 3.4).

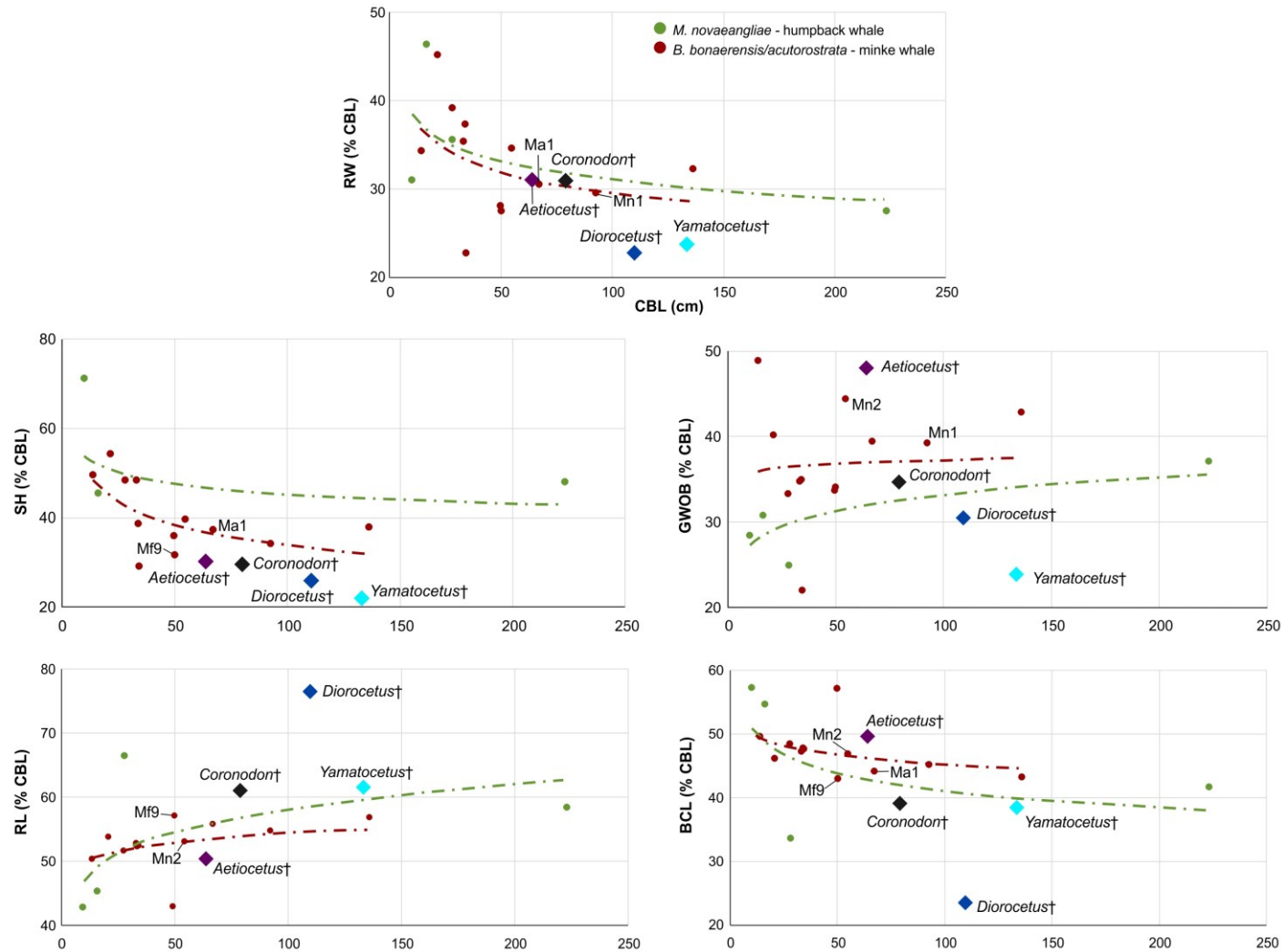


Figure 3.4 – 2D changes in proportions of each variable relative to skull length. Ratios of measurements relative to CBL on Y axis, CBL on X axis. Circles=specimens of minke and humpback whales, diamonds=fossil specimens. Color legend in RW is the same for all plots.

This evidence seems to suggest that these taxa had a similar growth pattern to modern whales, but they did not reach the mature proportions of these living species, making modern rorquals peramorphic relative to these stem mysticetes, as proposed by Tsai and Fordyce (2014). *Yamatocetus*† and *Diorocetus*† instead have distinct skull proportions for RW, GWOB and SH. Considering RL and BCL relative to skull length, *Diorocetus*† appears to have a long rostrum and short braincase compare to skull length, while *Yamatocetus*† appears similar in this aspect to postnatal minke and humpback. This might be caused by a closer phylogenetic relationship, and possibly overlapping feeding adaptations, between *Yamatocetus*† and similar Eomysticetidae† and modern rorquals.

Analyzing the 3D skull shape changes during growth in minke and humpback whales relative to its size (Fig. 3.5), both species have similar coefficients and show isometric growth, with the calculated coefficients not significantly different from 1 (Table 3.4).

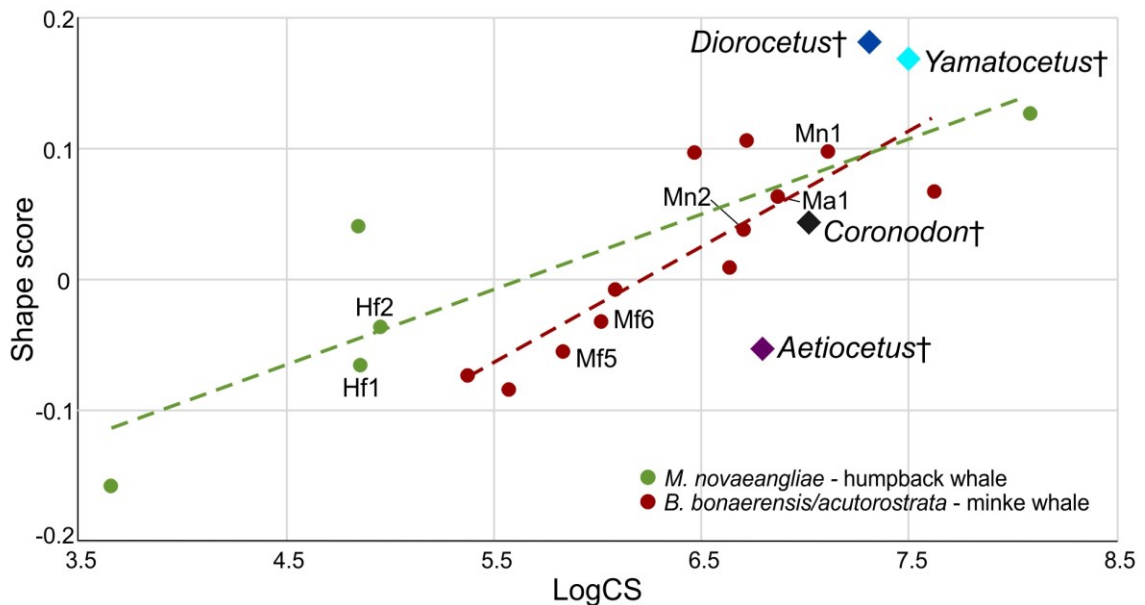


Figure 3.5 – 3D changes in skull shape relative to skull size. Shape score on Y axis, size as LogCS on X axis. Circles=specimens of minke and humpback whales, diamonds=fossil specimens. Color legend is the same as Fig. 3.4.

Table 3.4 – 3D allometric coefficients and growth patterns in minke (M) and humpback (H) whales.

Species	<i>a</i>	<i>b</i>	t-test p-value	Growth pattern relative to LogCS
<i>Megaptera novaeangliae</i>	1.093	-0.325	0.214	Isometric
<i>Balaenoptera acutorostrata/bonaerensis</i>	1.060	-0.552	0.068	Isometric

p-value<0.05 corresponds to  $\alpha \neq 1$  in t-test. Significant values in bold.

The position of the fossil taxa relative to the living species is in line with the pattern observed for the 2D analyses. *Yamatocetus*† and *Diorocetus*† plot separately from modern specimens, with higher shape score values. This might be due to their longer rostrum relative to braincase. *Aetiocetus*† and *Coronodon*† instead have a similar skull shape to fetal specimens of both minke and humpback whales. This again points to a possible peramorphic heterochronic change in the growth of modern species relative to their ancestors. A slower growth rate or shorter developmental time in these earlier stem Mysticeti lineages could explain their skull shape, while later toothless lineages would have acquired a positive allometric growth in the rostral region only, explaining their different rostrum and braincase ratios relative to skull length and unique shape scores. All these hypotheses are preliminary and should be tested with a larger sample size to study the growth pattern of other mysticete families (e.g. Balaenidae). However, they represent a starting point to interpret the results of more comprehensive 3D GM analyses.

### **Skull shape variation and modularity in the evolution of Mysticeti**

#### *Principal Component Analyses*

The PCA analysis conducted on the whole skull configuration “by specimen” dataset after allometric correction found 21 principal components, with the first eight describing 95% of the variation. The scatter plot of points and complete PCA results can be found in Figure S3.3 and Table S3.4 (Appendix F). After conducting a PCA analysis also on the “by species” dataset for this configuration corrected for allometry, the scores from this second PCA were applied to the



“by specimen” dataset to conduct the bgPCA analysis. Eight components were identified by the bgPCA, with bgPC1 and bgPC2 representing most of the total variation (46.3%) (Table 3.5).

Table 3.5 – bgPCA principal components for both configurations. Components ordered according to the amount of variation they represent, from largest to smallest.

<u>Whole skull configuration</u>		<u>Rostrum-only configuration</u>	
Principal Component	% Total Variance	Principal Component	% Total Variance
bgPC1	26.20	bgPC4	28.85
bgPC2	20.17	bgPC1	21.49
bgPC4	18.94	bgPC2	18.01
bgPC3	15.12	bgPC3	13.57
bgPC5	10.70	bgPC5	5.62
bgPC6	4.06	bgPC6	5.51
bgPC8	3.32	bgPC7	4.81
bgPC7	1.52	bgPC8	2.14

To better visualize and interpret the phylogenetic relationships among the data, the topologies presented in Figure 3.3 were tested for correlation with the PCA scores. None of the tested trees was found to be significantly correlated with the data, which is probably an effect of the dimensionality reduction caused by the methodology used. The topology with the shortest tree length was found to be Tree1, which positions the gray whale as sister taxon to all rorquals and *Diorocetus*† as the ancestor of all crown mysticetes, as show in the phylogeny proposed by Marx (2011) (Table 3.6).

Table 3.6 – Scores for topologies mapped on bgPCA for both configurations. Trees ordered by tree length, from shortest to longest.

<u>Whole skull configuration</u>			<u>Rostrum-only configuration</u>		
Topology	Tree length	p-value	Topology	Tree length	p-value
Tree1	0.089	0.058	Tree1	0.071	<b>0.002</b>
Tree2	0.091	0.114	Tree2	0.073	<b>0.005</b>
Tree3	0.093	0.176	Tree3	0.075	<b>0.012</b>
Tree5	0.094	0.194	Tree5	0.076	<b>0.016</b>
Tree4	0.097	0.377	Tree4	0.079	<b>0.029</b>
Tree6	0.098	0.361	Tree6	0.079	<b>0.028</b>

Significant p-values (p<0.05) in bold

Evaluating the results of the bgPCA with Tree1 (Fig. 3.6), specimens of modern taxa tend to occupy the same area of the morphospace with the exception of the pygmy right whale.

This species appears to have a slender braincase (bgPC2) and elongated rostrum (bgPC1). It also presents a relative high degree of telescoping (bgPC2), with the anterior edge of the supraoccipital reaching more anteriorly relative to the other specimens. Telescoping is mostly correlated with ontogenetic age as seen in Chapter Two, therefore modern species represented by postnatal specimens will appear more derived in this aspect. However, the peculiar shape of the

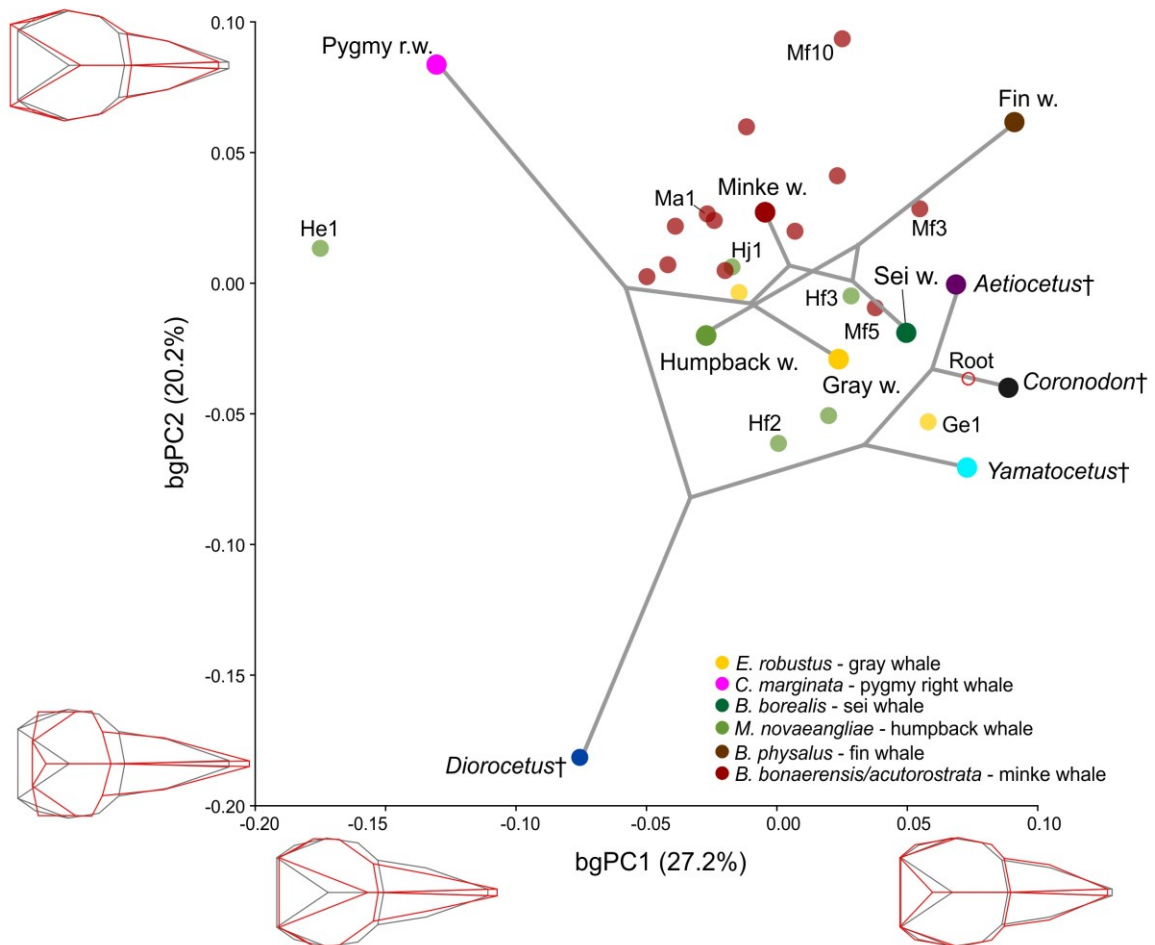


Figure 3.6 – bgPCA plot for the whole skull configuration. Tree topology from Tree1 in gray. Species averages in full color, single specimens in transparency. Average shape at 0 on both axes in light gray wireframe, shape at maximum and minimum values of axes in red wireframe. Color of taxa follows Fig. 3.3. Specimens code as in Table 3.1.

rostrum is the feature that clearly distinguishes this species, and it is connected to its feeding adaptation. The pygmy right whale has been interpreted as skim filter feeder, due to its arched and narrow rostrum, However these characters are not as pronounced as in the other skim feeder family Balaenidae (Bouetel, 2005, Werth et al., 2018). The gray whale, while also having a different filter feeding mode compared to rorquals, plots closer to the other modern species of this family, as only a few characters differentiate the general skull shape of this species from Balaenopteridae (Bouetel, 2005). Adding additional gray whale specimens to the dataset might differentiate it more from other taxa. Rorquals plot on the positive or slightly negative side of bgPC1 and bgPC2, displaying a broader rostrum, which is a key part of their lunge filter feeding adaptation (Bouetel, 2005, Werth and Ito, 2017, Werth et al., 2018). Older specimens of Balaenopteridae have scores near 0 for both components (e.g. Ma1, Hj1), with younger specimens scattered around them, mostly with more positive (e.g. Mf10) or more negative (e.g. Hf2) values of bgPC2. The extreme low value of He1 for bgPC1 is probably an effect of specimen deformation or might be due to the incomplete ossification of skull elements and the different growth observed in the embryonic stages (see Chapter Two). In this context, it is possible to interpret the position of the fossil taxa in the morphospace, especially by comparing their scores with the ones of modern samples at different stages of development (Fig. 3.7). *Diorocetus*† appears to have low values of both bgPC1 and bgPC2, indicating a very elongated and narrow rostrum but low levels of telescoping. Its distance from modern taxa is probably indicative of the presence of autoapomorphic traits, and possibly of a differential developmental trajectory of its rostrum relative to the braincase. *Yamatocetus*† and *Coronodon*† have similar values of bgPC1, plotting closer to each other. But while *Yamatocetus*† has lower values of bgPC2 reflecting its slender rostrum, *Coronodon*† has comparable values to early fetal specimens of living species. *Aetiocetus*†, which is believed to have intermediate skull adaptations between

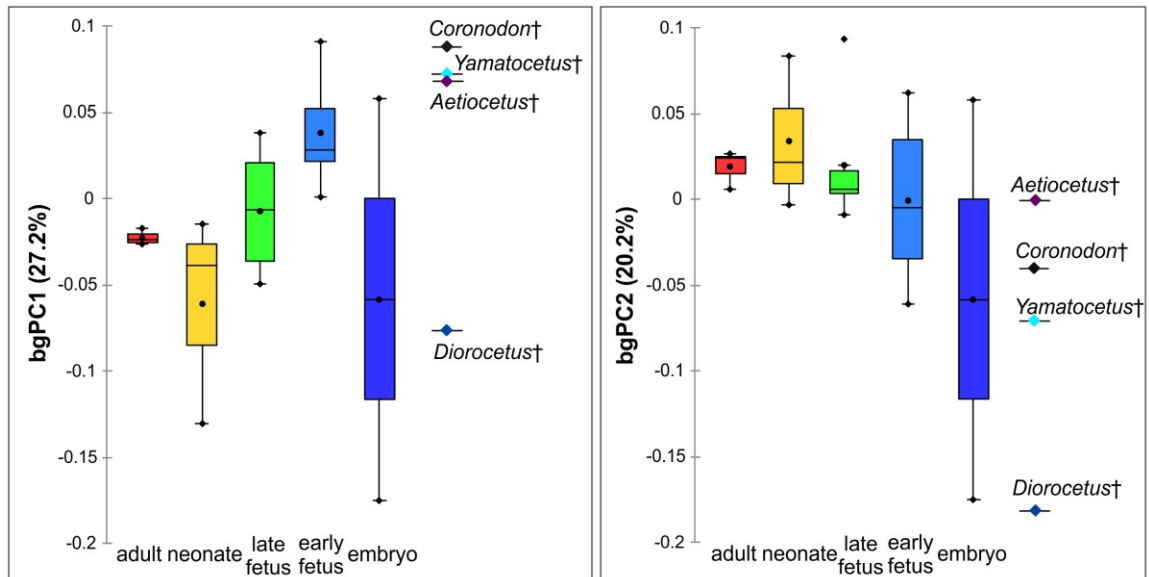


Figure 3.7 – Box plots comparing variation of bgPC1 and bgPC2 for ontogenetic age and fossil specimens in the whole skull configuration. Box=interquartile range for each ontogenetic stage, circle=mean, line=median, whiskers and diamonds=minimum/maximum. Fossil species are represented by a diamond as only one sample of each is included in the analysis and there is no variation. Color of taxa follows Fig. 3.3.

raptorial stem mysticetes like *Coronodon*† and later diverging toothless taxa as *Yamatocetus*† (e.g. Deméré et al., 2008, Marx et al., 2015), has a similar bgPC1 score to these taxa but a markedly higher bgPC2. Its values for this component are in the range of the ones observed in early fetal specimens of extant taxa, due to low levels of telescoping, a broad but short rostrum, and laterally oriented postglenoid process of the squamosal (visible on the sides of the braincase). These results are in line with what was observed in the 2D and 3D allometric analyses, with *Coronodon*† and *Aetiocetus*† resembling in certain elements fetal specimens of modern rorquals, while the toothless stem taxa have a unique skull shape. Given the position of the root of the tree and the distribution of the samples on the plot based on their ontogenetic age, it can be inferred that modern taxa and *Diorocetus*† present a combination of traits not seen in the ancestors, which they develop in later ontogenetic stages. A peramorphic shape transformation during evolution can explain this pattern. *Diorocetus*† and the pygmy right likely had a differential pattern of development of the rostrum relative to other taxa. However, incomplete

fossil and ontogenetic sampling does not allow to elaborate this further. The unexpected resemblance of the skulls of *Aetiocetus*† and of fetal Balaenopteridae specimens also implies that there might be a strong phylogenetic link between Aetiocetidae† and crown Mysticeti.

The same analyses were performed on the rostrum-only landmark configuration. The PCA conducted on the “by specimen” dataset after allometric correction found 15 components, and the first eight represent over 95% of the total variation, presented in Appendix F (Fig. S3.4, Table S3.4). When the scores from the PCA conducted on the “by species” dataset were applied on the “by specimen” dataset, eight components were identified in the resulting bgPCA. bgPC4 and bgPC1 represent most of the variation (50.4%) and will be used to describe the shape change (Table 3.5). As the bgPCA does not have all the properties that apply to standard PCAs, it is possible that the first two components would not describe the majority of the variation, as in this case (Mitteroecker and Bookstein, 2011). Tree1 resulted to be significantly correlated and have the best fit (shortest tree length) to the data, similar to the results in the whole skull configuration. All other topologies were also significantly correlated but resulted in longer tree lengths (Table 3.6). The scatter plots of the bgPCA with Tree1 displays similar patterns as those described for the whole skull analysis (Fig. 3.8). The pygmy right whale plots in a separate area of the morphospace, distant from the other taxa. The extremely low value of bgPC1 are reflective of its elongated and narrow rostrum, while the score for bgPC4 is more in line with the rest of the data. The gray whale plots in the same area as rorqual whales, with values close to 0. This is again likely due to incomplete sampling that does not capture well the morphological differences between the two families. Rorqual specimens are scattered between slightly negative and positive values of both axes. It is interesting to notice that the rostral shape seems to be able to capture interspecific differences. Minke whales’ specimens occupy values from -0.05 (Mf9) to +0.08 (Mf4) on both axes, with adult specimens in the middle of the distribution (e.g. Ma2),

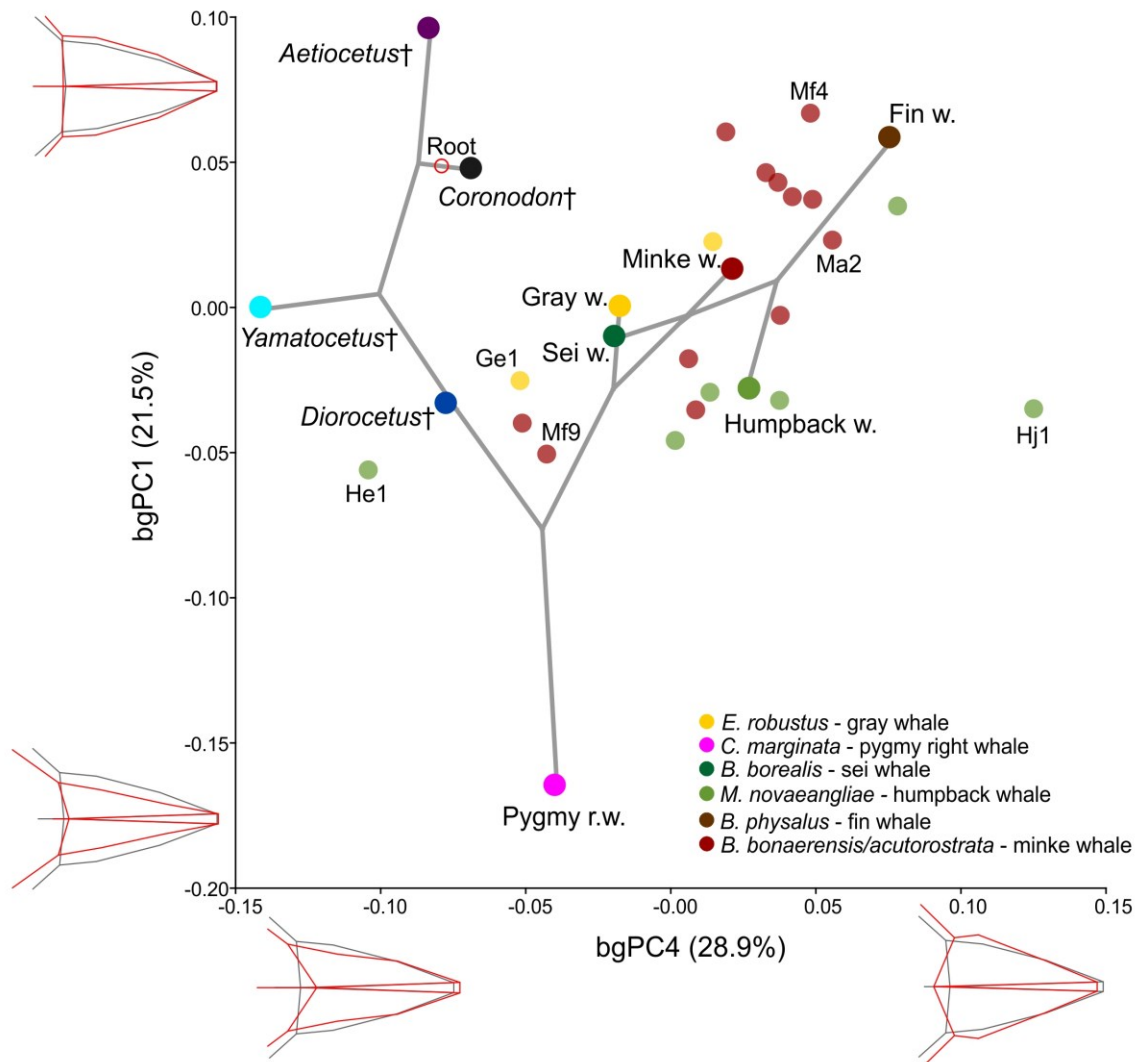


Figure 3.8 – bgPCA plot for the rostrum-only configuration. Tree topology from Tree1 in gray. Species averages in full color, single specimens in transparency. Average shape at 0 on both axes in light gray wireframe, shape at maximum and minimum values of axes in red wireframe. Color of taxa follows Fig. 3.3. Specimens code as in Table 3.1.

while the humpback samples, excluding He1, occupy only the positive area of bgPC4, with the postnatal specimen Hj1 having the highest score. The rostrum of minke whales appears to become longer and slender during development (bgPC1), while in the humpback whale there is a marked increase in width relative to its length (bgPC4). This pattern might be due to the overall allometric scaling of the buccal cavity to the size of the animal recorded in Balaenopteridae (Pyenson et al., 2013, Goldbogen and Madsen, 2018, Kahane-Rapport and Goldbogen, 2018).

As the humpback whale is almost two times bigger than the minke whales, its proportionally wider rostrum is probably connected to this scaling pattern. However, it is somewhat surprising that this pattern is recognizable already from the early fetal stages of development, implying that early changes in ontogeny have a strong impact on the different rostral morphologies and feeding adaptations observed in the adults, also for closely species with similar filter feeding styles. All fossil specimens have very low values of bgPC4, showing almost no overlap on this axis with modern species independently of ontogenetic stage (Fig. 3.9). This is likely due to the anterior positioning of the nasal bones in fossil specimens, which is related to telescoping. *Diorocetus*† is closer to *Yamatocetus*† than in the whole skull configuration, as these taxa share a similar relatively long rostrum, as shown by negative and slightly negative values of bgPC1. *Coronodon*† and *Aetiocetus*† have instead positive scores for this component, with *Aetiocetus*† displaying a relatively broad and blunt rostrum.

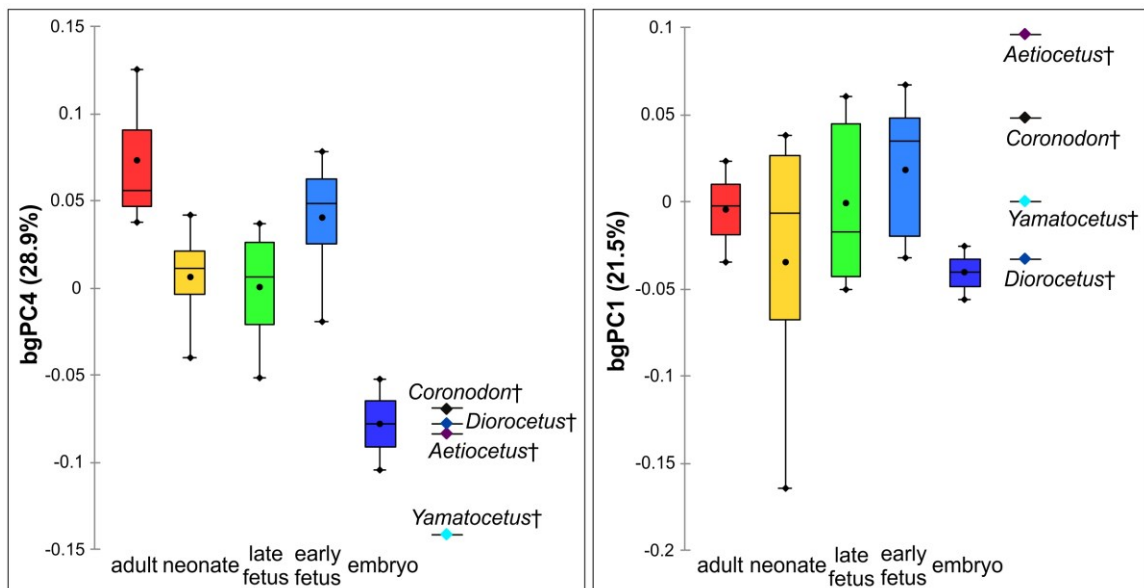


Figure 3.9 – Box plots comparing variation of bgPC1 and bgPC2 for ontogenetic age and fossil specimens in the rostrum-only configuration. Box=interquartile range for each ontogenetic stage, circle=mean, line=median, whiskers and diamonds=minimum/maximum. Fossil species are represented by a diamond as only one sample of each is included in the analysis and there is no variation. Color of taxa follows Fig. 3.3.

While *Diorocetus*† and *Yamatocetus*† have values of bgPC1 comparable to neonate and adults of living species, *Coronodon*† and *Aetiocetus*† have more extreme scores not observed in the ontogeny of modern taxa sampled. This pattern suggests that a major shift in rostral shape occurred independently from the braincase in conjunction with the loss of functional dentition. It also confirms that early toothless mysticetes were likely employing a feeding strategy similar to modern taxa, probably due to the acquisition of well-developed baleen.

#### *Modularity and Partial Least Square analyses*

Before conducting the PLS analysis using the whole skull configuration data after allometric correction, a modularity analysis was conducted to test whether the braincase and rostrum can be compared as relatively independent evolutionary units (modules). RV coefficient is usually high in mammalian skulls, including in Odontoceti, indicating that braincase and rostrum tend to evolve and grow at the same rate (Goswami, 2007, del Castillo et al., 2017). However, if the calculated RV coefficient for the *a priori* hypothesis is falls in the bottom 5% of values, the two partitions can still be analyzed independently, as they are less connected than other parts of the skull. The partition hypothesis tested had an RV score ( $RV_h=0.432$ ) slightly greater than the lowest possible score computed for all the partitions tested ( $RV_{min}=0.426$ ).  $RV_h$  was also in the bottom 5% of calculated coefficients ( $RV_h>1.14\%$ ) (Fig. 3.10). Given this result, it is possible to compare the shape changes in the rostrum relative to the braincase in evolution, as they occur relatively independently.

The PLS analysis between the rostrum and the braincase on the “by specimen” dataset found that the blocks are significantly correlated ( $p<0.001$ ), as expected by being two parts of the skull (del Castillo et al., 2017), and most of the variation between these two elements is explained by the first component PLS1 (77.2%). To better understand the interspecific relationships, PLS1



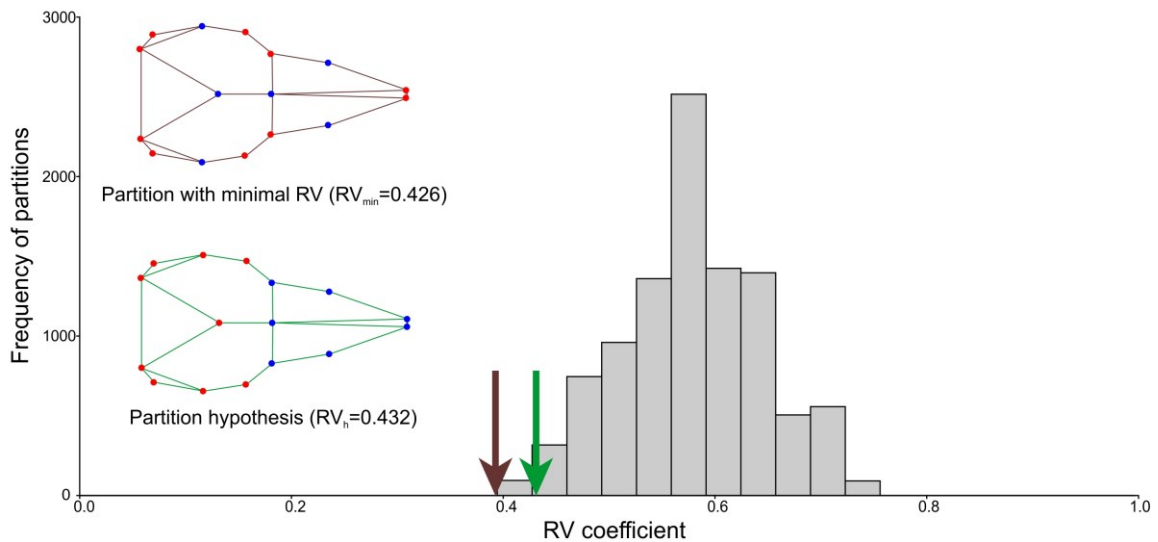


Figure 3.10 – Distribution of RV coefficients for rostrum and braincase modularity analysis. Brown arrow=minimum RV coefficient, green arrow=RV coefficient for partition hypothesis. Distribution of landmark between partitions are figured for the minimum RV (brown wireframe) and for the hypothesis (green wireframe). Partition1 landmarks=red, partition2=blue.

scores were mapped on the tree topologies. Tree1 again was significantly correlated and the shortest among the topologies tested. Tree2 was also significantly associated with the data but had a longer tree length. All other phylogenies tested were not significantly correlated (Table 3.7). Analyzing the resulting relationships among taxa when plotting Tree1 on the PLS1 plot (Fig. 3.11), several interesting patterns on the shape transformation of rostrum relative to the braincase can be described that were not immediately apparent by looking at the bgPCA analyses. The pygmy right whale has a relative braincase-to-rostrum shape ratio similar to fetal specimens of minke whale (Mf9) and to the gray whale embryo (Ge1), with a lower vertex and narrow braincase, and a relatively slender rostrum. This shows that overall the skull proportions of this species are comparable to the ones of other modern mysticetes lineages, despite it seemingly presenting a radically different skull shape. As the pygmy right whale is not unequivocally the ancestor of gray and rorqual whales, it is not possible to speculate on the heterochronic relationships among these groups based on the recovered scores.

Table 3.7 – Scores for topologies mapped on PLS1. Trees ordered by tree length, from shortest to longest. Significant p-values ( $p < 0.05$ ) in bold.

Topology	Tree length	p-value
Tree1	0.090	<b>0.020</b>
Tree2	0.091	<b>0.036</b>
Tree3	0.095	0.090
Tree5	0.096	0.106
Tree4	0.098	0.197
Tree6	0.099	0.185

Mature rorqual specimens have lower scores for both PLS blocks, with a broad braincase and a wide and long rostrum with straight margins. The postnatal humpback whale (Hj1) has a lower score on both axes compared to adult minke whales (e.g. Ma2). This might relate to the different rostral shapes of these species, which is mostly caused by the allometric scaling of the buccal cavity (Goldbogen et al., 2012, Kahane-Rapport and Goldbogen, 2018). The fin whale early fetus occupies an intermediate position between the older specimens of minke and humpback whales. This would suggest that the scaling pattern is already visible in early developmental stages, and that adult fin whales would occupy even more negative areas of the morphospace. These inferences are in line with the results of the rostrum-only bgPCA. Among fossils, *Yamatocetus*† and *Diorocetus*† have extremely high values of PLS1 for both components, due to their slender skull, low level of telescoping and elongated rostrum. *Coronodon*† is positioned closer to modern taxa, with an overall wider skull. *Aetiocetus*† also in this analysis plots in the opposite quadrant of toothless mysticetes, more closely resembling in the relative rostrum and braincase shapes fetal specimens of humpback whale (Hf1 and Hf2) and other rorquals such as the minke and the sei whale. Its broad and blunt but straight rostrum and wide braincase are probably driving this relationship. Overall, this PLS analysis confirms observations made both using 2D measurements and 3D data. Early toothless mysticetes present several autapomorphic traits that characterize their area of the morphospace, with a very elongated

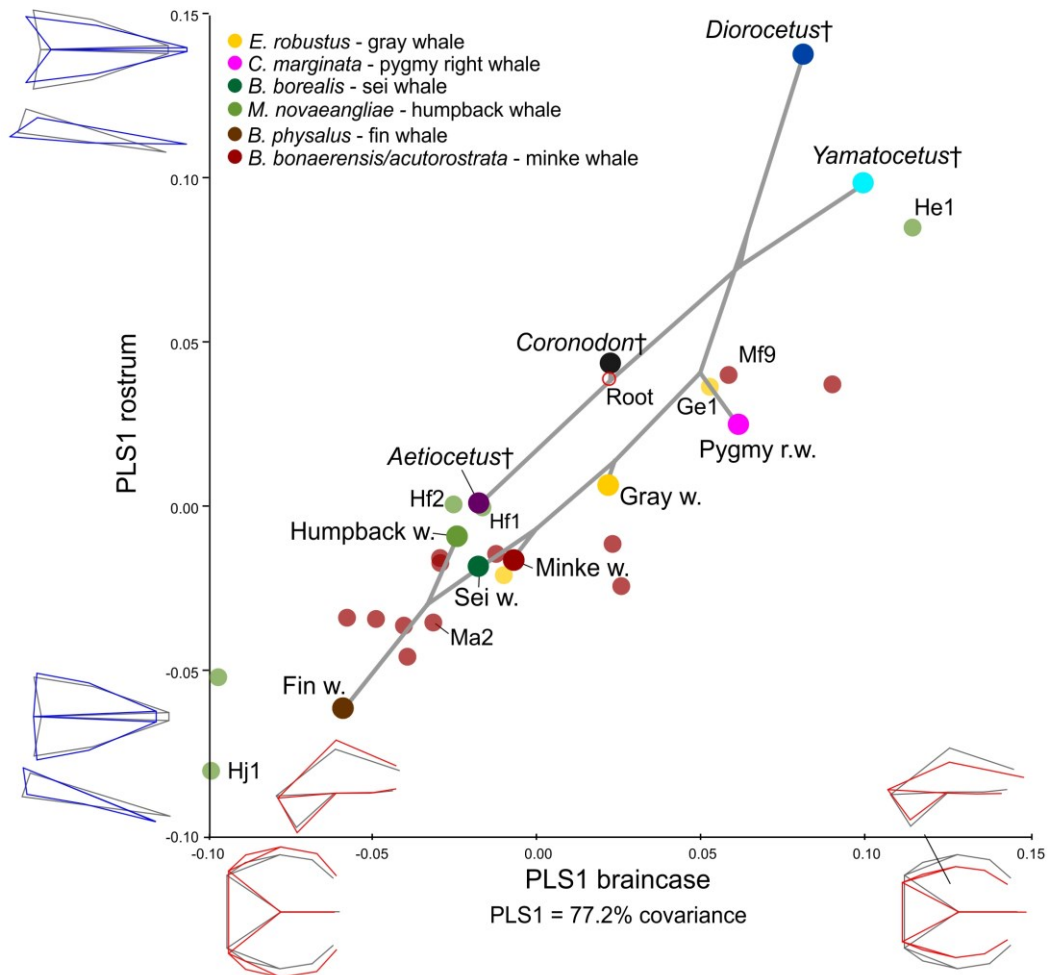


Figure 3.11 – PLS1 analysis plot, comparing scores from the two partitions (rostrum and braincase). Tree topology from Tree1 in gray. Species averages in full color, single specimens in transparency. Average shape at 0 on both axes in light gray wireframe. Shape at maximum and minimum values of Y axes in blue wireframe (rostrum) and of X axes in red (braincase). Color of taxa follows Fig. 3.3. Specimens code as in Table 3.1.

rostrum but smaller and less telescoped braincase. *Coronodon*†, and *Aetiocetus*† in particular, instead to have relative rostral and braincase shapes compatible with fetal specimens of modern species. This plausibly indicates a close phylogenetic relationship between these extinct taxa and extant ones. An acceleration of development in shape (peramorphosis) was likely involved in the evolution of the adaptations that characterize later diverging lineages, with first the rostrum showing increased growth rates, followed by the braincase in the crown group.

By the specimens' arrangement on the PLS plot, it is possible to assume that the evolution and growth of rostrum and braincase occur at similar rates and that their shapes are highly correlated. The regression analysis of the scores of the two partitions (Fig. 3.12) found that they are significantly correlated ( $p < 0.001$ ), with a regression coefficient close to 1 (1.021), indicating an isometric relationship between the two partitions. This is different from the result of the same analysis for the minke whale specimens presented in Chapter Two, as the development of those species the slope was significantly higher than  $45^\circ$ , with the braincase growing faster than the rostrum. The present trajectory is probably mostly influenced by disparity of relationship between rostrum and braincase shape among fossil and modern species.

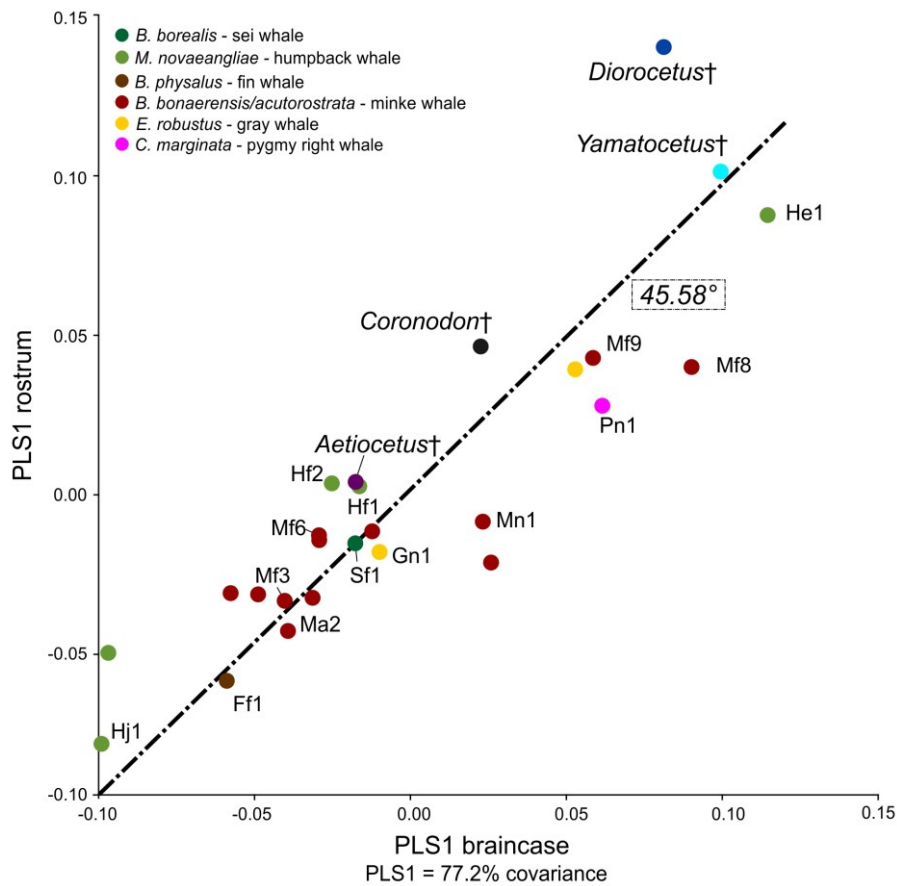


Figure 3.12 – Regression of PLS1 scores of rostrum and braincase. Axes as PLS1 plot. Dash-dotted line=regression line drawn according to the angle calculated using the coefficient provided in the Results. Slope angle is indicated on graph. Color of taxa follows Fig. 3.3. Specimens code as in Table 3.1.

While minke whales' specimens are scattered mostly around the center of the distribution independently of their age, humpback specimens show a clear trend, with younger specimen having positive values and older specimens moving to negative values. This could be due to different sampling between the two species but could also be an indicator that they have different growth patterns as discussed previously. All fossil taxa show a higher degree of shape change in the rostrum relative to the braincase, falling on the left side of the regression line. This implies that modifications in the rostrum were more prevalent in the early evolution of mysticetes, with the braincase changing more slowly. While *Coronodon*†, *Yamatocetus*† and *Diorocetus*† have values that are not close to what is observed in the rest of the dataset, *Aetiocetus*† plots once again close to fetal humpback specimens (Hf1, Hf2) and in proximity of other specimens of different species and ages (e.g. Mf6, Sf1). This is again confirmation that this taxon has an intermediate relationship between rostrum and braincase compatible with what is seen in the ontogeny of modern mysticetes. This evidence supports the hypotheses that *Aetiocetus*† has a strong evolutionary connection with crown Mysticeti and that peramorphism in skull shape can explain the transition from the fossil morphologies to the anatomy observed in modern species.

### **Heterochrony and evolution of the skull in Cetartiodactyla**

Changes in mode and tempo of skull shape growth characterize fetal and postnatal developmental stages, but the ossification sequence of single bone elements, which mostly takes place in the embryonic period, can influence this process on a deeper level by constraining how much time and space each element can use to develop, and how it interacts with surrounding structures (Goswami, 2007). To analyze these shifts in ossification sequence, it is necessary to use a broader scale, as many of these events are highly conserved in all mammals and even amniotes (Smith, 1997, Bininda-Emonds et al., 2003). Therefore, the data obtained by analyzing the development of mysticetes (humpback whale) must be put in the larger context of the

evolution of Cetartiodactyla to find answers to more general questions, such as how Cetacea were able to change their skull to adapt to life in water, for example by developing telescoping, and how can Odontoceti and Mysticeti have evolved such diverse feeding adaptations and associated skull shapes. By reconstructing changes in the developmental sequence of selected species of Cetartiodactyla during their evolution using maximum parsimony, it is possible to highlight some of the major shifts that occurred during the evolution of this clade. Using ACCTRAN character optimization (Fig. 3.13, Appendix E), several delays in the ossification sequence appear to define Cetacea and the different species considered inside the group. The clade as a whole is characterized by an early onset of the ossification of the exoccipital. The clade Odontoceti has an acceleration in the ossification of the lacrimal and parietal, while it shows a delay for the vomer, ectotympanic and teeth mineralization. The early ossification of the exoccipital might be connected with the peculiar cervical vertebrae anatomy that is observed in modern cetaceans, as they have stiffer necks with compressed and sometimes fused cervical vertebrae to swim more efficiently (Spoor et al., 2002, Thewissen et al., 2009). The ectotympanic in Mysticeti is overall thicker (higher degree of pachyostosis) and relatively larger than in Odontoceti (Luo, 1998, Thewissen et al., 2009), which can explain the earlier ossification of this element in baleen whales. It is interesting however to note that teeth begin to form later in toothed whales, even if they mostly maintain a functional dentition postnatally. The early onset of tooth mineralization in Mysticeti might be connected with the need of leaving time for the extra developmental steps of tooth resorption and baleen development later in the gestation, as it was noted when analyzing ossification patterns qualitatively in Chapter Two. The pantropical spotted dolphin (*S. attenuata*) and the sperm whale (*P. macrocephalus*) present very distinct ossification sequences as shown by large numbers of heterochronies on the respective branches.

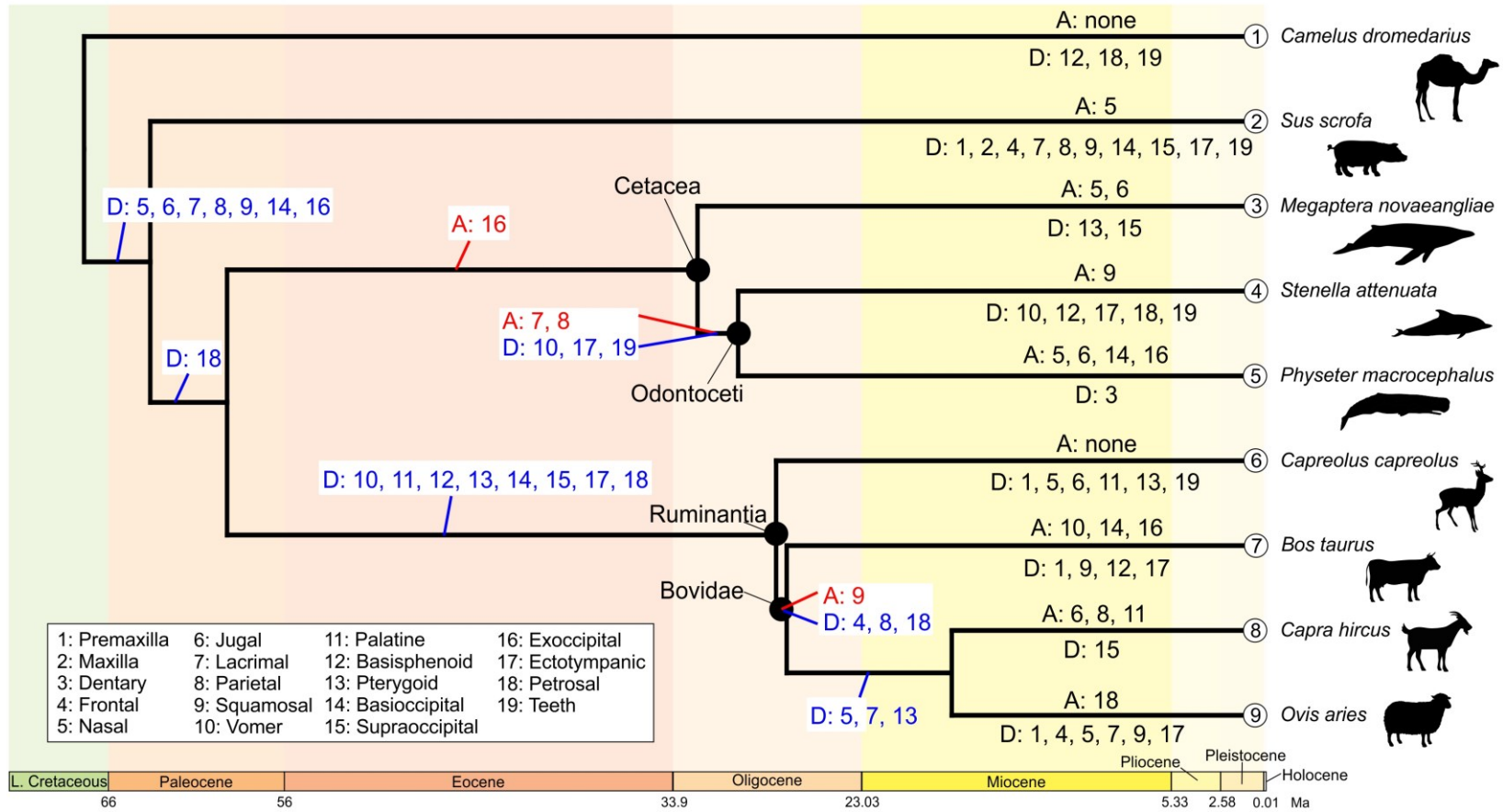


Figure 3.13 – Heterochronic changes in skull ossification sequence of Cetartiodactyla using ACCTRAN character optimization. Bone elements and teeth are represented by their character number (see legend in figure). On internal branches, acceleration in red and delays in blue. On tip branches, acceleration on the top and delays on the bottom. Taxa numbers and silhouettes will be used throughout this section.

The acceleration in the development of many elements in the sperm whale might be connected with its large size compared to the dolphin. For terrestrial taxa, it is interesting to note that the clade Ruminantia is characterized by delayed development of eight skull elements, indicating that this clade has a unique developmental pattern compared to other terrestrial artiodactyls and Cetacea. Toothed and baleen whales might have been hypothesized to possess more drastic changes in the ossification sequences given their radically different lifestyle and head shape, but ruminants appear more derived overall. Domestication of some of these taxa, cattle (*B. taurus*), goats (*C. hircus*) and sheep (*O. aries*), could play a role in this pattern, as also the domestic pig (*S. scrofa*) appears to have several unique changes on its branch (Owen et al., 2014). Adding more wild taxa could solve this issue by allowing for a better comparison with Cetacea. The dromedary (*C. dromedarius*), despite being a partially domesticated species (Kadim et al., 2008), appears to have a conserved ossification sequences, with only three elements showing characteristic heterochronic changes. The DELTRAN character optimization produced a more conservative estimate of transformations on the intermediate branches, with most of the changes occurring toward the tips, as expected when using this algorithm (Fig. 3.14, Appendix E). However, especially when analyzing developmental sequences, both methods should be considered equally (Agnarsson and Miller, 2008, Sánchez-Villagra et al., 2008). In this optimization, Cetacea is characterized not only by an acceleration of the development of the exoccipital, but also by a delayed onset of ossification of the petrosal. This is an important difference, as the petrosal in Cetacea is highly derived for hearing underwater, starting from early Archeocetes, and it appears that modification in its development played a major role in the evolution of modern auditory structures in whales and dolphins (Yamato and Pyenson, 2015, Churchill et al., 2016, Ekdale, 2016). Mysticeti and Odontoceti only have one recognizable heterochronic shift between them, the delayed ossification of the lacrimal.



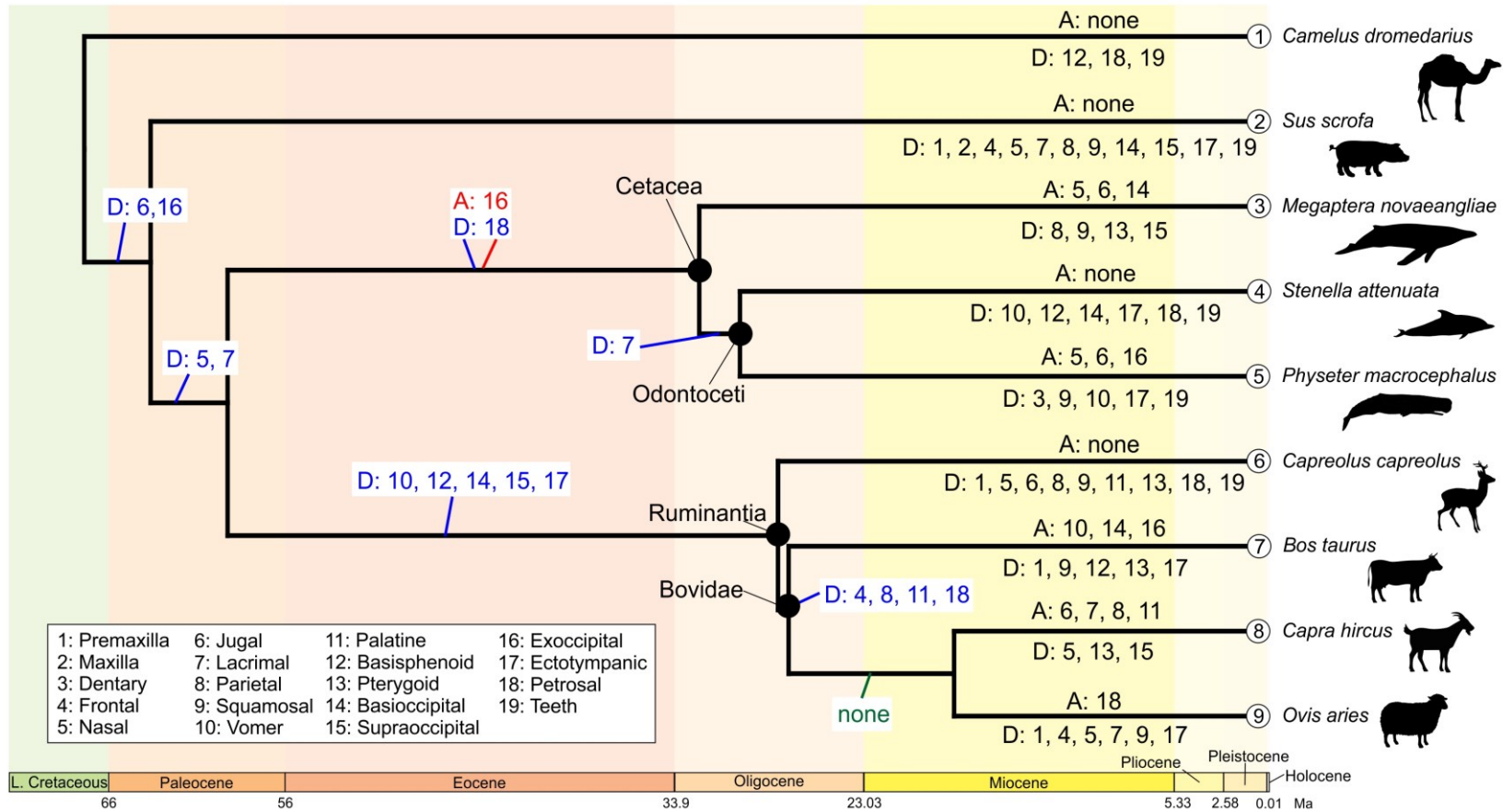


Figure 3.14 – Heterochronic changes in skull ossification sequence of Cetartiodactyla using DELTRAN character optimization. Bone elements and teeth are represented by their character number (see legend in figure). On internal branches, acceleration in red and delays in blue, no changes in green. On tip branches, acceleration on the top and delays on the bottom. Taxa numbers and silhouettes as in Fig. 3.13.

However, the branches leading to the sperm whale and the pantropical spotted dolphin have a more homogenous number of changes. The humpback whale (*M. novaeangliae*) also has more changes recorded on its branch. It is interesting to notice that in both optimizations the supraoccipital ossification is delayed in this representative of Mysticeti compared to Odontoceti. Its timing of ossification has biological significance, as an early onset was hypothesized to be linked to higher EQ (encephalization quotient) by Koyabu et al. (2014). This bone qualitatively appeared to start ossifying at the same time in both groups (see Chapter Two). However, these quantitative analyses show that there is a clear delay in the ossification of this bone in the humpback whale, and possibly all baleen whales, which is expected given their lower EQ relative to toothed whales (Lanzetti et al., 2018, Lanzetti, in press). Ruminantia maintain a relative high number of heterochronies that characterize them as a clade. No change in ossification sequence is present on the branch leading to goats and sheep. These taxa are closely related and both domesticated, therefore this is not completely unexpected especially under DELTRAN assumptions. The changes leading to the pig and dromedary are overall conserved compared to the ACCTRAN reconstruction. From both these analyses, the dromedary appears to be a reliable outgroup for future studies, while the pig and other domesticated species should be considered with caution when compared to Cetacea, as they have a high number of unique heterochronies.

When trying to infer the relationship among taxa using the ontogenetic sequences instead of reconstructing character changes on a known phylogeny, it is possible to understand which sequences more closely resemble each other and how this might be connected with the biology and evolutionary history of the organism (Fig. 3.14). In this instance, both ACCTRAN and DELTRAN optimization produced the same results in number and position of changes (Appendix E).

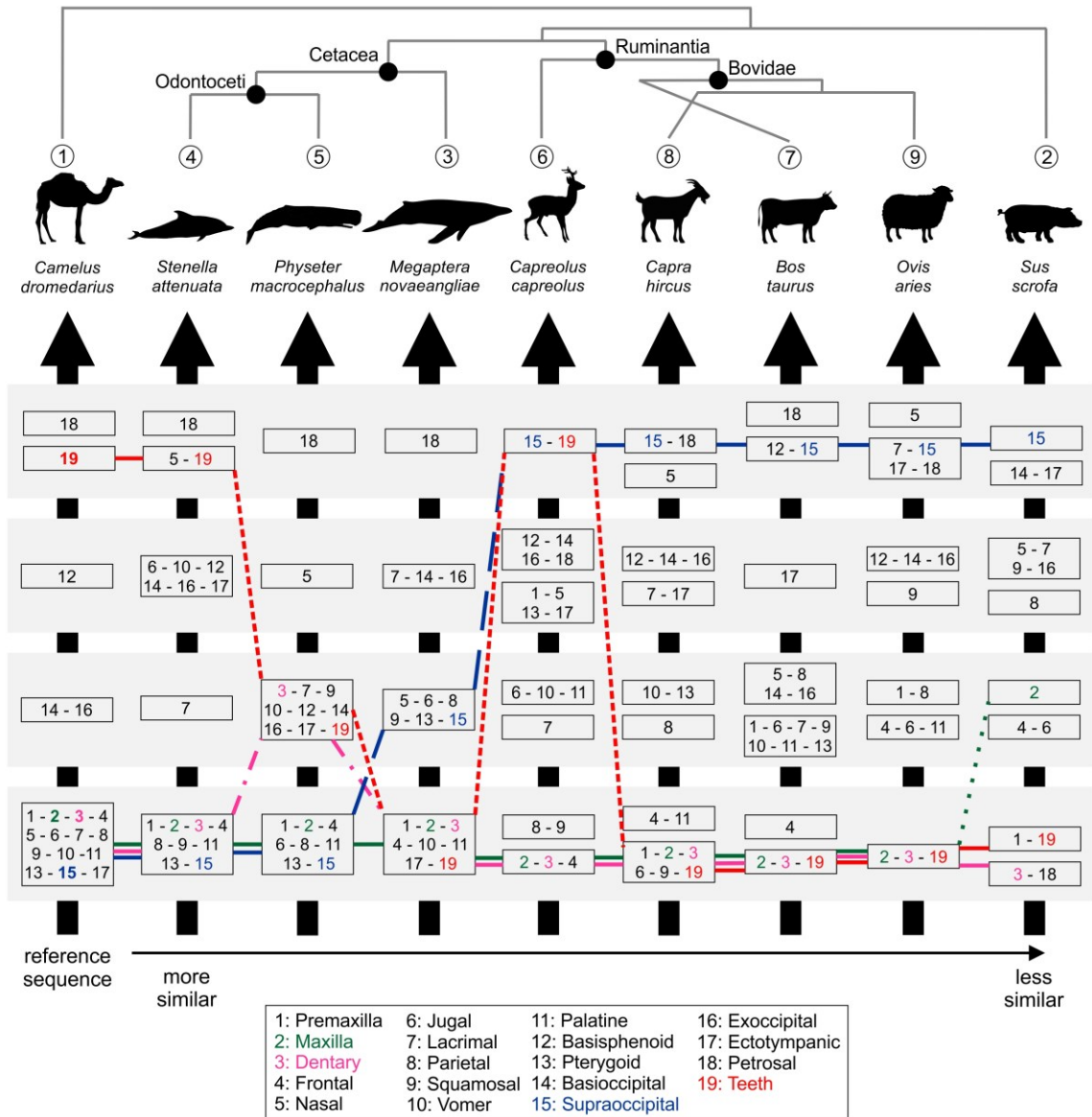


Figure 3.15 – Skull ossification sequences of Cetartiodactyla from more to less similar, starting from the dromedary on the left. Bone elements and teeth are represented by their character number (see legend in figure). Green lines=changes in ossification maxilla, pink=dentary, blue=supraoccipital, red=teeth. Phylogenetic relationships are shown at the top, using taxa numbers as in Fig. 3.13.

Overall, Cetacea have a relative conserved ossification sequence compared to the reference taxon, the dromedary. Bovidae (cattle, goats, sheep) and the pig present a similar and higher number of heterochronies, despite their phylogenetic distance. This is probably an effect of domestication as hypothesized earlier. Following changes in the onset of ossification and

mineralization of elements of interest in this study, important observations can be made. The maxilla, which forms most of the rostrum in Cetacea, and dentary have an early and overall conserved onset of ossification in all taxa. This is expected for dermal bones, and it has been shown that these elements present a conserved early ossification among all mammals (Smith, 1997, Koyabu et al., 2014). Interestingly, the sperm whale and the pig present a slightly delayed onset of ossification of one of these bones, dentary and maxilla respectively. While this might be an artifact of incomplete ontogenetic sampling, especially in the case of the sperm whale, it would be interesting to add more related taxa to the dataset (e.g. pygmy sperm whale and wild boar) to test if this pattern is connected to the evolution of the lineage and investigate the possible functional implications. Tooth mineralization timing is more variable, with the dromedary, the pantropical spotted dolphin and the roe deer presenting a late start of this process, while the other taxa have an early onset of mineralization. It is not clear from this analysis if this pattern is due to phylogeny or to other factors, therefore it will be examined more closely using phylogenetic comparative methods later. However, it qualitatively appears to not be related with the ossification timing of maxilla and dentary, even if these bones surround the teeth and form the alveolar canal. The relationship between ossification in these elements is also tested later using phylogenetic independent contrasts and ancestral state reconstruction methods. As heterochrony in supraoccipital ossification was hypothesized to play an important role in the evolution of EQ of mammals (Koyabu et al., 2014), also the pattern of changes for this bone was traced. By comparing the sequences, it appears that in Cetartiodactyla an early onset of ossification of the supraoccipital represents the ancestral state for the clade, given what is observed in the dromedary. This state might have been conserved in early Cetaceans and it is still present in Odontoceti, while Mysticeti such as the humpback whale evolved a slightly delayed onset of ossification of this element. All other taxa examined have a very late onset of ossification, which

apparently evolved convergently in pigs and ruminants. Combining this evidence with the results of the heterochrony analyses, it is possible that the relatively early ossification of the supraoccipital in the humpback whale is due to developmental constraints rather than related to its EQ, which is low compared to smaller odontocetes (Lanzetti et al., 2018, Lanzetti, in press), with Odontoceti maintaining that possibly aided the evolution of their bigger brains.

The relationship between ossification heterochrony of the supraoccipital and EQ, as well as of maxilla, dentary and tooth mineralization, can be better analyzed using squared-change parsimony ancestral state reconstruction (ASR) and Felsenstein's phylogenetic independent contrasts (PIC), to understand the possible connection between these ontogenetic changes and the evolution of the different adaptations of Cetacea. Comparing the reconstructed timing of formation for maxilla and dentition (Fig. 3.16), the maxilla presents a constant early ossification in all taxa except for the pig, while tooth mineralization is more variable. A similar trend is recognizable contrasting the dentary ossification and teeth mineralization patterns (Fig. 3.17), with a conserved early ossification of the bone with the exception of the sperm whale, where it is slightly delayed. The standardized PIC analysis found that there is a significant correlation between the reconstructed ancestral states at the internal nodes of the maxilla and the teeth, but between dentary and teeth or the two bony elements (see Fig. 3.16-3.17 captions for values). These results might imply a biological reason for the connection between timing of tooth mineralization and maxilla ossification that is absent for the dentary and therefore goes beyond phylogenetic constraint. Early tooth formation could also be correlated with adult dental pattern of the taxa. The differences among Cetacea might be caused by their diverse postnatal tooth numbers: while the pantropical spotted dolphin has the characteristic polyodont dentition of dolphins, with over 40 cone shaped teeth per side in both jaws, the sperm whale only has functional teeth in the dentary, and the humpback whale bears baleen (see Chapter One).

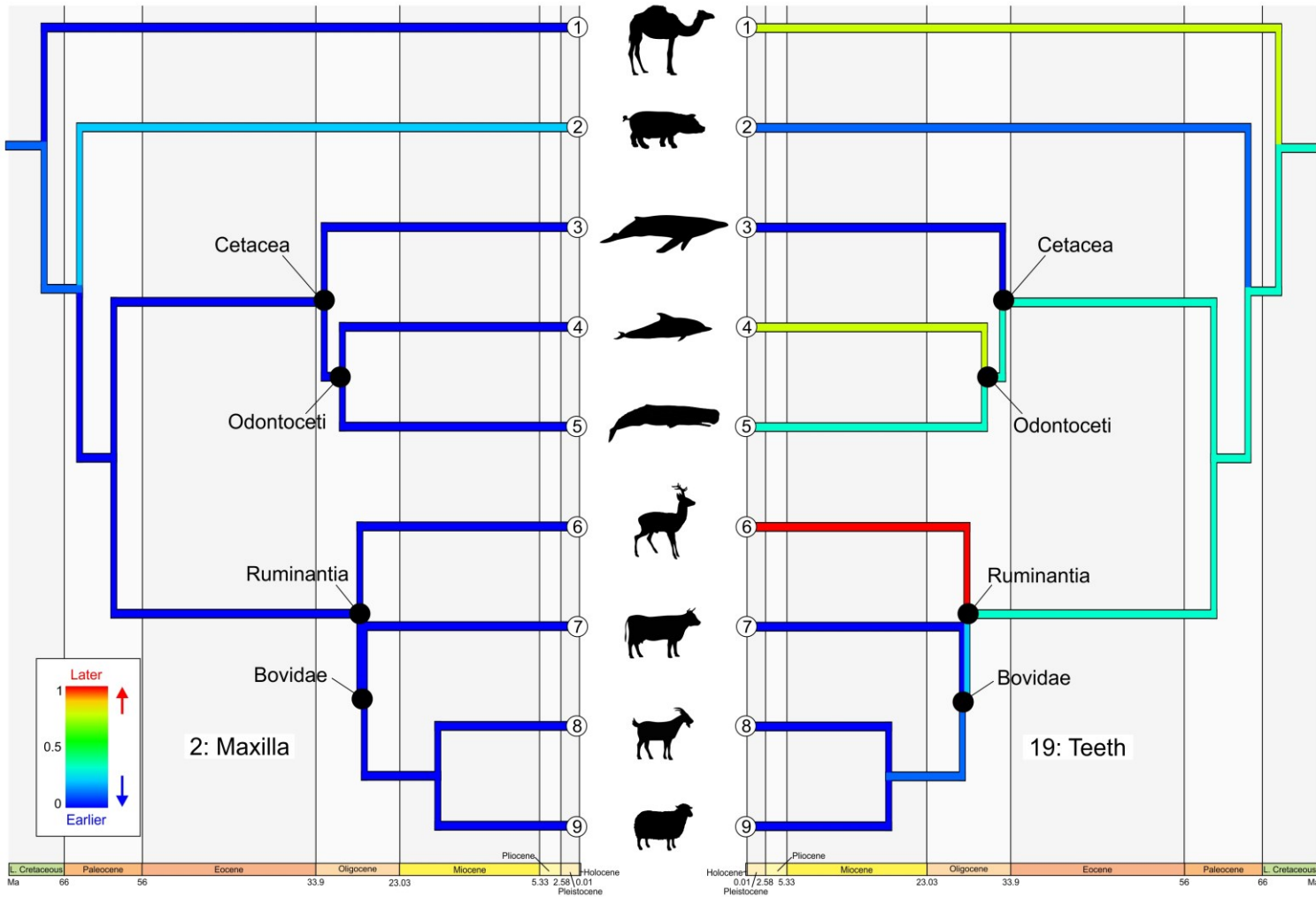


Figure 3.16 – Ancestral state reconstruction of timing of ossification of maxilla (left) and of tooth mineralization (right). A significant correlation was recovered between the changes in the two characters (Pearson's coefficient=0.980,  $p < 0.0001$ ). Warmer colors indicate later onset, cooler colors earlier. Taxa numbers and silhouettes as in Fig. 3.13.

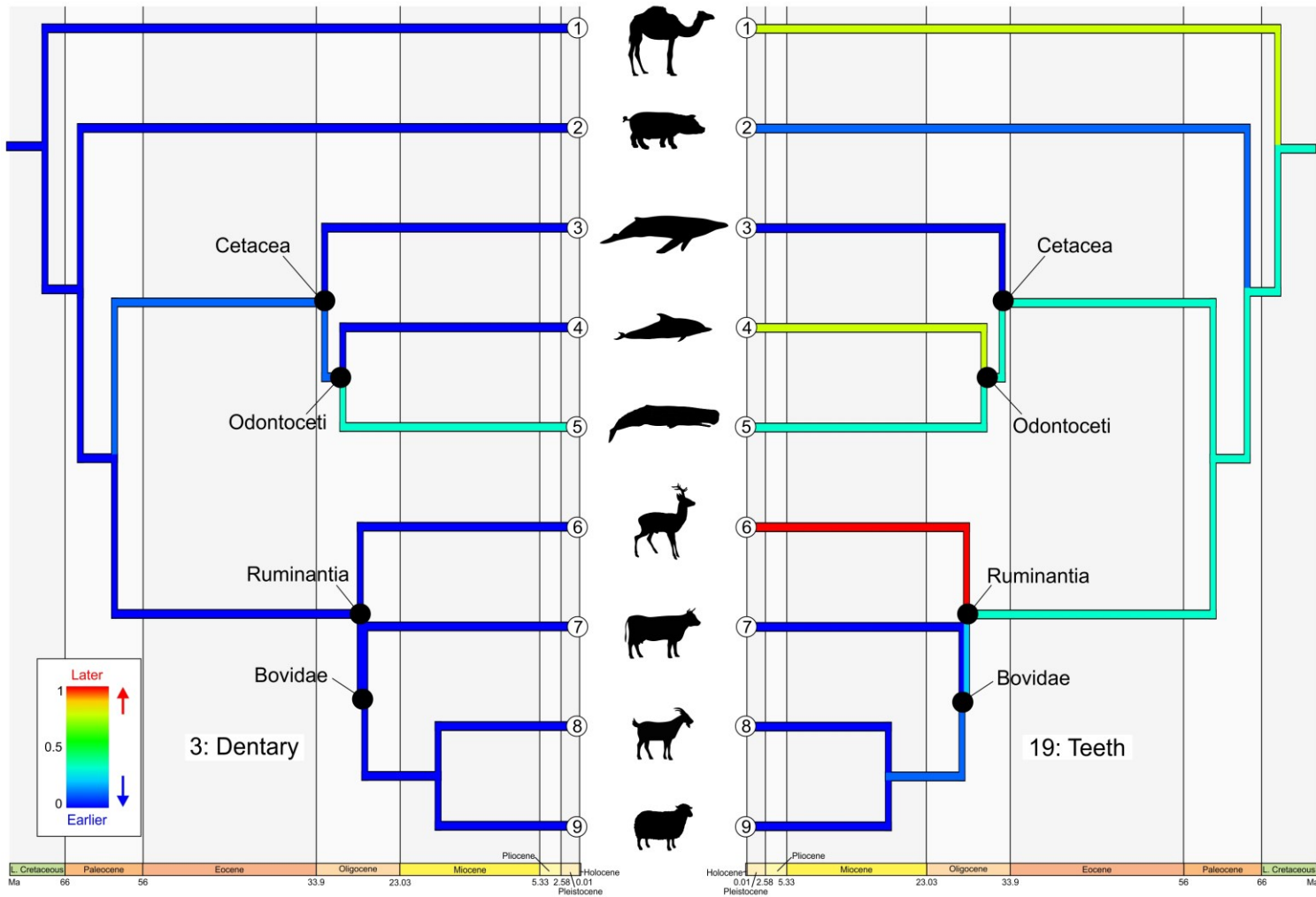


Figure 3.17 – Ancestral state reconstruction of timing of ossification of dentary (left) and of tooth mineralization (right). No significant correlation was recovered between the changes in the two characters (Pearson's coefficient=0.206,  $p=0.624$ ). Warmer colors indicate later onset, cooler colors earlier. Taxa numbers and silhouettes as in Fig. 3.13.

Bovidae, which also have an early onset of tooth mineralization, have an incomplete adult dentition in the upper jaw, lacking canines and incisor that are replaced in adult by a horny dental pad (*pulvinus dentalis*) (Witter et al., 2003, Schaller and Constantinescu, 2007, Berkovitz and Shellis, 2018). However, all ruminants have this characteristic dentition and hard palate, including the roe deer (Sempere et al., 1996, Pérez et al., 2012, Berkovitz and Shellis, 2018), which is reconstructed to have a later tooth formation based on evidence from other species (Kierdorf et al., 2012). On the opposite end, the pig has relatively early mineralization but it does bear a complete adult dentition, with incisors, canines, molars, premolars (Berkovitz and Shellis, 2018). Therefore, while an early onset of mineralization seems connected with partial or complete tooth resorption in Cetacea, the pattern in other artiodactyls needs to be investigated more closely. A larger dataset including other cetacean and terrestrial species is needed to test this correlation in detail. As for the relationship between timing of supraoccipital ossification and EQ (Fig. 3.18), the standardized PIC analysis found a significant correlation between the two variables (see Fig. 3.18 caption for values), in line with findings of Koyabu et al. (2014). However, analyzing the distribution of these traits on the tree, it seems that phylogenetic constraint might still play a role in the relative timing of ossification of the supraoccipital, as noted early based on the results of MP reconstructions. The early ossification could be a plesiomorphic trait in Cetartiodactyla, and Cetacea, which have the largest brains among living animals (Ridgway et al., 2017), might have retained this characteristic independently of their EQ. More cetacean species with different body and brain sizes need to be added to this dataset in order to test this hypothesis.



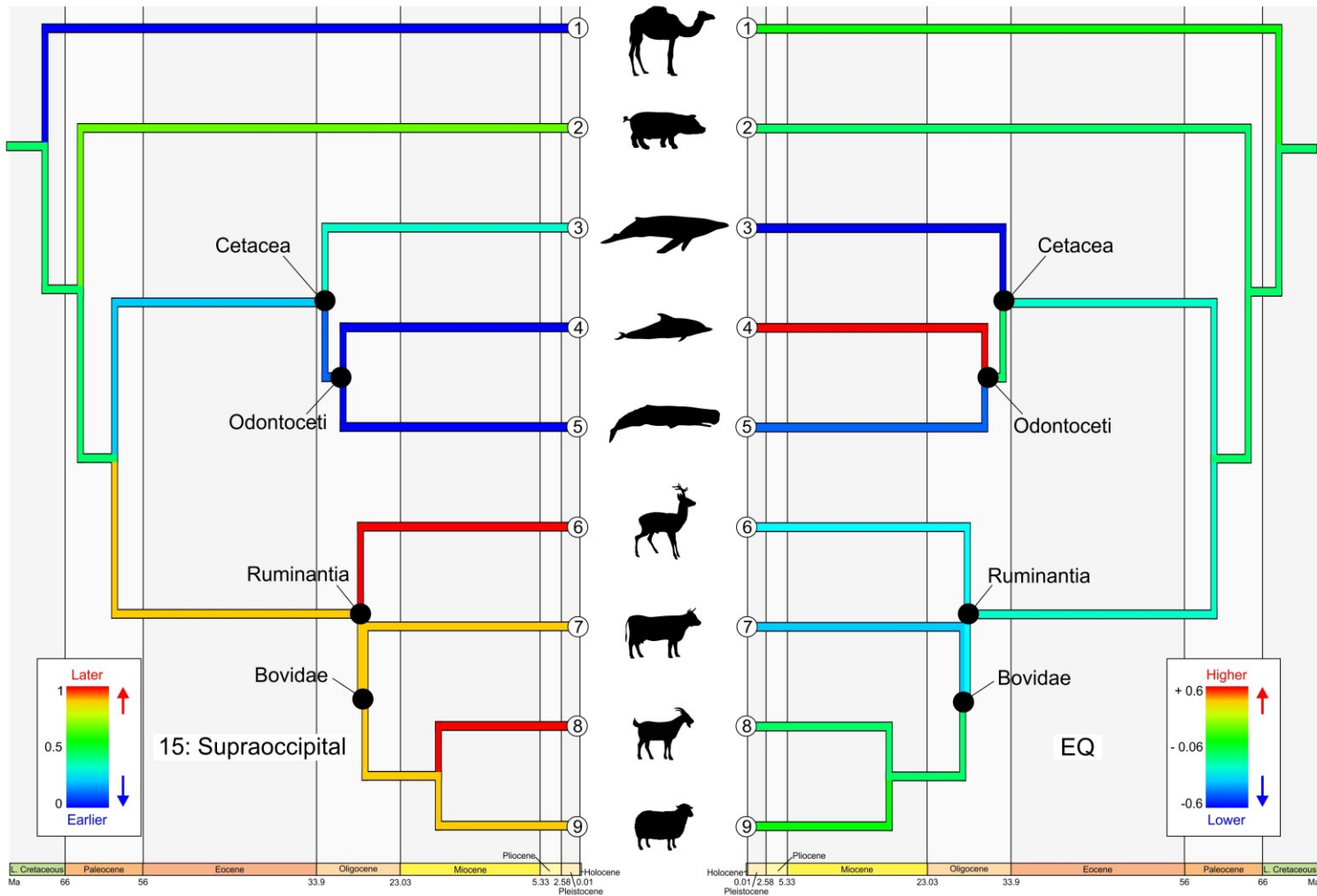


Figure 3.18 – Ancestral state reconstruction of timing of ossification of supraoccipital (left) and EQ values (right). A significant correlation was recovered between the changes in the two characters (Pearson's coefficient=0.972,  $p < 0.0001$ ). Warmer colors indicate later onset or higher value, cooler colors earlier onset or lower value. Taxa numbers and silhouettes as in Fig. 3.13.

## **Discussion**

### **Allometric growth in modern Mysticeti**

In order to identify the role of development in the evolution of a lineage, it is important to have a clear understanding of the allometric growth patterns that characterize its living species (Piras et al., 2010, Morris et al., 2019). Analyzing changes in size of skull components in the humpback and minke whales, most elements present isometric growth relative to total skull length for both species, with the exception of the rostrum and braincase of the humpback whale that show positive and negative allometric trends respectively (Fig. 3.4). Considering the results of previous studies (Nakamura and Kato, 2014, Franci and Berta, 2018), it is possible that the prenatal growth pattern of the minke whale is different from the postnatal one. In mice (Wilson, 2011) and humans (Sardi et al., 2007), different allometric trajectories between prenatal and postnatal ontogeny have been identified in several regions of the skull, providing an interesting precedent for the observations made on these species. More specimens should be added to this study and the minke whale species should be analyzed separately to test this hypothesis. The humpback whale sample is also uneven, with only one postnatal specimen and five embryonic and fetal specimens. The allometric trajectory of the postnatal growth of this species might therefore be driving the results, eliminating the possible discrepancies between patterns observed in the minke whales. A larger dataset is needed to investigate prenatal and postnatal growth in the humpback whale separately, as allometric studies have never been conducted for this genus of Balaenopteridae.

The overall skull shape presents isometric growth relative to size, with the humpback whale growing at a faster rate than the minke (Fig. 3.5, Table 3.4). While this shape growth pattern seems consistent with the recorded allometric growth in size, when the rostrum and braincase are analyzed separately opposite trends are recorded. As presented in Chapter Two, in

the minke whales the rostrum and braincase shape grow isometrically relative to skull size, but the braincase shows faster development compared to the rostrum. In the analysis of allometric size increase, the rostrum resulted to have a faster growth rate relatively to the braincase, as detected by the allometric coefficients (Table 3.3). Therefore, the rostrum appears to mostly change its size while the braincase undergoes major shape transformations, possibly related to telescoping. While it was not possible to test differences in shape growth between rostrum and braincase in the humpback whale due to the limited sample size, the similarity of the patterns in 3D overall shape development and 2D allometric growth point to the conclusion that these two species have similar overall trends. However, it is noticeable that the humpback whale appears to undergo a higher rate of shape change in rostrum and braincase, as illustrated in the PLS plot (Fig. 3.11). These interspecific differences might be caused by distinct trends of shape and size growth in these two skull components. These slight changes in growth trajectories among species, along with different rates of overall skull shape development, might be connected with the allometric scaling observed in the feeding apparatus of modern rorquals (Goldbogen et al., 2012, Kahane-Rapport and Goldbogen, 2018).

Taken as a whole, these novel results demonstrate that there is a disparity of growth patterns between shape and size in the skull of rorqual whales. While the rostrum has a rapid increase in size, it has a slower shape change both relative to its size and skull size (Fig. 3.19). The braincase does not elongate at the same rate as the rostrum, but it changes shape faster than its size, producing discordant allometric patterns. This can be explained by the fact that, while in the braincase several major bone elements change position to achieve telescoping, the rostrum remains relatively conserved, just elongating and decreasing its width. The earlier onset of ossification in the dermal bones can also play a role, by allowing more time for the

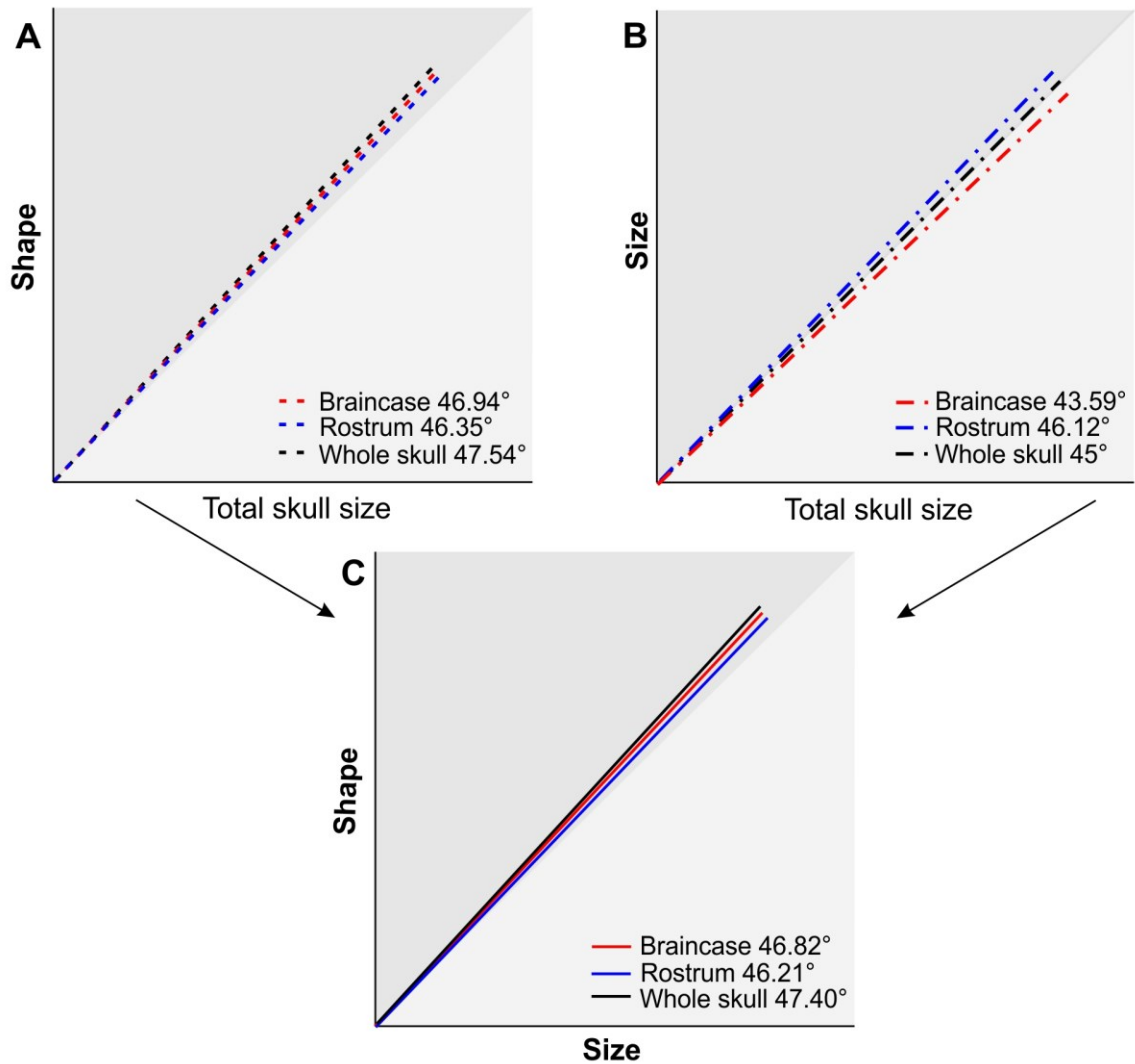


Figure 3.19 – Allometric trajectories in the growth of the skull, rostrum and braincase of the minke whales. A: changes in 3D shape relative to skull size (LogCS), B: changes in 2D length relative to total skull length (LogCBL), C: changes in 3D shape relative to changes in 2D size of each element. The slope angles provided were calculated using the allometric coefficients of the regressions. A higher slope angle corresponds to a faster growth rate.

maxilla and premaxilla to fully develop their shape before the neurocranial bones, which then have to grow at a faster rate to reach maturity at the same time. The relatively low integration development in these two skull components as described by the RV coefficient (Fig. 3.10) also points to the fact that modularity does not pose a constraint on the differential morphological development and evolution of these two regions (Klingenberg, 2009, Goswami

and Polly, 2010a). Differential growth rates between the braincase and rostrum can facilitate species diversification, by allowing different species to evolve diverging skull shapes by modifying the rate of shape change between rostrum and braincase, while maintaining a conserved growth trajectory.

Given these observations, mosaic heterochrony, where changes in shape and size in separate parts of the skull, here braincase and rostrum, occur at different rates (Sydney et al., 2012), are a significant component of the development of the modern baleen whale skull, and possibly played a key role in the evolution of this lineage and the progressive acquisition of filter feeding adaptations. This was also found to be the case in at least one genus of dolphins (*Sotalia* spp. – Sydney et al., 2012), and it is also possibly present in other oceanic dolphins (*Sagmatias* spp. – del Castillo et al., 2017, Vollmer et al., 2019), and porpoises (Galatius et al., 2011). This process could be responsible for the onset of the differential allometric scaling patterns that are observed among different species with disparate feeding (Nakamura et al., 2012, Werth et al., 2018). As many other elements in modern mysticete anatomy appear to be allometrically scaled to body size, such as mandibular length (Pyenson et al., 2013), fluke and flipper length (Kahane-Rapport and Goldbogen, 2018), and filtration area (Kahane-Rapport and Goldbogen, 2018, Werth et al., 2018), differential growth between size and shape might be influencing the development and evolution of many different features in this lineage.

Additional data from species with diverse feeding adaptations are needed to validate these hypotheses. In particular, this dataset is focused on Balaenopteridae, as this is the most speciose family of mysticetes (Gatesy et al., 2013, Berta et al., 2016). However more significant patterns might be recovered when comparing the developmental trajectories of shape and size among multiple families. For example, the pygmy right whale appears to follow a potentially different developmental path and allometric scaling pattern in the skull relative to rorqual whales, as it was

recently shown for its baleen filtration area (Kahane-Rapport and Goldbogen, 2018). Balaenidae, which are skim filter feeders more specialized than this species (Berta et al., 2016, Kahane-Rapport and Goldbogen, 2018), need to be considered in future analyses as well. The gray whale sample size should also be expanded to capture the differences between this species and rorquals. This species only has a few peculiar features in postnatal skull anatomy (Bouetel, 2005, Werth et al., 2018), and genetic data place it as a member of the Balaenopteridae family, indicating relatively recent adaptation to its unique filter feeding style (McGowen et al., 2009, Marx and Fordyce, 2015). Studying the prenatal developmental pattern of this species might bear unique insight in the impact of ontogeny in the diversification of baleen whales, given its overall conserved morphology and recent divergence time.

### **Implications of developmental data for the evolution of filter feeding**

#### *Ontogenetic data informs the phylogeny of Mysticeti*

While it is not possible to infer the feeding strategy of fossil taxa using present fetal morphologies, it is important to highlight the similar patterns that are observable in the ontogeny and the evolution of baleen whales, both qualitatively and quantitatively, as this can inform the phylogenetic relationship in this clade as well as help interpret certain aspects of the anatomy of fossil taxa. From quantitative analyses of skull shape, this study was able to show, using both 2D measurements and 3D shape analyses, that the skulls of two early toothed stem-mysticetes (*Coronodon*† and *Aetiocetus*†) share similar proportions and characteristics with those of fetal specimens of modern Balaenopteridae. In particular, these taxa present a relatively short and broad rostrum, with a braincase of equal length, similar to neonatal minke whales (Fig. 3.4). They also have low levels of telescoping in combination with a blunt and straight rostrum, and this shape combination mostly resembles instead what is observed in late and early fetal development of several species of rorquals (Figs. 3.5 – 3.7, 3.11, 3.12). However, their rostral shape alone is

markedly different from those of modern specimens, possibly due to their different feeding adaptations (Figs. 3.8, 3.9). The two toothless taxa examined, *Yamatocetus*† and *Diorocetus*†, appear instead to have a unique skull shape, with a combination of a small braincase and low levels of telescoping combined with a narrow, long and flat rostrum (Figs. 3.5 – 3.7, 3.11, 3.12). When observing the rostrum alone, some overlap in shape can be seen between these taxa and many specimens of living species at different stages of development (Figs. 3.8, 3.9). Therefore, toothed and toothless stem-mysticetes appear to have followed different patterns of skull shape evolution. Rather than presenting a continuous shape change from the earliest fossil to living species, there is an abrupt transition between tooth-bearing lineages and toothless ones.

Surprisingly However, toothed fossils appear to have more in common with developing modern taxa than toothless specimens. This bears clear phylogenetic implications: while it was never debated that a complex trait such as baleen would evolved only once in the Mysticeti lineage, many authors argued that Aetiocetidae† and other similar taxa are very likely representative of a distinct lineage that only shared a distant common ancestor with toothless mysticetes (Marx et al., 2016, Peredo and Uhen, 2016a, Peredo et al., 2018b). These results show that there is a tight link between skull shape of adult toothed mysticetes and developing modern taxa, implying the presence of a direct common ancestor between the two lineages. Comparable findings have helped consolidate previous phylogenetic hypotheses and understand the developmental drivers of major evolutionary transition in other groups such as birds (Bhullar et al., 2012, Botelho et al., 2014, Smith-Paredes et al., 2018) and crocodiles (Piras et al., 2010, Foth et al., 2017). Similarly, the present results can provide a new framework to interpret the anatomy observed in fossil specimens of Mysticeti. Aside from the direct conclusion of this study, including samples of different ontogenetic ages in macroevolutionary analyses might be the best approach to answer the many open questions regarding the teeth-to-baleen transition.

### *Heterochronic patterns in the evolution of filter feeding*

Using these observations, it is possible to determine the major heterochronic patterns in skull shape growth and evolution that characterized the dietary shifts in Mysticeti and the teeth-to-baleen transition. A reconstruction of possible growth trajectories in braincase and rostral shape in fossil taxa relative to the minke whales is provided in Fig. 3.20. *Aetiocetus*† and *Coronodon*† might have presented similar growth rates in shape and size of both regions of the skull. This, combined with the numerous juvenile aspects in their skull anatomy, points to the fact that present mysticete morphologies were achieved by a progressive acceleration of development or peramorphism. Aetiocetidae† and Mammalodontidae† have previously been hypothesized to present paedomorphic traits (Sanders and Barnes, 2002, Fitzgerald, 2010, Marx et al., 2015), and the present results are in line with these observations. However, as heterochrony is established based on the ancestral condition of that lineage (Gould, 1977, McNamara, 1986), it would be incorrect to judge the level of maturity of skull features of extinct taxa based on extant ones. Therefore, the most correct interpretation is that at least modern Balaenopteridae, the focus of this study, present a peramorphic skull shape compared to early toothed Mysticeti. Acceleration and extension of developmental time and events are not only observable in skull shape, but also in other anatomical traits. This hypothesis of peramorphism could explain the progressive loss of teeth and evolution of organized baleen plates in the lineage. Longer developmental time and more rapid ossification of skull bones and early tooth mineralization could have allowed for the progressive loss of teeth in the adults and the formation of the baleen rack. As tooth resorption and baleen formation only occur in the last stages of gestation in modern species, it is conceivable that the accelerated last portion of the gestation seen presently is connected with the teeth to baleen transition.



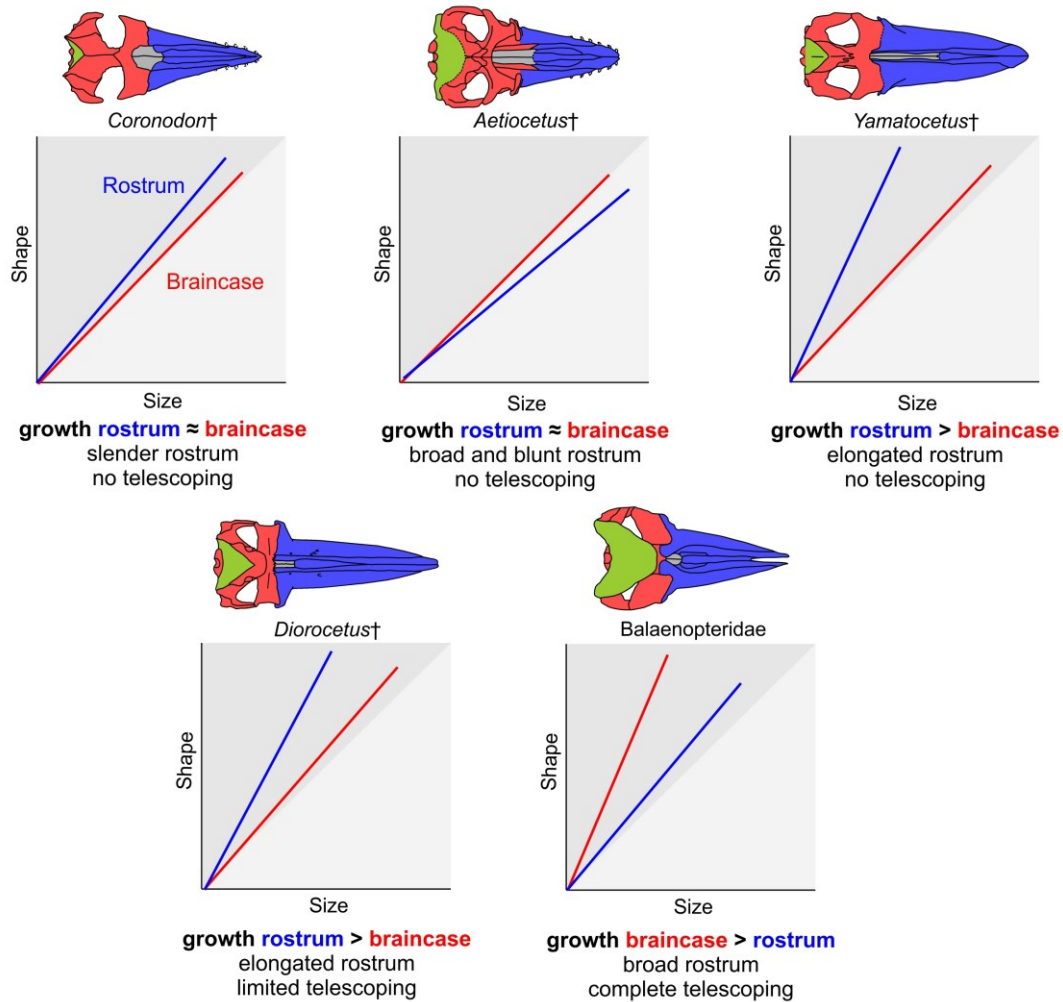


Figure 3.20 – Hypothesized allometric growth trajectories of rostrum and braincase and skull shape changes in fossil Mysticeti, compared to minke whales. Growth rates relative to size are estimated based on the adult proportions of the taxa and they are only used to illustrate and qualitatively compare the changes among different lineages. Braincase=red, rostrum=blue, supraoccipital=green, nasals=gray.

Filter feeders could have progressively evolved starting from forms that were born at an intermediate stage, still bearing teeth but with small keratinous structures that were only partially developed, and that therefore adopted a mixed feeding strategy, using both the ancestral raptorial and suction feeding and some measure of filter feeding, as it was previously hypothesized by Deméré and Berta (2008). Natural selection could have acted to favor organisms bearing progressively more complex proto-baleen and reduced dentition, until it was abandoned completely in favor of baleen racks. This slow adaptive process in the evolution of filter feeding in mysticetes is confirmed by several lines of evidence (Clementz et al., 2014, Berta et al., 2016, Peredo et al., 2018a), and was probably driven by a rapidly changing marine ecosystem and with the availability of the planktivorous filter feeding trophic niche that was left mostly empty by the extinction of specialized bony fishes and Mesozoic marine reptiles at the end of the Cretaceous period (Marx and Uhen, 2010, Friedman, 2012, Motani et al., 2015, Berta and Lanzetti, in press). It appears unlikely based on the present developmental evidence that some mysticetes were obligate highly specialized suction feeders as modern Ziphiidae (Peredo et al., 2017, Peredo et al., 2018b). There is no ontogenetic stage where teeth are completely resorbed in the absence of clear baleen structures, and the skull shape of toothed fossil taxa is compatible with the development of modern mysticetes, lacking characteristics that would make them seem specialized suction feeders. These fossil stem mysticetes would also have to have evolved these specialized feeding style in less than 1 Ma according to present phylogenetic inference and dating (Fig. 1), while, for example, the fossil record of Ziphiidae shows that this strategy evolved progressively in over 7 Ma (Chapter One). Early diverging odontocetes were also concurrently adopting suction feeding strategies in the same areas where these early mysticetes lived, and they could have presented direct competitors for food resources (Fordyce, 1980, Tsai and Fordyce, 2016). More research is needed on the development of the hyoid bone, which is directly connected with lingual

musculature and suction feeding in modern Cetacea (Hocking et al., 2017, Kienle et al., 2017, Berta and Lanzetti, in press), to fully confirm this hypothesis, as well as closer reexamination and quantitative analyses of additional fossil specimens. Overall, given the current evidence it is more appropriate to suggest that the teeth were slowly replaced by baleen, and that they became vestigial in the adults before disappearing completely.

While peramorphosis is connected with overall skull shape changes in the evolution of Mysticeti, heterochronic processes operated at different rates on the rostrum and braincase, as proposed to explain the disparity in modern species (Fig. 3.20). Intermediate toothless taxa, *Yamatocetus*† and *Diorocetus*†, present a long rostrum but low levels of telescoping, indicating that peramorphosis was acting prevalently on the anterior portion of the skull. In the evolution of Mysticeti the rostrum became more elongated at first to accommodate the baleen plates, and only after the braincase started increasing telescoping and modifying its shape. Differential patterns of evolution of braincase and rostrum would explain the isometric trends between these two components observed in the complete dataset (Fig. 3.12), while in modern minke whale ontogeny the two structures present a positive allometric growth pattern relative to each other (Chapter Two). The elongation of the rostrum also requires mostly changes in scaling rather than shape changes, while telescoping is primarily a radical change in bone positioning and shape, as highlighted by the different growth rates of size and shape of these structures (Fig. 3.19). Therefore, intermediate toothless taxa skull anatomy is a product of mosaic heterochrony, with higher peramorphic rates only present in the rostral region. An elongated buccal cavity might be necessary to be a successful filter feeder, as this skull morphology was also independently evolved in other suspension feeders such as bony fishes (Friedman et al., 2010, Friedman, 2012) and marine reptiles (Motani et al., 2015).

Telescoping, however, is a unique feature of modern Cetacea that evolved convergently in both toothed and baleen whale through different mechanisms (Miller, 1923, Churchill et al., 2018, Roston and Roth, 2019), and is not directly related to filter feeding, but it is probably connected with changes in the respiratory apparatus to allow the fully dorsal positioning of the blowhole (Heyning and Mead, 1990). The acceleration in growth rate in the final stages of gestation in modern mysticete might also be connected with these changes in the neurocranium, as telescoping was shown in this study to mostly be completed during prenatal development, while positive allometric growth of the rostrum can continue postnatally during weaning (Nakamura and Kato, 2014, Franci and Berta, 2018). This disassociated development in size and shape might also be responsible for the apparent pedomorphic traits recognized in the pygmy right whale by Tsai and Fordyce (2014). They mostly based their conclusion on the relatively low degree of movement of the supraoccipital and nasal bones during the ontogeny of this species, which causes adults to have very similar shapes to neonates and juveniles. It is noticeable, however, that this taxon does not have almost any skull shape features in common with rorquals or gray whales, but instead presents a characteristic anteriorly elongated supraoccipital shield and a short and curved rostrum. A slower rate of the braincase shape development after an initial fast growth relative to the rostrum could produce the peculiar and relatively neotenic appearance of the skull of the pygmy right whale. More data on the development of this enigmatic species needs to be collected in order to understand the different developmental patterns that characterize it. However, mosaic heterochrony, with peramorphic rostral elongation and different rates of shape change in the braincase, is maintained in this taxon and in Balaenidae, playing an important role in the diversification and feeding adaptation of modern mysticete families.

## **Heterochrony in the origin and diversification of Cetacea**

The later onset of telescoping in both evolution and development in Mysticeti is remarkably different from what is observed in Odontoceti. While stem lineages of baleen whales presented very little evidence of telescoping, early diverging toothed whales already showed several features that characterize modern taxa, including a low degree of overlap in the neurocranial bones, possibly connected with the rapid evolution of echolocation in this lineage (Miller, 1923, Whitmore and Sanders, 1976, Uhen, 2008, Churchill et al., 2016, Churchill et al., 2018). During the Oligocene epoch (33.9-23.03 Ma), stem fossil members of Odontoceti reached the same level of telescoping observed in modern taxa, while Mysticeti only started showing a similar neurocranial bone arrangement after the evolution of the crown group families in the Miocene (23.03-5.33 Ma) (Marx and Fordyce, 2015, Churchill et al., 2018). The adult arrangement in the neurocranial bones in modern toothed and baleen whales is also markedly different. Odontocetes present an almost complete overlap of the maxilla with the frontal and very small, globular nasal bones. Instead, Mysticeti have the characteristic infraorbital process of the maxilla that prevents this complete overlap from occurring, and they also have antero-posteriorly elongated nasal bones (Miller, 1923, Roston and Roth, 2019). As seen in Chapter Two, the different bone arrangement in the braincase is already recognizable in the early fetal stages of toothed and baleen whales, with an early ossification of the infraorbital process of the maxilla preventing the posterior movement of the maxilla in minke and humpback whale fetuses. An earlier onset of nasals ossification can also contribute to develop their elongated shape in Mysticetes (Fig. 3.15). Overall, it is likely that the different bone arrangement observed in the braincase of Odontoceti is due to a markedly different allometric pattern, where the braincase shape change is markedly higher than in Mysticeti from early ontogeny. Instead, since having an elongated rostrum and large mouth is a prerequisite for filter feeding in baleen whales, their

growth starts with an increase in size and shape change in the anterior region of the skull which is then followed by braincase shape transformations. This is in line with previous hypotheses formulated by the only comparative study by Armfield et al. (2011), where they compared allometric trajectories in the growth of external anatomical features of the head of pantropical spotted dolphins and bowhead whales. An earlier onset in the evolutionary history of odontocetes of this relatively accelerated shape change trend can explain why the earliest member of this group already possessed a telescoped skull. Further morphometric studies including archaeocetes, the common ancestors of both toothed and baleen whales, as well modern and fossil odontocetes at different stages of development are needed to test whether their allometric growth patterns are indeed different from mysticetes and if this differential growth between braincase and rostrum could be detected also in early Cetacea (Churchill et al., 2018).

While it is likely that different allometric growth characterizes the two major groups of Cetacea, their ossification sequences appear to be relatively conserved both relative to each other and to other artiodactyls, especially in the facial region (Fig. 3.13-3.15). They both follow the expected mammalian pattern, with dermal bones ossifying earlier than endochondral elements (Smith, 1997, Koyabu et al., 2011, Koyabu et al., 2014). As neurocranial bones are mostly endochondral, their relatively delayed ossification could explain why the shape change in this region must be more rapid than in the rostrum, which is composed of dermal bones, as seen in Mysticeti. However, this also implies that most of the shape change occurs in the later parts of the gestation, when the single bone elements have mostly completed ossification in all lineages, including terrestrial ones. Therefore, the suture ossification timing must be what is driving the differentiation in shape development between Cetacea and terrestrial artiodactyls, as well as between toothed and baleen whales. This is in line with what was previously hypothesized using qualitative evidence (Lanzetti et al., 2018, Roston and Roth, 2019). A dataset coding the timing of

suture closure instead of the ossification sequence is probably the best way to understand the differences between aquatic and terrestrial taxa, and to identify major differences among cetaceans that drive differential telescoping.

Analyzing heterochronies in ossification sequences in Cetacea compared to terrestrial artiodactyls, in both ACCTRAN and DELTRAN parsimony analysis an acceleration of ossification of the exoccipital characterized the clade, while in most other taxa the ossification of this element is delayed relative to the reference sequence (Fig. 3.13-3.14). This heterochrony is the only one that is consistently recovered independently of the algorithm used and therefore warrants further scrutiny. The exoccipital is the bone element that forms the condylar processes, which articulate with the atlas. The *foramen magnum* is formed between the condylar processes and it surrounds the main blood vessels and nerves that connect the brain to the spinal column and the rest of the body (Mead and Fordyce, 2009). In Cetacea, the size of the *foramen magnum*, as well as the shape of the condylar processes, is used to estimate age and relative body size of modern taxa (e.g. Nakamura and Kato, 2014) and it is an important character for phylogenetic inference of fossils (e.g. Geisler and Sanders, 2003). While it is not clear why toothed and baleen whales present a high morphological variability of this trait, it is possible to hypothesize that the earlier onset of the ossification of the exoccipital might be connected with these observations. Moreover, toothed and baleen whales present cervical vertebrae that are antero-posteriorly compressed and fused together in many species during postnatal ontogeny (Buchholtz and Schur, 2004). This is believed to be an adaptation to life in water, which requires a stiffer neck to avoid excessive oscillation of the head during swimming, and it is also recorded in other marine mammals (Buchholtz et al., 2007), extinct marine reptiles (Mulder, 2001), as well as in the fossil ancestors of Cetacea, archaeocetes (Buchholtz, 2001). An earlier onset of ossification of the exoccipital might be part of the set of changes that allowed this adaptation to evolve, as the

condylar process directly articulate with the cervical vertebrae. However, more research on the postcranial ossification sequence of Cetacea and other artiodactyla is needed to test this hypothesis.

While it was not recovered as a characteristic heterochrony of this clade, Cetacea, and Odontoceti in particular, present an early ossification of the supraoccipital (Fig. 3.15). Koyabu et al. (2014) correlated this trait with a higher EQ, and while this study recovers the same significant relationship (Fig. 3.18), it is worth noting that in Cetartiodactyla this might represent the ancestral trait for the group. This implies that in Cetacea this was maintained as a plesiomorphic characteristic, which then likely facilitated the increase in brain size and the relatively higher EQ observed in most modern toothed whales. An ancestral early ossification of the supraoccipital would also explain why baleen and toothed whales with a notably lower EQ (e.g. sperm whale, humpback whale) at least partially retain this characteristic. The fact that all modern cetaceans retained this plesiomorphic state might be related to the convergent evolution of telescoping, as the anterior progression of the supraoccipital shield is a notable part of this process (Miller, 1923, Churchill et al., 2018, Roston and Roth, 2019). All other terrestrial taxa have a notably late ossification of this bone, with the exception of the dromedary, which might also have conserved this as a plesiomorphic state despite its low EQ (Figs. 3.15, 3.18). An expanded dataset that includes ossification sequences of more species of Cetacea and of early-diverging artiodactyls is needed to test this possible connection.

Most of the changes in the ossification sequences of the taxa examined are recorded for neurocranial bones that undergo endochondral ossification. However, changes in ossifications of dermal bones that make up the oral cavity could provide more insights in the evolution of different feeding styles in Cetacea. The start of tooth mineralization could also be connected to the high dentition variability and tooth loss in this clade. When analyzing the timing of



ossification of the maxilla and dentary relative to the initiation of tooth mineralization, the maxilla was found to be connected with teeth formation, while the dentary was not (Fig. 3.16-3.17). In studies of laboratory mice, the presence of a well-developed dentition was found to be correlated with proper development of the maxilla but not of the mandible (Paradis et al., 2013, Phen et al., 2018). Therefore, it is possible that the onset of formation of teeth and maxilla are more tightly linked than teeth and dentary in mammals in general (Paradis et al., 2013), as exemplified in these analyses of Cetartiodactyla. The close connection between maxilla development and tooth formation might also be responsible for the retention of rudimentary tooth germs in baleen whales and toothed whales with reduced dentition. As both upper and lower dentition are produced by the same developmental pathways (Jernvall and Thesleff, 2000, Tummers and Thesleff, 2009), the necessity to develop tooth germs to progress the development of the upper jaw would cause the retention of dentition in the lower jaw as well. At the same time, in baleen whales the resorption of dentition before birth might have allowed for the rostral shape to develop new shapes free of the constraints imposed by dentition, as seen in the fossil record, with toothless taxa presenting a very different rostral shape than their toothed ancestors (Fig. 3.20). The connection between teeth and jaws shape should also be validated in these non-model organisms, for example by quantifying skull shape variation in modern and fossil Cetartiodactyla to test if adult dentition has an impact on maxilla and dentary shape. A closer inspection of the genetic bases of tooth development and of the ossification sequence of more toothed and baleen whales could also illuminate whether the retention of rudimentary teeth has an impact on rostral and mandibular growth and on the feeding adaptations of these taxa.

Tooth germ development has also been connected with baleen formation on a gene regulatory level (Thewissen et al., 2017). It is then possible that an early mineralization of tooth germs is necessary for their resorption and replacement as exemplified by the sperm whale, the humpback whale and some terrestrial artiodactyls. Modern ruminants, such as sheep, cattle and goats, have a horny dental pad made of keratin that replaces their upper incisors (Cutress, 1972, Pérez et al., 2012, Berkovitz and Shellis, 2018). However, they still develop rudimentary tooth germs in ontogeny that are then resorbed before birth (Witter and Mísek, 1999, Witter et al., 2003). While the ancestor of ruminants and cetaceans retained upper incisors (Webb and Taylor, 1980), it is conceivable that the developmental pathways that bring the formation of both baleen and horny dental pads are partially shared among Cetartiodactyla, as they derive from a common ancestor. Further research on the molecular composition and development of these structures is needed to assess homology. However, adding more taxa to this study dataset would be a first step in this direction, making it possible to test whether tooth resorption is indeed correlated with the formation of keratinous structures in this clade.

## Conclusions

In this Chapter, newly collected quantitative information detailing the modifications in skull shape during ontogeny and evolution in Mysticeti and the changes in ossification sequence of Cetartiodactyla were presented. These new data were then connected to the available qualitative information on the development of modern species of baleen whales and observations on the anatomy of related fossil taxa to understand how changes in development influenced the evolution of new feeding and lifestyle adaptations. In particular, the examination of skull shape changes through developmental and evolutionary time, both using 2D measurements and 3D GM analyses, demonstrated that a general acceleration of developmental rate (peramorphosis) of the shape and size of braincase and rostrum is responsible for modern mysticete anatomical features. The two skull components appear to have shifting allometric relationships both in the ontogeny of modern species and in cetacean evolution, showing a pattern of mosaic heterochrony. First, the rostrum increased its growth rate in shape and size, resulting in taxa with a very elongated rostrum and therefore larger buccal cavities than the ancestors. This was probably directly correlated with the loss of permanent dentition and the adoption of a bulk filter feeding strategy. In crown Mysticeti, the rate of shape development of the braincase increased, and, at least in Balaenopteridae, it now surpasses the one of the rostrum. This change is connected with an increased level of telescoping, with the supraoccipital shield reaching further anteriorly and the nasals being moved posteriorly relative to their position in stem mysticetes. While it is not possible to directly correlate adult morphology of extinct taxa with the anatomy of fetuses and juveniles of extant baleen whales, the neotenic appearance of early mysticetes such as Aetiocetidae† might be connected with their feeding adaptation. These taxa had not yet acquired the higher rostral growth rate associated with bulk filter feeding and toothless taxa but probably had proto-baleen structures and well-developed teeth in the adults, with a blunt and short rostrum.

This was due to shorter and slower development, as modern taxa need to undergo additional ontogenetic stages to resorb teeth and develop a full baleen rack with an elongated rostrum.

Only a few heterochronies, as changes in the timing of onset of ossification of skull bone elements, characterize Cetacea relative to other artiodactyl species examined. An earlier start of ossification of the exoccipital seems to be a distinctive trait of this clade and might be connected with changes in their neck morphology related to swimming. Another neurocranial element, the supraoccipital, begins ossification relatively early in Cetacea, particularly in Odontoceti. This appears to be the plesiomorphic state for all artiodactyls and might have allowed the evolution of bigger brains relative to body size in many toothed whale species as well as the evolution of telescoping. The facial bones that are directly correlated with feeding adaptations present a conserved early onset of ossification in all examined taxa. Small differences in maxilla ossification seem connected with initiation of tooth mineralization, but this is not the case for the dentary. This pattern can be explained by the tighter link between upper jaw formation and tooth mineralization, which was not recovered for the mandible. Timing of tooth mineralization also appears connected with the absence of adult dentition, with taxa that partially or completely lack permanent dentition having an earlier onset of tooth development. However, this is just an observation that needs to be tested further with quantitative methods on a larger dataset. Nonetheless, the connection between tooth formation and upper jaw ossification is possibly one of the causes of the retention of rudimentary tooth germs in fetal mysticetes, as well as their role in the baleen formation signaling pathway.

In sum, this study represents the first step towards a deeper understanding of the developmental patterns connected to Cetacea evolution, particularly in regard to mysticete feeding adaptations. Future work will need to test these hypotheses using a larger dataset of 3D skull morphology data to quantify the difference in shape rate development of the different parts

of the skull that characterize odontocetes and mysticetes, as well as how they differ from their terrestrial relatives. Collecting data on the timing of suture closure instead of onset of ossification on a larger number of taxa might bring to light more key differences between Cetacea and other artiodactyls, illuminating how transformation in the developmental sequences of the skull contributed to the transition from a terrestrial to an aquatic environment. Novel methods will allow larger scale studies also on unique groups such as Cetacea, making it possible to test the preliminary hypotheses formulated in this study.

## Literature cited

- Addinsoft** (2019) XLSTAT statistical and data analysis solution. Long Island, New York, NY: Addinsoft
- Agnarsson I, Miller Ja** (2008) Is ACCTRAN better than DELTRAN? *Cladistics*, **24**, 1032-1038.
- Alberch P** (1985) Problems with the interpretation of developmental sequences. *Syst Zool*, **34**, 46-58.
- Alberch P, Gould SJ, Oster GF, Wake DB** (1979) Size and shape in ontogeny and phylogeny. *Paleobiology*, **5**, 296-317.
- Armfield BA, George JC, Vinyard CJ, Thewissen JGM** (2011) Allometric patterns of fetal head growth in mysticetes and odontocetes: comparison of *Balaena mysticetus* and *Stenella attenuata*. *Mar Mamm Sci*, **27**, 819-827.
- Armfield BA, Zheng Z, Bajpai S, Vinyard CJ, Thewissen JGM** (2013) Development and evolution of the unique cetacean dentition. *PeerJ*, **1**, e24.
- Bebej RM, Smith KM** (2017) Lumbar mobility in archaeocetes (Mammalia: Cetacea) and the evolution of aquatic locomotion in the earliest whales. *Zool J Linn Soc*, **182**, 695-721.
- Berkovitz B, Shellis P** (2018) Cetartiodactyla: Artiodactyla. In *The Teeth of Mammalian Vertebrates*, pp. 223-248. London: Academic Press.
- Berta A, Lanzetti A** (IN REVIEW) Feeding in marine mammals: an integration of evolution and ecology through time. *Palaeontol Electron*.
- Berta A, Lanzetti A, Ekdale EG, Deméré TA** (2016) From teeth to baleen and raptorial to bulk filter feeding in mysticete cetaceans: the role of paleontological, genetic, and geochemical data in feeding evolution and ecology. *Integr Comp Biol*, **56**, 1271-1284.
- Bhullar B-AS, Marugán-Lobón J, Racimo F, et al.** (2012) Birds have paedomorphic dinosaur skulls. *Nature*, **487**, 223-226.
- Bhullar BA, Hanson M, Fabbri M, Pritchard A, Bever GS, Hoffman E** (2016) How to make a bird skull: major transitions in the evolution of the avian cranium, paedomorphosis, and the beak as a surrogate hand. *Integr Comp Biol*, **56**, 389-403.
- Bininda-Emonds ORP, Cardillo M, Jones KE, et al.** (2007) The delayed rise of present-day mammals. *Nature*, **446**, 507-512.
- Bininda-Emonds ORP, Jeffrey JE, Richardson MK** (2003) Is sequence heterochrony an important evolutionary mechanism in mammals? *J Mamm Evol*, **10**, 335-361.

- Bisconti M** (2015) Anatomy of a new cetotheriid genus and species from the Miocene of Herentals, Belgium, and the phylogenetic and palaeobiogeographical relationships of Cetotheriidae s.s. (Mammalia, Cetacea, Mysticeti). *J Syst Palaeontol*, **13**, 377-395.
- Boessenecker RW** (2013) Pleistocene survival of an archaic dwarf baleen whale (Mysticeti: Cetotheriidae). *Naturwissenschaften*, **100**, 365-371.
- Boessenecker RW, Fordyce RE** (2015a) Anatomy, feeding ecology, and ontogeny of a transitional baleen whale: a new genus and species of Eomysticetidae (Mammalia: Cetacea) from the Oligocene of New Zealand. *PeerJ*, **3**, e1129-e1129.
- Boessenecker RW, Fordyce RE** (2015b) A new genus and species of eomysticetid (Cetacea: Mysticeti) and a reinterpretation of 'Mauicetus lophocephalus' Marples, 1956: transitional baleen whales from the upper Oligocene of New Zealand. *Zool J Linn Soc*, **175**, 607-660.
- Boessenecker RW, Fordyce RE** (2016) A new eomysticetid from the Oligocene Kokoamu Greensand of New Zealand and a review of the Eomysticetidae (Mammalia, Cetacea). *J Syst Palaeontol*, DOI: 10.1080/14772019.2016.1191045.
- Botelho JF, Ossa-Fuentes L, Soto-Acuña S, et al.** (2014) New developmental evidence clarifies the evolution of wrist bones in the dinosaur–bird transition. *PLoS Biol*, **12**, e1001957.
- Bouetel VV** (2005) Phylogenetic implications of skull structure and feeding behavior in balaenopterids (Cetacea, Mysticeti). *J Mammal*, **86**, 139-146.
- Buchholtz EA** (2001) Vertebral osteology and swimming style in living and fossil whales (Order: Cetacea). *J Zool*, **235**, 175-190.
- Buchholtz Ea** (2007) Modular evolution of the cetacean vertebral column. *Evol Dev*, **9**, 278-289.
- Buchholtz EA, Booth AC, Webbink KE** (2007) Vertebral anatomy in the Florida manatee, *Trichechus manatus latirostris*: a developmental and evolutionary analysis. *Anat Rec*, **290**, 624-637.
- Buchholtz Ea, Schur Sa** (2004) Vertebral osteology in Delphinidae (Cetacea). *Zool J Linn Soc*, **140**, 383-401.
- Cheverud JM** (1982) Relationships among ontogenetic, static, and evolutionary allometry. *Am J Phys Anthropol*, **59**, 139-149.
- Churchill M, Geisler JH, Beatty BL, Goswami A** (2018) Evolution of cranial telescoping in echolocating whales (Cetacea: Odontoceti). *Evolution*, **72**, 1092-1108.
- Churchill M, Martinez-caceres M, de Muizon C, et al.** (2016) The origin of high-frequency hearing in whales. *Curr Biol*, **26**, 1-6.

- Cignoni P, Callieri M, Corsini M, Dellepiane M, Ganovelli F, Ranzuglia G** (2008) MeshLab: an open-source mesh processing tool. (eds Scarano V, Chiara RD, Erra U), pp. 129-136. Eurographics Italian Chapter Conference.
- Clauss M, Steuer P, Müller D, Codron D, Hummel J** (2013) Herbivory and body size: allometries of diet quality and gastrointestinal physiology, and implications for herbivore ecology and dinosaur gigantism. *PLoS ONE*, **8**, e68714.
- Clementz MT, Fordyce RE, Peek SL, Fox DL** (2014) Ancient marine isoscapes and isotopic evidence of bulk-feeding by Oligocene cetaceans. *Palaeogeogr, Palaeoclimatol, Palaeoecol*, **400**, 28-40.
- Collareta A, Lambert O, Landini W, et al.** (2017) Did the giant extinct shark *Carcharocles megalodon* target small prey? Bite marks on marine mammal remains from the late Miocene of Peru. *Palaeogeogr, Palaeoclimatol, Palaeoecol*, **469**, 84-91.
- Collareta A, Landini W, Lambert O, et al.** (2015) Piscivory in a Miocene Cetotheriidae of Peru: first record of fossilized stomach content for an extinct baleen-bearing whale. *Sci Nat*, **102**, 70.
- Cutress TW** (1972) The incisive apparatus of the sheep. *Res Vet Sci*, **13**, 74-78.
- Davies JL, Guiler ER** (1957) A note on the pygmy right whale, *Caperea marginata* Gray. *Proc Zool Soc Lond*, **129**, 579-589.
- del Castillo DL, Viglino M, Flores DA, Cappozzo HL** (2017) Skull ontogeny and modularity in two species of *Lagenorhynchus*: morphological and ecological implications. *J Morphol*, **278**, 203-214.
- Deméré TA, Berta A** (2008) Skull anatomy of the Oligocene toothed mysticete *Aetiocetus weltoni* (Mammalia; Cetacea): implications for mysticete evolution and functional anatomy. *Zool J Linn Soc*, **154**, 308-352.
- Deméré TA, McGowen MR, Berta A, Gatesy J** (2008) Morphological and molecular evidence for a stepwise evolutionary transition from teeth to baleen in mysticete whales. *Syst Biol*, **57**, 15-37.
- Denoël M, Ficetola GF, Ćirović R, et al.** (2009) A multi-scale approach to facultative paedomorphosis of European newts (Salamandridae) in the Montenegrin karst: distribution pattern, environmental variables, and conservation. *Biol Conserv*, **142**, 509-517.
- Drake AG, Klingenberg CP** (2008) The pace of morphological change: historical transformation of skull shape in St. Bernard dogs. *Proc R Soc Lond B Biol Sci*, **275**, 71-76.
- Duncan RP, Blackburn TM, Worthy TH** (2002) Prehistoric bird extinctions and human hunting. *Proc R Soc Lond B Biol Sci*, **269**, 517-521.



- Ekdale E, Deméré TA, Berta A** (2015) Vascularization of the gray whale palate (Cetacea, Mysticeti, *Eschrichtius robustus*): soft tissue evidence for an alveolar source of blood to baleen. *Anat Rec*, **298**, 691-702.
- Ekdale EG** (2016) Morphological variation among the inner ears of extinct and extant baleen whales (Cetacea: Mysticeti). *J Morphol*, **277**, 1599-1615.
- El Adli JJ, Deméré TA, Boessenecker RW** (2014) *Herpetocetus morrowi* (Cetacea: Mysticeti), a new species of diminutive baleen whale from the Upper Pliocene (Piacenzian) of California, USA, with observations on the evolution and relationships of the Cetotheriidae. *Zool J Linn Soc*, **170**, 400-466.
- Fahlke JM, Hampe O** (2015) Cranial symmetry in baleen whales (Cetacea, Mysticeti) and the occurrence of cranial asymmetry throughout cetacean evolution. *Sci Nat*, **102**, 58.
- FEI VSG** (2018) Avizo Lite: 3D analysis software for scientific and industrial data, version 9.5. Berlin: Konrad-Zuse-Zentrum für Informationstechnik
- Fitzgerald EMG** (2010) The morphology and systematics of *Mammalodon colliveri* (Cetacea: Mysticeti), a toothed mysticete from the Oligocene of Australia. *Zool J Linn Soc*, **158**, 367-476.
- Fitzgerald EMGG** (2006) A bizarre new toothed mysticete (Cetacea) from Australia and the early evolution of baleen whales. *Proc R Soc Lond B Biol Sci*, **273**, 2955-2963.
- Fordyce RE** (1980) Whale evolution and Oligocene southern ocean environments. *Palaeogeogr, Palaeoclimatol, Palaeoecol*, **31**, 319-336.
- Fordyce RE, Marx FG** (2013) The pygmy right whale *Caperea marginata*: the last of the cetotheres. *Proc R Soc Lond B Biol Sci*, **280**, 20122645.
- Fordyce RE, Marx FG** (2016) Mysticetes baring their teeth: a new fossil whale, *Mammalodon hakataramea*, from the Southwest Pacific. *Mem Mus Vic*, **74**, 107-116.
- Fordyce RE, Marx FG** (2018) Gigantism precedes filter feeding in baleen whale evolution. *Curr Biol*, **28**, 1670-1676.
- Foth C, Fernandez Blanco MV, Bona P, Scheyer TM** (2017) Cranial shape variation in jacarean caimanines (Crocodylia, Alligatoroidea) and its implications in the taxonomic status of extinct species: the case of *Melanosuchus fisheri*. *J Morphol*, **279**, 259-273.
- Franci G, Berta A** (2018) Relative growth of the skull of the common minke whale (*Balaenoptera acutorostrata*) using a 3D laser surface scanner. *Aquat Mamm*, **44**, 529-537.
- Friedman M** (2012) Parallel evolutionary trajectories underlie the origin of giant suspension-feeding whales and bony fishes. *Proc R Soc Lond B Biol Sci*, **279**, 944-951.

- Friedman M, Shimada K, Martin LD, et al.** (2010) 100-million-year dynasty of giant planktivorous bony fishes in the Mesozoic seas. *Science*, **327**, 990-993.
- Fröbisch NB, Carroll RL, Schoch RR** (2007) Limb ossification in the Paleozoic branchiosaurid *Apateon* (Temnospondyli) and the early evolution of preaxial dominance in tetrapod limb development. *Evol Dev*, **9**, 69-75.
- Galatius A** (2010) Paedomorphosis in two small species of toothed whales (Odontoceti): how and why? *Biol J Linn Soc*, **99**, 278-295.
- Galatius A, Berta A, Frandsen MS, Goodall RNP** (2011) Interspecific variation of ontogeny and skull shape among porpoises (Phocoenidae). *J Morphol*, **272**, 136-148.
- Galatius a, Kinze CC** (2003) Ankylosis patterns in the postcranial skeleton and hyoid bones of the harbour porpoise (*Phocoena phocoena*) in the Baltic and North Sea. *Can J Zool*, **81**, 1851-1861.
- Gatesy J** (2009) Whales and even-toed ungulates (Cetartiodactyla). In *The Timetree of Life* (eds Hedges SB, Kumar S), pp. 511-515. New York: Oxford University Press.
- Gatesy J, Berta A, Demere TA, Ekdale EG, El Adli JJ, McGowen MR** (2018) Contrasting interpretations of the teeth to baleen transition in mysticete cetaceans. *J Vert Paleontol, Program and Abstracts*, 132.
- Gatesy J, Geisler JH, Chang J, et al.** (2013) A phylogenetic blueprint for a modern whale. *Mol Phylogen Evol*, **66**, 479-506.
- Geisler JH** (2018) Evolution: more mysticete mysteries. *Curr Biol*, **28**, R603-R605.
- Geisler JH, Boessenecker RW, Brown M, Beatty BL** (2017) The origin of filter feeding in whales. *Curr Biol*, **27**, 2036-2042.
- Geisler JH, Sanders AE** (2003) Morphological evidence for the phylogeny of Cetacea. *J Mamm Evol*, **10**, 23-129.
- Gioncada A, Collareta A, Gariboldi K, et al.** (2016) Inside baleen: exceptional microstructure preservation in a late Miocene whale skeleton from Peru. *Geology*, **44**, G38216.1.
- Gol'din P, Startsev D** (2014) *Brandtocetus*, a new genus of baleen whales (Cetacea, Cetotheriidae) from the late Miocene of Crimea, Ukraine. *J Vert Paleontol*, **34**, 419-433.
- Gol'din P, Steeman ME, Sanders AE, et al.** (2015) From problem taxa to problem solver: a new miocene family, Tranatocetidae, brings perspective on baleen whale evolution. *PLoS ONE*, **10**, e0135500.
- Goldbogen JA, Calambokidis J, Croll DA, et al.** (2012) Scaling of lunge-feeding performance in rorqual whales: mass-specific energy expenditure increases with body size and progressively limits diving capacity. *Funct Ecol*, **26**, 216-226.

- Goldbogen JA, Madsen PT** (2018) The evolution of foraging capacity and gigantism in cetaceans. *J Exp Biol*, **221**, jeb166033.
- Goldbogen JA, Potvin J, Shadwick RE** (2010) Skull and buccal cavity allometry increase mass-specific engulfment capacity in fin whales. *Proc R Soc Lond B Biol Sci*, **277**, 861-868.
- Goswami A** (2007) Cranial modularity and sequence heterochrony in mammals. *Evol Dev*, **9**, 290-298.
- Goswami A, Polly PD** (2010a) The influence of modularity on cranial morphological disparity in carnivora and primates (Mammalia). *PLoS ONE*, **5**, e9517.
- Goswami A, Polly PD** (2010b) Methods for studying morphological integration and modularity. *Paleo Soc Pap*, **16**, 213-243.
- Gould SJ** (1977) *Ontogeny and phylogeny*, Harvard University Press, USA.
- Haeckel EH** (1866) *Generelle Morphologie der Organismen*, 2 Bde. Georg Reimer, Berlin.
- Hampe O, Baszio S** (2010) Relative warps meet cladistics: a contribution to the phylogenetic relationships of baleen whales based on landmark analyses of mysticete crania. *Bull Geosci*, **85**, 199-218.
- Harrison L, Larsson H** (2008) Estimating evolution of temporal sequence changes: a practical approach to inferring ancestral developmental sequences and sequence heterochrony. *Syst Biol*, **57**, 378-387.
- Herridge VL, Lister AM** (2012) Extreme insular dwarfism evolved in a mammoth. *Proc R Soc Lond B Biol Sci*, **279**, 3193-3200.
- Heyning JE, Mead JG** (1990) Evolution of the nasal anatomy of cetaceans. In *Sensory abilities of cetaceans* (eds Thomas JA, Kastelein RA), pp. 67-79. Boston: Springer.
- Hocking DP, Marx FG, Park T, Fitzgerald EMG, Evans AR** (2017) A behavioural framework for the evolution of feeding in predatory aquatic mammals. *Proc R Soc Lond B Biol Sci*, **284**, 20162750.
- Jeffery JE, Bininda-Emonds ORP, Coates MI, Richardson MK** (2002a) Analyzing evolutionary patterns in amniote embryonic development. *Evol Dev*, **4**, 292-302.
- Jeffery JE, Richardson MK, Coates MI, Bininda-Emonds ORP** (2002b) Analyzing developmental sequences within a phylogenetic framework. *Syst Biol*, **51**, 478-91.
- Jernvall J, Thesleff I** (2000) Reiterative signaling and patterning during mammalian tooth morphogenesis. *Mech Dev*, **92**, 19-29.
- Kadim IT, Mahgoub O, Purchas RW** (2008) A review of the growth, and of the carcass and meat quality characteristics of the one-humped camel (*Camelus dromedaries*). *Meat Sci*, **80**, 555-569.

- Kahane-Rapport SR, Goldbogen JA** (2018) Allometric scaling of morphology and engulfment capacity in rorqual whales. *J Morphol*, **279**, 1256–1268.
- Karlsen K** (1962) Development of tooth germs and adjacent structures in the whalebone whale (*Balaenoptera physalus*). *Hval skrif*, **45**, 5-56.
- Kienle SS, Law CJ, Costa DP, Berta A, Mehta RS** (2017) Revisiting the behavioural framework of feeding in predatory aquatic mammals. *Proc R Soc Lond B Biol Sci*, **284**, 20171035.
- Kierdorf H, Hommelsheim S, Kierdorf U** (2012) Development of the permanent mandibular cheek teeth in fallow deer (*Dama dama*). *Anat Histol Embryol*, **41**, 419-427.
- Klingenberg CP** (1998) Heterochrony and allometry: the analysis of evolutionary change in ontogeny. *Biol Rev Camb Philos Soc*, **73**, 79-123.
- Klingenberg CP** (2005) Developmental constraints, modules, and evolvability. In *Variations* (eds Hallgrímsson B, Hall BK), pp. 219-247. Cambridge: Academic Press.
- Klingenberg CP** (2009) Morphometric integration and modularity in configurations of landmarks: tools for evaluating a priori hypotheses. *Evol Dev*, **11**, 405-421.
- Klingenberg CP** (2011) MORPHOJ: an integrated software package for geometric morphometrics. *Mol Ecol Resour*, **11**, 353-357.
- Klingenberg CP, Gidaszewski NA** (2010) Testing and quantifying phylogenetic signals and homoplasy in morphometric data. *Syst Biol*, **59**, 245-261.
- Klingenberg CP, Marugán-Lobón J** (2013) Evolutionary covariation in geometric morphometric data: Analyzing integration, modularity, and allometry in a phylogenetic context. *Syst Biol*, **62**, 591-610.
- Koyabu D, Endo H, Mitgutsch C, et al.** (2011) Heterochrony and developmental modularity of cranial osteogenesis in lipotyphlan mammals. *EvoDevo*, **2**, 21-21.
- Koyabu D, Werneburg I, Morimoto N, et al.** (2014) Mammalian skull heterochrony reveals modular evolution and a link between cranial development and brain size. *Nat Commun*, **5**, 3625-3625.
- Kuzmin AA** (1976) Embryogenesis of the osseous skull of the sperm whale. *Investig Cetacea*, **7**, 187-202.
- Lanzetti A** (in press) Prenatal developmental sequence of the skull of minke whales and its implications for the evolution of mysticetes and the teeth-to-baleen transition. *J Anat*.
- Lanzetti A, Berta A, Ekdale EG** (2018) Prenatal development of the humpback whale: growth rate, tooth loss and skull shape changes in an evolutionary framework. *Anat Rec*, <https://doi.org/10.1002/ar.23990>.

- Livezey BC** (1993) An ecomorphological review of the dodo (*Raphus cucullatus*) and solitaire (*Pezophaps solitaria*), flightless Columbiformes of the Mascarene Islands. *J Zool*, **230**, 247-292.
- Luo ZX** (1998) Homology and transformation of cetacean ectotympanic structures. In *The Emergence of Whales* (ed Thewissen JGM), pp. 270-277. New York, NY: Springer.
- Maddison WP** (1991) Squared-change parsimony reconstructions of ancestral states for continuous-valued characters on a phylogenetic tree. *Syst Biol*, **40**, 304-314.
- Maddison WP, Maddison DR** (2018) Mesquite: a modular system for evolutionary analysis. Version 3.6. <http://mesquiteproject.org>
- Marx FG** (2011) The more the merrier? A large cladistic analysis of mysticetes, and comments on the transition from teeth to baleen. *J Mamm Evol*, **18**, 77-100.
- Marx FG, Collareta A, Gioncada A, et al.** (2017a) How whales used to filter: exceptionally preserved baleen in a Miocene cetotheriid. *J Anat*, **231**, 212-220.
- Marx FG, Fordyce RE** (2015) Baleen boom and bust: a synthesis of mysticete phylogeny, diversity and disparity. *Roy Soc Open Sci*, **2**, 140434.
- Marx FG, Fordyce RE** (2016) A link no longer missing: new evidence for the cetotheriid affinities of *Caperea*. *PLoS ONE*, **11**, e0164059.
- Marx FG, Hocking DP, Park T, Ziegler T, Evans AR, Fitzgerald EMG** (2016) Suction feeding preceded filtering in baleen whale evolution. *Mem Mus Vic*, **75**, 71-82.
- Marx FG, Lambert O, de Muizon C** (2017b) A new Miocene baleen whale from Peru deciphers the dawn of cetotheriids. *Roy Soc Open Sci*, **4**, 170560.
- Marx FG, Post K, Bosselaers M, Munsterman DK** (2019) A large Late Miocene cetotheriid (Cetacea, Mysticeti) from the Netherlands clarifies the status of Tranatocetidae. *PeerJ*, **7**, e6426.
- Marx FG, Tsai C-h, Fordyce RE** (2015) A new Early Oligocene toothed 'baleen' whale (Mysticeti: Aetiocetidae) from western North America: one of the oldest and the smallest. *Roy Soc Open Sci*, **2**, 150476.
- Marx FG, Uhen MD** (2010) Climate, critters, and cetaceans: cenozoic drivers of the evolution of modern whales. *Science*, **327**, 993-996.
- Maxwell EE, Harrison LB** (2009) Methods for the analysis of developmental sequence data. *Evol Dev*, **11**, 109-119.
- McGowen MR** (2011) Toward the resolution of an explosive radiation—a multilocus phylogeny of oceanic dolphins (Delphinidae). *Mol Phylogen Evol*, **60**, 345-57.

- McGowen MR, Spaulding M, Gatesy J** (2009) Divergence date estimation and a comprehensive molecular tree of extant cetaceans. *Mol Phylogen Evol*, **53**, 891-906.
- McKinney ML** (1988) Classifying heterochrony. In *Heterochrony in evolution* (ed McKinney ML), pp. 17-34. New York: Springer.
- McNamara KJ** (1986) A guide to the nomenclature of heterochrony. *J Paleontol*, **60**, 4-13.
- McNamara KJ, McKinney ML** (2005) Heterochrony, disparity, and macroevolution. *Paleobiology*, **31**, 17-26.
- Mead JG, Fordyce RE** (2009) The therian skull: a lexicon with emphasis on the odontocetes. *Smithson Contrib Zool*, **627**, 1-249.
- Mellor L, Cooper LN, Torre J, Brownell RL** (2009) Paedomorphic ossification in porpoises with an emphasis on the vaquita (*Phocoena sinus*). *Aquat Mamm*, **35**, 193-202.
- Midford PE, Garland TJ, Maddison WP** (2005) PDAP Package of Mesquite.
- Miller GS** (1923) The telescoping of the cetacean skull. *Smit Misc Coll*, **76**, 1-71.
- Mitteroecker P, Bookstein F** (2011) Linear discrimination, ordination, and the visualization of selection gradients in modern morphometrics. *Evol Biol*, **38**, 100-114.
- Monteiro-Filho ELdA, Monteiro LR, Dos Reis SF** (2002) Skull shape and size divergence in dolphins of the genus *Sotalia*: a tridimensional morphometric analysis. *J Mammal*, **83**, 125-134.
- Morris ZS, Vliet KA, Abzhanov A, Pierce SE** (2019) Heterochronic shifts and conserved embryonic shape underlie crocodylian craniofacial disparity and convergence. *Proc R Soc Lond B Biol Sci*, **286**, 20182389.
- Motani R, Chen X-H, Jiang D-Y, Cheng L, Tintori A, Rieppel O** (2015) Lunge feeding in early marine reptiles and fast evolution of marine tetrapod feeding guilds. *Sci Rep*, **5**, 8900.
- Mulder EWA** (2001) Co-ossified vertebrae of mosasaurs and cetaceans: implications for the mode of locomotion of extinct marine reptiles. *Paleobiology*, **27**, 724-734.
- Nakamura G, Kato H** (2014) Developmental changes in the skull morphology of common minke whales *Balaenoptera acutorostrata*. *J Morphol*, **275**, 1113-1121.
- Nakamura G, Kato H, Fujise Y** (2012) Relative growth of the skull of the common minke whale *Balaenoptera acutorostrata* from the North Pacific in comparison to other *Balaenoptera* species. *Mamm Study*, **37**, 105-112.
- Okazaki Y** (2012) A new mysticete from the upper Oligocene Ashiya Group, Kyushu, Japan and its significance to mysticete evolution. *Bull Kitakyushu Mus Nat Hist*, **10**, 129-152.

- Olori JC** (2013) Ontogenetic sequence reconstruction and sequence polymorphism in extinct taxa: an example using early tetrapods (Tetrapoda: Lepospondyli). *Paleobiology*, **39**, 400-428.
- Olsson L, Levit GS, Hoßfeld U** (2017) The “Biogenetic Law” in zoology: from Ernst Haeckel’s formulation to current approaches. *Theory Biosci*, **136**, 19-29.
- Owen J, Dobney K, Evin A, Cucchi T, Larson G, Strand Vidarsdottir U** (2014) The zooarchaeological application of quantifying cranial shape differences in wild boar and domestic pigs (*Sus scrofa*) using 3D geometric morphometrics. *J Archaeol Sci*, **43**, 159-167.
- Paradis MR, Raj MT, Boughner JC** (2013) Jaw growth in the absence of teeth: the developmental morphology of edentulous mandibles using the p63 mouse mutant. *Evol Dev*, **15**, 268-279.
- Pavey CR** (1992) The occurrence of the pigmy right whale, *Caperea marginata* (Cetacea: Neobalaenidae), along the Australian coast. *Aust Mammal*, **15**, 1-6.
- Peredo CM, Peredo JS, Pyenson ND** (2018a) Convergence on dental simplification in the evolution of whales. *Paleobiology*, **44**, 434-443.
- Peredo CM, Pyenson ND, Boersma AT** (2017) Decoupling tooth loss from the evolution of baleen in whales. *Front Mar Sci*, **4**, 1-11.
- Peredo CM, Pyenson ND, Marshall CD, Uhen MD** (2018b) Tooth loss precedes the origin of baleen in whales. *Curr Biol*, **28**, 3992-4000.
- Peredo CM, Uhen MD** (2016a) Exploration of marine mammal paleogeography in the Northern Hemisphere over the Cenozoic using beta diversity. *Palaeogeogr, Palaeoclimatol, Palaeoecol*, **449**, 227-235.
- Peredo CM, Uhen MD** (2016b) A new basal chaemysticete (Mammalia: Cetacea) from the Late Oligocene Pysht Formation of Washington, USA. *Pap Palaeontol*, **2**, 533-554.
- Pérez W, Michel V, Jerbi H, Vazquez N** (2012) Anatomy of the mouth of the giraffe (*Giraffa camelopardalis rothschildi*). *Int J Morphol*, **30**, 322-329.
- Phen A, Greer J, Uppal J, Der J, Boughner JC** (2018) Upper jaw development in the absence of teeth: new insights for craniodental evo-devo integration. *Evol Dev*, **20**, 146-159.
- Piras P, Colangelo P, Adams DC, et al.** (2010) The *Gavialis-Tomistoma* debate: the contribution of skull ontogenetic allometry and growth trajectories to the study of crocodylian relationships. *Evol Dev*, **12**, 568-579.
- Pyenson ND, Goldbogen JA, Shadwick RE** (2013) Mandible allometry in extant and fossil Balaenopteridae (Cetacea: Mammalia): the largest vertebrate skeletal element and its role in rorqual lunge feeding. *Biol J Linn Soc*, **108**, 586-599.

- Pyenson ND, Goldbogen JA, Vogl AW, Szathmary G, Drake R, L., Shadwick RE** (2012) Discovery of a sensory organ that coordinates lunge feeding in rorqual whales. *Nature*, **485**, 498.
- Pyenson ND, Vermeij GJ** (2016) The rise of ocean giants: maximum body size in Cenozoic marine mammals as an indicator for productivity in the Pacific and Atlantic oceans. *Biol Lett*, **12**, 2016-2019.
- Ridgway SH, Carlin KP, Van Alstyne KR, Hanson AC, Tarpley RJ** (2017) Comparison of dolphins' body and brain measurements with four other groups of cetaceans reveals great diversity. *Brain Behav Evol*, **88**, 235-257.
- Rohlf FJ, Slice D** (1990) Extensions of the procrustes method for the optimal superimposition of landmarks. *Syst Zool*, **39**, 40-59.
- Roston RA, Roth VL** (2019) Cetacean skull telescoping brings evolution of cranial sutures into focus. *Anat Rec*, <https://doi.org/10.1002/ar.24079>.
- Sánchez-Villagra MR, Goswami A, Weisbecker V, Mock O, Kuratani S** (2008) Conserved relative timing of cranial ossification patterns in early mammalian evolution. *Evol Dev*, **10**, 519-530.
- Sander PM, Christian A, Clauss M, et al.** (2011) Biology of the sauropod dinosaurs: the evolution of gigantism. *Biol Rev*, **86**, 117-155.
- Sanders AE, Barnes LG** (2002) Paleontology of the Late Oligocene Ashley and Chandler Bridge Formations of South Carolina, 3: Eomysticetidae, a new family of primitive mysticetes (Mammalia: Cetacea). *Smithson Contrib Paleobiol*, **93**, 313-356.
- Sardi ML, Ventrice F, Ramírez Rozzi F** (2007) Allometries throughout the late prenatal and early postnatal human craniofacial ontogeny. *Anat Rec*, **290**, 1112-1120.
- Sawamura H** (2008) The origin of baleen whale-comparative morphology of the toothed mysticetes and the minke whale fetuses. *J Fos Res*, **40**, 120-130.
- Schaller O, Constantinescu GM** (2007) *Illustrated veterinary anatomical nomenclature Latin-English*, Georg Thieme Verlag, Stuttgart.
- Sempere AJ, Sokolov VE, Danilkin AA** (1996) *Capreolus capreolus*. *Mamm Species*, 1-9.
- Slater GJ, Goldbogen J, Pyenson ND** (2017) Independent evolution of baleen whale gigantism linked to Plio-Pleistocene ocean dynamics. *Proc R Soc Lond B Biol Sci*, **284**, 20170546.
- Smith-Paredes D, Núñez-León D, Soto-Acuña S, O'Connor J, Botelho JF, Vargas AO** (2018) Dinosaur ossification centres in embryonic birds uncover developmental evolution of the skull. *Nature*, **2**, 1966-1973.
- Smith KK** (1997) Comparative patterns of craniofacial development in eutherian and metatherian mammals. *Evolution*, **51**, 1663-1678.



- Smith KK** (2002) Sequence heterochrony and the evolution of development. *J Morphol*, **252**, 82-97.
- Smith KK** (2003) Time's arrow: heterochrony and the evolution of development. *Int J Dev Biol*, **621**, 613-621.
- Spoor F, Bajpai S, Hussain ST, Kumar K, Thewissen JGM** (2002) Vestibular evidence for the evolution of aquatic behaviour in early cetaceans. *Nature*, **417**, 163-166.
- Swofford DL** (2003) PAUP\*: Phylogenetic Analysis Using Parsimony (\*and Other Methods). Version 4. Sinauer Associates, Sunderland, Massachusetts.
- Sydney NV, Machado FA, Hingst-Zaher E** (2012) Timing of ontogenetic changes of two cranial regions in *Sotalia guianensis* (Delphinidae). *Mamm Biol*, **77**, 397-403.
- Thewissen JGM, Cohn MJ, Stevens LS, Bajpai S, Heyning J, Horton WE** (2006) Developmental basis for hind-limb loss in dolphins and origin of the cetacean bodyplan. *Proc Natl Acad Sci USA*, **103**, 8414-8418.
- Thewissen JGM, Cooper LN, Behringer RR** (2012) Developmental biology enriches paleontology. *J Vert Paleontol*, **32**, 1223-1234.
- Thewissen JGM, Cooper LN, George JC, Bajpai S** (2009) From land to water: the origin of whales, dolphins, and porpoises. *Evolution*, **2**, 272-288.
- Thewissen JGM, Fish FE** (1997) Locomotor evolution in the earliest cetaceans: functional model, modern analogues, and paleontological evidence. *Paleobiology*, **23**, 482-490.
- Thewissen JGM, Hieronymus TL, George JC, Suydam R, Stimmelmayer R, McBurney D** (2017) Evolutionary aspects of the development of teeth and baleen in the bowhead whale. *J Anat*, **230**, 549-566.
- Tsai C-H, Fordyce RE** (2018) A new archaic baleen whale *Toipahautea waitaki* (early Late Oligocene, New Zealand) and the origins of crown Mysticeti. *Roy Soc Open Sci*, **5**, 172453.
- Tsai C-H, Kohno N** (2016) Multiple origins of gigantism in stem baleen whales. *Naturwissenschaften*, **103**, 89-89.
- Tsai CH, Fordyce RE** (2014) Disparate heterochronic processes in baleen whale evolution. *Evol Biol*, **41**, 299-307.
- Tsai CH, Fordyce RE** (2016) Archaic baleen whale from the Kokoamu Greensand: earbones distinguish a new late Oligocene mysticete (Cetacea: Mysticeti) from New Zealand. *J R Soc N Z*, **46**, 117-138.
- Tummers M, Thesleff I** (2009) The importance of signal pathway modulation in all aspects of tooth development. *J Exp Zool Part B*, **312**, 309-319.

- Uhen MD** (2008) A new xenorophus- like odontocete cetacean from the oligocene of North Carolina and a discussion of the basal odontocete radiation. *J Syst Palaeontol*, **6**, 433-452.
- Vollmer NL, Ashe E, Brownell RL, et al.** (2019) Taxonomic revision of the dolphin genus *Lagenorhynchus*. *Mar Mamm Sci*, **00**, 1-101.
- Walsh BM, Berta A** (2011) Occipital ossification of balaenopteroid mysticetes. *Anat Rec*, **294**, 391-398.
- Wang S, Stiegler J, Wu P, et al.** (2017) Heterochronic truncation of odontogenesis in theropod dinosaurs provides insight into the macroevolution of avian beaks. *PNAS*, **114**, 10930-10935.
- Webb SD, Taylor BE** (1980) The phylogeny of hornless ruminants and a description of the cranium of *Archaeomeryx*. *Bull Am Mus Nat Hist*, **167**, 117-158.
- Webster M, David Sheets H** (2010) A practical introduction to landmark-based geometric morphometrics. *Paleo Soc Pap*, 163-188.
- Werth AJ, Ito H** (2017) Sling, scoop, and squirter: anatomical features facilitating prey transport, processing, and swallowing in rorqual whales (Mammalia: Balaenopteridae). *Anat Rec*, **300**, 2070-2086.
- Werth AJ, Potvin J, Shadwick RE, Jensen MM, Cade DE, Goldbogen JA** (2018) Filtration area scaling and evolution in mysticetes: trophic niche partitioning and the curious cases of sei and pygmy right whales. *Biol J Linn Soc*, **125**, 264-279.
- Weston EM, Lister AM** (2009) Insular dwarfism in hippos and a model for brain size reduction in *Homo floresiensis*. *Nature*, **459**, 85-88.
- Whitmore FC, Sanders AE** (1976) Review of the Oligocene Cetacea. *Syst Zool*, **25**, 304-320.
- Wiens JJ, Bonett RM, Chippindale PT** (2005) Ontogeny discombobulates phylogeny: paedomorphosis and higher-level salamander relationships. *Syst Biol*, **54**, 91-110.
- Wilson LAB** (2011) Comparison of prenatal and postnatal ontogeny: cranial allometry in the African striped mouse (*Rhabdomys pumilio*). *J Mammal*, **92**, 407-420.
- Witter K, Matulova P, Misek I** (2003) Three-dimensional reconstruction studies and morphometric analysis of rudimental tooth primordia in the upper incisor region of the sheep (*Ovis aries*, Ruminantia). *Arch Oral Biol*, **48**, 15-24.
- Witter K, Misek I** (1999) Time programme of the early tooth development in the domestic sheep (*Ovis aries*, Ruminantia). *Acta Vet Brno*, **68**, 3-8.
- Yamato M, Pyenson ND** (2015) Early development and orientation of the acoustic funnel provides insight into the evolution of sound reception pathways in cetaceans. *PLoS ONE*, **10**, e0118582.

**Yoshida K, Kimura T, Hasegawa Y** (2003) New cetothere (Cetacea: Mysticeti) from the Miocene Chichibumachi Group, Japan. *Bull Saitama Mus Nat Hist*, **20-21**, 1-10.

## Conclusions of the Dissertation

Among Mammalia, Cetacea present unique adaptations to the aquatic environment, which also include extreme cases of tooth reduction and loss. In Chapter One, I qualitatively demonstrated that the dentition and feeding apparatus of Odontoceti is highly variable, with many instances of convergent evolution. This pattern is likely caused by the relaxation of selective pressures on these traits, followed by adaptations to similar environments and feeding modes. Beaked whales (Ziphiidae) are one of the best examples of this high morphological variability of dentition in toothed whales. Sexual selection and competition for food resources contributed to the reacquisition of full adult dentition in the Tasman's beaked whale (*Tasmacetus*), while all other living beaked whales only display erupted teeth modified as mandibular tusks.

While all toothed whales have been shown to retain adult dentition in some form, living Mysticeti completely lack this trait and have instead evolved baleen, keratinous plates that aid in bulk filter feeding. Evolution of this novel trait and associated feeding mode is correlated with developmental and genetic changes. Combining novel data collected for gene *C4orf26* and a review of the literature on tooth- and enamel-related gene evolution in modern baleen whales and description of tooth morphology in fossils, it is possible to hypothesize that the loss of tooth function, accompanied by a loss of the enamel cap, as also seen in some modern toothed whales with reduced dentition, preceded the complete loss of adult dentition. This second step was likely related to the acquisition of baleen plates and the switch to specialized bulk filter feeding. This genetic pattern of tooth loss can also explain the lack of enamel in the fetal tooth germs and differences in their morphology among families.

These documented genetic modifications and subsequent loss of teeth co-occurred with major transformations in the skull anatomy of mysticetes. Developmental data can show how these changes occur in modern taxa and serve as a parallel for evolution. By analyzing in detail

teeth and skull ontogeny of minke and humpback whales, I observed that tooth germs appear in the very early fetal stages, then, at least in minke whales, after mid-gestation a denser material, interpreted as a precursor of baleen development and referred as “baleen rudiments”, starts developing medially to the resorbing tooth buds. In the very last portion of gestation, the transversal process of the baleen is erupted, starting at the posterior end, and no tooth germs are present. Quantitative investigation of skull shape changes shows that ontogeny potentially played a key role in the evolution of other characteristic traits of this lineage related to filter feeding, such as their large buccal cavity and elongated rostrum. Variations in the timing of development between different regions of the skull, mainly rostrum and braincase, likely contributed to the evolution of modern mysticetes anatomy.

These hypotheses were tested by directly comparing the skull anatomy of modern fetal specimens to adult fossils. Results show that toothed stem-mysticetes share similar rostral and braincase shape with neonatal and late fetal specimens of modern taxa. This suggests that living species go through additional ontogenetic steps compared to their ancestors to obtain their distinctive head shape, such as an elongated rostrum and marked overlapping of the neurocranial bones (telescoping). This reveals that a general acceleration of developmental rate (peramorphosis) of the shape and size of braincase and rostrum is likely responsible for modern mysticetes anatomical features. However they happened at different times. First, the rostrum increased its growth rate in shape and size, resulting in taxa with a very elongated rostrum and therefore larger buccal cavities than the ancestors. This was probably directly correlated with the loss of permanent dentition and the adoption of a bulk filter feeding strategy. In crown Mysticeti, the rate of shape development of the braincase increased, and, at least in Balaenopteridae, it now surpasses the one of the rostrum. This change relates to an increased level of telescoping, with the

supraoccipital shield reaching further anteriorly and the nasals being moved posteriorly relative to their position in stem mysticetes.

While the pattern of skull development in mysticetes is quite unique, they present a conserved ossification sequence relative to toothed whales and terrestrial artiodactyls. Almost no changes are quantitatively identifiable in the timing of ossification of facial bones that comprise the feeding apparatus among these groups. Instead, the timing of tooth mineralization appears connected with the absence of adult dentition, with taxa that partially or completely lack permanent dentition having an earlier onset of tooth development.

In sum, this study represents the first step towards a deeper understanding of the developmental patterns connected to tooth loss in baleen whales and evolution of bulk filter feeding. Complex pleiotropic effects at the genetic level are responsible for the retention of rudimentary tooth germs in the fetal stages of mysticetes development. Moreover, a connection between tooth formation and jaw ossification is possibly an additional cause, given the highly conserved ossification sequence of these bones among distantly related taxa. As tooth germs and baleen rudiments overlap for a part of prenatal development, it is also likely that tooth germs also play a role in baleen formation. This evidence reaffirms the idea that the transition from teeth to baleen in the evolution of Mysticeti was a step-wise process, with teeth first losing their function after the first appearance of proto-baleen and then becoming rudimentary as more mutations accumulated in the gene regions responsible for their development. Skull shape changes accompanied this process, first with an elongation of the rostrum, a key adaption for bulk filter feeding, and then with telescoping of the braincase bones in modern lineages.

Future work will need to test these hypotheses using a larger dataset of 3D skull morphology data to quantify the difference in shape rate development of the different parts of the skull that characterize odontocetes and mysticetes, as well as how they differ from their terrestrial

relatives. Data on the ontogenetic transformation of other families of modern baleen whales are also needed to highlight how development influences the present diversity of morphologies and feeding modes. Histological analyses can also help confirm the composition of the developing baleen tissue and clarify its relationship with the tooth germs. Sequencing of additional genes related to tooth formation will also help pinpoint when the complex transition started and what gene regions are primary responsible for it, allowing to apply this finding to other lineages of toothless mammals. With a wider availability of digitization techniques and of advanced computing methods, it will be increasingly easier to incorporate multiple lines of evidence in evolutionary studies, making it possible to formulate and test novel hypotheses on the developmental mechanisms at the base of macroevolutionary transition as those that occur in Cetacea.

## **APPENDICES**



## Appendix A: Supplementary Methods/Results for Chapter One

### Sources used to collect tooth counts data in Cetacea (Table S1.1)

- Archer FI, Perrin WF** (1999) *Stenella coeruleoalba*. *Mamm Species*, **603**, 1-9.
- Balcomb KCI** (1989) Baird's beaked whale - *Berardius bairdii* Stejneger, 1883: Arnoux's beaked whale - *Berardius arnouxii* Duvernoy, 1851. In *Handbook of Marine Mammals: River Dolphins and larger Toothed Whales* (eds Ridgway SH, Harrison R), pp. 261-288. London: Academic Press.
- Bannister JL** (2018) Baleen whales (Mysticetes). In *Encyclopedia of Marine Mammals* (eds Würsig B, Thewissen JGM, Kovacs KM), pp. 62-69. London: Academic Press.
- Bearzi G, Reeves RR, Remonato E, Pierantonio N, Airoidi S** (2011) Risso's dolphin *Grampus griseus* in the Mediterranean Sea. *Mamm Biol*, **76**, 385-400.
- Beasley I, Robertson KM, Arnold PW** (2005) Description of a new dolphin, the australian snubfin dolphin *Orcaella heinsohni* sp. n. (Cetacea, Delphinidae). *Mar Mamm Sci*, **21**, 365-400.
- Bernard HJ, Reilly SB** (1998) Pilot whales - *Globicephala* Lesson, 1828. In *Handbook of Marine Mammals: the Second Book of Dolphins and the Porpoises* (eds Ridgway SH, Harrison R), pp. 245-280. London: Elsevier Ltd.
- Berrow S, Cotton DCF** (1990) White-sided dolphin *Lagenorhynchus acutus* (Gray). *Ir Nat J*, **23**, 333-335.
- Best P** (1988) The external appearance of Heaviside's dolphin, *Cephalorhynchus heavisidii* (Gray, 1828). *Rep Int Whal Comm Spec Issue*, **9**, 279-299.
- Best PB, Shaughnessy PD** (1981) First record of the melon-headed whale *Peponocephala electra* from South Africa. *Annals of South African Museum*, **83**, 33-47.
- Best RC, Da Silva VMF** (1993) *Inia geoffrensis*. *Mamm Species*, **426**, 1-8.
- Bloodworth BE, Odell DK** (2008) *Kogia breviceps* (Cetacea: Kogiidae). *Mamm Species*, **819**, 1-12.
- Boschma H** (1951) Rows of small teeth in ziphioid whales. *Zool Meded*, **31**, 139-148.
- Brownell RL, Herald ES** (1972) *Lipotes vexillifer*. *Mamm Species*, **10**, 1-4.
- Brownell RLJ** (1983) *Phocoena sinus*. *Mamm Species*, 1-1.
- Brownell RLJ** (1989) Franciscana - *Pontoporia blainvillei* (Gervais and d'Orbigny, 1844). In *Handbook of Marine Mammals: River Dolphins and larger Toothed Whales* (eds Ridgway SH, Harrison R), pp. 45-68. London: Academic Press.

- Brownell RLJ, Walker WA, Forney KA** (1998) Pacific white-sided dolphin - *Lagenorhynchus obliquidens* Gill, 1865. In *Handbook of Marine Mammals: the Second Book of Dolphins and the Porpoises* (eds Ridgway SH, Harrison R), pp. 57-84. London: Elsevier Ltd.
- Charlton-Robb K, Gershwin L-A, Thompson R, Austin J, Owen K, McKechnie S** (2011) A new dolphin species, the Burrunan dolphin *Tursiops australis* sp. nov., endemic to southern Australian coastal waters. *PloS ONE*, **6**, e24047.
- Cipriano F** (2009) Atlantic white-sided dolphin *Lagenorhynchus acutus*. In *Encyclopedia of Marine Mammals* (eds Perrin WF, Wursig B, Thewissen JGM), pp. 56-58. London: Academic Press.
- Da Silva VMF, Best RC** (1994) Tucuxi - *Sotalia fluviatilis* (Gervais, 1853). In *Handbook of Marine Mammals: the First Book of Dolphins* (eds Ridgway SH, Harrison R), pp. 43-69. London: Academic Press.
- Da Silva VMF, Best RC** (1996) *Sotalia fluviatilis*. *Mamm Species*, **527**, 1-7.
- Dalebout M, Ross JB, Scott Baker C** (2003) Appearance, distribution, and genetic distinctiveness of Longman's beaked whale (*Indopacetus pacificus*). *Mar Mamm Sci*, **19**, 421-461.
- Dalebout ML, Scott Baker C, Steel D, et al.** (2014) Resurrection of *Mesoplodon hotaula* Deraniyagala 1963: a new species of beaked whale in the tropical Indo-Pacific. *Mar Mamm Sci*, **30**, 1081-1108.
- Dalebout ML, Steel D, Baker CS** (2008) Phylogeny of the beaked whale genus *Mesoplodon* (Ziphiidae: Cetacea) revealed by nuclear introns: implications for the evolution of male tusks. *Syst Biol*, **57**, 857-75.
- Fraser FC, Noble BA** (1968) Skull of *Lagenorhynchus cruciger* from Livingston Island, South Shetland Island. *Br Antarct Surv Bull*, **15**, 29-38.
- Goodall RNP** (1994) Commerson's dolphin - *Cephalorhynchus commersonii* (Lacepede, 1804). In *Handbook of Marine Mammals: the First Book of Dolphins* (eds Ridgway SH, Harrison R), pp. 241-268. London: Academic Press.
- Goodall RNP** (2009a) Hourglass dolphin *Lagenorhynchus cruciger*. In *Encyclopedia of Marine Mammals* (eds Perrin WF, Wursig B, Thewissen JGM), pp. 573-576. London: Academic Press.
- Goodall RNP** (2009b) Spectacled porpoise *Phocoena dioptrica*. In *Encyclopedia of Marine Mammals* (eds Perrin WF, Wursig B, Thewissen JGM), pp. 1087-1091. London: Academic Press.
- Goodall RNP, Galeazzi AR, Leatherwood S, et al.** (1988a) Studies of Commerson's dolphins, *Cephalorhynchus commersonii*, off Tierra del Fuego, 1976-1984, with a review of information on the species in the South Atlantic. *Rep Int Whal Comm Spec Issue*, **9**, 3-70.

- Goodall RNP, Norris KS, Galeazzi AR, Oporto JA, Cameron IS** (1988b) On the Chilean dolphin, *Cephalorhynchus eutropia* (Gray, 1846). *Rep Int Whal Comm Spec Issue*, **9**, 197-257.
- Goodall RNP, Norris KS, Schevill WE, et al.** (1997) Review and update of the biology of Peale's dolphins, *Lagenorhynchus australis*. International Whaling Commission, 777-796.
- Goodall RNP, Schiavini ACM** (1995) On the biology of the spectacled porpoise, *Australophocaena dioptrica*. *Rep Int Whal Comm Spec Issue*, **16**, 411-453.
- Heyning JE** (1989) Cuvier's beaked whale - *Ziphius cavirostris* Cuvier, 1823. In *Handbook of Marine Mammals: River Dolphins and larger Toothed Whales* (eds Ridgway SH, Harrison R), pp. 289-308. Academic Press.
- Heyning JE, Dahleim ME** (1988) *Orcinus orca*. *Mamm Species*, **304**, 1-9.
- Heyning JE, Perrin WF** (1994) Evidence for two species of common dolphins (genus *Delphinus*) from the eastern north pacific. *Contrib Sci (Los Angel)*, **442**, 1-35.
- Jefferson TA** (1988) *Phocoenoides dalli*. *Mamm Species*, **319**, 1-7.
- Jefferson TA, Barros NB** (1997) *Peponocephala electra*. *Mamm Species*, **553**, 1-6.
- Jefferson TA, Curry BE** (2003) *Stenella clymene*. *Mamm Species*, **726**, 1-5.
- Jefferson TA, King SK** (2004) *Neophocaena phocaenoides*. *Mamm Species*, **746**, 1-12.
- Jefferson TA, Leatherwood S** (1994) *Lagenodelphis hosei*. *Mamm Species*, **470**, 1-5.
- Jefferson TA, Newcomer MW** (1993) *Lissodelphis borealis*. *Mamm Species*, **425**, 1-6.
- Jefferson TA, van Waerebeek K** (2004) Geographic variation in skull morphology of humpback dolphins (*Sousa* spp.). *Aquat Mamm*, **30**, 3-17.
- Kinze CC** (2009) White-beaked dolphin *Lagenorhynchus albirostris*. In *Encyclopedia of Marine Mammals* (eds Perrin WF, Wursig B, Thewissen JGM), pp. 1255-1258. London: Academic Press.
- Mead JG** (1989a) Bottlenose whales - *Hyperoodon ampullatus* (Forster, 1770) and *Hyperoodon planifrons* Flower, 1882. In *Handbook of Marine Mammals: River Dolphins and larger Toothed Whales* (eds Ridgway SH, Harrison R), pp. 321-348. London: Academic Press.
- Mead JG** (1989b) Shepherd's beaked whale - *Tasmacetus shepherdi* Olivier, 1937. In *Handbook of Marine Mammals: River Dolphins and larger Toothed Whales* (eds Ridgway SH, Harrison R), pp. 309-320. London: Academic Press.
- Mead JG, Payne RS** (1975) A specimen of the Tasman beaked whale, *Tasmacetus shepherdi*, from Argentina. *American Society of Mammalogists*, **56**, 213-218.

- Newcomer MW, Jefferson TA, Brownell RL, Brownell Jr RL** (1996) *Lissodelphis peronii*. *Mamm Species*, **531**, 1-5.
- Nweeia MT, Eichmiller FC, Hauschka PV, et al.** (2012) Vestigial tooth anatomy and tusk nomenclature for *Monodon monoceros*. *Anat Rec*, **295**, 1006-1016.
- Odell DK, McClune K** (1998) False killer whale - *Pseudorca crassidens* (Owen, 1846). In *Handbook of Marine Mammals: the Second Book of Dolphins and the Porpoises* (eds Ridgway SH, Harrison R), pp. 213-244. London: Elsevier Ltd.
- Oliver WRB** (1937) *Tasmacetus shepherdi*: a new genus and species of beaked whale from New Zealand. *Proc of Zool Soc Lond*, **3**, 371-381.
- Olson PA** (2009) Pilot whales (*Globicephala melas* and *G. macrorhynchus*). In *Encyclopedia of Marine Mammals* (eds Perrin WF, Wursig B, Thewissen JGM), pp. 847-852. London: Academic Press.
- Peixun C** (1989) Baiji - *Lipotes vexillifer* Miller, 1918. In *Handbook of Marine Mammals: River Dolphins and larger Toothed Whales* (eds Ridgway SH, Harrison R), pp. 25-44. London: Academic Press.
- Perrin WF** (1998) *Stenella longirostris*. *Mamm Species*, **599**, 1-7.
- Perrin WF** (2001) *Stenella attenuata*. *Mamm Species*, **683**, 1-8.
- Perrin WF** (2002) *Stenella frontalis*. *Mamm Species*, **702**, 1-6.
- Perryman WL, Au DWK, Leatherwood S, Van Waerebeek K** (1994) Melon headed whale - *Peponocephala electra* Gray, 1846. In *Handbook of Marine Mammals: the First Book of Dolphins* (eds Ridgway SH, Harrison R), pp. 363-386. London: Academic Press.
- Read AJ** (1998) Harbour porpoise - *Phocoena phocoena* (Linnaeus, 1758). In *Handbook of Marine Mammals: the Second Book of Dolphins and the Porpoises* (eds Ridgway SH, Harrison R), pp. 323-356. London: Elsevier Ltd.
- Reeves RR, Brownell RLJ** (1989) Susu - *Platanista gangetica* (Roxburgh, 1801) and *Platanista minor* Owen, 1853. In *Handbook of Marine Mammals: River Dolphins and larger Toothed Whales* (eds Ridgway SH, Harrison R), pp. 69-100. London: Academic Press.
- Reeves RR, Smeenk C, Brownell Jr RL, Kinze CC** (1998a) Atlantic white-sided dolphin - *Lagenorhynchus acutus* (Gray, 1828). In *Handbook of Marine Mammals: the Second Book of Dolphins and the Porpoises* (eds Ridgway SH, Harrison R), pp. 31-56. London: Elsevier Ltd.
- Reeves RR, Smeenk C, Kinze CC, Brownell Jr RL, Lien J** (1998b) White-beaked dolphin - *Lagenorhynchus albirostris* Gray, 1846. In *Handbook of Marine Mammals: the Second Book of Dolphins and the Porpoises* (eds Ridgway SH, Harrison R), pp. 1-30. London: Elsevier Inc.
- Reeves RR, Tracey S** (1980) *Monodon monoceros*. *Mamm Species*, **127**, 1-7.

- Reyes JC, van Waerebeek K** (1995) Aspects of the biology of Burmeister's porpoise from Peru. *Rep Int Whal Comm Spec Issue*, **16**, 349-364.
- Rice DW** (1989) Sperm whale - *Physeter macrocephalus* Linnaeus, 1758. In *Handbook of Marine Mammals: River Dolphins and larger Toothed Whales* (eds Ridgway SH, Harrison R), pp. 177-234. London: Academic Press.
- Ross JB, Leatherwood S** (1994) Pigmy killer whale - *Feresa attenuata* Gray, 1874. In *Handbook of Marine Mammals: the First Book of Dolphins* (eds Ridgway SH, Harrison R), pp. 387-404. Academic Press.
- Slooten E, Dawson M** (1994) Hector's dolphin - *Cephalorhynchus hectori* (van Beneden, 1881). In *Handbook of Marine Mammals: the First Book of Dolphins* (eds Ridgway SH, Harrison R), pp. 311-334. London: Academic Press.
- Stacey PJ, Arnold PW** (1999) *Orcaella brevirostris*. *Mamm Species*, **616**, 1-8.
- Stacey PJ, Leatherwood S, Baird RW** (1994) *Pseudorca crassidens*. *Mamm Species*, **456**, 1-6.
- Stewart BE, Stewart REA** (1989) *Delphinapterus leucas*. *Mamm Species*, **336**, 1-8.
- van Bree PJH, Nijssen H** (1964) On three specimens of *Lagenorhynchus albirostris* Gray, 1846 (Mammalia, Cetacea). *Beaufortia*, **11**, 85-93.
- van Waerebeek K, van Breet PJH, Best PB** (1995) On the identity of *Prodelphinus petersii* Lutken, 1889 and records of dusky dolphin *Lagenorhynchus obscurus* (Gray, 1828) from the Southern Indian and Atlantic oceans. *S Afr J Mar Sci*, **16**, 25-35.
- Walker WA, Leatherwood S, Goodrich KR, Perrin WF, Stroud RK** (1986) Geographical variation and biology of the Pacific white-sided dolphin, *Lagenorhynchus obliquidens*, in the north-eastern Pacific. In *Research on dolphins* (eds Bryden MM, Harrison R), pp. 441-465. Oxford: Clarendon Press.
- West KL, Mead JG, White W** (2011) *Steno bredanensis* (Cetacea: Delphinidae). *Mamm Species*, **43**, 177-189.

### Matrix for ancestral state reconstruction of tooth counts in Cetacea

Character coding: 0 (absent), 1 (1-5), 2 (6-10), 3 (11-15), 4 (16-20), 5 (21-25), 6 (26-30), 7 (31-35), 8 (36-40), 9 (41-45), A (46-50), B (51-55)

Taxon	Upper Jaw	Lower Jaw
Mysticeti	0	0
<i>Berardius arnuxii</i>	0	1
<i>Berardius bairdii</i>	0	1
<i>Cephalorhynchus commersonii</i>	7	7
<i>Cephalorhynchus eutropia</i>	7	7
<i>Cephalorhynchus heavisidii</i>	5	5
<i>Cephalorhynchus hectori</i>	6	6
<i>Delphinapterus leucas</i>	2	2
<i>Delphinus capensis</i>	B	B
<i>Delphinus delphis</i>	A	A
<i>Feresa attenuata</i>	2	3
<i>Globicephala macrorhynchus</i>	2	2
<i>Globicephala melas</i>	3	3
<i>Grampus griseus</i>	0	1
<i>Hyperoodon ampullatus</i>	0	1
<i>Hyperoodon planifrons</i>	0	1
<i>Indopacetus pacificus</i>	0	1
<i>Inia geoffrensis</i>	6	6
<i>Kogia breviceps</i>	0	3
<i>Kogia sima</i>	0	2
<i>Lagenodelphis hosei</i>	8	8
<i>Lagenorhynchus acutus</i>	7	7
<i>Lagenorhynchus albirostris</i>	6	5
<i>Lagenorhynchus australis</i>	7	7
<i>Lagenorhynchus cruciger</i>	6	7
<i>Lagenorhynchus obliquidens</i>	6	6
<i>Lagenorhynchus obscurus</i>	6	6
<i>Lipotes vexillifer</i>	7	7
<i>Lissodelphis borealis</i>	9	A
<i>Lissodelphis peronii</i>	9	9
<i>Mesoplodon</i> sp.	0	1
<i>Monodon monoceros</i>	1	0
<i>Neophocaena phocaenoides</i>	4	4
<i>Orcaella brevirostris</i>	4	4
<i>Orcaella heinsohni</i>	4	4
<i>Orcinus orca</i>	3	3
<i>Peponocephala electra</i>	5	5
<i>Phocoena dioptrica</i>	4	4
<i>Phocoena phocoena</i>	5	5
<i>Phocoena sinus</i>	4	4
<i>Phocoena spinipinnis</i>	4	4
<i>Phocoenoides dalli</i>	6	6
<i>Physeter macrocephalus</i>	0	5
<i>Platanista gangetica</i>	7	7
<i>Pontoporia blainvillei</i>	B	B
<i>Pseudorca crassidens</i>	2	2
<i>Sotalia fluviatilis</i>	7	7

<i>Sotalia guianensis</i>	7	7
<i>Sousa chinensis</i>	7	7
<i>Stenella attenuata</i>	9	9
<i>Stenella clymene</i>	A	9
<i>Stenella coeruleoalba</i>	A	A
<i>Stenella frontalis</i>	8	7
<i>Stenella longirostris</i>	B	B
<i>Steno bredanensis</i>	5	5
<i>Tasmacetus shepherdi</i>	4	5
<i>Tursiops aduncus</i>	5	5
<i>Tursiops truncatus</i>	5	5
<i>Ziphius cavirostris</i>	0	1

### Matrix for ancestral state reconstruction of dentition state in Ziphiidae

Character coding: 0 (present), 1 (absent), 2 (tusks only), ? (unknown)

†: fossil taxa

Taxon	Upper jaw	Lower jaw
<i>Africanacetus</i> †	1	?
<i>Aporotusrec</i> †	1	?
<i>Archaeoziphius</i> †	?	2
<i>Berardius</i>	1	2
<i>Beneziphius</i> †	0/1	?
<i>Chavziphius</i> †	0	0
<i>Chimuziphius</i> †	?	?
<i>Choneziphius</i> †	1	?
<i>Eurhinodelphis</i> †	0	0
<i>Globicetus</i> †	1	?
<i>Hyperoodon</i>	1	2
<i>Ihlengesi</i> †	1	?
<i>Imocetus</i> †	1	?
<i>Indopacetus</i>	1	2
<i>Izikoziphius</i> †	1	?
<i>Mesoplodon</i>	1	2
<i>Messapicetus</i> †	0	0
<i>Microberardius</i> †	?	?
<i>Nazcacetus</i> †	1	?
<i>Nenga</i> †	1	?
<i>Ninoziphius</i> †	0	0
<i>Notoziphius</i> †	0	?
<i>Pterocetus</i> †	1	?
<i>Schizodelphis</i> †	0	0
<i>Squalodon</i> †	0	0
<i>Squaloziphius</i> †	?	?
<i>Tasmacetus</i>	0	0
<i>Tusciziphius</i> †	1	?
<i>Waipatia</i> †	0	0
<i>Xhosacetus</i> †	1	?
<i>Ziphius</i>	1	2
<i>Ziphiodelphis</i> †	0	0
<i>Ziphirostrum</i> †	0/1	?

## Appendix B: Supplementary Tables/Figures for Chapter One

Table S1.1 – Tooth counts for all modern species of Cetacea, listed by family. Species in gray are not included in the phylogeny. Published averages are in bold, other averages were calculated using published data. List of references in Appendix A.

Common name	Genus	species	Upper jaw			Lower jaw			References	Notes
			min	avg	max	min	avg	max		
Commerson's dolphin	<i>Cephalorhynchus</i>	<i>commersonii</i>	28	<b>31</b>	34	26	<b>31</b>	35	Goodal et al. (1988a), Goodal (1994)	
Chilean's dolphin	<i>Cephalorhynchus</i>	<i>eutropia</i>	28	<b>31</b>	34	29	<b>31</b>	33	Goodal et al. (1988b)	
Heaviside's dolphin	<i>Cephalorhynchus</i>	<i>heavisidii</i>	22	25	28	22	25	28	Best (1988)	
Hector's dolphin	<i>Cephalorhynchus</i>	<i>hectori</i>	24	<b>28</b>	32	24	<b>28</b>	32	Slooten and Dawson (1994)	
Long-beaked common dolphin	<i>Delphinus</i>	<i>capensis</i>	47	<b>53</b>	59	47	<b>51</b>	55	Heyning and Perrin (1994)	
Short-beaked common dolphin	<i>Delphinus</i>	<i>delphis</i>	42	<b>49</b>	54	41	<b>49</b>	53	Heyning and Perrin (1994)	
Pygmy killer whale	<i>Feresa</i>	<i>attenuata</i>	8	<b>10</b>	11	10	<b>12</b>	13	Ross and Leatherwood (1994)	
Short-finned pilot whale	<i>Globicephala</i>	<i>macrorhynchus</i>	7	8	9	7	8	9	Olson (2009), Bernard and Reilly (1998)	
Long-finned pilot whale	<i>Globicephala</i>	<i>melas</i>	9	11	12	9	11	12	Olson (2009), Bernard and Reilly (1998)	
Risso's dolphin	<i>Grampus</i>	<i>griseus</i>	0	0	0	2	5	7	Bearzi et al. (2011)	occasionally 2 vestigial teeth in upper jaw
Fraser's dolphin	<i>Lagenodelphis</i>	<i>hosei</i>	36	40	44	34	39	44	Jefferson and Leatherwood (1994)	
Atlantic white-sided dolphin	<i>Lagenorhynchus</i>	<i>acutus</i>	30	35	40	31	35	38	Cipriano (2009), Reeves et al. (1998a), Berrow and Cotton (1990)	
White-beaked dolphin	<i>Lagenorhynchus</i>	<i>albirostris</i>	23	26	28	22	25	28	Kinze (2009), Reeves et al. (1998b), van Bree and Nijssen (1964)	



Peale's dolphin	<i>Lagenorhynchus</i>	<i>australis</i>	28	32	36	27	32	36	Fraser and Noble (1968), Goodall et al. (1997)
Hourglass dolphin	<i>Lagenorhynchus</i>	<i>cruciger</i>	25	30	34	27	31	35	Goodall (2009a), Fraser and Noble (1968)
Pacific white-sided dolphin	<i>Lagenorhynchus</i>	<i>obliquidens</i>	24	<b>30</b>	36	23	<b>30</b>	35	Brownell et al. (1998), Walker et al. (1986)
Dusky dolphin	<i>Lagenorhynchus</i>	<i>obscurus</i>	27	<b>30</b>	34	26	<b>30</b>	34	van Waerebeek et al. (1995)
Northern right whale dolphin	<i>Lissodelphis</i>	<i>borealis</i>	37	45	52	42	48	54	Jefferson and Newcomer (1993)
Southern right whale dolphin	<i>Lissodelphis</i>	<i>peronii</i>	37	44	50	37	44	50	Newcomer et al. (1996)
Irrawaddy dolphin	<i>Orcaella</i>	<i>brevirostris</i>	13	17	20	12	16	19	Stacey and Arnold (1999)
Australian snubfin dolphin	<i>Orcaella</i>	<i>heinsohni</i>	11	18	22	14	17	19	Beasley et al. (2005)
Killer whale	<i>Orcinus</i>	<i>orca</i>	10	12	14	10	12	14	Heyning and Dahlheim (1988)
Melon-headed whale	<i>Peponocephala</i>	<i>electra</i>	20	23	26	22	24	25	Best and Shaughnessy (1981), Perryman et al. (1994), Jefferson and Barros (1997)
False killer whale	<i>Pseudorca</i>	<i>crassidens</i>	7	<b>8</b>	10	8	<b>9</b>	10	Odell & McClune (1996), Stacey et al. (1994)
Tucuxi	<i>Sotalia</i>	<i>fluviatilis</i>	28	32	35	26	31	35	Da Silva and Best (1994), Da Silva and Best (1996)
Guiana dolphin	<i>Sotalia</i>	<i>guanensis</i>	30	33	36	30	33	36	Da Silva and Best (1994)
Indo-Pacific humpback dolphin	<i>Sousa</i>	<i>chinensis</i>	31	<b>35</b>	38	29	<b>33</b>	38	Jefferson and van Waerebeek (2004)
Indian Ocean humpback dolphin	<i>Sousa</i>	<i>plumbea</i>	33	<b>37</b>	39	32	<b>35</b>	37	Jefferson and van Waerebeek (2004)
Atlantic humpback dolphin	<i>Sousa</i>	<i>teuszii</i>	27	<b>30</b>	32	28	<b>29</b>	31	Jefferson and van Waerebeek (2004)

Pantropical spotted dolphin	<i>Stenella</i>	<i>attenuata</i>	35	42	48	34	41	47	Perrin (2001)	
Clymene dolphin	<i>Stenella</i>	<i>clymene</i>	39	46	52	39	44	48	Jefferson and Curry (2003)	
Striped dolphin	<i>Stenella</i>	<i>coeruleoalba</i>	38	49	59	37	46	55	Archer and Perrin (1999)	
Atlantic spotted dolphin	<i>Stenella</i>	<i>frontalis</i>	32	37	42	30	35	40	Perrin (2002)	
Spinner dolphin	<i>Stenella</i>	<i>longirostris</i>	44	54	64	42	52	62	Perrin (1998)	
Rough-toothed dolphin	<i>Steno</i>	<i>bredanensis</i>	19	23	26	19	24	28	West et al. (2011)	
Indo-Pacific bottlenose dolphin	<i>Tursiops</i>	<i>aduncus</i>	21	<b>23</b>	25	22	<b>24</b>	27	Charlton-Robb et al. (2011)	
Burrunan dolphin	<i>Tursiops</i>	<i>australis</i>	22	<b>24</b>	28	21	<b>23</b>	26	Charlton-Robb et al. (2011)	
Common bottlenose dolphin	<i>Tursiops</i>	<i>truncatus</i>	20	<b>23</b>	26	20	<b>22</b>	25	Charlton-Robb et al. (2011)	
Amazon river dolphin	<i>Inia</i>	<i>geoffrensis</i>	22	29	35	22	29	35	Best and Da Silva (1993)	shape and size gradient, bigger teeth in posterior part of jaws
La Plata river dolphin	<i>Pontoporia</i>	<i>blainvillei</i>	53	56	58	51	54	56	Brownell (1989)	
Chinese river dolphin	<i>Lipotes</i>	<i>vexillifer</i>	30	32	34	32	34	36	Peixun (1989), Brownell and Herald (1972)	
South Asian river dolphin	<i>Platanista</i>	<i>gangetica</i>	26	33	39	26	31	35	Reeves and Brownell (1989)	
Indo-pacific finless porpoise	<i>Neophocaena</i>	<i>phocaenoides</i>	15	19	22	15	19	22	Jefferson and King (2004)	
Spectacled porpoise	<i>Phocoena</i>	<i>dioptrica</i>	16	<b>20</b>	26	17	<b>20</b>	23	Goodall and Schiavini (1995), Goodall (2009b)	
Harbour porpoise	<i>Phocoena</i>	<i>phocoena</i>	21	25	29	20	25	29	Read (1998), Jefferson and King (2004)	
Vaquita	<i>Phocoena</i>	<i>sinus</i>	18	20	22	17	19	20	Brownell (1983)	

Burmeister's porpoise	<i>Phocoena</i>	<i>spinipinnis</i>	10	17	23	14	19	23	Reyes and van Waerebeck (1995)	
Dall's porpoise	<i>Phocoenoides</i>	<i>dalli</i>	23	26	28	24	26	28	Jefferson (1988)	
Beluga	<i>Delphinapterus</i>	<i>leucas</i>	8	9	10	8	9	10	Reeves and Tracey (1980), Stewart and Stewart (1989)	teeth partially lost during life, very thin enamel, up to 40 vestigial teeth per row, less dentition in females 6 cheek teeth present in fetal stages in addition to 2 in the front in both jaws, only these 2 in the upper jaw (maxilla)
Narwhal	<i>Monodon</i>	<i>monoceros</i>	0	1	2	0	0	0	Reeves and Tracey (1980), Nweeia et al. (2011)	present in adult, the first one develops more, the other vestigial, in males usually the left one forms the tusk, in females remain unerupted but present in adult
Sperm whale	<i>Physeter</i>	<i>macrocephalus</i>	0	0	0	20	23	26	Rice (1989)	17/29 max, eruption at puberty (8 years), bigger in old males, maxillary teeth rarely erupt, at least 11 present in most specimens, more difficult to find in females

Pigmy sperm whale	<i>Kogia</i>	<i>breviceps</i>	0	0	0	12	14	16	Bloodworth and Odell (2008)	rare but sometimes vestigial teeth present in upper jaw
Dwarf sperm whale	<i>Kogia</i>	<i>sima</i>	0	0	0	7	10	12	Bloodworth and Odell (2008)	rare but sometimes vestigial teeth present in upper jaw
Arnoux's beaked whale	<i>Berardius</i>	<i>arnuxii</i>	0	0	0	2	2	2	Balcomb (1989)	both sexes erupt, first: tip of mandible, lateral, triangular, big, second: smaller and conical
Baird's beaked whale	<i>Berardius</i>	<i>baiardii</i>	0	0	0	2	2	2	Balcomb (1989)	both sexes erupt, first: tip of mandible, lateral, triangular, big, second: smaller and conical
Northern bottlenose whale	<i>Hyperoodon</i>	<i>ampullatus</i>	0	0	0	1	2	2	Mead (1989a), Boschma (1951)	males only, tip of mandible, conical, small, second pair smaller, 10-20 vestigial in both jaws found often
Southern bottlenose whale	<i>Hyperoodon</i>	<i>planifrons</i>	0	0	0	1	2	2	Mead (1989a), Boschma (1951)	males only, tip of mandible, conical, small, second pair smaller, 10-20 vestigial in both jaws found often
Longman's beaked whale	<i>Indopacetus</i>	<i>pacificus</i>	0	0	0	1	1	1	Dalebout et al. (2003)	males only, tip of mandible, small and conical

Sowerby's beaked whale	<i>Mesoplodon</i>	<i>bidens</i>	0	0	0	1	1	1	Dalebout et al. (2008)	males only, first third mandible, flat, small, pointed backwards
Andrews' beaked whale	<i>Mesoplodon</i>	<i>bowdoini</i>	0	0	0	1	1	1	Dalebout et al. (2008)	males only, almost middle mandible, big
Hubb's beaked whale	<i>Mesoplodon</i>	<i>carlhubbsi</i>	0	0	0	1	1	1	Dalebout et al. (2008)	males only, first third mandible, lateral, flat, big, pointed backwards
Blainville's beaked whale	<i>Mesoplodon</i>	<i>densirostris</i>	0	0	0	1	1	1	Dalebout et al. (2008)	males only, mandible has a 90° angle in the middle where teeth are, lateral, flat, big
Gervais' beaked whale	<i>Mesoplodon</i>	<i>europaeus</i>	0	0	0	1	1	1	Dalebout et al. (2008)	males only, first third of mandible, triangular, small
Ginkgo-toothed beaked whale	<i>Mesoplodon</i>	<i>ginkgodens</i>	0	0	0	1	1	1	Dalebout et al. (2008)	males only, almost middle mandible, lateral, flat, big
Gray's beaked whale	<i>Mesoplodon</i>	<i>grayi</i>	0	0	0	1	1	1	Dalebout et al. (2008)	males only, first third mandible, lateral, big
Hector's beaked whale	<i>Mesoplodon</i>	<i>hectori</i>	0	0	0	1	1	1	Dalebout et al. (2008)	males only, tip of mandible, small, triangular
Deraniyagala's beaked whale	<i>Mesoplodon</i>	<i>hotaula</i>	0	0	0	1	1	1	Dalebout et al. (2014)	males only, almost middle mandible, lateral, flat, tilted a little backwards
Strap-toothed whale	<i>Mesoplodon</i>	<i>layardii</i>	0	0	0	1	1	1	Dalebout et al. (2008)	males only, almost middle mandible, lateral, flat, very big, tilted backwards

True's beaked whale	<i>Mesoplodon</i>	<i>mirus</i>	0	0	0	1	1	1	Dalebout et al. (2008)	males only, tip of mandible, small, conical
Perrin's beaked whale	<i>Mesoplodon</i>	<i>perrini</i>	0	0	0	1	1	1	Dalebout et al. (2008)	males only, tip of mandible, big, triangular
Pigmy beaked whale	<i>Mesoplodon</i>	<i>peruvianus</i>	0	0	0	1	1	1	Dalebout et al. (2008)	males only, first third mandible, mandible has crest where teeth are, small, conical
Stejneger's beaked whale	<i>Mesoplodon</i>	<i>stejnegeri</i>	0	0	0	1	1	1	Dalebout et al. (2008)	males only, almost middle mandible, lateral, big, conical, straight
Spade-toothed whale	<i>Mesoplodon</i>	<i>traversii</i>	0	0	0	1	1	1	Dalebout et al. (2008)	males only, almost middle mandible, lateral, flat, big, tilted backwards
Shepherd's beaked whale	<i>Tasmacetus</i>	<i>shepherdi</i>	17	19	21	18	23	28	Mead (1989b), Oliver (1937), Mead and Payne (1975)	both sexes erupt, more developed in males, anterior pair of mandible only
Cuvier's beaked whale	<i>Ziphius</i>	<i>cavirostris</i>	0	0	0	1	1	1	Heyning (1989)	males erupted and bigger, conical, small
Bowhead whale	<i>Balaena</i>	<i>mysticetus</i>	0			0			Bannister (2018)	males only, tip of mandible, conical, small
Southern right whale	<i>Eubalaena</i>	<i>australis</i>	0			0			Bannister (2018)	possess baleen plates in upper jaw, all teeth resorb before birth
			0			0				possess baleen plates in upper jaw, all teeth resorb before birth

North Atlantic right whale	<i>Eubalaena</i>	<i>glacialis</i>	0	0	Bannister (2018)	possess baleen plates in upper jaw, all teeth resorb before birth
Pygmy right whale	<i>Caperea</i>	<i>marginata</i>	0	0	Bannister (2018)	possess baleen plates in upper jaw, all teeth resorb before birth
Grey whale	<i>Eschrichtius</i>	<i>robustus</i>	0	0	Bannister (2018)	possess baleen plates in upper jaw, all teeth resorb before birth
Common minke whale	<i>Balaenoptera</i>	<i>acutorostrata</i>	0	0	Bannister (2018)	possess baleen plates in upper jaw, all teeth resorb before birth
Antarctic minke whale	<i>Balaenoptera</i>	<i>bonaerensis</i>	0	0	Bannister (2018)	possess baleen plates in upper jaw, all teeth resorb before birth
Sei whale	<i>Balaenoptera</i>	<i>borealis</i>	0	0	Bannister (2018)	possess baleen plates in upper jaw, all teeth resorb before birth
Bryde's whale	<i>Balaenoptera</i>	<i>edeni</i>	0	0	Bannister (2018)	possess baleen plates in upper jaw, all teeth resorb before birth
Blue whale	<i>Balaenoptera</i>	<i>musculus</i>	0	0	Bannister (2018)	possess baleen plates in upper jaw, all teeth resorb before birth
Omura's whale	<i>Balaenoptera</i>	<i>omurai</i>	0	0	Bannister (2018)	possess baleen plates in upper jaw, all teeth resorb before birth

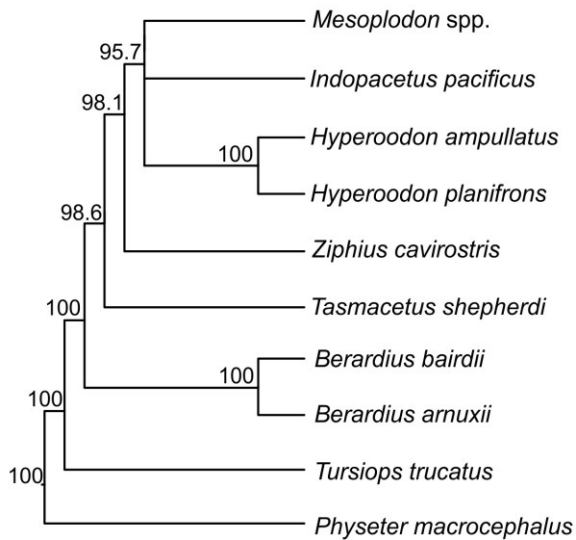
Fin whale	<i>Balaenoptera</i>	<i>physalus</i>	0	0	Bannister (2018)	possess baleen plates in upper jaw, all teeth resorb before birth
Humpback whale	<i>Megaptera</i>	<i>novaeangliae</i>	0	0	Bannister (2018)	possess baleen plates in upper jaw, all teeth resorb before birth



Table S1.2 – Sources and GenBank accession numbers for the three mtDNA genes included in the total evidence phylogenetic analysis. Sequences were extracted from the supermatrix stored on TreeBase: <http://purl.org/phylo/treebase/phylovs/study/TB2:S10190>, published in McGowen et al. (2009). These sequences were used as reference to align the ones obtained from GenBank.

<b>Genus</b>	<b>species</b>	<b>CYTB</b>	<b>12S</b>	<b>16S</b>
<i>Berardius</i>	<i>bairdii</i>	McGowen et al. 2009	McGowen et al. 2009	McGowen et al. 2009
<i>Hyperoodon</i>	<i>ampullatus</i>	McGowen et al. 2009	McGowen et al. 2009	McGowen et al. 2009
<i>Indopacetus</i>	<i>pacificus</i>	KY364702.1	KY364702.1	KY364702.1
<i>Mesoplodon</i>	<i>bidens</i>	McGowen et al. 2009	McGowen et al. 2009	McGowen et al. 2009
<i>Physeter</i>	<i>macrocephalus</i>	McGowen et al. 2009	McGowen et al. 2009	McGowen et al. 2009
<i>Tasmacetus</i>	<i>shepherdi</i>	McGowen et al. 2009	McGowen et al. 2009	McGowen et al. 2009
<i>Tursiops</i>	<i>truncatus</i>	McGowen et al. 2009	EU557093	EU557093
<i>Ziphius</i>	<i>cavirostris</i>	LN997430.1	LN997430.1	LN997430.1

**A: no partitions**



**B: partition nu-mt DNA**

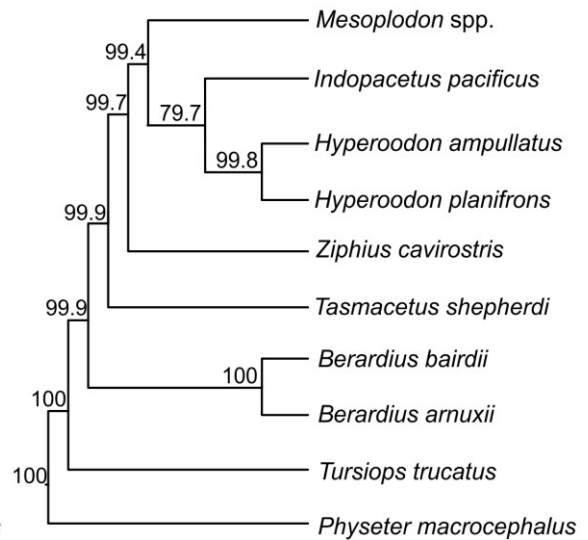


Fig. S1.1 – Molecular phylogenies of living species of Ziphiidae, obtained using maximum likelihood (RAxML). 14 of the 15 species of genus *Mesoplodon* were included in the analysis, but the genus is collapsed in one branch as their relationships are not the focus of the study. The only difference between when no partitions are considered (A) and considering nuDNA and mtDNA as separate partitions (B) is the position of *Indopacetus*. Bootstrap support values are indicated on nodes.

## Equal weighting

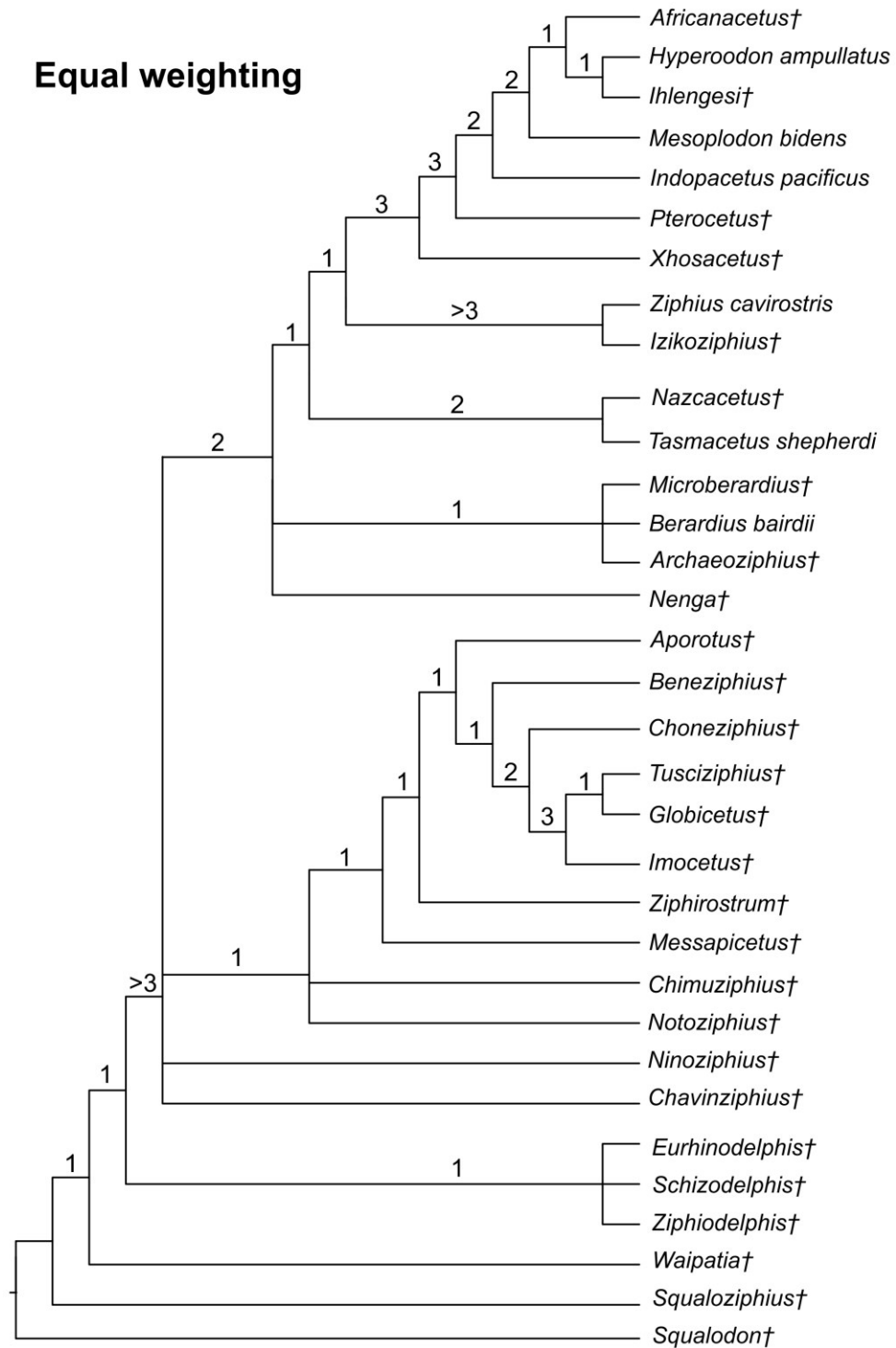


Fig. S1.2 – Total evidence phylogeny of living and fossil Ziphiidae, obtained using maximum parsimony (PAUP\*) with equal weighting of characters. Strict consensus of 55 equally parsimonious trees (tree length: 54664, CI: 0.722, RI: 0.671). *Squalodont†* was constrained as outgroup, *Tursiops* and *Physeter* were pruned from the tree after analysis. Decay index support values are indicated on branches.



## Appendix C: Supplementary Methods/Results for Chapter Two

### Sources used to compile growth curves and derived growth rates (Figs. 2.3-2.4-2.14 – Figs. S2.2-S2.3)

#### *Humpback whale*

**Hampe O, Franke H, Hipsley CA, Kardjilov N, Muller J** (2015) Prenatal cranial ossification of the humpback whale (*Megaptera novaeangliae*). *J Morphol*, **276**, 564-582.

**Ridewood WG** (1923) Observations on the skull in foetal specimens of whales of the genera *Megaptera* and *Balaenoptera*. *Philos Trans R Soc Lond B Biol Sci*, **211**, 209-272. (teeth development)

**Tomilin AG** (1967) *Mammals of the USSR and adjacent countries, Volume IX, Cetacea*, Israel Program for Scientific Translations, Jerusalem.

#### *Antarctic minke whale*

**Ishikawa H, Amasaki H** (1995) Development and physiological degradation of tooth buds and development of rudimental baleen plate in southern minke whale, *Balaenoptera acutorostrata*. *J Vet Med Sci*, **57**, 665-670. (teeth development, resorption, baleen development)

**Masaki Y** (1979) Yearly change of biological parameters for the Antarctic minke whale. International Whaling Commission, 375-395.

#### *Common minke whale*

**Ivashin MV, Mikhalev YA** (1978) To the problem of the prenatal growth of minke whales *Balaenoptera acutorostrata* of the Southern Hemisphere and of the biology of their reproduction. International Whaling Commission, 201-205.

**Tomilin AG** (1967) *Mammals of the USSR and adjacent countries, Volume IX, Cetacea*, Israel Program for Scientific Translations, Jerusalem.

#### *Sei whale*

**Tomilin AG** (1967) *Mammals of the USSR and adjacent countries, Volume IX, Cetacea*, Israel Program for Scientific Translations, Jerusalem.

#### *Fin whale*

**Karlsen K** (1962) Development of tooth germs and adjacent structures in the whalebone whale (*Balaenoptera physalus*). *Hval skrif*, **45**, 5-56. (teeth development and resorption)

**Ohsumi S, Nishiwaki M, Hibiya T** (1958) Growth of fin whale in the Northern Pacific. Whales Research Institute of Tokyo, 97-133.

**Van Dissel-Scherft MC, Vervoort W** (1954) Development of teeth in fetal *Balaenoptera physalus*. *Proc K Ned Akad Wet Ser C Biol Med Sci*, **57**, 196-210. (teeth development and resorption)

*Blue whale*

**Fudge DS, Szewciw LJ, Schwalb AN** (2009) Morphology and development of blue whale baleen: an annotated translation of Tycho Tullberg's classic 1883 paper. *Aquat Mamm*, **35**, 226-252. (baleen development)

**Tomilin AG** (1967) *Mammals of the USSR and adjacent countries, Volume IX, Cetacea*, Israel Program for Scientific Translations, Jerusalem.

*Gray whale*

**Rice DW** (1983) Gestation period and fetal growth of the gray whale. International Whaling Commission, 539-544.

*Spinner dolphin*

**Sterba O, Klima M, Schildger B** (2000) Embryology of dolphins: staging and ageing of embryos and fetuses of some Cetaceans. *Adv Anat Embryol Cell Biol*, **157**, 1-133.

*Short-beaked common dolphin*

**Sterba O, Klima M, Schildger B** (2000) Embryology of dolphins: staging and ageing of embryos and fetuses of some Cetaceans. *Adv Anat Embryol Cell Biol*, **157**, 1-133.

*Pantropical spotted dolphin*

**Perrin WF, Coe JM, Zweifel JR** (1976) Growth and reproduction of the spotted porpoise, *Stenella attenuata*, in the offshore eastern tropical pacific. *Fish Bull*, **74**, 229-269.

**Sterba O, Klima M, Schildger B** (2000) Embryology of dolphins: staging and ageing of embryos and fetuses of some Cetaceans. *Adv Anat Embryol Cell Biol*, **157**, 1-133.

*Sperm whale*

**Laws RM** (1959) The foetal growth rates of whales with special reference to the fin whale, *Balaenoptera physalus* Linn. *Disc Rep*, **29**, 281-308. (Northern Hemisphere data only)

*Cattle*

**Evans HE, Sack WO** (1973) Prenatal development of domestic and laboratory mammals: growth curves, external features and selected references. *Anat Histol Embryol*, **2**, 11-45.

**Lyne AG** (1960) Pre-natal growth of cattle. *Proc Aust Soc Anim Prod*, **3**, 153-161.

*Sheep*

**Evans HE, Sack WO** (1973) Prenatal development of domestic and laboratory mammals: growth curves, external features and selected references. *Anat Histol Embryol*, **2**, 11-45.

**Harris HA** (1937) The foetal growth of the sheep. *J Anat*, **71**, 516-527.

*Pig*

**Evans HE, Sack WO** (1973) Prenatal development of domestic and laboratory mammals: growth curves, external features and selected references. *Anat Histol Embryol*, **2**, 11-45.

**Marrable AW** (1971) *The embryonic pig: a chronological account*, Pitman Medical, London.

**Procrustes ANOVA between landmarks takes – humpback whale whole skull configuration**

This analysis takes into account the object symmetry in the data.

Classifiers used for the Procrustes ANOVA:

Individuals: From dataset

Centroid size:

Effect	SS	MS	df	F	P (param.)
Individual	164.584313	164.584313	1	0.00	0.9929
Residual	15698124.250842	1962265.531355	8		

Shape, Procrustes ANOVA:

Effect	SS	MS	df	F	P (param.)
Individual	0.00222569	0.0001059850	21	1.22	0.3323
Side	0.00636329	0.0003181643	20	3.65	0.0028
Ind * Side	0.00174266	0.0000871328	20	0.09	1.0000
Residual	0.30294348	0.0009236082	328		

Shape, MANOVA tests of effects:

*Not available due to low sample size*

**Procrustes ANOVA between landmarks takes – humpback whale rostrum-only configuration**

This analysis takes into account the object symmetry in the data.

Classifiers used for the Procrustes ANOVA:

Individuals: From dataset

Centroid size:

Effect	SS	MS	df	F	P (param.)
Individual	87.331237	87.331237	1	0.00	0.9915
Residual	7324507.102582	732450.710258	10		

Shape, Procrustes ANOVA:

Effect	SS	MS	df	F	P (param.)
Individual	0.00219475	0.0001463164	15	1.73	0.1552
Side	0.01847861	0.0013199004	14	15.65	<.0001
Ind * Side	0.00118099	0.0000843567	14	0.08	1.0000
Residual	0.28907731	0.0009968183	290		

Shape, MANOVA tests of effects:

*Not available due to low sample size*

**Procrustes ANOVA between landmarks takes – minke whales whole skull configuration**

This analysis takes into account the object symmetry in the data.

Classifiers used for the Procrustes ANOVA:  
Individuals: From dataset

Centroid size:

Effect	SS	MS	df	F	P (param.)
Individual	1.469389	1.469389	1	0.00	<b>0.9981</b>
Residual	5698502.087291	259022.822150	22		

Shape, Procrustes ANOVA:

Effect	SS	MS	df	F	P (param.)
Individual	0.00071703	0.0000341441	21	1.24	0.3188
Side	0.00161807	0.0000809033	20	2.93	0.0101
Ind * Side	0.00055201	0.0000276006	20	0.10	<b>1.0000</b>
Residual	0.25978814	0.0002880135	902		

Shape, MANOVA tests of effects:

Symmetric component of shape variation:

Effect	Pillai tr.	P (param.)
Individual	0.99	<b>0.1272</b>

Note: the test for 'Individual' used the symmetric component of the residual as the 'error' effect.

Asymmetry component of shape variation:

Effect	Pillai tr.	P (param.)
Ind * Side	0.90	<b>0.4375</b>



### Procrustes ANOVA between landmarks takes – rostrum-only configuration

This analysis takes into account the object symmetry in the data.

Classifiers used for the Procrustes ANOVA:

Individuals: From dataset

Centroid size:

Effect	SS	MS	df	F	P (param.)
Individual	32.443373	32.443373	1	0.00	<b>0.9867</b>
Residual	2508342.029782	114015.546808	22		

Shape, Procrustes ANOVA:

Effect	SS	MS	df	F	P (param.)
Individual	0.00401413	0.0002676085	15	4.26	0.0049
Side	0.00082114	0.0000586528	14	0.93	0.5494
Ind * Side	0.00087859	0.0000627564	14	0.12	<b>1.0000</b>
Residual	0.33827327	0.0005302089	638		

Shape, MANOVA tests of effects:

Symmetric component of shape variation:

Effect	Pillai tr.	P (param.)
Individual	0.61	<b>0.6284</b>

Note: the test for 'Individual' used the symmetric component of the residual as the 'error' effect.

Asymmetry component of shape variation:

Effect	Pillai tr.	P (param.)
Ind * Side	0.52	<b>0.7331</b>

## **Descriptions of fetal humpback and minke whale specimens**

The qualitative descriptions of the specimens are reported from Lanzetti et al. (2018) and Lanzetti (in press). They are arranged in ontogenetic order, from the youngest to the oldest specimen, Grouped by taxon, with the minke whale species labeled (Table 2.1). I first assess the stage of the specimen and identify its main characteristics, then provide a description of the external and internal anatomy, focusing on the ossifications and suture closure of skull bones. All major bone elements are visible in each specimen, despite limited image quality and preservation issues, which are also specified. The precise extent of the suture closure is sometimes hard to determine for the same reasons. A postnatal specimen of common minke whale also employed in GM analyses (Ma2) was used as comparison to establish the status of suture closure in the skull in mature individuals, along with evidence from the literature. When possible, also the postcranial ossification is described. The tooth germs and baleen tissues are described in a separate section. The Fetal Stages are determined based on previous work (Sterba et al., 2000, Thewissen and Heyning, 2007) or described in detail if new to this work. The specimens are compared to similar fetuses described in previous work (Table 2.5-2.6; Julin, 1880, Eschricht, 1849, Ridewood, 1923, Ishikawa and Amasaki, 1995, Sawamura, 2008, Hampe et al., 2015). Anatomical terminology for the skull bones follows Mead and Fordyce (2009). All the available measurements for each specimen are provided in Table S2.1 and in Table 2.7 for the tooth germs. For diceCT and CT methods, and other information on the specimens, refer to the Materials and Methods section. Specimens descriptions are accompanied by figures of the 3D internal skull structure except for Mf1.

## **Humpback whale specimens (from Lanzetti et al., 2018)**

### **He1 – AMNH232597 – TL 17 cm (Fig. 2.6)**

*Staging:* Carnegie stage 18/19

Digital ray 3<sup>rd</sup> longer than 2<sup>nd</sup>, globular fluke, distinct beak (Sterba et al. 2000, stage 6)

*External characteristics.* Tubercles are present on the tip of mandible and on the rostrum. A few tubercles are also present on the flippers. The phalanges are visible through the skin of the flippers. The fluke is paddle-like with an overall round shape. No hind limbs are visible externally, but an incision due to a previous dissection or damage near the reproductive slit could have obliterated them. The blowhole is located at approximately one-half the distance between the tip of the rostrum and the eye. The eyelids are present but not fused. No tactile hairs are visible macroscopically; the skin coloration with brown patches is probably due to preservation. The gingivae on the upper palate are mostly flat and no ridge is visible at this stage.

*Internal characteristics.*

*Intramembranous ossification of the skull.* Premaxillae have started ossifying in the central and posterior part of the rostrum and are hard to distinguish from the maxilla. The maxillae contribute most of the rostrum. The bones appear porous and rough overall. On the ventral side, part of the vomer and palatine are also ossified. The supraorbital process of the frontal is ossified.

Ossification has begun in the ectotympanic area where it is possible to distinguish two small laminae. Most of the posterior part of the dentaries is ossified, with the coronoid process clearly visible. The rami bend slightly medially and are well separated anteriorly.

*Endochondral ossification of the skull.* There is no clear indication of ossification in the neurocranium. Only the area of the supraoccipital appears denser than the surrounding areas.

*Tooth germs.* Tooth germs are present in both jaws. Each maxilla has a complete row with over 20 tooth germs. No tooth germs are present on the premaxilla. The maxillary germs are evenly

spaced overall across the entire length of the maxilla. Some of the maxillary tooth germs appear to be very close to each other, forming what in the literature is referred to as “double teeth” (Peredo et al. 2017). This morphology was first noticed by early authors and there was debate on how they originated (e.g. Owen 1845; Kukenthal 1893). It has been concluded that they form as a result of fusion between two germs that, as they grow, get closer and eventually partially fuse together (Van Dissel-Scherft and Vervoort 1954; Karlsen 1962; Peredo et al. 2017). If there was no visible gap between the two cusps, they were counted as one unit. In the lower jaw, there are fewer tooth germs with fewer than 10 per side. Tooth germs are mostly concentrated in the mid portion of the jaw, with a large gap between the mainGroup at the middle of the jaw and those few positioned closer to the tip.

*Postcranial skeleton.* Vertebral centra appear denser but not ossified, and a similar condition is seen in the ribs. Rudimentary limb bones are recognizable and mostly ossified, while the forelimbs are only cartilaginous at this stage.

*Comparisons.* The total length of He1 is between specimens IV and V of Hampe et al. (2015), and the degree of ossification is consistent with that described by those authors. Hampe et al. also found no ossification of the squamosal or endochondral bones. They did not observe tooth germs, However this might be due to either the preservation of their specimens or resolution of their CT images. Hampe et al. did not employ diceCT in contrast to our study. Specimen X of Ridewood (1923) is slightly smaller than He1 in total length. Which skull elements were ossified in Ridewoods’ specimens is unclear, but overall the rostrum seems to be in a more advanced ossification stage than the neurocranium, as we observe in He1. Ridewood (1923) observed complete tooth rows in both upper and lower jaws with more than 30 tooth germs per maxilla, and a similar number can be found in the mandibular rami. Ridewood also noticed that some tooth germs in the upper jaw appear as “double teeth” and the lower teeth are more widely

spaced. The higher number of tooth germs found by Ridewood is probably due to the fact that he dissected a fresh specimen and therefore was able to recover the smallest tooth germs that may not be resolved in the CT data.

**Hf1 – AMNH99602 – TL 31cm (Fig. 2.7)**

*Staging:* Carnegie stage 19/Fetal stage 20 – last embryonic stage, start of the fetal period

Digital ray 2<sup>nd</sup> longer than 3<sup>rd</sup>, rostrum with typical cetacean shape (Sterba et al. 2000, stages 7 and 8)

Revision to Thewissen and Heyning (2007): identification of this stage in the humpback is better characterized by posterior movement of the external nasal aperture that extends to its approximate adult position in the last one-third of the head. Hyperphalangy noted by Thewissen and Heyning was already clearly visible in the younger specimen He1, and therefore is not indicative of this stage.

*External characteristics.* Tubercles are present at the tips of both lower and upper jaws. Tubercles are more numerous and distinguishable on the flippers than they were in He1. The fluke has assumed a cetacean-like shape, with two wide triangular lobes on each side separated by a median notch, but it still does not present the typical morphology of this species. The blowhole is positioned posteriorly, and it is now approximately at two-thirds of the distance between the tip of the rostrum and the eye. The eyelids are not fused. No tactile hairs are visible macroscopically. The gingival ridge is a recognizable elevation on the lateral borders of the upper palate, between the internal palate surface and the lip.

*Internal characteristics.*

*Intramembranous ossification of the skull.* The premaxilla and maxilla are the same length, and the bones are porous obscuring the identity of foramina. Ossification of the frontal bone is more

expansive than in He1, with this bone extending both dorsally and posteriorly. There is a possible initial ossification of the parietal bone on the posterior edge of the frontal on the right side of the skull. The diagnostic mysticete trait, large infraorbital process of the maxilla (Deméré et al. 2005; Hampe et al. 2015), along with the nasal bones also are recognizable in Hf1. The nasals have a rhomboidal shape and are quite small compared to the skull size. The squamosal is also present with both zygomatic and postglenoid processes ossified. On the ventral surface, the palatine ossification has expanded, and the vomer is elongated anteriorly. The pterygoids have begun ossification. The ectotympanic remains a thin horseshoe-shaped lamina. The mandibular rami are more ossified anteriorly than in He1, and they still retain a similar straight orientation as in the previous stage. The left ramus appears shorter due to breakage.

*Endochondral ossification of the skull.* Most endochondral elements have begun to ossify. The supraoccipital is present at the posterior end of the skull as a rectangular plate, apparently not articulated with other bones. Initial ossification of the basisphenoid and basioccipital.

*Tooth germs.* In the maxilla, 24 tooth germs are observed on the left side but only 22 on the right side. Some are “double teeth”, but overall they are evenly spaced. On the lower jaw, 11 tooth germs are on the left side, while on right side none are recognizable. This might be an artifact of preservation or in CT scanning. The tooth germs appear more evenly spaced than in He1, and they are only present in the anterior 2/3 of the mandible.

*Postcranial bones.* The ribs are not ossified, and they appear as dense cartilage. Ossification has begun near the center of vertebrae and the atlas. The forelimb bones are also still cartilaginous, while the pelvic bones and hind limb remnants are still clearly recognizable.

*Comparisons.* Hf1 is slightly larger in total length than specimen VI of Hampe et al. (2015). The extent of ossification is mostly similar, except that the parietal is not clearly recognizable in Hf1, which might be due to either preservation or intraspecific variation. Also, postcranial ossification

in specimen VI of Hampe et al. (2015) is more advanced. Those authors did not recognize tooth germs but rather a row of possible alveoli in the dentaries. They hypothesized that the tooth germs had already been resorbed, given that they only found alveoli a smaller specimen, which is in an early embryonic stage, but this would contradict evidence from previous authors (Eschricht 1849; Ridewood 1923). Hampe et al. (2015) concluded that the dentin layers might not be dense enough to be shown in the CT scan. This might be the case especially after preservation in formalin and ethanol, which is known to deteriorate tissues (Simmons 1995). The use of the iodine stain clearly helps visualizing the dentin layer even when degraded. Ridewood (1923) does not describe a specimen of comparable size.

#### **Hf2 – UCB123560 – TL ?39 cm (Fig. 2.8)**

*Note:* the present length of the specimen might be an underestimate – antero-posterior compression of body due to improper storage.

*Staging:* Fetal stage 20

Eyelids completely fused, fluke shape more developed both in width and length (Sterba et al. 2000, stages 7 and 8)

*External characteristics.* Tubercles on the rostrum, mandible, and flippers are more prominent than in younger specimens. The flippers are also more elongated and start assuming the proportions characteristic of this species. The fluke has a triangular shape. The blowhole is in a similar position as the previous stage. The gingival ridge is prominent and well visible especially around the mid-length of the upper palate.

*Internal characteristics.*

*Intramembranous ossification of the skull.* The bones are smoother than in earlier stages, and the sutures are more easily identifiable. The premaxilla and maxilla are the same length. On the

maxilla, three infraorbital foramina are present on each side. The palatine is completely ossified, as well as the vomer and the pterygoids. The ventral side of the rostrum is therefore mostly complete. The frontal is expanded dorsally. Posterior to the frontal, an ossification center is observed in a homologous position to the interparietal in odontocetes (Mead and Fordyce 2009; Moran et al. 2011). We therefore identify this ossifying element as the interparietal. Small portions of the parietal bone are recognizable laterally on the right side of the skull. The frontal fontanelle at the center of the neurocranium is smaller as a result of the increased ossification of these elements. The dorsal portion of the squamosal is also ossified. The nasal bones are larger than in the previous stage and are elongated antero-dorsally. The ectotympanic now has assumed a sigmoid shape, and it is thicker and wider overall. The mandibular rami are completely ossified except at the anteriormost point. They also start to curve laterally as is characteristic in mysticetes.

*Endochondral ossification of the skull.* The supraoccipital is extended dorsally and laterally. The first ossification of the exoccipital is recognizable on the ventral side in the area of the paraoccipital process. The basioccipital is visible posterior to the basisphenoid. Small hyoid elements can also be identified at the posterior end of the skull.

*Tooth germs.* In the maxilla, 28 tooth germs are visible on the right side and 26 on the left. A few “double teeth” are also present in this specimen. They occupy the entire length of the bone and are homogeneous in size. As indicated in the earlier specimens, no tooth germs are present on the premaxilla. The alveolar groove is more easily identifiable as a result of its degree of ossification, but it still does not cover the tooth germs laterally and it is wide and deep. In the lower jaw, 11 tooth germs are present on the right side and 16 on the left. On the left side they occupy the entire length of the mandibular ramus, while on the right side only the anterior and middle part of the ramus have tooth germs. Again, this may be due to either an artifact of preservation or CT



scanning. The lower tooth germs are smaller than the corresponding tooth germs in the upper jaw, and all of the tooth germs show a size gradient in being smaller rostrally and becoming progressively larger moving caudally. No “double teeth” are recognizable in the lower jaw of Hf2.

*Postcranial bones.* The vertebral centra are ossified, and the dorsal processes of the vertebrae have started to ossify. The atlas and the other cervical vertebrae appear to be less ossified than the rest of the column. The ribs appear to be ossified. Ossification has begun in the centers of the scapula, radius and ulna on both sides of the body. The hind limb remnants are not recognizable in this specimen possibly due to the effect compression during preservation.

*Comparisons.* This specimen stage of development is more advanced than all the specimens described by Hampe et al. (2015). Specimen Y of Ridewood (1923) is about 40 cm in length and has similar ossification levels as Hf2. That skull is not figured by Ridewood and only few details on the individual bones are provided. More information can be found on the tooth germs of this specimen. Ridewood reported a higher number of tooth germs in the lower jaw, as well as in the upper jaw, compared to our observations. This might be due to preservation or intraspecific variation, as Ridewood commented that Eschricht (1849) found an even larger number of tooth germs in his partial description of humpback whale fetuses. Ridewood also observed the tooth germs in the lower jaw to be smaller than in the upper jaw, as well as being smaller at the rostral tip of the dentaries and larger at the posterior end. Ridewood only found “double teeth” in the maxilla as we also observed.

### **Hf3 – SDNHM25552 – TL 70 cm (Fig. S2.5)**

*Staging:* Fetal stage 22

Separated eyelids (Sterba et al. 2000, stage 12)

Revision to Thewissen and Heyning (2007): we propose that this stage also is further characterized in Balaenopteridae by the beginning of development of throat grooves. This is also the first stage where tactile hairs are clearly visible macroscopically.

*External characteristics.* The tubercles are more prominent on lower and upper jaws especially at the tip and small tactile hairs are recognizable in this area as well. The throat grooves first appear as they start developing from the tip of lower jaw. The flippers are even more elongated than in earlier stages. The fluke has a triangular shape, but the posterior border is curved. The gingival ridge is wider than in previous specimens, but it exhibits shallow grooves on the surface especially at the anterior part of the palate.

*Internal characteristics.*

*Intramembranous ossification of the skull.* The surfaces of the bones are smooth, the fontanelle is smaller than in previous stages, and the sutures between bones in the neurocranium are starting to close significantly. The premaxilla is distinguishable and completely ossified. The maxilla seems to have suffered from preservation issues given that it appears to be ossified only on the lateral edges and minimally in the center. This might be a result of decalcification due to long term storage in formalin (Simmons 1995). The observed ossification likely is not an artifact of incomplete iodine staining because this specimen was also scanned before the staining with similar lack of resolution of the rostrum. No foramina are recognizable on the maxilla for this reason. The vomer and palatine are also not recognizable. The nasal bones are in contact with the frontal laterally and dorsally. The parietal is almost in contact with the interparietal laterally. The squamosal is articulated with the rest of the skull by contact with the parietal. The shape of the ectotympanic is more defined but only the ventral side is ossified. The mandibular rami have the same length as maxilla and premaxilla, but the anterior one-third is not well preserved and

broken. The typical curvature is even more marked at this stage, and the posterior end has reached its complete shape.

*Endochondral ossification of the skull.* The supraoccipital is mostly complete and even more expanded dorsally and anteriorly than in earlier stages. The exoccipital has reached the ventral side of the supraoccipital. The basisphenoid is recognizable, but it is in close proximity with the anterior end of the basioccipital. The basioccipital is extended posteriorly and nearly contacting the exoccipital. The hyoid elements appear larger than they did in earlier stages.

*Tooth germs.* On the upper jaw, 29 tooth germs are present on the left side and 26 on the right, all on the maxilla. They are the same size along the row, with again some “double teeth”. They also occupy the entire length of the bone as seen in previous stages. On the lower jaw, there are 15 and 13 tooth germs on the left and right side, respectively. They are only recognizable in the anterior and median portion. They are again smaller than in the upper jaw, and also smaller at tips.

*Postcranial bones.* The ribs, scapula, humerus, radius and ulna are completely ossified, as are most phalanges and carpals. The vertebral centra are large and assume the antero-posterior compressed shape that characterizes Cetacea. The dorsal processes of the vertebrae continue to ossify on both sides of the bones, and the cervical vertebrae are still less defined and without their centra. The hind limb remnants not clearly identifiable in this specimen.

*Comparisons.* Hf3 is of comparable length to specimen Z described by Ridewood (1923). The stage of ossification is similar overall. Ridewood described a pronounced antero-dorsal position of the supraoccipital, which in his specimen hides the parietal in posterior view. The parietal is still visible from that angle in Hf3. With regard to tooth germs, Ridewood counted a higher number on each row, but the germs are still only present in the maxilla. He also confirmed the presence of “double teeth” at this stage. The tooth germs appear to be developing at this stage in Ridewood’s specimen, and some of them show very small cusps, but they are too small to be

identified with certainty. In the lower jaw, Ridewood observed a similar number of tooth germs as in the upper jaw. The tooth germs in the lower jaw appear to be larger than those in the upper jaw in his specimen.

#### **Hf4 – ZMCU-CN15 – TL 103cm (Fig. 2.10)**

*Note:* only the skull was CT scanned. The posterior part of the neurocranium, and the posterior end of the left mandibular ramus were not recovered in the scan due to the inclination of the head during its storage.

*Staging:* Fetal stage 24

This new stage is defined by the full development of the throat grooves, extending to at least the insertion of forelimb. This trait can be used to stage balaenopterid specimens only as extensive throat grooves are absent in other extant mysticetes.

*External characteristics.* The tubercles are clearly distinguishable on both the rostrum and dentary. Tactile hairs are also in higher number than in previous stages. The eyes are completely open. The flippers are more elongated, but they still retain similar proportions to total body length as previous stages (around 20%, while in the adult they range between 28% and 34% (Clapham and Mead 1999). The posterior end of the fluke starts showing the characteristic irregular tubercles of this species. The characteristic hump can also be seen at two-thirds of the total length of the specimen on the dorsal side. The gingival ridge is now mostly absent, and a groove has formed along the posterior portion of the palate, while the anterior part is mostly flat.

*Internal characteristics.*

*Intramembranous ossification of the skull.* The bones at this stage have reached the expected smooth surface. The maxilla and premaxilla are completely ossified and with a clearly distinguishable suture. The premaxilla is longer than the maxilla. More foramina (6-8) are

recognizable on the dorsal side of maxilla, and they are possibly connected with the foramina visible on the posterior portion of the palatine. The ventral side of the skull is mostly ossified with only the vomer still having cartilaginous portions. The nasal bones are elongated antero-posteriorly and slightly more posteriorly positioned, however they still do not contact the frontal dorsally. The frontal is mostly ossified and is sutured with the parietal. It is still possible to recognize a small suture on the dorsal end of the right parietal that could be the remaining visible portion of the interparietal. The dorsal fontanelle is still open at the contact between the parietal, frontal and supraoccipital. The jugal is distinguishable for the first time. On the right lateral side of the skull it a small bone at the anterior contact between the jugal, the frontal and the infraorbital process of the maxilla that we interpret as the lacrimal is observed. The curvature of the dentary is more prominent, and the rami are fully ossified. The anterior tips of the jaws are closer together due to the formation of the ligamentous symphysis.

*Endochondral ossification of the skull.* The supraoccipital is positioned anteriorly and has developed the characteristic triangular end that is typical of postnatal balaenopterids.

*Tooth germs.* 40 tooth germs can be found on the right side of the maxilla, and 41 on the left side – the highest number observed among all specimens described here. The higher number of tooth germs in Hf4 is probably due to the more complete ossification of the alveolar groove that makes it easier to isolate the germs in CT images, and the result of higher mineralization of the germs in this later fetus. Four to five “double teeth” are found in each row. The size of the tooth germs is consistent through the row and the average size of the teeth is proportionally smaller compared to the skull than in earlier stages. The alveolar groove is still prominent, wide and open, but the edges are straight. In the lower jaw, 36 and 38 tooth germs are visible in the left and right sides, respectively. They are smaller than in the upper jaw, and show a size gradient, with the smaller germs found at the anterior tips of the mandible. They are not present in the posterior most

portion of the mandibular rami. Some “double teeth” are present on each side. The alveolar groove appears shallower in the lower jaw as well.

*Comparisons.* This is the first fetal specimen of humpback of this size formally described since the work of Eschricht (1849), who focused on the description of the tooth germs. In a specimen with a total length of 115 cm, Eschricht found tooth germs with signs of resorption. It is difficult to identify signs of resorption in tooth germs using the CT scans. However, because Hf4 has an even higher number of tooth germs present for the entire length of the jaws compared with the previous stages, and that their size is not significantly decreased, we conclude that they are not yet in resorption.

## **Minke whale specimens (from Lanzetti, in press)**

### **Mf1 – NSMT27154 – TL 28 cm – Antarctic m.w. (not figured)**

*Note:* given low CT scan resolution, even after the iodine staining, it was not possible to segment internal structures and bones for a 3D model, therefore no accurate ossification stage description of individual bones was possible.

*Staging:* Fetal Stage 20/21

Eyelids fused, umbilical hernia retracted/tactile hair present, blowhole in the last one-third of head (Sterba et al. (2000): stages 7, 8 and 9).

Revision to Thewissen and Heyning (2007) and Lanzetti et al. (2018): as presented for the humpback fetuses, FS21 is better characterized by the posterior movement of the external nasal aperture towards its approximate adult position, in the last one-third of the head.

#### *External characteristics*

Few tactile hairs are present on rostrum. The blowhole is positioned in posterior third of the head similar to the adult. The flippers are elongated but still short in proportion to total body length; a small dorsal fin is present. The fluke has two distinct lobes and a medial notch, but it still has a rounded shape (longer than wide – Thewissen and Heyning, 2007). The gingival ridge (gum) is clearly visible for entire length of the rostrum between palate and lip.

#### *Internal characteristics*

*Intramembranous ossification of the skull.* Few skull elements are recognizable in the CT images: a little piece of the anterior portion of neurocranium and parts of maxilla and premaxilla are ossified, as well as the mandible in certain portions.

*Endochondral ossification of the skull.* No portion of the supraoccipital or other parts of the posterior part of the neurocranium are visible.

*Tooth germs.* No tooth germs are visible. This might be due to their small size, which is expected to be less than or equal to the slice thickness (0.5 mm) based on the relative size of tooth buds to head length of humpback specimens at this stage (Lanzetti et al., 2018) and on the other specimens of this growth series.

*Postcranial bones.* Vertebral centra are visible along the spine; incipient ossification in forelimb bones is also recognizable.

*Comparisons.* Tooth germs should be present at this stage according to Ishikawa and Amasaki (1995), which found visible tooth germs starting from specimens of 8.3 cm in total length. In a similar specimen that they described (n. 16 – 24.1 cm TL) they found a full row of tooth germs in both lower and upper jaws.

**Mf2 – NSMT27149 — TL 41 cm – Antarctic m.w. (Fig. S2.4)**

*Note:* given low CT scan resolution, even after the iodine staining, it was not possible to segment internal structures and bones for a 3D model, therefore no accurate ossification stage description of individual bones was possible.

*Staging:* Fetal Stage 21/22

Tactile hair present, eyelids separated, blowhole in the last one-third of head/throat grooves present (Sterba et al. (2000): stages 9 and 12).

Revision to Thewissen and Heyning (2007) and Lanzetti et al. (2018): as seen in the humpback fetuses, FS22 can be further characterized in Balaenopteridae by the beginning of development of throat grooves. In this specimen body coloration is also visible, as reported by Thewissen and Heyning (2007), probably due to good preservation conditions.

*External characteristics.* Tactile hairs are present on both rostrum and mandible. The flippers are more elongated anteroposteriorly; the back fin is more elevated. The fluke has more defined and



elongated lobes that However it still lacks many important characteristics. Throat grooves are well developed under the buccal cavity and start reaching faintly beyond the flippers, denoting a very rapid development from the previous stage. The gingival ridge is well defined for the entire rostral length similar to Mf1.

*Internal characteristics*

*Intramembranous ossification of the skull.* Partial ossification is recognizable in the maxilla and premaxilla, in parts of the skull roof and in the dentary.

*Endochondral ossification of the skull.* The supraoccipital appears to have started ossifying at the posterior end of the skull.

*Tooth germs.* Tooth germs are clearly visible in the CT images, and they appear more abundant in the upper jaw than in the lower jaw (20-30 u.j., 10-20 l.j. per side).

*Postcranial bones.* Vertebral centra and spinal processes are clearly recognizable throughout the length of the spine. The forelimb bones are also clearly identifiable.

*Comparisons.* Ishikawa and Amasaki (1995) found tooth germs in comparable numbers to the ones observed here in a 42 cm TL specimen (n. 18) in both jaws. Julin (1880) described a mandible of similar length (8.4 cm) from a minke whale, but it is unknown if it belonged to an Antarctic or common minke whale. This author found 41 tooth germs per side in this lower jaw and described heterodont teeth in the middle and posterior portion of the tooth row. The dentary presented a continuous and advanced ossification.

**Mf3 – ZMCU-CN6x – TL 48 cm – common m.w. (Fig. 2.9)**

*Staging:* Fetal Stage 21/22

Tactile hair present, eyelids separated, blowhole in the last one-third of head/throat grooves present (Sterba et al. (2000): stages 9 and 12).

Revision to Thewissen and Heyning (2007) and Lanzetti et al. (2018): see Mf2

*External characteristics.* Only few tactile hairs are recognizable on the head of this specimen due to partial skin removal. The flippers are elongated compared to the previous specimen and they are getting closer to the length and width proportions expected for the species. The back fin is larger and starts assuming the typical hook-like shape. The fluke lobes are more developed but still present a simple triangular shape with straight edges. The throat grooves are only visible under the buccal cavity and so appear less developed than in Mf2: this might be due to intraspecific differences in development or variability in developmental timing of this feature, but might also be an artifact of the shirking caused by ethanol preservation. The gingival ridge is present but not clearly marked as in previous specimens: it does not look elevated from palate and upper lip is retracted, probably due to shrinking.

*Internal characteristics*

*Intramembranous ossification of the skull.* All bones present irregular and rough surfaces. Premaxilla and maxilla are mostly ossified with foramina well visible in the posterior portion. The rostrum presents a distinct dorso-ventral curvature especially in the anterior part. A very prominent infraorbital process is present but not connected to the frontal bone. Nasal bones start ossifying and have a small triangular shape. The frontal is well developed and close to the parietal posteriorly. The parietal is well ossified with only a small gap between its lateral and dorsal sides, which ossify separately. The interparietal bone is clearly recognizable at the top of the skull and its starting to connect with parietal. The squamosal is well ossified and in contact with the parietal. Pterygoid, palatine and vomer are recognizable and most of their surfaces are ossified. The vomer ossification is still progressing in the anterior portion of the rostrum. The pterygoid hamuli still lack the posterior portion. Jugal and lacrimal bones are recognizable on both sides and appear well ossified. The ectotympanic has 3-dimensional shape but is still not ossified in

most of the posterior and ventral portion. The mandible appears completely ossified with prominent lateral curvature, but the anterior symphysis is still well separated, and no evidence of the ligament are present.

*Endochondral ossification of the skull.* The supraoccipital shield is well formed. It is ossifying towards the anterior end of the skull and only a small portion is visible in posterior view. It also does not have the characteristic triangular shape. A small crest is present at the center, oriented antero-posteriorly (sagittal crest). Exoccipital processes are ossified on both sides. Basioccipital and basisphenoid are present. Hyoid bones are recognizable, but still small and far apart.

*Tooth germs.* No clear rows of tooth germs are recognizable possibly due to the absence of iodine stain and to the scan resolution (slice thickness 0.6 mm). Some tooth germs can probably be identified in the dentary. The alveolar groove in the maxilla is well developed and deep, as is the mandibular canal. This feature indicates the probable presence of tooth germs, as well as the presence of a full tooth row in both jaws of Mf2.

*Postcranial bones.* The forelimb bones (radius, ulna, humerus and scapula) all started ossifying. The ribs are mostly ossified as well. The vertebral centra are well ossified and assumed the typical rounded and compressed cetacean shape in the posterior portion of the body. The vertebral processes have started ossifying as well. No hind limbs elements are visible.

*Comparisons.* As stated for Mf2, Ishikawa and Amasaki (1995) found tooth germs in both jaws in a specimen of similar length (n. 18), and Julin (1880) describes them for a mandible of comparable size, which is additional confirmation that this specimen probably has full rows of tooth germs as well. Eschricht (1849) also noted the presence of the interparietal bone in a smaller (23 cm TL) fetus of minke whale, which he later reported to be fused with parietal and rest of the skull roof bones in a specimen of around 190 cm TL.

**Mf4 – NSMT “blue10” – TL 72 cm – Antarctic m.w. (Fig. S2.6)**

*Note:* only the head region was CT scanned for this and all the following specimens due to size and CT scan resolution constraints

*Staging:* Fetal Stage 23/24

Pigmentation present, throat grooves well developed, reach below the flippers.

Revision to Thewissen and Heyning (2007) and Lanzetti et al. (2018): this specimen confirms the observation done on a humpback specimen at a similar stage of the gestation about the development of throat grooves, which become longer and more pronounced. The pigmentation was noted at stage 23 by Thewissen and Heyning (2007) and its well visible on the entire body in this specimen probably because of the formalin preservation.

*External characteristics.* The specimen presents cuts in the lower jaw and a section is missing from the left mandibular ramus, but it is in overall good conditions. The tactile hairs are present at the tip of the mandible and rostrum. The flipper is more elongated and with length and width proportion similar to its final proportions. The back fin is also more developed but still not assumed its characteristic shape. The lobes of the fluke are laterally elongated, but they are still triangular and with straight sides. The throat grooves are deep and numerous and reach well below the flipper. The gingival ridge is well defined through the upper jaw.

*Internal characteristics*

*Intramembranous ossification of the skull.* All bones have a spongy appearance, due to preservation conditions and development. Premaxilla and maxilla appear to be almost completely ossified especially in the posterior part where the foramina are also visible, with the upper jaw being the same length as the mandible, while in previous stages the dentary was always slightly longer than the rostrum. The infraorbital process of the maxilla still doesn't contact the frontal. The frontal is ossified and very close to contacting the nasals medially. The nasal bones are

bigger and elongated posteriorly even if they are still not as long as in adult mysticetes. The parietal is in contact with the frontal on the left side, but still is not completely ossified laterally on both. In Mf3 the parietal is more complete: this difference can be due to both a developmental timing difference among specimens or an interspecific difference, given that the two specimens belong to different minke whale species. The interparietal is clearly recognizable at the top of the skull, and it is in contact with the supraoccipital posteriorly, but not with any other element. The squamosal is completely ossified and contacts the parietal. The lacrimal bone is ossified and visible on both sides, while the jugal is only visible on one probably due to the specimen inclination in the CT scan machine. On the ventral side, the vomer, palatine, pterygoids and palatine process of maxilla are mostly ossified and more compact, even if some portions of the vomer and maxilla are still missing anteriorly and the hamule are not complete. The ectotympanic is mostly ossified, but still lacks articulation with skull posteriorly and part of its ventro-lateral portion (outer lip). The mandible has a prominent lateral curvature, and the two rami are closer together even if limited conclusions can be drawn about the presence of the symphysis given the not optimal preservation conditions of the lower jaw.

*Endochondral ossification of the skull.* The supraoccipital reaches the interparietal anteriorly at the top of the skull. A faint crest is visible in the center. The exoccipital is more ossified but it is still not contacting the squamosal. Basisphenoid and basioccipital are mostly complete, but they still do not contact with dermal bones of the skull. It is important to remember that the sutures between the supraoccipital and exoccipital, exoccipital and basioccipital, and basioccipital and basisphenoid only ossify after birth, and they are an important part of assessing the maturity of postnatal specimens (Walsh and Berta, 2011). The periotic bones at this stage is clearly recognizable inside the ectotympanic complex and ossified. The hyoid bones are more ossified, but still appear as small conical or prismatic elements far apart from each other.

*Tooth germs.* Few tooth germs (3 on left side and 12 on right side) are recognizable in the upper jaw. They are small but evenly spaced in the portions where they are visible. It is likely that the CT scan resolution limitations are preventing the observation of the full tooth row. The upper alveolar groove is in fact still wide for the entire length of the maxilla. While no tooth germs are visible on the dentary, the mandibular alveolar groove is deep and well defined, so probably tooth germs are present in the lower jaw as well.

*Comparisons.* Ishikawa and Amasaki (1995) found complete rows of tooth germs in a specimen only slightly smaller (66 cm TL – n.20), but they did not comment on whether they showed signs of resorption. Eschricht (1849) found more than 40 teeth in each side of the jaws in a specimen only slightly larger than this (87 cm TL – 6.5 months f.c.) and he hypothesized that the maximum development of teeth in the minke whale – probably examining common minke whale fetuses – occurs in fetuses between 74 cm and 96 cm TL. Based on these observations by multiple authors and the visible bony correlates, this specimen most definitively has complete tooth rows on both upper and lower jaws.

**Mf5 – NSMT “white11” – TL 110 cm – Antarctic m.w. (Fig. S2.7)**

*Note:* this specimen is in overall poor preservation conditions, with dried out skin and many cuts on rostrum.

*Staging:* Fetal Stage 25 (?)

Thick “baleen gum” develops medial to gingival ridge

Notes on staging: since this specimen is in poor preservation conditions, I do not base the new fetal stage 25 on this specimen description. For a description of this stage, see next specimen Mf6.

*External characteristics.* At this stage, the body starts is more elongated relative to the head, as it is expected mysticetes. Tactile hairs are abundant on head and skin coloration present on the entire body. The flippers are longer and closer to their final proportions. The back fin has assumed its typical pronounced “hook” shape. The fluke now presents a laterally elongated shape more similar to the adult, but the preservation conditions of the specimen do not allow assessment of the shape of the edges and its precise proportions. The throat grooves appear deteriorated, but they seem to extend to well below the flippers. The gingival ridge is not recognizable anymore, instead a gingival groove is visible in the first third of the rostrum. Moving posteriorly, the groove shifts laterally and on the medial side an enlarged gum is present, slightly elevated from the palate and separated from the lip by the groove. This enlarged posterior gum might be an indication of baleen formation, given its expanded medial position compared to the gingival ridge that hosted the tooth buds (Thewissen et al., 2017).

*Internal characteristics*

*Intramembranous ossification of the skull.* All bones have irregular surfaces and spongy appearance, probably due in part to the poor conditions of this specimen. Premaxilla and maxilla appear ossified, but the anterior, lateral and ventral portions are particularly degraded, and no foramina are visible. The infraorbital process appears to contact the frontal laterally, but there is still a visible gap between this process and the medial side of the frontal. The nasal bones are bigger and slightly more elongated posteriorly. The frontal now contacts the nasals laterally and posteriorly the gap is greatly reduced. The parietal is mostly complete laterally and sutured with the interparietal dorsally, which is in turn harder to recognize. The palatine, vomer and pterygoid are highly degraded even if they are apparently present. The squamosal is sutured with the parietal, but a gap is still visible on one side. Both lacrimal and jugal are not distinguishable to due preservation issues. The ectotympanic bone is still not completely ossified posteriorly and

ventro-laterally. The mandible presents a prominent curvature, but it is dislocated and degraded anteriorly and with signs of previous dissections, therefore the symphysis is not visible.

*Endochondral ossification of the skull.* The supraoccipital has expanded posteriorly, while anteriorly it contacts interparietal and parietal. The sagittal crest is marked in the posterior portion. The exoccipital is now ossified beyond the condylar processes and it is closer to the supraoccipital dorsally. The basioccipital and basisphenoid are completely ossified, but it is unclear whether they are in contact with the surrounding bones due to the poor conditions of the specimen. Also, a completely ossified periotic is recognizable. Hyoid elements are bigger and more defined, with the thyrohyoids, basihyoid and stylohyoids displaying distinct morphologies.

*Tooth germs.* At least 5 small tooth germs are recognizable on each side of the upper jaw, even if the state of preservation of the specimen makes it hard to identify them. The alveolar canal on the upper jaw is present. However it is hard to determine its size given the extended bone degradation. Sparse tooth germs are also visible in the lower jaw. The alveolar canal is present but shallower especially in the posterior portion of the dentary.

*Comparisons.* Ishikawa and Amasaki (1995) observed degrading tooth buds in their specimens of 90 cm and 112 cm TL (n.21 and n.22), However they still counted a full row of tooth germs in both lower and upper jaws, with over 30 germs per side. In these two specimens, they also point out the presence of “rudiments of baleen”. Given that the authors do not provide any additional description of this structure and the poor condition of this specimen, I will not discuss the possible start of baleen formation here (see Mf6).

**Mf6 – NSMT “white15” – TL 110 cm – Antarctic m.w. (Fig. 2.11)**

*Note:* this specimen has the same total length as Mf5, but it is particularly well preserved.

*Staging:* Fetal Stage 25



Thick “baleen gum” develops medial to gingival ridge

Notes on staging: this new fetal stage is characterized by the development of a thick gum in the medial part of the palate, especially visible in the posterior portion of the upper jaw (“baleen gum”),

that progressively becomes smaller moving anteriorly. In the anterior one-third of the rostrum, only a groove is visible between the palate and the lip.

*External characteristics.* Numerous tactile hairs are present on the rostrum forming rows. The specimen presents extensive body coloration, with the ventral area being lighter than the dorsal area, as typical in most baleen whales. The flippers are close to expected proportions with a length of about four times their width. The back fin also assumed the characteristically hooked shape. The fluke is larger, with more elongated lobes and undulated edges. As described in the fetal stage characterization, the gingival groove is well visible in the anterior part of the rostrum, while a thick gum is present at the posterior end.

*Internal characteristics*

*Intramembranous ossification of the skull.* The bones have a smoother appearance, indicating both an advanced ossification and the good preservation status of the specimen. The rostrum overall is mostly flat, presenting a less marked dorso-ventral curvature, while until Mf4 (stage 23/24) the curvature was still very prominent especially at the anterior tip. Premaxilla and maxilla are well ossified. The anteriormost portion is still spongy in appearance, probably due to the ongoing elongation of the rostrum. Multiple foramina are visible in the posterior third of the maxilla. A gap is still present between the infraorbital process and the frontal, which is also a probable indication that the skull is still elongating and changing shape. The nasals are more elongated posteriorly. The frontal is closing its medial gap and it is now in proximity with the nasals posteriorly. The lacrimal and jugal are ossified and visible on both sides. The interparietal

is sutured with the parietals but its borders are still recognizable. The parietals are completely ossified also laterally and are sutured with the squamosal and supraoccipital. The vomer and palatine are clearly visible in this specimen, and they are mostly ossified with the anterior part of the vomer being still incomplete as expected, given that the same condition is observed in the maxilla and premaxilla. The pterygoid is compact with the hamuli being mostly complete also at the posterior end. The ectotympanic still has an unossified portion postero-ventrally but is now completely ossified posteriorly and very close to the base of the squamosal. The dentary presents a pronounced lateral curvature and a small ridge in the posterior one-third on the lateral side. The two rami appear close together and probably articulated with the cartilaginous symphysis, However cartilage is not clearly recognizable in the CT images without a contrast method.

*Endochondral ossification of the skull.* The supraoccipital is in contact with the interparietal anteriorly and expanded posteriorly towards the exoccipital. On the posterior part, a small sagittal crest is still present. The exoccipital is expanded dorsally and is now articulated with the squamosal laterally. The basioccipital and basisphenoid are completely ossified but still a small gap is visible between these elements and the dermal bones. The periotic is now clearly sutured with the skull, with no visible gap, as expected in this species (Yamato et al., 2012). The hyoid elements are bigger and more defined.

*Tooth germs/baleen rudiments.* A complete tooth row is recognizable in the right upper jaw with 30-35 tooth germs. Some of these germs are very small, but they are all conical and evenly spaced. On the left upper jaw, only 12 tooth germs are visible, mostly in the anterior and posterior end of the tooth row. The alveolar canal is smaller overall. In the mandible, only 3-4 very small tooth germs are recognizable at the anterior tip of both rami. The alveolar canal is shallower and narrow especially posteriorly, as the mandibular canal internally. While the low number of tooth germs visible is probably an artifact of the scanning, it is clear that they are particularly small at

this stage, especially compared to the size of the skull. A denser material is recognizable in the scans that does not contact the rostral bones inside the medial part of the alveolar ridge. This material is present mostly in the posterior part of the rostrum, where most of the foramina are located and also where externally the enlarged gum is visible. I hypothesize that this tissue might be a precursor of the baleen, and it is visible in the CT scans as the baleen plates are, given the higher density of keratin compared to regular soft tissue.

*Comparisons.* The number of tooth germs in the right upper jaw is comparable with was found by Ishikawa and Amasaki (1995) in their specimen n.22 (112 cm TL). Their observation of “rudiments of baleen” might correspond to the denser material in the posterior portion of the upper jaw, However they did not provide details on this structure.

**Mf7 – NSMT27171 – TL 121 cm – Antarctic m.w. (Fig. 2.12)**

*Staging:* Fetal Stage 26

Ridge (keel) forms at the center of the baleen gums.

Notes on staging: this new stage is characterized by the formation of a distinct cartilaginous ridge at the center of the baleen gum. It is most prominent at the posterior end of the rostrum. The gingival groove still borders the baleen gum laterally and it is the only structure present at tip of the rostrum.

*External characteristics.* Many tactile hairs are recognizable on the head of the specimen. The body keeps elongating in comparison to the skull. The flipper now has also acquired asymmetrical borders on the left and right sides. The back fin presents a more marked hook shape and it is growing. The fluke lobes are markedly curved towards the body. The throat grooves did not grow in length, but they are deeper. As described for the definition of this fetal stage, the

baleen gum now presents a ridge in the center, and it is only visible in the posterior part of the upper jaw and fades away towards the tip.

*Internal characteristics*

*Intramembranous ossification of the skull.* The bones are less spongy overall but there are still sign of elongation of the rostrum with less marked ossification in the anterior portion. The premaxilla is longer than maxilla. They are mostly ossified, and foramina are visible in the posterior portion. The nasals are elongated and are close to contacting the frontal posteriorly. The right and left frontal are sutured medially. There is still a gap laterally with the infraorbital processes, showing that skull shape is still in development. The lacrimal is now in contact with the infraorbital process of the maxilla and the preorbital process of the frontal. The jugals are visible on both sides but do not appear to articulate with any of the orbital bones. On the dorsal surface of the skull, no more fontanelles are visible, with the interparietal not recognizable anymore due to its fusion with the parietal and frontal. The parietal is mostly complete laterally even if a small gap persists on one side. Comparing this with the state in the younger samples, it appears that the fusion of the two parts of parietal appears to be highly variable from specimen to specimen and between sides. The bone is sutured to the squamosal on both sides. On the ventral side of the skull, the vomer is only visible in the posterior end of the skull, possibly due to CT images resolution and to the ongoing elongation of the rostrum. The palatine and pterygoid still have a spongy appearance but are mostly ossified with the hamuli close to contacting the basisphenoid. The ectotympanic is close to be complete with only a small portion left to ossify laterally and ventrally on the posterior end of the outer lip. Its posterior process is clearly in contact with the squamosal. It now also shows a markedly higher density compared to the rest of the skull. The dentary has a progressively more marked lateral curvature. It presents a small ridge

laterally in the posterior portion near the coronoid process. Clear evidence of the cartilaginous symphysis is visible at the anterior tip of the rami given the arrangement and shape of the bones. *Endochondral ossification of the skull.* The supraoccipital partially overlaps the interparietal at its anterior end, and it is sutured to the frontal laterally. The sagittal crest has now disappeared. The exoccipital is fused to the squamosal laterally and it reduced the gap with the supraoccipital dorsally. The basioccipital still does not seem to contact any dermal bones, while the basisphenoid contacts the squamosal laterally and its close to contacting the pterygoid anteriorly. The periotic now has an enlarged “bubble-like” appearance typical of adult mysticetes and its denser than the surrounding bones. The hyoid elements are bigger but still far apart. While it is known that the basihyoid and thyrohyoids are ossified in a single element in the adults, it is probable that the ossification of the cartilage between them only starts after birth at the juvenile stage, even if direct evidence of this process for Balaenopteridae in particular is lacking (Omura, 1964, Werth, 2007).

*Tooth germs/baleen rudiments.* Only a few tooth germs are recognizable in this specimen (less than 10 per side in the upper jaw and less than 5 per side in lower jaw). The visible tooth germs occur at the posterior end of the jaw mostly, and they are very small relatively to the increasing head size. In the upper jaw, their position at the center of the alveolar canal makes it plausible that they occupy the elevated ridge visible externally in the posterior part of the gums. The alveolar canal in the lower jaw is shallower and narrow along the entire length of the rami. In the upper palate, a denser material not contacting the bone is again present. The material appears to be mostly medio-dorsal to the remaining tooth germs. At this stage it is recognizable along most of the length of the rostrum, However it appears more developed posteriorly and in this region it also expands ventrally beyond the ossified margin of the maxilla. This might be correlated to the steep gum margins observed externally in the posterior third of the upper jaw.

*Comparisons.* Ishikawa and Amasaki (1995) described the dentition and baleen rudiments in a specimen only slightly larger than this (149 cm TL, n.23). It still had over 30 tooth buds in each side of both jaws, but it also had the baleen rudiments, However none of these findings are figured. Sawamura (2008) described and figured the gums of an Antarctic minke whale fetus of 145 cm TL. This fetus presented a similar medial ridge in the posterior part of the gums as the specimen I describe here, with some tooth buds still contained in the ridge. He only conducted a macroscopical dissection, therefore he does not notice the presence of denser materials in this region. However, he describes an increased number of blood vessels and nerves medial to the tooth germs, and he connects this to the start of the formation of baleen in the most posterior third of the rostrum. The validity of this connection is confirmed by the results of a more recent study on baleen formation on a molecular level (Thewissen et al., 2017). These authors found that higher concentration of the signaling protein associated with baleen formation (FGF-4) is found near small vessels in the medial portion of the gums, especially in the posterior portion of the palate.

**Mf8 – ZMCU-CN4x – TL 125 cm – common m.w. (Fig. S2.8)**

*Staging:* Fetal Stage 26

Ridge (keel) forms at the center of the baleen gums.

Notes on staging: this specimen is older than Mf7 since it is a common minke whale, which has smaller body length and shorter gestation time. At this late stage of gestation, the difference between the two species in gestational age is particularly marked given the acceleration of growth that happens in the last third of the pregnancy. However, I did not find any additional characteristic and therefore I characterize this specimen with the same fetal stage as Mf7.

*External characteristics.* The body proportions of this specimen are hard to assess due to deformation in preservation and a deep cut under the throat. There is also a rope that runs through the mouth and around the neck, but overall the specimen is in good conditions. The body coloration is recognizable, even if the specimen has acquired a yellow-brown color due to ethanol preservation. A few tactile hairs are visible on the head. The flippers have assumed the expected proportions and have now uneven anterior and posterior borders. The back fin is also taller and with the typical hook-like shape. The fluke has assumed the characteristic shape for this species, with wavy margins and elongated lobes. The throat grooves are deep and well develop until their posterior end, between the flippers and umbilicus. The gingival groove is marked on the lateral sides of the gums. The baleen gums are now larger and present for almost the entire rostral length. The medial ridge is very marked with steep sides in the posterior half of the upper jaw. After this it becomes smaller then fades away in the anterior one-third of the gums. It is However more developed than in the previous specimen.

*Internal characteristics*

*Intramembranous ossification of the skull.* The bones appear smoother at this stage, signaling the proximity to the end of the gestation. The rostrum is now mostly dorso-ventrally flattened as expected in Balaenopteridae, and clearly longer than the dentary. The premaxilla is only slightly longer than the maxilla. The elongation seems to have stopped or decreased in magnitude given the fact that the anterior tip of these bones is compact. Foramina are visible in the posterior half of the rostrum in dorsal view. The nasals are extremely elongated posteriorly, and they are almost completely sutured to the frontal. There is still a gap present between the infraorbital process of the maxilla and the frontal, but it is smaller, also in line with the decrease in rostral elongation. The frontal and parietal are completely ossified and sutured together with no visible gaps. The interparietal is now completely unrecognizable at the top of the skull. The squamosal is

completely sutured to parietal laterally. The jugal and lacrimal are articulated to the anterior end of the orbit. The vomer and palatine are almost entirely ossified. The pterygoid hamuli are now complete and in contact with the basisphenoid. The ectotympanic is close to be complete, However a small segment remains to be ossified on the ventrolateral side in posterior view. It is clearly articulated with the squamosal posteriorly. The left ramus of the mandible is broken near the anterior end, but this does not compromise the articulation. The mandibular rami are clearly connected by a symphysis, likely cartilaginous, given their proximity to each other and articulation angle. The lateral ridge is mostly prominent in the region of the coronoid process, then fades away moving posteriorly and anteriorly.

*Endochondral ossification of the skull.* The supraoccipital is elongated anteriorly reaching around mid-length of the supraorbital process of the frontal. A groove has developed medially in the posterior portion of the bone, where the sagittal crest was observed in younger specimens. The exoccipital is more developed, and its fused to the squamosal. The gaps between the exoccipital and the other endochondral bones in the neurocranium are significantly reduced. No major changes occurred in the basioccipital and basisphenoid except that the latter is now more tightly articulated with the dermal bones. The petrotic did not changed externally. The hyoid bones were not recovered in the CT scan.

*Tooth germs/baleen rudiments.* Very recognizable tooth germs are present in both upper (24 on the left, 21 on the right) and lower jaws (15 on the left, 14 on the right). In the upper jaw, they are distributed evenly in the entire tooth row, and they are of similar size and evenly spaced even if there are some gaps in the row. In the lower jaw, they are only present in the posterior two-thirds of the mandibular rami. They are of slightly different shapes, with one or two “double teeth” (very close together tooth buds, sometimes interpreted as multicuspid teeth – Thewissen et al., 2017). The lower alveolar canal is shallow and very narrow. Also in this specimen, a denser



material is visible medially in the upper alveolar canal. This canal is now very narrow and, in some areas, filled with this material. The material does not contact the maxilla. In some regions it engulfs the tooth germs. It is spatially related with the dorsal foramina: in the posterior part where the foramina occur it is denser and directly below them. It is closer to the lateral margin of the alveolar canal where the external elevated ridge is present. All these characteristics allow to hypothesize that this material is connected with baleen formation, possibly being baleen proteins starting to form.

*Comparisons.* The comparative observation made for Mf7 are also valid for this specimen even if it is of a different species. Ishikawa and Amasaki (1995) and Sawamura (2008) both were describing Antarctic minke whale specimens, but this specimen shows that, while the developmental timing might be different, this crucial teeth-to-baleen transitional phase seems to be conserved between the two species (Table 4). The presence of the denser material in this fetus, as well as its abundance in the posterior part of the rostrum, prove that it is not a scanning artifact or something due to specimens' degradation, but it might indeed be a sign of developing baleen as presented in specimen n.23 by Ishikawa and Amasaki (1995). The interparietal is not recognizable anymore at this stage, sooner than observed by Eschricht (1849), who described this element in a larger specimen of this species (195 cm TL).

**Mf9 – NSMT27175 – TL 182 cm – Antarctic m.w. (Fig. S2.9)**

*Staging:* Fetal Stage 27

Transversally oriented rows of connective tissue and baleen visible.

Notes on staging: this new stage is characterized by the presence of the transversal ridges that will form the base of the baleen plates visible in the gums of the upper jaw. They are present for the entire length of the palate except at the anterior end. It is known that this structure represents

developing baleen thanks to the work on blue whale fetuses of Tullberg (1883) (translated and commented by Fudge et al., 2009).

*External characteristics.* The specimen is exteriorly in good conditions, with only a hole left probably from a hook that was placed in the middle of the palate. The body appears elongated compared to the head more resembling newborn proportions. Body coloration is very resembling of the adult. Tactile hairs are short but present in large numbers on the head. All appendages (flippers, back fin, fluke) are now of the shape and size expected for this species. The throat grooves are deeper and reach the umbilicus. The gingival groove is very steep and runs deep between the lateral side of the connective tissue and the lip. The transversal rows of connective tissue (transversal process of baleen) seem to have “erupted” from the center of the gum towards the sides given the medial depression. They are particularly visible in the posterior half of the rostrum, and they become shallower moving anteriorly.

*Internal characteristics*

*Intramembranous ossification of the skull.* All the bones have a “bubbly” appearance. This is different from the spongy appearance of the developing embryos and it is probably due to partial dissolution of the bony tissue by the formalin medium, which in time it is known to form formic acid, a known decalcifying agent (Fox et al., 1985). The premaxilla and maxilla appear completely ossified even on the anterior end. The skull has assumed the typical triangular shape in dorsal view, with a flat rostrum. The nasals contact the frontals posteriorly. The suturing between frontals and parietal is complete and the bone margins are not recognizable anymore, even if this might be partially due to preservation and CT imaging quality, as sometimes the contact is visible in postnatal specimens. The gap between the infraorbital process and the frontal is still present but small, indicating that skull shape is still developing. The squamosal is fused to the rest of the skull and its zygomatic process now contacts the postorbital process of the frontal.

The lacrimal is sutured to the preorbital process of the frontal, while the jugals are not visible in the CT images. The vomer and palatine process of the maxilla are mostly ossified, but certain areas of the palate and the tip of the rostrum display incomplete ossification. The palatine and pterygoid are completely ossified. The pterygoid is now sutured with the basisphenoid for the entire length of the contact. The ectotympanic is complete posteriorly, and the posterior suture with the squamosal is expanded. The bones of this region remain thicker and denser than surrounding ones. The mandibular rami have now assumed the expected degree of lateral curvature, and they are united at the anterior end by a large symphysis.

*Endochondral ossification of the skull.* The supraoccipital has progressed anteriorly and it is tightly sutured to the frontal dorsally. It has assumed its typical triangular shape. The exoccipital ossification has progressed both dorsally and ventrally, and the gap between the bones of the neurocranium is now significantly reduced. The basioccipital and basisphenoid did not significantly change. They are completely sutured to the dermal bones anteriorly and laterally. The periotic did not change externally. The hyoid elements are bigger but remain unfused. The basihyoid was not visible in the CT scans.

*Baleen.* No tooth germs are visible indicating that most likely they were completely resorbed before this stage. The alveolar canal is narrow but still visible, especially in the posterior part of the rostrum where the baleen transversal ridges are visible externally. The lower alveolar canal is shallow but present up until the anterior portion of the rami. The baleen are present and recognizable in the CT scan as a structure of intermediate density between the soft tissues and the bone. They do not present any apparent physical connection with the alveolar groove or other palatal structures, but they are recognizable dorsally up to the lateral margins of the maxilla. They are thicker in the posterior end of the jaw.

*Comparisons.* Ishikawa and Amasaki (1995) also found only baleen in the biggest specimen they examined (182 cm TL – n.24), However they do not present illustrations of this stage. Sawamura (2008) described and figured the baleen ridge of a 175 cm TL fetus, which resembles very closely the one in this specimen. He found the transverse process was mostly developed in the posterior half of the upper jaws and very small baleen bristles that here are probably lost due to preservation. This author noted during dissection that the baleen seems to form from the alveolar ridge, therefore from a part of the periodontal tissue, claiming a deep connection between teeth and baleen development. The baleen would start developing medially to the tooth germs near the posterior end of the palate in regions of the periodontal tissue rich of nerve endings and blood vessels. This hypothesis has been confirmed by Thewissen et al. (2017) that found that baleen co-opts the same signaling proteins used for teeth development and forms from the medial region of the periodontal tissue.

**Mf10 – NSMT27174 – TL 212.5 cm – Antarctic m.w. (Fig. 2.13)**

*Staging:* Fetal Stage 27

Transversally oriented rows of connective tissue and baleen visible.

*External characteristics.* The specimen presents a hole in the center of the palate probably due to a hook, and signs of sectioning of the baleen ridge in certain sections of the upper jaw, but it is overall well preserved. The head-to-body proportion is now very similar to the one observed in neonates of this species. Tactile hairs are very short but distributed on the entire head, especially concentrated at the tip of the mandible. Body coloration closely resembles the one of neonates and adults. Flippers, back fin, and fluke have now assumed their final shape. The throat grooves are deep and also in this specimen are elongated till the umbilicus. The gums present visible transversal processes of baleen. The transversal rows of baleen tissue are visible for most of the

palate, with only the anterior tip lacking them. It has a deep groove at the center, and it again looks like the connective tissue was erupted from the center towards the sides of the gums. It is more developed at the posterior end of the upper jaw. No bristles are preserved. The gingival groove is very deep dividing a steep lateral side of the emerging baleen tissue and the medial margin of the lip. The groove is shallower at the tip where the gums are not enlarged since the baleen are not erupted.

*Internal characteristics*

*Intramembranous ossification of the skull.* This specimen presents evidence of decalcification due to formalin preservation with the bones having rough edges and a bubbly appearance as Mf9. The rostrum has acquired the typical triangular and flat shape of this species. The premaxilla is ossified and as long as the dentary, while the maxilla seems to lack several portions especially towards the anterior end of the rostrum. This might be due to either continued elongation of the bone or to decalcification. The nasals are elongated and in contact with the frontal posteriorly. The gap between the infraorbital process and the frontal is only present on the right side, signaling that the bone arrangement is close to complete. All the major dermal bones of the neurocranium are sutured together and no gaps are visible also laterally. The zygomatic process of the squamosal is in contact with the postorbital process of the frontal on one side. Lacrimal and jugal are not visible in the CT images. On the ventral side, the vomer is mostly ossified while the palatine process of the maxilla lacks large portions likely due to decalcification. The palatine and pterygoids are well ossified and sutured the surrounding bones. The ectotympanic did not went through any major exterior changes. The mandible has a marked lateral curvature and it is also curved ventrally in the last one third. The lateral ridge is smaller but still visible in the region of the coronoid process.

*Endochondral ossification of the skull.* The supraoccipital is completely sutured to the parietal and frontal with no gaps visible and reaches around the middle of the orbit. The exoccipital has expanded and now the gap with the basioccipital is very small. No changes occurred to basioccipital, basisphenoid and petrotic externally. The hyoid elements are larger, but the basihyoid was not recovered in the CT scan also in this specimen. This likely indicates that it is far apart from the thyrohyoids, suggesting that indeed the elements that fuse together only do so after birth, as hypothesized based on other mysticetes (Werth, 2007).

*Baleen.* No tooth germs are visible. The transverse ridge of baleen reaches almost the tip of the rostrum on both sides. This baleen ridge is wider posteriorly and becomes progressively smaller moving anteriorly. It does not appear to have any physical contact with the bones or the alveolar canal. The canal is narrower but still well defined, on the left side, while it is not possible to identify it on the right side due to preservation issues. The lower alveolar canal is shallower but still recognizable for the entire length of the dentary. It is well separated for most of the length of the mandible from the internal mandibular canal.

*Comparisons.* This specimen is longer than any other specimen ever described for this species. The baleen ridge resembles morphologically the one described for MF9 and the one examined by Sawamura (2008) in a fetus of 175 cm TL. It confirms However the observations made by this author about the progression of baleen development: the posterior portion of the palate presents the more developed transversal ridges, and the development proceed anteriorly compared to the previous specimen.

## Literature cited

- Amasaki H, Ishikawa H, Daigo M** (1989) Development of the external genitalia in fetuses of the southern minke whale, *Balaenoptera acutorostrata*. *Acta Anat*, **135**, 142-148.
- Clapham PJ, Mead JG** (1999) *Megaptera novaeangliae*. *Mamm Species*, **604**, 1-9.
- Deméré TA, Berta A, McGowen MR** (2005) The taxonomic and evolutionary history of fossil and modern balaenopteroid mysticetes. *J Mamm Evol*, **12**, 99-143.
- Eschricht DF** (1849) *Zoologisch-anatomisch-physiologische Untersuchungen über die nordischen Wallthiere*, Verlag von Leopold Voss, Leipzig.
- Fox CH, Johnson FB, Whiting J, Roller PP** (1985) Formaldehyde fixation. *J Histochem Cytochem*, **33**, 845-853.
- Fudge DS, Szewciw LJ, Schwalb AN** (2009) Morphology and development of blue whale baleen: An annotated translation of Tycho Tullberg's classic 1883 paper. *Aquat Mamm*, **35**, 226-252.
- Hampe O, Franke H, Hipsley CA, Kardjilov N, Muller J** (2015) Prenatal cranial ossification of the humpback whale (*Megaptera novaeangliae*). *J Morphol*, **276**, 564-582.
- Ishikawa H, Amasaki H** (1995) Development and physiological degradation of tooth buds and development of rudimental baleen plate in southern minke whale, *Balaenoptera acutorostrata*. *J Vet Med Sci*, **57**, 665-670.
- Julin C** (1880) Recherches sur l'ossification du maxillaire inferieur et sur la constitution du systeme dentaire chez le foetus de la Balaenoptera rostrata. *Arch Biol*, **1**, 75-136.
- Lanzetti A** (in press) Prenatal developmental sequence of the skull of minke whales and its implications for the evolution of mysticetes and the teeth-to-baleen transition. *J Anat*.
- Lanzetti A, Berta A, Ekdale EG** (2018) Prenatal development of the humpback whale: growth rate, tooth loss and skull shape changes in an evolutionary framework. *Anat Rec*, <https://doi.org/10.1002/ar.23990>.
- Mead JG, Fordyce RE** (2009) The therian skull: a lexicon with emphasis on the odontocetes. *Smithson Contrib Zool*, **627**, 1-249.
- Omura H** (1964) A systematic study of the hyoid bones in the baleen whale. Whales Research Institute of Tokyo, 149-170.
- Ridewood WG** (1923) Observations on the skull in foetal specimens of whales of the genera *Megaptera* and *Balaenoptera*. *Philos Trans R Soc Lond B Biol Sci*, **211**, 209-272.
- Simmons JE** (1995) Storage in fluid preservatives. In *Storage of Natural History Collections: A Preventive Conservation Approach* (eds Rose CL, Hawks CA, Genoways HH), pp. 161-186. New York: Society for the Preservation of Natural History Collections.
- Sterba O, Klima M, Schildger B** (2000) Embryology of dolphins: staging and ageing of embryos and fetuses of some cetaceans. *Adv Anat Embryol Cell Biol*, **157**, 1-133.
- Thewissen JGM, Heyning J** (2007) Embryogenesis and development in *Stenella attenuata* and other cetaceans. In *Reproductive Biology and Phylogeny of Cetacea* (ed Miller DL), pp. 307-329. Boca Raton: CRC Press.

- Thewissen JGM, Hieronymus TL, George JC, Suydam R, Stimmelmayer R, McBurney D** (2017) Evolutionary aspects of the development of teeth and baleen in the bowhead whale. *J Anat*, **230**, 549-566.
- Tullberg T** (1883) Bau und Entwicklung der Barten bei *Balaenoptera sibbaldii*. *Nov Acta Reg Soc Scie Ups*, **3**, 1-36.
- Walsh BM, Berta A** (2011) Occipital ossification of balaenopteroid mysticetes. *Anat Rec*, **294**, 391-398.
- Werth AJ** (2007) Adaptations of the cetacean hyolingual apparatus for aquatic feeding and thermoregulation. *Anat Rec*, **290**, 546-568.
- Yamato M, Ketten DR, Arruda J, Cramer S, Moore K** (2012) The auditory anatomy of the minke whale (*Balaenoptera acutorostrata*): a potential fatty sound reception pathway in a baleen whale. *Anat Rec*, **295**, 991-998.



**Discriminant Function Analysis between specimens of humpback whale – whole skull configuration**

Comparison: Hf1 -- Hj1

Difference between means:

Procrustes distance: 0.27149558

Mahalanobis distance: 5.1737

T-square: 26.7671, P-value (parametric): 0.2637

P-values for permutation tests (1000 permutation runs):

Procrustes distance: 0.3600

T-square: 0.3600

(Note: The permutation test using the T-square statistic is equivalent to a test using Mahalanobis distance.)

Classification/misclassification tables

Group 1: Hf1

Group 2: Hj1

From discriminant function:

True	Allocated to		
Group	Group 1	Group 2	Total
Group 1	2	0	2
Group 2	0	2	2

From cross-validation:

True	Allocated to		
Group	Group 1	Group 2	Total
Group 1	1	1	2
Group 2	1	1	2

Comparison: He1 -- Hj1

Difference between means:

Procrustes distance: 0.30700503

Mahalanobis distance: 1.4288

T-square: 2.0415, P-value (parametric): 0.7035

P-values for permutation tests (1000 permutation runs):

Procrustes distance: 0.3480

T-square: 0.6920

(Note: The permutation test using the T-square statistic is equivalent to a test using Mahalanobis distance.)

Classification/misclassification tables

Group 1: He1

Group 2: Hj1

From discriminant function:

True	Allocated to		
Group	Group 1	Group 2	Total
Group 1	2	0	2
Group 2	0	2	2

From cross-validation:

True	Allocated to		
Group	Group 1	Group 2	Total
Group 1	1	1	2
Group 2	0	2	2

Comparison: H<sub>j1</sub> -- H<sub>f3</sub>

Difference between means:

Procrustes distance: 0.19746428

Mahalanobis distance: 4.3062

T-square: 18.5438, P-value (parametric): 0.3120

P-values for permutation tests (1000 permutation runs):

Procrustes distance: 0.3340

T-square: 0.3340

(Note: The permutation test using the T-square statistic is equivalent to a test using Mahalanobis distance.)

Classification/misclassification tables

Group 1: H<sub>j1</sub>

Group 2: H<sub>f3</sub>

From discriminant function:

True	Allocated to		
Group	Group 1	Group 2	Total
Group 1	2	0	2
Group 2	0	2	2

From cross-validation:

True	Allocated to		
Group	Group 1	Group 2	Total
Group 1	2	0	2
Group 2	1	1	2

Comparison: H<sub>j1</sub> -- H<sub>f2</sub>

Difference between means:

Procrustes distance: 0.23223400

Mahalanobis distance: 1.4354

T-square: 2.0603, P-value (parametric): 0.7018

P-values for permutation tests (1000 permutation runs):

Procrustes distance: 0.3400

T-square: 0.6930

(Note: The permutation test using the T-square statistic is equivalent to a test using Mahalanobis distance.)

Classification/misclassification tables

Group 1: Hj1

Group 2: Hf2

From discriminant function:

True	Allocated to		
Group	Group 1	Group 2	Total
Group 1	2	0	2
Group 2	1	1	2

From cross-validation:

True	Allocated to		
Group	Group 1	Group 2	Total
Group 1	1	1	2
Group 2	2	0	2

### **Discriminant Function Analysis between specimens of humpback whale – rostrum-only configuration**

Comparison: Hf1 -- Hj1

Difference between means:

Procrustes distance: 0.22840536

Mahalanobis distance: 3.6416

T-square: 13.2612, P-value (parametric): 0.3620

P-values for permutation tests (1000 permutation runs):

Procrustes distance: 0.3410

T-square: 0.3410

(Note: The permutation test using the T-square statistic is equivalent to a test using Mahalanobis distance.)

Classification/misclassification tables

Group 1: Hf1

Group 2: Hj1

From discriminant function:

True	Allocated to		
Group	Group 1	Group 2	Total
Group 1	2	0	2
Group 2	0	2	2

From cross-validation:

True	Allocated to		
Group	Group 1	Group 2	Total
Group 1	2	0	2
Group 2	0	2	2

Comparison: He1 -- Hj1

Difference between means:

Procrustes distance: 0.28835696

Mahalanobis distance: 5.3144

T-square: 28.2429, P-value (parametric): 0.2572

P-values for permutation tests (1000 permutation runs):

Procrustes distance: 0.3210

T-square: 0.3210

(Note: The permutation test using the T-square statistic is equivalent to a test using Mahalanobis distance.)

Classification/misclassification tables

Group 1: He1

Group 2: Hj1

From discriminant function:

True Group	Allocated to		Total
	Group 1	Group 2	
Group 1	2	0	2
Group 2	0	2	2

From cross-validation:

True Group	Allocated to		Total
	Group 1	Group 2	
Group 1	2	0	2
Group 2	1	1	2

Comparison: Hj1 -- Hf4

Difference between means:

Procrustes distance: 0.13827637

Mahalanobis distance: 4.6321

T-square: 21.4561, P-value (parametric): 0.2920

P-values for permutation tests (1000 permutation runs):

Procrustes distance: 0.3260

T-square: 0.3260

(Note: The permutation test using the T-square statistic is equivalent to a test using Mahalanobis distance.)

Classification/misclassification tables

Group 1: Hj1

Group 2: Hf4

From discriminant function:

True Group	Allocated to		Total
	Group 1	Group 2	
Group 1	2	0	2
Group 2	0	2	2

From cross-validation:

True	Allocated to		
Group	Group 1	Group 2	Total
Group 1	1	1	2
Group 2	0	2	2

Comparison: H<sub>j1</sub> -- H<sub>f3</sub>

Difference between means:

Procrustes distance: 0.28525849

Mahalanobis distance: 2.9110

T-square: 8.4740, P-value (parametric): 0.4370

P-values for permutation tests (1000 permutation runs):

Procrustes distance: 0.3250

T-square: 0.3250

(Note: The permutation test using the T-square statistic is equivalent to a test using Mahalanobis distance.)

Classification/misclassification tables

Group 1: H<sub>j1</sub>

Group 2: H<sub>f3</sub>

From discriminant function:

True	Allocated to		
Group	Group 1	Group 2	Total
Group 1	2	0	2
Group 2	0	2	2

From cross-validation:

True	Allocated to		
Group	Group 1	Group 2	Total
Group 1	1	1	2
Group 2	0	2	2

Comparison: H<sub>j1</sub> -- H<sub>f2</sub>

Difference between means:

Procrustes distance: 0.15870574

Mahalanobis distance: 2.0564

T-square: 4.2288, P-value (parametric): 0.5666

P-values for permutation tests (1000 permutation runs):

Procrustes distance: 0.3160

T-square: 0.3160

(Note: The permutation test using the T-square statistic is equivalent to a test using Mahalanobis distance.)

Classification/misclassification tables

Group 1: Hj1

Group 2: Hf2

From discriminant function:

True	Allocated to		
Group	Group 1	Group 2	Total
Group 1	2	0	2
Group 2	0	2	2

From cross-validation:

True	Allocated to		
Group	Group 1	Group 2	Total
Group 1	0	2	2
Group 2	0	2	2

### **Discriminant Function Analysis between growth stages of minke whales – whole skull configuration**

Comparison: adult -- earlyFetus

Difference between means:

Procrustes distance: 0.15029277

Mahalanobis distance: 0.6226

T-square: 0.3877, P-value (parametric): 0.9152

P-values for permutation tests (1000 permutation runs):

Procrustes distance: 0.3410

T-square: 1.0000

(Note: The permutation test using the T-square statistic is equivalent to a test using Mahalanobis distance.)

Classification/misclassification tables

Group 1: adult

Group 2: earlyFetus

From discriminant function:

True	Allocated to		
Group	Group 1	Group 2	Total
Group 1	1	1	2
Group 2	0	2	2

From cross-validation:

True	Allocated to		
Group	Group 1	Group 2	Total
Group 1	1	1	2
Group 2	0	2	2

Comparison: adult -- lateFetus

Difference between means:

Procrustes distance: 0.08403352

Mahalanobis distance: 2.8946

T-square: 12.5682, P-value (parametric): 0.8585

P-values for permutation tests (1000 permutation runs):

Procrustes distance: 0.3950

T-square: 0.1710

(Note: The permutation test using the T-square statistic is equivalent to a test using Mahalanobis distance.)

Classification/misclassification tables

Group 1: adult

Group 2: lateFetus

From discriminant function:

True Group	Allocated to Group 1	Group 2	Total
Group 1	2	0	2
Group 2	0	6	6

From cross-validation:

True Group	Allocated to Group 1	Group 2	Total
Group 1	1	1	2
Group 2	2	4	6

Comparison: adult -- neonate

Difference between means:

Procrustes distance: 0.03777683

Mahalanobis distance: 0.3853

T-square: 0.1485, P-value (parametric): 0.9648

P-values for permutation tests (1000 permutation runs):

Procrustes distance: 1.0000

T-square: 1.0000

(Note: The permutation test using the T-square statistic is equivalent to a test using Mahalanobis distance.)

Classification/misclassification tables

Group 1: adult

Group 2: neonate

From discriminant function:

True Group	Allocated to Group 1	Group 2	Total
Group 1	1	1	2
Group 2	1	1	2

From cross-validation:

True	Allocated to		
Group	Group 1	Group 2	Total
Group 1	0	2	2
Group 2	1	1	2

Comparison: earlyFetus -- lateFetus

Difference between means:

Procrustes distance: 0.11133318

Mahalanobis distance: 2.9097

T-square: 12.6999, P-value (parametric): 0.8568

P-values for permutation tests (1000 permutation runs):

Procrustes distance: 0.1750

T-square: 0.2310

(Note: The permutation test using the T-square statistic is equivalent to a test using Mahalanobis distance.)

Classification/misclassification tables

Group 1: earlyFetus

Group 2: lateFetus

From discriminant function:

True	Allocated to		
Group	Group 1	Group 2	Total
Group 1	2	0	2
Group 2	0	6	6

From cross-validation:

True	Allocated to		
Group	Group 1	Group 2	Total
Group 1	0	2	2
Group 2	2	4	6

Comparison: earlyFetus -- neonate

Difference between means:

Procrustes distance: 0.14995491

Mahalanobis distance: 1.6604

T-square: 2.7570, P-value (parametric): 0.6484

P-values for permutation tests (1000 permutation runs):

Procrustes distance: 0.3160

T-square: 0.3160

(Note: The permutation test using the T-square statistic is equivalent to a test using Mahalanobis distance.)



Classification/misclassification tables

Group 1: earlyFetus

Group 2: neonate

From discriminant function:

True	Allocated to		
Group	Group 1	Group 2	Total
Group 1	2	0	2
Group 2	1	1	2

From cross-validation:

True	Allocated to		
Group	Group 1	Group 2	Total
Group 1	1	1	2
Group 2	2	0	2

Comparison: lateFetus -- neonate

Difference between means:

Procrustes distance: 0.07604568

Mahalanobis distance: 4.3198

T-square: 27.9916, P-value (parametric): 0.7000

P-values for permutation tests (1000 permutation runs):

Procrustes distance: 0.5320

T-square: 0.1170

(Note: The permutation test using the T-square statistic is equivalent to a test using Mahalanobis distance.)

Classification/misclassification tables

Group 1: lateFetus

Group 2: neonate

From discriminant function:

True	Allocated to		
Group	Group 1	Group 2	Total
Group 1	6	0	6
Group 2	0	2	2

From cross-validation:

True	Allocated to		
Group	Group 1	Group 2	Total
Group 1	6	0	6
Group 2	1	1	2

### **Discriminant Function Analysis between growth stages of minke whales – rostrum-only configuration**

Comparison: adult -- earlyFetus

Difference between means:

Procrustes distance: 0.16158639

Mahalanobis distance: 1.4641

T-square: 2.1436, P-value (parametric): 0.6947

P-values for permutation tests (1000 permutation runs):

Procrustes distance: 0.3310

T-square: 0.3310

(Note: The permutation test using the T-square statistic is equivalent to a test using Mahalanobis distance.)

Classification/misclassification tables

Group 1: adult

Group 2: earlyFetus

From discriminant function:

True	Allocated to		
Group	Group 1	Group 2	Total
Group 1	2	0	2
Group 2	1	1	2

From cross-validation:

True	Allocated to		
Group	Group 1	Group 2	Total
Group 1	2	0	2
Group 2	2	0	2

Comparison: adult -- lateFetus

Difference between means:

Procrustes distance: 0.07776725

Mahalanobis distance: 1.9123

T-square: 5.4855, P-value (parametric): 0.9572

P-values for permutation tests (1000 permutation runs):

Procrustes distance: 0.5790

T-square: 0.3990

(Note: The permutation test using the T-square statistic is equivalent to a test using Mahalanobis distance.)

Classification/misclassification tables

Group 1: adult

Group 2: lateFetus

From discriminant function:

True	Allocated to		
Group	Group 1	Group 2	Total
Group 1	2	0	2
Group 2	1	5	6

From cross-validation:

True	Allocated to		
Group	Group 1	Group 2	Total
Group 1	1	1	2
Group 2	4	2	6

Comparison: adult -- neonate

Difference between means:

Procrustes distance: 0.05370058

Mahalanobis distance: 0.7298

T-square: 0.5326, P-value (parametric): 0.8887

P-values for permutation tests (1000 permutation runs):

Procrustes distance: 1.0000

T-square: 1.0000

(Note: The permutation test using the T-square statistic is equivalent to a test using Mahalanobis distance.)

Classification/misclassification tables

Group 1: adult

Group 2: neonate

From discriminant function:

True	Allocated to		
Group	Group 1	Group 2	Total
Group 1	1	1	2
Group 2	0	2	2

From cross-validation:

True	Allocated to		
Group	Group 1	Group 2	Total
Group 1	0	2	2
Group 2	1	1	2

Comparison: earlyFetus -- lateFetus

Difference between means:

Procrustes distance: 0.11892149

Mahalanobis distance: 2.5843

T-square: 10.0180, P-value (parametric): 0.8932

P-values for permutation tests (1000 permutation runs):

Procrustes distance: 0.1820

T-square: 0.3570

(Note: The permutation test using the T-square statistic is equivalent to a test using Mahalanobis distance.)

Classification/misclassification tables

Group 1: earlyFetus

Group 2: lateFetus

From discriminant function:

True	Allocated to		
Group	Group 1	Group 2	Total
Group 1	2	0	2
Group 2	1	5	6

From cross-validation:

True	Allocated to		
Group	Group 1	Group 2	Total
Group 1	0	2	2
Group 2	1	5	6

Comparison: earlyFetus -- neonate

Difference between means:

Procrustes distance: 0.17076361

Mahalanobis distance: 2.3686

T-square: 5.6103, P-value (parametric): 0.5126

P-values for permutation tests (1000 permutation runs):

Procrustes distance: 0.3290

T-square: 0.3290

(Note: The permutation test using the T-square statistic is equivalent to a test using Mahalanobis distance.)

Classification/misclassification tables

Group 1: earlyFetus

Group 2: neonate

From discriminant function:

True	Allocated to		
Group	Group 1	Group 2	Total
Group 1	2	0	2
Group 2	0	2	2

From cross-validation:

True	Allocated to		
Group	Group 1	Group 2	Total
Group 1	1	1	2
Group 2	1	1	2

Comparison: lateFetus – neonate

Difference between means:

Procrustes distance: 0.08545708

Mahalanobis distance: 2.8131

T-square: 11.8705, P-value (parametric): 0.8678

P-values for permutation tests (1000 permutation runs):

Procrustes distance: 0.5210

T-square: 0.1400

(Note: The permutation test using the T-square statistic is equivalent to a test using Mahalanobis distance.)

Classification/misclassification tables

Group 1: lateFetus

Group 2: neonate

From discriminant function:

True	Allocated to		
Group	Group 1	Group 2	Total
Group 1	6	0	6
Group 2	0	2	2

From cross-validation:

True	Allocated to		
Group	Group 1	Group 2	Total
Group 1	3	3	6
Group 2	1	1	2

## Appendix D: Supplementary Tables/Figures for Chapter Two

Table S2.1 – Detailed external measurements of the specimens of humpback whale less than 100 cm and minke whales less than 120 cm in TL, as in Lanzetti et al. (2018) and Lanzetti (in press). All measurements in cm.

	He1	Hf1	Hf2	Hf3	Mf1	Mf2	Mf3	Mf4	Mf5	Mf6	Mf7
Sex	U	M	F	M	F	M	M	M	F	F	M
<i>Total length</i>	17	31	239	70	28	41	48	74	110	110	115
<i>Distance tip of snout to blowhole</i>	1.5	4.5	5	7.6	4	6	5	9	16	13	15.5
<i>eye</i>	3	7	7.5	12	5.5	7.5	9	15	20	23	25.5
<i>Lower jaw length</i>	3	6	8.5	13	5.5	7.5	10	15	23	24	28
<i>width (max)</i>	2	3.3	5	9.3	4.25	7	7	12	20	21	24
<i>Circumference at blowhole</i>	5.21	5.5	13	23	9.5	14	23	27.5	58	51	60
<i>Flipper</i>											
<i>anterior length</i>	2.6	7.5	8	12.5	4	4.75	6	9.5	14	18.5	18.5
<i>width at body</i>	0.7	1.5	1.5	3	1	2.5	2.5	4	4	5	4.5
<i>Fluke</i>											
<i>anterior length</i>	1.2	5.5	6.5	13.5	4.5	8.5	10	17	19	30	24

Table S2.2 – PCA principal components for both configurations for the “by specimen” dataset. Components ordered according to the amount of variation they represent, from largest to smallest.

<u>Whole skull configuration</u>		<u>Rostrum-only configuration</u>	
Principal Component	% Total Variance	Principal Component	% Total Variance
PC1	51.732	PC1	62.937
PC2	22.850	PC2	17.370
PC3	10.246	PC3	6.614
PC4	7.671	PC4	5.262
PC5	3.424	PC5	2.941
PC6	1.374	PC6	2.180
PC7	1.285	PC7	1.310
PC8	0.660	PC8	0.692
PC9	0.349	PC9	0.320
PC10	0.254	PC10	0.223
PC11	0.156	PC11	0.151

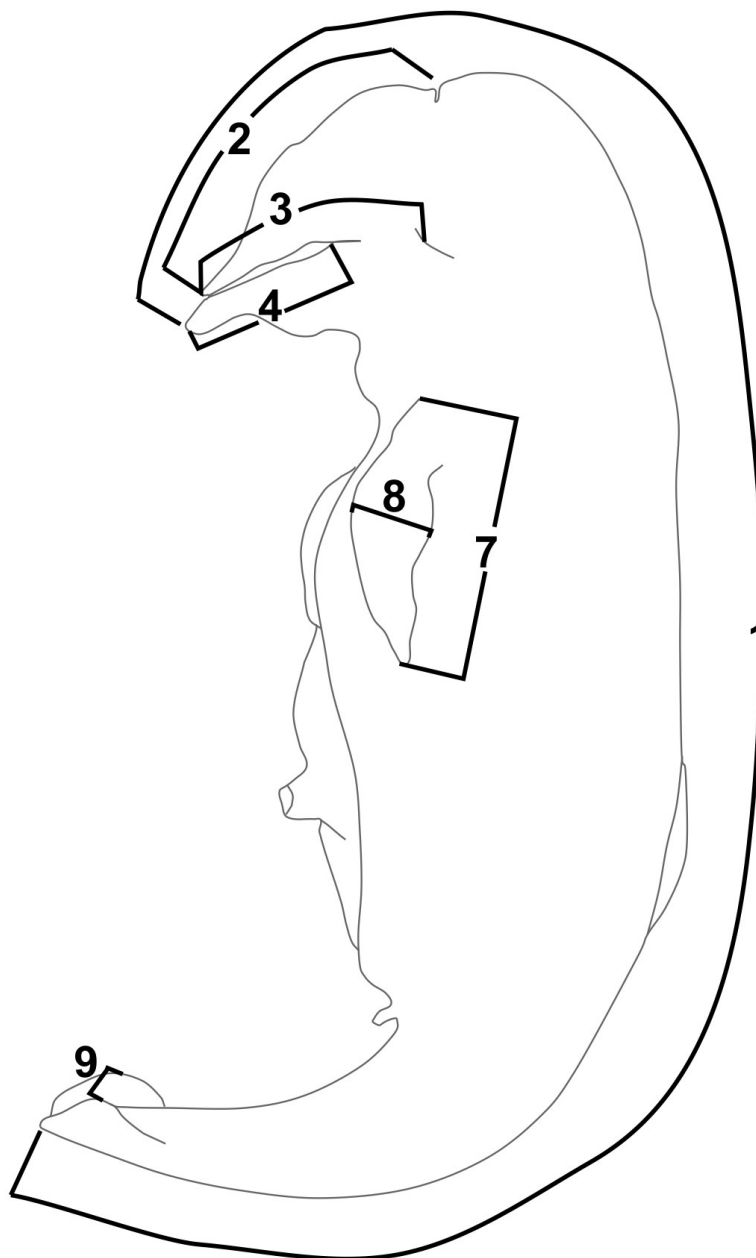


Figure S2.1 – Measurements taken on specimens less than 1 m/1.21 m in length, 1: total length (TL), 2: distance tip of snout to blowhole, 3: distance tip of snout to eye, 4: lower jaw length, 5: lower jaw width, 6: circumference at blowhole, 7: flipper length (anterior), 8: flipper width at body, 9: fluke length (anterior). Measurement 5 and 6 not figured. Measurement 9 was taken while flattening the fluke from the left to the right tip. Measurements selected from Durham (1980), figure modified from Sterba et al. (2000). From Lanzetti et al. (2018).

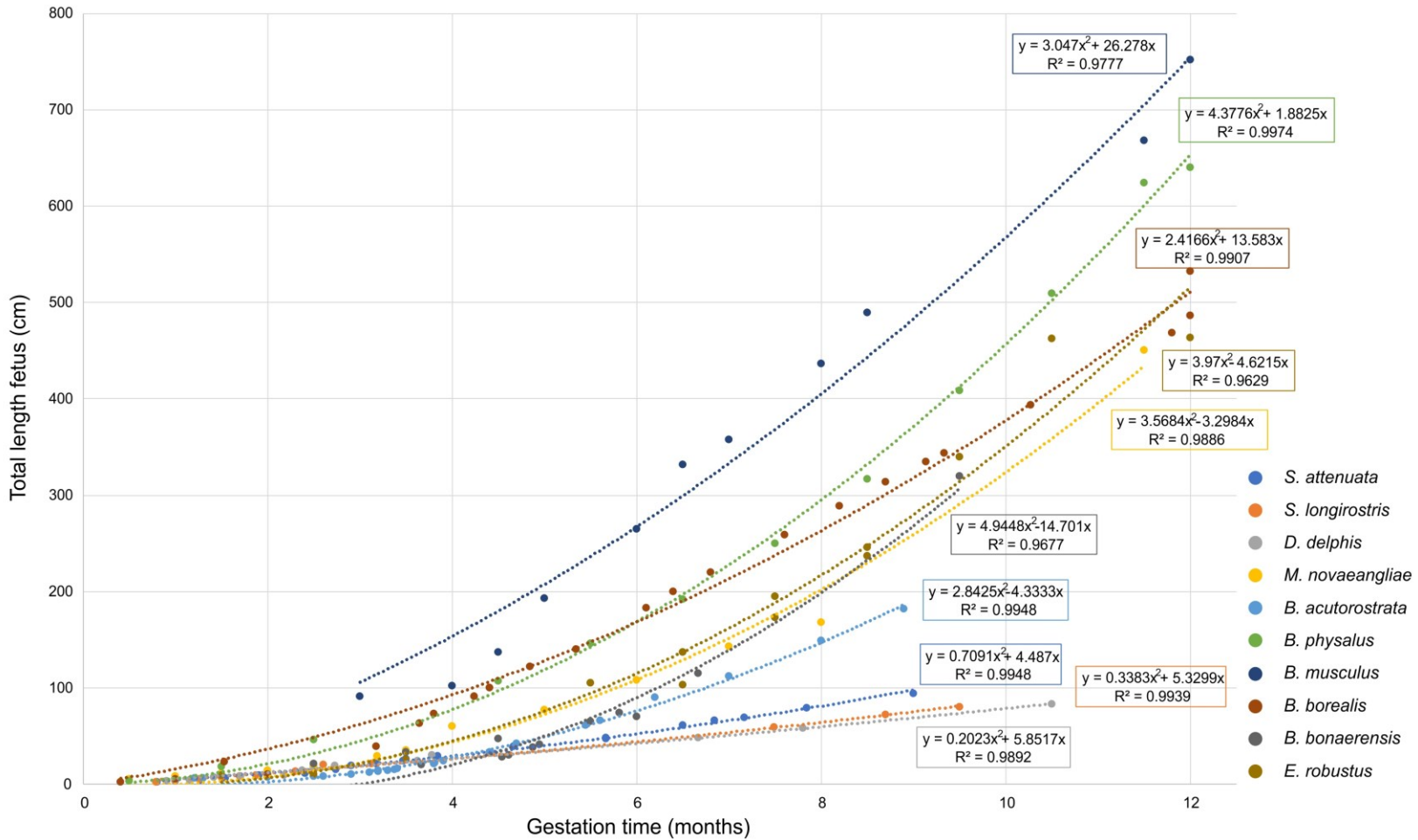


Figure S2.2 – Calculated growth trajectories, using total length (cm) and estimated gestational age (months), for seven mysticetes species and three dolphin species. Circles=specimens used to build the curve for each species. Equations and R<sup>2</sup> values are reported for each species on the graph. Data sources listed in Appendix C.



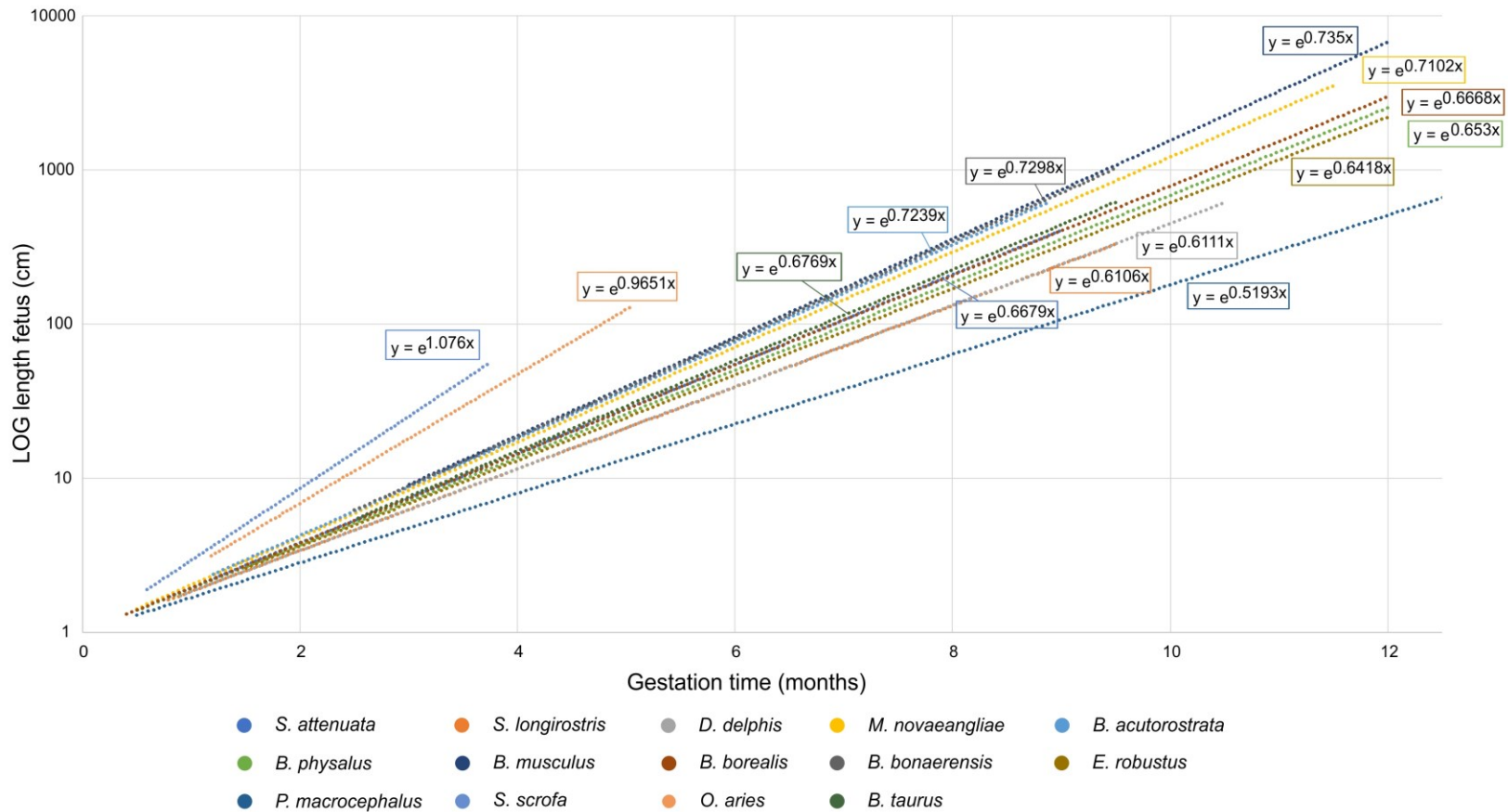


Figure S2.3 – Calculated growth rates, using the LOG-transformed length (cm) and estimated gestational age (months), for seven mysticetes species, four odontocete species, and three terrestrial artiodactyls. Equations indicating the growth rate for each species are presented on the chart. Data sources listed in Appendix C.

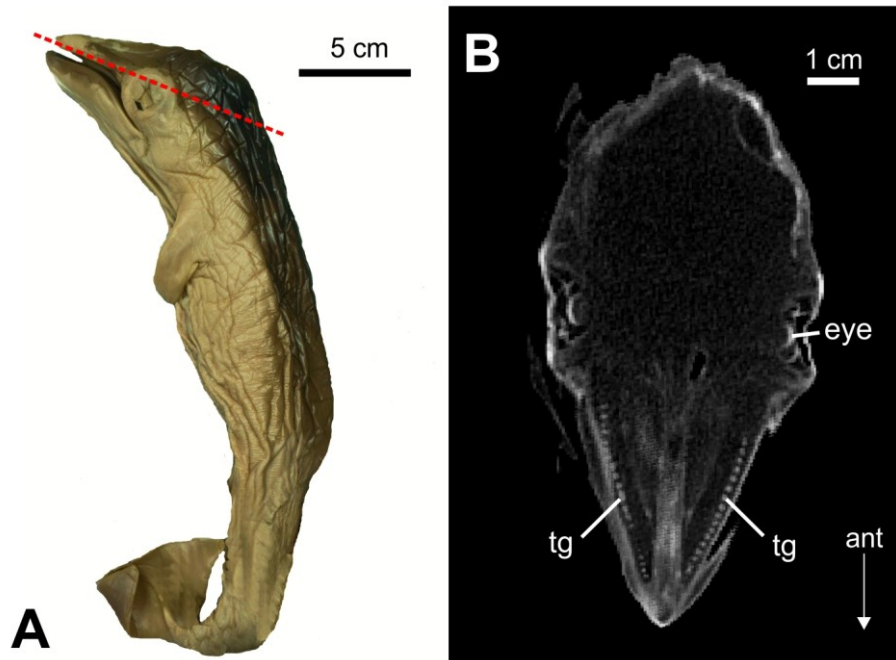


Figure S2.4 – Mf2 (NSMT27149; TL 41 cm) external morphology and longitudinal CT image of the rostrum A: left lateral view of external morphology, B: CT slice of longitudinal section of rostrum of Mf2. Red dashed line in A represents CT slice location and orientation. tg: tooth germs. Form Lanzetti (in press).

Figure S2.5 (next page) – Hf3 (SDNHM25552, TL 70cm) external and internal morphology, A: left lateral view, B: left lateral view of 3D rendering of the internal morphology, C: head in dorsal view, D: head in ventral view, E: head in right dorso-lateral view, F: head in postero-ventral view. Ossified skull bones in yellow, tooth germs in red, nasal bones in green, ossified postcranial elements in purple. Ossified elements and tooth germs are labeled in the figures. Abbreviations for Figures S2.5-S2.9: b, baleen; bhy, basihyoid; bo, basioccipital; br, baleen rudiments; bs, basisphenoid; cp, coronoid process (dentary); d, dentary (=mandibular rami); dif, dorsal infraorbital foramina; ect, ectotympanic; eo, exoccipital; f, frontal; h, humerus; hy, indeterminate hyoid elements; ip, infraorbital process (maxilla); j, jugal; inp, interparietal; l, lacrimal; m, maxilla; ms, mandibular symphysis; n, nasal; p, parietal; pe, pelvic elements; pg, postglenoid process (squamosal); ph, phalanges; pl, palatine; plp, palatine process (maxilla); pm, premaxilla; pt, pterygoid; ra, radius; rc, rib cage; sc, scapula; shy, stylohyoid; so, supraoccipital; sop, supraorbital process (frontal); sq, squamosal; tg, tooth germs; thy, thyrohyoid; ul, ulna; v, vomer; vr, vertebrae; zp, zygomatic process (squamosal). From Lanzetti et al. (2018).

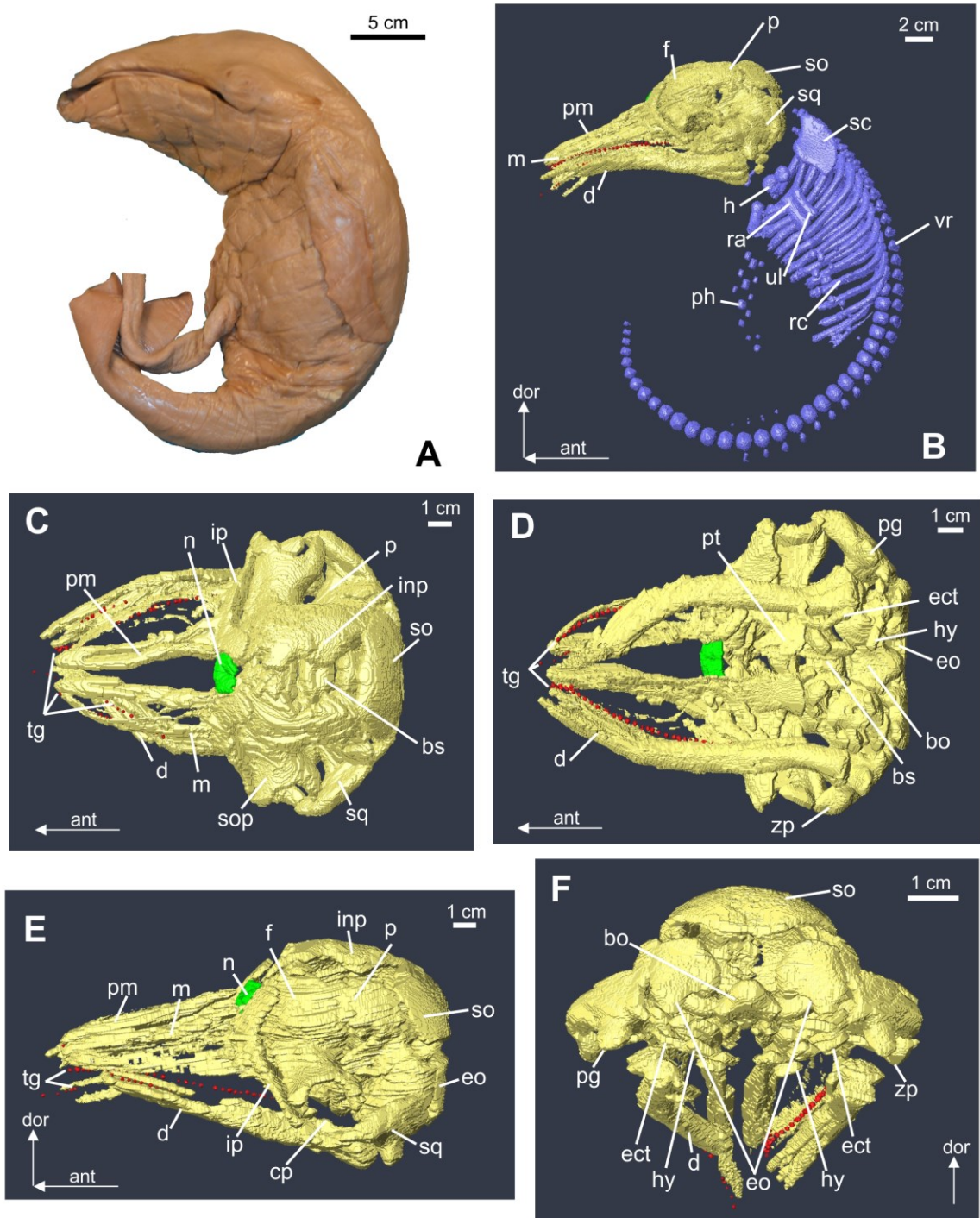


Figure S2.5 – Hf3 (SDNHM25552, TL 70cm) external and internal morphology Complete caption previous page.

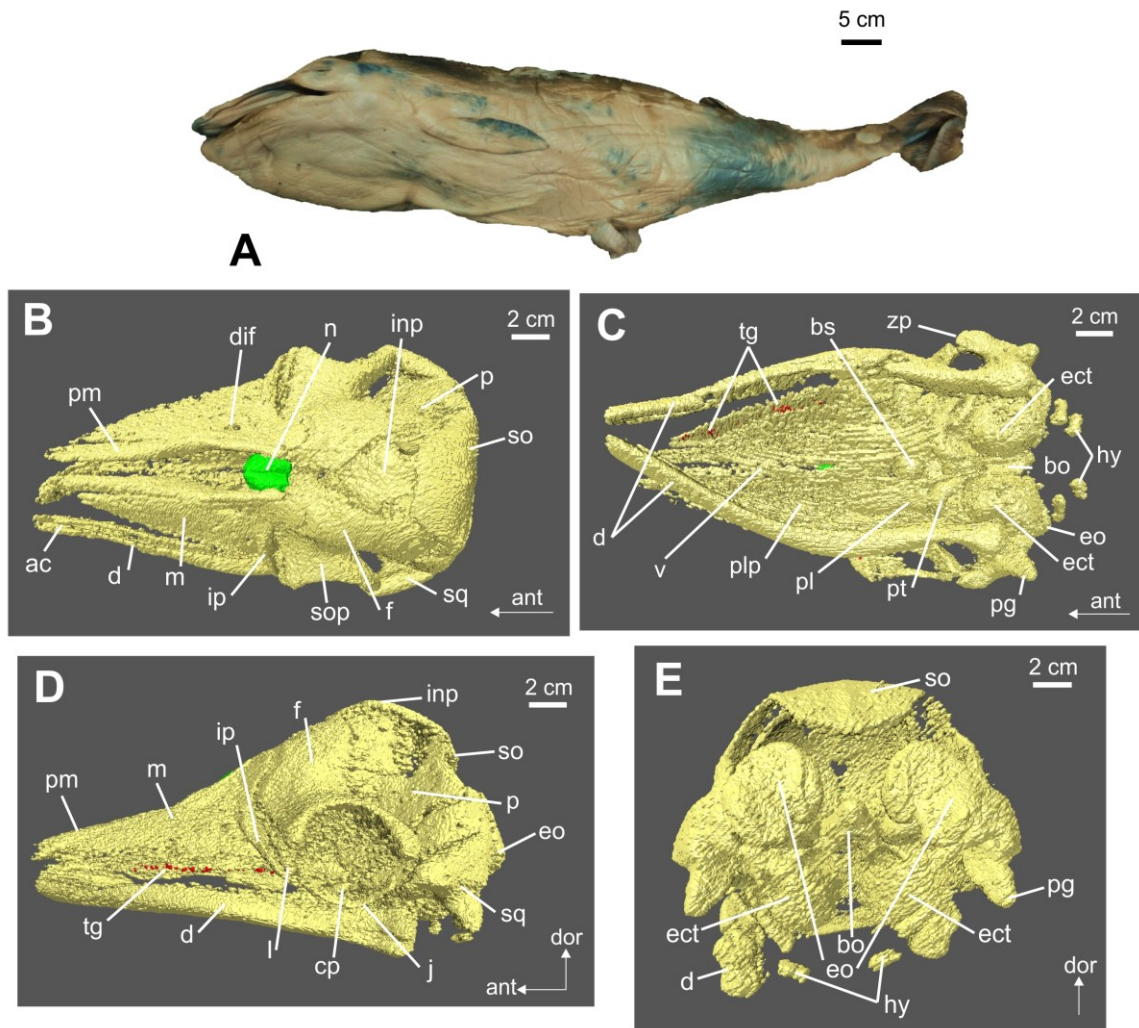


Figure S2.6 – Mf4 (NSMTblue10, TL 72 cm) external and internal morphology. A: left lateral view of external morphology, B: dorsal view of 3D rendering of the internal morphology of head, C: head in ventral view, D: head in left lateral view, E: head in postero-ventral view. Ossified skull bones in yellow, nasal bones in green, tooth germs in red. Ossified elements and tooth germs are labeled in the figures. Abbreviations listed in page 366 (Fig. S2.5). Form Lanzetti (in press).



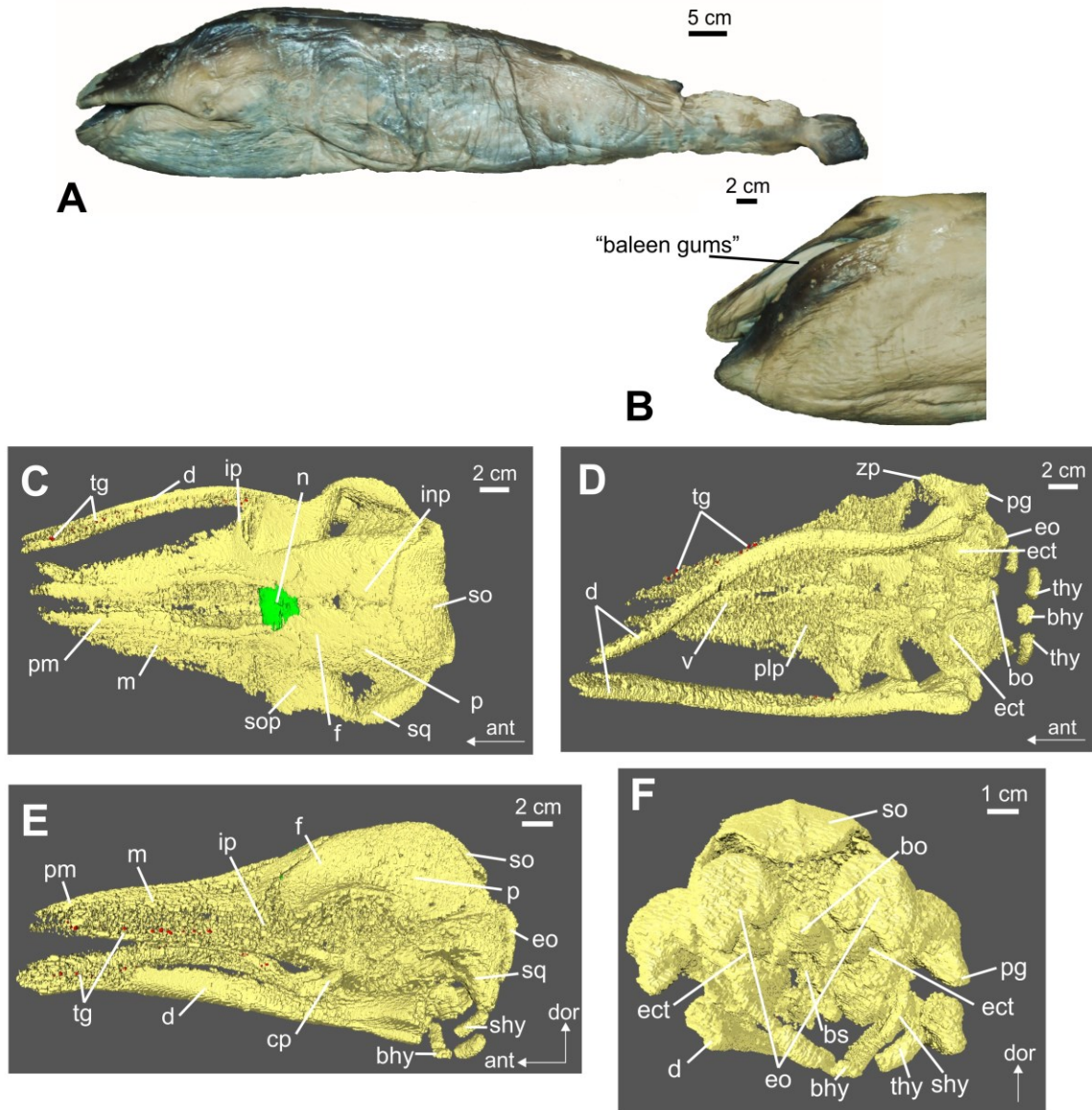


Figure S2.7 – Mf5 (TzMwhite11, TL 110 cm) external and internal morphology, A: left lateral view of external morphology, B: left lateral close-up view of head, C: cross section of 3D rendering of internal morphology of head, D: head in dorsal view, E: head in ventral view, F: head in left lateral view, G: head in postero-ventral view. Ossified skull bones in yellow, nasal bones in green, tooth germs in red. Ossified elements and tooth germs are labeled in the figures. Abbreviations listed in page 366 (Fig. S2.5). Form Lanzetti (in press).

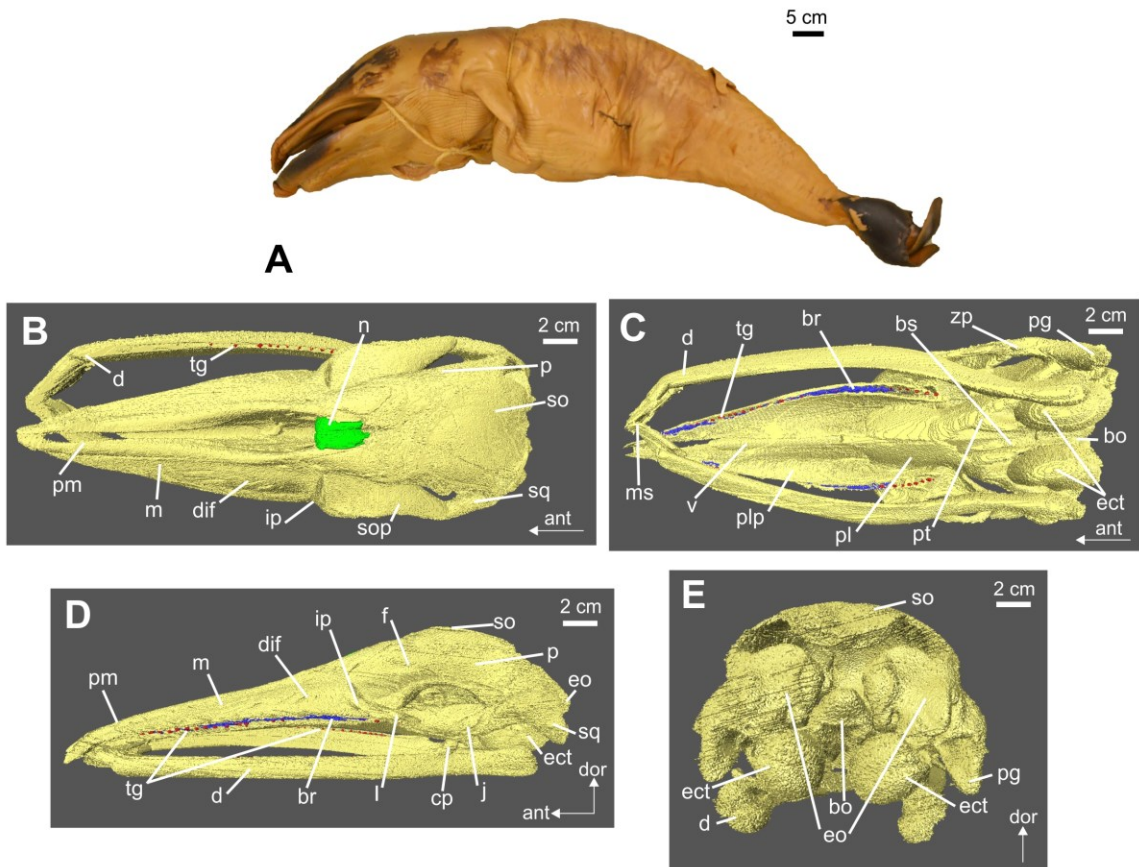


Figure S2.8 – Mf8 (ZMCU-CN4x; TL 125 cm) external and internal morphology, A: left lateral view of external morphology, B: dorsal view of 3D rendering of internal morphology of head, C: head in ventral view, D: head in left lateral view, E: head in postero-ventral view. Ossified skull bones in yellow, nasal bones in green, tooth germs in red. Ossified elements and tooth germs are labeled in the figures. Abbreviations listed in page 366 (Fig. S2.5). Form Lanzetti (in press).

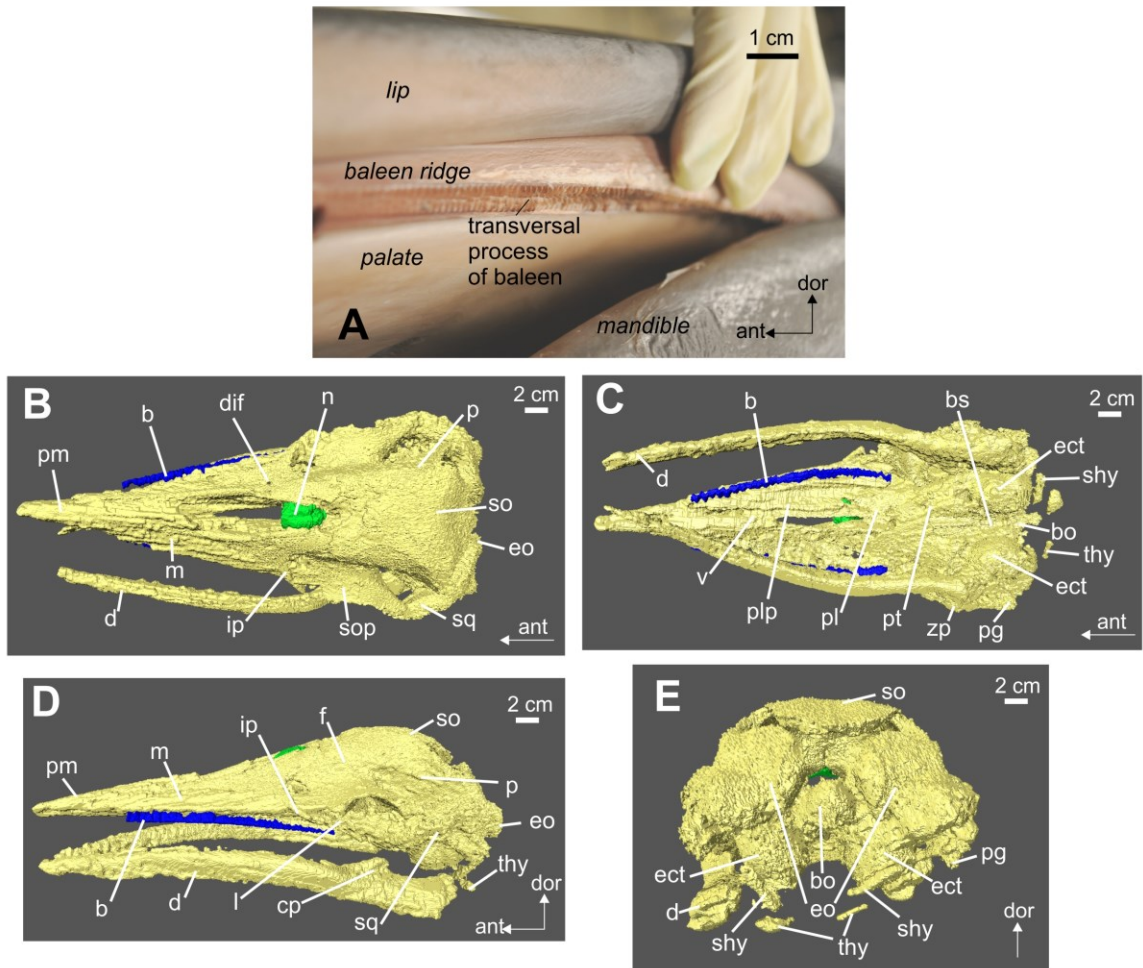


Figure S2.9 – Mf9 (TMZ27175; TL 182 cm) external and internal morphology, A: close-up view of baleen ridge, B: dorsal view of 3D rendering of internal morphology of head, C: head in ventral view, D: head in left lateral view, D: head in postero-ventral view. Ossified skull bones in yellow, nasal bones in green, baleen in blue. Ossified elements and baleen are labeled in the figures. Abbreviations listed in page 366 (Fig. S2.5). Form Lanzetti (in press).

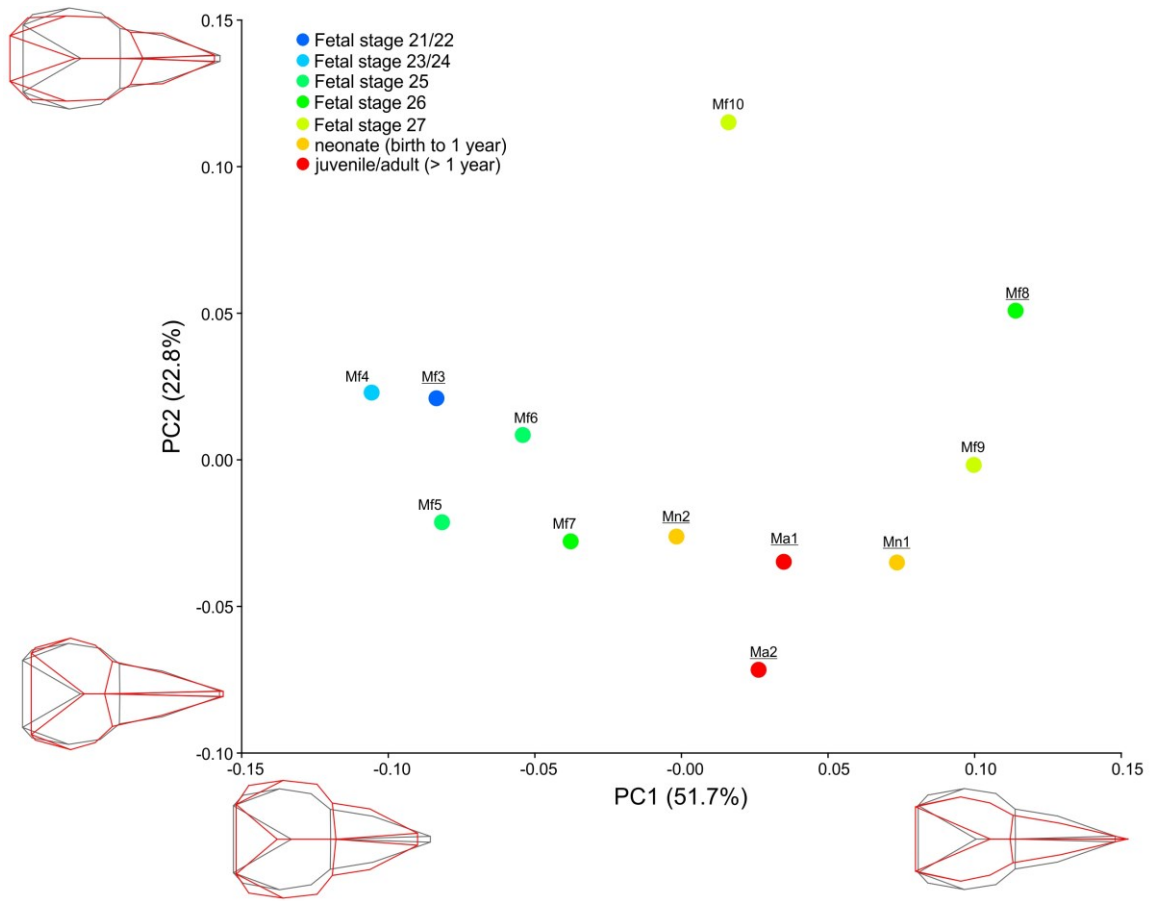


Figure S2.10 – PCA plot for the whole skull configuration of the “by specimen” dataset. Average shape at 0 on both axes in light gray wireframe, shape at maximum and minimum values of axes in red wireframe. Specimens colored according to developmental stage. Specimens codes as in Table 2.1, with common minke whale samples underlined.



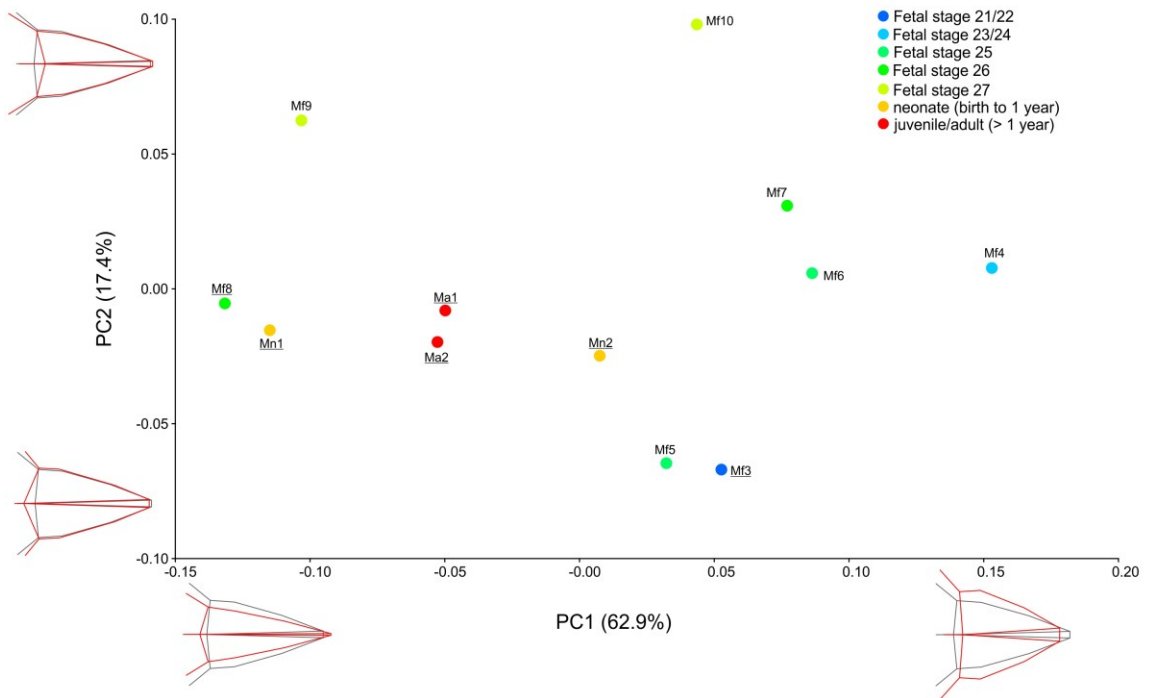


Figure S2.11 – PCA plot for the rostrum-only configuration of the “by specimen” dataset. Average shape at 0 on both axes in light gray wireframe, shape at maximum and minimum values of axes in red wireframe. Specimens colored according to developmental stage. Specimens codes as in Table 2.1, with common minke whale samples underlined.

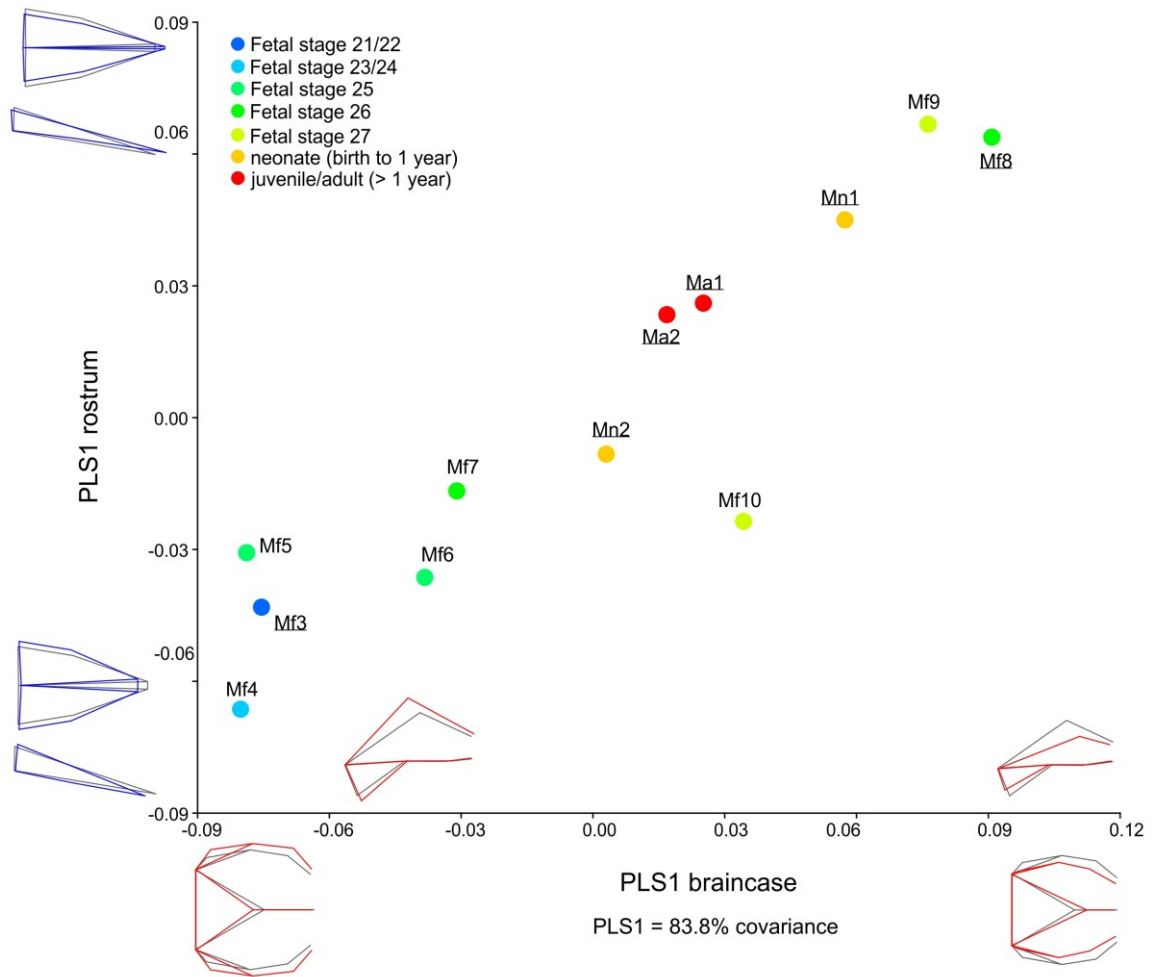


Figure S2.12 – PLS1 analysis plot, comparing scores from the two partitions (rostrum and braincase), for the “by specimen” dataset. Average shape at 0 on both axes in light gray wireframe. Shape at maximum and minimum values of Y axes in blue wireframe (rostrum) and of X axes in red (braincase). Specimens colored according to developmental stage. Specimens codes as in Table 2.1, with common minke whale samples underlined.

## Appendix E: Supplementary Methods/Results for Chapter Three

### Procrustes ANOVA between landmarks takes – whole skull configuration

This analysis takes into account the object symmetry in the data.

Classifiers used for the Procrustes ANOVA:

Individuals: From dataset

Centroid size:

Effect	SS	MS	df	F	P (param.)
Individual	18.847965	18.847965	1	0.00	<b>0.9953</b>
Residual	27125529.404	542510.5881	50		

Shape, Procrustes ANOVA:

Effect	SS	MS	df	F	P (param.)
Individual	0.00192779	0.0000917995	21	0.91	0.5821
Side	0.00309941	0.0001549704	20	1.54	0.1706
Ind * Side	0.00201099	0.0001005493	20	0.15	<b>1.0000</b>
Residual	1.36801728	0.0006673255	2050		

Shape, MANOVA tests of effects:

Symmetric component of shape variation:

Effect	Pillai tr.	P (param.)
Individual	0.21	<b>0.9866</b>

Note: the test for 'Individual' used the symmetric component of the residual as the 'error' effect.

Asymmetry component of shape variation:

Effect	Pillai tr.	P (param.)
Ind * Side	0.37	0.5817

### Procrustes ANOVA between landmarks takes – rostrum-only configuration

This analysis takes into account the object symmetry in the data.

Classifiers used for the Procrustes ANOVA:

Individuals: From dataset

Centroid size:

Effect	SS	MS	df	F	P (param.)
Individual	1.310317	1.310317	1	0.00	<b>0.9982</b>
Residual	12825442.533192	246643.125638	52		

Shape, Procrustes ANOVA:

Effect	SS	MS	df	F	P (param.)
Individual	0.00321749	0.0002144996	15	2.50	0.0470
Side	0.00728288	0.0005202058	14	6.07	0.0009
Ind * Side	0.00119896	0.0000856400	14	0.10	<b>1.0000</b>
Residual	1.33100843	0.0008826316	1508		

Shape, MANOVA tests of effects:

Symmetric component of shape variation:

Effect	Pillai tr.	P (param.)
Individual	0.10	<b>0.9955</b>

Note: the test for 'Individual' used the symmetric component of the residual as the 'error' effect.

Asymmetry component of shape variation:

Effect	Pillai tr.	P (param.)
Ind * Side	0.19	0.7891

**Relative timing of onset of ossification (ranks) in the cranial elements and teeth for all species examined.**

Species	Reference	1	2	3	4	5	6	7	8	9	10	11	12	13	14	15	16	17	18	19*	rmax
<i>Bos taurus</i>	Koyabu et al. (2014)	3	1	1	2	4	3	3	4	3	3	3	7	3	4	7	4	6	8	1	8
<i>Camelus dromedarius</i>	Kanan (1962)	1	1	1	1	1	1	1	1	1	1	1	3	1	2	1	2	1	5	4	5
<i>Capra hircus</i>	Koyabu et al. (2014)	1	1	1	2	7	1	5	3	1	4	2	6	4	6	8	6	5	8	1	8
<i>Capreolus capreolus</i>	Koyabu et al. (2014)	5	1	1	1	5	4	3	2	2	4	4	6	5	6	7	6	5	6	7	7
<i>Dama dama</i>	Koyabu et al. (2014)	2	2	1	2	2	2	2	2	2	2	2	2	2	2	2	2	2	2	3	3
<i>Megaptera novaeangliae</i>	This study	1	1	1	1	2	2	3	2	2	1	1	2	2	3	2	3	1	4	1	4
<i>Ovis aries</i>	Harris (1937)	4	1	1	3	8	3	7	4	5	?	3	6	?	6	7	6	7	7	1	8
<i>Physeter macrocephalus</i>	Kuzmin (1976)	1	1	2	1	3	1	2	1	2	2	1	2	1	2	1	2	2	4	2	4
<i>Stenella attenuata</i>	Moran, et al. (2011)	1	1	1	1	4	3	2	1	1	3	1	3	1	3	1	3	3	5	4	5
<i>Sus scrofa</i>	Hodges (1953)	2	4	1	3	6	3	6	5	6	?	?	?	?	7	8	6	7	12	3	12

1: Premaxilla; 2: Maxilla; 3: Dentary; 4: Frontal; 5: Nasal; 6: Jugal; 7: Lacrimal; 8: Parietal; 9: Squamosal; 10: Vomer; 11: Palatine; 12: Basisphenoid; 13: Pterygoid; 14: Basisoccipital; 15: Supraoccipital; 16: Exoccipital; 17: Ectotympanic; 18: Petrosal; 19: Teeth\*; rmax: max number of ranks for the species. *D. dama* is in gray as it was not possible to use it following analyses as rmax=3.

377

\*Sources for teeth mineralization, with notes

<i>B. taurus</i>	Soana et al. (1997)	
<i>C. dromedarius</i>	Kanan (1962)	
<i>Ca. hircus</i>	Witter and Misek (1999), Witter et al. (2003)	estimated based on <i>O. aries</i>
<i>Cap. capreolus</i>	Short (1970), Kierdorf et al. (2012)	estimated based on <i>D.dama</i> , <i>Odocoileus virginianus</i> and <i>Od. hemionus</i>
<i>D. dama</i>	Kierdorf et al. (2012)	
<i>M. novaeangliae</i>	This study	
<i>O. aries</i>	Witter and Misek (1999), Witter et al. (2003)	
<i>P. macrocephalus</i>	Nishiwaki et al. (1963)	
<i>S. attenuata</i>	Moran et al. (2011)	
<i>Sus scrofa</i>	Bivin and Mc Clure (1976)	

### **Complete sources for teeth mineralization**

**Bivin WS, Mc Clure RC** (1976) Deciduous tooth chronology in the mandible of the domestic pig. *J Dent Res*, **55**, 591-597.

**Kanan CV** (1962) Observations on the development of the osteocranium in *Camelus dromedarius*. *Acta Zool*, **43**, 297-310.

**Kierdorf H, Hommelsheim S, Kierdorf U** (2012) Development of the permanent mandibular cheek teeth in fallow deer (*Dama dama*). *Anat Histol Embryol*, **41**, 419-427.

**Moran MM, Nummela S, Thewissen JGM** (2011) Development of the skull of the pantropical spotted dolphin (*Stenella attenuata*). *Anat Rec*, **294**, 1743-1756.

**Nishiwaki M, Ohsumi S, Maeda Y** (1963) Change of form in the sperm whale accompanied with growth. Whales Research Institute of Tokyo, 1-17.

**Short C** (1970) Morphological development and aging of mule and white-tailed deer fetuses. *J Wildl Manage*, **34**, 383-388.

**Soana S, Bertoni G, Gnudi G, Botti P** (1997) Anatomo-radiographic study of prenatal development of bovine fetal teeth. *Anat Histol Embryol*, **26**, 107-113.

**Witter K, Matulova P, Misek I** (2003) Three-dimensional reconstruction studies and morphometric analysis of rudimental tooth primordia in the upper incisor region of the sheep (*Ovis aries*, Ruminantia). *Arch Oral Biol*, **48**, 15-24.

**Witter K, Misek I** (1999) Time programme of the early tooth development in the domestic sheep (*Ovis aries*, Ruminantia). *Acta Vet Brno*, **68**, 3-8.

**Matrix of transformed ranks and EQ values for the taxa examined used in the ASR analyses**

Species	1	2	3	4	5	6	7	8	9	10	11	12	13	14	15	16	17	18	19	20
<i>B. taurus</i>	0.29	0.00	0.00	0.14	0.43	0.29	0.29	0.43	0.29	0.29	0.29	0.86	0.29	0.43	0.86	0.43	0.71	1.00	0.00	-0.39
<i>C. dromedarius</i>	0.00	0.00	0.00	0.00	0.00	0.00	0.00	0.00	0.00	0.00	0.00	0.50	0.00	0.25	0.00	0.25	0.00	1.00	0.75	-0.05
<i>Ca. hircus</i>	0.00	0.00	0.00	0.14	0.86	0.00	0.57	0.29	0.00	0.43	0.14	0.71	0.43	0.71	1.00	0.71	0.57	1.00	0.00	-0.14
<i>Cap. capreolus</i>	0.67	0.00	0.00	0.00	0.67	0.50	0.33	0.17	0.17	0.50	0.50	0.83	0.67	0.83	1.00	0.83	0.67	0.83	1.00	-0.22
<i>M. novaeangliae</i>	0.00	0.00	0.00	0.00	0.33	0.33	0.67	0.33	0.33	0.00	0.00	0.33	0.33	0.67	0.33	0.67	0.00	1.00	0.00	-0.59
<i>O. aries</i>	0.43	0.00	0.00	0.29	1.00	0.29	0.86	0.43	0.57	?	0.29	0.71	?	0.71	0.86	0.71	0.86	0.86	0.00	-0.02
<i>P. macrocephalus</i>	0.00	0.00	0.33	0.00	0.67	0.00	0.33	0.00	0.33	0.33	0.00	0.33	0.00	0.33	0.00	0.33	0.33	1.00	0.33	-0.42
<i>S. attenuata</i>	0.00	0.00	0.00	0.00	0.75	0.50	0.25	0.00	0.00	0.50	0.00	0.50	0.00	0.50	0.00	0.50	0.50	1.00	0.75	0.55
<i>Sus scrofa</i>	0.09	0.27	0.00	0.18	0.45	0.18	0.45	0.36	0.45	?	?	?	?	0.55	0.64	0.45	0.55	1.00	0.18	-0.15

1: Premaxilla; 2: Maxilla; 3: Dentary; 4: Frontal; 5: Nasal; 6: Jugal; 7: Lacrimal; 8: Parietal; 9: Squamosal; 10: Vomer; 11: Palatine; 12: Basisphenoid; 13: Pterygoid; 14: Basisoccipital; 15: Supraoccipital; 16: Exoccipital; 17: Ectotympanic; 18: Petrosal; 19: Teeth\*; 20: EQ (Encephalization Quotient – brain size relative to body mass in adults)

### **Brownian motion model test**

*Absolute value of contrast vs. standard deviation – PDAP (Midford et al., 2005)*

2-tailed test p-value of the analysis for each character indicates fit of the model to the data: significant values ( $p < 0.05$ ) indicate lack of fit.

#### Maxilla (character 2)

X Axis - Square root of sum of corrected branch lengths  
Y Axis - Maxilla (Absolute value of standardized contrast (Maxilla))  
Number of data points: 8  
Minimum of X,Y coordinates: 5.966573556070519, 0.0  
Maximum of X,Y coordinates: 9.402009444831176, 0.028901571194077956  
Mean of X,Y coordinates: 7.665177944634213, 0.004590540856150941  
Variance of X,Y coordinates: 1.8846512975327734, 1.0398740010147004E-4  
Covariance: 0.008864446051150164  
Pearson Product-Moment Correlation Coefficient: 0.6332070437767767  
Reduced Major Axis.  
Slope: 0.0074280506450531405  
Y Intercept: -0.052346789119936336  
Major Axis.  
Slope: 0.00470364945664374  
Y Intercept: -0.03146376921820536  
Least Squares Regression.  
Slope: 0.004703493989978279  
Intercept: -0.03146257753855013  
R Squared: 0.40095116028852484  
t: 2.003965529168819  
F: 4.015877842096865  
d.f.: 6  
p-value:  
**2-tailed: 0.09191984468025294**  
1-tailed: 0.04595992234012647

#### Dentary (character 3)

X Axis - Square root of sum of corrected branch lengths  
Y Axis - Dentary (Absolute value of standardized contrast (Dentary))  
Number of data points: 8  
Minimum of X,Y coordinates: 5.966573556070519, 0.0  
Maximum of X,Y coordinates: 9.402009444831176, 0.04260281680828159  
Mean of X,Y coordinates: 7.665177944634213, 0.011040130532244109  
Variance of X,Y coordinates: 1.8846512975327734, 2.271324586207767E-4  
Covariance: 0.0028472187685122446  
Pearson Product-Moment Correlation Coefficient: 0.13761498683160928



Reduced Major Axis.

Slope: 0.010978022007933672

Y Intercept: -0.07310836163867808

Major Axis.

Slope: 0.0015109189966008541

Y Intercept: -5.413324366296147E-4

Least Squares Regression.

Slope: 0.0015107403540589224

Intercept: -5.399631097572682E-4

R Squared: 0.018937884600663993

t: 0.3403244140278737

F: 0.11582070678341562

d.f.: 6

p-value:

**2-tailed: 0.7452110625968429**

1-tailed: 0.37260553129842144

### Supraoccipital (character15)

X Axis - Square root of sum of corrected branch lengths

Y Axis - Supraoccipital (Absolute value of standardized contrast (Supraoccipital))

Number of data points: 8

Minimum of X,Y coordinates: 5.966573556070519, 0.0

Maximum of X,Y coordinates: 9.402009444831176, 0.09262647277953089

Mean of X,Y coordinates: 7.665177944634213, 0.032591854618904834

Variance of X,Y coordinates: 1.8846512975327734, 9.67614117078284E-4

Covariance: 0.01842991664143722

Pearson Product-Moment Correlation Coefficient: 0.43157548676927737

Reduced Major Axis.

Slope: 0.022658731545424908

Y Intercept: -0.14109135467647366

Major Axis.

Slope: 0.009783039963449827

Y Intercept: -0.04239688754040588

Least Squares Regression.

Slope: 0.00977895309629112

Intercept: -0.04236556097639842

R Squared: 0.18625740078013872

t: 1.171895450719398

F: 1.373338947416821

d.f.: 6

p-value:

**2-tailed: 0.28566157075735665**

1-tailed: 0.14283078537867833

### Teeth (character19)

X Axis - Square root of sum of corrected branch lengths  
Y Axis - Teeth (Absolute value of standardized contrast (Teeth))  
Number of data points: 7  
Minimum of X,Y coordinates: 6.48074069840786, 0.0  
Maximum of X,Y coordinates: 9.410291104903319, 0.1543033499620919  
Mean of X,Y coordinates: 8.041166831187919, 0.05031718260290791  
Variance of X,Y coordinates: 1.3775405111288797, 0.002918169871534713  
Covariance: -0.04055408190020717  
Pearson Product-Moment Correlation Coefficient: -0.6396274588019856  
Reduced Major Axis.  
Slope: -0.04602598534656334  
Y Intercept: 0.42041980934443424  
Major Axis.  
Slope: -0.029476347840374922  
Y Intercept: 0.28734141316148837  
Least Squares Regression.  
Slope: -0.02943948404607989  
Intercept: 0.28704498524153094  
R Squared: 0.40912328605348575  
t: -1.8606456163709135  
F: 3.462002109720297  
d.f.: 5  
p-value:  
**2-tailed: 0.12186962151823402**  
1-tailed: 0.06093481075911701

### EQ (character 20)

X Axis - Square root of sum of corrected branch lengths  
Y Axis - EQ (Absolute value of standardized contrast (EQ))  
Number of data points: 8  
Minimum of X,Y coordinates: 5.966573556070519, 0.0024194058100441072  
Maximum of X,Y coordinates: 9.402009444831176, 0.12522646152737313  
Mean of X,Y coordinates: 7.665177944634213, 0.03983136036915785  
Variance of X,Y coordinates: 1.8846512975327734, 0.0023354993145301337  
Covariance: -0.013913601908180473  
Pearson Product-Moment Correlation Coefficient: -0.20971727080469538  
Reduced Major Axis.  
Slope: -0.035202569790466896  
Y Intercept: 0.3096653219214914  
Major Axis.  
Slope: -0.007391343043562948  
Y Intercept: 0.09648732004790209  
Least Squares Regression.  
Slope: -0.007382586861768516  
Intercept: 0.09642020235633195

R Squared: 0.04398133367376993  
t: -0.5253837505752775  
F: 0.27602808536854545  
d.f.: 6  
p-value:  
**2-tailed: 0.6181575482391901**  
1-tailed: 0.30907877411959506

### **Felsenstein's phylogenetic independent contrasts**

*X positivized contrasts vs. Y contrasts – PDAP (Midford et al., 2005)*

2-tailed test p-value of the analysis of the contrasts for each pair of characters indicates if the variation at internal nodes in state of the two characters are significantly correlated ( $p < 0.05$ ).

#### Teeth vs. Maxilla (ch.19 vs. ch. 2)

X Axis - Teeth (Positivized Contrasts - CAUTION if any values are zero)  
Y Axis - Maxilla (Contrasts Positivized on the X variable (Garland et al.1992))  
Number of contrasts: 8  
Minimum of X,Y coordinates: 0.0, -0.028901571194077956  
Maximum of X,Y coordinates: 0.15943513555149275, 0.0  
Mean of X,Y coordinates: zero, zero  
Variance of X,Y coordinates: 0.005281827371570752,1.2807090336088833E-4  
Covariance: -1.1859005901796538E-4  
Pearson Product-Moment Correlation Coefficient: -0.14418860739239375  
Reduced Major Axis. Slope: -0.1557159626701496  
Y Intercept: zero  
Major Axis.  
Slope: -0.022998241224990734  
Y Intercept: zero  
Least Squares Regression.  
Slope: -0.02245246780617484  
Intercept: zero  
R Squared: 0.020790354501757865  
t: -0.38551575034697555  
F: 0.14862239376559158  
d.f.: 7  
p-value:  
2-tailed: 0.7113029955330821  
1-tailed: 0.35565149776654104  
Number of Y contrasts > 0 : 0  
Number of Y contrasts < 0 : 2  
Number of Y contrasts = 0 : 6  
**Sign test 2-tailed : 0.5**  
1-tailed : 0.25

Teeth vs. Dentary (ch.19 vs. ch. 3)

X Axis - Teeth (Positivized Contrasts - CAUTION if any values are zero)  
Y Axis - Dentary (Contrasts Positivized on the X variable (Garland et al.1992))  
Number of contrasts: 8  
Minimum of X,Y coordinates: 0.0, -0.04260281680828159  
Maximum of X,Y coordinates: 0.15943513555149275, 0.02342842566269143  
Mean of X,Y coordinates: zero, zero  
Variance of X,Y coordinates: 0.005281827371570752, 3.6642900967104954E-4  
Covariance: -7.898753530278874E-5  
Pearson Product-Moment Correlation Coefficient: -0.05677688171383026  
Reduced Major Axis. Slope: -0.26339214736675814  
Y Intercept: zero  
Major Axis.  
Slope: -0.01606525929210373  
Y Intercept: zero  
Least Squares Regression.  
Slope: -0.014954584795394174  
Intercept: zero  
R Squared: 0.003223614297146273  
t: -0.1504602178448511  
F: 0.022638277153920052  
d.f.: 7  
p-value:  
2-tailed: 0.8846453516917382  
1-tailed: 0.4423226758458691  
Number of Y contrasts > 0 : 3  
Number of Y contrasts < 0 : 2  
Number of Y contrasts = 0 : 3  
**Sign test 2-tailed :1.0**  
1-tailed : 0.5

EQ vs. Supraoccipital (ch. 20 vs. ch.15)

X Axis - EQ (Positivized Contrasts - CAUTION if any values are zero)  
Y Axis - Supraoccipital (Contrasts Positivized on the X variable (Garland et al.1992))  
Number of contrasts: 8  
Minimum of X,Y coordinates: 0.0024194058100441072, -0.09262647277953089  
Maximum of X,Y coordinates: 0.12522646152737313, 0.013319968217292899  
Mean of X,Y coordinates: zero, zero  
Variance of X,Y coordinates: 0.004148684764653241, 0.0021815901027923733  
Covariance: -8.360216069365232E-4  
Pearson Product-Moment Correlation Coefficient: -0.2778917836666328  
Reduced Major Axis. Slope: -0.7251558570548715  
Y Intercept: zero  
Major Axis.  
Slope: -0.367579165108212  
Y Intercept: zero

Least Squares Regression.

Slope: -0.20151485455328405

Intercept: zero

R Squared: 0.07722384342942265

t: -0.7653790035528318

F: 0.5858050190795258

d.f.: 7

p-value:

2-tailed: 0.4690606264505922

1-tailed: 0.2345303132252961

Number of Y contrasts > 0 : 2

Number of Y contrasts < 0 : 5

Number of Y contrasts = 0 : 1

**Sign test 2-tailed : 0.4531250000000001**

1-tailed : 0.22656250000000006

**Heterochrony analysis of developmental sequences – parsimony ACCTRAN  
(PAUP\* – Swofford, 2003)**

Tree description:

Optimality criterion = parsimony

Character-status summary:

Of 19 total characters:

All characters are of type 'unord'

All characters have equal weight

5 characters are parsimony-uninformative

Number of parsimony-informative characters = 14

Gaps are treated as "missing"

Character-state optimization: Accelerated transformation (ACCTRAN)

AncStates = "standard"

Tree length = 82

Consistency index (CI) = 0.8171

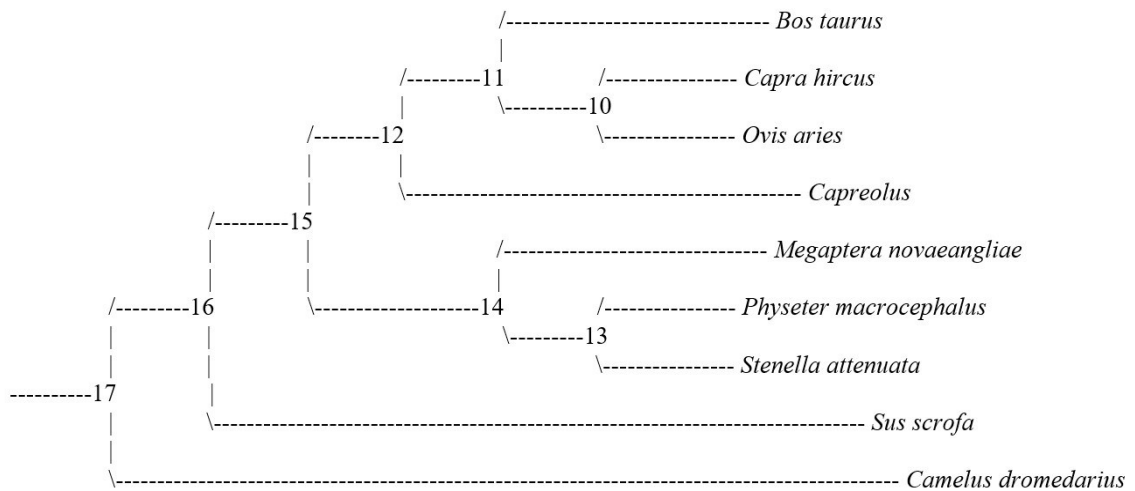
Homoplasy index (HI) = 0.1829

CI excluding uninformative characters = 0.7692

HI excluding uninformative characters = 0.2308

Retention index (RI) = 0.4444

Rescaled consistency index (RC) = 0.3631



Apomorphy lists:

Branch	Character	Steps	CI	Change
node_17 --> node_16	5 (Nasal)	1	1.000	1 --> 4
	6 (Jugal)	1	0.600	1 --> 3
	7 (Lacrimal)	1	1.000	1 --> 3
	8 (Parietal)	1	0.800	1 --> 2
	9 (Squamosal)	1	0.667	1 --> 2
	14 (Basioccipital)	1	0.800	2 --> 3
node_16 --> node_15	16 (Exoccipital)	1	0.750	2 --> 6
	18 (Petrosal)	1	0.833	1 --> 4
node_15 --> node_12	10 (Vomer)	1	0.750	1 ==> 4
	11 (Palatine)	1	1.000	1 --> 3
	12 (Basisphenoid)	1	0.750	2 --> 6
	13 (Pterygoid)	1	1.000	1 --> 3
	14 (Basioccipital)	1	0.800	3 --> 6
	15 (Supraoccipital)	1	0.750	1 ==> 7
	17 (Ectotympanic)	1	0.833	1 ==> 5
	18 (Petrosal)	1	0.833	4 --> 6
node_12 --> node_11	4 (Frontal)	1	0.667	1 ==> 2
	8 (Parietal)	1	0.800	2 --> 4
	9 (Squamosal)	1	0.667	2 --> 1
node_11 --> <i>Bos taurus</i>	18 (Petrosal)	1	0.833	6 --> 8
	1 (Premaxilla)	1	1.000	1 ==> 3
	9 (Squamosal)	1	0.667	1 --> 3
	10 (Vomer)	1	0.750	4 ==> 3
	12 (Basisphenoid)	1	0.750	6 ==> 7
	14 (Basioccipital)	1	0.800	6 ==> 4
node_11 --> node_10	16 (Exoccipital)	1	0.750	6 ==> 4
	17 (Ectotympanic)	1	0.833	5 ==> 6
	5 (Nasal)	1	1.000	4 --> 7
	7 (Lacrimal)	1	1.000	3 --> 5
node_10 --> <i>Capra hircus</i>	13 (Pterygoid)	1	1.000	3 --> 4
	6 (Jugal)	1	0.600	3 ==> 1
	8 (Parietal)	1	0.800	4 ==> 3
node_10 --> <i>Ovis aries</i>	11 (Palatine)	1	1.000	3 ==> 2
	15 (Supraoccipital)	1	0.750	7 ==> 8
	1 (Premaxilla)	1	1.000	1 ==> 4
	4 (Frontal)	1	0.667	2 ==> 3
	5 (Nasal)	1	1.000	7 --> 8
node_10 --> <i>Ovis aries</i>	7 (Lacrimal)	1	1.000	5 --> 7
	9 (Squamosal)	1	0.667	1 --> 5
	17 (Ectotympanic)	1	0.833	5 ==> 7
	18 (Petrosal)	1	0.833	8 ==> 7
	1 (Premaxilla)	1	1.000	1 ==> 5
	5 (Nasal)	1	1.000	4 ==> 5
node_12 --> <i>Capreolus capreolus</i>	6 (Jugal)	1	0.600	3 ==> 4
	11 (Palatine)	1	1.000	3 --> 4
	13 (Pterygoid)	1	1.000	3 --> 5
	19 (Teeth)	1	0.600	1 --> 7
	16 (Exoccipital)	1	0.750	6 ==> 3
node_15 --> node_14	16 (Exoccipital)	1	0.750	6 ==> 3
node_14 --> <i>Megaptera novaeangliae</i>	5 (Nasal)	1	1.000	4 ==> 2

	6 (Jugal)	1	0.600	3 ==> 2
	13 (Pterygoid)	1	1.000	1 ==> 2
	15 (Supraoccipital)	1	0.750	1 ==> 2
node_14 --> node_13	7 (Lacrimal)	1	1.000	3 ==> 2
	8 (Parietal)	1	0.800	2 --> 1
	10 (Vomer)	1	0.750	1 --> 2
	17 (Ectotympanic)	1	0.833	1 --> 2
	19 (Teeth)	1	0.600	1 --> 2
node_13 --> <i>Physeter macrocephalus</i>	3 (Dentary)	1	1.000	1 ==> 2
	5 (Nasal)	1	1.000	4 ==> 3
	6 (Jugal)	1	0.600	3 ==> 1
	14 (Basioccipital)	1	0.800	3 --> 2
	16 (Exoccipital)	1	0.750	3 ==> 2
node_13 --> <i>Stenella attenuata</i>	9 (Squamosal)	1	0.667	2 --> 1
	10 (Vomer)	1	0.750	2 --> 3
	12 (Basisphenoid)	1	0.750	2 --> 3
	17 (Ectotympanic)	1	0.833	2 --> 3
	18 (Petrosal)	1	0.833	4 --> 5
	19 (Teeth)	1	0.600	2 --> 4
node_16 --> <i>Sus scrofa</i>	1 (Premaxilla)	1	1.000	1 ==> 2
	2 (Maxilla)	1	1.000	1 ==> 4
	4 (Frontal)	1	0.667	1 ==> 3
	5 (Nasal)	1	1.000	4 --> 6
	7 (Lacrimal)	1	1.000	3 --> 6
	8 (Parietal)	1	0.800	2 --> 5
	9 (Squamosal)	1	0.667	2 --> 6
	14 (Basioccipital)	1	0.800	3 --> 7
	15 (Supraoccipital)	1	0.750	1 ==> 8
	17 (Ectotympanic)	1	0.833	1 ==> 7
	19 (Teeth)	1	0.600	1 --> 2
node_17 --> <i>Camelus dromedarius</i>	12 (Basisphenoid)	1	0.750	2 --> 3
	18 (Petrosal)	1	0.833	1 --> 5
	19 (Teeth)	1	0.600	1 --> 4



**Heterochrony analysis of developmental sequences – parsimony DELTRAN  
(PAUP\* – Swofford, 2003)**

Tree description:

Optimality criterion = parsimony

Character-status summary:

Of 19 total characters:

All characters are of type 'unord'

All characters have equal weight

5 characters are parsimony-uninformative

Number of parsimony-informative characters = 14

Gaps are treated as "missing"

Character-state optimization: Delayed transformation (DELTRAN)

AncStates = "standard"

Tree length = 82

Consistency index (CI) = 0.8171

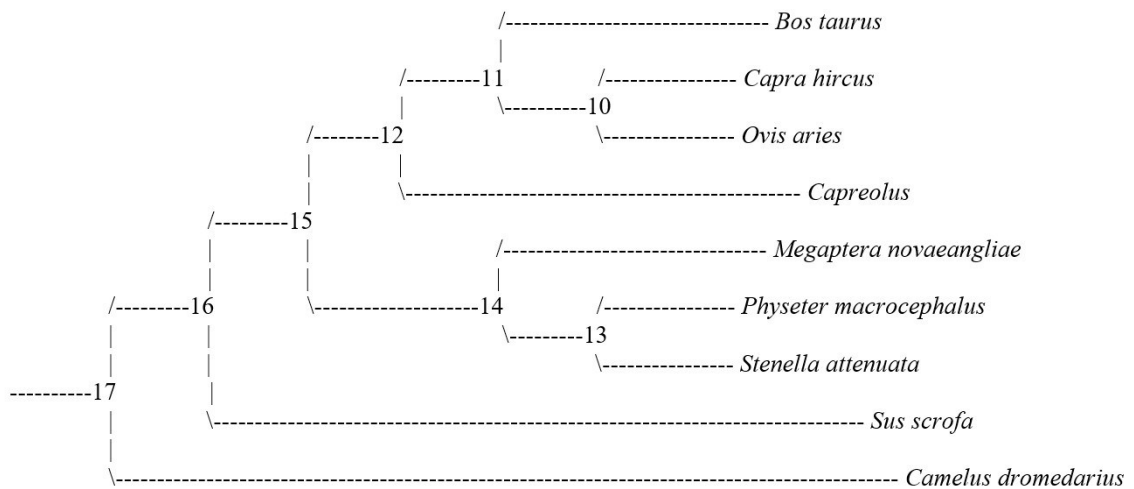
Homoplasy index (HI) = 0.1829

CI excluding uninformative characters = 0.7692

HI excluding uninformative characters = 0.2308

Retention index (RI) = 0.4444

Rescaled consistency index (RC) = 0.3631



Apomorphy lists:

Branch	Character	Steps	CI	Change
node_17 --> node_16	6 (Jugal)	1	0.600	1 --> 3
	16 (Exoccipital)	1	0.750	2 --> 6
node_16 --> node_15	5 (Nasal)	1	1.000	1 --> 4
	7 (Lacrimal)	1	1.000	1 --> 3
node_15 --> node_12	10 (Vomer)	1	0.750	1 ==> 4
	12 (Basisphenoid)	1	0.750	2 --> 6
	14 (Basioccipital)	1	0.800	2 --> 6
	15 (Supraoccipital)	1	0.750	1 ==> 7
	17 (Ectotympanic)	1	0.833	1 ==> 5
node_12 --> node_11	4 (Frontal)	1	0.667	1 ==> 2
	8 (Parietal)	1	0.800	1 --> 4
	11 (Palatine)	1	1.000	1 --> 3
	18 (Petrosal)	1	0.833	1 --> 8
node_11 --> <i>Bos taurus</i>	1 (Premaxilla)	1	1.000	1 ==> 3
	9 (Squamosal)	1	0.667	1 --> 3
	10 (Vomer)	1	0.750	4 ==> 3
	12 (Basisphenoid)	1	0.750	6 ==> 7
	13 (Pterygoid)	1	1.000	1 --> 3
	14 (Basioccipital)	1	0.800	6 ==> 4
	16 (Exoccipital)	1	0.750	6 ==> 4
	17 (Ectotympanic)	1	0.833	5 ==> 6
node_10 --> <i>Capra hircus</i>	5 (Nasal)	1	1.000	4 --> 7
	6 (Jugal)	1	0.600	3 ==> 1
	7 (Lacrimal)	1	1.000	3 --> 5
	8 (Parietal)	1	0.800	4 ==> 3
	11 (Palatine)	1	1.000	3 ==> 2
	13 (Pterygoid)	1	1.000	1 --> 4
	15 (Supraoccipital)	1	0.750	7 ==> 8
	17 (Ectotympanic)	1	0.833	5 ==> 6
node_10 --> <i>Ovis aries</i>	1 (Premaxilla)	1	1.000	1 ==> 4
	4 (Frontal)	1	0.667	2 ==> 3
	5 (Nasal)	1	1.000	4 --> 8
	7 (Lacrimal)	1	1.000	3 --> 7
	9 (Squamosal)	1	0.667	1 --> 5
	17 (Ectotympanic)	1	0.833	5 ==> 7
	18 (Petrosal)	1	0.833	8 ==> 7
	19 (Teeth)	1	0.600	1 --> 7
node_12 --> <i>Capreolus capreolus</i>	1 (Premaxilla)	1	1.000	1 ==> 5
	5 (Nasal)	1	1.000	4 ==> 5
	6 (Jugal)	1	0.600	3 ==> 4
	8 (Parietal)	1	0.800	1 --> 2
	9 (Squamosal)	1	0.667	1 --> 2
	11 (Palatine)	1	1.000	1 --> 4
	13 (Pterygoid)	1	1.000	1 --> 5
	18 (Petrosal)	1	0.833	1 --> 6
node_15 --> node_14	16 (Exoccipital)	1	0.750	6 ==> 3
	18 (Petrosal)	1	0.833	1 --> 4
node_14 --> <i>Megaptera novaeangliae</i>	5 (Nasal)	1	1.000	4 ==> 2
	6 (Jugal)	1	0.600	3 ==> 2

	8 (Parietal)	1	0.800	1 --> 2
	9 (Squamosal)	1	0.667	1 --> 2
	13 (Pterygoid)	1	1.000	1 ==> 2
	14 (Basioccipital)	1	0.800	2 --> 3
	15 (Supraoccipital)	1	0.750	1 ==> 2
node_14 --> node_13	7 (Lacrimal)	1	1.000	3 ==> 2
node_13 --> <i>Physeter macrocephalus</i>	3 (Dentary)	1	1.000	1 ==> 2
	5 (Nasal)	1	1.000	4 ==> 3
	6 (Jugal)	1	0.600	3 ==> 1
	9 (Squamosal)	1	0.667	1 --> 2
	10 (Vomer)	1	0.750	1 --> 2
	16 (Exoccipital)	1	0.750	3 ==> 2
	17 (Ectotympanic)	1	0.833	1 --> 2
	19 (Teeth)	1	0.600	1 --> 2
node_13 --> <i>Stenella attenuata</i>	10 (Vomer)	1	0.750	1 --> 3
	12 (Basisphenoid)	1	0.750	2 --> 3
	14 (Basioccipital)	1	0.800	2 --> 3
	17 (Ectotympanic)	1	0.833	1 --> 3
	18 (Petrosal)	1	0.833	4 --> 5
	19 (Teeth)	1	0.600	1 --> 4
node_16 --> <i>Sus scrofa</i>	1 (Premaxilla)	1	1.000	1 ==> 2
	2 (Maxilla)	1	1.000	1 ==> 4
	4 (Frontal)	1	0.667	1 ==> 3
	5 (Nasal)	1	1.000	1 --> 6
	7 (Lacrimal)	1	1.000	1 --> 6
	8 (Parietal)	1	0.800	1 --> 5
	9 (Squamosal)	1	0.667	1 --> 6
	14 (Basioccipital)	1	0.800	2 --> 7
	15 (Supraoccipital)	1	0.750	1 ==> 8
	17 (Ectotympanic)	1	0.833	1 ==> 7
	19 (Teeth)	1	0.600	1 --> 2
node_17 --> <i>Camelus dromedarius</i>	12 (Basisphenoid)	1	0.750	2 --> 3
	18 (Petrosal)	1	0.833	1 --> 5
	19 (Teeth)	1	0.600	1 --> 4

**Similarity of developmental sequences – parsimony ACCTRAN/DELTRAN  
(PAUP\* – Swofford, 2003)**

Heuristic search settings:

Optimality criterion = parsimony

Character-status summary:

Of 19 total characters:

All characters are of type 'unord'

All characters have equal weight

5 characters are parsimony-uninformative

Number of parsimony-informative characters = 14

Gaps are treated as "missing"

Starting tree(s) obtained via stepwise addition

Addition sequence: simple (reference taxon = *Camelus dromedarius*)

Number of trees held at each step = 1

Branch-swapping algorithm: tree-bisection-reconnection (TBR) with reconnection limit = 8

Steepest descent option not in effect

Initial 'Maxtrees' setting = 100

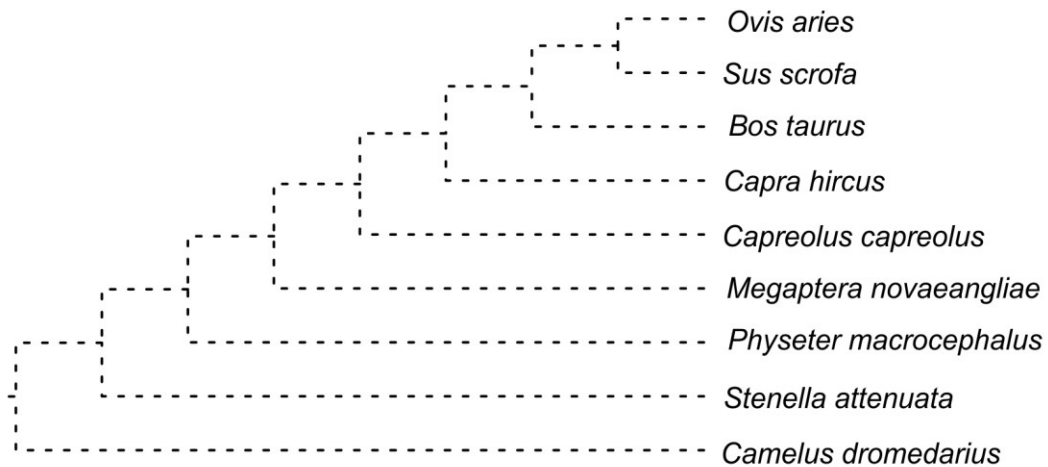
Branches collapsed (creating polytomies) if maximum branch length is zero

'MulTrees' option in effect

No topological constraints in effect

Trees are unrooted

Character-state optimization: Accelerated transformation (ACCTRAN)



Tree length = 74

Consistency index (CI) = 0.9054

Homoplasy index (HI) = 0.0946

CI excluding uninformative characters = 0.8772

HI excluding uninformative characters = 0.1228

Retention index (RI) = 0.7407

Rescaled consistency index (RC) = 0.6707

Heuristic search settings:

Optimality criterion = parsimony

Character-status summary:

Of 19 total characters:

All characters are of type 'unord'

All characters have equal weight

5 characters are parsimony-uninformative

Number of parsimony-informative characters = 14

Gaps are treated as "missing"

Starting tree(s) obtained via stepwise addition

Addition sequence: simple (reference taxon = *Camelus dromedarius*)

Number of trees held at each step = 1

Branch-swapping algorithm: tree-bisection-reconnection (TBR) with reconnection limit = 8

Steepest descent option not in effect

Initial 'Maxtrees' setting = 100

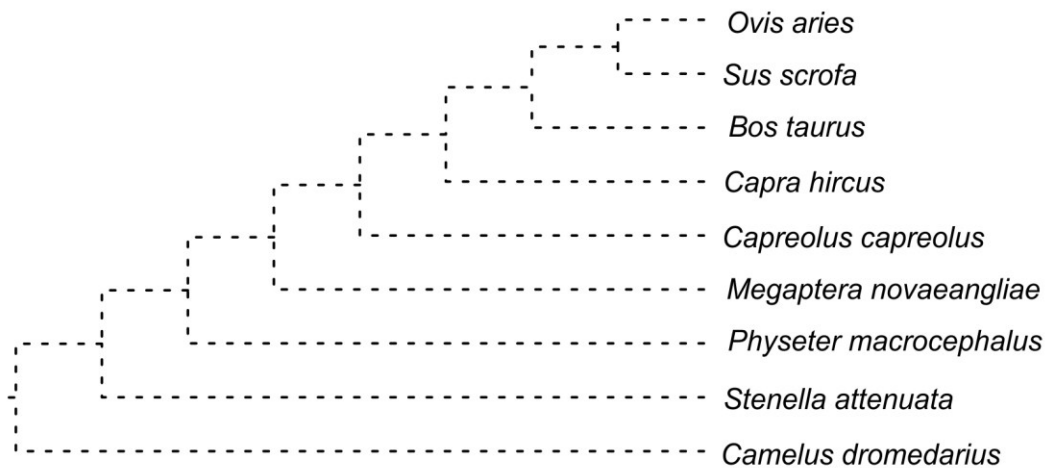
Branches collapsed (creating polytomies) if maximum branch length is zero

'MulTrees' option in effect

No topological constraints in effect

Trees are unrooted

Character-state optimization: Delayed transformation (DELTRAN)



Tree length = 74

Consistency index (CI) = 0.9054

Homoplasy index (HI) = 0.0946

CI excluding uninformative characters = 0.8772

HI excluding uninformative characters = 0.1228

Retention index (RI) = 0.7407

Rescaled consistency index (RC) = 0.6707

## Appendix F: Supplementary Tables/Figures for Chapter Three

Table S3.1 – Equations and p-value of the regressions of skull measurements on CBL for 2D allometric analysis. Significant values ( $p < 0.05$ ) in bold. All variables are log-transformed.

Minke whales	p-value
RW = $-0.732970657063805 + 0.893459386408622 * \text{CBL}$	< <b>0.0001</b>
RL = $-0.791698954067928 + 1.03983954270856 * \text{CBL}$	< <b>0.0001</b>
GWOB = $-1.05194707880379 + 1.01470917227361 * \text{CBL}$	< <b>0.0001</b>
SH = $-0.226180728437348 + 0.81563321533882 * \text{CBL}$	< <b>0.0001</b>
BCL = $-0.573856776565702 + 0.952328453007315 * \text{CBL}$	< <b>0.0001</b>
Humpback whale	p-value
RW = $-0.757738418391704 + 0.908754117864469 * \text{CBL}$	0.093639
RL = $-1.07091219220744 + 1.09840586009484 * \text{CBL}$	<b>0.001661</b>
GWOB = $-1.42371734201319 + 1.08113413200942 * \text{CBL}$	<b>0.006811</b>
SH = $-0.34753027913382 + 0.921933335189547 * \text{CBL}$	0.084451
BCL = $-0.321520741228645 + 0.897797000736778 * \text{CBL}$	<b>0.001044</b>

Table S3.2 – Landmarks used in GM analyses as depicted in Figure S3.1. Reported from Table 2.3.

<b>A</b>	<u>Landmarks whole skull configuration</u>	<b>B</b>	<u>Landmarks rostrum only configuration</u>
1, 12*	anteriormost point of premaxilla	1, 10*	anteriormost point of premaxilla
2, 11*	lateral midpoint of maxilla	2, 9	lateral one-third of maxilla
3, 10*	antorbital notches	3, 8	lateral two-thirds of maxilla
4, 9*	anterolateral point of the supraorbital process of frontal	4, 7*	antorbital notches
5, 8	posterolateral point of the supraorbital process of frontal	5, 6*	anterolateral point of the supraorbital process of frontal
6, 7*	posterolateral end of the exoccipital	11*	anteromedial point of nasal
13*	anteromedial point of nasal	12	posterior end of nasals
14*	apex of supraoccipital		
15, 16	posteroventral edge of postglenoid process of the squamosal		

\*=landmarks from Tsai and Fordyce (2014)

Table S3.3 – Equations and p-value of the regressions of skull shape (whole skull configuration) score on size (LogCS) for 3D allometric analysis.

Species	Regression equation	p-value
Minke whales	Shape score = $-0.325240348077869+5.80157536748848E-02*\text{LogCS}$	<b>0.001</b>
Humpback whale	Shape score = $-0.552049273152472+8.88679643708869E-02*\text{LogCS}$	<b>0.044</b>

Significant values ( $p<0.05$ ) in bold.

Table S3.4– PCA principal components for both configurations. Components ordered according to the amount of variation they represent, from largest to smallest.

<u>Whole skull configuration</u>		<u>Rostrum-only configuration</u>	
Principal Component	% Total Variance	Principal Component	% Total Variance
PC1	32.400	PC1	41.173
PC2	24.898	PC2	19.719
PC3	14.930	PC3	15.153
PC4	7.472	PC4	6.804
PC5	5.856	PC5	5.287
PC6	4.828	PC6	3.756
PC7	3.212	PC7	2.499
PC8	1.921	PC8	2.244
PC9	1.252	PC9	1.118
PC10	0.964	PC10	0.863
PC11	0.710	PC11	0.487
PC12	0.426	PC12	0.430
PC13	0.372	PC13	0.280
PC14	0.267	PC14	0.125
PC15	0.171	PC15	0.063
PC16	0.137		
PC17	0.073		
PC18	0.057		
PC19	0.030		
PC20	0.015		
PC21	0.009		

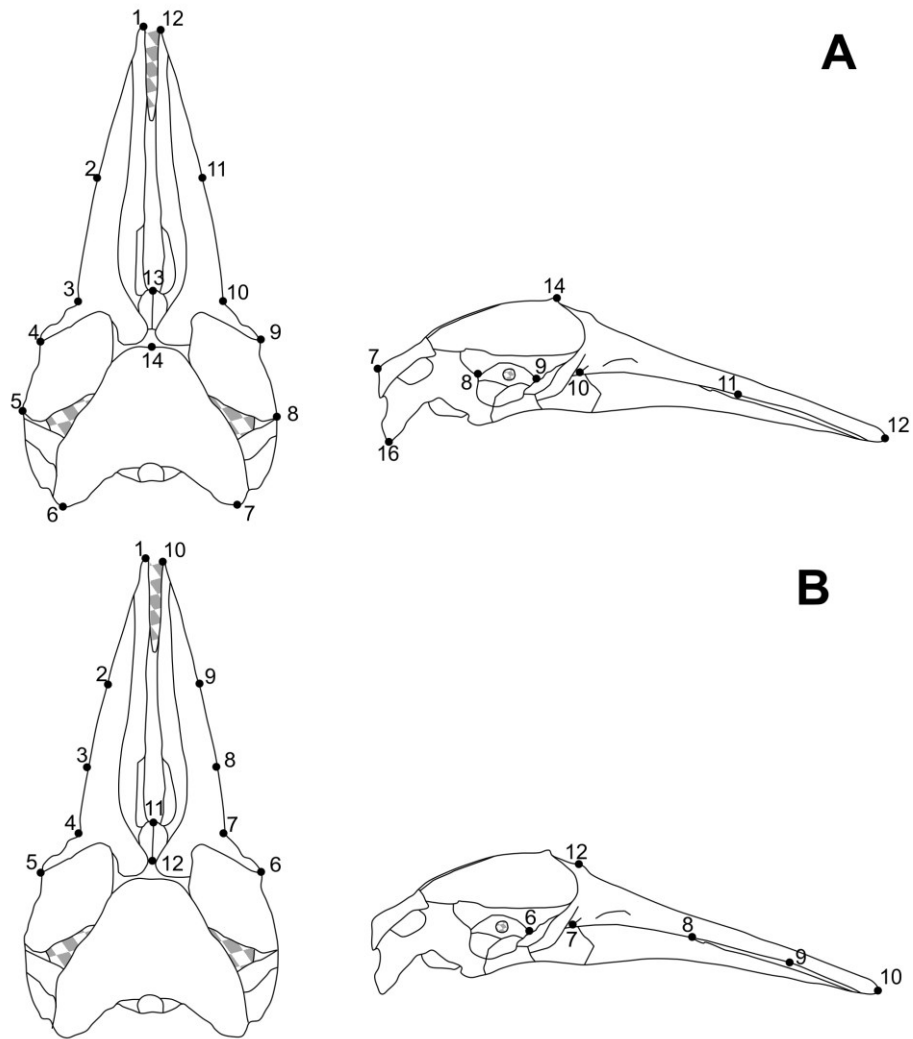


Fig. S3.1 – Selected landmarks for the 16-landmark whole skull configuration (A) and the 12-landmark rostrum-only configuration (B) in dorsal and right lateral view of a skull of an adult minke whale. Original of the skull from Nakamura and Kato (2014), figure modified from Lanzetti et al. (2018). Reported from Fig. 2.2.



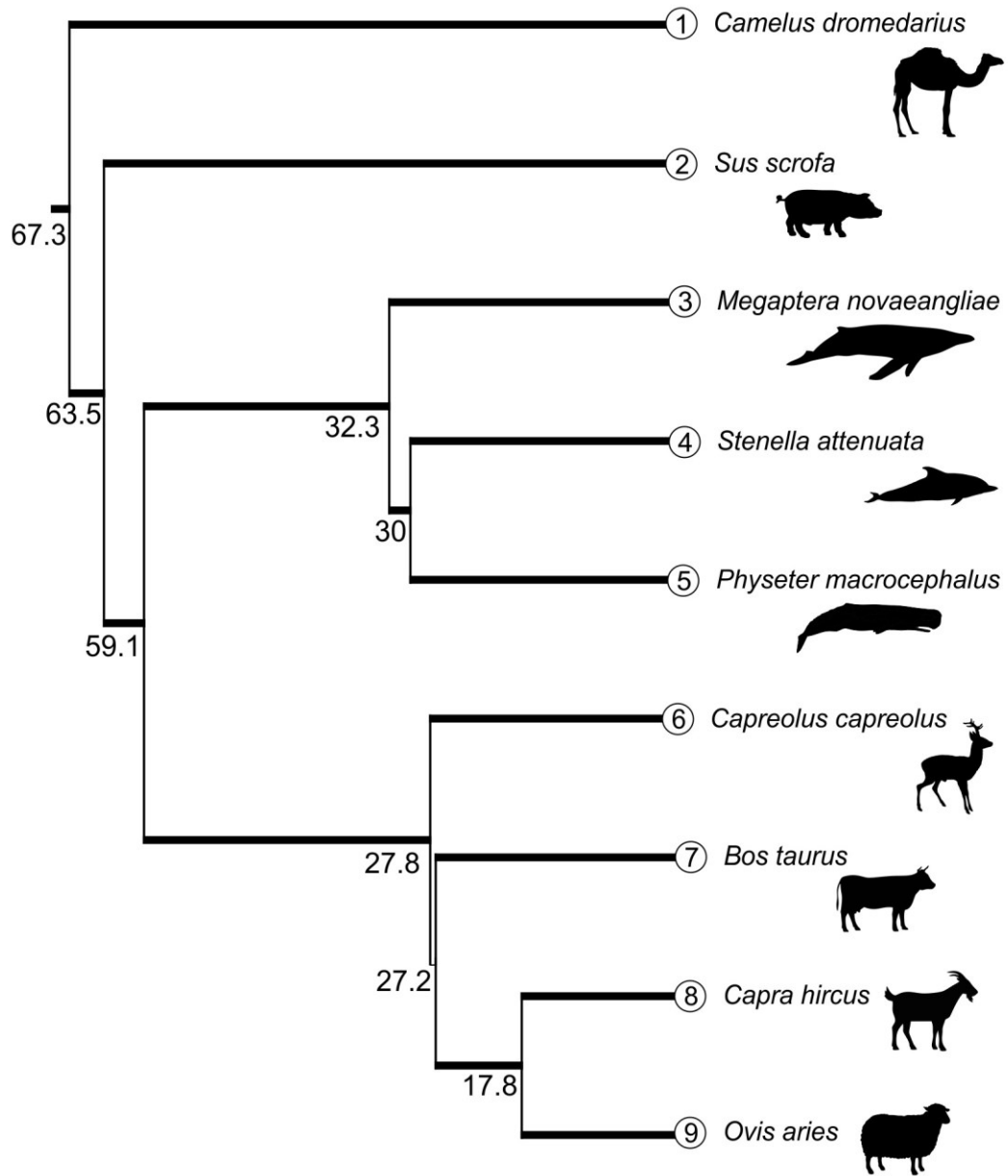


Fig. S3.2 – Tree topology used for ASR analyses of heterochony of the ossification sequence. For consistency with Koyabu et al. (2014), topology and node dates are based on this work and the missing species (*M.novaeangliae* and *P. macrocephalus*) are placed according to Gatesy (2009). The node ages of these taxa were selected based on the date of divergence of the clade they belong to (Mysticeti and Physeteridae) as reported in the reference paper. Node dates placed on the tree are in Ma.

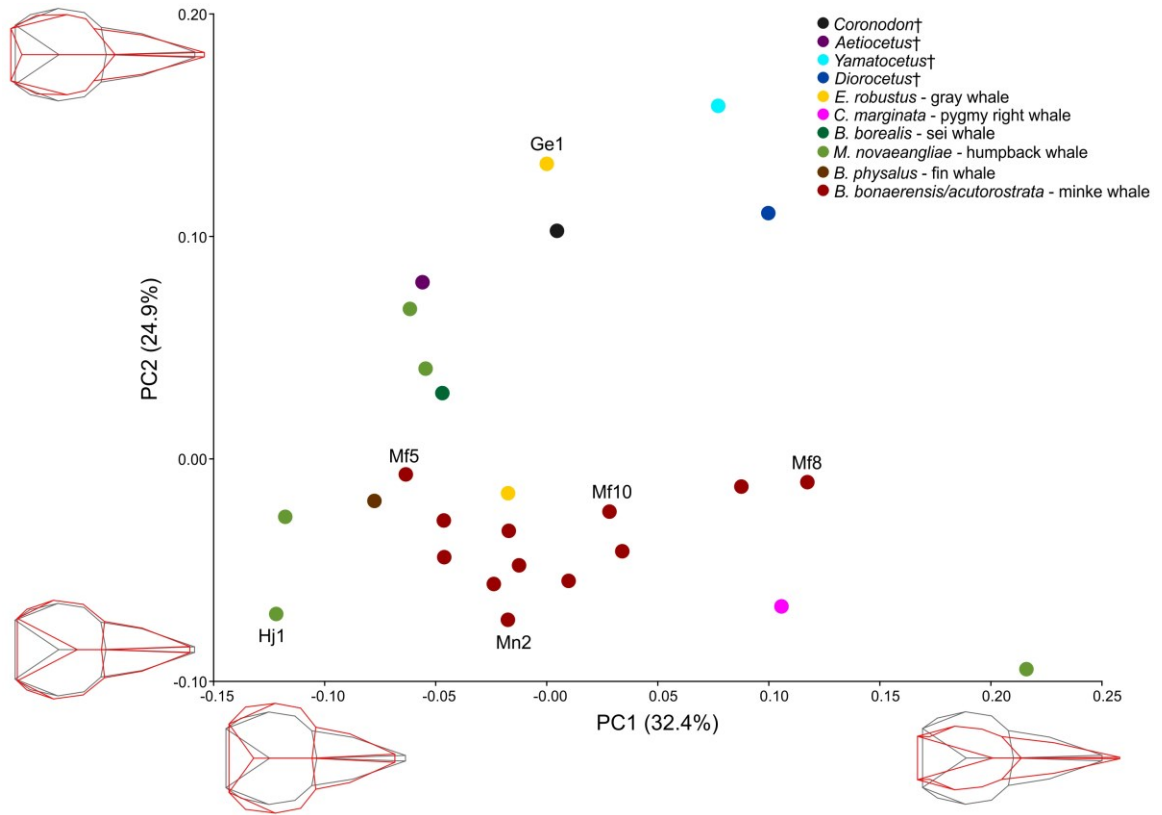


Figure S3.3 – PCA plot for the whole skull configuration. Average shape at 0 on both axes in light gray wireframe, shape at maximum and minimum values of axes in red wireframe. Color of taxa follows Fig. 3.3. Specimens code as in Table 3.1.

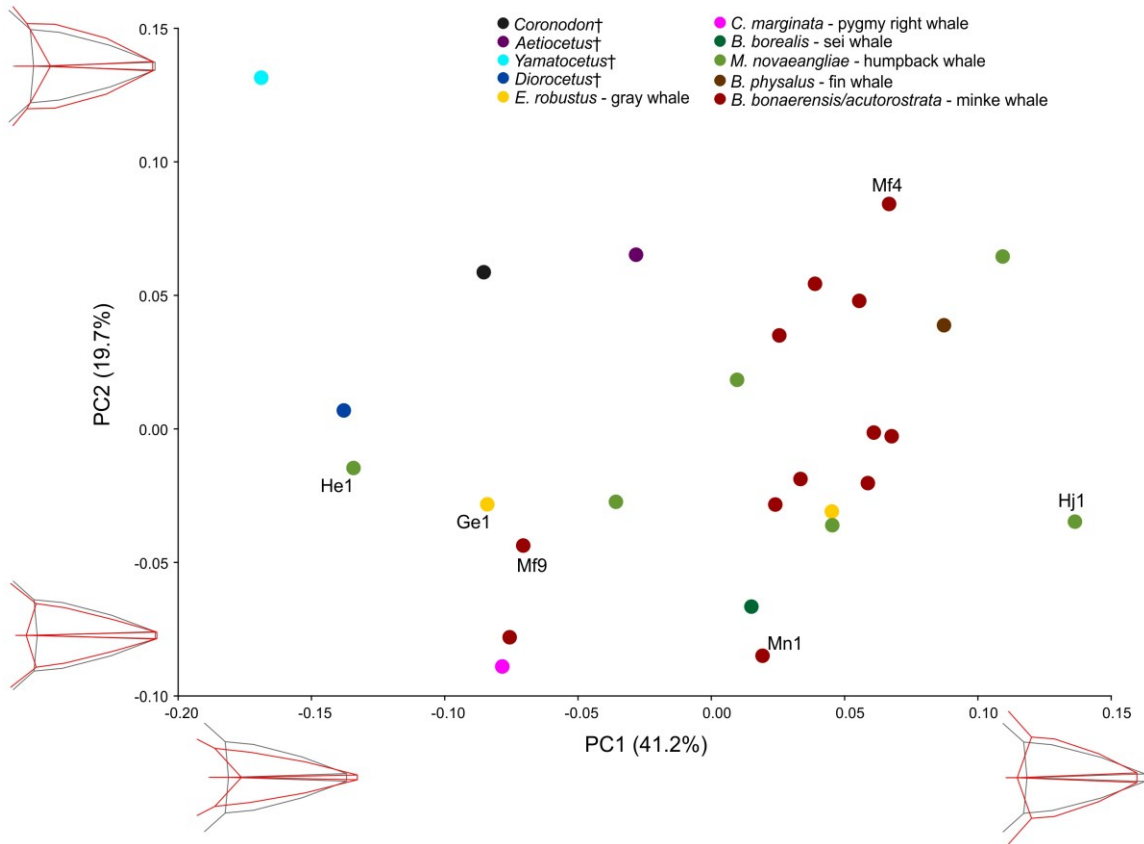


Figure S3.4 – PCA plot for the rostrum-only configuration. Average shape at 0 on both axes in light gray wireframe, shape at maximum and minimum values of axes in red wireframe. Color of taxa follows Fig. 3.3. Specimens code as in Table 3.1.